

Klaatu Verata Ni...

University of Alberta

Rational Design of an HIV-1 Vaccine using a Filamentous Phage Carrier

by

Justin James Bailey

A thesis submitted to the Faculty of Graduate Studies and Research
in partial fulfillment of the requirements for the degree of

Doctor of Philosophy

Department of Chemistry

©Justin James Bailey
Spring 2013
Edmonton, Alberta

Permission is hereby granted to the University of Alberta Libraries to reproduce single copies of this thesis and to lend or sell such copies for private, scholarly or scientific research purposes only. Where the thesis is converted to, or otherwise made available in digital form, the University of Alberta will advise potential users of the thesis of these terms.

The author reserves all other publication and other rights in association with the copyright in the thesis and, except as herein before provided, neither the thesis nor any substantial portion thereof may be printed or otherwise reproduced in any material form whatsoever without the author's prior written permission.

Abstract

Glycans are a diverse and integral component of all biological organisms, making them an ideal target for vaccine development. Carbohydrates often act as weak antigens, lacking the T cell epitopes required to recruit T cell help which is vital to develop a strong and long lasting protective antibody response. Chemical conjugation of glycan antigens to a protein carrier to elicit T cell help has been a successful strategy to improve the strength of the immune response towards glycan-derived haptens. The hapten-carrier concept has been successfully used for numerous synthetic glycoconjugate vaccines now approved for human use.

HIV-1 appears to be an ideal candidate for developing a glycoconjugate vaccine as the exposed HIV-1 envelope protein, gp120, is one of the most heavily *N*-glycosylated proteins known. Glycoconjugate vaccines displaying the glycans of gp120 have thus far failed to elicit protective antibodies that bind to gp120 or neutralize viruses bearing HIV-1 Env. The lack of cross reactivity has been attributed to an inability of the glycoconjugate vaccines to faithfully mimic the carbohydrate-dense gp120 surface.

Described herein is the synthesis of two mannosyl thiol analogues of gp120 glycans, their chemical conjugation to a filamentous phage carrier, and the LC-UV-MS methodology developed to characterize the resulting glycoconjugates. The mannosyl thiols provide access to highly reactive linker chemistry while maintaining a minimal linker length, which may be essential to mimic the limited flexibility of the tightly packed glycans of gp120. Filamentous phage possess a structurally homogenous, repeating surface with closely spaced, solvent exposed amines available for conjugation. This arrangement is ideal for mimicking the glycan shield of gp120. Coupling of mannosyl thiol analogues to the phage carrier produced a densely glycosylated surface where over

80% of the 8,100+ conjugation sites of the phage were occupied, as was determined to an unprecedented level of clarity by LC-UV-MS. The phage glycoconjugates were shown to interact with anti-HIV-1 glycan-specific antibody 2G12 with 0.5 nM avidity, ranking it as one of the best 2G12-binding antigenic mimics described thus far. Mice immunized with the phage glycoconjugates elicited high titres of carbohydrate-specific antibodies that were unable to cross react with gp120.

Acknowledgements

I would first like to thank my research supervisor, Professor David R. Bundle for his leadership and guidance during the years I have spent at the University of Alberta. I joined the Bundle group under the recommendation of my first chemistry mentor, Dr. Lois Browne and was unaware at the time of what a top notch research group I had become a part of. Together, these two mentors have been a significant guiding force in my life.

I would also like to thank Professor Jamie K. Scott of Simon Fraser University for the opportunity to work on developing a filamentous phage glycoconjugate vaccine for HIV-1. This project took me a lot farther down the rabbit hole than I initially anticipated, which may be partly due to the creative freedom I was given. What was supposed to be a quick and easy project of *'creating α -linked mannosides, which is like shooting fish in a barrel'*, ended up being a five year test of sanity, endurance and exciting breakthroughs.

This project would not have been as successful without the assistance of the exceptional support staff in the Department of Chemistry at the University of Alberta. Angie Morales-Izquierdo, Randy Whittal and Béla Reiz of the mass spectrometry facility were instrumental to the success of my project. I will also cherish the many impromptu NMR lessons from Mark Miskolzie, even though they never seem to fully sink in.

I would like to thank all the Bundle group members for their friendship and comradery over the years. Of all the group members, Joanna Sadowska in particular stands out. Thank you for your support and putting up with my relentless ELISA requests. The grad school experience would not have been complete without the Friday BBQs in the middle of campus, laboratory 'safety meetings', the constant distraction of wilderness adventure, and the general harassment of the beloved post docs. The friendships gained while in grad school have left me with many fond memories.

Lastly, I would like to thank my family for their love and support over the years.

Table of Contents

CHAPTER 1: Design of a Synthetic HIV-1 Carbohydrate Vaccine	1
Preface	1
Part I: Carbohydrate-based Vaccine Design	1
Carbohydrates in Biological Systems	1
History of Carbohydrate Vaccines	7
Immune Response to Carbohydrate Antigens	8
Immunoglobulin Diversity and Recognition	13
Glycoconjugate Vaccine Carriers	17
Glycoconjugation Techniques	21
Part II: Human Immunodeficiency Virus Vaccine Design	27
HIV and AIDs	27
HIV Molecular Epidemiology	28
HIV Life Cycle	31
Structural Biology of HIV Env Glycoproteins	34
History of HIV Glycoconjugate Vaccine Design	44
Phase III Vaccine Trials	48
Glycans of the gp120 Glycan Shield	50
Part III: Scope of Project	54
Preface	54
Ff Phage Biology	55
Filamentous Phage as a Vaccine Carrier	58
Synthetic Glycan Antigens to Represent the gp120 Glycans	61
Linker Strategy	63
Concluding Remarks	64
References	66
CHAPTER 2: Synthesis of Oligo-Mannopyranosyl Thiol Analogues of the High-Mannose Oligosaccharides Found on HIV-1 gp120	104
Part I: Synthetic Aspects of Carbohydrate Chemistry	104
Introduction to Carbohydrate Chemistry	104
Glycoside Formation	106

The Anomeric Effect	108
Neighbouring Group Participation	109
Synthesis of Mannosyl Thiols	110
Part II: Synthesis of Mannosyl Thiol Analogues	115
Retrosynthetic Analysis	115
Synthesis of Mannosyl Donor Building Block 5	120
Synthesis of 3,6-Dihydroxy Mannoside Building Block 4	122
Synthesis of Mannosyl Disulfide Building Block 3	124
Synthesis of Tetrasaccharide 32	131
Synthesis of Pentasaccharide 38	133
Deprotection of Tetrasaccharide 32 and Pentasaccharide 38	135
Synthesis of Azidomethyl 1-Thio-Mannopyranosides	139
References	143
CHAPTER 3: Conjugation of the Oligo-Mannose Analogues to Filamentous Phage and their Characterization	153
Part I: Refining Conjugation Methodology	153
Preface	153
Purification of Filamentous Phage	153
Quantifying Conjugations to Filamentous Phage	155
Optimization of Linker Additions	160
Determining the Sites of pVIII Conjugation	163
Optimization of Glycoconjugation Reactions	167
Part II: Preparation of Glycoconjugates for Vaccination	172
Tetra- and Pentasaccharide Glycoconjugations	172
β -Glucan Conjugations	174
Analysis of Phage Integrity	176
References	180
CHAPTER 4: Immunization Studies	186
Part I: Binding Studies of Phage Glycoconjugates	186
Preparation of Ubiquitin and BSA Glycoconjugates	186
Ubiquitin Glycoconjugate Binding Studies	187
Phage Glycoconjugate Binding Studies	189

Part II: Mouse Immunizations	192
ELISA Titrations of Mouse Sera	192
Concluding remarks	199
References	201
CHAPTER 5: Closing Remarks and Future Directions	203
References	206
CHAPTER 6: Experimental	207
Methods	207
Compounds	215
References	260
Appendices	261
Appendix List	261
Appendix A1	262
Appendix A2	286
Appendix A3	292
Appendix A4	293

List of Figures

Figure 1. Glycan biosynthetic pathways.	3
Figure 2. <i>N</i> -linked glycan biosynthetic pathway.	6
Figure 3. Representation of glycopeptide MHC presentation and the TD/TI immune responses.	11
Figure 4. B cell maturation.	14
Figure 5. Antibody recombination.	15
Figure 6. A model of the antibody antigen-binding site.	16
Figure 7. An example of a heterobifunctional linker.	25
Figure 8. HIV-1 and HIV-2 groups and subtypes.	29
Figure 9. Global distribution of HIV-1 group M subtypes and recombinants from 2004 to 2007.	30
Figure 10. HIV life cycle.	32
Figure 11. Diagrams of the structure of the gp120.	35
Figure 12. Model of the induced conformational change of gp120 upon binding CD4.	37
Figure 13. The crystal structure of gp120 _{SIV} in an unliganded conformation (PDB: 2BF1) and gp120 _{HIV} bound to CD4 in the CD4-induced conformation (PDB: 2B4C).	38
Figure 14. Model of virus-mediated membrane fusion, based on studies of the influenza virus hemagglutinin and HIV gp41 crystal structures.	39
Figure 15. NMR structure of trimeric SIV gp41 ectodomain in the postfusion six-helix bundle conformation (PDB: 2EZR).	40
Figure 16. Principle of tomography.	41
Figure 17. The 3-dimensional reconstruction of the HIV-1 _{JR-FL} Env structure at ~11 Å resolution.	42
Figure 18. Mapping of the Env protomer.	43
Figure 19. Structures of typical HIV-1 high-mannose oligosaccharides that were examined for their affinity to 2G12 by competitively inhibiting 2G12-binding to immobilized gp120 in an ELISA.	45
Figure 20. Oligomannose structures that were evaluated for their ability to inhibit binding to 2G12 to immobilized gp120 in an ELISA.	46
Figure 21. Glycoconjugates used as immunogens in animal studies.	47
Figure 22. <i>N</i> -linked glycan processing in the secretory system.	51
Figure 23. MALDI-TOF MS analyses of the <i>N</i> -linked glycans ([M+Na] ⁺ ions)	52
Figure 24. Divergence of gp120 glycosylation from host cell glycosylation.	53
Figure 25. Ff phage structure.	56
Figure 26. Ff phage life cycle.	57
Figure 27. The structure and assembly of the major coat protein pVIII of the f1.K phage (modified from PDB: 2C0W).	59
Figure 28. A modeled comparison of the surface amines of the f1.K and Qβ capsids.	60
Figure 29. A comparison of the glycan density of an f1.K glycoconjugate and gp120.	61
Figure 30. The target 1-thio mannosides for the HIV-1 vaccine.	62

Figure 31. Two short amine and thiol reactive linkers.	63
Figure 32. Representations of glucose.	104
Figure 33. Early glycosylation reactions performed by Michael (A), Fischer (B) and Koenigs-Knorr (C).	107
Figure 34. Reaction at the anomeric center.	108
Figure 35. The origins of the anomeric effect.	109
Figure 36. Biomolecular mechanism of the Koenigs-Knorr glycosylation of a 1,2- <i>trans</i> glycosyl donor.	110
Figure 37. Three methods used to install an anomeric thiol.	112
Figure 38. Common methods of forming unsymmetrical disulfides.	114
Figure 39. The complexities of thiol-disulfide exchange.	114
Figure 40. SDS-PAGE of f1.K phage purified by CsCl, Zeba™ Spin Desalting column or Detoxi-Gel™ endotoxin removing column.	154
Figure 41. Diagram of the LC-UV-ESI-MS system.	158
Figure 42. The LC-UV chromatogram of the pVIII coat protein of f1.K phage.	158
Figure 43. The LC-UV chromatogram of f1.K phage conjugated with linker 54.	159
Figure 44. Nomenclature of fragment ions from MS/MS of a peptide.	164
Figure 45. The LC-UV chromatogram of f1.K-(4- <i>yne</i>) linker conjugate.	164
Figure 46. A selection of the fragment ions obtained from the MS/MS results displayed over the pVIII _{f1.K} sequence for the conjugates of peaks 1-3	165
Figure 47. A selection of the fragment ions obtained from the MS/MS analysis are displayed over the pVIII _{f1.K} sequence for the conjugates of peaks 4 and 5	166
Figure 48. The LC-UV chromatogram of f88-(4- <i>yne</i>) and a comparison of the pVIII sequence of f1.K and f88.	167
Figure 49. LC-UV-ESI-MS analysis of f1.K-SIA-Mono glycoconjugate.	168
Figure 50. Reaction scheme for the initial monosaccharide conjugations to f1.K phage.	169
Figure 51. LC-UV chromatograms of the f1.K-SIA-Penta and f1.K-SIA-Tetra conjugates, and a representative deconvoluted mass chromatogram.	173
Figure 52. Agarose gel electrophoresis analysis of phage DNA on a 0.8% agarose gel in 4x GBB buffer.	177
Figure 53. Analysis of phage protein using a modified SDS-PAGE system.	178
Figure 54. Transmission electron micrographs of f1.K phage particles.	179
Figure 55. LC-UV and LC-MS chromatograms obtained from Ub-SIA-Tetra.	187
Figure 56. ELISA results of labeled ConA titrated against ubiquitin glycoconjugates and gp120.	188
Figure 57. ELISA results of antibody 2G12 titrated against ubiquitin glycoconjugates and gp120.	189
Figure 58. ELISA results of ConA titrated against the phage tetra- and pentasaccharide glycoconjugates.	190
Figure 59. ELISA results of antibody 2G12 titrated against the phage tetra- and pentasaccharide glycoconjugates.	191

Figure 60. Titration of immune sera against ubiquitin glycoconjugates.	193
Figure 61. Titration of immune sera against BSA glycoconjugates.	194
Figure 62. Sera analysis for crossreactive anti-gp120 antibodies.	196
Figure 63. Sera analysis of mice immunized with phage conjugates treated with polymixin B.	198

List of Schemes

Scheme 1. An example of the coupling strategy using the SIA crosslinker and mannopyranosyl thiol 2.	64
Scheme 2. Retrosynthesis of tetrasaccharide 1 and pentasaccharide 2.	115
Scheme 3. Utilizing stannylidene chemistry for temporary 3,6-di- <i>O</i> -protection to allow for the installation of more permanent 2,4-di- <i>O</i> -protection.	117
Scheme 4. Regioselective opening on benzylidene acetals to achieve 2,4-di- <i>O</i> -protection of mannose.	117
Scheme 5. Kong's one-pot method to produce a 3,6-differentially protected mannoside.	118
Scheme 6. Retrosynthetic elaboration of building blocks A and C to the synthetic targets 3 and 4.	119
Scheme 7. Retrosynthetic elaboration of the donor building block B to imidate 5.	120
Scheme 8. Synthesis of triacetyl mannose orthoester 8.	120
Scheme 9. Synthesis of mannose donor building block 5.	121
Scheme 10. The disarming effects of the ester protecting groups reduce the susceptibility of donor 5 towards acidic activation and trichloroacetamide formation (A) while increasing its susceptibility to basic degradation and reversion to trichloroacetonitrile (B).	122
Scheme 11. Synthesis of allyl mannopyraonside 12.	122
Scheme 12. Attempted one-pot synthesis of the 2,4-di- <i>O</i> -benzoylated intermediates 13 and 14.	123
Scheme 13. Synthesis of 3,6-dihydroxy building block 4.	124
Scheme 14. Preparation of diisopropyl- <i>N</i> -(<i>tert</i> -butylsulfanyl)hydrazodicarboxylate 15.	124
Scheme 15. Synthesis of mercapto- <i>tert</i> -butyl 1-thio-mannoside 17.	125
Scheme 16. Deacetylation of mannosides 17.	125
Scheme 17. Structures of reagents explored to increase tritylation yield.	126
Scheme 18. Comparison of conditions explored to increase the yield of trityl ether formation of mannosyl disulfide 19.	127
Scheme 19. Silylation and benzoylation of intermediate 19 to produce the 3,6-differentially protected building block 3.	128
Scheme 20. Synthesis and investigation of the acetylated analogue of building block 3.	129
Scheme 21. Regioselective protection of intermediate 18.	130
Scheme 22. Regioselective glycosylation of triol 25 to produce disaccharide 26.	130
Scheme 23. Synthesis of the disaccharide acceptor 29.	132
Scheme 24. Synthesis of protected tetrasaccharide analogue 32.	133
Scheme 25. Synthesis of acceptor disaccharide 34.	134
Scheme 26. Synthesis of 3,6-branched trisaccharide donor 37.	135
Scheme 27. Glycosylation of disaccharide 34 to form the pentasaccharide target 38.	135

Scheme 28. Reduction and deacetylation of 17 to produce 1-thio- β -mannopyranose 39.	137
Scheme 29. Deprotection of tetrasaccharide 32 to yield the target tetrasaccharide 1.	138
Scheme 30. Deprotection of pentasaccharide 38 to yield the target pentasaccharide 2.	139
Scheme 31. Formation of the azidomethyl monosaccharide 44.	140
Scheme 32. Formation of azidomethyl tetrasaccharide 47.	141
Scheme 33. Formation of azidomethyl pentasaccharide 50.	142
Scheme 34. The crosslinkers evaluated in the phage conjugation studies.	160
Scheme 35. Preparation of the azide-functionalized β -glucan 56.	175
Scheme 36. A concise oligomannose synthetic scheme	204

List of Tables

Table 1. Examples of functional groups used in conjugation reactions.	23
Table 2. Average bond energies and lengths of sulfur and oxygen with silicon and carbon.	113
Table 3. Glycosylation conditions explored for the coupling of donor 5 and acceptor 25.	131
Table 4. Conditions investigated for the disulfide reduction of 18 to form the free thiol 39.	136
Table 5. The effects of pH and reaction time on the loading of the 2-alkynyl linker on f1.K phage.	162
Table 6. The effects of linker equivalents on the degree of conjugation using the 4-alkynyl crosslinker 54 and f88 phage.	162
Table 7. Linker addition results of f1.K and f88 phage.	163
Table 8. Conjugations of mannose monosaccharides to f1.K phage.	170
Table 9. Glycoconjugation results of f1.K and f88 phage linker conjugates with tetra- and pentasaccharide.	174
Table 10. Degree of conjugation of the heterogenous linker addition of SIA and 4-alkynyl crosslinker 54 to f1.K phage.	175
Table 11. Results of the f1.K conjugation to tetrasaccharide, pentasaccharide and β -glucan 56.	176

Abbreviations

Ac	acetyl
AcOH	acetic acid
Ac ₂ O	acetic anhydride
BF ₃ ·OEt ₂	boron tetrahydrofuran complex
[bmim]BF ₄	1-butyl-3-methylimidazolium tetrafluoroborate
Bn	benzyl
<i>t</i> -BuSH	2-methyl-2-propanethiol
Bz	benzoyl
BzCl	benzoyl chloride
DCM	dichloromethane
DEA	diethylamine
DEAD	diethyl azodicarboxylate
DIAD	diisopropyl azodicarboxylate
DMAP	4-dimethylaminopyridine
DMF	dimethylformamide
EtOAc	ethyl acetate
Et ₃ SiH	triethylsilane
FeCl ₃	iron(III) chloride
Fmoc	9-fluorenylmethyloxycarbonyl
FmocCl	9-fluorenylmethyloxycarbonyl chloride
gCOSY	gradient –selected correlation spectroscopy
HBr	hydrobromic acid
HF	hydrofluoric acid
¹ H NMR	proton nuclear magnetic resonance

MeOH	methanol
NaOMe	sodium methoxide
NaSAc	sodium thioacetate
Piv	pivaloyl
PivCl	pivaloyl chloride
R _f	retardation factor
TBDMSCl	<i>tert</i> -butylchlorodimethylsilane
TBDPSCl	<i>tert</i> -butylchlorodiphenylsilane
TDSCl	dimethylthexylsilyl chloride
TEA	triethylamine
TFA	trifluoroacetic acid
TLC	thin layer chromatography
TMSOTf	trimethylsilyl trifluoromethanesulfonate
Tr	trityl or triphenylmethyl
TrCl	triphenylmethyl chloride
TrCl-DMAP	4-dimethylamino- <i>N</i> -triphenylmethylpyridinium chloride

CHAPTER 1: Design of a Synthetic HIV-1 Carbohydrate Vaccine

Preface

Despite the successes of modern medicine and drug development, treating disease can require significant financial resources, extended treatment times and suffering of the afflicted. A more effective method for disease control is through vaccination as it offers long term preventative protection to the population. Vaccines function by presenting an antigen to the immune system in order to safely build up immunity in preparation for future encounters with the same antigen. Prophylactic vaccines typically contain a dead or attenuated pathogen or immunogenic proteins, glycoproteins or polysaccharides that are associated with the pathogen. Carbohydrates are present on the surface of every cell and pathogen and are often structurally distinct, which is ideal for vaccine design. Advances in both glycomics and carbohydrate synthesis in the last 30 years have made it much easier to deduce the complex structures of naturally occurring glycans and to synthesize workable quantities of pure and structurally defined oligosaccharides for biological study. Synthetic saccharides have since been incorporated into vaccines as haptens, adjuvants, and as cell-specific targeting motifs.

This introductory chapter provides a thorough background of the concepts intrinsic to the rational design of a carbohydrate-based vaccine against HIV-1, focusing on the topics of bioorganic chemistry, immunology and structural biology.

Part I: Carbohydrate-based Vaccine Design

Carbohydrates in Biological Systems

Carbohydrates are one of the four fundamental classes of biomolecules, along with lipids, nucleic acids and amino acids. As an integral part of all organisms, carbohydrates are directly involved in many extra- and intra-cellular processes. On the surfaces of mammalian and bacterial cells, carbohydrates are found attached to proteins and lipids which are involved in cell signaling, molecular recognition and adhesion events.¹ Within the cell, glycan modifications of proteins often directly influence the synthesis, stability, recognition and regulation of proteins and their

interactions with other biomolecules.² Carbohydrate interactions with receptor proteins such as lectins, enzymes, hormones, toxins, antibodies, bacteria and viruses play crucial roles in host-pathogen interaction, immunity and disease progression.³ With such physiologically important functions under the influence of glycans, it is clear that carbohydrates are promising candidates in drug development.

Of all biomolecules, carbohydrates are arguably the most abundant and structurally diverse biomolecule found in nature.⁴ The extraordinary complexity of glycan structures arises from a combination of multiple available linkage points, the stereochemistry of the linkages, and the opportunity for branching. In contrast to protein complexity, two identical amino acids can only produce a single dipeptide whereas two identical hexose monosaccharides can produce 11 different disaccharides. The disparity between protein and polysaccharide complexity is exponential. Four different amino acids may produce 24 different tetrapeptides, but four different hexose monosaccharides may form 35,560 distinct tetrasaccharides.⁵ Thus, carbohydrates encode an immense amount of biological information. The abundance and high diversity of carbohydrate structures found on the exterior of microbes and viruses makes them attractive targets for vaccine development.

Despite the complexity of oligosaccharide structures, they are not produced by a template encoded by the genome, but are instead produced by glycosyltransferase and glycosidase enzymes in the secretory pathway. Glycosyltransferases mediate the transfer of activated glycans to acceptor molecules such as proteins, lipids or another glycans. Glycosidases function opposite to glycosyltransferases, catalyzing the cleavage of specific glycosidic linkages. Although it may appear counterproductive, both enzymes collaborate to determine the structural outcome in pathways of glycan biosynthesis. Glycan assembly proceeds sequentially where glycosyltransferase/glycosidases rely on the glycan structure produced by the previous enzyme in the biosynthetic pathway in order to produce the substrate for the next enzyme in the sequence.⁶ In this way, as proteins and lipids transit through the endoplasmic reticulum (ER) and Golgi apparatus, the glycans they bare become increasingly oligomeric and complex. Glycan biosynthesis exhibits species-specific and even cell type-specific diversity.⁷ Even within a specific cell type, glycoconjugates are typically produced as mixtures of glycoforms, where the

glycan structures and glycosylations patterns differ while the carrier structure remains the same.⁸ In eukaryotes, the glycome consists primarily of glycolipids, glycoproteins and glycosaminoglycans (proteoglycans) (Figure 1).⁹

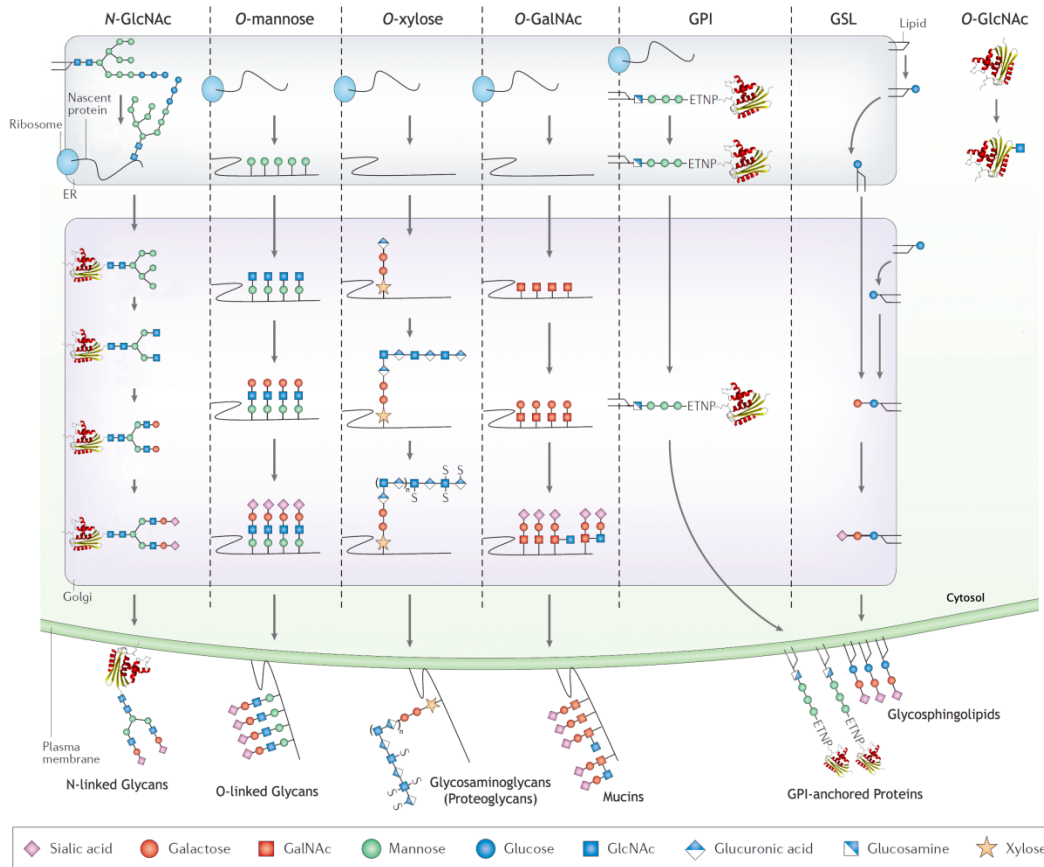


Figure 1. Glycan biosynthetic pathways. The dotted lines separate the pathways and are used to represent the inner membrane of the ER and Golgi apparatus. Proteins may also contain multiple types of glycans, although only one glycan type per protein is shown here for simplicity. The *N*-linked pathway begins with the transfer of a preformed glycan to the nascent protein soon after emerging from the ribosome. The glycan is further modified in both the ER and Golgi. *O*-mannosylation begins in the ER with further elongation occurring in the Golgi. *O*-xylose and *O*-GalNAc-linked glycan assembly occurs exclusively in the Golgi. GPI anchors are assembled in the ER where proteins are attached soon after translation. GSLs begin their synthesis on the cytoplasmic side of the ER after which the glycolipid precursor flips into the lumen and is extended with additional sugars in the Golgi. ETNP: ethanolamine phosphate, S: sulfate. Adapted by permission from Macmillan Publishers Ltd: *Nature Reviews Genetics*, 7, 537-551, ©2006.

Glycolipids fall into two structurally defined categories, either glycosphingolipids (GSLs) or glycosylphosphatidylinositols (GPIs). Both are found on the outer leaflet of the plasma membrane. Glycosphingolipids are characterized by an *O*-linkage between glucose or galactose and ceramide which are further elongated to produce a diverse array of GSLs. They are typically found clustered in lipid rafts where they mediate cell

signaling and recognition on the cell surface.¹⁰ Glycosylphosphatidylinositols are composed of a phosphatidylinositol membrane anchor attached to a short glycan core containing mannose and glucosamine. Proteins are linked at their C-terminus through a phosphodiester linkage of phosphoethanolamine to this core glycan. GPI-anchored proteins are involved in intracellular protein sorting and signaling pathways.¹¹

Glycoproteins are defined by the type of linkage between the glycan and amino acid. There are 13 monosaccharides and 8 amino acids that can be involved in the initial glycosidic linkage, and though many permutations of the glycan-amino acid linkage can form, certain linkages are more prevalent than others.¹² *N*- and *O*-linked glycans are linked through the asparagine nitrogen and either the serine or threonine hydroxyl, respectively, and are the most common protein glycosylations in mammalian cells. Other linkages, such as *C*-linked glycans which are linked through the C2 atom of tryptophan, are less common.¹³

O-glycans are attached through serine and threonine and can be further subdivided into groups based on the initiating glycan of the chain. *O*-linked glycoproteins initiated with GalNAc are characteristic of mucins.¹⁴ Mucins are highly glycosylated trans-membrane proteins that function as cellular lubricants through their high hydrophilicity. *O*-mannose linked glycans are predominantly found in the brain, nerve and muscle tissues of mammals.¹⁵ *O*-glycosylation of serine/threonine with single GlcNAc has been shown to modulate protein activity.¹⁶ *O*-GlcNAc modification is unique as it takes place in the cytoplasm and nucleus rather than in the secretory pathway, and often competes for the same posttranslational modification sites as phosphorylation.¹⁷

Glycosaminoglycans are a subset of *O*-glycosylation, linked to proteins through xylose to serine residues. These glycans tend to be long and linear with many repeating disaccharide units that are often further modified by sulfation. Heparin, heparan sulfate, chondroitin sulfate and dermatan sulfate are all glycosaminoglycans. They are used in extracellular structural roles, such as in cartilage, as well as being involvement in signal transduction and regulatory processes.¹⁸

N-glycans are the most widely distributed class of glycans, being found across all domains of life.^{12, 19} In eukaryotes, *N*-glycans are linked by β -GlcNAc to asparagine in the

consensus sequence Asn-X-Ser/Thr, where X can be any amino acid but proline. The consensus sequence is universal for *N*-glycosylation, although the initiating glycan linkage can vary in prokaryotes.¹⁹ *N*-linked glycosylation differs significantly from other glycan biosynthetic pathways as the glycan is sequentially assembled on a dolichyl pyrophosphate carrier and then transferred *en bloc* onto newly made proteins, rather than being assembled on the protein itself (Figure 2).²⁰ In the majority of eukaryotes, the conserved Glc₃Man₉GlcNAc₂ oligosaccharide is cotranslationally transferred to proteins.²¹ The addition of this oligosaccharide has been shown to contribute to thermodynamic stability and solubility of nascent proteins, leading to improved rates of protein folding.²²⁻²⁴ The terminal glucoses and mannoses in the structure also interact with lectins in the ER which serve to direct proteins to folding, secretion or degradation pathways.²⁵⁻²⁷ After transfer to the Golgi apparatus, a core glycan is created by glycosidases that trim off successive mannose residues (Figure 2) followed by further elaboration into complex structures specific to the cell.

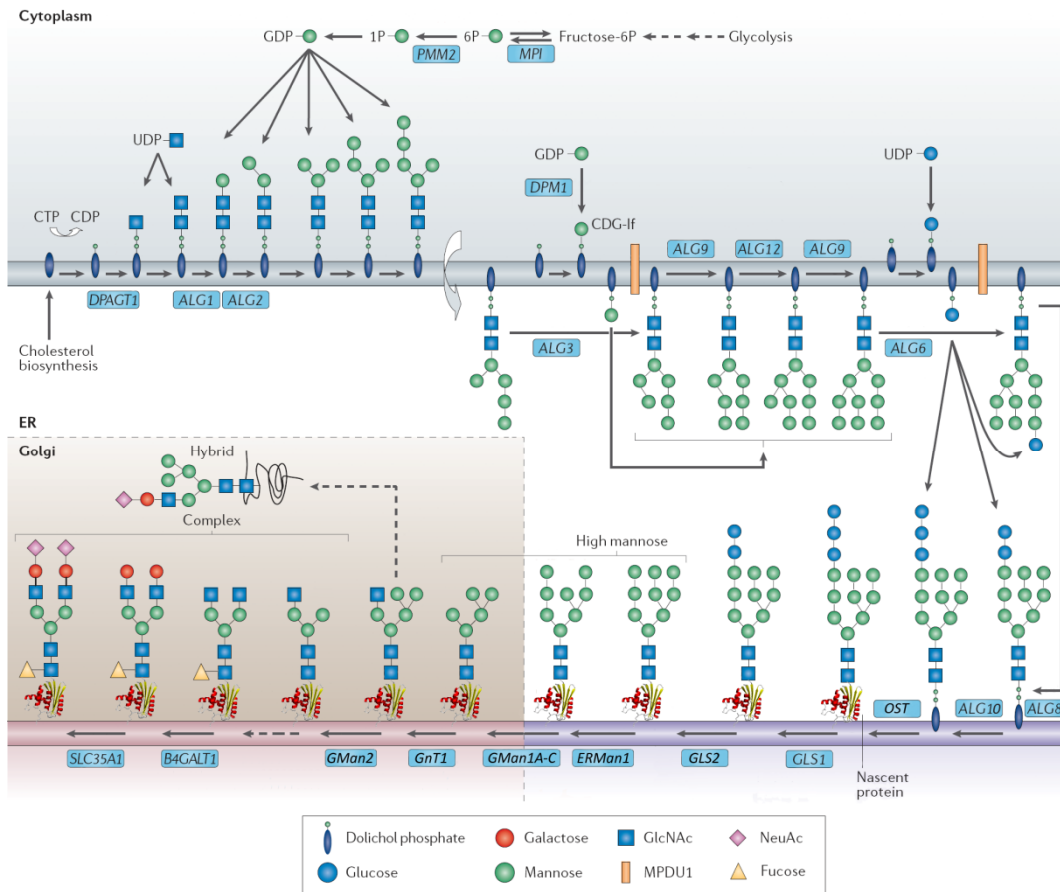


Figure 2. *N*-linked glycan biosynthetic pathway. Dolichol in the cytoplasmic side of the ER membrane is sequentially glycosylated using nucleoside phosphate monosaccharide donors to form the $\text{Man}_5\text{GlcNAc}_2$ structure. The dolichol conjugate then flips into the ER lumen where it is further elaborated using dolichol-phosphate monosaccharide donors. The resulting $\text{Glc}_3\text{Man}_9\text{GlcNAc}_2$ structure is transferred *en bloc* by an oligosaccharidetransferase (OST) complex to asparagine of a nascent protein. The resulting glycoprotein is trimmed to the $\text{Man}_8\text{GlcNAc}_2$ and transferred to the Golgi apparatus. In eukaryotes, this high mannose structure is further trimmed down to $\text{Man}_5\text{GlcNAc}_2$ and sequentially glycosylated to form a hybrid or complex glycan. Complex-type glycans no mannose residues other than the trimannosyl core while hybrid-type glycans retain additional mannose residues. Adapted by permission from Macmillan Publishers Ltd: *Nature Reviews Genetics*, 7, 537-551, ©2006.

Viruses, which rely on host-cell biosynthetic pathways to replicate, utilize host-cell glycosylation pathways to produce primarily *N*-linked viral glycoproteins.²⁸ The glycosylation patterns on viral proteins reflects that of the host cell from which the virus was derived. Glycosylation of viral proteins influences many aspects of the viral life cycle such as receptor binding,²⁹ membrane fusion,³⁰ intracellular transport,³¹ viral assembly/release³² and immune evasion.³³ Enveloped viruses, such as HIV, hepatitis C virus and influenza A virus, are particularly reliant on envelope protein glycosylation for resisting antibody (Ab) neutralization and host-cell entry.³⁴⁻³⁷

History of Carbohydrate Vaccines

The use of carbohydrates to induce immunity is a relatively new strategy, even though Heidelberger and Avery revealed in 1923 that pneumococcal antigens targeted by the immune system were capsular polysaccharide.³⁸ Tillet and Francis took this work a step further and showed that intradermal injection of only pneumococcal polysaccharide would provoke an immune response in individuals suffering from lobar pneumonia.³⁹ In 1944, the first carbohydrate vaccine, consisting of four types of pneumococcal capsule polysaccharides, was tested in 8,000 men in an army air force technical school, roughly half the school population.⁴⁰ The vaccine not only provided significant protection to the immunized students, it also greatly reduced the incidence of pneumonia in the non-immunized, since fewer vaccinated men now carried pneumococcus. Unfortunately, interest in carbohydrate vaccines was lost due to the advent of penicillin during this same period. A steady increase in antibiotic resistance brought back a renewed interest in disease prevention and in 1983, PneumoVax™, the first commercial polysaccharide vaccine, was launched. The vaccine consisted of capsular polysaccharides from 14 serotypes of *Streptococcus pneumoniae*, which has since increased to include 23 serotypes.⁴¹ While this vaccine protects adults against 90% of all infections, the immune response is poor in high risk groups such as children under the age of two, the elderly and the immunocompromised.^{42, 43} Furthermore, immunity only lasts 5-6 years as polysaccharide alone is unable to elicit T-cell help and, subsequently, generates poor B-cell memory.⁴⁴⁻⁴⁶ Polysaccharide vaccines against other encapsulated pathogens, such as *Neisseria meningitidis* and *Haemophilus influenzae* have similar efficacies.⁴⁷

Polysaccharide immunogenicity can be enhanced through conjugation to an immunogenic carrier protein, as was reported by Avery and Goebel in 1931.⁴⁸ Immunization with glycoconjugates provokes a T-cell dependent response,⁴⁹ providing lifelong protection of adults and all persons of high risk.⁵⁰ Glycoconjugate vaccines against *S. pneumoniae*, *N. meningitidis* and *H. influenzae* are currently available, which alleviate the shortcomings of their polysaccharide vaccine counterpart. The *H. influenzae* is currently the only synthetic carbohydrate vaccine on the market, although

development of synthetic carbohydrate vaccines against many other pathogens is in progress.⁵¹

Of growing interest are therapeutic vaccines, which involve production of an immune response against an already existing disease. Carbohydrate vaccines in immunotherapy have primarily been directed against cancers.⁵²⁻⁵⁵ The unregulated growth of cancer cells influences the expression of glycosyltransferases, which can result in the up or down regulation of glycan expression,^{56, 57} produce incomplete glycans or even neoglycans.^{58, 59} The aberrant expression of these self-antigens could be exploited by the immune system to differentiate healthy cells from tumor cells.⁶⁰ Cancer immunotherapy has shown cytotoxicity against tumor cells, although in clinical trials this response was not effective enough to significantly enhance patient survival.⁶¹⁻⁶³ Overcoming immunotolerance of tumor-associated self-antigens remains a challenge.⁶⁴

Carbohydrates have also been exploited in vaccine design as a ligand component to target lectin receptors on antigen-presenting cells. Such an approach has been used to deliver antigens to dendritic cells and macrophages by targeting mannose receptor (CD206) which binds oligosaccharides containing terminal mannose residues.^{65, 66} The resulting antibody response was superior in comparison to control vaccines that lacked the mannose ligands. Other carbohydrate-specific lectins found on antigen-presenting cells, such as DC-SIGN^{67, 68} and Dectin-1⁶⁹, have displayed potential for *in vivo* targeting in vaccine delivery as well.

Immune Response to Carbohydrate Antigens

The immune system is a network of cells, tissues, and organs that defends an organism against a wide range of infectious agents. Immunological protection is achieved through innate immunity and adaptive immunity. The innate immune response is the body's first line of defense, composed of systems and components that are present before infection. These include the body's epithelial barriers, the complement system, inflammatory responses and a variety of leukocytes such as Natural killer (NK) cells, mast cells, neutrophils and dendritic cells. The innate response proceeds very rapidly and in a non-specific manner which is in contrast to the adaptive

response which can take days to weeks to become effective and is highly specific to the invading pathogen. The adaptive response can either be of humoral (antibody-mediated) or cellular (cell-mediated) nature. Antibodies are produced by B lymphocytes and cell-mediated immunity is coordinated by T lymphocytes.

Antigen-presenting cells (APCs), which include dendritic cells, macrophages and B cells, bridge the innate and adaptive immune responses.⁷⁰ Dendritic cells (DCs) are the most effective APCs, possessing the broadest range of antigen presentation, as well as cytokine secretion.⁷¹ They migrate through the body where they serve as sentinels for foreign antigens. Pathogens are identified by APCs through pattern recognition receptors (PRRs), such as Toll-like receptors (TLRs) and C-type lectins, which recognize conserved structural components of microbes that are foreign to the host; lipopolysaccharide is an example of one such pathogen-associated molecular pattern (PAMP). Pathogen interaction with PRRs triggers intracellular signaling cascades that lead to proinflammatory responses, increased antigen presentation, cytokine production, and upregulation of co-receptors.^{70, 72} Antigen is internalized by DCs through phagocytosis or receptor-mediated endocytosis and then processed for loading onto major histocompatibility complex (MHC) receptor proteins which are shuttled to the cell surface.⁷³ DCs then migrate from the periphery to lymphoid tissues where they can present antigen to immature lymphocytes. T-cell receptors (TCRs), found on the surface of T cells, are able to recognize antigens bound to MHC molecules, and thereby activate the adaptive immune system. The interaction between antigen and the specific PRR that was involved in DC maturation will have far reaching effects into how the adaptive immune response develops.⁷⁴

There are two classes of MHC receptors that interact directly with TCRs and either the CD8 or CD4 co-receptor (Figure 3). Class I MHC activates cytotoxic T lymphocytes (CTL, CD8+ T cells) which destroy cells that are infected by viruses or bacteria, or are damaged in some other way.⁷⁵ Class I MHC is expressed on nearly every cell in the body and is used to present intracellular antigens, such as self-derived antigens or antigens from intracellular pathogens. When CTLs encounter a foreign antigen on a class I MHC receptor of an infected cell, they kill the cell with the release of cytotoxins such as perforins and granzymes. Class II MHC is used exclusively by APCs for

presenting antigens that are taken up from the extracellular environment. Class II MHC presentation activates naive helper T cells (CD4+ cells) which cause them to proliferate and differentiate into helper subtypes. Evidence suggests that APCs provide the main influence in determining the subtype of proliferating helper T cells during class II MHC presentation.^{74, 76-78} In the classic 1986 model,^{79, 80} differentiation to type 1 helper T cells (Th1) cells activate macrophages and CTLs, and differentiation to Th2 cells stimulate B cell proliferation and antibody class switching. New helper T cells are continually being defined outside the Th1/Th2 model,⁸¹ such as T follicular cells (Tfh),⁸²⁻⁸⁴ Th9⁸⁵, Th17,⁸⁶ and Th22,^{87, 88} which has led some to question the continued use of the simplistic 25 year old paradigm.^{89, 90}

Helper T cells, especially Tfh, are important for inducing high-affinity Ab producing B cells to differentiate into long-lived plasma B cells⁹¹ and memory B cells.^{81, 92} Long-term immunological memory, as well as immunoglobulin (Ig) class switching to more specialized antibody types, is a defining characteristic of T cell dependent (TD) responses.⁹³ In contrast, T cell independent (TI) responses have been thought to lack memory B cell production and Ig class switching, although this has frequently been challenged.⁹⁴⁻⁹⁶ It has been shown that B-cells can produce memory without T cell help, although of a different quality, which is discussed more in the next section. In general, TD responses are more effective, and well-documented, at producing lifelong memory cells and protective secondary responses in vaccine development.

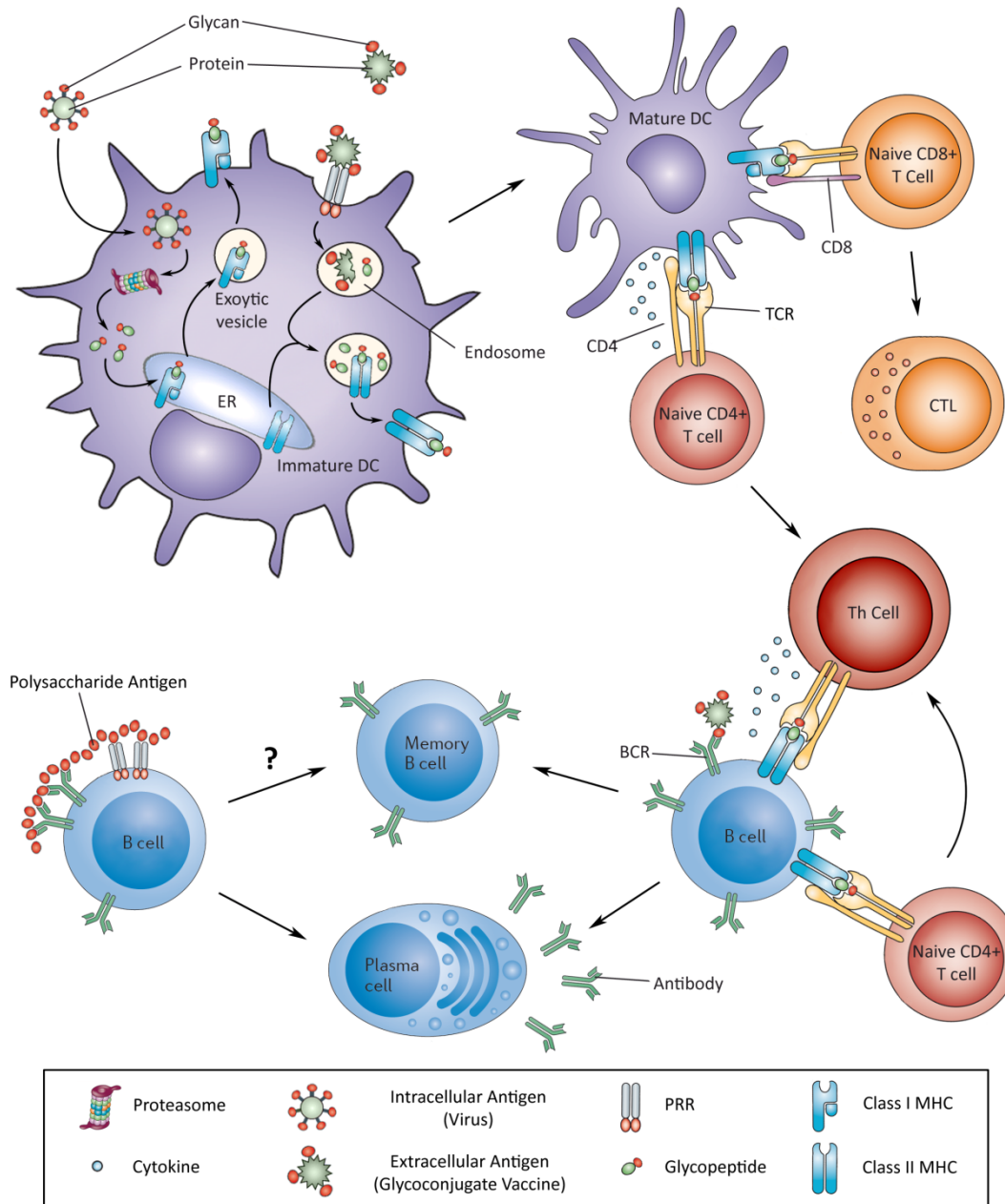


Figure 3. Representation of glycopeptide MHC presentation and the TD/TI immune responses. Class I MHC molecules present glycopeptides derived from intracellular pathogens in the cytosol that have been degraded by the proteasome. Presentation of the class I MHC-glycopeptide complex to naïve CD8+ T cells produces a cellular immune response. Class II MHC presentation of glycopeptides from extracellular antigens induce the maturation of naïve CD4+ T cells into a helper T cells. The cytokine profile of the APC will determine the phenotype of the helper T cell. Stimulation of B cells via activated helper T cells triggers TD proliferation and differentiation into long-lived memory B cells and plasma cells. Polysaccharide alone can also activate B cells through carbohydrate specific BCRs and PRRs, although the effectiveness of a TI response appears insufficient to provide lifelong protection.

TI responses activate B cells through TLRs and the crosslinking of B cell receptors (BRCs) by polymeric antigens with repeating units such as polysaccharides (Figure 3).⁹⁷

Carbohydrate antigens can be converted to TD immunogens by conjugation to a protein carrier in order to access class II MHC presentation for T cell help. In this way, the immune response can be directed towards a carbohydrate while circumventing the disadvantages of a TI response. Glycoconjugates taken up by APCs are digested by proteases in endosomal compartments to yield glycan-peptide fragments. The peptide portion binds class II MHC in the endosome, leaving the carbohydrate distal to the MHC binding groove.⁹⁸ The glycopeptide-MHC complex is presented to the TCR of CD4+ T cells, which recognizes the glycan specifically. MHC-mediated activation of the T cell, along with co-stimulation, results in cytokine release and B cell maturation with consequent Ig class switching. The most common APCs for T cell activation are DCs. Naïve B cells, which also express class II MHC, are thought to be able to activate naïve helper T cells, although their effectiveness has long been questioned.⁹⁹ While it has been shown that naïve B cells, despite expressing lesser numbers of class II MHC,¹⁰⁰ are able to poorly activate helper T cells,¹⁰¹ they are also known to induce T cell tolerance.¹⁰²⁻¹⁰⁵ It is obvious that our understanding of B cells functioning as APCs requires further investigation.

Effective conjugate vaccines require the use of adjuvants to provide the danger signal that accompanies natural infection.¹⁰⁶ Adjuvants enhance the immune response through their interaction with the innate immune system, either acting as ligands for PRRs or directly interacting with signaling pathways that provoke an inflammatory response.^{107, 108} The result is an increase in magnitude of the adaptive response, both in the rate of the response and in antibody titre. Adjuvants can also alter the cytokine profile leading to the qualitative alteration of the adaptive response.¹⁰⁹ Choice of adjuvant can be exploited to effectively stimulate specific helper T cells in order to get the desired immune response. Currently aluminum salts (alum) are the only adjuvant approved for use by the FDA, but this is primarily due to the fact that alum has been safely used for over 80 years, predating the founding of the FDA.¹¹⁰ Squalene and the detoxified LPS derivative monophosphoryl lipid A (MPL) have been approved for adjuvant use throughout Europe. A multitude of adjuvants have been used in clinical trials, including Freund's adjuvant which consists of heat-killed *Mycobacterium tuberculosis*, flagellin from *Salmonella typhimurium* and the saponins QS-21 and GPI-0100.¹⁰⁹ Carbohydrates can also act as potent adjuvants themselves, with β -glucans,

mannans, chitans, lipopolysaccharide and glycosylated mycobacterial components all able to interact with various PRRs.¹¹⁰

The objective of vaccination is to generate B and T cell memory so that the immune system can rapidly clear the immunizing antigen when re-encountered.^{111, 112} T cell help and the selection of high-affinity B cells for memory progression and lifelong antibody production are paramount to this paradigm. Circulating preexisting antibody is especially important for protective immunity against viruses like HIV that can establish a latent infection if initial acquisition is not blocked. Due to the observed successes of glycoconjugate vaccines, conjugation to carrier proteins in order to elicit TD immunological responses continues to be the standard in carbohydrate vaccine development.⁵¹

Immunoglobulin Diversity and Recognition

Antibodies, also known as immunoglobulins (Igs), display an evolving morphology that is linked to the life cycle of B cells. The BCR of naïve B cells is a membrane-bound Ig that is able to bind a specific cognate antigen. Once a naïve B cell is activated, it undergoes a series of genetic and phenotypic changes that may eventually lead to the release of unbound Ig.¹¹³ B cells in the marginal zone of the spleen or lymph nodes are primarily activated in a TI manner, such as through interaction with polysaccharides (Figure 4A). B cells activated in this way are deprived of the conditions that lead to Ig class switching and extensive affinity maturation. This results in differentiation into Ig-producing plasma cells that continue to produce low affinity IgM and, perhaps more importantly, into memory B cells that appear to be unable to live indefinitely. Naïve B cells that are partially activated via APC presentation migrate to the T-B zone border in lymphatic tissue where they rapidly proliferate and undergo productive interactions with T cells (Figure 4B). Some of these B cells continue to proliferate and differentiate into short lived plasma cells without much affinity maturation and class switching. Concurrently, some activated B and T cells migrate into germinal centers where B cells undergo extensive proliferation, somatic hypermutation (SHM) and antigen-affinity driven selection. B cells that gain affinity through SHM are able to outcompete their less avid peers for the necessary survival signals.¹¹⁴ Over time the germinal center is populated with high affinity B cells which can then further

differentiate into long lived memory and short lived plasma B cells.¹¹⁵ These plasma cells can access survival niches in the bone marrow where they can survive indefinitely, secreting protective antibodies for long term protection.

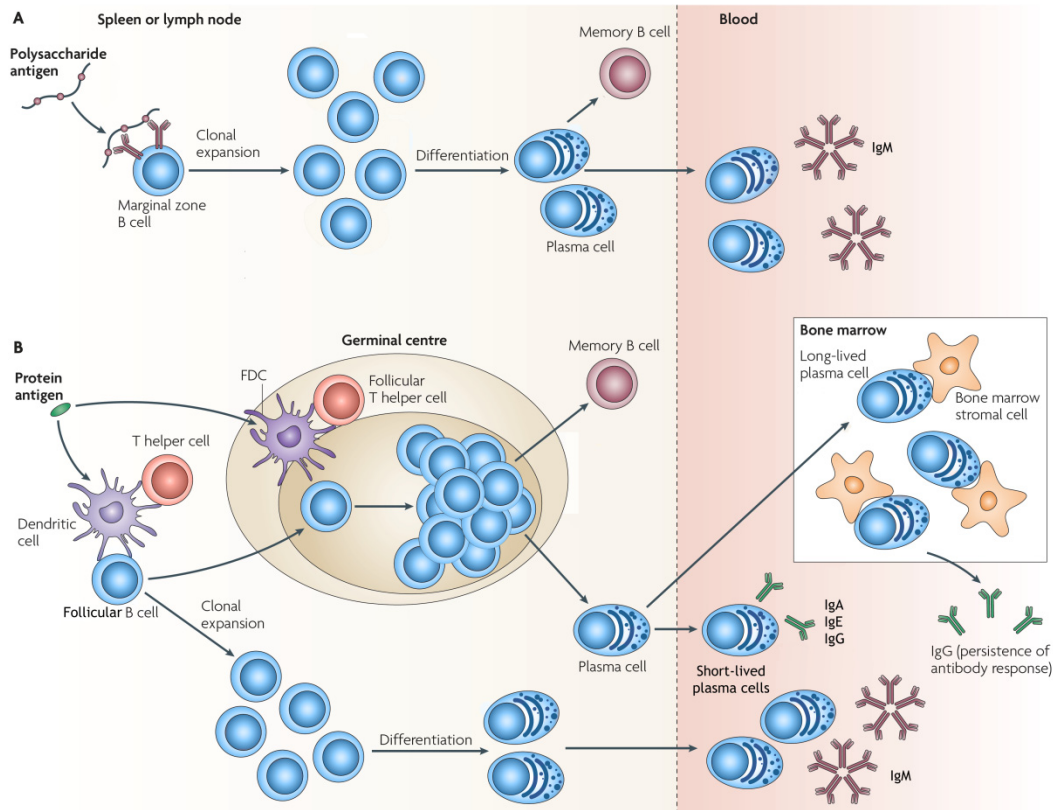


Figure 4. B cell maturation. A| Polysaccharides provoke marginal zone B cells to proliferate and differentiate into short lived, low affinity plasma and memory B cells. B| Proteins presented by APC can activate follicular B and T cells. Such activated B cells can either differentiate into low affinity and plasma cells or migrate to germinal centers where they undergo extensive affinity maturation and class switching. These high affinity B cells can further differentiate into long lived memory B cells and plasma cells. Adapted by permission from Macmillan Publishers Ltd: *Nature Reviews Immunology*, 9, 185-194, ©2009.

IgGs are large Y-shaped proteins that recognize cognate antigens via the antigen-binding sites on the tips of each arm (Figure 5B). IgGs are composed of two heavy chains (H) and two light chains (L) that are linked through disulfide bonds. Both chains contain variable (V) and constant (C) regions. Individual B cells are only able to produce one distinct type of Ig, although it is estimated that 10^{11} IgGs with unique antigen-binding sites can exist. Such diversity is accomplished through the genetic recombination of one of the variable (V), diversity (D) and joining (J) exons that are encoded in the Ig heavy and light chain variable regions (Figure 5A).¹¹⁶ The recombination process is imprecise,

leading to the further diversification of the V(D)J segment through the removal of nucleotides at the site of recombination and the addition of non-templated nucleotides into the exon junctions.^{117, 118} Thus, the initial heterogeneity of Ig antigen-binding sites is generated through the combinations of V, D and J segments and in the way in which they join. The VDJ sequence can undergo further antigen-driven gene diversification through SHM, which introduces point mutations into the V-region exons at high rates.¹¹⁹ SHM is the defining event of germinal centers that enables the selection of B cells that produce higher affinity antibodies.

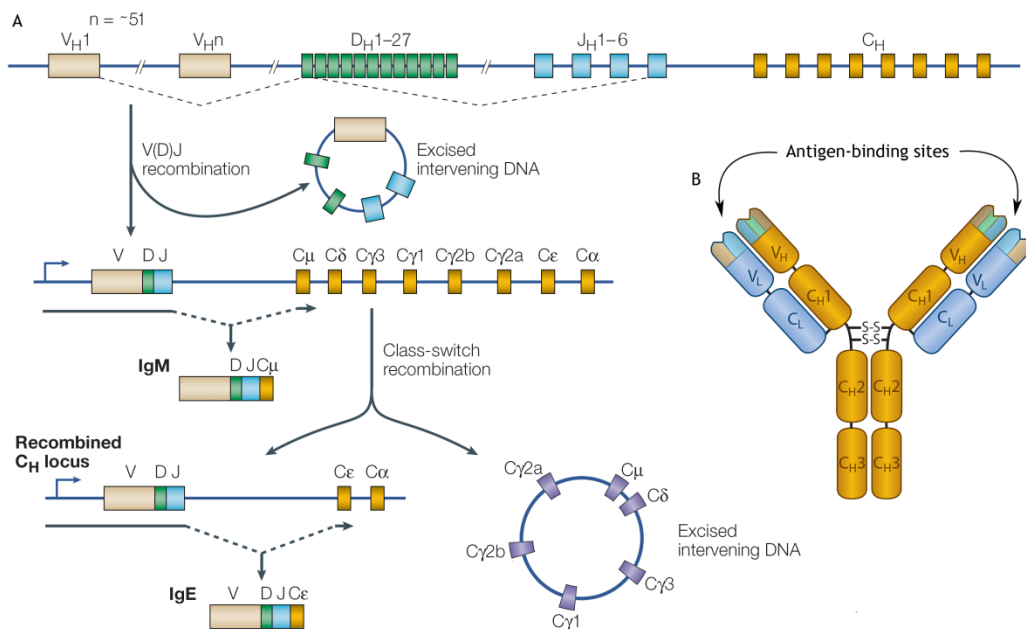


Figure 5. Antibody recombination. A) Organization of the germ-line gene segments of the immunoglobulin heavy chain. DNA recombination of the V, D and J exons form the unique antigen-binding sites on the heavy chain. Light chain recombination proceeds similar to the heavy chain, although there is no D sequence. Transcription across the locus is driven by a promoter upstream of the VDJ sequence which facilitates the synthesis of a μ heavy chain. CSR exchanges the C_{μ} region exon of the heavy chain with an alternative set of downstream constant region exons. B) A model depicting a transcribed antibody is shown here. The heavy chains are shown in gold and the light chains are shown in light blue. The antigen-binding site is composed of the VDJ sequence of the heavy chain and the VJ sequence of the light chain.

Class-switch recombination (CSR) is a genetic process by which antigen-stimulated B cells switch from the initial production of IgM to Igs that have more specialized roles.^{120, 121} CSR exchanges the initially expressed heavy chain constant region exon of IgM and IgD with an alternate downstream constant region exon (Figure 5A). The resulting Ig expression retains the same variable region and antigen specificity but has a secondary heavy chain isotype that possess different effector functions.

The five mammalian isotypes of Ig are known as IgA, IgD, IgE, IgG and IgM. IgM and IgD both function as BCRs in the B cell membrane and are the first secreted antibodies to be produced during an immune response, during which there is limited affinity maturation.¹²² IgM is secreted as a pentameric Ig, which allows for greater avidity for multivalent antigens and other unique properties.¹²³ IgD doesn't appear to play a direct role in antigen clearance as little secreted IgD is found in human serum, although it has recently been shown to play minor immunomodulatory roles.¹²⁴ IgA is the predominant Ig found in mucosal areas such as the gut and respiratory tract and exists as a dimer.¹²⁵ IgE is involved in parasitic immunity and allergen recognition. IgG provides the majority of antibody-based immunity and is the Ig response desired from immunization.

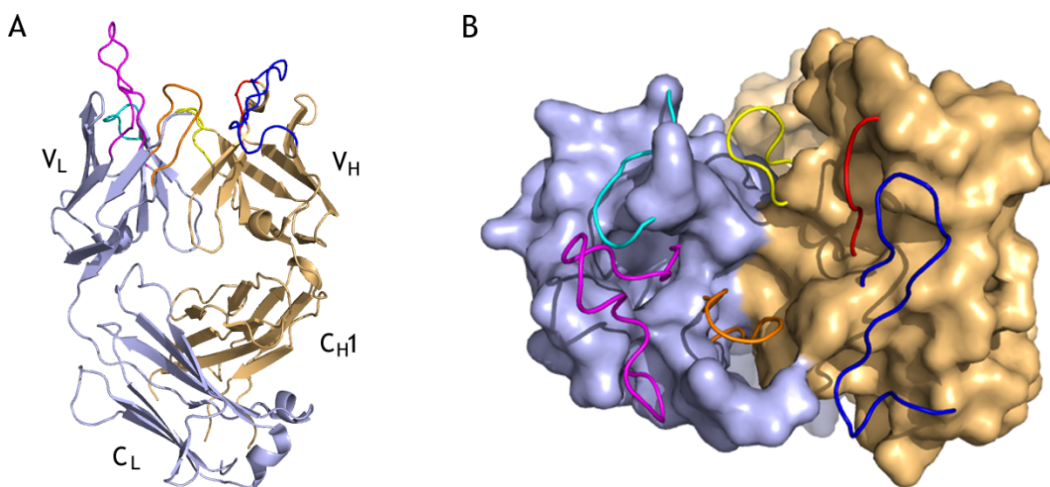


Figure 6. A model of the antibody antigen-binding site. **A|** A ribbon model of the antigen-binding fragment (Fab) of an antibody is shown with the heavy chain in gold and light chain in blue. Each chain of the Fab contains two β -sandwich structures. The antigen-binding site is composed of the colored loops. **B|** A space filling model of the Fab is shown, looking down on the antigen-binding site. The CDRs of both models are colored as follows: CDR H1: red, CDR H2: blue, CDR H3: yellow, CDR L1: magenta, CDR L2: cyan, CDR L3: orange. Modeled from PDB ID: 1H3P.

Carbohydrate antigens typically display lower binding affinity to immunoglobulins than protein antigens. In contrast to peptides that have rich structural and chemical diversity in their functional groups, carbohydrates primarily display only hydroxyl and amine groups for Ig recognition. Ig recognition is thus achieved through a combination of hydrogen bonding to the sugar hydroxyls and van der Waals interactions of the hydrophobic sugar faces with aromatic amino acid side chains.¹²⁶ The binding sites for carbohydrates are predominantly found in shallow indentations formed by the

loops at the ends of β -sheets on protein surfaces.¹²⁷ The antigen-binding site of Igs is formed by the loops of two β -sandwich structures of the heavy and light chain variable regions (Figure 6A). These loops are referred to as complementarity determining regions (CDRs). Both the light and heavy chains contribute three CDRs, named L1, L2, L3 and H1, H2, H3 respectively. CDR L/H1 and CDR L/H2 are encoded by the V sequence, whereas CDR L/H3 includes the V, D (heavy chain only) and J sequence. CDR H3 in particular displays the largest variability in its length, sequence and structure and is suitably centrally located within the antibody-binding site (Figure 6B).^{128, 129} Studies have shown that CDR H3 is the dominant determinant of specificity in the recognition and binding of antigens.¹³⁰ The CDR1 and CDR2 sequences, originating from the germline V sequences, display more cross-reactive recognition of antigens.

Glycoconjugate Vaccine Carriers

Proteins are the most commonly utilized carriers in glycoconjugate vaccines primarily for their ability to elicit TD responses. Protein carriers can also offer additional benefits such as mitogenic activity and adjuvant-like properties that enhance the immune response.¹³¹⁻¹³⁵ While a wide variety of proteins have been utilized as carriers in a research environment, only a few have been approved for human use. Such approval generally requires a safe record of injection into host subjects, extensive knowledge of the protein structure and consistent hapten conjugation to yield near homologous characterizable conjugates. The choice of carrier can also affect the immunological outcome of vaccines,¹³⁶ although comparative studies often yield conflicting results and are difficult to interpret due to the coexistence of other variables such as conjugation technique, adjuvant type, glycan composition and vaccination protocol.¹³⁵⁻¹⁴⁰

The five main carrier proteins used in commercially available vaccines today are tetanus toxoid (TT), diphtheria toxoid (DT), cross-reactive material 197 (CRM₁₉₇), *N. meningitides* outer membrane protein complex (OMPC), and non-typeable *H. influenzae* (Hib) derived protein D (PD). The first utilized carrier proteins, DT and TT, were chosen due to their safety track record accumulated from their use in tetanus and diphtheria vaccinations dating back to the 1920's.^{141, 142} CRM₁₉₇ is a nontoxic mutant of DT, containing a single missense G52E mutation which eliminates its destructive enzymatic

activity.¹⁴³ Without the need for detoxification, CRM₁₉₇ is thought to have better intact helper T cell epitopes over the chemically treated toxoids.¹⁴⁴ This may be the reason why CRM₁₉₇ conjugate vaccines against bacterial influenza and meningococcal disease have demonstrated superior immunogenicity in infants over similar vaccines utilizing DT carriers.^{137, 145, 146} OMPC glycoconjugates have displayed enhanced immunogenicity over the toxoid carriers which is attributed to OMPC's additional engagements with the immune system.^{135, 147} OMPC is recognized by TLRs on macrophages and dendritic cells, inducing cytokine production that enhances the B cell immune response.^{134, 148} OMPC has also been shown to interact with B cells directly to up-regulate costimulatory ligand expression and providing mitogenic stimuli.^{133, 134} These additional interactions with the immune system may account for why a single inoculation of OMPC Hib glycoconjugate vaccine is able to induce protective levels of anti-Hib polysaccharide antibodies, whereas similar CRM₁₉₇ and DT conjugates require multiple booster immunizations.^{135, 138} The repeated use of the same carrier for different glycoconjugate vaccines can lead to immune interferences which can impact the immunogenicity of concurrent or subsequent vaccinations.^{149, 150} For this reason, as well as its proven safety record in *H. influenzae* vaccines and known structural homogeneity, PD has been employed as a glycoconjugate vaccine carrier.^{151, 152} As an interesting side effect, pneumococcal polysaccharide conjugates of PD, which is derived from *H. influenzae*, have been shown to induce immunity against both *S. pneumoniae* and *H. influenzae*.^{153, 154}

Many other proteins are used routinely for glycoconjugate vaccines in a research environment. Two carriers of interest are keyhole limpet hemocyanin (KLH) and N19. KLH is a carrier protein isolated from the mollusk *Megathera crenulata* that has potent immunological properties. Glycoconjugates of KLH have been able to elicit antibody responses against haptens that are poorly immunogenic, such as self-antigens that are frequently used in cancer therapeutic vaccines.¹³⁹ The large complicated heterogeneous structure of KLH has impeded its approval as a vaccine carrier in North America, although it has been approved for use in Europe and Asia. N19 is a designer protein born out of the need for a new carrier construct to avoid the risk of carrier-specific suppression.¹⁵⁵ N19 is composed of 19 peptide sequences derived from antigens to which the human population is frequently exposed. The peptide sequences liberated upon cellular processing are able to bind a wide range of class II MHC

molecules and are recognized by T helper cells. Glycoconjugates of N19 using Hib and meningococcal oligosaccharides produced competitive results when compared to similar vaccines utilizing classical carriers.^{155, 156}

Fully synthetic glycoconjugate vaccines utilizing synthetically made peptide carriers have been produced to overcome some drawbacks of protein carriers.¹⁵⁷ Peptides have the benefits of being easier to purify and characterize, and allow for controlled hapten addition to produce well defined structures. Peptides can also be tailored for loading onto class I or class II MHC to direct either a cellular or humoral response. Despite the advantages peptide carriers offer, a peptide epitope taken out of context of the whole antigen brings with it challenges. Peptides may not follow the same processing pathways as their native protein equivalent, leading to loading onto the unintended MHC class and producing an unexpected type of immune response. Peptide epitopes also need to be relevant to a broad population of MHC allotypes and require predictable cellular processing in order to assure the desired T cell epitope is presented. Promiscuous peptide epitopes that can be presented by a wide range of MHC molecules have been identified, although predicting peptide processing remains difficult.¹⁵⁸ Peptides are also poorly immunogenic due to their size and simplicity. This has been alleviated through advances in adjuvants, conjugation to TLR ligands and direct delivery to dendritic cells *in vitro*.¹⁵⁷

Viral nanoparticles (VNPs) and virus-like particles (VLPs) have also been used as scaffolds for displaying carbohydrates haptens in vaccine design.¹⁵⁹⁻¹⁶² VNPs are whole virus particles that characteristically are unable to replicate in mammals, such as plant viruses and bacteriophage. VLPs consist of the envelopes or capsids from viruses without the viral genome or any infectious viral components. The viral capsids (VCs) of VNPs and VLPs are composed of structural proteins that assemble in a highly organized manner. VLPs have been FDA approved and are used in hepatitis B virus (HBV) and human papillomavirus (HPV) vaccines. VCs used to present antigens have been shown to provide immunologically superior responses, even without adjuvant,¹⁶³ than carriers that provide less organized presentation.¹⁶⁴⁻¹⁶⁷ The demonstrated safety, immunogenicity and structural definition have made VCs attractive carriers for antigen presentation.

The highly ordered structure of VCs, as well as their particulate nature, provides many advantages to stimulating the immune system. It has been shown that the immune system is primed to recognize and respond to antigens that are the size of viruses.¹⁶⁸ VCs interact with many APCs through PRRs which leads to effective priming of both humoral and cellular immune responses.^{169, 170} The VC, being composed of protein, provides a route for attached glycans to induce TD B cell responses. VCs can also provoke TI stimulation of B cells through the cross-linking of BCRs and TCRs by the patterned presentation of glycan antigens. Interestingly, viral displays of antigen can induce class switching to IgG earlier and with much higher titres than antigen displayed on smaller carriers.^{164, 171, 172} The increased class switching efficiency is thought to be a consequence of the synergistic activation of B cells through both TLRs and BCRs, bridging the TI and TD responses.^{165, 173, 174}

Other carrier strategies have been devised to include TLR interaction and adjuvant-like properties. Dendrimeric carriers that cluster glycan haptens present the glycans in a somewhat repetitive manner which may be favourable for uptake and presentation by APCs, much like virus particles. Glycodendrimers have been able to elicit immune responses that are much more efficient than their monomeric equivalents.^{175, 176} Dendrimer structures are fully synthetic and must include helper T cell epitopes in order to be immunogenic.¹⁷⁶ Lipopeptides have been used as immunogenic carriers that include inherent adjuvant properties. TLRs on APCs recognize lipopeptides which simultaneously incites cytokine release and internalization of the glycolipid conjugate for processing and presentation. The desired immune response can be tailored by modification of the helper T cell peptide epitope, the external adjuvant and through multivalent presentation.¹⁷⁶ Most interestingly, zwitterionic polysaccharides (ZPSs) have recently been used as immunogenic carriers. In 2004, Kasper and co-workers demonstrated that ZPSs are able to bind class II MHC molecules and elicit a TD immune response similar to that of exogenous protein.¹⁷⁷ ZPS has since been used as a carrier for a tumor-associated carbohydrate antigen for the development of an entirely synthetic carbohydrate vaccine.^{178, 179} ZPS has been suggested to be a promising carrier substitute for proteins in anti-cancer vaccines as an immune response against the carrier protein may suppress the already weak antibody development against the self-carbohydrate hapten.^{150, 180}

Glycoconjugation Techniques

Many methodologies and synthetic strategies have been developed to couple carbohydrates to proteins and peptides.¹⁸¹⁻¹⁸³ The most commonly employed conjugation methods are through chemical ligation techniques which offer the greatest flexibility with respect to structural modifications. Enzymatic methods have also been used to modify existing carbohydrates on proteins/peptide scaffold as well as to form carbohydrate-amino acid linkages.

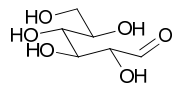
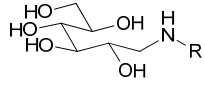
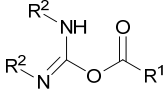
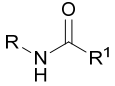
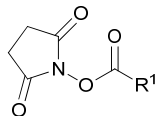
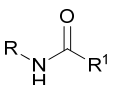
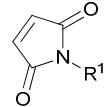
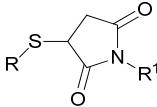
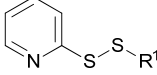
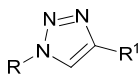
While enzymatic synthesis can efficiently form specific glycosidic linkages under mild conditions with no need for protection/deprotection strategies, often expensive enzymes are required that are available for a relatively small number of reactions and are unsuitable for large scale preparations of glycoconjugates.¹⁸⁴ Molecular biology techniques have taken enzymatic synthesis one step further through the manipulation of glycoconjugates *in vivo*, although controlling the biosynthetic glycosylation products has been difficult. Advances in the past decade in biosynthetic regulation and recombinant DNA technology have produced successful biological platforms for controlled glycoconjugate production.¹⁸⁴⁻¹⁸⁹ By modifying the genes involved in glycosylation pathways of bacteria or yeast, or inserting entire cassettes encoding foreign glycosylation pathways, glycoprotein expression systems have been developed to produce customized glycosylation.¹⁹⁰

Glycopeptide/protein assembly follows two general approaches: the elongation of an existing glycan-bound amino acid or the direct attachment of the entire carbohydrate to an amino acid. The latter approach is employed for the majority of glycoconjugate synthesis. The rest of this section will focus on chemical ligation techniques that are used for the convergent assembly of synthesized carbohydrates to protein.

Carbohydrates and their protein and peptide carriers contain natural reactive centers that can be exploited for chemical ligation. The amino acid side chains of proteins and peptides provide some functional groups that can be used for indiscriminant conjugation. The most commonly utilized functional groups are the amino group of the N-terminus and the ϵ -amine of lysine. Amino groups tend to be

accessible on the protein surface due to their positive charge at physiological pH. The carboxyls of the C-terminus, aspartic acid and glutamic acid are also utilized as functional groups for conjugation but require chemical activation prior to coupling. Like amines, the charged, hydrophilic nature of carboxyls favors surface expression on proteins where they can be hydrated by the aqueous environment. Cysteine thiols are the strongest protein nucleophile and can also be used for conjugation. Cysteine residues are frequently found as disulfides with another cysteine residue which play important roles in protein structure and conformation. Accessing cysteine thiols and disulfides for conjugation can be difficult as they are usually located within the core of the protein. In contrast to amino acids, carbohydrates impart mostly indiscriminate alcohol groups and, if the reducing end is free, an aldehyde for conjugation. To increase the breadth of reactive functional groups, carbohydrates are frequently synthesized with functionalized aglycones. Peptides have also been synthesized to incorporate unnatural amino acids that contain unique functional groups to provide selective chemical functionalities for conjugation.¹⁹¹⁻¹⁹⁶ Unnatural amino acids have been incorporated into proteins for glycoconjugation but have yet to gain widespread use due to the inconvenience of producing and purifying these unnatural proteins.¹⁹⁷⁻²⁰¹

Table 1. Examples of functional groups used in conjugation reactions.

Reaction	Nucleophile	Electrophile	Product
Reductive amination	$R-NH_2$		
Oxime formation	$R-O-NH_2$	R^1-CHO	$R-O-N=N-R^1$
Hydrazone formation	$R-NH-NH_2$	R^1-CHO	$R-NH-N=N-R^1$
Carbodiimide coupling	$R-NH_2$		
Reactive (NHS) ester	$R-NH_2$		
Thioalkylation	$R-SH$	$Br-CH_2-C(=O)-R^1$	$R-S-CH_2-C(=O)-R^1$
Thiol addition	$R-SH$		
Disulfide exchange	$R-SH$		$R-S-S-R^1$
Thiol-ene	$R-SH$	$CH_2=CH-R^1$	$R-S-CH_2-CH_2-R^1$
CuAAC	$R-N=N=N^+$	$C\equiv C-R^1$	

The most direct conjugation method is through reductive amination of the open chain aldehyde from the reducing end of the carbohydrate with protein amino groups. This has been particularly useful due to the high abundance of surface lysines. However, reductive amination is slow and inefficient, requiring large excesses of carbohydrate and long reaction times for completion.²⁰² The loss of conformation of the reducing saccharide is also a drawback, especially in small oligomers, since it may be important for epitope recognition.^{203, 204} For these reasons, aglycone linkers with more

reactive functional groups are usually installed at the reducing end of carbohydrates during synthesis. The functionality of the aglycone is often decided before synthesis although linkers are often able to be modified late in the synthesis to allow for a broad selection of conjugation techniques. Aldehydes, amines, carboxylic acids, thiols and azides are commonly used functional groups in conjugation reactions (Table 1).

Ideal conjugation reactions are highly selective, simple orthogonal reactions that do not yield side products and are highly efficient under mild conditions.²⁰⁵ One of the most selective and efficient reactions used for chemical conjugation is the Cu(I) catalyzed azide-alkyne cycloaddition (CuAAC) reaction between an azide and alkyne to form a 1,2,3,-triazole.²⁰⁶ Since it was introduced in 2002, CuAAC chemistry has been extensively used in medicinal chemistry for conjugation reactions with overwhelming success.²⁰⁷ Thiols have also demonstrated click-like reaction efficiencies with reactive alkenes under free-radical conditions.²⁰⁸ Thiols are also versatile nucleophiles and have been reacted preferentially with haloacetyls, maleimides and other free thiols. Carboxylic acids activated as *N*-Hydroxysuccinimide (NHS) esters react preferentially with amines and are frequently used for conjugation to proteins. NHS esters bearing an orthogonal reactive group can also be used to functionalize the surface amines of proteins for reaction with complementary functionalized carbohydrates. Heterobifunctional crosslinkers function in this way, containing two or more reactive centers capable of chemically attaching specific functional groups (Figure 7). A variety of bifunctional linkers are commercially available for reaction between many functional group combinations.

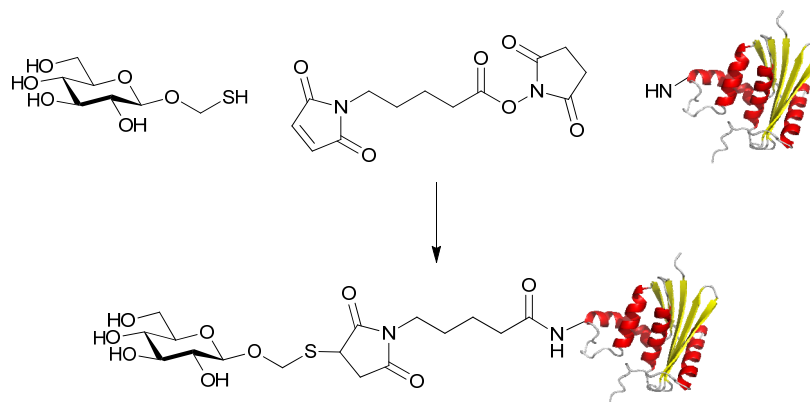


Figure 7. An example of a heterobifunctional linker. The *N*-(δ -maleimidopentanyloxy) succinimide ester cross linker contains a thiol-reactive maleimide group on one end and an amine-reactive NHS ester on the opposite end.

The spacer arm of the linker is an important consideration for glycoconjugate vaccine design. Ideally the spacer should be immunologically silent to maintain the antibody response focused on the carbohydrate hapten and avoid epitope suppression. Longer linkers can alleviate steric hindrance that might impede coupling between large molecules, but present a more accessible linker epitope to the immune system. Rigid, constrained linkers in particular have been shown to elicit a significant amount of undesirable antibodies. In the case of an Le^y conjugate vaccine, a rigid cyclic maleimide linker produced a strong IgM and IgG response against the linker, while a more flexible alkyl maleimide linker helped direct the humoral response towards the carbohydrate hapten.²⁰⁹ In contrast to this observation, a rigid linker has been shown to generate higher IgM and IgG titers over a short flexible linker which only produced low levels of IgM and no detectable IgG Abs.²¹⁰ Furthermore, while flexible linear linkers are shown to be less immunogenic, linear linkers that incorporate unique functionalities such as the hydrazido or maleimido groups, have been revealed to create unwanted neoepitopes that diminish the amount and affinity of the humoral response to the carbohydrate hapten.²¹¹⁻²¹³ Such discrepancies may be due to the relatively low antigenicity of carbohydrate haptens compared to that of the spacer. In order to increase the immunogenic focus onto the hapten, the Bundle group has used a stereodiversified linker strategy, where a carbohydrate hapten is linked through a set of structurally distinct linkers.²¹⁴ A small increase in antibody titres against a disaccharide antigen was

observed using this technique, suggesting that affinity maturation selects for B cells that better recognize the constant carbohydrate hapten portion of the glycoconjugate.

Part II: Human Immunodeficiency Virus Vaccine Design

HIV and AIDs

In 1981 an unusual pattern of disease began to emerge in the United States as Kaposi's Sarcoma, a rare form of lung cancer, and opportunistic diseases such as pneumonia were increasing in the homosexual community. Although many unfounded assumptions and theories were made during this time as to the cause of the disease;²¹⁵⁻²¹⁷ it was eventually recognized that the underlying problem was a defective immune system.²¹⁸ The depletion of CD4+ T-helper cells was known to be the cause of immunosuppression, with transmission of the disease thought to be spread by an unknown virus, as the routes of transmission were similar to that of hepatitis B virus.²¹⁸ As study of the increasing numbers of immunocompromised individuals grew to include intravenous drug users,²¹⁹ hemophiliacs,²²⁰ Haitians,²²¹ females^{222, 223} and infants,²²⁴ many names were given to the disease, with *acquired immunodeficiency syndrome* (AIDS) eventually being settled upon.²¹⁸

With reports of the AIDS epidemic increasing throughout the world, it wasn't until 1983 that the human immunodeficiency virus (HIV) was first recognized as the cause of AIDS.²²⁵ Barré-Sinoussi and Montagnier received the Nobel Prize in Medicine in 2008 for this discovery. Since the discovery of HIV, there has been an estimated 60 million people infected worldwide with 25 million who have since died from AIDS.²²⁶ Although the current pandemic is believed to have silently started in the 1970's, the earliest direct evidences of an HIV infection in humans have been found in a plasma sample from 1959²²⁷ and a lymph node biopsy from 1960.²²⁸ These virus samples have not only directly provided an early time frame for HIV infection in humans, but they have been used to facilitate molecular clock analyses of HIV to push back the origin of HIV in humans to between 1884 and 1924.²²⁹

It has been generally accepted that HIV originated through viral zoonosis of simian immunodeficiency virus (SIV) to humans.^{230, 231} Phylogenetic analysis indicates that multiple interspecies transmission events from nonhuman primates have introduced two genetically distinct types of HIV to humans.²³² HIV type 1 (HIV-1) has been concluded to have originated from chimpanzees (SIV_{CPZ}) of west-central Africa²³³

and HIV type 2 (HIV-2) to have originated from sooty mangabeys (SIV_{SM}) in western Africa.²³⁴ Both types of HIV cause clinically indistinguishable AIDS and are transmitted through blood, sexual contact, and from mother to child. HIV-2, however, is less virulent and the progression to AIDS is much slower than that of HIV-1.²³⁵

HIV infection can be classified into four progressive stages towards AIDS.²³⁶ Primary HIV infection is the first stage, where infected individuals experience flu-like symptoms or no symptoms at all. During this stage, HIV is abundant in the peripheral blood and the adaptive immune system begins to respond to the virus by producing HIV-specific antibodies (Abs), a process known as seroconversion. The first stage typically lasts a few weeks, which is then followed by the asymptomatic stage. An infected individual can look and feel healthy for many years while in the asymptomatic stage, although they may complain of swollen glands due to the shift of the virus from the blood to the lymph nodes. Eventually, the immune system becomes overrun by HIV as the virus gradually mutates and becomes more pathogenic and the body fails to keep up with replacing lost CD4+ T cells. In this third stage, the symptomatic stage, opportunistic infections emerge and retroviral therapy would begin. When CD4+ cell counts within the blood drop to less than 200/ μ L, the infected individual enters the last stage which is known as AIDS where severe opportunistic infections and cancers tend to prevail.

HIV Molecular Epidemiology

HIV-1 and HIV-2 are further divided into genetically distinct lineages arising from individual zoonotic transmission events throughout the last century (Figure 8). HIV-1 is split into groups M (main), N (non-M, non-O), O (outlier) and P and HIV-2 into epidemic groups A and B and non-epidemic groups C-G.^{235, 237} The contribution of each viral group to the current pandemic varies considerably. HIV-1 group M is the oldest HIV lineage in humans and accounts for more than 90 percent of HIV-1 infections globally; the remaining infections arise from HIV-1 groups N, O, P and HIV-2, which are all primarily restricted to Africa.²²⁶ The predominant HIV-1 group M virus has since diversified within the human population to give rise to nine genetically distinct subtypes (A-D, F-H, J and K), as well as at least 48 hybrid viruses known as circulating recombinant forms (CRFs).²³⁸

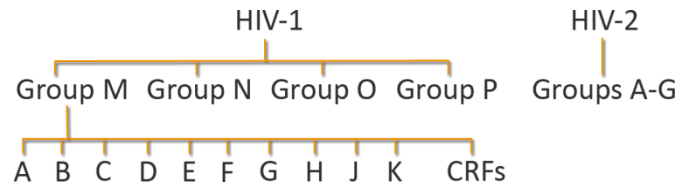


Figure 8. HIV-1 and HIV-2 groups and subtypes. Groups arise from individual cross-over events of SIV from nonhuman primates to humans while the Group M subtypes arise from mutations of the virus within humans.

The group M subtypes and CRFs have distinct global distribution patterns (Figure 9).²³⁸ In particular, subtype A is predominant in central/east Africa and the former Soviet Union. Subtype B is the main genetic variant in the Americas, Europe and Australia. Subtype C is predominant in Africa and eastern Asia. Much of our understanding of HIV-1 disease progression and derives from studies in the developed world where HIV infection is almost exclusively subtype B. The HIV-1 subtypes differ phenotypically which may lead to variances in pathogenicity,²³⁹ such as differences in the progression to AIDS^{240, 241}, mode of transmission²⁴², and plasma viral load.^{242, 243} For instance, there is a general trend that subtype D is associated with faster progression to AIDS than subtype A in populations with both circulating viruses.^{240, 244-246} Studies of phenotypic variance between subtypes are difficult though, as localized populations infected with two or more HIV-1 subtypes are predominantly located in resource-poor parts of the world (Figure 9). In addition, the increasing availability of retroviral treatment makes such studies less ethically feasible.

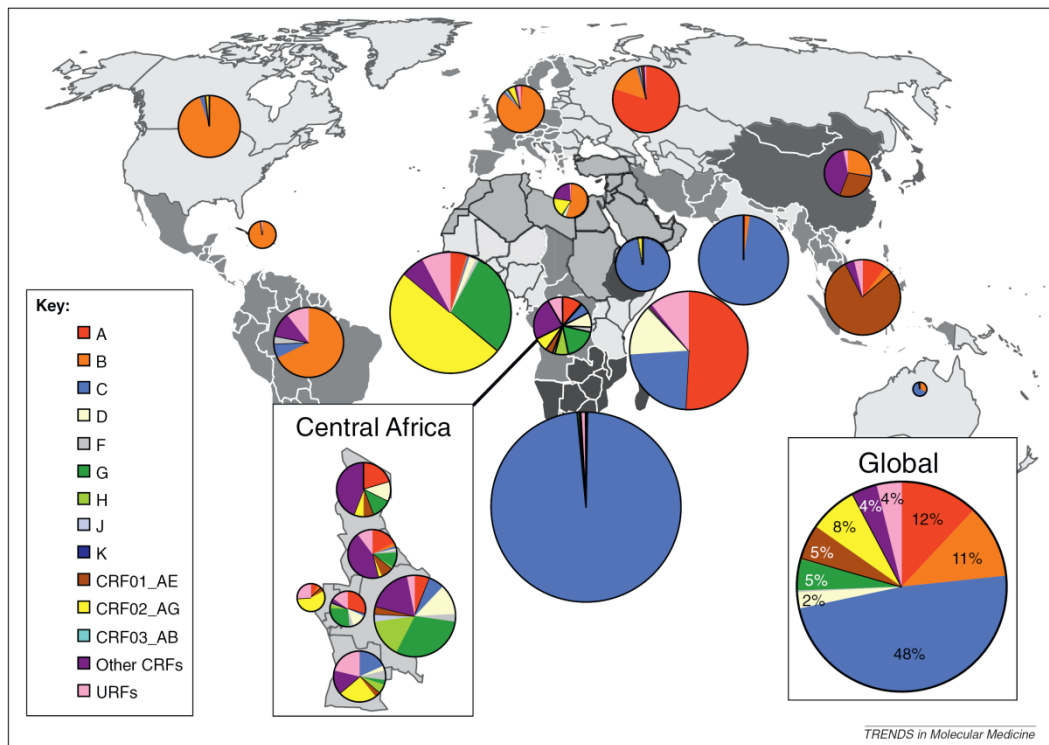


Figure 9. Global distribution of HIV-1 group M subtypes and recombinants from 2004 to 2007. The relative areas of the pie charts represent the relative number of people living with HIV in each area of the world. Reprinted from *Trends in Molecular Medicine*, 18, 182-192, ©2012 with permission from Elsevier.

HIV and AIDs are predominantly managed by highly active antiretroviral therapy (HAART), which has transformed AIDS from an inevitable fatal condition to a chronic, manageable disease. HAART decreases the viral load and allows for the rebuilding and maintaining of the immune system; however it does not eradicate the virus and requires strict life-long adherence to the antiviral regimen. The antiretroviral drugs are directed against the viral reverse transcriptase, protease, integrase and fusion protein (gp41) as well as the cellular coreceptor, CCR5, used for viral entry. The HAART regimen pairs up two reverse transcriptase inhibitors with one or two of the other inhibitors, which defends against resistance by suppressing HIV replication as much as possible. When to start treatment has been a subject of debate as drug toxicity, pill burden and risk of developing drug-resistant HIV have dissuaded early starts, pushing treatment back until the onset of AIDS when CD4+ cells fall below 200 cells/ μL . However, recent studies have been gathering beneficial evidence for initiating treatment before the CD4+ cell count declines to below 350/ μL .²⁴⁷ Alternative treatments to small molecule antiviral drugs

are also being explored, such as monoclonal antibody therapies²⁴⁸ and lectins that target the glycosylated envelope of HIV-1.²⁴⁹

HIV Life Cycle

HIV is a lentivirus, a genus of viruses within the Retroviridae family that is characterized by its long incubation period. Like all retroviruses, HIV carries its genetic material as RNA which must be duplicated within the host cell to produce a DNA copy of its genome. The DNA replicant of the viral genome is incorporated into the host's DNA and the virus thereafter replicates as part of the host cell's genome. Unlike most retroviruses which rely on the disassembly of the nuclear envelope during mitosis to gain entry to the nucleus,²⁵⁰ lentiviruses are unique in that they are able to infect non-dividing cells.²⁵¹⁻²⁵³ It is HIV's ability to infect cells that are arrested in the cell cycle that may account for its very high replication rate observed in HIV-infected individuals.^{254, 255}

HIV begins its life cycle by gaining entry into the target macrophage or CD4+ T cell through the high-affinity binding of the viral surface glycoprotein gp120 to the CD4 receptor (Figure 10, step 1).^{256, 257} This binding interaction induces a conformational change in gp120 to expose a secondary binding domain for the target chemokine receptor CCR5 or CXCR4.²⁵⁸⁻²⁶¹ This triggers further conformational changes which ultimately lead to the fusion of the viral and host cell membranes and entry of the viral capsid into the cytoplasm (Figure 10, step 2).^{262, 263} Viral phenotypes are designated by their coreceptor specificity: R5 for CCR5-using viruses, X4 for CXCR4-using viruses and R5X4 for dual-tropic viruses or viral populations that use both coreceptors.²⁶⁴ Over 90% of primary HIV infection occurs with R5 virus while X4 viruses emerge during the late stage of infection,²⁶⁵⁻²⁶⁷ presumably through mutation.²⁶⁸ It is unclear whether the evolution towards CXCR4 use is the cause or the consequence of disease progression,²⁶⁹ but it is noted that strains that use CXCR4 earlier and more frequently in infection progress more rapidly to AIDS.^{244, 270}

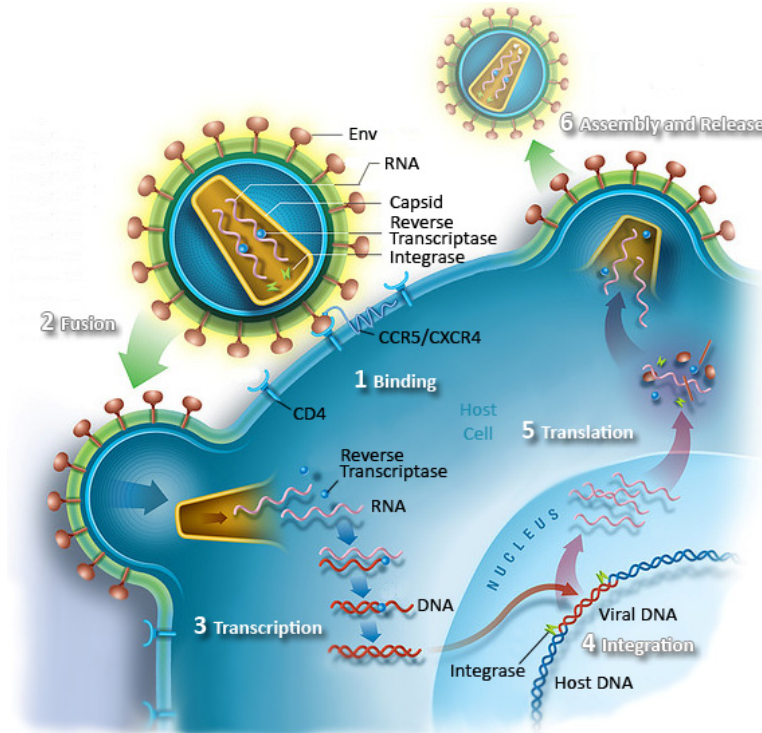


Figure 10. HIV life cycle. 1. The Env protein on the surface of the virus binds to CD4 of the host cell and undergoes a conformational change, allowing for binding to the secondary receptor, CCR5 or CXCR4. 2. The viral envelope fuses with the cell membrane and the viral RNA genome and proteins enter the cytoplasm. 3. HIV reverse transcriptase produces a complementary double-stranded DNA copy the viral RNA. 4. HIV integrase allows the viral DNA to integrate into the hosts genome as a provirus. 5. Provirus is transcribed to viral RNA, and viral proteins are translated. 6. Viral RNA and proteins assemble into viral particles and the virus buds out of the cell.

Once in the cytoplasm the viral capsid is disassembled, releasing the single-stranded positive-sense RNA (ss(+)) genome and various viral proteins such as reverse transcriptase, integrase, protease and regulatory proteins (Figure 10, step 3). The reverse transcriptase liberates the RNA genome from the attached viral proteins and copies it into a complementary DNA (cDNA) molecule. This process is extremely error-prone,²⁷¹ resulting in mutations that can cause drug resistance and allow escape from the host immune response. The reverse transcriptase also acts as a ribonuclease and DNA polymerase, degrading the viral RNA and creating a sense DNA from the antisense cDNA. The newly formed double stranded viral DNA is transported to the nucleus where it is integrated into the host chromosomal DNA using the viral enzyme, integrase (Figure 10, step 4).²⁷²

The integrated viral DNA lies dormant in the latent stage of HIV infection. Transcription of the provirus relies on cellular transcription factors, such as NF- κ B, that are upregulated when the host cell becomes activated.²⁷³ The transcribed mRNA is spliced and exported from the nucleus to the cytoplasm where they are translated into the regulatory proteins Tat and Rev.²⁷⁴ Tat vastly increases the efficiency of viral transcription and Rev binds to full length viral mRNAs and enables the export of the unspliced and singly spliced RNA from the nucleus (Figure 10, step 5).²⁷⁵⁻²⁷⁷ The full length mRNA encodes the entire viral genome, allowing for the translation of the Env and Gag proteins. The Env glycoprotein complex makes up the viral envelope and the Gag proteins play numerous roles in the assembly, maturation and release of the viral particles.^{278, 279} The viral proteins congregate at the plasma membrane where the virus is assembled and released through budding (Figure 10, step 6).^{278, 280-282} A mature viral particle will consist of ~10 Env proteins embedded in the viral envelop which is derived from the host plasma membrane.²⁸³ The viral envelope surrounds the spherical viral matrix, which further encases the viral capsid that contains two copies of the viral ssRNA and multiple copies of viral enzymes.

HIV can infect new host cells through either a cell-free route or through cell-to-cell contact.²⁸⁴ Cell-free viral dispersal enables host-to-host transmission and infection of distant tissues but exposes the free virions to various biophysical, kinetic and immunological barriers.²⁸⁵ Direct infection of neighbouring cells through points of cell-to-cell contact, known as virological synapses,²⁸⁶⁻²⁸⁹ is much more efficient and avoids many extracellular obstacles to infection.²⁹⁰ Cell-to-cell infection, as well as viral latency, has been used to explain why HIV is able to continue ongoing replication in patients receiving antiretroviral therapy.²⁹¹ It has also been recently shown that while naturally occurring antibodies can neutralize free viruses and block their transmission to uninfected cells, these same antibodies are dramatically less potent inhibitors of cell-to-cell transmission.²⁹² Thus, the design of an HIV vaccine to establish a standing arsenal of neutralizing antibodies is therefore paramount to sterilize and abort an impending infection before the complexities of cell-to-cell transmission can arise.

Structural Biology of HIV Env Glycoproteins

HIV-1 vaccine development has revolved around the elicitation of broadly neutralizing antibodies against the only exposed viral epitope, the envelope glycoprotein Env.²⁹³ The Env spike is a complex of two non-covalently associated trimers of glycoproteins gp120 and gp41 that protrudes from the viral surface.^{283, 294-296} Antibodies directed towards Env are vital for interrupting virus-receptor binding and fusion events, thus making Env the ideal target for neutralization.²⁹⁷ The structural biology of HIV-1 proteins has been extensively studied in an effort to develop HIV-1 therapeutics and vaccines.²⁹⁸

Env is translated as the polyprotein precursor gp160 in the ER of the host cell. During transcription gp160 is extensively modified by *N*-linked glycosylation with minor *O*-linked glycosylation.^{299, 300} Monomeric gp160 oligomerizes in the ER to form a trimer which is thought to be a required step to facilitate the subsequent trafficking to the Golgi complex.^{301, 302} As gp160 progresses through the Golgi, the high-mannose oligosaccharide side chains gained in the ER are processed and gp160 is proteolytically cleaved by cellular furin to yield the mature gp120 and gp41 Env subunits.³⁰³ Both subunits remain associated through noncovalent interactions, with the mature Env spike consisting of three heavily glycosylated gp120 subunits resting on three gp41 transmembrane stalks.³⁰⁴⁻³⁰⁶ Proteolytic processing of gp160 is essential for the fusogenic activity of Env.³⁰⁷ The mature gp120/gp41 complex is then trafficked from the Golgi to the plasma membrane surface via the secretory pathway.³⁰⁸

gp120

A number of structures of gp120 have been solved by X-ray crystallography. The solved structures have so far been limited to the gp120 'core', from which the surface glycans and variable regions are removed to reduce the conformational flexibility and heterogeneity that inhibit crystallization. The majority of these core structures are in complex with CD4,^{260, 309-312} neutralizing antibodies³¹³⁻³¹⁶ and small molecule ligands.³¹⁷⁻³²⁰ These studies have provided a wealth of information on the mechanism of gp120 interactions with other molecules and its inherent conformational plasticity.

Comparison of gp120 gene sequences from multiple HIV-1 isolates revealed extensive nucleotide substitutions and deletions/insertions concentrated within five hypervariable regions (Figure 11A, B).^{321, 322} These variable regions, labeled V1 through V5, also correspond to antigenic sites of gp120.³²³ The overall envelope structure is highly conserved outside of the variable regions. HIV-1 gp120 contains 18 cysteine residues which form disulfide bridges that are crucial to the formation of Env tertiary structure.²⁹⁹ Several of these disulfide bonds are responsible for delimiting the V1-V4 regions, forming variable loops (Figure 11B). The exposed surface of gp120 contains 20-35 *N*-linked glycosylation sites that mask the protein surface from immune recognition,³²⁴ contribute to protein folding,³²⁵ and help virions bind to the host surface.³²⁶ Approximately half of the molecular mass of gp120 is attributed to *N*-linked glycans,³²⁷ making it one of the most heavily glycosylated proteins known.

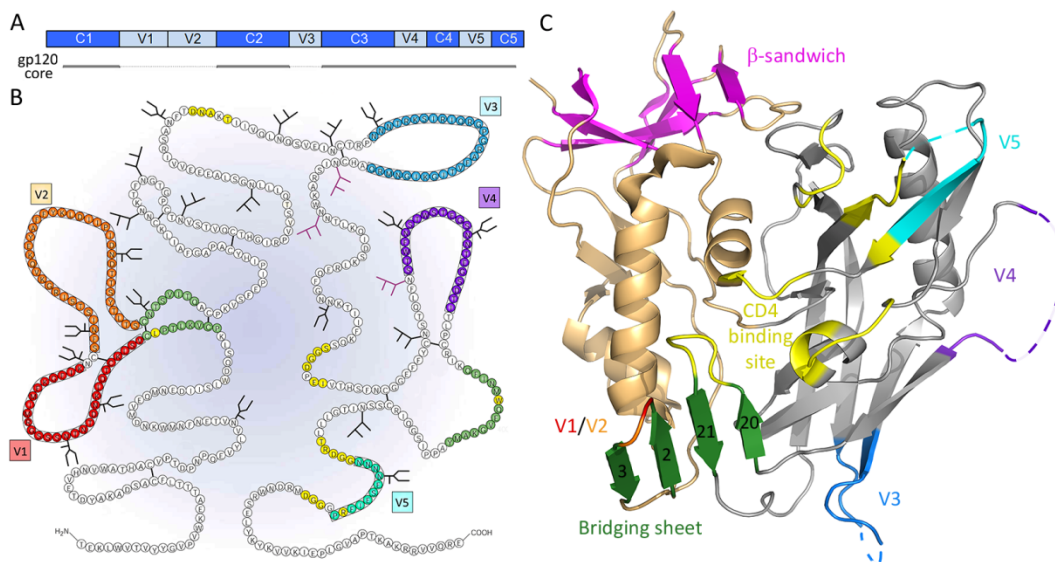


Figure 11. Diagrams of the structure of the gp120. A| Diagram of the sequence elements of gp120 and the core structure used to obtain crystal structures. B| Schematic layout of gp120.^{299, 323} The glycosylation sites containing high-mannose type or hybrid type oligosaccharide structures are indicated by the branched structures.³²⁸ The carbohydrates involved in Ab 2G12 binding are shown in purple. The bridging sheet is colored in green. Contact residues for CD4 are colored in yellow, based on crystal structure analyses.^{260, 329} C| The CD4-bound conformation of gp120, using the same color scheme as in B (PDB: 3TGQ). The outer domain is portrayed in grey and the inner domain in gold. The gp41 interacting site, the β -sandwich, is colored in pink. The V1-V3 loops were truncated to obtain a crystal structure.

The five loop regions play major roles in infectivity, transmission and resistance to neutralization. The V1/V2 loop is the most variable in loop length, ranging from 50 to 90 amino acids. Increases in length and variation in glycosylation pattern of the V1/V2

loop have been correlated with disease progression and neutralization resistance.³³⁰⁻³³⁹ These changes allow for the masking of neutralization-sensitive epitopes such as the conserved CD4 binding site, coreceptor binding site and bridging sheet.^{331, 332, 337, 340-355} The protective effect imparted by lengthier V1/V2 loops appears to also diminish infectivity as circulating viruses with shorter V1/V2 loops and fewer glycosylations are preferentially transmitted or have a selective advantage in early infection,³⁵⁶⁻³⁵⁹ suggesting that increases in V1/V2 length and glycosylation arise from immunological pressure at the cost of decreasing virulence. The V1/V2 region is not functionally essential to HIV-1, as viruses with the V1/V2 region removed are still able to replicate.^{340, 342, 349, 360-364}

The third variable region, V3, of gp120 is an ~35 amino acid loop that binds the coreceptor CCR5 or CXCR4,^{365, 366} triggering fusion of the Env complex with the host cell.³⁶⁷ The V3 loop is consistent in length but is highly variable in sequence and frequently glycosylated. Mutations within the V3 loop facilitate escape from V3-directed neutralizing antibodies,^{368, 369} and are responsible for the evolved switching of coreceptor specificity.³⁷⁰⁻³⁷³ The V3 loop masks potential antigenic sites on gp120,³⁷⁴ and its own antigenic sites are masked by glycans and neighbouring V1/V2 loops.^{355, 375, 376} The V3 loop is conformationally flexible, adopting a conformation close to the gp120 core in the CD4-unbound state, and protruding out towards the target cell membrane to form the coreceptor binding site upon CD4 binding (Figure 12).³⁷⁷ The V3 loop, along with the V1/V2 loop, do not play a direct role in CD4 binding, as gp120 variants with these regions deleted still bind CD4 with high affinity.^{360, 378} Various analogies have been made between the secondary structure of V3 and the natural chemokine ligands of the transmembrane coreceptors CCR5 and CXCR4,^{323, 379} although the semblance has been debatable.³⁸⁰ The most unabated common structural feature is the overall net positive charge,^{365, 366, 376, 381-384} which interact with GAGs and the negatively charged extracellular surface of the coreceptors.³⁸⁵⁻³⁸⁷

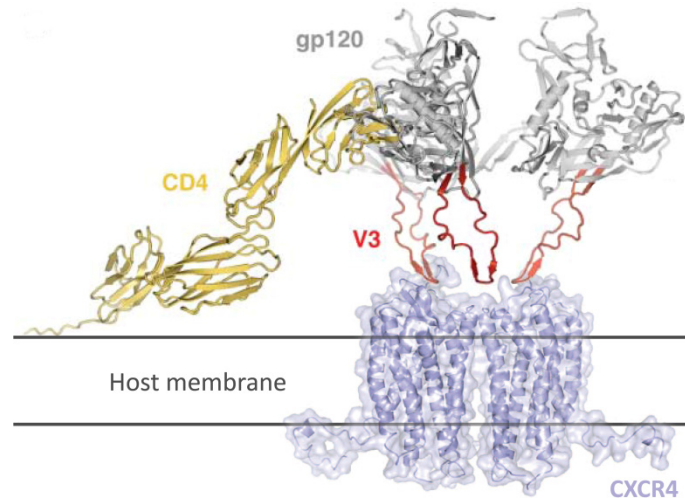


Figure 12. Model of the induced conformational change of gp120 upon binding CD4. Upon CD4 binding, the V3 loop becomes more exposed to interact with the coreceptor CCR5 or CXCR4.^{377, 388}

The V4 and V5 loops vary heavily in length and glycosylation. Their function has not been clearly identified as they do not appear to interfere with either CD4 binding or with any other known biological function of gp120.^{368, 389, 390} V4 has been postulated to exist solely to facilitate viral escape as a hypervariable component of the glycan shield.³⁹¹⁻³⁹³ The V5 region functions similarly, although its close proximity to the CD4-binding site (Figure 13) appears to influence gp120-CD4 binding, viral fusion and escape from CD4-binding Abs.^{377, 393-396} Significant increases in the net positive charge of the V5 loop were also found in the HIV variants from individuals with late disease,³³⁹ suggesting the possible formation of an alternative site for coreceptor binding.

The core of gp120 is relatively conserved when compared to the five variable regions.^{329, 397-399} The core is organized into an inner domain that interacts with neighbouring gp120 in the Env trimeric structure and gp41, and an outer domain that protrudes from the Env spike and carries the bulk of the glycosylation sites.²⁶⁰ Crystallographic and biochemical studies have revealed large conformational changes in the gp120 core induced by CD4 binding. To date, crystallographic information of the prestructured, unbound form of trimeric gp120 has been elusive. However, the crystal structure of the unliganded form of a gp120_{SIV} monomer has been solved, revealing a structurally invariant outer domain with a markedly different conformation and arrangement of the inner domain and bridging sheet domains compared to CD4-bound gp120_{HIV} monomeric structures (Figure 13).⁴⁰⁰ Longstanding dogma held that CD4

binding induces the formation of a large internal cavity on gp120 formed by the inner, outer, and bridging sheet domains (Figure 11C, Figure 13).^{304, 401, 402} The bridging sheet domain is a four-stranded antiparallel β -sheet composed of the $\beta 2/\beta 3$ strands from the inner domain and $\beta 20/\beta 21$ strands from the outer domain. This doctrine has been challenged as recent crystal structures of unliganded gp120 revealed that gp120 can spontaneously adopt the CD4-bound conformation when not restricted by the presence of the V1, V2, and V3 loops.³¹⁹ Molecular dynamics simulations reveal strong interactions between the V3 loop with the $\beta 2/\beta 3$ strands, preventing the formation of the bridging sheet.⁴⁰³ Thus, the CD4-bound conformation of gp120 represents a ground state for the core, with the variable loops and quaternary interactions restraining the unliganded conformation of gp120 from snapping into the CD4-bound conformation.³¹⁹ This has interesting implications to the neutralization capabilities of naturally occurring Abs, as recognition of epitopes on such a spring-loaded, unliganded conformation of gp120 could spontaneously induce a conformational change that could distort the recognized epitope, dislodging the bound antibody from gp120.

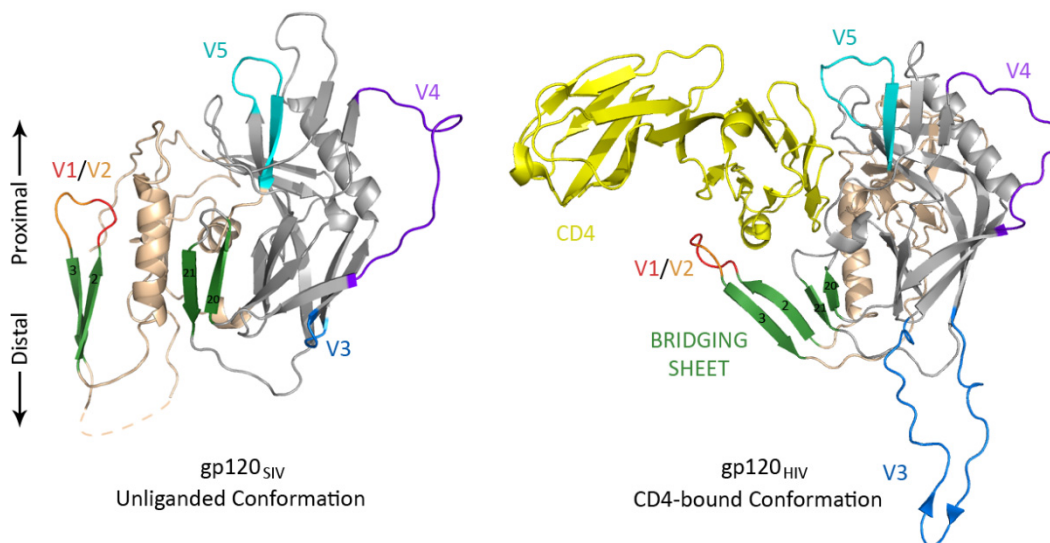


Figure 13. The crystal structure of gp120_{SIV} in an unliganded conformation (PDB: 2BF1) and gp120_{HIV} bound to CD4 in the CD4-induced conformation (PDB: 2B4C). The variable V1, V2 loops, as well as the N- and C-terminal segments, have been truncated in both structures, as well as the V3 loop for gp120_{SIV}. The inner domain (light gold) undergoes extensive conformational rearrangement upon CD4 binding.

gp41

Fusion of the viral envelope with the plasma membrane of the host cell is mediated by the Env transmembrane glycoprotein gp41. Gp41 is comprised of six distinct functional domains: the fusion peptide, N-terminal heptad repeat (HR1), disulfide-bonded bridging loop, C-terminal heptad repeat (HR2), membrane-proximal external region (MPER) and the transmembrane domain (Figure 14).²⁹⁴ The fusion peptide is a hydrophobic region as the N-terminal that inserts into the host cell membrane and is required for fusion.^{404, 405} Both HR regions exist as α -helices composed of repeating sequences of hydrophobic amino acids (heptad repeat) which allow for the formation of the coiled coil structural motif of gp41. The disulfide-bridging loop functions as the hinge between the two HRs and may play a role in lipid merging.⁴⁰⁶ The MPER is an α -helical extension of HR2 that is highly conserved and plays a crucial role in the fusion of the viral and cellular membranes.⁴⁰⁷⁻⁴⁰⁹ The C-terminal region of the ectodomain contains 3-4 closely spaced, highly conserved *N*-linked glycosylation sites that are not necessary for viral fusion and replication,^{410, 411} but are shown to mask the exposed MPER and neighbouring regions from antibody recognition.^{411, 412}

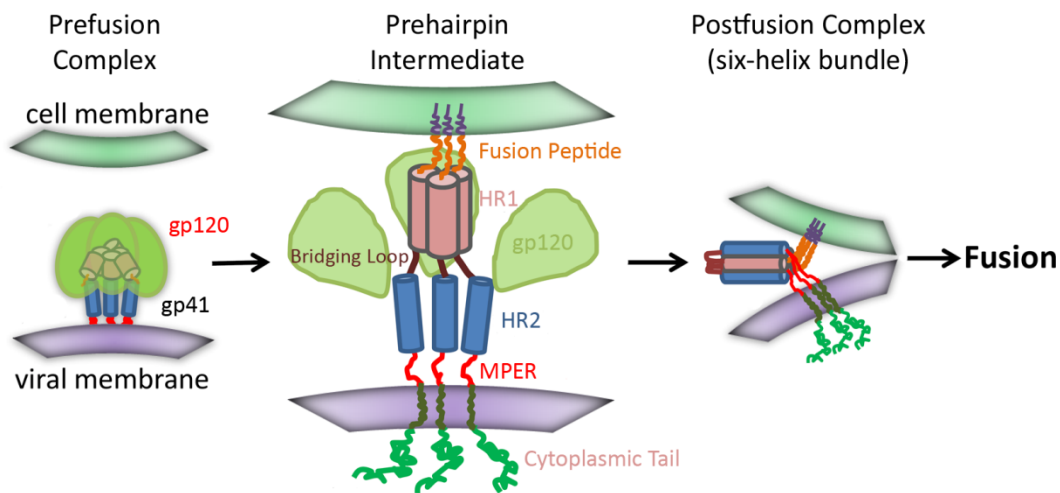


Figure 14. Model of virus-mediated membrane fusion, based on studies of the influenza virus hemagglutinin and HIV gp41 crystal structures.^{295, 413} Adapted from *The Journal of Biological Chemistry*, 2012, 288, 234-246 with permission.

The function of gp41 is thought to be analogous to the fusion proteins of other enveloped viruses such as influenza hemagglutinin (HA), Ebola GP2 and paramyxovirus F protein.⁴¹⁴⁻⁴¹⁶ The structure of the gp41 trimer exists in three conformations: the

prefusion conformation, prehairpin intermediate, and the postfusion conformation. The structure of the gp41 ectodomain (extracellular domain) has been determined by NMR spectroscopy and X-ray crystallography, but only in the postfusion conformation (Figure 15).^{294, 295, 417, 418} The metastable prefusion and prehairpin intermediate conformations have eluded crystallographers and so the gp41 fusion mechanism has been largely inferred from influenza HA fusion as outlined in Figure 14.⁴¹⁹ The initial prefusion conformation of gp41 is held in a high energy state through its interactions with gp120. Conformational changes within the gp120 trimer, induced by coreceptor binding, weaken interactions between gp120 and gp41, allowing the N-terminal HR1 region to fully extend and insert the fusion peptide into the target membrane.^{256, 294, 295} This extended conformation of gp41 is referred to as the prehairpin intermediate.^{256, 419} Subsequent folding back of the HR2 region onto the fully extend HR1 coiled coil creates an extremely thermostable six-helix bundle,^{294, 295, 414, 420} which brings the viral membrane and cellular membrane together to promote fusion. The energy required for viral-cell membrane fusion derives from the sequential transitions that gp41 undergo, from the high-energy unliganded prefusion state to the low-energy six-helix bundle.^{415, 421}

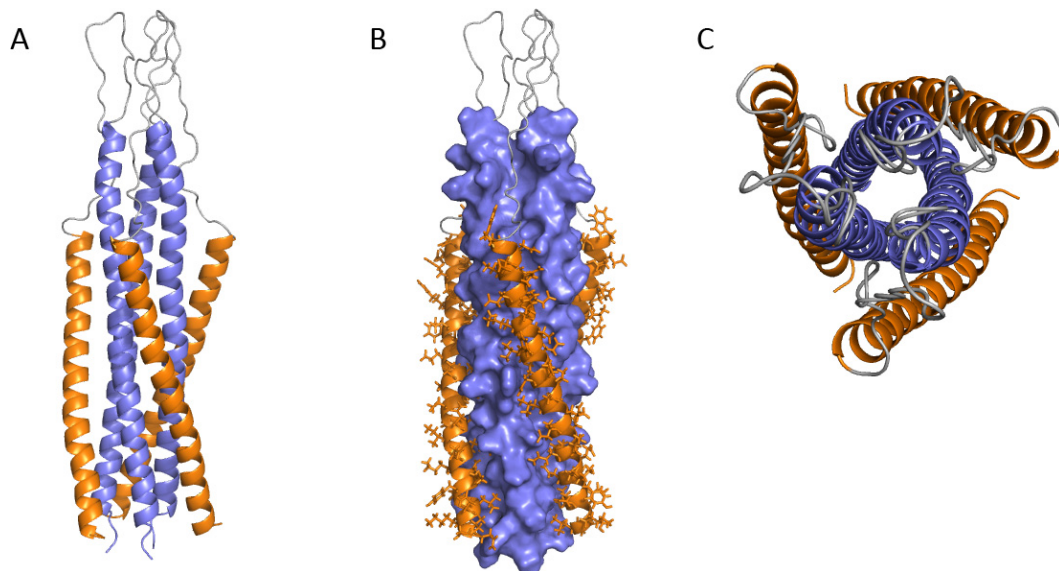


Figure 15. NMR structure of trimeric SIV gp41 ectodomain in the postfusion six-helix bundle conformation (PDB: 2EZR).⁴¹⁷ The bridging loop is colored in grey, HR1 in blue and HR2 in gold. A| Secondary structure illustrating the coiled coil structural motif. B| Space filling model of the HR1 trimer illustrating the the binding for the HR2 side chains. C| Top down view of the six-helix bundle.

Env Quaternary Structure

Obtaining a crystal structure of the complete Env spike has been problematic, owing to the heavy glycosylation, structural plasticity and metastable nature of the Env trimer. X-ray crystallography has shed much light on the structures of the monomeric gp120 core in the CD4-bound state and the ectodomain of gp41 trimers in the postfusion six-helix bundle. There is much value in understanding the assembly of the Env trimer in its natural unliganded state, as this represents the major target for most neutralizing antibodies. Cryo-electron tomography (cryoET) has stepped up to fill the void of structural information, allowing for the visualization of the Env spike in both its liganded and unliganded conformation.^{283, 422-428} With this technique, multiple cryo-electron microscope images are obtained of the Env spike from different angles and added together to reconstruct the 3-dimensional morphology (Figure 16).⁴²⁹ Most structural models of Env obtained from cryoET have been at 20-30 Å resolution which has been too low to reveal the organization of gp120 and gp41. Recently, a cryo-electron microscopy (cryoEM) model of the unliganded, membrane-bound HIV-1 Env trimer has been obtained at 11 Å resolution (Figure 17),⁴²⁸ providing insight into the architectural organization of the gp120 and gp41 subunits.

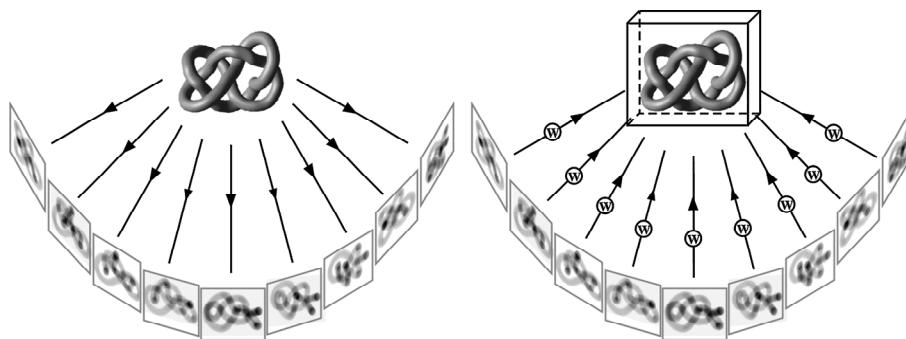


Figure 16. Principle of tomography. Left| Projections of the specimen were recorded from different directions by tilting the specimen holder. Right| The 3-dimensional reconstruction of the specimen can be deduced from the 2-dimensional projections. Reprinted from *Annual Review of Biochemistry*, 2005, 74, 833-865 with permission.

The Env trimer has an overall tetrahedral shape with a pronounced interior void as seen in Figure 17. Although it is not possible to distinguish secondary structures, the orientation of the subunits is apparent. The monomers of gp41 are associated as a coiled coil in the viral membrane and then dissociate to branch out to form three lobes

consisting of each gp120 subunit. Narrow interprotomer contact points at the base of the membrane suggest further interactions between the gp41 ectodomains. The interdomain cavity that is observed in the crystal structure of gp120 is also a prominent structural feature in the cryoEM map, providing a reference point for fitting the crystal structure of the HIV-1 gp120 core into the cryoEM map (Figure 17B). The size and shape of the gp120 crystal structure segments in the restructured Env model corresponds well with the inner and outer domain segments of gp120 X-ray crystal structures.*

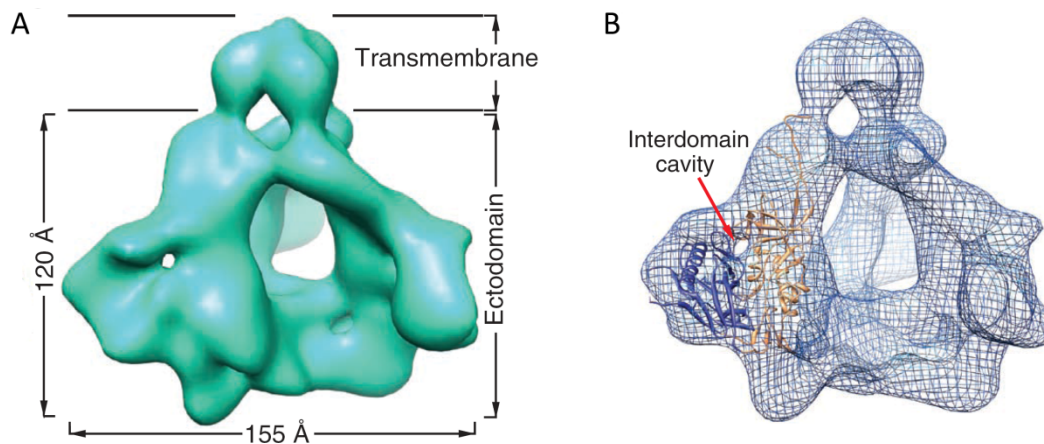


Figure 17. The 3-dimensional reconstruction of the HIV-1_{JR-FL} Env structure at ~11 Å resolution. The cytoplasmic tail was truncated to improve Env expression yields. A| Env is shown as a solid surface viewed from a perspective parallel to the viral membrane. The approximate boundaries of the transmembrane region and ectodomain are indicated. B| Env is represented as a mesh with the CD4-bound gp120 core crystal structure (PDB: 3JWD)³¹² modeled in one of the lobes. The outer domain is shown in blue and the inner domain in gold. The gp120 core is missing the V1, V2 and V3 variable regions. Reprinted by permission from Macmillan Publishers Ltd: *Nat Struct Mol Biol*, 19, 893-899, ©2012.

The cryoEM reconstruction appears to be of sufficient quality to allow for the mapping of the segments of Env that make biological sense and are compatible with available structural information (Figure 18A, B). The gp41 ectodomain can be partitioned into two discrete segments, but lacks the detail to define the secondary structure of HR1 and the fusion peptide in this prefusion conformation. The gp120-gp140 interface is exclusive to the inner domain of gp120 which is consistent with the literature.³¹² The

* To date, only ligand-bound conformations of HIV-1 gp120 have been visualized by crystallography. The cryoET structure was produced from the unliganded conformation of Env, and thus the ligand-bound gp120 core was best fitted with the inner and outer domain orientated independent of each other. The rearranged fitting of the inner and outer domains support the observation that gp120 exists in different conformations in its unbound and CD4-bound states.

V1/V2 and V3 loops, which are truncated in crystal structures of monomeric gp120, are shown here extending from the inner and outer domains towards a central triangular junction at the membrane-distal apex of the spike. (Figure 18D, E). This arrangement explains how the V3 loop can simultaneously make intramolecular contact with the V1/V2 loop to suppress bridging sheet formation,^{319, 403} and intermolecularly shield the V1/V2 loop of neighboring gp120 monomers from neutralization.^{355, 375}

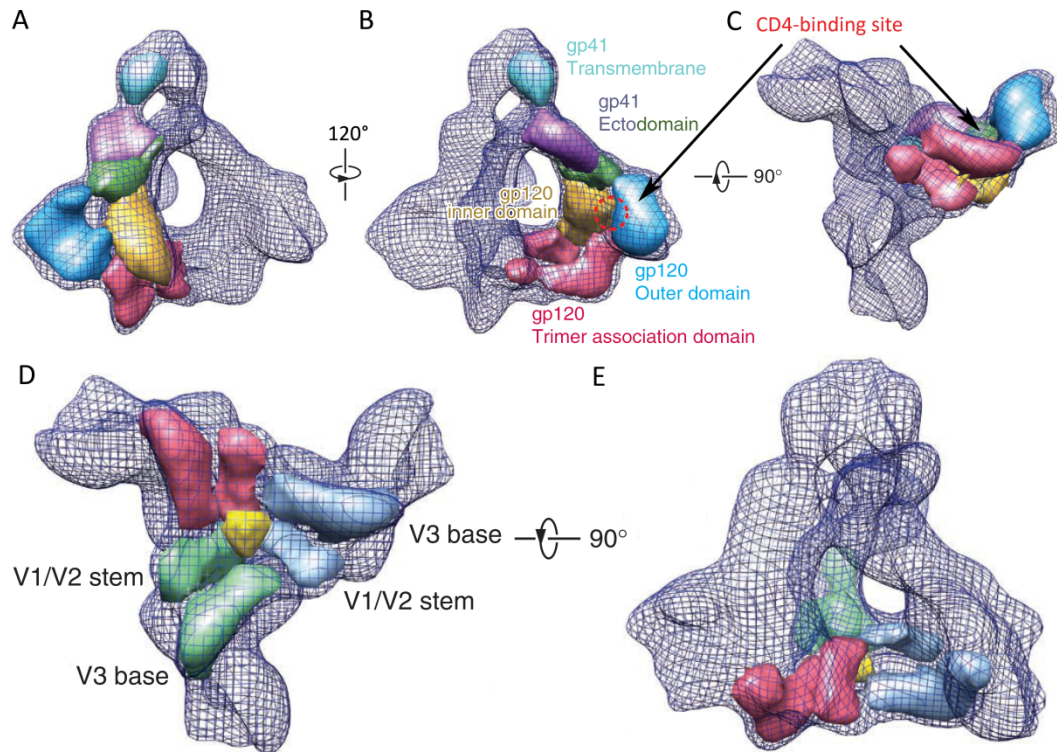


Figure 18. Mapping of the Env protomer. A & B | The mapped segmentations of one Env protomer are shown as solid surfaces wrapped in the surface mesh, viewed from a perspective parallel to the viral membrane. The CD4-binding site is represented by the dashed red circle. C | The segmentation viewed from the perspective of the target cell. D & E | The gp120 trimer-association domains of each protomer displayed as solid surfaces, illustrating their arrangement with respect to one another. The approximate positions of the V1/V2 stem and V3 base of two protomers are labeled. The central triangular junction is colored yellow. Reprinted by permission from Macmillan Publishers Ltd: *Nat Struct Mol Biol*, 19, 893-899, ©2012.

The cryoEM map of Env reveals additional structural insights into the mechanics of the viral spike. The prefusion conformation of gp41 in the unliganded Env trimer is very different than the low-energy state postfusion conformation. In the unliganded Env structure, gp120 appears to clasp gp41, keeping the gp41 ectodomains away from each other, suppressing the formation of the stable six-helix bundle (Figure 18B). Thus, with gp41 held in a metastable conformation by gp120, and gp120 preference to adopt

the downstream CD4-bound conformation,^{319, 403} the viral spike appears to be spring-loaded for cell entry. The open structure is also unusual among viral envelope glycoproteins,⁴¹⁹ which minimizes the protein contacts between the subunits, allowing for easier conformational changes. Formation of such an unstable quaternary structure could only occur during the assembly of the gp160 proprotein trimer complex early in the secretory pathway.³⁰⁷ Thus, proteolytic cleavage of gp160 into the gp120 and gp41 subunits during the last step of Env processing serves to prime the delicate Env complex.

The unusual topology of the viral spike also likely contributes to HIV-1 immune evasion and persistence. The variable domains and the glycan shield mask much of the accessible outer surface, while the conserved CD4-binding site is positioned on the inward-facing side of the protomeric lobes (Figure 18B, C). Such an orientation limits the accessibility of antibodies to these surfaces through steric hinderance by the adjacent protomer. The tetrahedral shape also imposes an acute angle between the viral membrane and the Env spike, further limiting antibody binding by means of steric clash with the viral membrane. Antibody binding to a metastable structure is also a challenge in itself, as binding-induced conformation changes could restructure the surface epitope to which the antibody is bound. However, antibodies have been shown to neutralize HIV inducing the dissociation of gp120 from the envelope timer.⁴³⁰ This is thought to occur by inducing a conformational change in Env through antibody binding.

History of HIV Glycoconjugate Vaccine Design

Antigenic variation of HIV-1 is a major hurdle in the development of an effective broadly neutralizing HIV-1 vaccine. The amino acid sequence can vary by 30% between individuals and as much as 10% within individuals.²³¹ Thus a protective HIV-1 vaccine has to be able to elicit a response against a structure, or variety of structures that are present on all quasispecies of HIV-1. The glycan shield of gp120 is attractive in this regard, as while the N-linked glycosylation sites are prone to mutagenesis, the enzymatic activities present in the host cell secretory pathway determines the glycan structures. With carbohydrates accounting for half of the molecular weight of gp120 and covering the majority of its surface area, they make for an attractive target for vaccine development.

Identification of conserved and accessible epitopes on HIV-1 Env has been an essential step in vaccine development. Broadly neutralizing antibodies isolated from cells of chronically infected HIV-1 patients have provided important clues for rational immunogen design. For some time, only a small number of broadly neutralizing antibodies have been isolated and characterized,³²³ consisting of antibodies 2F5, Z13e1 and 4E10 that bind the MPER,⁴³¹⁻⁴³⁴ antibody b12 that binds the CD4-binding site,^{435, 436} and antibody 2G12 that binds the glycans of the outer domain of gp120.^{328, 437-441} Considerably more broad and potent antibodies have been recently isolated which include the VRC series antibodies (VRC01-03) that target the CD4-binding site,^{99, 227-229} the MPER-specific antibody 10E8,⁴⁴² and the glycan-dependent antibodies PG9, PG16 and PGT series (PGT121-137 and PGT141-145).⁴⁴³⁻⁴⁴⁹

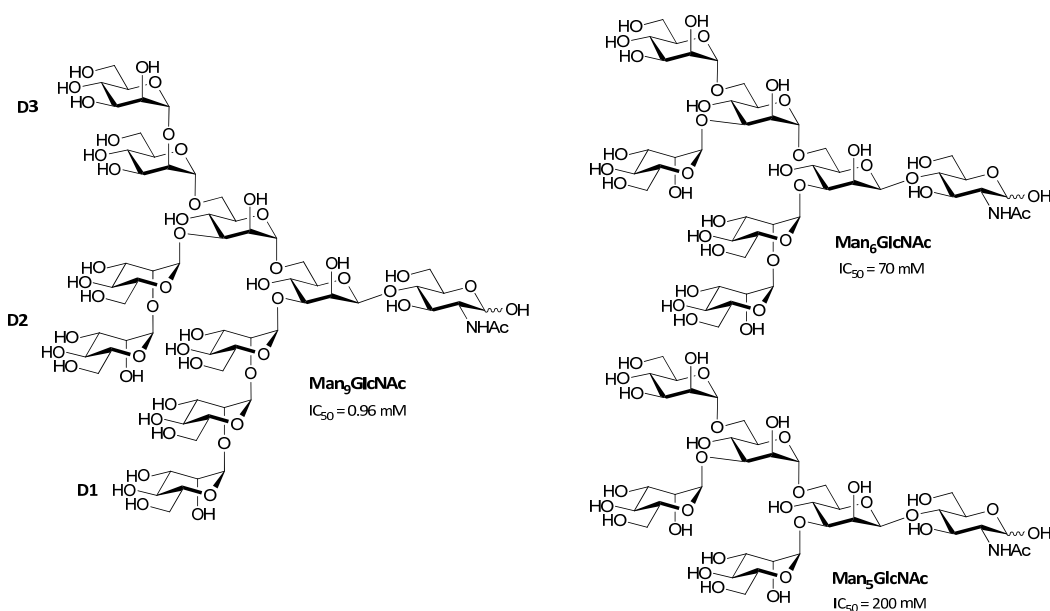


Figure 19. Structures of typical HIV-1 high-mannose oligosaccharides that were examined for their affinity to 2G12 by competitively inhibiting 2G12-binding to immobilized gp120 in an ELISA.⁴⁵⁰

The carbohydrates involved in 2G12 binding have been used as the basis of many microbial,^{441, 451-453} synthetic,^{440, 454-457} and recombinant glycoconjugate^{453, 458, 459} vaccines against HIV-1. Early mutagenesis and crystallography studies revealed that 2G12 binds primarily $\text{Man}\alpha 1 \rightarrow 2\text{Man}$ moieties of oligomannose structures that are densely clustered around the *N*-glycosylation sites of N295, N332, N339, and N391. The optimal oligomannose epitopes for 2G12 recognition have been deduced via competitive enzyme-linked immunosorbent assay (ELISA) experiments.^{440, 450, 460} It has

been observed that Man₉GlcNAc was 74-fold and 210-fold more effective at inhibiting 2G12 binding to immobilized gp120 than Man₆GlcNAc and Man₅GlcNAc oligosaccharides, illustrating the importance of the terminal Man α 1 \rightarrow 2Man linkages for 2G12 recognition (Figure 19).⁴⁵⁰ The binding epitope of 2G12 has been further dissected by evaluating the relative inhibitory activities of synthetic oligomannosides in a similar competition ELISA (Figure 20).⁴⁴⁰ The Man₄ structure, which mimics the D1 arm, and the Man₅ structure, which mimics the D2 and D3 arms, displayed equivalent inhibitory activities as the native Man₉GlcNAc₂ structure. The apparent affinity of the Man₄ structure for 2G12 and its simplistic synthesis have made it a particularly attractive immunogen in vaccine design.

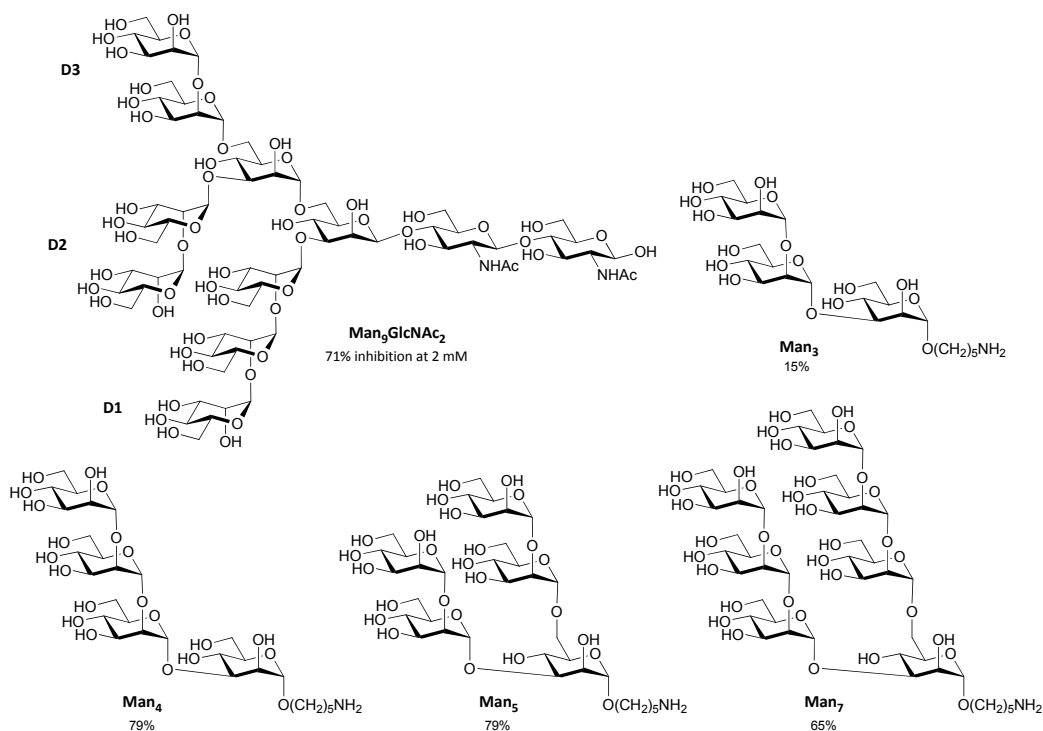


Figure 20. Oligomannose structures that were evaluated for their ability to inhibit binding to 2G12 to immobilized gp120 in an ELISA.⁴⁴⁰ The relative inhibitory values at 2 mM are listed under the structures.

Proper presentation of oligomannose structures in designed immunogens is thought to be crucial to elicit 2G12-like antibodies by vaccination. On gp120 the glycans are densely clustered which provides a unique surface for antibody recognition. The importance of glycan clustering to 2G12-binding is apparent from the mM binding affinities observed with individual synthetic oligomannosides and Man₉GlcNAc₂ structures which pale in comparison to the nM binding affinity of 2G12 to gp120.^{440, 450}

Many scaffolds have been utilized to cluster synthetic oligomannoses in order to recreate the glycan epitope of gp120, including BSA,⁴⁵⁴ cholic acid,⁴⁶¹ dendrimers,⁴⁶² DNA,⁴⁶³ polyamidoamine,⁴⁵⁵ gold nanoparticles,⁴⁶⁴ galactose,⁴⁶⁵ cyclic peptides,^{466, 467} and virus particles.¹⁶² In all cases, clustering the glycans greatly increased affinity to 2G12 compared to individual glycans, suggesting that the clustering of oligomannose structures is essential to mimicking the glycan shield of gp120. Glycan clustering may also be essential to breaking self-tolerance, as while high-mannose oligosaccharides are self glycans that are native to the secretory pathway, they are not commonly presented on the surfaces of mammalian cells or found in serum, and have not been described in such densely packed formations as observed with gp120.⁴⁶⁸⁻⁴⁷⁰

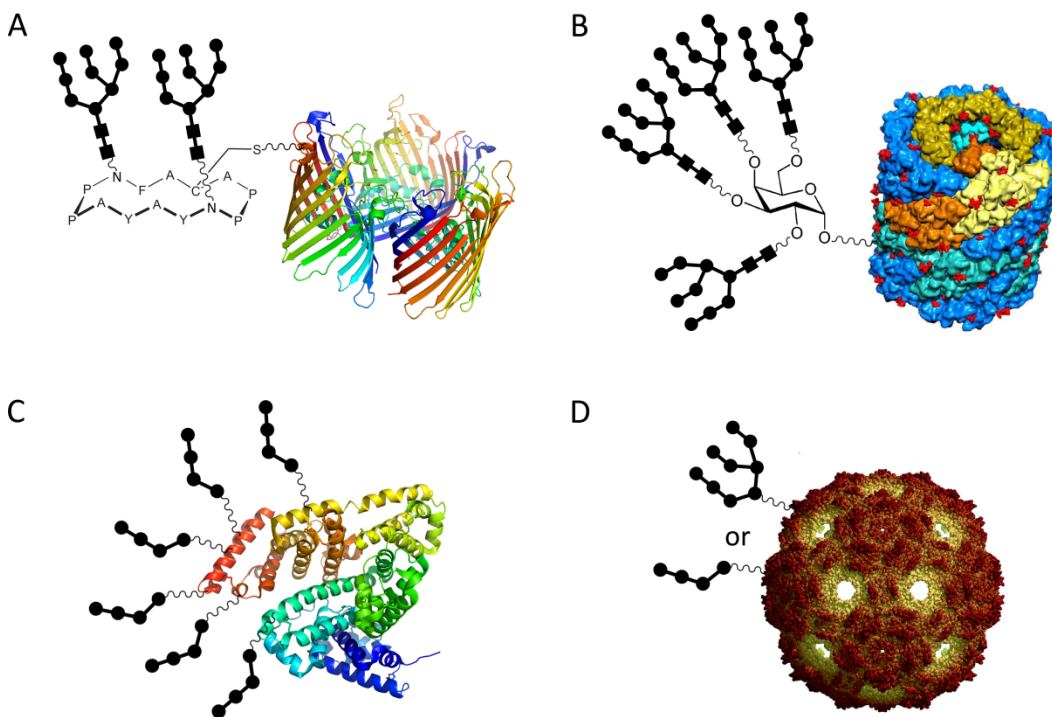


Figure 21. Glycoconjugates used as immunogens in animal studies. A| A cyclic peptide-based Man₉GlcNAc₂ divalent construct conjugated to OMPC.⁴⁶⁶ Contains between 2,000-3,000 mol of peptide per mol of carrier complex. B| Galactose-scaffolded Man₉GlcNAc₂ tetravalent construct conjugated to KLH.⁴⁶⁵ Contains ~15% carbohydrate. C| The synthetic Man₄ neoglycan conjugated to BSA.⁴⁵⁴ Contains 14 Man₄ oligomers per BSA. D| Synthetic Man₄ or Man₉ conjugated to Qβ bacteriophage.¹⁶² Contains between 400-500 tetra- or nonasaccharide per viral particle. Structural formulae symbols: ■ GlcNAc, ● Man.

Four synthetic glycoconjugates (Figure 21) have been evaluated in animal vaccination studies. The full Man₉GlcNAc₂ structure has been used in two of the animal studies, either clustered on a cyclic peptide (Figure 21A) or on a galactose scaffold

(Figure 21B). These frameworks were further conjugated to OMPC or KLH to enhance their immunogenicity. The Man₉GlcNAc₂ cyclic peptide conjugate (Figure 21A) produced a moderate carbohydrate-specific response, although much of the antibody response was directed towards the linker structure.⁴⁶⁶ Moderate carbohydrate-specific antibody responses were observed with the galactose-scaffolded Man₉GlcNAc₂ construct (Figure 21B),⁴⁶⁵ although in both cases the antibodies produced were poorly cross-reactive with recombinant Env. These studies demonstrate the difficulty of producing an immune response to the Man₉GlcNAc structure, even when clustered.

Linear neoglycan Man₄ and Man₉ structures have also been used in glycoconjugate vaccines with BSA and/or Q β bacteriophage (Figure 21C, D). Both glycoconjugates were able to elicit high titres of anti-mannose antibodies, but displayed no cross-reactivity with Env.^{162, 454} Interestingly, the serum of rabbits immunized with these conjugates bound a variety of synthetic mannose structures, but did not bind any high-mannose structures that included the chitobiose core. Furthermore, the anti-glycan portion of the immune sera and 2G12 did not appear to interfere with each other's binding to immobilized Q β glycoconjugates in competition ELISAs, signifying that the serum antibodies recognize a different carbohydrate epitope than 2G12. Taken together, these observations suggest that these high-mannose structures may be presented in a different conformation when chitobiose is present and that 2G12 glycan recognition is somewhat flexible, as long as it forms a clustered epitope of Man α 1 \rightarrow 2Man motifs.

Phase III Vaccine Trials

Despite the enormous effort that has gone into the development of an HIV vaccine, few have made it to clinical trials. The HIV vaccines that have proceeded to clinical trials are predominantly subunit vaccines that contain individual parts of HIV, DNA vaccines that introduce viral genes into host cells for viral protein expression, and recombinant vector vaccines that use attenuated non-HIV viruses that carry copies of HIV genes. While many of these vaccines have progressed through Phase I and II clinical

trials, so far only VaxGen's AIDS-VAX[®] vaccine has made it to Phase III testing.[†] The early vaccine formula consisted of a mixture of recombinant gp120 from the MN strain of subtype B and either the subtype B strain GNE8 or subtype E strain A244.^{471, 472} The AIDS-VAX[®] B/B formula was used in the North American and Netherlands Vax004 trial,⁴⁷³ and the B/E formula in the Thailand Vax003 trial,⁴⁷⁴ tailored to the local epidemiology. In both trials no overall protection was observed despite the test subjects eliciting high titers of Env binding antibodies.^{475, 476}

A more recent efficacy trial has been completed in Thailand (RV144), which used a heterologous prime-boost immunization regimen⁴⁷⁷ where the subjects were first immunized with a recombinant canarypox vector that encoded the gp120, gag and protease genes of HIV-1 followed by booster immunizations with AIDS-VAX B/E.⁴⁷⁸ The results of the RV144 revealed modest (26-31%) but statistically significant protection from HIV infection, making it the first demonstration that vaccination could protect humans from HIV-1 infection. Follow-up studies of the RV144 trial have commenced, probing for details of the antibody response that evoked protection,^{476, 479} and examining the structure of the immunogens that produced the response.⁴⁸⁰ Analysis of plasma from RV144 participants revealed that the vaccine failed to induce broadly neutralizing antibodies, suggesting that the protective effect was achieved via non-neutralizing[‡] or weakly neutralizing antibodies.⁴⁷⁶ The MN and A244 strains of recombinant gp120 used in the RV144 and Vax003 trials exhibited extensive differences in glycoform, exhibiting the largest disparity in net charge due to sialic acid incorporation.⁴⁸⁰ These differences in glycosylation influenced the affinity of broadly neutralizing antibodies to the recombinant gp120. With the glycosylation profile of gp120 playing such an important role in Env recognition, it is important to establish exactly what glycans are present on naturally occurring HIV-1 Env produced by their native cell targets.

[†] Phase I trials are conducted on small numbers of healthy adults to primarily evaluate the safety of the vaccine. Phase II trials involve larger numbers of volunteers (50-500) to generate additional safety data as well as information for refining the dosage and immunization schedule. Phase III trials are conducted to assess vaccine efficacy.

[‡] While neutralizing antibodies bind Env in way that impedes viral entry, non-neutralizing antibodies are able to bind Env but do not interfere with entry into the target cell. The roles of non-neutralizing antibodies in infection and disease progression are just beginning to be investigated.⁴⁸¹⁻⁴⁸³

Glycans of the gp120 Glycan Shield

The glycosylation profile of recombinant gp120, which is produced in a multitude of cell lines, has been defined for many strains of HIV.^{299, 480, 484-492} Common to all these analyses is the observation of high-mannose glycans and complex-type glycans that exist in discrete domains on the gp120 surface.^{484, 486, 492-494} There are at least 24 potential *N*-linked glycosylation sites on gp120 for any given Env,^{486, 493, 495-497} and while it was once believed that all glycosylation sites were occupied, recent reports have indicated otherwise.^{489, 492} The number of unoccupied glycosylation sites, as well as the glycan type occupying each glycosylation site, has also been shown to differ between and within HIV-1 clades and subtypes.⁴⁸⁹ Furthermore, the glycosylation of recombinant gp120 has been shown to vary significantly when expressed in different cell lines,^{490, 491} as the structure, composition, and heterogeneity of the attached glycans depend on the cellular system used for their expression.⁴⁹⁶ These differences in glycoforms are known to influence immunogenicity and antibody recognition.^{480, 490, 491, 493, 494} Despite the inconsistencies of glycosylation between cell lines, recombinant gp120 used in immunizations, such as in the Thailand phase III trials or in antibody detection assays, are typically produced in easy to maintain cell lines with high rates of protein synthesis, such as Chinese hamster ovary cells (CHO), human embryonic kidney cells (293T) and insect cells (Sf2), rather than in the natural host cells of HIV.⁴⁹⁸⁻⁵⁰² This raises questions about the use of glycan structures elucidated from recombinant gp120 derived from nonnative host cells as targets in synthetic glycoconjugate vaccines, as well as the reliability of ELISAs employing recombinant gp120 to assess antibody cross reactivity, both of which may partially explain the short comings of the HIV-1 vaccine attempts to date.

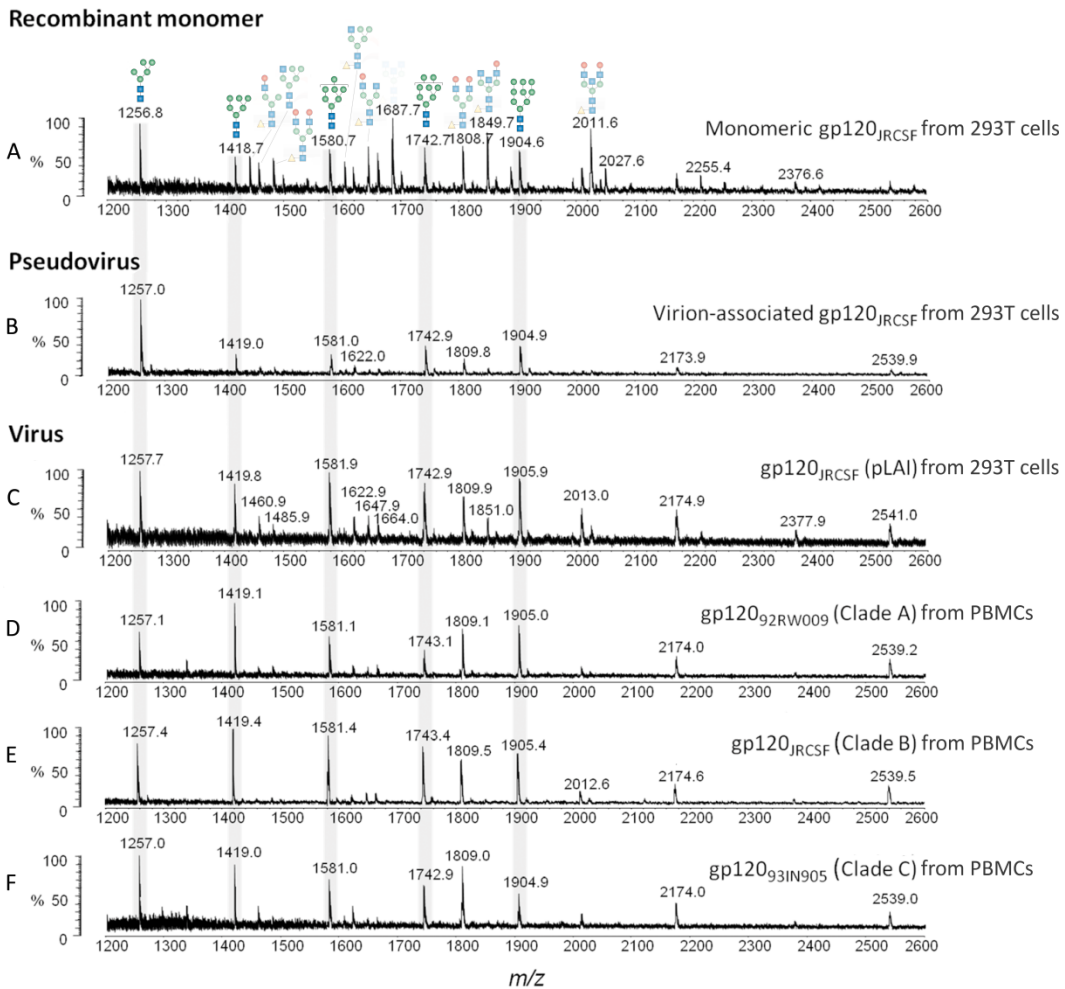


Figure 23. MALDI-TOF MS analyses of the *N*-linked glycans ($[M+Na]^+$ ions), released from: **A**) recombinant monomeric gp120_{JRCSF} expressed in HEK 293T cells; **B**) gp120_{JRCSF} isolated from pseudovirus generated by transfection of HEK 293T cells with plasmids expressing the virus backbone and functional envelope; **C**) gp120_{JRCSF} isolated from replication competent viral particles generated by transfection of HEK 293T cells with a molecular clone plasmid; **D**, **E** and **F**) gp120 from three HIV-1 clades obtained by infection of human PBMCs. Symbols used for the structural formulae: ● Gal, ■ GlcNAc, ● Man, ▲ Fuc. Adapted from *PLoS ONE* 2011, 6, e23521.

The abundance of high-mannose glycans found on envelope-derived gp120 represents a divergence from typical mammalian posttranslational glycan processing, where high-mannose glycans are nearly universally processed further to hybrid and complex-type glycans. The primary reason for this divergence is thought to derive from steric factors that hinder glycosidase activity,^{486, 504} which is supported by the differences in glycosylation profiles between recombinant monomeric gp120 and virion-associated gp120. The early Man₉GlcNAc₂ glycan intermediate is processed by the ER and Golgi α -mannosidases to yield Man₅GlcNAc₂ (Figure 22). This processing is

incomplete however, as the dense clustering of *N*-glycans hinders enzymatic access, giving rise to a $\text{Man}_{6,9}\text{GlcNAc}_2$ patch that is intrinsic to both monomeric and trimeric gp120 (Figure 24). Virion-associated gp120 retains an additional $\text{Man}_{5,9}\text{GlcNAc}_2$ population as a consequence of the additional steric factors from trimerization (Figure 24). Further downstream processing in the medial and trans-Golgi generate complex-type glycans from $\text{Man}_5\text{GlcNAc}_2$, although a significant population of $\text{Man}_5\text{GlcNAc}_2$ remains unprocessed, either due steric to constraints that restrict *N*-acetylglucosaminyltransferase (GnT1) access or by circumventing the medial-Golgi resident enzymes entirely.

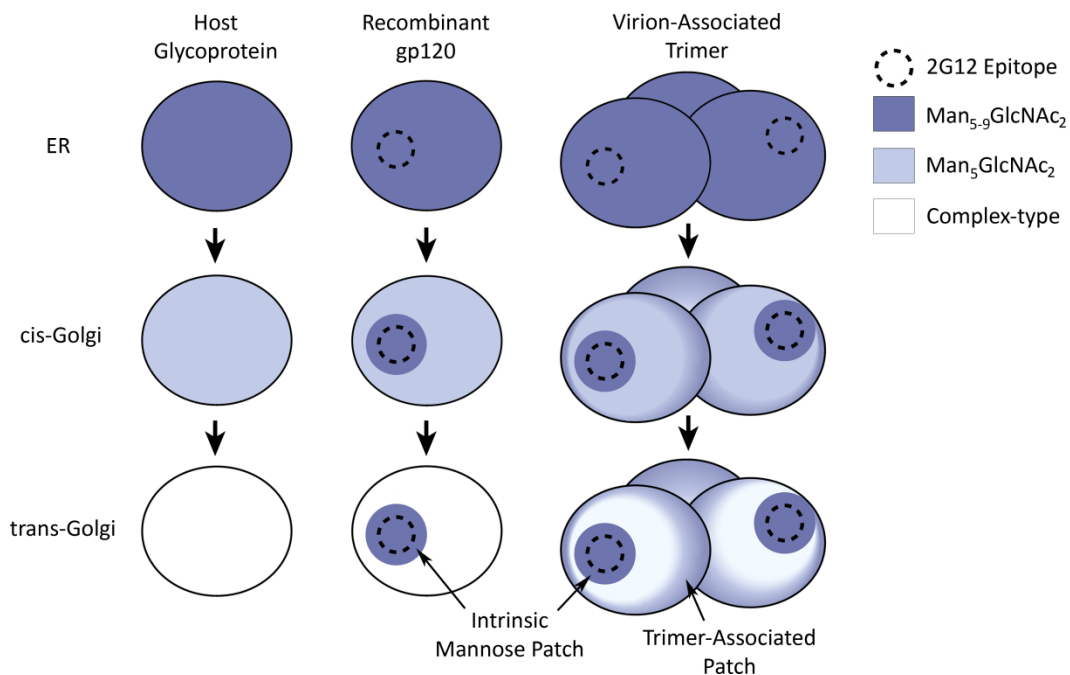


Figure 24. Divergence of gp120 glycosylation from host cell glycosylation. Following removal of terminal α -linked glucose residues in the ER, folded glycoproteins contain exclusively oligomannose glycans. As glycoproteins transit through the ER and cis-Golgi, $\text{Man}\alpha 1 \rightarrow 2\text{Man}$ termini are removed by mannosidases to yield $\text{Man}_5\text{GlcNAc}_2$. However, an oligomannose cluster intrinsic to both monomeric gp120 and oligomeric gp120 resists this glycan processing, leaving behind a patch of $\text{Man}_{5,9}\text{GlcNAc}_2$ that is recognized by antibody 2G12.⁴³⁸ Steric hindrance from trimerization further limits $\text{Man}\alpha 1 \rightarrow 2\text{Man}$ trimming leading to an additional trimer-associated population of $\text{Man}_{5,9}\text{GlcNAc}_2$. The exposed $\text{Man}_5\text{GlcNAc}_2$ glycans are processed by GnT1 and subsequent enzymes as they pass through the medial and trans-Golgi to form complex-type glycans. Adapted from *PLoS ONE* 2011, 6, e23521.

Part III: Scope of Project

Preface

Much effort has been expended on producing an effective HIV-1 vaccine glycoconjugate that protects against infection. The traditional approach of glycoconjugate vaccine design, where a carbohydrate component of the target is conjugated to a carrier protein, has thus far failed to elicit neutralizing antibody responses against HIV-1. The field of HIV-1 vaccine design has thus turned to rational, structure-based design strategies.⁵⁰⁶

While the glycan shield is a relatively conserved feature of the HIV Env spike, targeting these glycans is innately problematic since carbohydrate antigens generally elicit weak immune responses with little class switching or establishment of B cell memory. A number of reasons contribute to this limited response. A lack of CD4+ T cell help for carbohydrate antigens requires the B cells to become activated through the poorly understood CD4-independent mechanisms. The low affinity of carbohydrate-protein interactions hinders B cell recognition and activation. The carbohydrates on gp120 are also self-glycans, causing the immune system to be tolerant of these types of structures. A rationally designed HIV-1 must consider these problems, which are discussed in the proceeding sections. The approach taken in this work focused on three key areas:

- 1) An immunogenic carrier that directs the immune response towards the carbohydrate antigen
- 2) Display the appropriate immunogenic HIV-1 glycan structures
- 3) Accurate mimicry of the gp120 glycan clusters

The carbohydrate carrier plays the most important role in this design as its topology determines how the glycans are presented and interact with the immune system. An effective carrier would also direct the immune response towards the weakly immunogenic self-glycans. To this end, Professor Jamie K. Scott from Simon Fraser University approached us with the idea of coating filamentous bacteriophage with gp120 glycans. She has demonstrated that a phage carrier can better focus the antibody response towards a conjugated hapten than a traditional protein carrier such as

ovalbumin.⁵⁰⁷ She has also engineered a phage with increased amino functionalities on the major coat protein,⁵⁰⁷ establishing a repetitive landscape of conjugation points that could scaffold glycans to mimic the glycosylated surface of gp120. Filamentous phage also have inherent immunological properties that make them ideal vaccine carriers, such as being self-adjuncting,¹⁶⁹ inducing class switching to IgG,¹⁶⁴ and eliciting CD4+ T cell help to form immunological memory.⁵⁰⁸ Filamentous phage appear to be a superlative carrier for an HIV-1 glycoconjugate vaccine.

Ff Phage Biology

The F-specific filamentous (Ff) phage is an Inovirus, a genus of viruses within the Inoviridae family that form flexuous filamentous particles which infect enterobacteria.⁵⁰⁹ Infection with Ff phage is not lethal but does decrease the growth rate of the host cell. The most thoroughly investigated of the Ff viruses are the M13, f1 and fd phages, which infect F⁺ and Hfr strains of *Escherichia coli* via recognition of the F-pili on the cell surface.^{510, 511} These three bacteriophage are closely related, possessing 98% sequence homology and identical morphology,^{512, 513} and can be thought of as mutants of the same virus.

The phage structure is simplistic, consisting of single-stranded DNA genome packaged within a tubular capsid consisting of ~2700 copies of the major coat protein pVIII (Figure 25).⁵¹⁴ The termini of the filament contain five copies of the paired minor coat proteins, pVII/pIX and pIII/pVI.^{515, 516} The coat proteins are small and hydrophobic with the exception of pIII which is large and mostly hydrophilic. The ~6400 nucleotide genome is relatively small, composed of only 11 genes,⁵¹⁷ and tolerates insertions into non-essential regions well.⁵¹⁸ This has proven advantageous for numerous studies and applications such as phage display,⁵¹⁹⁻⁵²² where proteins and peptides are fused onto phage coat proteins to study protein-ligand interactions, DNA cloning and sequencing,^{523, 524} and in nanomaterial fabrication,^{525, 526} where semiconducting/magnetic nanowires have been constructed using M13 as a biological template.

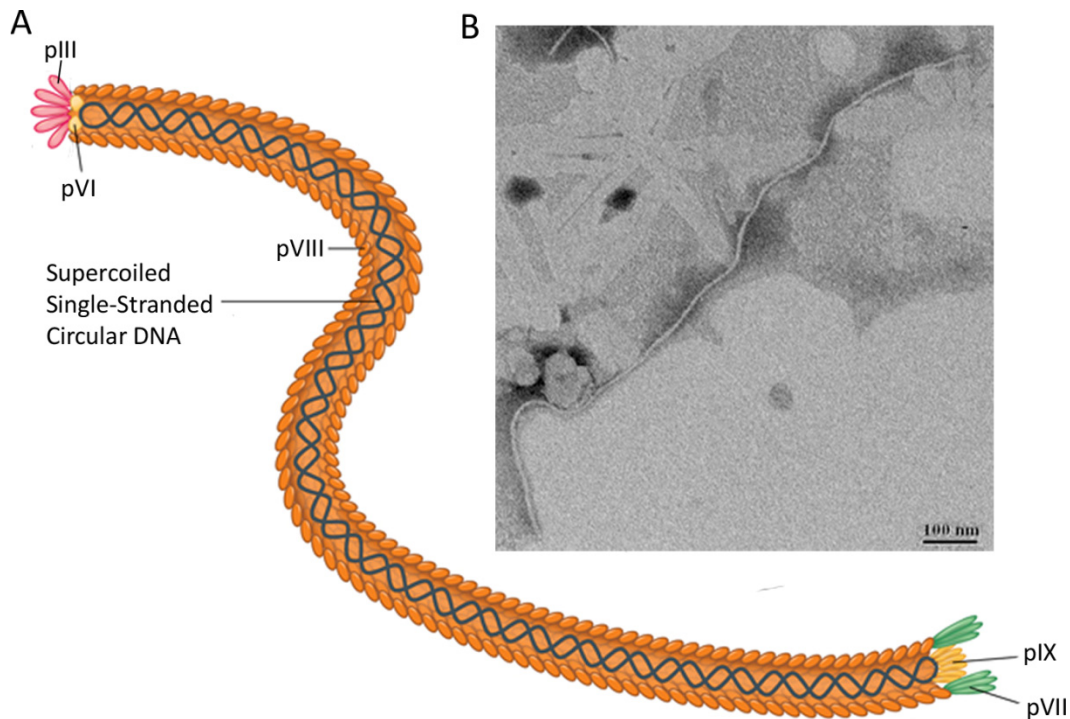


Figure 25. Ff phage structure. A| The pIII coat protein on the end of the phage is responsible for binding to the F-pilus to enter the host cell. The 'opposite' end, capped with pIX and pVII emerges from the host cell. Adapted from W.W. Norton & Company, *Microbiology: An Evolving Science, 2nd Ed*, ©2010 with permission. B| A filamentous phage particle as imaged from an electron microscope (TEM).

The general stages of the Ff phage life cycle are: infection and entry, replication of the viral genome, and assembly and release of the progeny particles from the host (Figure 26). Ff infection of *E. coli* starts by adsorption of the phage to the F-pilus via the N2 domain of the pIII coat protein causing the pilus to retract.⁵²⁷ The retracted pilus ushers the N1 domain of pIII into the periplasm where it interacts with the co-receptor TolA.^{528, 529} Conformational rearrangement of pIII exposes the C domain's hydrophobic membrane anchor α -helix, leading to the uncoating of the virion and DNA entry into the host cell cytoplasm.⁵³⁰ The hydrophobic helix inserts into the cytoplasmic membrane allowing for the subsequent entry of phage DNA into the cytoplasm and integration of pVIII into the inner membrane.

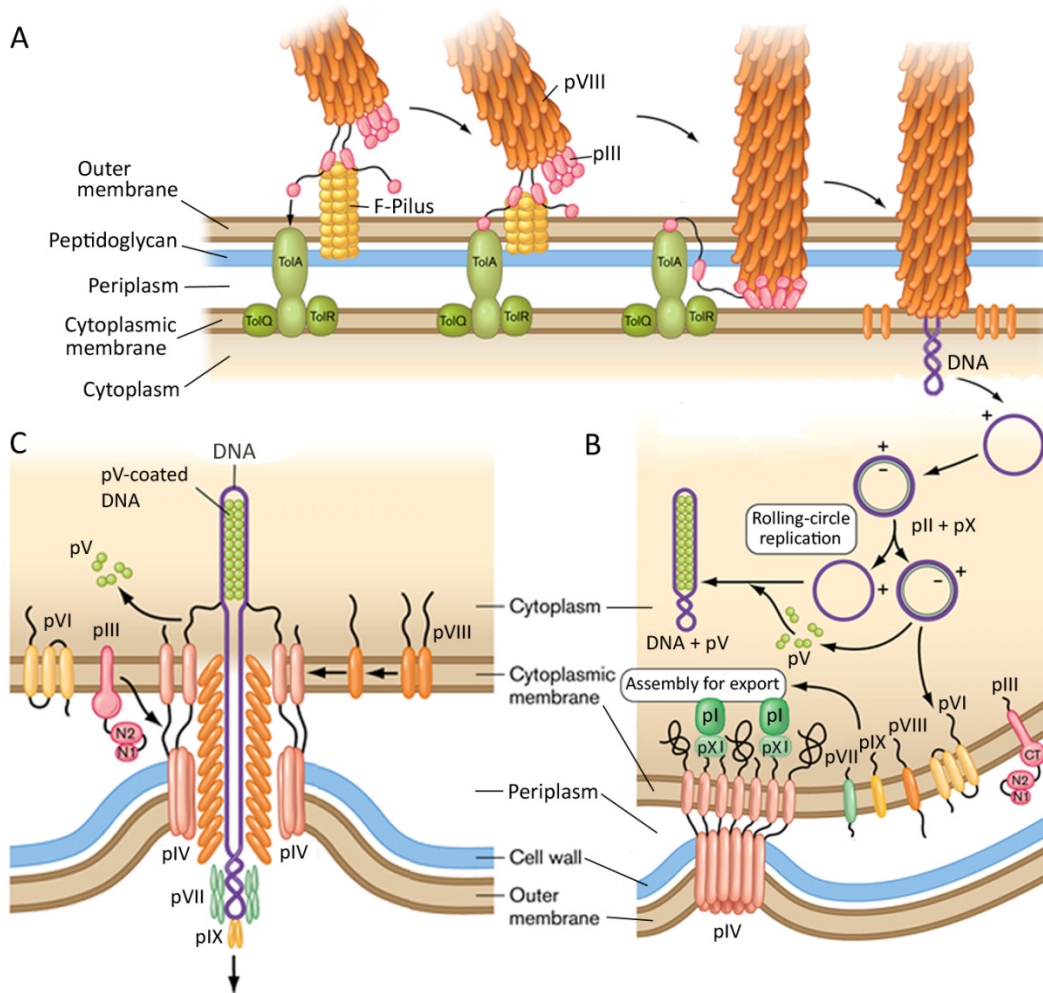


Figure 26. Ff phage life cycle. A) The phage binds to the host F-pilus and TolA coreceptor via the coat protein pIII. A hydrophobic portion of pIII inserts itself into the inner membrane leading to the distribution of coat proteins and release of its genome into the cytoplasm. B) The single stranded DNA genome is replicated and translated with host enzymes to produce phage proteins. New (+) strands of DNA are produced through rolling-circle replication and complexed with pV in preparation for packaging. C) The DNA-pV complex interacts with the pIV pore complex via its hairpin packaging signal and is exuded from the pore, replacing pV with the pVIII coat protein along the way. Adapted from W.W. Norton & Company, *Microbiology: An Evolving Science, 2nd Ed*, ©2010 with permission.

Following entry into the cytoplasm, the single-stranded DNA genome (+) strand serves as a template to synthesize the (-) DNA strand, yielding a double-stranded circle known as the replicative form. The replicative form DNA serves as a template for expression of phage genes and additional (+) strands for packaging into phage. The phage proteins that are involved in replication remain in the cytoplasm whereas all other proteins are targeted to the cytoplasmic membrane (Figure 26B).^{531, 532} New (+) strands are duplicated through rolling-circle replication, requiring pII to cleave the (+) strand to allow host cell DNA polymerase to replicate new (+) strands.⁵³³ The newly

synthesized (+) strands are used as templates for (-) strand replication to increase the copy number of (+) strand DNA early in infection, whereas late in infection these positive strands are coated with pV which collapses the DNA into a rod for phage assembly.

The progeny ssDNA, coated with pV, contains an exposed packaging signal, a hairpin loop, that is recognized by pI, pII and pIX in the cytoplasmic membrane.⁵³⁴ A phage assembly complex forms around a pore composed of pIV that extends through all layers of the cellular envelope (Figure 26C).⁵³⁵ Positive charges within the pore help draw in the negatively charged DNA and pV is replaced by major coat protein pVIII as the virion is extruded from the pore. When the DNA is completely coated with pVIII, the minor coat proteins pIII and pVI are added to the virion end and the virion is released.

Filamentous Phage as a Vaccine Carrier

The major coat protein, pVIII, dominates the phage architecture with ~2700 copies compared to 3-5 copies each of the minor coat proteins. pVIII is an α -helical protein composed of 50 amino acids. The helix possesses three distinct regions of polarity: the exposed N-terminal region amphipathic region, the central hydrophobic region that remains buried against the hydrophobic regions of neighbouring pVIII subunits, and the C-terminal region carries positively charged lysines that interact with the negatively charged DNA backbone within the center of the phage (Figure 27A, B).⁵³⁶⁵³⁷ The pVIII subunits form an overlapping helical array around the DNA core (Figure 27C).⁵³⁷ The completely assembled phage is ~60 Å in diameter and ~900 nm long, with the length of the phage dependent on the length of the genome.⁵³⁸

The phage architecture is predominantly held together by hydrophobic interactions between the coat protein subunits.^{539, 540} This is illustrated by the virus's sensitivity to detergents and organic solvents, especially chloroform.^{541, 542} Outside of lipophilic agents, Ff phages are exceptionally resilient, surviving prolonged incubation at 75 °C, high salt concentrations, 8M urea, and a pH range between 2 to 11.5.^{510, 543, 544} Purified phage are able to be stored indefinitely at moderate temperatures without losing infectivity.⁵⁴⁵ The Ff phages durability and resilience towards chemical manipulation^{536, 546-550} are favourable characteristics for a biological carrier to possess.

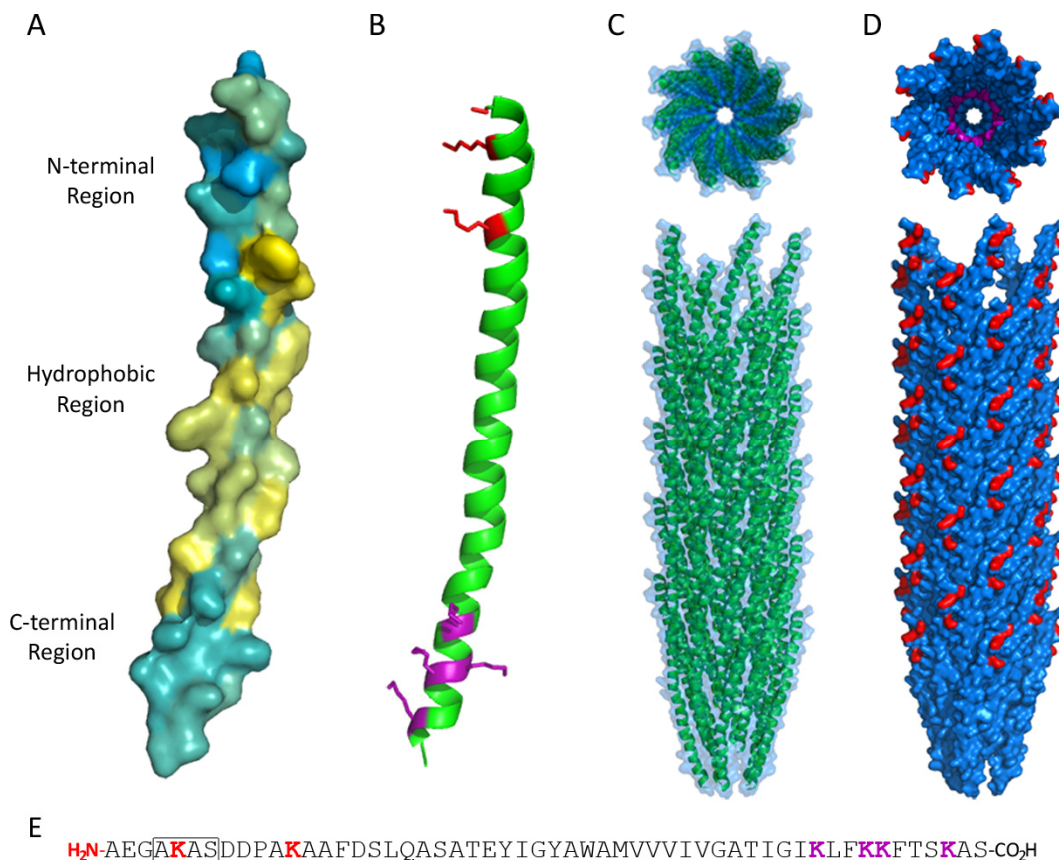


Figure 27. The structure and assembly of the major coat protein pVIII of the f1.K phage (modified from PDB: 2C0W). A| A surface model of pVIII where the hydrophobic regions are represented in yellow and the polar regions represented in blue. B| A cartoon representation of the helical structure of pVIII. The N-terminal amine and adjacent lysines are colored in red. The C-terminus lysines are colored in purple. C| A section of the assembled phage modeled with a transparent surface to expose the pVIII subunits. The top view is of the phage along the fibre axis and the bottom view is perpendicular to this axis. D| A surface model of the phage where the exposed terminal amine and lysines are colored in red. E| The sequence of pVIII of f1.K. The sequence of wt f1 phage was engineered to include the four-residue insert highlighted with the box.⁵⁰⁷ The N-terminal amine and lysines follow the same color scheme as in B and D.

The f1.K phage carrier used in this project is an f1 phage that has been engineered by Jamie Scott's lab to include an additional exposed lysine on the N-terminus (Figure 27E) for conjugation.⁵⁰⁷ The three exposed amines of each individual pVIII subunit form a cluster of conjugation sites on the phage surface (green circles, Figure 28A). These clusters are situated 25-40 Å away from each other in a repeating diamond pattern around the phage. The range of distances observed between the reactive amines on the f1.K capsid are comparable to the amine spacing observed on the Q β icosahedral virus capsid scaffold used by M.G. Finn and D.R. Burton in their HIV-1 glycoconjugate vaccine candidate (Figure 28B).¹⁶² However, a more evenly distributed

geometrical arrangement of amines is observed on f1.K, with less unadorned surface area. Thus, as a glycoconjugate carrier, the f1.K capsid should be more occluded by carbohydrate than what is achievable with the Q β scaffold, which is advantageous for mimicking the thoroughly shielded surface of gp120. A tightly glycosylated surface also conceals protein epitopes of the f1.K capsid, allowing the immune response to focus on the carbohydrate hapten.

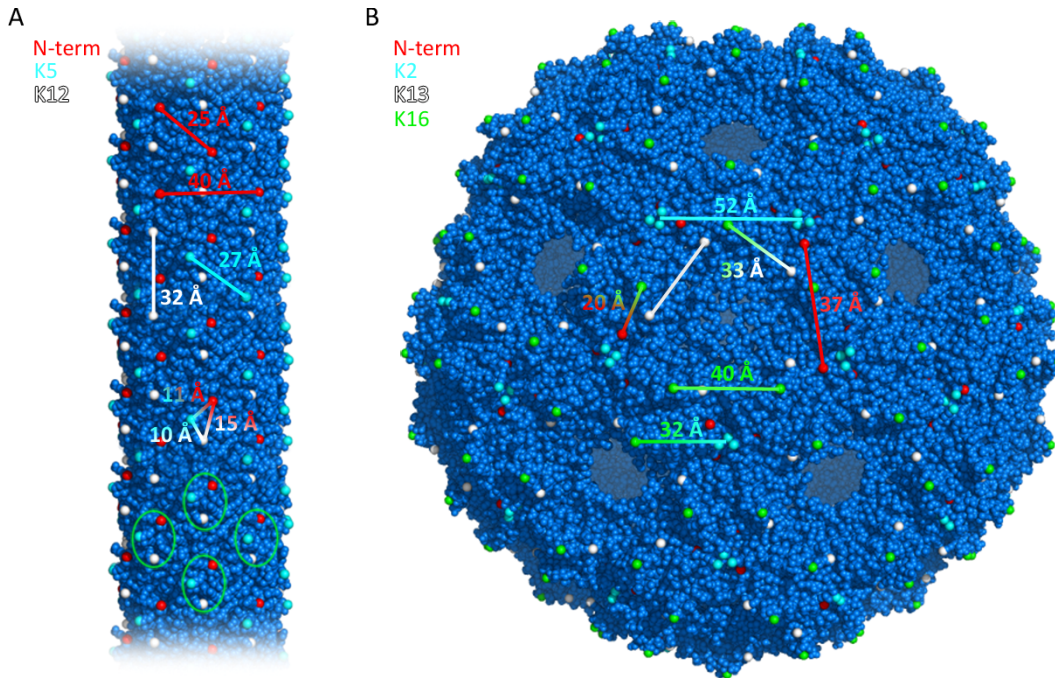


Figure 28. A modeled comparison of the surface amines of the f1.K and Q β capsids. A | A fragment of the f1.K capsid with the exposed amines colored in red, cyan and white. Model adapted from PDB: 2C0W. B | Q β icosahedral virus capsid with the exposed amines colored in red, cyan, white and green. Model adapted from PDB: 1QBE.

The distances between glycan conjugation sites on the f1.K capsid are appropriate for interaction with 2G12.⁴³⁹ On gp120, even though the *N*-glycosylation sites frequently change in response to immunological pressure,^{368, 551, 552} an overall minimum density of glycans is maintained with an optimal distance of 20-40 Å between glycosylation sites.³⁹² Modeling the f1.K capsid with a Man₅ glycan attached to the surface exposed amines reveals a densely glycosylated surface that is comparable to the glycan shield of gp120 (Figure 29). The diameter of the f1.K increases by ~40 Å with the attached glycans, becoming comparable in size to the ~160 Å diameter of the HIV-1 Env trimer.⁴²⁸ The f1.K filamentous phage is thus an exceptional mimic in both glycosylation density and size.

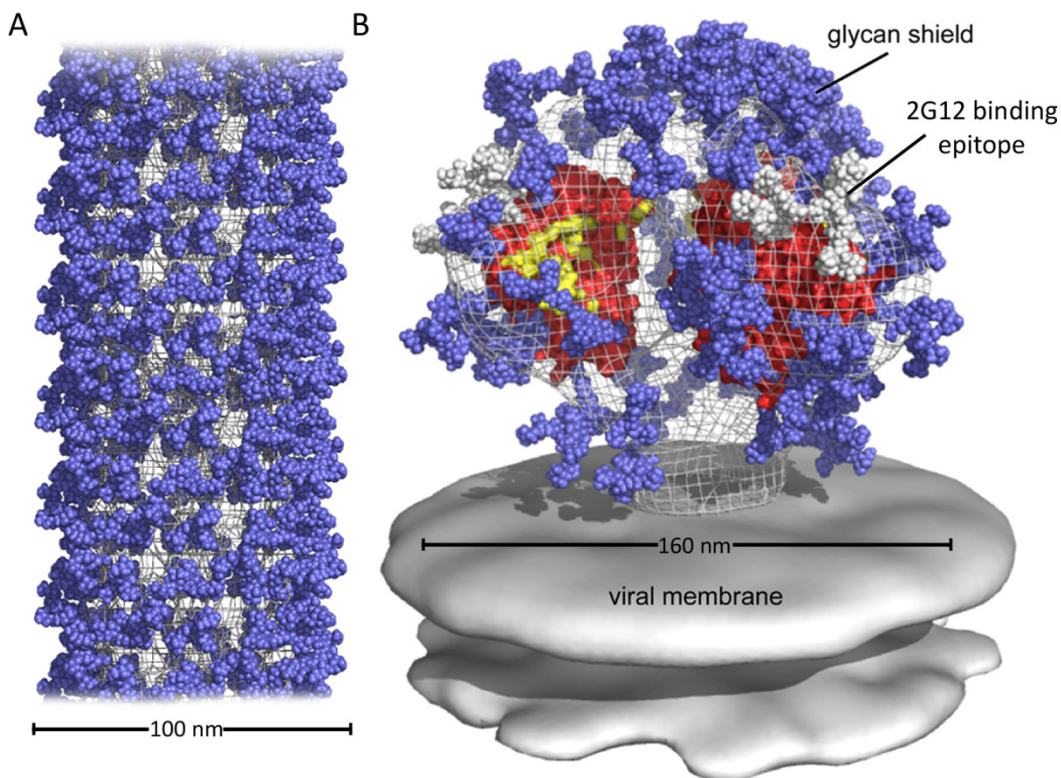


Figure 29. A comparison of the glycan density of an f1.K glycoconjugate and gp120. A| A model of a fragment of the f1.K capsid with a Man_5 glycan conjugated to the three exposed amines of every pVIII subunit. Glycans are shown in purple. The model was constructed in pymol based on the PDB: 2C0W structure. Glycan structures were constructed with the Glycam Biomolecule Builder. B| The HIV-1 envelop trimer is shown with the crystal structure of the b12-bound monomeric gp120 core³¹⁰ fitted within a cryo-electron tomographic density map.⁴²³ Glycans are shown in purple, with the white glycan cluster representing the 2G12 binding epitope. The CD4 binding site is shown in yellow. Image obtained from http://www.scrips.edu/news/press/images/burton_dennis/burton_image.jpg.

Synthetic Glycan Antigens to Represent the gp120 Glycans

The oligomannose glycans observed on the native virions are the most obvious target for a carbohydrate-based HIV-1 vaccine.^{503, 505} The excessive amount of high-mannose glycans on gp120 is disproportionate to the glycans found on mammalian cells, which are mostly complex type, making them somewhat foreign to the human immune system and a good immunological target. Recent evidence has correlated immunogenicity and the ability to elicit a wide breadth of neutralizing antibodies to epitopes composed of high-mannose glycans.^{493, 553} Additionally, mucosal transmission of HIV-1 is well known to be restricted to a small subset of viruses amongst the breadth of quasispecies present in the infected donor.^{336, 356, 554-556} These founder viruses have more high-mannose glycans compared to chronic viruses and are highly conserved, even

between clades.⁴⁹² Thus, high-mannose glycan are ideal antigenic targets to prevent HIV-1 infection.

The linear Man_4 structure that mimics the D1 arm of $\text{Man}_9\text{GlcNAc}_2$ has been used in many glycoconjugates to assess the effectiveness of various scaffolds to effectively cluster oligomannose structures for 2G12 recognition.^{162, 454, 462, 467, 557} Even though it is not a natural occurring *N*-linked glycan, it binds 2G12 with affinities comparable to the naturally derived $\text{Man}_9\text{GlcNAc}_2$ glycan (Figure 20).^{440, 460} The Man_4 structure is therefore an ideal initial synthetic target to assess the potential of the filamentous phage carrier to mimic the glycan presentation of gp120. For this project, the GlcNAc_2 core is excluded due to the difficulty in synthesizing chitobiose.^{558, 559} To compensate for the loss of the chitobiose and to maintain the natural topology of the glycan, a short rigid linker was used in place of GlcNAc_2 , and the oligomannan connected to the linker via a β -linkage, as it would naturally occur. This linker strategy is in contrast to the glycans linked via α -linkages to long flexible linkers that have been employed in previous HIV-1 glycoconjugates vaccines, which have failed to invoke crossreactivity.^{162, 454} To facilitate a short linker strategy and provide the means for a highly reactive conjugation, the tetramannosyl thiol **1** (Figure 30) was envisioned. The replacement of the anomeric alcohol with a thiol creates a reactive nucleophilic glycan that is useful in a number of linker strategies (TABLE 1) without the added length of a traditional aglycone spacer.

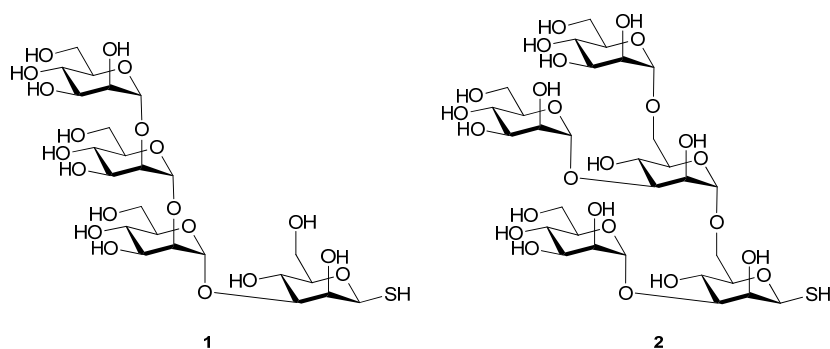


Figure 30. The target 1-thio mannosides for the HIV-1 vaccine.

The $\text{Man}_5\text{GlcNAc}_2$ structure is also of particular interest due to the recent discovery of the PG9, PG16 and PGT128 which recognize glycan-dependent epitopes on gp120 that contain $\text{Man}_5\text{GlcNAc}_2$.^{443, 448, 449, 560} These glycan-dependent antibodies

appear to be common in early infection,⁵⁶¹ supporting the use of their recognized glycans as target epitopes for immunization. The Man₅GlcNAc₂ glycan is also a predominant in the glycoform of gp120 as revealed by mass spectroscopy (Figure 23).^{503, 505} To date, the Man₅GlcNAc₂ has not been used as a hapten in an HIV-1 glycoconjugate vaccine in any published immunization studies. For these combined reasons, the Man₅ structure **2** (Figure 30) was chosen as an additional synthetic target.

Linker Strategy

The linker strategy must be reactive and selective enough in order to facilitate the high degree of conjugation required to mimic the gp120 glycan shield. High conjugation efficiency is also important to maintain low glycan equivalents in conjugation reaction since there are 8,000+ conjugation sites per phage. A short, rigid heterobifunctional linker with reactivity towards amines and thiols was needed. The amine reactive end would consist of an NHS ester, which is the standard strategy for conjugation to biological amines. For the thiol reactive end, two chemistries were chosen. The first being the haloacetyl displacement reaction, which was chosen because of its efficiency and selectivity for reaction with thiols.⁵⁶² The shortest possible linker with these functionalities is *N*-succinimidyl iodoacetate (SIA) (Figure 31), which produces a linker arm of only two carbons long.

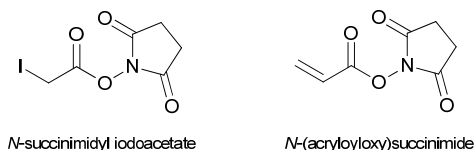
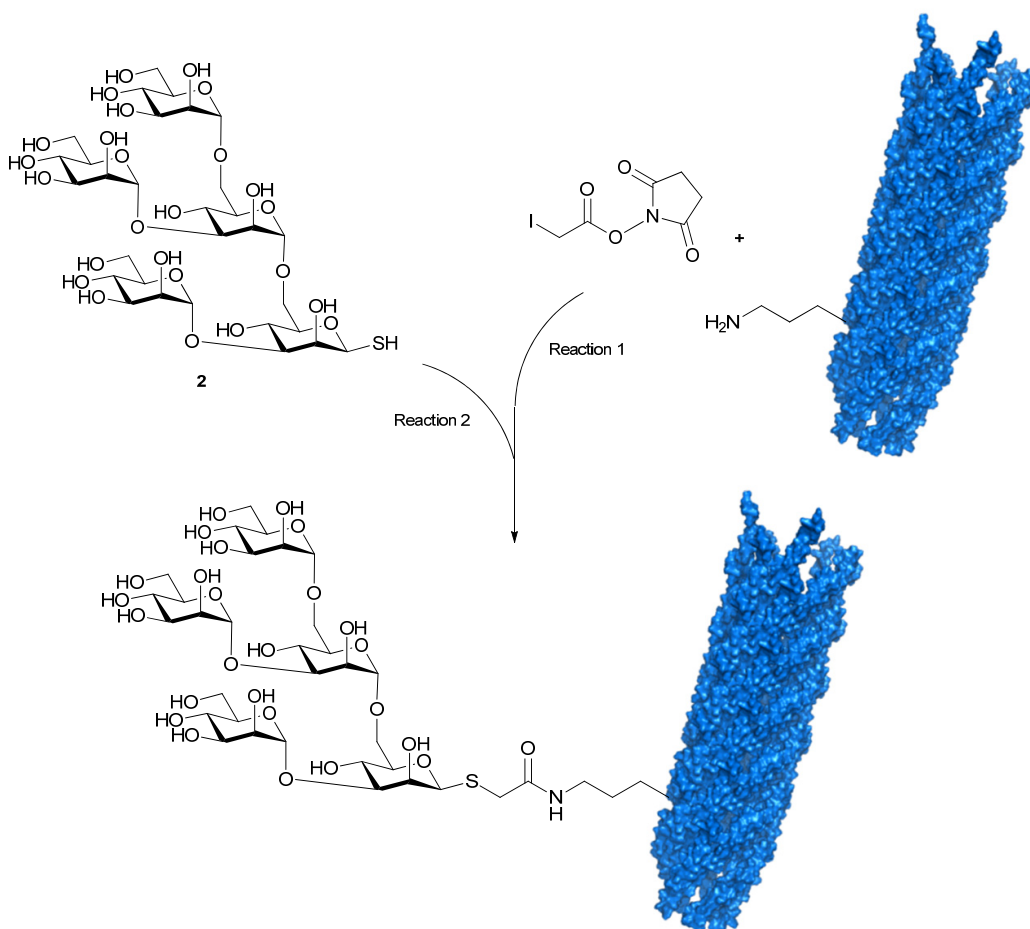


Figure 31. Two short amine and thiol reactive linkers.

The second chemistry chosen was the thiol-ene click reaction. The thiol-ene reaction is known for achieving quantitative yields, requiring small amounts of catalysts, and being very selective.²⁰⁸ It also has the added advantage that the alkene functionality is relatively inert compared to the activated iodoacetyl, which allows linker-conjugated phage to be stored for periods of time without degradation. The linker with the smallest spacer that contains the NHS ester and alkene functionalities is *N*-(acryloyloxy)succinimide (Figure 31). With both linkers, the exposed amines of the phage surface would be first reacted with the linker to produce the linker-functionalized

phage, which would then be reacted with the mannosyl thiols to produce the phage glycoconjugates (Scheme 1).



Scheme 1. An example of the coupling strategy using the SIA crosslinker and mannosyl thiol 2.

Concluding Remarks

The project started out with the synthesis of the glycan targets without much concern about how exactly these conjugates would be characterized. This project branched out along the way to investigate an additional interesting linker strategy opportunity, determine the exact sites on pVIII that were being conjugated, and included some *in vivo* vaccination strategies involving β -glucans. In Chapter 2, the synthesis of the tetrasaccharide and pentasaccharide glycans **1** and **2** are described. Since the degree of conjugation needed to be assessed accurately, and the common biological techniques used to quantify conjugation efficiency were not meticulous enough for this project, LC-UV-MS was explored as a quantification technique for this

project. This work, along with the conjugation and purification of the phage conjugates, are described in Chapter 3. Finally, the immunochemistry and animal immunization studies are discussed in Chapter 4.

References

1. K. Ohtsubo, J. D. Marth, *Cell* **2006**, *126*, 855-867.
2. P. M. Rudd, T. Elliott, P. Cresswell, I. A. Wilson, R. A. Dwek, *Science* **2001**, *291*, 2370-2376.
3. Y. van Kooyk, G. A. Rabinovich, *Nat. Immunol.* **2008**, *9*, 593-601.
4. J. R. Bishop, P. Gagneux, *Glycobiology* **2007**, *17*, 23R-34R.
5. N. Sharon, H. Lis, *Sci. Am.* **1993**, *268*, 82-89.
6. H. Schachter, *Glycoconj. J.* **2000**, *17*, 465-483.
7. K. Yamashita, A. Hitoi, N. Tateishi, T. Higashi, Y. Sakamoto, A. Kobata, *Arch. Biochem. Biophys.* **1983**, *225*, 993-996.
8. K. Yamashita, K. Totani, Y. Iwaki, I. Takamisawa, N. Tateishi, T. Higashi, Y. Sakamoto, A. Kobata, *J. Biochem. (Tokyo)* **1989**, *105*, 728-735.
9. E. Reynders, F. Foulquier, W. Annaert, G. Matthijs, *Glycobiology* **2011**, *21*, 853-863.
10. S. Degroote, J. Wolthoorn, G. van Meer, *Semin. Cell Dev. Biol.* **2004**, *15*, 375-387.
11. A. M. Wu, *Glycosyl phosphatidylinositol-linked glycoconjugates: Structure, biosynthesis and function*, in K. Hwa, *Molecular Immunology of Complex Carbohydrates-2*, **2001**, p. 207-214
12. R. G. Spiro, *Glycobiology* **2002**, *12*, 43R-56R.
13. T. de Beer, J. F. G. Vliegthart, A. Loeffler, J. Hofsteenge, *Biochemistry (Mosc.)* **1995**, *34*, 11785-11789.
14. D. J. Gill, H. Clausen, F. Bard, *Trends Cell Biol.* **2011**, *21*, 149-158.
15. M. Lommel, S. Strahl, *Glycobiology* **2009**, *19*, 816-828.
16. C. R. Torres, G. W. Hart, *J. Biol. Chem.* **1984**, *259*, 3308-3317.
17. E. J. Kim, *Molecules* **2011**, *16*, 1987-2022.

18. L. Schaefer, R. M. Schaefer, *Cell Tissue Res.* **2010**, *339*, 237-246.
19. F. Schwarz, M. Aebi, *Curr. Opin. Struct. Biol.* **2011**, *21*, 576-582.
20. P. Burda, M. Aebi, *Biochimica et Biophysica Acta (BBA) - General Subjects* **1999**, *1426*, 239-257.
21. C. Ruiz-Canada, D. J. Kelleher, R. Gilmore, *Cell* **2009**, *136*, 272-283.
22. S. R. Hanson, E. K. Culyba, T. L. Hsu, C. H. Wong, J. W. Kelly, E. T. Powers, *Proc. Natl. Acad. Sci. U. S. A.* **2009**, *106*, 3131-3136.
23. D. Shental-Bechor, Y. Levy, *Proceedings of the National Academy of Sciences* **2008**, *105*, 8256-8261.
24. E. K. Culyba, J. L. Price, S. R. Hanson, A. Dhar, C. H. Wong, M. Gruebele, E. T. Powers, J. W. Kelly, *Science* **2011**, *331*, 571-575.
25. M. Aebi, R. Bernasconi, S. Clerc, M. Molinari, *Trends Biochem. Sci.* **2010**, *35*, 74-82.
26. A. Helenius, M. Aebi, *Annu. Rev. Biochem.* **2004**, *73*, 1019-1049.
27. J. Roth, C. Zuber, S. Park, I. Jang, Y. Lee, K. G. Kysela, V. Le Fourn, R. Santimaria, B. Guhl, J. W. Cho, *Mol. Cells* **2010**, *30*, 497-506.
28. D. J. Vigerust, V. L. Shepherd, *Trends Microbiol.* **2007**, *15*, 211-218.
29. Y. Abe, E. Takashita, K. Sugawara, Y. Matsuzaki, Y. Muraki, S. Hongo, *J. Virol.* **2004**, *78*, 9605-9611.
30. H. C. Aguilar, K. A. Matreyek, C. M. Filone, S. T. Hashimi, E. L. Levrony, O. A. Negrete, A. Bertolotti-Ciarlet, D. Y. Choi, I. McHardy, J. A. Fulcher, S. V. Su, M. C. Wolf, L. Kohatsu, L. G. Baum, B. Lee, *J. Virol.* **2006**, *80*, 4878-4889.
31. A. Beyene, A. Basu, K. Meyer, R. Ray, *Virology* **2004**, *324*, 273-285.
32. S. L. Hanna, T. C. Pierson, M. D. Sanchez, A. A. Ahmed, M. M. Murtadha, R. W. Doms, *J. Virol.* **2005**, *79*, 13262-13274.
33. F. Helle, G. Duverlie, J. Dubuisson, *Viruses-Basel* **2011**, *3*, 1909-1932.

34. A. Goffard, N. Callens, B. Bartosch, C. Wychowski, F. L. Cosset, C. Montpellier, J. Dubuisson, *J. Virol.* **2005**, *79*, 8400-8409.
35. P. C. Reading, J. L. Miller, E. M. Anders, *J. Virol.* **2000**, *74*, 5190-5197.
36. D. G. Nguyen, J. E. K. Hildreth, *Eur. J. Immunol.* **2003**, *33*, 483-493.
37. M. Zhang, B. Gaschen, W. Blay, B. Foley, N. Haigwood, C. Kuiken, B. Korber, *Glycobiology* **2004**, *14*, 1229-1246.
38. M. Heidelberger, O. T. Avery, *The Journal of Experimental Medicine* **1923**, *38*, 73-79.
39. W. S. Tillett, T. Francis, *J. Exp. Med.* **1929**, *50*, 687-U152.
40. C. M. Macleod, R. G. Hodges, M. Heidelberger, W. G. Bernhard, *J. Exp. Med.* **1945**, *82*, 445-465.
41. J. B. Robbins, R. Austrian, C. J. Lee, S. C. Rastogi, G. Schiffman, J. Henrichsen, P. H. Makela, C. V. Broome, R. R. Facklam, R. H. Tiesjema, J. C. Parke, *J. Infect. Dis.* **1983**, *148*, 1136-1159.
42. S. Kruetzmann, M. M. Rosado, H. Weber, U. Germing, O. Tournilhac, H. H. Peter, R. Berner, A. Peters, T. Boehm, A. Plebani, I. Quinti, R. Carsetti, *J. Exp. Med.* **2003**, *197*, 939-945.
43. C.-A. Siegrist, R. Aspinall, *Nature Reviews Immunology* **2009**, *9*, 185-194.
44. S. Segal, A. J. Pollard, *Br. Med. Bull.* **2004**, *72*, 65-81.
45. A. Gonzalez-Fernandez, J. Faro, C. Fernandez, *Vaccine* **2008**, *26*, 292-300.
46. G. B. Lesinski, M. A. Westerink, *Current drug targets. Infectious disorders* **2001**, *1*, 325-334.
47. Á. González-Fernández, J. Faro, C. Fernández, *Vaccine* **2008**, *26*, 292-300.
48. O. T. Avery, W. F. Goebel, *The Journal of Experimental Medicine* **1931**, *54*, 437-447.
49. G. Ada, D. Isaacs, *Clin. Microbiol. Infect.* **2003**, *9*, 79-85.
50. A. Weintraub, *Carbohydr. Res.* **2003**, *338*, 2539-2547.

51. L. Morelli, L. Poletti, L. Lay, *European Journal of Organic Chemistry* **2011**, 5723-5777.
52. G. Ragupathi, F. Koide, P. O. Livingston, Y. S. Cho, A. Endo, Q. Wan, M. K. Spassova, S. J. Keding, J. Allen, O. Ouerfelli, R. M. Wilson, S. J. Danishefsky, *J. Am. Chem. Soc.* **2006**, *128*, 2715-2725.
53. J. Zhu, Q. Wan, D. Lee, G. Yang, M. K. Spassova, O. Ouerfelli, G. Ragupathi, P. Damani, P. O. Livingston, S. J. Danishefsky, *J. Am. Chem. Soc.* **2009**, *131*, 9298-9303.
54. G. Ragupathi, S. F. Slovin, S. Adluri, D. Sames, I. J. Kim, H. M. Kim, M. Spassova, W. G. Bornmann, K. O. Lloyd, H. I. Scher, P. O. Livingston, S. J. Danishefsky, *Angewandte Chemie-International Edition* **1999**, *38*, 563-566.
55. S. F. Slovin, G. Ragupathi, S. Adluri, G. Ungers, K. Terry, S. Kim, M. Spassova, W. G. Bornmann, M. Fazzari, L. Dantis, K. Olkiewicz, K. O. Lloyd, P. O. Livingston, S. J. Danishefsky, H. I. Scher, *Proc. Natl. Acad. Sci. U. S. A.* **1999**, *96*, 5710-5715.
56. S. L. Zhang, C. CordonCardo, H. S. Zhang, V. E. Reuter, S. Adluri, W. B. Hamilton, K. O. Lloyd, P. O. Livingston, *Int. J. Cancer* **1997**, *73*, 42-49.
57. S. L. Zhang, H. S. Zhang, C. CordonCardo, V. E. Reuter, A. K. Singhal, K. O. Lloyd, P. O. Livingston, *Int. J. Cancer* **1997**, *73*, 50-56.
58. Y. S. Kim, G. R. Deng, *Gastroenterology* **2008**, *135*, 305-309.
59. R. Kannagi, J. Yin, K. Miyazaki, M. Izawa, *Biochimica Et Biophysica Acta-General Subjects* **2008**, *1780*, 525-531.
60. A. J. Vangsted, H. Clausen, T. B. Kjeldsen, T. White, B. Sweeney, S. Hakomori, L. Drivsholm, J. Zeuthen, *Cancer Res.* **1991**, *51*, 2879-2884.
61. L. A. Holmberg, D. V. Oparin, T. Gooley, K. Lilleby, W. Bensinger, M. A. Reddish, G. D. MacLean, B. M. Longenecker, B. M. Sandmaier, *Bone Marrow Transplant.* **2000**, *25*, 1233-1241.
62. G. D. Maclean, M. Reddish, R. R. Koganty, T. Wong, S. Gandhi, M. Smolenski, J. Samuel, J. M. Nabholtz, B. M. Longenecker, *Cancer Immunology Immunotherapy* **1993**, *36*, 215-222.
63. A. Franco, *Anticancer Agents Med. Chem.* **2008**, *8*, 86-91.

64. S. F. Slovin, S. J. Keding, G. Ragupathi, *Immunol. Cell Biol.* **2005**, *83*, 418-428.
65. H.-L. Jiang, M. L. Kang, J.-S. Quan, S. G. Kang, T. Akaike, H. S. Yoo, C.-S. Cho, *Biomaterials* **2008**, *29*, 1931-1939.
66. S. Jain, P. Singh, V. Mishra, S. P. Vyas, *Immunol. Lett.* **2005**, *101*, 41-49.
67. L. Yang, H. Yang, K. Rideout, T. Cho, K. Il Joo, L. Ziegler, A. Elliot, A. Walls, D. Yu, D. Baltimore, P. Wang, *Nat. Biotechnol.* **2008**, *26*, 326-334.
68. A. Kretz-Rommel, F. Qin, N. Dakappagari, R. Torensma, S. Faas, D. Wu, K. S. Bowdish, *J. Immunother.* **2007**, *30*, 715-726.
69. J. H. Xie, L. Guo, Y. Y. Ruan, H. Y. Zhu, L. Wang, L. Zhou, X. J. Yun, J. X. Gu, *Biochem. Biophys. Res. Commun.* **2010**, *391*, 958-962.
70. A. Iwasaki, R. Medzhitov, *Science* **2010**, *327*, 291-295.
71. R. M. Steinman, *Nat. Med.* **2007**, *13*, 1155-1159.
72. C. J. Hertz, S. M. Kiertscher, P. J. Godowski, D. A. Bouis, M. V. Norgard, M. D. Roth, R. L. Modlin, *The Journal of Immunology* **2001**, *166*, 2444-2450.
73. M. Cella, F. Sallusto, A. Lanzavecchia, *Curr. Opin. Immunol.* **1997**, *9*, 10-16.
74. G. H. Huang, Y. Y. Wang, H. B. Chi, *Cell. Mol. Immunol.* **2012**, *9*, 287-295.
75. P. Brossart, M. J. Bevan, *Blood* **1997**, *90*, 1594-1599.
76. R. A. Maldonado, D. J. Irvine, R. Schreiber, L. H. Glimcher, *Nature* **2004**, *431*, 527-532.
77. S. L. Reiner, F. Sallusto, A. Lanzavecchia, *Science* **2007**, *317*, 622-625.
78. B. Leon, A. Ballesteros-Tato, J. L. Browning, R. Dunn, T. D. Randall, F. E. Lund, *Nat. Immunol.* **2012**, *13*, 681-690.
79. T. R. Mosmann, H. Cherwinski, M. W. Bond, M. A. Giedlin, R. L. Coffman, *The Journal of Immunology* **1986**, *136*, 2348-2357.
80. R. L. Coffman, J. Carty, *J. Immunol.* **1986**, *136*, 949-954.

81. E. K. Deenick, C. S. Ma, R. Brink, S. G. Tangye, *Curr. Opin. Immunol.* **2011**, *23*, 111-118.
82. D. Breitfeld, L. Ohl, E. Kremmer, J. Ellwart, F. Sallusto, M. Lipp, R. Forster, *J. Exp. Med.* **2000**, *192*, 1545-1551.
83. P. Schaerli, K. Willimann, A. B. Lang, M. Lipp, P. Loetscher, B. Moser, *The Journal of Experimental Medicine* **2000**, *192*, 1553-1562.
84. E. K. Deenick, C. S. Ma, *Immunology* **2011**, *134*, 361-367.
85. M. Veldhoen, C. Uyttenhove, J. van Snick, H. Helmby, A. Westendorf, J. Buer, B. Martin, C. Wilhelm, B. Stockinger, *Nat. Immunol.* **2008**, *9*, 1341-1346.
86. E. V. Acosta-Rodriguez, G. Napolitani, A. Lanzavecchia, F. Sallusto, *Nat. Immunol.* **2007**, *8*, 942-949.
87. T. Duhon, R. Geiger, D. Jarrossay, A. Lanzavecchia, F. Sallusto, *Nat. Immunol.* **2009**, *10*, 857-863.
88. S. Trifari, C. D. Kaplan, E. H. Tran, N. K. Crellin, H. Spits, *Nat. Immunol.* **2009**, *10*, 864-871.
89. A. J. M. van Oosterhout, A. C. Motta, *Eur. Respir. J.* **2005**, *25*, 591-593.
90. R. L. Coffman, *Nat. Immunol.* **2006**, *7*, 539-541.
91. I. J. Amanna, M. K. Slifka, *Immunol. Rev.* **2010**, *236*, 125-138.
92. C. G. Vinuesa, S. G. Tangye, B. Moser, C. R. Mackay, *Nature Reviews Immunology* **2005**, *5*, 853-865.
93. L. J. McHeyzer-Williams, M. G. McHeyzer-Williams, *Annu. Rev. Immunol.* **2005**, *23*, 487-513.
94. T. V. Obukhanych, M. C. Nussenzweig, *The Journal of Experimental Medicine* **2006**, *203*, 305-310.
95. T. Defrance, M. Taillardet, L. Genestier, *Curr. Opin. Immunol.* **2011**, *23*, 330-336.
96. K. L. Good-Jacobson, D. M. Tarlinton, *Int. Immunol.* **2012**, *24*, 403-408.

97. D. J. Rawlings, M. A. Schwartz, S. W. Jackson, A. Meyer-Bahlburg, *Nature Reviews Immunology* **2012**, *12*, 282-294.
98. F. Y. Avci, X. Li, M. Tsuji, D. L. Kasper, *Nat. Med.* **2011**, *17*, 1602-1609.
99. J. D. Ashwell, *The Journal of Immunology* **1988**, *140*, 3697-3700.
100. J. Delon, N. Bercovici, G. Raposo, R. Liblau, A. Trautmann, *The Journal of Experimental Medicine* **1998**, *188*, 1473-1484.
101. M. Gunzer, C. Weishaupt, A. Hillmer, Y. Basoglu, P. Friedl, K. E. Dittmar, W. Kolanus, G. Varga, S. Grabbe, *Blood* **2004**, *104*, 2801-2809.
102. E. E. Eynon, D. C. Parker, *The Journal of Experimental Medicine* **1992**, *175*, 131-138.
103. E. Fuchs, P. Matzinger, *Science* **1992**, *258*, 1156-1159.
104. G. Raimondi, I. Zanoni, S. Citterio, P. Ricciardi-Castagnoli, F. Granucci, *The Journal of Immunology* **2006**, *176*, 4012-4020.
105. P. Reichardt, B. Dornbach, S. Rong, S. Beissert, F. Gueler, K. Loser, M. Gunzer, *Blood* **2007**, *110*, 1519-1529.
106. C. Musselli, P. O. Livingston, G. Ragupathi, *J. Cancer Res. Clin. Oncol.* **2001**, *127*, R20-R26.
107. A. S. McKee, M. K. L. MacLeod, J. W. Kappler, P. Murrack, *BMC Biol.* **2010**, *8*,
108. *The Inflammasomes: Guardians of the Body*, in F. Martinon, A. Mayor, J. Tschopp, *Annu. Rev. Immunol.*, **2009**, p. 229-265
109. R. L. Coffman, A. Sher, R. A. Seder, *Immunity* **2010**, *33*, 492-503.
110. N. Petrovsky, P. D. Cooper, *Expert Rev. Vaccines* **2011**, *10*, 523-537.
111. R. Ahmed, D. Gray, *Science* **1996**, *272*, 54-60.
112. S. A. Plotkin, *Clin. Vaccine Immunol.* **2010**, *17*, 1055-1065.
113. T. W. LeBien, T. F. Tedder, *Blood* **2008**, *112*, 1570-1580.
114. M. J. Shlomchik, F. Weisel, *Immunol. Rev.* **2012**, *247*, 52-63.

115. D. Zotos, D. M. Tarlinton, *Trends Immunol.* **2012**, *33*, 281-288.
116. D. Jung, F. W. Alt, *Cell* **2004**, *116*, 299-311.
117. F. W. Alt, D. Baltimore, *Proceedings of the National Academy of Sciences* **1982**, *79*, 4118-4122.
118. T. Komori, A. Okada, V. Stewart, F. W. Alt, *Science* **1993**, *261*, 1171-1175.
119. F. N. Papavasiliou, D. G. Schatz, *Cell* **2002**, *109*, S35-S44.
120. J. Chaudhuri, F. W. Alt, *Nat. Rev. Immunol.* **2004**, *4*, 541-552.
121. Z. Xu, H. Zan, E. J. Pone, T. Mai, P. Casali, *Nat. Rev. Immunol.* **2012**, *12*, 517-531.
122. R. Geisberger, M. Lamers, G. Achatz, *Immunology* **2006**, *118*, 429-437.
123. M. R. Ehrenstein, C. A. Notley, *Nat. Rev. Immunol.* **2010**, *10*, 778-786.
124. K. Chen, A. Cerutti, *Immunol. Rev.* **2010**, *237*, 160-179.
125. B. J. Underdown, J. M. Schiff, *Annu. Rev. Immunol.* **1986**, *4*, 389-417.
126. W. I. Weis, K. Drickamer, *Annu. Rev. Biochem.* **1996**, *65*, 441-473.
127. H. Hashimoto, *Cell. Mol. Life Sci.* **2006**, *63*, 2954-2967.
128. C. Chothia, A. M. Lesk, A. Tramontano, M. Levitt, S. J. Smith-Gill, G. Air, S. Sheriff, E. A. Padlan, D. Davies, W. R. Tulip, P. M. Colman, S. Spinelli, P. M. Alzari, R. J. Poljak, *Nature* **1989**, *342*, 877-883.
129. B. Al-Lazikani, A. M. Lesk, C. Chothia, *J. Mol. Biol.* **1997**, *273*, 927-948.
130. J. L. Xu, M. M. Davis, *Immunity* **2000**, *13*, 37-45.
131. M. A. Liu, A. Friedman, A. I. Oliff, J. Tai, D. Martinez, R. R. Deck, J. T. C. Shieh, T. D. Jenkins, J. J. Donnelly, L. A. Hawe, *Proc. Natl. Acad. Sci. U. S. A.* **1992**, *89*, 4633-4637.
132. J. R. Harris, W. Gebauer, M. Adrian, J. Markl, *Micron* **1999**, *30*, 597-623.

133. L. M. Wetzler, Y. Ho, H. Reiser, L. W. Wetzler, *The Journal of Experimental Medicine* **1996**, *183*, 1151-1159.
134. D. M. Ambrosino, D. Bolon, H. Collard, R. Van Etten, M. V. Kanchana, R. W. Finberg, *The Journal of Immunology* **1992**, *149*, 3978-3983.
135. J. J. Donnelly, R. R. Deck, M. A. Liu, *The Journal of Immunology* **1990**, *145*, 3071-3079.
136. X. Wu, T. Lipinski, F. R. Carrel, J. J. Bailey, D. R. Bundle, *Org. Biomol. Chem.* **2007**, *5*, 3477-3485.
137. M. D. Decker, K. M. Edwards, R. Bradley, P. Palmer, *The Journal of Pediatrics* **1992**, *120*, 184-189.
138. D. M. Granoff, S. J. Holmes, *Vaccine* **1991**, *9*, Supplement 1, S30-S34.
139. Z. Yin, X. Huang, *Journal of Carbohydrate Chemistry* **2012**, *31*, 143-186.
140. M. Knuf, F. Kowalzik, D. Kieninger, *Vaccine* **2011**, *29*, 4881-4890.
141. J. G. FitzGerald, *Can. Med. Assoc. J.* **1927**, *17*, 524-529.
142. P. Descombey, *C. R. Seances Soc. Biol. Fil.* **1924**, *91*, 239-241.
143. T. Uchida, A. M. Pappenheimer, R. Greany, *J. Biol. Chem.* **1973**, *248*, 3838-3844.
144. M. Porro, M. Saletti, L. Nencioni, L. Tagliaferri, I. Marsili, *J. Infect. Dis.* **1980**, *142*, 716-724.
145. P. K. P. F. K. J. Snape Md, et al., *JAMA: The Journal of the American Medical Association* **2008**, *299*, 173-184.
146. H. R. Shinefield, *Vaccine* **2010**, *28*, 4335-4339.
147. T. H. Wu, X. X. Gu, *Infect. Immun.* **1999**, *67*, 5508-5513.
148. E. Latz, J. Franko, D. T. Golenbock, J. R. Schreiber, *The Journal of Immunology* **2004**, *172*, 2431-2438.
149. M. Burrage, A. Robinson, R. Borrow, N. Andrews, J. Southern, J. Findlow, S. Martin, C. Thornton, D. Goldblatt, M. Corbel, D. Sesardic, K. Cartwright, P. Richmond, E. Miller, *Infect. Immun.* **2002**, *70*, 4946-4954.

150. R. Dagan, J. Poolman, C. A. Siegrist, *Vaccine* **2010**, *28*, 5513-5523.
151. H. Janson, L. O. Hedén, A. Forsgren, *Infect. Immun.* **1992**, *60*, 1336-1342.
152. A. Forsgren, K. Riesbeck, *Clin. Infect. Dis.* **2008**, *46*, 726-731.
153. R. Prymula, P. Peeters, V. Chrobok, P. Kriz, E. Novakova, E. Kaliskova, I. Kohl, P. Lommel, J. Poolman, J. P. Prieels, L. Schuerman, *Lancet* **2006**, *367*, 740-748.
154. M. Toropainen, A. Raitolehto, I. Henckaerts, D. Wauters, J. Poolman, P. Lestrade, H. Kayhty, *Infect. Immun.* **2008**, *76*, 4546-4553.
155. F. Falugi, R. Petracca, M. Mariani, E. Luzzi, S. Mancianti, V. Carinci, M. L. Melli, O. Finco, A. Wack, A. Di Tommaso, M. T. De Magistris, P. Costantino, G. Del Giudice, S. Abrignani, R. Rappuoli, G. Grandi, *Eur. J. Immunol.* **2001**, *31*, 3816-3824.
156. K. Baraldo, E. Mori, A. Bartoloni, F. Norelli, G. Grandi, R. Rappuoli, O. Finco, G. Del Giudice, *Infect. Immun.* **2005**, *73*, 5835-5841.
157. A. W. Purcell, J. McCluskey, J. Rossjohn, *Nat. Rev. Drug Discov.* **2007**, *6*, 404-414.
158. R. Singh, S. Singh, P. K. Sharma, U. P. Singh, D. E. Briles, S. K. Hollingshead, J. W. Lillard, Jr., *PLoS ONE* **2010**, *5*, e9432.
159. E. M. Plummer, M. Manchester, *Wiley Interdisciplinary Reviews-Nanomedicine and Nanobiotechnology* **2011**, *3*, 174-196.
160. E. Kaltgrad, S. Sen Gupta, S. Punna, C. Y. Huang, A. Chang, C. H. Wong, M. G. Finn, O. Blixt, *Chembiochem* **2007**, *8*, 1455-1462.
161. A. Miermont, H. Barnhill, E. Strable, X. Lu, K. A. Wall, Q. Wang, M. G. Finn, X. Huang, *Chemistry – A European Journal* **2008**, *14*, 4939-4947.
162. R. D. Astronomo, E. Kaltgrad, A. K. Udit, S. K. Wang, K. J. Doores, C. Y. Huang, R. Pantophlet, J. C. Paulson, C. H. Wong, M. G. Finn, D. R. Burton, *Chem. Biol.* **2010**, *17*, 357-370.
163. M. Visciano, M. Tagliamonte, M. Tornesello, F. Buonaguro, L. Buonaguro, *J. Transl. Med.* **2012**, *10*, 1-9.

164. J. Denis, N. Majeau, E. Acosta-Ramirez, C. Savard, M.-C. Bedard, S. Simard, K. Lecours, M. Bolduc, C. Pare, B. Willems, N. Shoukry, P. Tessier, P. Lacasse, A. Lamarre, R. Lapointe, C. Lopez Macias, D. Leclerc, *Virology* **2007**, *363*, 59-68.
165. D. R. Milich, A. McLachlan, *Science* **1986**, *234*, 1398-1401.
166. W. Baschong, L. Hasler, M. Häner, J. Kistler, U. Aebi, *J. Struct. Biol.* **2003**, *143*, 258-262.
167. M. F. Bachmann, H. Hengartner, R. M. Zinkernagel, *Eur. J. Immunol.* **1995**, *25*, 3445-3451.
168. T. Fifis, A. Gamvrellis, B. Crimeen-Irwin, G. A. Pietersz, J. Li, P. L. Mottram, I. F. C. McKenzie, M. Plebanski, *J. Immunol.* **2004**, *173*, 3148-3154.
169. P. Lenz, C. D. Thompson, P. M. Day, S. M. Bacot, D. R. Lowy, J. T. Schiller, *Clin. Immunol.* **2003**, *106*, 231-237.
170. C. Ruedl, T. Storni, F. Lechner, T. Bächli, M. F. Bachmann, *Eur. J. Immunol.* **2002**, *32*, 818-825.
171. A. Jegerlehner, T. Storni, G. Lipowsky, M. Schmid, P. Pumpens, M. F. Bachmann, *Eur. J. Immunol.* **2002**, *32*, 3305-3314.
172. M. F. Bachmann, R. M. Zinkernagel, *Annu. Rev. Immunol.* **1997**, *15*, 235-270.
173. D. R. Milich, M. Chen, F. Schödel, D. L. Peterson, J. E. Jones, J. L. Hughes, *Proceedings of the National Academy of Sciences* **1997**, *94*, 14648-14653.
174. E. J. Pone, H. Zan, J. S. Zhang, A. Al-Qahtani, Z. M. Xu, P. Casali, *Crit. Rev. Immunol.* **2010**, *30*, 1-29.
175. C. Brocke, H. Kunz, *Bioorg. Med. Chem.* **2002**, *10*, 3085-3112.
176. T. C. Shiao, R. Roy, *New Journal of Chemistry* **2012**, *36*, 324-339.
177. B. A. Cobb, O. Wang, A. O. Tzianabos, D. L. Kasper, *Cell* **2004**, *117*, 677-687.
178. R. De Silva, D. Appulage, H. Pietraszkiewicz, K. Bobbitt, J. Media, J. Shaw, F. Valeriote, P. Andreana, *Cancer Immunol. Immunother.* **2012**, *61*, 581-585.
179. R. A. De Silva, Q. Wang, T. Chidley, D. K. Appulage, P. R. Andreana, *J. Am. Chem. Soc.* **2009**, *131*, 9622-9623.

180. M. P. Schutze, C. Leclerc, M. Jolivet, F. Audibert, L. Chedid, *The Journal of Immunology* **1985**, *135*, 2319-2322.
181. D. P. Gamblin, E. M. Scanlan, B. G. Davis, *Chem. Rev.* **2009**, *109*, 131-163.
182. T. Buskas, S. Ingale, G. J. Boons, *Glycobiology* **2006**, *16*, 113R-136R.
183. D. R. Bundle, *New frontiers in the Chemistry of Glycoconjugate Vaccines*, in F. Bagnoli, R. Rappuoli, *Vaccine Design: Innovative Approaches and Novel Strategies*, Caister Academic Press, **2011**, p. 69-107
184. J. R. Rich, S. G. Withers, *Nat. Chem. Biol.* **2009**, *5*, 206-215.
185. M. Wacker, D. Linton, P. G. Hitchen, M. Nita-Lazar, S. M. Haslam, S. J. North, M. Panico, H. R. Morris, A. Dell, B. W. Wren, M. Aebi, *Science* **2002**, *298*, 1790-1793.
186. J. A. Prescher, D. H. Dube, C. R. Bertozzi, *Nature* **2004**, *430*, 873-877.
187. C. H. Röhrig, O. A. Retz, L. Hareng, T. Hartung, R. R. Schmidt, *Chembiochem* **2005**, *6*, 1805-1816.
188. S. Wildt, T. U. Gerngross, *Nature Reviews Microbiology* **2005**, *3*, 119-128.
189. M. F. Feldman, M. Wacker, M. Hernandez, P. G. Hitchen, C. L. Marolda, M. Kowarik, H. R. Morris, A. Dell, M. A. Valvano, M. Aebi, *Proc. Natl. Acad. Sci. U. S. A.* **2005**, *102*, 3016-3021.
190. D. Zha, *Glycoengineered Yeast as an Alternative Monoclonal Antibody Discovery and Production Platform*, **2012**
191. D. P. Galonić, W. A. van der Donk, D. Y. Gin, *J. Am. Chem. Soc.* **2004**, *126*, 12712-12713.
192. Y. Zhu, W. A. van der Donk, *Org. Lett.* **2001**, *3*, 1189-1192.
193. X. Zhu, R. R. Schmidt, *Chemistry – A European Journal* **2004**, *10*, 875-887.
194. S. Peluso, B. Imperiali, *Tetrahedron Lett.* **2001**, *42*, 2085-2087.
195. S. Groothuys, B. H. M. Kuijpers, P. Quaedflieg, H. Roelen, R. W. Wiertz, R. H. Blaauw, F. L. van Delft, F. Rutjes, *Synthesis-Stuttgart* **2006**, 3146-3152.

196. G. J. McGarvey, T. E. Benedum, F. W. Schmidtman, *Org. Lett.* **2002**, *4*, 3591-3594.
197. E. J. Grayson, G. J. L. Bernardes, J. M. Chalker, O. Boutureira, J. R. Koepe, B. G. Davis, *Angewandte Chemie-International Edition* **2011**, *50*, 4127-4132.
198. H. Liu, L. Wang, A. Brock, C.-H. Wong, P. G. Schultz, *J. Am. Chem. Soc.* **2003**, *125*, 1702-1703.
199. E. Strable, D. E. Prasuhn, A. K. Udit, S. Brown, A. J. Link, J. T. Ngo, G. Lander, J. Quispe, C. S. Potter, B. Carragher, D. A. Tirrell, M. G. Finn, *Bioconjug. Chem.* **2008**, *19*, 866-875.
200. S. I. Van Kasteren, H. B. Kramer, D. P. Gamblin, B. G. Davis, *Nat. Protoc.* **2007**, *2*, 3185-3194.
201. G. J. L. Bernardes, J. M. Chalker, J. C. Errey, B. G. Davis, *J. Am. Chem. Soc.* **2008**, *130*, 5052-+.
202. J. C. Gildersleeve, O. Oyelaran, J. T. Simpson, B. Allred, *Bioconjug. Chem.* **2008**, *19*, 1485-1490.
203. J. Poolman, C. Frasch, A. Nurkka, H. Kayhty, R. Biemans, L. Schuerman, *Clin. Vaccine Immunol.* **2011**, *18*, 327-336.
204. I. Ohtsuka, Y. Sadakane, M. Higuchi, N. Hada, J. Hada, N. Kakiuchi, A. Sakushima, *Bioorg. Med. Chem.* **2011**, *19*, 894-899.
205. H. C. Kolb, M. G. Finn, K. B. Sharpless, *Angewandte Chemie International Edition* **2001**, *40*, 2004-2021.
206. V. V. Rostovtsev, L. G. Green, V. V. Fokin, K. B. Sharpless, *Angewandte Chemie International Edition* **2002**, *41*, 2596-2599.
207. J. L. Hou, X. F. Liu, J. Shen, G. L. Zhao, P. G. Wang, *Expert Opinion on Drug Discovery* **2012**, *7*, 489-501.
208. C. E. Hoyle, C. N. Bowman, *Angewandte Chemie International Edition* **2010**, *49*, 1540-1573.
209. T. Buskas, Y. Li, G.-J. Boons, *Chemistry – A European Journal* **2004**, *10*, 3517-3524.

210. G. Ragupathi, P. P. Deshpande, D. M. Coltart, H. M. Kim, L. J. Williams, S. J. Danishefsky, P. O. Livingston, *Int. J. Cancer* **2002**, *99*, 207-212.
211. A. Bartoloni, F. Norelli, C. Ceccarini, R. Rappuoli, P. Costantino, *Vaccine* **1995**, *13*, 463-470.
212. A. Cox, F. St. Michael, D. Neelamegan, S. Lacelle, C. Cairns, M. Giuliani, A. Biolchi, J. Hoe, E. Moxon, J. Richards, *Glycoconj. J.* **2010**, *27*, 643-648.
213. C. Boeckler, B. Frisch, S. Muller, F. Schuber, *J. Immunol. Methods* **1996**, *191*, 1-10.
214. T. Lipinski, T. Luu, P. Kitov, A. Szpacenko, D. Bundle, *Glycoconj. J.* **2011**, *28*, 149-164.
215. M. S. Gottlieb, R. Schroff, H. M. Schanker, J. D. Weisman, P. T. Fan, R. A. Wolf, A. Saxon, *N. Engl. J. Med.* **1981**, *305*, 1425-1431.
216. G. M. Shearer, U. Hurtenbach, *Immunol. Today* **1982**, *3*, 153-154.
217. J. J. Goedert, W. C. Wallen, D. L. Mann, D. M. Strong, C. Y. Neuland, M. H. Greene, C. Murray, J. F. Fraumeni, W. A. Blattner, *Lancet* **1982**, *1*, 412-416.
218. J. L. Marx, *Science* **1982**, *217*, 618-621.
219. B. Moll, E. E. Emeson, C. B. Small, G. H. Friedland, R. S. Klein, I. Spigland, *Clin. Immunol. Immunopathol.* **1982**, *25*, 417-423.
220. K. C. Davis, C. R. Horsburgh, U. Hasiba, A. L. Schocket, C. H. Kirkpatrick, *Ann. Intern. Med.* **1983**, *98*, 284-286.
221. J. Vieira, E. Frank, T. J. Spira, S. H. Landesman, *N. Engl. J. Med.* **1983**, *308*, 125-129.
222. C. Harris, C. B. Small, R. S. Klein, G. H. Friedland, B. Moll, E. E. Emeson, I. Spigland, N. H. Steigbigel, *N. Engl. J. Med.* **1983**, *308*, 1181-1184.
223. H. Masur, M. A. Michelis, G. P. Wormser, S. Lewin, J. Gold, M. L. Tapper, J. Giron, C. W. Lerner, D. Armstrong, U. Setia, J. A. Sender, R. S. Siebken, P. Nicholas, Z. Arlen, S. Maayan, J. A. Ernst, F. P. Siegal, S. Cunningham-Rundles, *Ann. Intern. Med.* **1982**, *97*, 533-539.

224. A. Rubinstein, M. Sicklick, A. Gupta, L. Bernstein, N. Klein, E. Rubinstein, I. Spigland, L. Fruchter, N. Litman, H. Lee, M. Hollander, *Jama-Journal of the American Medical Association* **1983**, *249*, 2350-2356.
225. F. Barré-Sinoussi, J. C. Chermann, F. Rey, M. T. Nugeyre, S. Chamaret, J. Gruest, C. Dauguet, C. Axlerblin, F. Vezinetbrun, C. Rouzioux, W. Rozenbaum, L. Montagnier, *Science* **1983**, *220*, 868-871.
226. UNAIDS Report on the Global AIDS Epidemic 2010, Geneva, **2010**
227. T. Zhu, B. T. Korber, A. J. Nahmias, E. Hooper, P. M. Sharp, D. D. Ho, *Nature* **1998**, *391*, 594-597.
228. M. Worobey, M. Gemmel, D. E. Teuwen, T. Haselkorn, K. Kunstman, M. Bunce, J.-J. Muyembe, J.-M. M. Kabongo, R. M. Kalengayi, E. Van Marck, M. T. P. Gilbert, S. M. Wolinsky, *Nature* **2008**, *455*, 661-664.
229. M. Worobey, M. Gemmel, D. E. Teuwen, T. Haselkorn, K. Kunstman, M. Bunce, J. J. Muyembe, J. M. M. Kabongo, R. M. Kalengayi, E. Van Marck, M. T. P. Gilbert, S. M. Wolinsky, *Nature* **2008**, *455*, 661-U657.
230. B. H. Hahn, G. M. Shaw, K. M. De Cock, P. M. Sharp, *Science* **2000**, *287*, 607-614.
231. J. Hemelaar, *Trends Mol. Med.* **2012**, *18*, 182-192.
232. P. M. Sharp, B. H. Hahn, *Cold Spring Harbor Perspectives in Medicine* **2011**, *1*,
233. F. Gao, E. Bailes, D. L. Robertson, Y. L. Chen, C. M. Rodenburg, S. F. Michael, L. B. Cummins, L. O. Arthur, M. Peeters, G. M. Shaw, P. M. Sharp, B. H. Hahn, *Nature* **1999**, *397*, 436-441.
234. P. Lemey, O. G. Pybus, B. Wang, N. K. Saksena, M. Salemi, A. M. Vandamme, *Proc. Natl. Acad. Sci. U. S. A.* **2003**, *100*, 6588-6592.
235. R. Kannangai, S. David, G. Sridharan, *Indian Journal of Medical Microbiology* **2012**, *30*, 6-15.
236. World Health Organization, Interim WHO clinical staging of HIV/AIDS and HIV/AIDS case definitions for surveillance, **2005**
237. D. L. Robertson, J. P. Anderson, J. A. Bradac, J. K. Carr, B. Foley, R. K. Funkhouser, F. Gao, B. H. Hahn, M. L. Kalish, C. Kuiken, G. H. Learn, T. Leitner, F. McCutchan, S. Osmanov, M. Peeters, D. Pieniazek, M. Salminen, P. M. Sharp, S. Wolinsky, B. Korber, *Science* **2000**, *288*, 55.

238. D. M. Tebit, E. J. Arts, *Lancet Infect. Dis.* **2011**, *11*, 45-56.
239. R. M. Lynch, T. Shen, S. Gnanakaran, C. A. Derdeyn, *AIDS Res. Hum. Retroviruses* **2009**, *25*, 237-248.
240. N. Kiwanuka, O. Laeyendecker, M. Robb, G. Kigozi, M. Arroyo, F. McCutchan, L. A. Eller, M. Eller, F. Makumbi, D. Birx, F. Wabwire-Mangen, D. Serwadda, N. K. Sewankambo, T. C. Quinn, M. Wawer, R. Gray, *J. Infect. Dis.* **2008**, *197*, 707-713.
241. P. J. Kanki, D. J. Hamel, J. L. Sankale, C. C. Hsieh, I. Thior, F. Barin, S. A. Woodcock, A. Gueye-Ndiaye, E. Zhang, M. Montano, T. Siby, R. Marlink, I. Ndoye, M. E. Essex, M. Souleymane, *J. Infect. Dis.* **1999**, *179*, 68-73.
242. T. C. Quinn, M. J. Wawer, N. Sewankambo, D. Serwadda, C. J. Li, F. Wabwire-Mangen, M. O. Meehan, T. Lutalo, R. H. Gray, G. Rakai Project Study, *N. Engl. J. Med.* **2000**, *342*, 921-929.
243. D. J. Hu, S. Vanichseni, T. D. Mastro, S. Raktham, N. L. Young, P. A. Mock, S. Subbarao, B. S. Parekh, L. Srisuwanvilai, R. Sutthent, C. Wasi, W. Heneine, K. Choopanya, *AIDS* **2001**, *15*, 683-691.
244. P. Kaleebu, N. French, C. Mahe, D. Yirrell, C. Watera, F. Lyagoba, J. Nakiyingi, A. Rutebemberwa, D. Morgan, J. Weber, C. Gilks, J. Whitworth, *J. Infect. Dis.* **2002**, *185*, 1244-1250.
245. P. Kaleebu, A. Ross, D. Morgan, D. Yirrell, J. Oram, A. Rutebemberwa, F. Lyagoba, L. Hamilton, B. Biryahwaho, J. Whitworth, *AIDS* **2001**, *15*, 293-299.
246. A. Vasan, B. Renjifo, E. Hertzmark, B. Chaplin, G. Msamanga, M. Essex, W. Fawzi, D. Hunter, *Clin. Infect. Dis.* **2006**, *42*, 843-852.
247. V. Jain, S. Deeks, *Curr. HIV/AIDS Rep.* **2010**, *7*, 60-68.
248. W. Z. Chen, D. S. Dimitrov, *AIDS Res. Hum. Retroviruses* **2012**, *28*, 425-434.
249. K. O. Francois, J. Balzarini, *Med. Res. Rev.* **2012**, *32*, 349-387.
250. T. Roe, T. C. Reynolds, G. Yu, P. O. Brown, *EMBO J.* **1993**, *12*, 2099-2108.
251. J. B. Weinberg, T. J. Matthews, B. R. Cullen, M. H. Malim, *The Journal of Experimental Medicine* **1991**, *174*, 1477-1482.
252. P. Lewis, M. Hensel, M. Emerman, *EMBO J.* **1992**, *11*, 3053-3058.

253. A. Fassati, *Retrovirology* **2006**, *3*, 74.
254. D. D. Ho, A. U. Neumann, A. S. Perelson, W. Chen, J. M. Leonard, M. Markowitz, *Nature* **1995**, *373*, 123-126.
255. X. Wei, S. K. Ghosh, M. E. Taylor, V. A. Johnson, E. A. Emini, P. Deutsch, J. D. Lifson, S. Bonhoeffer, M. A. Nowak, B. H. Hahn, M. S. Saag, G. M. Shaw, *Nature* **1995**, *373*, 117-122.
256. D. C. Chan, P. S. Kim, *Cell* **1998**, *93*, 681-684.
257. R. Wyatt, J. Sodroski, *Science* **1998**, *280*, 1884-1888.
258. Q. J. Sattentau, J. P. Moore, F. Vignaux, F. Traincard, P. Pognard, *J. Virol.* **1993**, *67*, 7383-7393.
259. R. W. Doms, S. C. Peiper, *Virology* **1997**, *235*, 179-190.
260. P. D. Kwong, R. Wyatt, J. Robinson, R. W. Sweet, J. Sodroski, W. A. Hendrickson, *Nature* **1998**, *393*, 648-659.
261. Q. J. Sattentau, J. P. Moore, *The Journal of Experimental Medicine* **1991**, *174*, 407-415.
262. M. Bosch, P. Earl, K. Fagnoli, S. Picciafuoco, F. Giombini, F. Wong-Staal, G. Franchini, *Science* **1989**, *244*, 694-697.
263. K. Miyauchi, Y. Kim, O. Latinovic, V. Morozov, G. B. Melikyan, *Cell* **2009**, *137*, 433-444.
264. E. A. Berger, R. W. Doms, E. M. Fenyo, B. T. M. Korber, D. R. Littman, J. P. Moore, Q. J. Sattentau, H. Schuitemaker, J. Sodroski, R. A. Weiss, *Nature* **1998**, *391*, 240-240.
265. P. Gorry, P. Ancuta, *Curr. HIV/AIDS Rep.* **2011**, *8*, 45-53.
266. G. J. Moyle, A. Wildfire, S. Mandalia, H. Mayer, J. Goodrich, J. Whitcomb, B. G. Gazzard, *J. Infect. Dis.* **2005**, *191*, 866-872.
267. T. F. Zhu, H. M. Mo, N. Wang, D. S. Nam, Y. Z. Cao, R. A. Koup, D. D. Ho, *Science* **1993**, *261*, 1179-1181.

268. E. M. Bunnik, L. C. Swenson, D. Edo-Matas, W. Huang, W. Dong, A. Frantzell, C. J. Petropoulos, E. Coakley, H. Schuitemaker, P. R. Harrigan, A. B. van 't Wout, *PLoS Pathog.* **2011**, *7*, e1002106.
269. C. Verhofstede, M. Nijhuis, L. Vandekerckhove, *Curr. Opin. HIV AIDS* **2012**, *7*, 432-439.
270. W. Huang, S. H. Eshleman, J. Toma, S. Fransen, E. Stawiski, E. E. Paxinos, J. M. Whitcomb, A. M. Young, D. Donnell, F. Mmiro, P. Musoke, L. A. Guay, J. B. Jackson, N. T. Parkin, C. J. Petropoulos, *J. Virol.* **2007**, *81*, 7885-7893.
271. B. D. Preston, B. J. Poiesz, L. A. Loeb, *Science* **1988**, *242*, 1168-1171.
272. K. D. Jayappa, Z. Ao, X. Yao, *Int. J. Biochem. Mol. Biol.* **2012**, *3*, 70-85.
273. J. Hiscott, H. Kwon, P. Génin, *The Journal of Clinical Investigation* **2001**, *107*, 143-151.
274. D. F. Purcell, M. A. Martin, *J. Virol.* **1993**, *67*, 6365-6378.
275. V. W. Pollard, M. H. Malim, *Annu. Rev. Microbiol.* **1998**, *52*, 491-532.
276. K. Strebel, *AIDS* **2003**, *17*, S25-S34.
277. S. Debaisieux, F. Rayne, H. Yezid, B. Beaumelle, *Traffic* **2012**, *13*, 355-363.
278. E. O. Freed, *Virology* **1998**, *251*, 1-15.
279. T. Takemura, T. Murakami, *Frontiers in Microbiology* **2012**, *3*,
280. C. S. Adamson, E. O. Freed, *Adv. Pharmacol.* **2007**, *55*, 347-387.
281. P. D. Bieniasz, *Cell Host Microbe* **2009**, *5*, 550-558.
282. N. Jouvenet, S. J. D. Neil, C. Bess, M. C. Johnson, C. A. Virgen, S. M. Simon, P. D. Bieniasz, *PLoS Biol.* **2006**, *4*, e435.
283. P. Zhu, E. Chertova, J. Bess, J. D. Lifson, L. O. Arthur, J. Liu, K. A. Taylor, K. H. Roux, *Proceedings of the National Academy of Sciences* **2003**, *100*, 15812-15817.
284. I. Puigdomenech, M. Massanella, C. Cabrera, B. Clotet, J. Blanco, *Retrovirology* **2009**, *6*, 89.

285. Q. Sattentau, *Nat Rev Micro* **2008**, *6*, 815-826.
286. D. McDonald, L. Wu, S. M. Bohks, V. N. KewalRamani, D. Unutmaz, T. J. Hope, *Science* **2003**, *300*, 1295-1297.
287. C. Jolly, Q. J. Sattentau, *Traffic* **2004**, *5*, 643-650.
288. Q. J. Sattentau, *Viruses* **2010**, *2*, 1306-1321.
289. W. Mothes, N. M. Sherer, J. Jin, P. Zhong, *J. Virol.* **2010**, *84*, 8360-8368.
290. D. S. Dimitrov, R. L. Willey, H. Sato, L. J. Chang, R. Blumenthal, M. A. Martin, *J. Virol.* **1993**, *67*, 2182-2190.
291. A. Sigal, J. T. Kim, A. B. Balazs, E. Dekel, A. Mayo, R. Milo, D. Baltimore, *Nature* **2011**, *477*, 95-98.
292. I. A. Abela, L. Berlinger, M. Schanz, L. Reynell, H. F. Gunthard, P. Rusert, A. Trkola, *PLoS Pathog.* **2012**, *8*,
293. F. Barin, M. McLane, J. Allan, T. Lee, J. Groopman, M. Essex, *Science* **1985**, *228*, 1094-1096.
294. D. C. Chan, D. Fass, J. M. Berger, P. S. Kim, *Cell* **1997**, *89*, 263-273.
295. W. Weissenhorn, A. Dessen, S. C. Harrison, J. J. Skehel, D. C. Wiley, *Nature* **1997**, *387*, 426-430.
296. M. Farzan, H. Choe, E. Desjardins, Y. Sun, J. Kuhn, J. Cao, D. Archambault, P. Kolchinsky, M. Koch, R. Wyatt, J. Sodroski, *J. Virol.* **1998**, *72*, 7620-7625.
297. S. Ugolini, I. Mondor, P. W. H. I. Parren, D. R. Burton, S. A. Tilley, P. J. Klasse, Q. J. Sattentau, *The Journal of Experimental Medicine* **1997**, *186*, 1287-1298.
298. A. Engelman, P. Cherepanov, *Nature Reviews Microbiology* **2012**, *10*, 279-290.
299. C. K. Leonard, M. W. Spellman, L. Riddle, R. J. Harris, J. N. Thomas, T. J. Gregory, *J. Biol. Chem.* **1990**, *265*, 10373-10382.
300. H. B. Bernstein, S. P. Tucker, E. Hunter, J. S. Schutzbach, R. W. Compans, *J. Virol.* **1994**, *68*, 463-468.

301. P. L. Earl, R. W. Doms, B. Moss, *Proceedings of the National Academy of Sciences* **1990**, *87*, 648-652.
302. P. L. Earl, S. Koenig, B. Moss, *J. Virol.* **1991**, *65*, 31-41.
303. S. Hallenberger, V. Bosch, H. Angliker, E. Shaw, H.-D. Klenk, W. Garten, *Nature* **1992**, *360*, 358-361.
304. M. Kowalski, J. Potz, L. Basiripour, *Science* **1987**, *237*, 1351-1355.
305. S. C. Blacklow, M. Lu, P. S. Kim, *Biochemistry (Mosc.)* **1995**, *34*, 14955-14962.
306. M. Lu, S. C. Blacklow, P. S. Kim, *Nat. Struct. Mol. Biol.* **1995**, *2*, 1075-1082.
307. M. Moulard, E. Decroly, *Biochimica et Biophysica Acta (BBA) - Reviews on Biomembranes* **2000**, *1469*, 121-132.
308. M. A. Checkley, B. G. Luttge, E. O. Freed, *J. Mol. Biol.* **2011**, *410*, 582-608.
309. P. D. Kwong, R. Wyatt, S. Majeed, J. Robinson, R. W. Sweet, J. Sodroski, W. A. Hendrickson, *Structure* **2000**, *8*, 1329-1339.
310. T. Zhou, L. Xu, B. Dey, A. J. Hessel, D. Van Ryk, S.-H. Xiang, X. Yang, M.-Y. Zhang, M. B. Zwick, J. Arthos, D. R. Burton, D. S. Dimitrov, J. Sodroski, R. Wyatt, G. J. Nabel, P. D. Kwong, *Nature* **2007**, *445*, 732-737.
311. R. Diskin, P. M. Marcovecchio, P. J. Bjorkman, *Nat. Struct. Mol. Biol.* **2010**, *17*, 608-613.
312. M. Pancera, S. Majeed, Y.-E. A. Ban, L. Chen, C.-c. Huang, L. Kong, Y. D. Kwon, J. Stuckey, T. Zhou, J. E. Robinson, W. R. Schief, J. Sodroski, R. Wyatt, P. D. Kwong, *Proceedings of the National Academy of Sciences* **2010**, *107*, 1166-1171.
313. L. Chen, Y. Do Kwon, T. Zhou, X. Wu, S. O'Dell, L. Cavacini, A. J. Hessel, M. Pancera, M. Tang, L. Xu, Z.-Y. Yang, M.-Y. Zhang, J. Arthos, D. R. Burton, D. S. Dimitrov, G. J. Nabel, M. R. Posner, J. Sodroski, R. Wyatt, J. R. Mascola, P. D. Kwong, *Science* **2009**, *326*, 1123-1127.
314. C.-c. Huang, S. N. Lam, P. Acharya, M. Tang, S.-H. Xiang, S. S.-u. Hussan, R. L. Stanfield, J. Robinson, J. Sodroski, I. A. Wilson, R. Wyatt, C. A. Bewley, P. D. Kwong, *Science* **2007**, *317*, 1930-1934.

315. T. Q. Zhou, I. Georgiev, X. L. Wu, Z. Y. Yang, K. F. Dai, A. Finzi, Y. D. Kwon, J. F. Scheid, W. Shi, L. Xu, Y. P. Yang, J. A. Zhu, M. C. Nussenzweig, J. Sodroski, L. Shapiro, G. J. Nabel, J. R. Mascola, P. D. Kwong, *Science* **2010**, *329*, 811-817.
316. X. Wu, T. Zhou, J. Zhu, B. Zhang, I. Georgiev, C. Wang, X. Chen, N. S. Longo, M. Louder, K. McKee, S. O'Dell, S. Perfetto, S. D. Schmidt, W. Shi, L. Wu, Y. Yang, Z.-Y. Yang, Z. Yang, Z. Zhang, M. Bonsignori, J. A. Crump, S. H. Kapiga, N. E. Sam, B. F. Haynes, M. Simek, D. R. Burton, W. C. Koff, N. A. Doria-Rose, M. Connors, N. C. S. Program, J. C. Mullikin, G. J. Nabel, M. Roederer, L. Shapiro, P. D. Kwong, J. R. Mascola, *Science* **2011**, *333*, 1593-1602.
317. C.-c. Huang, F. Stricher, L. Martin, J. M. Decker, S. Majeed, P. Barthe, W. A. Hendrickson, J. Robinson, C. Roumestand, J. Sodroski, R. Wyatt, G. M. Shaw, C. Vita, P. D. Kwong, *Structure* **2005**, *13*, 755-768.
318. F. Stricher, C.-c. Huang, A. Descours, S. Duquesnoy, O. Combes, J. M. Decker, Y. Do Kwon, P. Lusso, G. M. Shaw, C. Vita, P. D. Kwong, L. Martin, *J. Mol. Biol.* **2008**, *382*, 510-524.
319. Y. D. Kwon, A. Finzi, X. Wu, C. Dogo-Isonagie, L. K. Lee, L. R. Moore, S. D. Schmidt, J. Stuckey, Y. Yang, T. Zhou, J. Zhu, D. A. Vicic, A. K. Debnath, L. Shapiro, C. A. Bewley, J. R. Mascola, J. G. Sodroski, P. D. Kwong, *Proceedings of the National Academy of Sciences* **2012**, *109*, 5663-5668.
320. J. M. LaLonde, Y. D. Kwon, D. M. Jones, A. W. Sun, J. R. Courter, T. Soeta, T. Kobayashi, A. M. Princiotto, X. Wu, A. Schön, E. Freire, P. D. Kwong, J. R. Mascola, J. Sodroski, N. Madani, A. B. Smith, *J. Med. Chem.* **2012**, *55*, 4382-4396.
321. R. L. Willey, R. A. Rutledge, S. Dias, T. Folks, T. Theodore, C. E. Buckler, M. A. Martin, *Proceedings of the National Academy of Sciences* **1986**, *83*, 5038-5042.
322. B. R. Starcich, B. H. Hahn, G. M. Shaw, *Cell* **1986**, *45*, 637-648.
323. S. Zolla-Pazner, *Nat. Rev. Immunol.* **2004**, *4*, 199-210.
324. D. C. Montefiori, W. E. Robinson, W. M. Mitchell, *Proceedings of the National Academy of Sciences* **1988**, *85*, 9248-9252.
325. H. Li, P. C. Chien Jr, M. Tuen, M. L. Visciano, S. Cohen, S. Blais, C. F. Xu, H. T. Zhang, C. E. Hioe, *J. Immunol.* **2008**, *180*, 4011-4021.
326. M. Raska, J. Novak, *Arch. Immunol. Ther. Exp. (Warsz.)* **2010**, *58*, 191-208.
327. J. S. Allan, J. E. Coligan, F. Barin, *Science* **1985**, *228*, 1091-1094.

328. R. W. Sanders, M. Venturi, L. Schiffner, R. Kalyanaraman, H. Katinger, K. O. Lloyd, P. D. Kwong, J. P. Moore, *J. Virol.* **2002**, *76*, 7293-7305.
329. J. M. Decker, F. Bibollet-Ruche, X. Wei, S. Wang, D. N. Levy, W. Wang, E. Delaporte, M. Peeters, C. A. Derdeyn, S. Allen, E. Hunter, M. S. Saag, J. A. Hoxie, B. H. Hahn, P. D. Kwong, J. E. Robinson, G. M. Shaw, *The Journal of Experimental Medicine* **2005**, *201*, 1407-1419.
330. C. Palmer, P. Balfe, D. Fox, J. C. May, R. Frederiksson, E. M. Fenyő, J. A. McKeating, *Virology* **1996**, *220*, 436-449.
331. B. Chackerian, L. M. Rudensey, J. Overbaugh, *J. Virol.* **1997**, *71*, 7719-7727.
332. D. G. Fox, P. Balfe, C. P. Palmer, J. C. May, C. Arnold, J. A. McKeating, *J. Virol.* **1997**, *71*, 759-765.
333. T. Shioda, S. Oka, X. Xin, H. Liu, R. Harukuni, A. Kurotani, M. Fukushima, M. K. Hasan, T. Shiino, Y. Takebe, A. Iwamoto, Y. Nagai, *J. Virol.* **1997**, *71*, 4871-4881.
334. S. Masciotra, S. M. Owen, D. Rudolph, C. F. Yang, B. Wang, N. Saksena, T. Spira, S. Dhawan, R. B. Lal, *AIDS* **2002**, *16*, 1887-1898.
335. K. M. Kitrinis, N. G. Hoffman, J. A. E. Nelson, R. Swanstrom, *J. Virol.* **2003**, *77*, 6811-6822.
336. B. Chohan, D. Lang, M. Sagar, B. Korber, L. Lavreys, B. Richardson, J. Overbaugh, *J. Virol.* **2005**, *79*, 6528-6531.
337. M. Sagar, X. Wu, S. Lee, J. Overbaugh, *J. Virol.* **2006**, *80*, 9586-9598.
338. P. R. Harrington, J. A. E. Nelson, K. M. Kitrinis, R. Swanstrom, *J. Virol.* **2007**, *81*, 5413-5417.
339. J. A. Cenci, L. Tivoschi, G. D' Avenio, P. Narino, S. Becattini, D. Bernasconi, M. Chiappi, L. La Torre, H. Sukati, E. Vardas, A. Lo Presti, E. Eleonora Cella, M. Ciccozzi, O. Picconi, P. Monini, B. Ensoli, S. Buttò, *J. AIDS Clinic. Res.* **2012**, *S8*, 006.
340. J. Cao, N. Sullivan, E. Desjardin, C. Parolin, J. Robinson, R. Wyatt, J. Sodroski, *J. Virol.* **1997**, *71*, 9808-9812.
341. T. Morikita, Y. Maeda, S. Fujii, S. Matsushita, K. Obaru, K. Takatsuki, *AIDS Res. Hum. Retroviruses* **1997**, *13*, 1291-1299.

342. L. Stamatatos, C. Cheng-Mayer, *J. Virol.* **1998**, *72*, 7840-7845.
343. A. Ly, L. Stamatatos, *J. Virol.* **2000**, *74*, 6769-6776.
344. B. Losman, A. Bolmstedt, K. Schonning, A. Bjorndal, C. Westin, E. M. Fenyo, S. Olofsson, *AIDS Res. Hum. Retroviruses* **2001**, *17*, 1067-1076.
345. W. E. Johnson, H. Sanford, L. Schwall, D. R. Burton, P. W. H. I. Parren, J. E. Robinson, R. C. Desrosiers, *J. Virol.* **2003**, *77*, 9993-10003.
346. K. S. Cole, J. D. Steckbeck, J. L. Rowles, R. C. Desrosiers, R. C. Montelaro, *J. Virol.* **2004**, *78*, 1525-1539.
347. A. Pinter, W. J. Honnen, Y. He, M. K. Gorny, S. Zolla-Pazner, S. C. Kayman, *J. Virol.* **2004**, *78*, 5205-5215.
348. P. Pugach, S. E. Kuhmann, J. Taylor, A. J. Marozsan, A. Snyder, T. Ketas, S. M. Wolinsky, B. T. Korber, J. P. Moore, *Virology* **2004**, *321*, 8-22.
349. C. J. Saunders, R. A. McCaffrey, I. Zharkikh, Z. Kraft, S. E. Malenbaum, B. Burke, C. Cheng-Mayer, L. Stamatatos, *J. Virol.* **2005**, *79*, 9069-9080.
350. C. Krachmarov, A. Pinter, W. J. Honnen, M. K. Gorny, P. N. Nyambi, S. Zolla-Pazner, S. C. Kayman, *J. Virol.* **2005**, *79*, 780-790.
351. C. P. Krachmarov, W. J. Honnen, S. C. Kayman, M. K. Gorny, S. Zolla-Pazner, A. Pinter, *J. Virol.* **2006**, *80*, 7127-7135.
352. J. Shibata, K. Yoshimura, A. Honda, A. Koito, T. Murakami, S. Matsushita, *J. Virol.* **2007**, *81*, 3757-3768.
353. L. K. Ching, G. Vlachogiannis, K. A. Bosch, L. Stamatatos, *J. Virol.* **2008**, *82*, 949-956.
354. M. J. van Gils, E. M. Bunnik, B. D. Boeser-Nunnink, J. A. Burger, M. Terlouw-Klein, N. Verwer, H. Schuitemaker, *J. Virol.* **2011**, *85*, 6986-6995.
355. P. Rusert, A. Krarup, C. Magnus, O. F. Brandenberg, J. Weber, A.-K. Ehlert, R. R. Regoes, H. F. Günthard, A. Trkola, *The Journal of Experimental Medicine* **2011**, *208*, 1419-1433.

356. C. A. Derdeyn, J. M. Decker, F. Bibollet-Ruche, J. L. Mokili, M. Muldoon, S. A. Denham, M. L. Heil, F. Kasolo, R. Musonda, B. H. Hahn, G. M. Shaw, B. T. Korber, S. Allen, E. Hunter, *Science* **2004**, *303*, 2019-2022.
357. K. Ritola, C. D. Pilcher, S. A. Fiscus, N. G. Hoffman, J. A. E. Nelson, K. M. Kitrinou, C. B. Hicks, J. J. Eron, R. Swanstrom, *J. Virol.* **2004**, *78*, 11208-11218.
358. S. D. W. Frost, Y. Liu, S. L. K. Pond, C. Chappay, T. Wrin, C. J. Petropoulos, S. J. Little, D. D. Richman, *J. Virol.* **2005**, *79*, 6523-6527.
359. Y. Liu, M. E. Curlin, K. Diem, H. Zhao, A. K. Ghosh, H. Zhu, A. S. Woodward, J. Maenza, C. E. Stevens, J. Stekler, A. C. Collier, I. Genowati, W. Deng, R. Zioni, L. Corey, T. Zhu, J. I. Mullins, *Virology* **2008**, *374*, 229-233.
360. R. Wyatt, N. Sullivan, M. Thali, H. Repke, D. Ho, J. Robinson, M. Posner, J. Sodroski, *J. Virol.* **1993**, *67*, 4557-4565.
361. R. Wyatt, J. Moore, M. Accola, E. Desjardin, J. Robinson, J. Sodroski, *J. Virol.* **1995**, *69*, 5723-5733.
362. L. Stamatatos, M. Wiskerchen, C. Cheng-Mayer, *AIDS Res. Hum. Retroviruses* **1998**, *14*, 1129-1139.
363. M. M. Laakso, F.-H. Lee, B. Haggarty, C. Agrawal, K. M. Nolan, M. Biscione, J. Romano, A. P. O. Jordan, G. J. Leslie, E. G. Meissner, L. Su, J. A. Hoxie, R. W. Doms, *PLoS Pathog.* **2007**, *3*, e117.
364. I. Bontjer, A. Land, D. Eggink, E. Verkade, K. Tuin, C. Baldwin, G. Pollakis, W. A. Paxton, I. Braakman, B. Berkhout, R. W. Sanders, *J. Virol.* **2009**, *83*, 368-383.
365. H. Choe, M. Farzan, Y. Sun, N. Sullivan, B. Rollins, P. D. Ponath, L. Wu, C. R. Mackay, G. LaRosa, W. Newman, N. Gerard, C. Gerard, J. Sodroski, *Cell* **1996**, *85*, 1135-1148.
366. F. Cocchi, A. L. DeVico, A. Garzino-Demo, A. Cara, R. C. Gallo, P. Lusso, *Nat. Med.* **1996**, *2*, 1244-1247.
367. J. P. Moore, S. G. Kitchen, P. Pugach, J. A. Zack, *AIDS Res. Hum. Retroviruses* **2004**, *20*, 111-126.
368. X. Wei, J. M. Decker, S. Wang, H. Hui, J. C. Kappes, X. Wu, J. F. Salazar-Gonzalez, M. G. Salazar, J. M. Kilby, M. S. Saag, N. L. Komarova, M. A. Nowak, B. H. Hahn, P. D. Kwong, G. M. Shaw, *Nature* **2003**, *422*, 307.

369. D. D. Richman, T. Wrin, S. J. Little, C. J. Petropoulos, *Proc. Natl. Acad. Sci. U. S. A.* **2003**, *100*, 4144-4149.
370. T. Shioda, S. Oka, S. Ida, K. Nokihara, H. Toriyoshi, S. Mori, Y. Takebe, S. Kimura, K. Shimada, Y. Nagai, *J. Virol.* **1994**, *68*, 7689-7696.
371. N. Shimizu, Y. Haraguchi, Y. Takeuchi, Y. Soda, K. Kanbe, H. Hoshino, *Virology* **1999**, *259*, 324-333.
372. S. Pöhlmann, C. Davis, S. Meister, G. J. Leslie, C. Otto, J. D. Reeves, B. A. Puffer, A. Papkalla, M. Krumbiegel, A. Marzi, S. Lorenz, J. Münch, R. W. Doms, F. Kirchhoff, *J. Virol.* **2004**, *78*, 3223-3232.
373. C. Pastore, A. Ramos, D. E. Mosier, *J. Virol.* **2004**, *78*, 7565-7574.
374. I. Kiszka, D. Kmiecik, J. Gzyl, T. Naito, E. Bolesta, A. Sieron, S. P. Singh, A. Srinivasan, G. Trinchieri, Y. Kaneko, D. Kozbor, *J. Virol.* **2002**, *76*, 4222-4232.
375. N. K. T. Back, L. Smit, J.-J. De Jong, W. Keulen, M. Schutten, J. Goudsmit, M. Tersmette, *Virology* **1994**, *199*, 431-438.
376. P. D. Kwong, R. Wyatt, Q. J. Sattentau, J. Sodroski, W. A. Hendrickson, *J. Virol.* **2000**, *74*, 1961-1972.
377. C.-c. Huang, M. Tang, M.-Y. Zhang, S. Majeed, E. Montabana, R. L. Stanfield, D. S. Dimitrov, B. Korber, J. Sodroski, I. A. Wilson, R. Wyatt, P. D. Kwong, *Science* **2005**, *310*, 1025-1028.
378. S. R. Pollard, M. D. Rosa, J. J. Rosa, D. C. Wiley, *EMBO J.* **1992**, *11*, 585-591.
379. M. Sharon, N. Kessler, R. Levy, S. Zolla-Pazner, M. Görlach, J. Anglister, *Structure* **2003**, *11*, 225-236.
380. O. Hartley, P. J. Klasse, Q. J. Sattentau, J. P. Moore, *AIDS Res. Hum. Retroviruses* **2005**, *21*, 171-189.
381. M. A. Jensen, F.-S. Li, A. B. van 't Wout, D. C. Nickle, D. Shriner, H.-X. He, S. McLaughlin, R. Shankarappa, J. B. Margolick, J. I. Mullins, *J. Virol.* **2003**, *77*, 13376-13388.
382. J. J. Dejong, A. Deronde, W. Keulen, M. Tersmette, J. Goudsmit, *J. Virol.* **1992**, *66*, 6777-6780.

383. T. Shioda, J. A. Levy, C. Cheng-Mayer, *Proceedings of the National Academy of Sciences* **1992**, *89*, 9434-9438.
384. Y. Isaka, A. Sato, S. Miki, S. Kawauchi, H. Sakaida, T. Hori, T. Uchiyama, A. Adachi, M. Hayami, T. Fujiwara, O. Yoshie, *Virology* **1999**, *264*, 237-243.
385. M. Patel, M. Yanagishita, G. Roderiquez, D. C. Bouhabib, T. Oravec, V. C. Hascall, M. A. Norcross, *AIDS Res. Hum. Retroviruses* **1993**, *9*, 167-174.
386. A. BreLOT, N. Heveker, K. Adema, M. J. Hosie, B. Willett, M. Alison, *J. Virol.* **1999**, *73*, 2576-2586.
387. I. Mondor, S. Ugolini, Q. J. Sattentau, *J. Virol.* **1998**, *72*, 3623-3634.
388. B. Wu, E. Y. T. Chien, C. D. Mol, G. Fenalti, W. Liu, V. Katritch, R. Abagyan, A. Brooun, P. Wells, F. C. Bi, D. J. Hamel, P. Kuhn, T. M. Handel, V. Cherezov, R. C. Stevens, *Science* **2010**, *330*, 1066-1071.
389. N. E. Kinsey, M. G. Anderson, T. J. Unangst, S. V. Joag, O. Narayan, M. C. Zink, J. E. Clements, *Virology* **1996**, *221*, 14-21.
390. P. L. Moore, E. S. Gray, I. A. Choge, N. Ranchobe, K. Mlisana, S. S. A. Karim, C. Williamson, L. Morris, T. Caprisa 002 Study, *J. Virol.* **2008**, *82*, 1860-1869.
391. X. Ren, J. Sodroski, X. Yang, *J. Virol.* **2005**, *79*, 5616-5624.
392. A. F. Y. Poon, F. I. Lewis, S. L. K. Pond, S. D. W. Frost, *PLoS Comput. Biol.* **2007**, *3*, e11.
393. E. Castro, M. Belair, G. P. Rizzardi, P. A. Bart, G. Pantaleo, C. Graziosi, *AIDS Res. Hum. Retroviruses* **2008**, *24*, 106-113.
394. D. Guo, X. Shi, K. Arledge, D. Song, L. Jiang, L. Fu, S. Zhang, X. Wang, L. Zhang, *Retrovirology* **2012**, *9*, P46.
395. D. Guo, X. Shi, K. C. Arledge, D. Song, L. Jiang, L. Fu, X. Gong, S. Zhang, X. Wang, L. Zhang, *J. Biol. Chem.* **2012**,
396. J. Sterjovski, M. J. Churchill, M. Roche, A. Ellett, W. Farrugia, S. L. Wesselingh, A. L. Cunningham, P. A. Ramsland, P. R. Gorry, *Virology* **2011**, *410*, 418-428.
397. I. Hötzel, W. P. Cheevers, *Virus Res.* **2000**, *69*, 47-54.

398. I. Hötzel, W. P. Cheevers, *J. Virol.* **2001**, *75*, 2014-2018.
399. N. W. Douglas, G. H. Munro, R. S. Daniels, *J. Mol. Biol.* **1997**, *273*, 122-149.
400. B. Chen, E. M. Vogan, H. Gong, J. J. Skehel, D. C. Wiley, S. C. Harrison, *Nature* **2005**, *433*, 834-841.
401. L. A. Lasky, G. Nakamura, D. H. Smith, C. Fennie, C. Shimasaki, E. Patzer, P. Berman, T. Gregory, D. J. Capon, *Cell* **1987**, *50*, 975-985.
402. U. Olshevsky, E. Helseth, C. Furman, J. Li, W. Haseltine, J. Sodroski, *J. Virol.* **1990**, *64*, 5701-5707.
403. I. H. Shrivastava, K. Wendel, J. M. LaLonde, *Biochemistry (Mosc.)* **2012**, *51*, 7783-7793.
404. W. R. Gallaher, *Cell* **1987**, *50*, 327-328.
405. H. Schaal, M. Klein, P. Gehrman, O. Adams, A. Scheid, *J. Virol.* **1995**, *69*, 3308-3314.
406. A. Ashkenazi, E. Merklinger, Y. Shai, *Biochemistry (Mosc.)* **2012**, *51*, 6981-6989.
407. K. Salzwedel, J. T. West, E. Hunter, *J. Virol.* **1999**, *73*, 2469-2480.
408. W. Shi, J. Bohon, D. P. Han, H. Habte, Y. Qin, M. W. Cho, M. R. Chance, *J. Biol. Chem.* **2010**, *285*, 24290-24298.
409. M. Montero, N. E. van Houten, X. Wang, J. K. Scott, *Microbiol. Mol. Biol. Rev.* **2008**, *72*, 54-84.
410. W. E. Johnson, J. M. Sauvron, R. C. Desrosiers, *J. Virol.* **2001**, *75*, 11426-11436.
411. E. Yuste, J. Bixby, J. Lifson, S. Sato, W. Johnson, R. Desrosiers, *J. Virol.* **2008**, *82*, 12472-12486.
412. G. Frey, J. Chen, S. Rits-Volloch, M. M. Freeman, S. Zolla-Pazner, B. Chen, *Nat. Struct. Mol. Biol.* **2010**, *17*, 1486-1491.
413. P. A. Bullough, F. M. Hughson, J. J. Skehel, D. C. Wiley, *Nature* **1994**, *371*, 37-43.
414. D. M. Eckert, P. S. Kim, *Annu. Rev. Biochem.* **2001**, *70*, 777-810.

415. R. Polly, *Mechanism of Membrane Fusion by Viral Envelope Proteins*, in S. C. Harrison, *Adv. Virus Res.*, Academic Press, **2005**, p. 231-261
416. R. A. Lamb, T. S. Jardetzky, *Curr. Opin. Struct. Biol.* **2007**, *17*, 427-436.
417. M. Caffrey, M. Cai, J. Kaufman, S. J. Stahl, P. T. Wingfield, D. G. Covell, A. M. Gronenborn, G. M. Clore, *EMBO J.* **1998**, *17*, 4572-4584.
418. V. Buzon, G. Natrajan, D. Schibli, F. Campelo, M. M. Kozlov, W. Weissenhorn, *PLoS Pathog.* **2010**, *6*, e1000880.
419. S. C. Harrison, *Nat. Struct. Mol. Biol.* **2008**, *15*, 690-698.
420. W. Weissenhorn, S. A. Wharton, L. J. Calder, P. L. Earl, B. Moss, E. Aliprandis, J. J. Skehel, D. C. Wiley, *EMBO J.* **1996**, *15*, 1507-1514.
421. S. Bjelić, I. Jelesarov, *Biophys. Chem.*
422. P. Zhu, J. Liu, J. Bess, E. Chertova, J. D. Lifson, H. Gris , G. A. Ofek, K. A. Taylor, K. H. Roux, *Nature* **2006**, *441*, 847-852.
423. J. Liu, A. Bartesaghi, M. J. Borgnia, G. Sapiro, S. Subramaniam, *Nature* **2008**, *455*, 109-113.
424. T. A. White, A. Bartesaghi, M. J. Borgnia, J. R. Meyerson, M. J. V. de la Cruz, J. W. Bess, R. Nandwani, J. A. Hoxie, J. D. Lifson, J. L. S. Milne, S. Subramaniam, *PLoS Pathog.* **2010**, *6*, e1001249.
425. S.-R. Wu, R. L ving, B. Lindqvist, H. Hebert, P. J. B. Koeck, M. S jberg, H. Garoff, *Proceedings of the National Academy of Sciences* **2010**, *107*, 18844-18849.
426. A. Harris, M. J. Borgnia, D. Shi, A. Bartesaghi, H. He, R. Pejchal, Y. Kang, R. Depetris, A. J. Marozsan, R. W. Sanders, P. J. Klasse, J. L. S. Milne, I. A. Wilson, W. C. Olson, J. P. Moore, S. Subramaniam, *Proceedings of the National Academy of Sciences* **2011**, *108*, 11440-11445.
427. G. Hu, J. Liu, K. A. Taylor, K. H. Roux, *J. Virol.* **2011**, *85*, 2741-2750.
428. Y. Mao, L. Wang, C. Gu, A. Herschhorn, S.-H. Xiang, H. Haim, X. Yang, J. Sodroski, *Nat. Struct. Mol. Biol.* **2012**, *19*, 893-899.
429. V. Lu i , F. F rster, W. Baumeister, *Annu. Rev. Biochem.* **2005**, *74*, 833-865.

430. C. R. Ruprecht, A. Krarup, L. Reynell, A. M. Mann, O. F. Brandenburg, L. Berlinger, I. A. Abela, R. R. Regoes, H. F. Günthard, P. Rusert, A. Trkola, *The Journal of Experimental Medicine* **2011**, *208*, 439-454.
431. T. Muster, F. Steindl, M. Purtscher, A. Trkola, A. Klima, G. Himmler, F. Rüker, H. Katinger, *J. Virol.* **1993**, *67*, 6642-6647.
432. M. B. Zwick, A. F. Labrijn, M. Wang, C. Spenlehauer, E. O. Saphire, J. M. Binley, J. P. Moore, G. Stiegler, H. Katinger, D. R. Burton, P. W. H. I. Parren, *J. Virol.* **2001**, *75*, 10892-10905.
433. C. E. Parker, L. J. Deterding, C. Hager-Braun, J. M. Binley, N. Schülke, H. Katinger, J. P. Moore, K. B. Tomer, *J. Virol.* **2001**, *75*, 10906-10911.
434. G. Stiegler, R. Kunert, M. Purtscher, S. Wolbank, R. Voglauer, F. Steindl, H. Katinger, *AIDS Res. Hum. Retroviruses* **2001**, *17*, 1757-1765.
435. D. Burton, J. Pyati, R. Koduri, S. Sharp, G. Thornton, P. Parren, L. Sawyer, R. Hendry, N. Dunlop, P. Nara, a. et, *Science* **1994**, *266*, 1024-1027.
436. E. O. Saphire, P. W. H. I. Parren, R. Pantophlet, M. B. Zwick, G. M. Morris, P. M. Rudd, R. A. Dwek, R. L. Stanfield, D. R. Burton, I. A. Wilson, *Science* **2001**, *293*, 1155-1159.
437. A. Trkola, M. Purtscher, T. Muster, C. Ballaun, A. Buchacher, N. Sullivan, K. Srinivasan, J. Sodroski, J. P. Moore, H. Katinger, *J. Virol.* **1996**, *70*, 1100-1108.
438. C. N. Scanlan, R. Pantophlet, M. R. Wormald, E. O. Saphire, R. Stanfield, I. A. Wilson, H. Katinger, R. A. Dwek, P. M. Rudd, D. R. Burton, *J. Virol.* **2002**, *76*, 7306-7321.
439. D. A. Calarese, C. N. Scanlan, M. B. Zwick, S. Deechongkit, Y. Mimura, R. Kunert, P. Zhu, M. R. Wormald, R. L. Stanfield, K. H. Roux, J. W. Kelly, P. M. Rudd, R. A. Dwek, H. Katinger, D. R. Burton, I. A. Wilson, *Science* **2003**, *300*, 2065-2071.
440. H.-K. Lee, C. N. Scanlan, C.-Y. Huang, A. Y. Chang, D. A. Calarese, R. A. Dwek, P. M. Rudd, D. R. Burton, I. A. Wilson, C.-H. Wong, *Angewandte Chemie International Edition* **2004**, *43*, 1000-1003.
441. D. C. Dunlop, C. Bonomelli, F. Mansab, S. Vasiljevic, K. J. Doores, M. R. Wormald, A. S. Palma, T. Feizi, D. J. Harvey, R. A. Dwek, M. Crispin, C. N. Scanlan, *Glycobiology* **2010**, *20*, 812-823.

442. J. Huang, G. Ofek, L. Laub, M. K. Louder, N. A. Doria-Rose, N. S. Longo, H. Imamichi, R. T. Bailer, B. Chakrabarti, S. K. Sharma, S. M. Alam, T. Wang, Y. Yang, B. Zhang, S. A. Migueles, R. Wyatt, B. F. Haynes, P. D. Kwong, J. R. Mascola, M. Connors, *Nature* **2012**, *advance online publication*,
443. L. M. Walker, S. K. Phogat, P.-Y. Chan-Hui, D. Wagner, P. Phung, J. L. Goss, T. Wrin, M. D. Simek, S. Fling, J. L. Mitcham, J. K. Lehrman, F. H. Priddy, O. A. Olsen, S. M. Frey, P. W. Hammond, P. G. P. Investigators, S. Kaminsky, T. Zamb, M. Moyle, W. C. Koff, P. Poignard, D. R. Burton, *Science* **2009**, *326*, 285-289.
444. K. J. Doores, D. R. Burton, *J. Virol.* **2010**, *84*, 10510-10521.
445. L. M. Walker, M. D. Simek, F. Priddy, J. S. Gach, D. Wagner, M. B. Zwick, S. K. Phogat, P. Poignard, D. R. Burton, *PLoS Pathog.* **2010**, *6*, e1001028.
446. L. M. Walker, M. Huber, K. J. Doores, E. Falkowska, R. Pejchal, J.-P. Julien, S.-K. Wang, A. Ramos, P.-Y. Chan-Hui, M. Moyle, J. L. Mitcham, P. W. Hammond, O. A. Olsen, P. Phung, S. Fling, C.-H. Wong, S. Phogat, T. Wrin, M. D. Simek, P. G. Principal Investigators, W. C. Koff, I. A. Wilson, D. R. Burton, P. Poignard, *Nature* **2011**, *477*, 466-470.
447. M. Bonsignori, K.-K. Hwang, X. Chen, C.-Y. Tsao, L. Morris, E. Gray, D. J. Marshall, J. A. Crump, S. H. Kapiga, N. E. Sam, F. Sinangil, M. Pancera, Y. Yongping, B. Zhang, J. Zhu, P. D. Kwong, S. O'Dell, J. R. Mascola, L. Wu, G. J. Nabel, S. Phogat, M. S. Seaman, J. F. Whitesides, M. A. Moody, G. Kelsoe, X. Yang, J. Sodroski, G. M. Shaw, D. C. Montefiori, T. B. Kepler, G. D. Tomaras, S. M. Alam, H.-X. Liao, B. F. Haynes, *J. Virol.* **2011**, *85*, 9998-10009.
448. J. S. McLellan, M. Pancera, C. Carrico, J. Gorman, J.-P. Julien, R. Khayat, R. Louder, R. Pejchal, M. Sastry, K. Dai, S. O'Dell, N. Patel, S. Shahzad-ul-Hussan, Y. Yang, B. Zhang, T. Zhou, J. Zhu, J. C. Boyington, G.-Y. Chuang, D. Diwanji, I. Georgiev, Y. Do Kwon, D. Lee, M. K. Louder, S. Moquin, S. D. Schmidt, Z.-Y. Yang, M. Bonsignori, J. A. Crump, S. H. Kapiga, N. E. Sam, B. F. Haynes, D. R. Burton, W. C. Koff, L. M. Walker, S. Phogat, R. Wyatt, J. Orwenyo, L.-X. Wang, J. Arthos, C. A. Bewley, J. R. Mascola, G. J. Nabel, W. R. Schief, A. B. Ward, I. A. Wilson, P. D. Kwong, *Nature* **2011**, *advance online publication*,
449. R. Pejchal, K. J. Doores, L. M. Walker, R. Khayat, P.-S. Huang, S.-K. Wang, R. L. Stanfield, J.-P. Julien, A. Ramos, M. Crispin, R. Depetris, U. Katpally, A. Marozsan, A. Cupo, S. Maloveste, Y. Liu, R. McBride, Y. Ito, R. W. Sanders, C. Ogohara, J. C. Paulson, T. Feizi, C. N. Scanlan, C.-H. Wong, J. P. Moore, W. C. Olson, A. B. Ward, P. Poignard, W. R. Schief, D. R. Burton, I. A. Wilson, *Science* **2011**, *334*, 1097-1103.
450. L.-X. Wang, J. Ni, S. Singh, H. Li, *Chem. Biol.* **2004**, *11*, 127-134.

451. D. C. Dunlop, A. Ulrich, B. J. Appelmelk, D. R. Burton, R. A. Dwek, N. Zitzmann, C. N. Scanlan, *AIDS* **2008**, *22*, 2214-2217.
452. R. J. Luallen, J. Lin, H. Fu, K. K. Cai, C. Agrawal, I. Mboudjeka, F.-H. Lee, D. Montefiori, D. F. Smith, R. W. Doms, Y. Geng, *J. Virol.* **2008**, *82*, 6447-6457.
453. R. J. Luallen, C. Agrawal-Gamse, H. Fu, D. F. Smith, R. W. Doms, Y. Geng, *Glycobiology* **2010**, *20*, 280-286.
454. R. D. Astronomo, H. K. Lee, C. N. Scanlan, R. Pantophlet, C. Y. Huang, I. A. Wilson, O. Blixt, R. A. Dwek, C. H. Wong, D. R. Burton, *J. Virol.* **2008**, *82*, 6359-6368.
455. A. Kabanova, R. Adamo, D. Proietti, F. Berti, M. Tontini, R. Rappuoli, P. Costantino, *Glycoconj. J.* **2010**, *27*, 501-513.
456. K. J. Doores, Z. Fulton, V. Hong, M. K. Patel, C. N. Scanlan, M. R. Wormald, M. G. Finn, D. R. Burton, I. A. Wilson, B. G. Davis, *Proc. Natl. Acad. Sci. U. S. A.* **2010**, *107*, 17107-17112.
457. *Carbohydrate-Based Vaccines against HIV/AIDS*, in W. Lai-Xi, *Glycobiology and Drug Design*, American Chemical Society, **2012**, p. 157-186
458. C. N. Scanlan, G. E. Ritchie, K. Baruah, M. Crispin, D. J. Harvey, B. B. Singer, L. Lucka, M. R. Wormald, P. Wentworth Jr, N. Zitzmann, P. M. Rudd, D. R. Burton, R. A. Dwek, *J. Mol. Biol.* **2007**, *372*, 16-22.
459. C. Agrawal-Gamse, R. J. Luallen, B. Liu, H. Fu, F.-H. Lee, Y. Geng, R. W. Doms, *J. Virol.* **2011**, *85*, 470-480.
460. D. A. Calarese, H. K. Lee, C. Y. Huang, M. D. Best, R. D. Astronomo, R. L. Stanfield, H. Katinger, D. R. Burton, C. H. Wong, I. A. Wilson, *Proc. Natl. Acad. Sci. U. S. A.* **2005**, *102*, 13372-13377.
461. H. Li, L.-X. Wang, *Org. Biomol. Chem.* **2004**, *2*, 483-488.
462. S. K. Wang, P. H. Liang, R. D. Astronomo, T. L. Hsu, S. L. Hsieh, D. R. Burton, C. H. Wong, *Proc. Natl. Acad. Sci. U. S. A.* **2008**, *105*, 3690-3695.
463. K. Gorska, K.-T. Huang, O. Chaloin, N. Winssinger, *Angewandte Chemie International Edition* **2009**, *48*, 7695-7700.

464. M. Marradi, P. Di Gianvincenzo, P. M. Enríquez-Navas, O. M. Martínez-Ávila, F. Chiodo, E. Yuste, J. Angulo, S. Penadés, *J. Mol. Biol.* **2011**, *410*, 798-810.
465. J. Ni, H. Song, Y. Wang, N. M. Stamatou, L.-X. Wang, *Bioconjug. Chem.* **2006**, *17*, 493-500.
466. J. G. Joyce, I. J. Krauss, H. C. Song, D. W. Opalka, K. M. Grimm, D. D. Nahas, M. T. Esser, R. Hrin, M. Feng, V. Y. Dudkin, M. Chastain, J. W. Shiver, S. J. Danishefsky, *Proceedings of the National Academy of Sciences* **2008**, *105*, 15684-15689.
467. J. Wang, H. Li, G. Zou, L.-X. Wang, *Org. Biomol. Chem.* **2007**, *5*, 1529-1540.
468. M. E. Taylor, *Biochem. Soc. Trans.* **1993**, *21*, 468-473.
469. G. R. Vasta, M. Quesenberry, H. Ahmed, N. O'Leary, *Dev. Comp. Immunol.* **1999**, *23*, 401-420.
470. W. I. Weis, M. E. Taylor, K. Drickamer, *Immunol. Rev.* **1998**, *163*, 19-34.
471. P. W. Berman, *AIDS Res. Hum. Retroviruses* **1998**, *14*, S277-S289.
472. P. W. Berman, W. Huang, L. Riddle, A. M. Gray, T. Wrin, J. Vennari, A. Johnson, M. Klaussen, H. Prashad, C. Köhne, C. deWit, T. J. Gregory, *Virology* **1999**, *265*, 1-9.
473. T. r. H. V. S. Group, *J. Infect. Dis.* **2005**, *191*, 654-665.
474. P. Pitisuttithum, P. Gilbert, M. Gurwith, W. Heyward, M. Martin, F. van Griensven, D. Hu, Jordan W. Tappero, B. V. E. Group, *J. Infect. Dis.* **2006**, *194*, 1661-1671.
475. P. B. Gilbert, M. L. Peterson, D. Follmann, M. G. Hudgens, D. P. Francis, M. Gurwith, W. L. Heyward, D. V. Jobes, V. Popovic, S. G. Self, F. Sinangil, D. Burke, P. W. Berman, *J. Infect. Dis.* **2005**, *191*, 666-677.
476. D. C. Montefiori, C. Karnasuta, Y. Huang, H. Ahmed, P. Gilbert, M. S. de Souza, R. McLinden, S. Tovanabutra, A. Laurence-Chenine, E. Sanders-Buell, M. A. Moody, M. Bonsignori, C. Ochsenbauer, J. Kappes, H. Tang, K. Greene, H. Gao, C. C. LaBranche, C. Andrews, V. R. Polonis, S. Rerks-Ngarm, P. Pitisuttithum, S. Nitayaphan, J. Kaewkungwal, S. G. Self, P. W. Berman, D. Francis, F. Sinangil, C. Lee, J. Tartaglia, M. L. Robb, B. F. Haynes, N. L. Michael, J. H. Kim, *J. Infect. Dis.* **2012**, *206*, 431-441.
477. S. Lu, *Curr. Opin. Immunol.* **2009**, *21*, 346-351.

478. S. Rerks-Ngarm, P. Pitisuttithum, S. Nitayaphan, J. Kaewkungwal, J. Chiu, R. Paris, N. Prensri, C. Namwat, M. de Souza, E. Adams, M. Benenson, S. Gurunathan, J. Tartaglia, J. G. McNeil, D. P. Francis, D. Stablein, D. L. Birx, S. Chunsuttiwat, C. Khamboonruang, P. Thongcharoen, M. L. Robb, N. L. Michael, P. Kunasol, J. H. Kim, *N. Engl. J. Med.* **2009**, *361*, 2209-2220.
479. N. Karasavvas, E. Billings, M. Rao, C. Williams, S. Zolla-Pazner, R. T. Bailer, R. A. Koup, S. Madnote, D. Arworn, X. Shen, G. D. Tomaras, J. R. Currier, M. Jiang, C. Magaret, C. Andrews, R. Gottardo, P. Gilbert, T. J. Cardozo, S. Rerks-Ngarm, S. Nitayaphan, P. Pitisuttithum, J. Kaewkungwal, R. Paris, K. Greene, H. Gao, S. Gurunathan, J. Tartaglia, F. Sinangil, B. T. Korber, D. C. Montefiori, J. R. Mascola, M. L. Robb, B. F. Haynes, V. Ngauy, N. L. Michael, J. H. Kim, M. S. de Souza, *AIDS Res. Hum. Retroviruses* **2012**, *28*, 1444-1457.
480. B. Yu, J. F. Morales, S. M. O'Rourke, G. P. Tatsuno, P. W. Berman, *PLoS ONE* **2012**, *7*, e43903.
481. V. Holl, M. Peressin, T. Decoville, S. Schmidt, S. Zolla-Pazner, A.-M. Aubertin, C. Moog, *J. Virol.* **2006**, *80*, 6177-6181.
482. M. Asmal, Y. Sun, S. Lane, W. Yeh, S. D. Schmidt, J. R. Mascola, N. L. Letvin, *J. Virol.* **2011**, *85*, 5465-5475.
483. D. R. Burton, A. J. Hessel, B. F. Keele, P. J. Klasse, T. A. Ketas, B. Moldt, D. C. Dunlop, P. Pognard, L. A. Doyle, L. Cavacini, R. S. Veazey, J. P. Moore, *Proceedings of the National Academy of Sciences* **2011**, *108*, 11181-11186.
484. T. Mizuochi, M. W. Spellman, M. Larkin, J. Solomon, L. J. Basa, T. Feizi, *Biochem. J.* **1988**, *254*, 599-603.
485. J.-C. Yeh, J. R. Seals, C. I. Murphy, H. van Halbeek, R. D. Cummings, *Biochemistry (Mosc.)* **1993**, *32*, 11087-11099.
486. X. Zhu, C. Borchers, R. J. Bienstock, K. B. Tomer, *Biochemistry (Mosc.)* **2000**, *39*, 11194-11204.
487. J. M. Cutalo, L. J. Deterding, K. B. Tomer, *J. Am. Soc. Mass Spectrom.* **2004**, *15*, 1545-1555.
488. S.-M. Kang, F. Shi Quan, C. Huang, L. Guo, L. Ye, C. Yang, R. W. Compans, *Virology* **2005**, *331*, 20-32.
489. E. P. Go, J. Irungu, Y. Zhang, D. S. Dalpathado, H.-X. Liao, L. L. Sutherland, S. M. Alam, B. F. Haynes, H. Desaire, *J. Proteome Res.* **2008**, *7*, 1660-1674.

490. M. Raska, K. Takahashi, L. Czernekova, K. Zachova, S. Hall, Z. Moldoveanu, M. C. Elliott, L. Wilson, R. Brown, D. Jancova, S. Barnes, J. Vrbkova, M. Tomana, P. D. Smith, J. Mestecky, M. B. Renfrow, J. Novak, *J. Biol. Chem.* **2010**, *285*, 20860-20869.
491. L. Kong, N. C. Sheppard, G. B. E. Stewart-Jones, C. L. Robson, H. Chen, X. Xu, G. Krashias, C. Bonomelli, C. N. Scanlan, P. D. Kwong, S. A. Jeffs, I. M. Jones, Q. J. Sattentau, *J. Mol. Biol.* **2010**, *403*, 131-147.
492. E. P. Go, G. Hewawasam, H.-X. Liao, H. Chen, L.-H. Ping, J. A. Anderson, D. C. Hua, B. F. Haynes, H. Desaire, *J. Virol.* **2011**, *85*, 8270-8284.
493. E. P. Go, Q. Chang, H.-X. Liao, L. L. Sutherland, S. M. Alam, B. F. Haynes, H. Desaire, *J. Proteome Res.* **2009**, *8*, 4231-4242.
494. J. M. Binley, Y.-E. A. Ban, E. T. Crooks, D. Eggink, K. Osawa, W. R. Schief, R. W. Sanders, *J. Virol.* **2010**, *84*, 5637-5655.
495. H. Geyer, C. Holschbach, G. Hunsmann, J. Schneider, *J. Biol. Chem.* **1988**, *263*, 11760-11767.
496. T. Mizuochi, T. J. Matthews, M. Kato, J. Hamako, K. Titani, J. Solomon, T. Feizi, *J. Biol. Chem.* **1990**, *265*, 8519-8524.
497. Y. Zhang, E. P. Go, H. Desaire, *Anal. Chem.* **2008**, *80*, 3144-3158.
498. M. Li, F. Gao, J. R. Mascola, L. Stamatatos, V. R. Polonis, M. Koutsoukos, G. Voss, P. Goepfert, P. Gilbert, K. M. Greene, M. Bilska, D. L. Kothe, J. F. Salazar-Gonzalez, X. Wei, J. M. Decker, B. H. Hahn, D. C. Montefiori, *J. Virol.* **2005**, *79*, 10108-10125.
499. S. Lu, *Springer Semin. Immunopathol.* **2006**, *28*, 255-265.
500. D. L. Kothe, J. M. Decker, Y. Li, Z. Weng, F. Bibollet-Ruche, K. P. Zammit, M. G. Salazar, Y. Chen, J. F. Salazar-Gonzalez, Z. Moldoveanu, J. Mestecky, F. Gao, B. F. Haynes, G. M. Shaw, M. Muldoon, B. T. M. Korber, B. H. Hahn, *Virology* **2007**, *360*, 218-234.
501. G. Sailaja, I. Skountzou, F.-S. Quan, R. W. Compans, S.-M. Kang, *Virology* **2007**, *362*, 331-341.
502. S. Wang, J. S. Kennedy, K. West, D. C. Montefiori, S. Coley, J. Lawrence, S. Shen, S. Green, A. L. Rothman, F. A. Ennis, J. Arthos, R. Pal, P. Markham, S. Lu, *Vaccine* **2008**, *26*, 1098-1110.

503. K. J. Doores, C. Bonomelli, D. J. Harvey, S. Vasiljevic, R. A. Dwek, D. R. Burton, M. Crispin, C. N. Scanlan, *Proceedings of the National Academy of Sciences* **2010**, *107*, 13800-13805.
504. D. Eggink, M. Melchers, M. Wuhler, T. van Montfort, A. K. Dey, B. A. Naaijken, K. B. David, V. Le Douce, A. M. Deelder, K. Kang, W. C. Olson, B. Berkhout, C. H. Hokke, J. P. Moore, R. W. Sanders, *Virology* **2010**, *401*, 236-247.
505. C. Bonomelli, K. J. Doores, D. C. Dunlop, V. Thaney, R. A. Dwek, D. R. Burton, M. Crispin, C. N. Scanlan, *PLoS ONE* **2011**, *6*, e23521.
506. P. D. Kwong, J. R. Mascola, G. J. Nabel, *Cold Spring Harbor Perspectives in Medicine* **2011**, *1*,
507. N. E. van Houten, M. B. Zwick, A. Menendez, J. K. Scott, *Vaccine* **2006**, *24*, 4188-4200.
508. A. E. Willis, R. N. Perham, D. Wraith, *Gene* **1993**, *128*, 79-83.
509. F. Rohwer, R. Edwards, *J. Bacteriol.* **2002**, *184*, 4529-4535.
510. D. A. Marvin, B. Hohn, *Bacteriol. Rev.* **1969**, *33*, 172-209.
511. I. Rasched, E. Oberer, *Microbiol. Rev.* **1986**, *50*, 401-427.
512. D. T. Denhardt, P. Model, *Crit. Rev. Microbiol.* **1975**, *4*, 161-223.
513. D. F. Hill, G. B. Petersen, *J. Virol.* **1982**, *44*, 32-46.
514. J. Newman, H. L. Swinney, L. A. Day, *J. Mol. Biol.* **1977**, *116*, 593-603.
515. R. A. Grant, T. C. Lin, W. Konigsberg, R. E. Webster, *J. Biol. Chem.* **1981**, *256*, 539-546.
516. C. W. Gray, R. S. Brown, D. A. Marvin, *J. Mol. Biol.* **1981**, *146*, 621-627.
517. E. Beck, B. Zink, *Gene* **1981**, *16*, 35-58.
518. R. Herrmann, K. Neugebauer, H. Zentgraf, H. Schaller, *Molecular and General Genetics MGG* **1978**, *159*, 171-178.
519. G. Smith, *Science* **1985**, *228*, 1315-1317.

520. J. K. Scott, G. P. Smith, *Science* **1990**, *249*, 386-390.
521. J. W. Kehoe, B. K. Kay, *Chem. Rev.* **2005**, *105*, 4056-4072.
522. A. Menendez, D. A. Calarese, R. L. Stanfield, K. C. Chow, C. N. Scanlan, R. Kunert, H. Katinger, D. R. Burton, I. A. Wilson, J. K. Scott, *The FASEB Journal* **2008**, *22*, 1380-1392.
523. F. Sanger, A. R. Coulson, B. G. Barrell, A. J. H. Smith, B. A. Roe, *J. Mol. Biol.* **1980**, *143*, 161-178.
524. C. Graham and A. M. Hill, *The Universal Primers and the Shotgun DNA Sequencing Method*, in J. Messing, *DNA Sequencing Protocols*, Humana Press, **2001**, p. 13-31
525. C. Mao, C. E. Flynn, A. Hayhurst, R. Sweeney, J. Qi, G. Georgiou, B. Iverson, A. M. Belcher, *Proceedings of the National Academy of Sciences* **2003**, *100*, 6946-6951.
526. C. Mao, D. J. Solis, B. D. Reiss, S. T. Kottmann, R. Y. Sweeney, A. Hayhurst, G. Georgiou, B. Iverson, A. M. Belcher, *Science* **2004**, *303*, 213-217.
527. J. M. Burke, C. P. Novotny, P. Fives-Taylor, *J. Bacteriol.* **1979**, *140*, 525-531.
528. L. Riechmann, P. Holliger, *Cell* **1997**, *90*, 351-360.
529. E. M. Click, R. E. Webster, *J. Bacteriol.* **1997**, *179*, 6464-6471.
530. N. J. Bennett, D. Gagic, A. J. Sutherland-Smith, J. Rakonjac, *J. Mol. Biol.* **2011**, *411*, 972-985.
531. H. Endemann, P. Model, *J. Mol. Biol.* **1995**, *250*, 496-506.
532. M. P. Rapoza, R. E. Webster, *J. Mol. Biol.* **1995**, *248*, 627-638.
533. F. M. Thomas, G. Klaus, *Nature* **1982**, *296*, 828-832.
534. M. Russel, P. Model, *J. Virol.* **1989**, *63*, 3284-3295.
535. D. K. Marciano, M. Russel, S. M. Simon, *Science* **1999**, *284*, 1516-1519.
536. J. ARMSTRONG, J. A. HEWITT, R. N. PERHAM, *EMBO J.* **1983**, *2*, 1641-1646.

537. D. A. Marvin, L. C. Welsh, M. F. Symmons, W. R. P. Scott, S. K. Straus, *J. Mol. Biol.* **2006**, 355, 294-309.
538. L. Specthrie, E. Bullitt, K. Horiuchi, P. Model, M. Russel, L. Makowski, *J. Mol. Biol.* **1992**, 228, 720-724.
539. K. Ikehara, H. Utiyama, M. Kurata, *Virology* **1975**, 66, 306-315.
540. Y. Nakashima, R. L. Wiseman, W. Konigsberg, D. A. Marvin, *Nature* **1975**, 253, 68-71.
541. M. Manning, S. Chrysogelos, J. Griffith, *J. Virol.* **1981**, 40, 912-919.
542. R. Marco, S. M. Jazwinski, A. Kornberg, *Virology* **1974**, 62, 209-223.
543. A. K. Dunker, R. W. Williams, W. L. Peticolas, *J. Biol. Chem.* **1979**, 254, 6444-6448.
544. X. Ji, J. Oh, A. K. Dunker, K. W. Hipps, *Ultramicroscopy* **1998**, 72, 165-176.
545. V. A. Petrenko, V. J. Vodyanoy, *J. Microbiol. Methods* **2003**, 53, 253-262.
546. I. Yacoby, I. Benhar, *Expert Opin. Drug Deliv.* **2008**, 5, 321-329.
547. S. A. Hilderbrand, K. A. Kelly, R. Weissleder, C.-H. Tung, *Bioconjug. Chem.* **2005**, 16, 1275-1281.
548. E. R. Goldman, M. P. Pazirandeh, J. M. Mauro, K. D. King, J. C. Frey, G. P. Anderson, *J. Mol. Recognit.* **2000**, 13, 382-387.
549. K. Li, Y. Chen, S. Li, H. G. Nguyen, Z. Niu, S. You, C. M. Mello, X. Lu, Q. Wang, *Bioconjug. Chem.* **2010**, 21, 1369-1377.
550. D. W. Domaille, J. H. Lee, J. N. Cha, *Chem. Commun. (Camb.)* **2013**, 49, 1759-1761.
551. D. C. Montefiori, M. Altfeld, P. K. Lee, M. Bilska, J. Zhou, M. N. Johnston, F. Gao, B. D. Walker, E. S. Rosenberg, *The Journal of Immunology* **2003**, 170, 3906-3914.
552. M. Choisy, C. H. Woelk, J.-F. Guégan, D. L. Robertson, *J. Virol.* **2004**, 78, 1962-1970.

553. C. L. Lavine, S. Lao, D. C. Montefiori, B. F. Haynes, J. G. Sodroski, X. Yang, t. N. C. f. H. A. V. *Immunology, J. Virol.* **2012**, *86*, 2153-2164.
554. T. Zhu, H. Mo, N. Wang, D. Nam, Y. Cao, R. Koup, D. Ho, *Science* **1993**, *261*, 1179-1181.
555. B. F. Keele, C. A. Derdeyn, *Curr. Opin. HIV AIDS* **2009**, *4*, 352-357
310.1097/COH.1090b1013e32832d32839fef.
556. J. F. Salazar-Gonzalez, M. G. Salazar, B. F. Keele, G. H. Learn, E. E. Giorgi, H. Li, J. M. Decker, S. Wang, J. Baalwa, M. H. Kraus, N. F. Parrish, K. S. Shaw, M. B. Guffey, K. J. Bar, K. L. Davis, C. Ochsenbauer-Jambor, J. C. Kappes, M. S. Saag, M. S. Cohen, J. Mulenga, C. A. Derdeyn, S. Allen, E. Hunter, M. Markowitz, P. Hraber, A. S. Perelson, T. Bhattacharya, B. F. Haynes, B. T. Korber, B. H. Hahn, G. M. Shaw, *The Journal of Experimental Medicine* **2009**, *206*, 1273-1289.
557. V. Y. Dudkin, M. Orlova, X. Geng, M. Mandal, W. C. Olson, S. J. Danishefsky, *J. Am. Chem. Soc.* **2004**, *126*, 9560-9562.
558. S. J. Danishefsky, S. Hu, P. F. Cirillo, M. Eckhardt, P. H. Seeberger, *Chemistry – A European Journal* **1997**, *3*, 1617-1628.
559. V. Y. Dudkin, J. S. Miller, S. J. Danishefsky, *Tetrahedron Lett.* **2003**, *44*, 1791-1793.
560. M. Pancera, J. S. McLellan, S. Shahzad-ul-Hussan, N. Doria-Rose, B. Zhang, Y. Yang, D. R. Burton, W. C. Koff, C. A. Bewley, P. D. Kwong, *Retrovirology* **2012**, *9*, 1-1.
561. I. Mikell, L. Stamatatos, *PLoS ONE* **2012**, *7*, e49610.
562. G. T. Hermanson, *Bioconjugate Techniques, 2nd ed.*, Academic Press: London, Amsterdam, Burlington, San Diego, **2008**

CHAPTER 2: Synthesis of Oligo-Mannopyranosyl Thiol Analogues of the High-Mannose Oligosaccharides Found on HIV-1 gp120

Part I: Synthetic Aspects of Carbohydrate Chemistry

Introduction to Carbohydrate Chemistry

The early days of carbohydrate chemistry were enormously challenging for synthetic chemists. The roots of carbohydrate synthesis dates back to the late 1800s where the structures of sugars were first being deduced through labourous chemical analysis. Emil Fischer joined the field of carbohydrate chemistry in 1884 and significantly advanced the knowledge of sugars, earning him the Nobel Prize in Chemistry in 1902. He is most noted for his logical application of an elaborate chemical methodology to elucidate the relative configurations of (+)-glucose and other hexose and pentose sugars in 1891.^{1, 2} There was still uncertainty regarding his structural assignments however. The absolute configuration of the sugars could not be determined at the chiral center furthest from the aldehyde (Figure 32A). Consequently, Fischer made the arbitrary choice to pick the D-series structure for all the studied aldohexoses, and his choice was eventually shown to be correct by X-ray diffraction studies in 1951.³

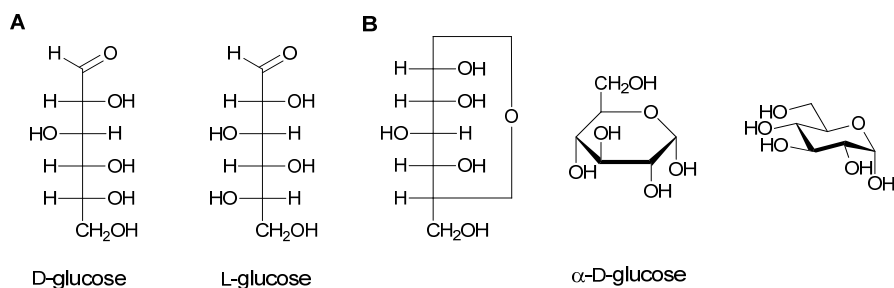


Figure 32. Representations of glucose. A| Fischer projections of acyclic D- and L-glucose. B| Cyclic representations of α -D-glucose displayed as a Fischer projection, Haworth projection, and chair conformation of from left to right.

The cyclic structure of sugars was another problem that was difficult to establish, as most work was done on the assumption of acyclic aldose structures. The first correctly proposed cyclic structure was by Tollens in 1883, who suggested a cyclic furanose ring for glucose, levulose and sucrose to explain the unusually low reactivity of

the sugar aldehyde.⁴ The findings of two forms of D-glucose in methylation⁵ and acylation^{6, 7} reactions, as well as the observed mutarotation⁸ of two isolated forms of crystalline D-glucose was explainable by the existence of a ring structure with an anomerizable hemiacetal carbon, although the specifics of such a structure remained unclear. It wasn't until 1926 that Haworth and others corrected the structure of glucose to a six-membered cyclic hemiacetal and introduced the three-dimensional Haworth projection to replace the dated cyclic Fischer projections (Figure 32B).^{9, 10} The Haworth projection was later updated to the present-day chair conformational drawing of sugar rings by Reeves in 1950.¹¹ Part of the Haworth legacy survives, as his suggestion that monosaccharides containing a tetrahydropyran system be termed pyranoses, and those with a tetrahydrofuran system furanoses, is still used today as an integral part of sugar nomenclature.¹²

As complex oligosaccharides and polysaccharides of biological relevance were being discovered throughout the twentieth century,¹³ the rudimentary chemical methods used to elucidate and synthesize carbohydrates required extensive and challenging experimental techniques. Improvements in instrumental methods such as HPLC,¹⁴ mass spectrometry (MS)^{15, 16} and NMR spectroscopy¹⁷ in the 1970's made possible the swift structural characterization of larger oligosaccharides. Advances in carbohydrate synthesis also started to emerge during this time, marked by the synthesis of the complex trisaccharide A and B blood group determinants by Raymond Lemieux and co-workers in 1975.¹⁸⁻²¹ This was accomplished through development of reliable methodologies for the stereospecific control of glycosidic linkage formation, and the structural analysis of both the protected intermediates and final synthetic targets by NMR spectroscopy. For the first time, the synthesis of oligosaccharides of sufficient complexity was achieved, opening the way for other laboratories to join in the effort. In the last two decades reliable techniques for the synthesis of complex glycans have advanced dramatically and with the exception of large oligomers (greater than octasaccharide lengths) synthesis of medium sized oligosaccharides are considered fairly routine.

An efficient synthesis of oligosaccharide targets requires control of the regioselective and stereoselective outcomes of reactions. Simple monosaccharides have

multiple hydroxyl groups available for reaction, and are commonly differentially protected to control the number of available hydroxyls for further manipulation. Protecting groups play an essential role in carbohydrate synthesis and an efficient synthetic strategy often relies on utilizing a minimal amount of high-yielding protecting group manipulations that have compatible chemistries. Fortunately, a wide range of protecting groups are available that offer a multitude of installation and cleavage conditions.²² The primary goal of protecting groups within carbohydrate synthesis is to restrict the number of reactive hydroxyls to allow for the regioselective reaction with a glycosyl donor. Glycosidic bond formation must not only be regioselective, but stereoselective as well. Many types of glycosyl donors and glycosylation strategies have been developed for this important class of reactions, and which are described in the following section.

Glycoside Formation

Glycosidic bond formation requires a glycosyl donor with an activated anomeric carbon, and a glycosyl acceptor with usually a single exposed hydroxyl group. The breadth of glycosyl donors has grown dramatically since the first glycosylations performed by Michael²³ and Fischer²⁴ at the end of the nineteenth century. Michael's glycosylation proceeded through the nucleophilic displacement of an anomeric halide with a phenolate (Figure 33A). Soon after, Fischer reported the glycosylation of simple, aliphatic alcohols with unprotected monosaccharides under harsh acidic conditions (Figure 33B). The anomeric mixture of furanosides and pyranosides obtained from the Fischer glycosylation underscores the complexity of the glycosylation process. The first controlled, general glycosylation procedure was reported in 1901 by Koenigs and Knorr who demonstrated the activation of glycosyl halides by heavy metal halophiles (Figure 33C). The milder reaction conditions allowed for the synthesis of more complex oligosaccharide products. Today there are many reactive donor types to choose from that react under a wide range of mild activating conditions. At present, the majority of oligosaccharide synthesis rely on trichloroacetimidate,²⁵ thioglycoside²⁶ and glycosyl sulfoxides²⁷ donors.

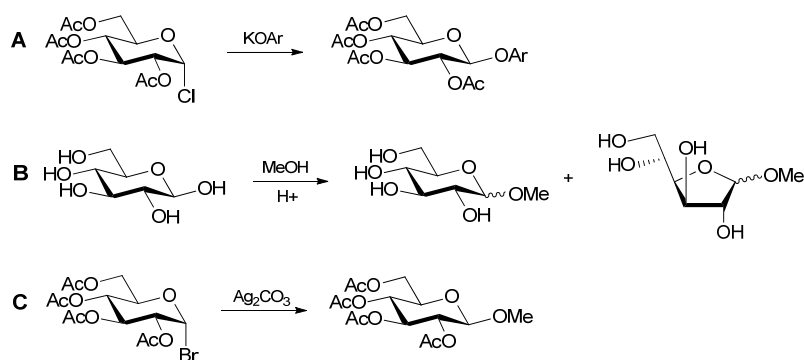


Figure 33. Early glycosylation reactions performed by Michael (A), Fischer (B) and Koenigs-Knorr (C).

Glycosylation reactions are inherently complex and the mechanism is not completely understood which can lead to unpredictable reaction outcomes.²⁸ In the Michael and Koenigs-Knorr glycosylations, the reaction proceeds through a concerted S_N2 mechanism (Figure 34A), leading to a predictable inversion in stereochemistry. Most modern donors proceed through more of a unimolecular S_N1 route (Figure 34B) which yields less predictable stereochemistry unless steps are taken to control the mechanism of formation. A 'pure' S_N1 glycosylation mechanism proceeds through the assisted departure of the anomeric leaving group by use of an appropriate promoter, which results in the formation of the oxocarbenium ion.^{**} The formation of the oxocarbenium ion is the rate limiting step and is typically irreversible. Nucleophilic attack by the glycosyl acceptor forms the new glycosidic linkage. The mechanism in which modern donors react more accurately falls at the border between S_N1 and S_N2 mechanisms.^{28, 29} This is because the oxocarbenium ion is never completely free as other reactive species are present in the reaction mixture, such as the counter ion of the promoter, the leaving group, neighbouring protecting groups and even the solvent. These additional interactions can significantly influence the stereoselective outcome of the glycosidic bond formation, some of which will be discussed in the subsequent sections.³⁰

^{**} Provided that the O2 substituents are non-participating.

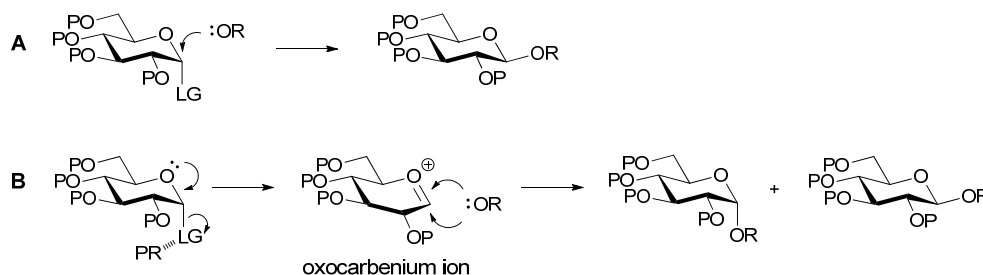


Figure 34. Reaction at the anomeric center. **A** | A nucleophilic alcohol displaces the leaving group (LG) in the S_N2 reaction mechanism. **B** | The S_N1 reaction mechanism starts with the promoter (PR) assisted departure of the anomeric LG resulting in the formation of an oxocarbenium cation. Nucleophilic attack on the top face will result in a β -linked product and an α -linked product from the bottom face. P : protecting group.

The Anomeric Effect

The anomeric effect was first observed by Edward³¹ in 1955 and later defined by Lemieux^{32, 33} as the preference of large electronegative constituents at C-1 of the pyranose ring to adopt an axial orientation. This appears to be counterintuitive as axially orientated substituents on cyclohexyl rings result in unfavourable 1,3-diaxial steric interactions (Figure 35A). Equatorially orientated substituents avoid such steric interactions and thus should be more energetically favourable. However, the ring oxygen within the pyranose ring provides additional thermodynamic stabilization to neighbouring axial substituents through the anomeric effect. The origins of the anomeric effect are thought to be controlled by two factors: an unfavourable dipole alignment between the ring oxygen and electronegative anomeric substituent when orientated in an equatorial configuration (Figure 35B), and the hyperconjugation of the axially orientated lone-pair electrons of the ring oxygen interacting with the periplanar anti-bonding σ^* orbital of an axial orientated substituent (Figure 35C). In the absence of nonparticipating factors in the reaction mixture, α -glycoside formation will be predominantly favored due to the anomeric effect.

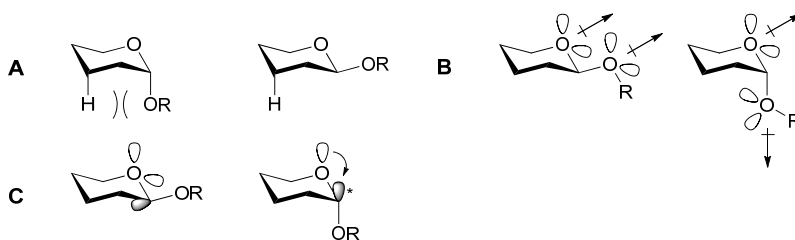


Figure 35. The origins of the anomeric effect. A| Axial orientated substituents on a six membered ring produce unfavourable 1,3-diaxial interactions which are alleviated in the equatorial orientation. B| Equatorial orientated substituents produce unfavourable dipole-dipole interactions with the ring oxygen lone pair. C| The axial anomer is stabilized through the delocalization of the axial lone pair electrons of the ring oxygen into the anti-bonding molecular orbital of the glycosidic linkage. This is not possible with the equatorial anomer.

Neighbouring Group Participation

As syntheses utilizing the Koenigs-Knorr glycosylation became more common, research groups started to notice that an acetate protecting group at C-2 seemed to effect the stereochemical outcome and byproduct formation of glycosylation reactions.^{29, 34} It was observed that basic or neutral glycosylations conditions could produce 1,2-orthoester byproducts, but only if the anomeric halogen and adjacent acetyl group were *trans* to each other. In addition to orthoester formation, 1,2-*trans* glycosyl donors could produce glycosylation products that retain their anomeric stereochemistry. To account for these observations, Isbell first proposed in 1940 that the nucleophile could attack the anomeric carbon of the intermediate acetoxonium ion intermediate of the orthoester reaction rather than the carbonyl carbon of the acetyl group (Figure 36).³⁴ Under acidic conditions, orthoester formation is in equilibrium with the acetoxonium intermediate which drives the reaction to form the 1,2-*trans* glycoside. Isbell's findings were later substantiated through Winstein's kinetic studies on neighbouring group participation which concluded that the unassisted departure of a leaving group to produce a free oxocarbenium intermediate would require much more energy than a concerted nucleophilic displacement via intramolecular participation.^{35, 36} Since most modern donors utilize leaving groups that more completely dissociate from the anomeric centre, neighbouring acyl groups will preferentially react with the free oxocarbenium ion regardless of the initial anomeric configuration. Thus, neighbouring group participation provides a reliable protocol for 1,2-*trans* glycosidic linkage formation.

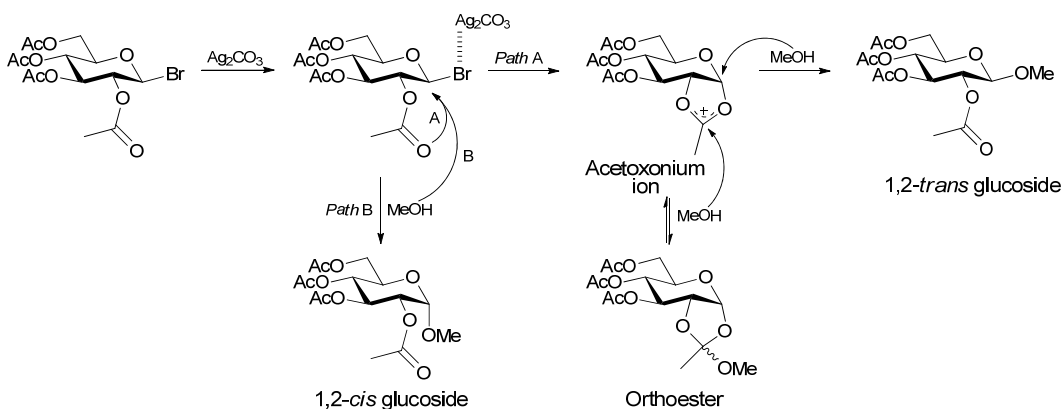


Figure 36. Biomolecular mechanism of the Koenigs-Knorr glycosylation of a 1,2-*trans* glycosyl donor. In the first step, the anomeric bromide complexes with the silver salt making it more susceptible to nucleophilic attack. An extramolecular nucleophile, such as methanol, can displace the bromide to yield a 1,2-*cis* product. The bromide can also be displaced by an intramolecular orthoester reaction with the neighbouring ester group on C-2 to produce an acetoxonium ion. An extramolecular nucleophile can either attack at the acetyl carbon or the anomeric carbon to produce an orthoester or 1,2-*trans* product, respectively.

Synthesis of Mannosyl Thiols

Since glycosyl thiols (also known as 1-thiosugars) are exploited extensively in this thesis, the following section deals at length with this topic.

Glycosyl thiols are beginning to see more use in the synthesis of thiooligosaccharides and *S*-glycoconjugates.³⁷⁻⁴³ This is in part due to the resistance to enzymatic and chemical hydrolysis of glycosidic linkages that are formed through a sulfur atom, rather than the natural oxygen atom.^{40, 44-48} An *S*-glycosidic linkage is also a good conformational mimic of a natural *O*-linkage, although an increase in flexibility about the anomeric linkage has been described.⁴⁹⁻⁵³ Owing to these properties, *S*-glycosides have been employed as biomimics of natural *O*-glycosides for biological applications, such as vaccine design,⁵⁴ where metabolic stability can prolong the life of the glycan *in vivo*, leading to an enhancement of biological activity. Outside of exploiting thiols for their stable glycosidic linkages, the high reactivity of thiols and their relative rarity in most biomolecules makes glycosyl thiols ideal for controlled glycoconjugation reactions.

A synthetic scheme involving a thiol group requires special considerations in order to avoid problems associated with their high reactivity; problems that are only

partially tamed though protection. Thiols are much more acidic (pK_a 10-11) than alcohols (pK_a 15-16), and thiolate anions are softer and consequently more nucleophilic than alkoxides. Thiols are also easily oxidized to disulfides, even from exposure to atmospheric oxygen, which can be straightforwardly reversed through reductive means. Thiols protected as thioethers are still susceptible to oxidation to sulfoxides and sulfones, and reduction back to a thioether is difficult and impractical. Oxidative conditions should thus be avoided in a thiol-containing synthetic scheme, as well as reductive conditions if a disulfide is part of the synthetic strategy. Degassing solvents to remove atmospheric oxygen and performing reaction under an inert gas may be required to avoid oxidation.

Glycosyl thiols are commonly made through the reaction of a glycosyl halide with a moderately stable thiol such as a thioacetate,^{55, 56} thiourea^{57, 58} or thiocyanate (Figure 37).^{59, 60} They can also be synthesized conventionally from normal glycosyl donors and the corresponding thiol acceptor. The *S*-acetate, *S*-alkyl thiouronium salt and *S*-cyanate groups that offer only temporary thiol protection due to their limited stabilities are often reprotected as a more stable thioether or disulfide when carried throughout longer syntheses. The stereochemistry of an anomeric thiol is retained during the reprotection as glycosyl thiols undergo a rate of mutarotation that is much slower than that of anomeric hydroxyls.^{38, 61} Thus, the desired anomeric configuration of a glycosyl thiol must be considered when the anomeric thiol is first installed. Pure β -glycosyl thiols are usually straightforward to obtain by treatment of α -glycosyl halides with the corresponding thiol in an S_N2 manner. α -Glycosyl thiols can be synthesized similarly by the displacement of β -glycosyl halides or the stereospecific ring opening of 1,6-anhydrosugars.^{55, 56, 62, 63} Neighbouring group participation can potentially override the displacement reaction of glycosyl halides, yielding glycosyl thiols that retain their original stereochemistry. *trans*-Mannosyl bromides treated with thiourea or potassium thiocyanate give mainly the α -mannosyl product through an S_N1 mechanism involving the attack of the sulfur nucleophile on the α -face of the intermediate isocarbenium ion (Figure 37A,B).⁶⁴ The same reaction with potassium thioacetate produces predominantly the β -product (Figure 37C).^{56, 65} This discrepancy may be due to the

higher nucleophilicity of the thioate which would more readily displace the anomeric halide.

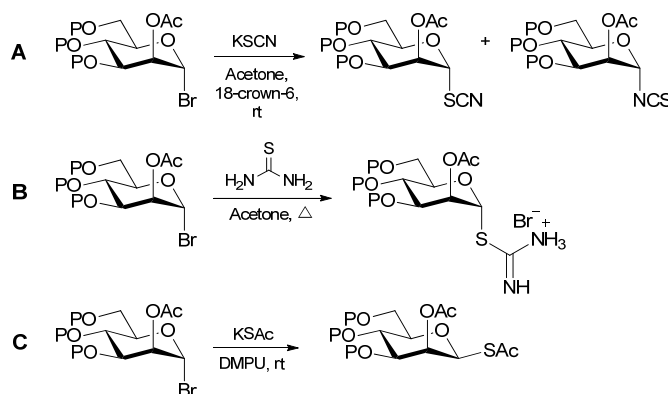


Figure 37. Three methods used to install an anomeric thiol. **A|and B|** Reaction of a glycosyl halide with potassium thiocyanate or thiourea produces predominantly the α -anomer. **C|** Reaction with potassium thioacetate produces primarily the β -anomer.

The protecting groups commonly used for hydroxyl protection are impractical for thiol protection due to sulfur's weak hold on most protecting groups. Silyl and alkyl/aryl/acyl protecting groups are held much more loosely by sulfur than oxygen (Table 2), eliminating silyl and ester protecting groups from practical application. Alkyl and aryl protecting groups, which can be difficult to remove from protected hydroxyls, find use in thiol protection. Popular *S*-protecting groups include the xanthenyl (Xan),⁶⁶ triphenylmethyl (Tr)⁶⁷ and benzyl (Bn) groups. These groups are commonly used in peptide synthesis and are not always compatible with carbohydrate synthesis. Xan installation requires strongly acidic conditions which may be incompatible with other protecting groups. The mild removal conditions (1% trifluoroacetic acid) for Xan also pose a problem as they mimic glycosylation conditions, limiting their potential to a temporary protecting group.⁶⁸ Trityl group installation can be troublesome and low yielding, and it is also removed by moderately acidic conditions.⁶⁹ *S*-benzyl groups are very stable to many conditions and easy to install, however they differ from *O*-benzyl removal in that hydrogenation cannot be utilized as the free thiol that is generated would poison the palladium catalyst. Removal is thus limited to dissolving metal reduction,^{70,71} treatment with hydrofluoric acid⁷² or electrolysis.⁷³

Table 2. Average bond energies and lengths of sulfur and oxygen with silicon and carbon.^{74, 75}

Bond	Bond Strength (kcal/mol)	Bond Length (pm)
O-Si	108	163
S-Si	70	200
O-C	86	143
S-C	65	182

Thiols can also be protected as disulfides at the expense of being unable to utilize reducing conditions for protecting group manipulation. Symmetrical disulfides can be formed by treating a thiol with an oxidizing reagent to form a disulfide with itself.⁷⁶ When a glycosyl thiol is protected this way, further manipulations of the carbohydrate may suffer in yield as each subsequent reaction would have to occur on both sides of the disulfide to be complete; a 75% yield for a manipulation on a saccharide could become a 50% yield when two saccharides are part of the same molecule. Problems may also arise as steric bulk increases with the cumulative addition of sizable protecting groups and additional sugars with subsequent glycosylations. The use of unsymmetrical disulfides can avoid these problems by utilizing small thiols to form the disulfide bond. An excess of protecting thiol must be used when forming the disulfide through oxidative means. Unsymmetrical disulfides can also be formed in a more direct and controlled manner by performing a thiol-disulfide exchange with the protecting thiol in its disulfide form,⁷⁷ utilizing azodicarboxylate transfer reagents,⁷⁷ or performing a thiol-disulfide exchange on glycosyl methanethiosulfonates (Figure 38).⁷⁸ Disulfide derivatives are relatively resistant to acids and bases, with decreasing stability in the following order: RSS*t*Bu > RSS*i*Pr > RSSEt. The *t*Bu also has the advantage of being resistant to unwanted thiol-disulfide exchange,⁷⁹ although there have been reported difficulties with reducing an *t*Bu disulfide, possibly due to its stability and steric bulk.⁸⁰

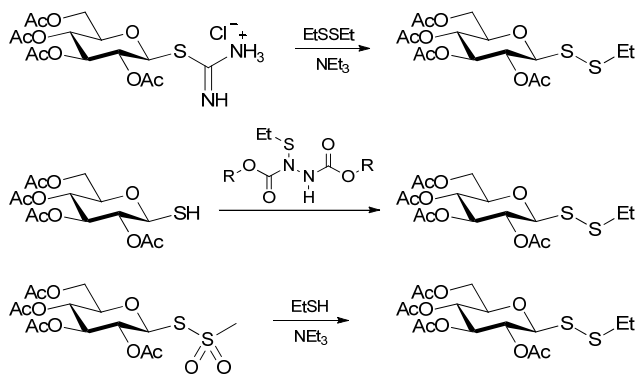


Figure 38. Common methods of forming unsymmetrical disulfides.

Disulfides are typically broken by thio-disulfide exchange or treatment with reducing agents. Thiol-disulfide exchange occurs through the $\text{S}_{\text{N}}2$ attack of a disulfide bond by a free thiol, forming a new disulfide and free thiol.⁸¹ The reaction is reversible and can potentially lead to a multiple of products (Figure 39). The equilibrium of the exchange is under control of steric factors and the relative nucleophilicities of the thiols generated during the exchange. In general, bulky and nucleophilic thiols form disulfides that are resistant to exchange. Dithiothreitol (DTT) and 2-mercaptoethanol are frequently used to reduce disulfides. DTT is especially useful, because once oxidized, it forms a stable six-membered ring with an internal disulfide bond, eliminating unwanted thiol-disulfide exchange.⁸² Any general reducing agent can be used to reduce a disulfide; however phosphines are commonly used as they preferentially reduce disulfides in most cases.⁸³ There have also been reports of desulfurization and complex mixtures being formed during reduction with phosphines,^{80, 84} although these are exceptions to the general rule.

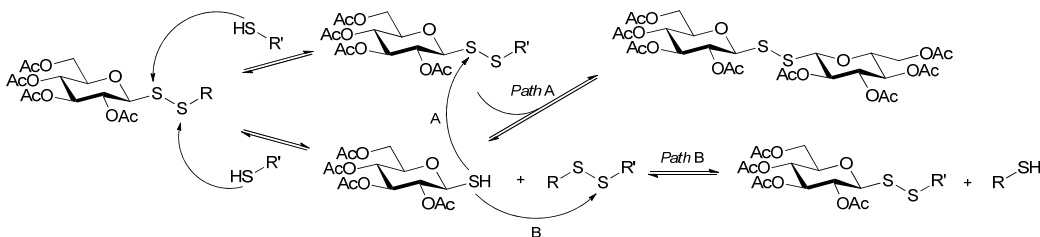
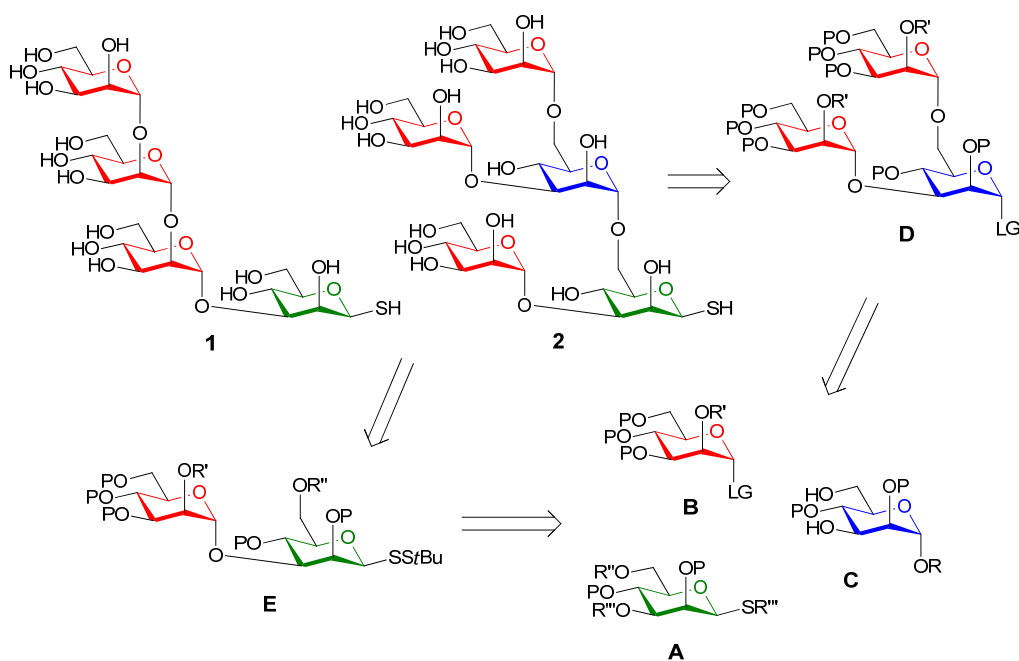


Figure 39. The complexities of thiol-disulfide exchange.

Part II: Synthesis of Mannosyl Thiol Analogues

Retrosynthetic Analysis

The synthesis of the tetra- and penta-mannopyranosyl thiol analogues **1** and **2** pose two synthetic challenges: 1) the installation and protection of the β -anomeric thiol and 2) protection of a glycosyl acceptor for creating 3,6-branched mannosides. Both the tetrasaccharide **1** and pentasaccharide **2** share common structural features that can be broken down into the monosaccharide building blocks **A**, **B** and **C** (Scheme 2). Since the thiol protection strategy will dictate the allowed protecting group chemistry, and limit the synthetic routes to 3,6-branched mannosides, the chemistry of the anomeric-thiol building block **A** was to be established first.



Scheme 2. Retrosynthesis of tetrasaccharide **1** and pentasaccharide **2**. **P**: global protecting group, **R**: temporary anomeric protecting group, **R'** and **R''**: temporary orthogonal protecting groups, **R'''**: thiol protecting group, **LG**: donor leaving group.

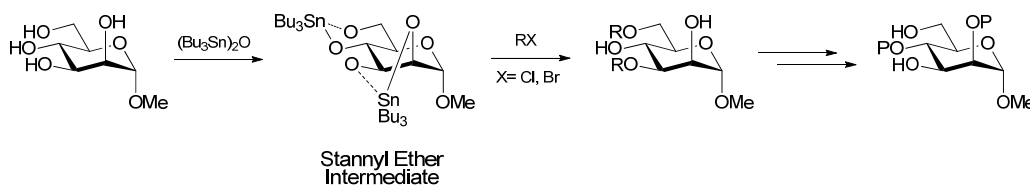
The most reliable method to produce a β -mannosyl thiol is through the S_N2 reaction of α -D-mannopyranosyl bromide with thioacetate.^{55, 56} Mannosyl bromides are commonly created through the reaction of peracetylated mannose with HBr in acetic acid. These conditions should be avoided late in the synthesis in order to maintain the integrity of the protecting groups and glycosidic linkages. A late-stage conversion of

larger oligosaccharides to glycosyl halides can be achieved using mild Vilsmeier-Haack reagents as long as the hemiacetal group can be accessed.^{85, 86} While this reaction is high yielding there is uncertainty that the subsequent nucleophilic attack of thioacetate would proceed smoothly on a larger and more complex mannoside. In an effort to eliminate uncertainty late in the synthetic scheme, the early installation of the anomeric thiol was chosen here despite the restrictions thiols place on the synthesis. The temporary *S*-acetate group will be selectively removed and the thiol protected as an unsymmetrical *tert*-butyl disulfide, which was the protecting group most tolerant to protecting group manipulations and glycosylation conditions when evaluated with other anomeric thiol protecting groups by Liang and coworkers.⁷⁹

There have been many approaches to the synthesis of 3,6-branched mannosides,^{56, 80, 87-108} driven particularly by the interest in synthesizing the *N*-linked glycans found on gp120. Both retrons **A** and **C** share this branching pattern, though the prior installation of the anomeric disulfide eliminates protection strategies that utilize 1,2-acetals^{80, 100, 101, 109} or glycols.^{92, 98, 110} The presence of the disulfide also eliminates the regioselective opening of 4,6-benzylidene acetals with reducing agents, which is a useful strategy for *O*4 and *O*6 protection.^{108, 111, 112} Elaborate protection strategies that would be difficult to adapt were not considered, such as the tethered cyclo-glycosylation of Lopez and coworkers.⁹⁶ A protection strategy with permanent protecting groups at *O*2 and *O*4 and orthogonal temporary protecting groups on *O*3 and *O*6 would allow for retron **A** to be used in the synthesis of both tetrasaccharide **1** and pentasaccharide **2**. Methods to produce 3,6-branched mannosides that are compatible with an anomeric disulfide are discussed below.

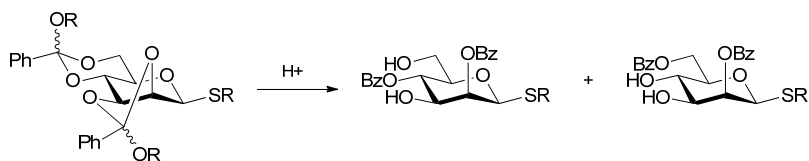
Ogawa was one of the first chemists to synthesize the high-mannose core structures of *N*-glycans, utilizing the regioselective enhancement of hydroxyl nucleophilicity through stannylidene chemistry.^{87, 88} Treating an unprotected sugar with dialkyltin oxide forms a dialkylstannyl ether intermediate, increasing the nucleophilicity of primary oxygen atoms and equatorial oxygen atoms that are coordinated to adjacent axial oxygen atoms on the ring.^{113, 114} In the case of mannose, treatment of the stannyl ether intermediates with alkyl or acyl halides preferentially forms 3,6-di-*O*-protected products. This method is typically used to temporarily protect

the 3,6-hydroxyls, allowing for easy protection of the 2,4-hydroxyls and subsequent removal of the temporary protecting groups for 3,6-*O*-glycosylation (Scheme 3).^{91, 99, 104, 115} Glycosyl halides can also be reacted with stannyl ethers to directly form 3,6-branched mannosides.⁸⁷ While these reaction schemes allow for convenient access to 3,6-branched mannosides, it is reportedly sluggish and low yielding (~30%) and has the additional downside of working with toxic alkyltin reagents that are sometimes difficult to remove from final products.^{87, 88, 108, 113}



Scheme 3. Utilizing stannylidene chemistry for temporary 3,6-di-*O*-protection to allow for the installation of more permanent 2,4-di-*O*-protection.

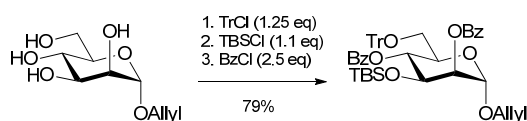
Another approach to achieve 2,4-di-*O*-protection is through the regioselective opening of benzylidene acetals.^{56, 90, 103, 106} Treatment of 2,3:4,6-di-*O*-alkoxybenzylidene-mannopyranosides with acid opens the 2,3-ortho-benzoate regioselectively to the 2-*O*-acyl derivative, whereas the 4,6-ortho-benzoate produces a mixture of 4-*O*- and 6-*O*-acyl derivatives (Scheme 4). This reaction was performed by the Bundle group on a somewhat similar 1-thio- β -mannopyranoside successfully, with no purification of the orthoester intermediate.⁵⁶ This reaction suffers similarly in yield as in the previously mentioned stannylidene method of obtaining 2,4-di-*O*-protected mannosides.



Scheme 4. Regioselective opening on benzylidene acetals to achieve 2,4-di-*O*-protection of mannose.

Multiple, higher yielding regioselective protection methods have been developed to access the 2,4-di-*O*-protection pattern.^{95, 107, 116} These methods rely on the increased reactivity of the primary 6-OH and equatorial 3-OH to achieve regioselective 3,6-di-*O*-protection without the use of toxic tin reagents. Large protecting groups can

increase regioselectivity, preferring reaction of the least hindered primary 6-OH, which helps constrain reaction of the neighbouring 4-OH. The preference of the 3-OH over the 2-OH is largely driven by the steric hindrance of the axial 2-OH and bulkier protecting groups will be more selective for the 3-OH. Trityl and bulky silyl groups have seen much success in this protection strategy,^{95, 108, 116, 117} and smaller groups like benzoates affording lesser regioselectivity.⁹⁴ Kong and coworkers have reported an elegant one-pot procedure to create 3,6-differentially protected mannosides in moderate yields.^{95, 117} In this protocol, allyl α -D-mannopyranoside is subjected to sequential addition of trityl chloride, *tert*-butyldimethylchlorosilane (TBDMSCl) and benzoyl chloride (BzCl) (Scheme 5). One column separation gave allyl 2,4-di-*O*-benzoyl-3-*O*-*tert*-butyldimethylsilyl-6-*O*-trityl- α -D-mannopyranoside in 79% yield. Such a synthon can be easily transformed into a free 3-, 6- or 3,6-di-*O*-acceptor by the selective or simultaneous removal of the trityl and silyl groups. The versatility and high yield of Kong's method makes it attractive for syntheses that comprise multiple core type structures.

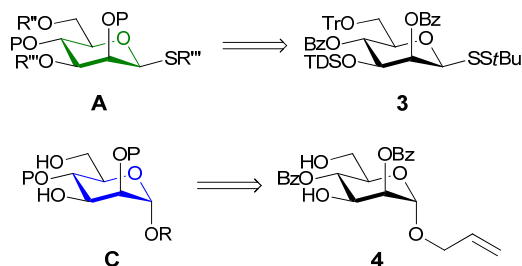


Scheme 5. Kong's one-pot method to produce a 3,6-differentially protected mannoside.¹¹⁷

The empirical rules that substantiate the regioselective 3,6-di-*O*-protection can also be applied to glycosylations on unprotected sugars, eliminating the need for a conventional multistep protection scheme. The regioselective outcome of glycosylations on minimally protected acceptors is still difficult to predict or to extrapolate trends as the donor chemistry, protecting groups, activating conditions, and anomeric configuration of the acceptor can all influence the reaction outcome.^{118, 119} Purification is also problematic as the byproducts with unwanted linkages may have similar retention times in flash chromatography. The glycosylation of mannose tetrols produces a mixture of 4,6-linked, 3,6-linked and 2,6-linked trimannosides that is able to be purified after the destruction of the 2,6-linked and 4,6-linked trisaccharides via periodate oxidation or following additional protection.^{89, 102} The yields using tetrol acceptors are quite low (17-33%), which demonstrates a lack of selectivity between the

2-, 3- and 4-hydroxyls. The selectivity can be significantly enhanced on acceptors where the 2-OH is locked as an orthoester, which is incompatible with a previously installed anomeric disulfide.⁹⁷

Of all these methods to produce the 3,6-branched mannosides, Kong's one-pot synthesis appears the most practical (Scheme 5), allowing for the efficient protection of both retrons **A** and **C**. This methodology accommodates 3,6-differential protection which enables retron **A** to be useful in the synthesis of both tetrasaccharide **1** and pentasaccharide **2**. Thus retrons **A** and **C** can be further refined to the building blocks **3** and **4**, respectively (Scheme 6).

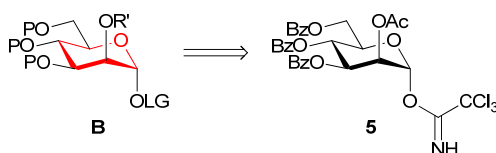


Scheme 6. Retrosynthetic elaboration of building blocks **A** and **C** to the synthetic targets **3** and **4**.

The order in which trisaccharide **1** and pentasaccharide **2** are assembled also warrants consideration. Tetrasaccharide **1** can be assembled in a step-wise linear fashion starting from the reducing terminus or through the addition of a trimannose Man α 1-2Man α 1-2Man donor to retron **A**. The later reaction has a reported lower yield and would require the synthesis of additional building blocks, leaving the iterative elongation more attractive.^{93, 104} Pentasaccharide **2** can be built via a 3,6-branched trimannoside donor and 1,3-linked disaccharide acceptor (Scheme 2, Retron **D** and **E**, respectively). While larger donors can lead to low glycosylation yields, syntheses using donors similar to donor **D** have proceeded in >65% yield.^{92, 117} Since glycosyl disulfides can be activated under similar conditions as thioglycosides, this discourages their use in this synthesis and trichloroacetimidates donors shall be used instead.

The elongation of the α -1,2-linked branches of **1** and **2** is a straightforward process guided by neighbouring group participation. The ester on the 2-OH should be removable after glycosylation to allow for the continued elongation of the D1 arm of tetrasaccharide **1**. Retron **5** (Scheme 7) has a well preceded synthetic

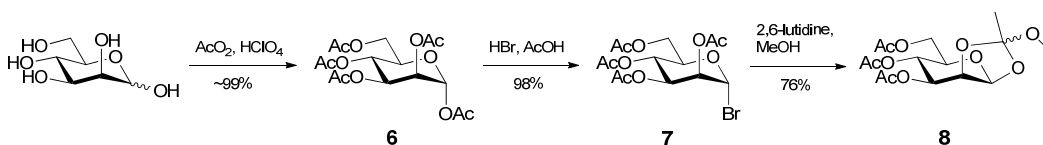
methodology¹²⁰ and allows for the selective removal of the 2-*O*-acetate in the presence of benzoates with HCl in methanol.^{121, 122} Removal of the acetate may become less selective as the number of competing benzoates grows with each glycosylation, although this is not seen in the literature.¹¹⁷ This could be avoided by the use of benzyl ethers which are inert to these conditions, but benzyl removal has limited compatibility with disulfides as previously discussed.¹²³ Thus, the donor building block **5** was chosen as the global mannosyl donor.



Scheme 7. Retrosynthetic elaboration of the donor building block **B** to imidate **5**.

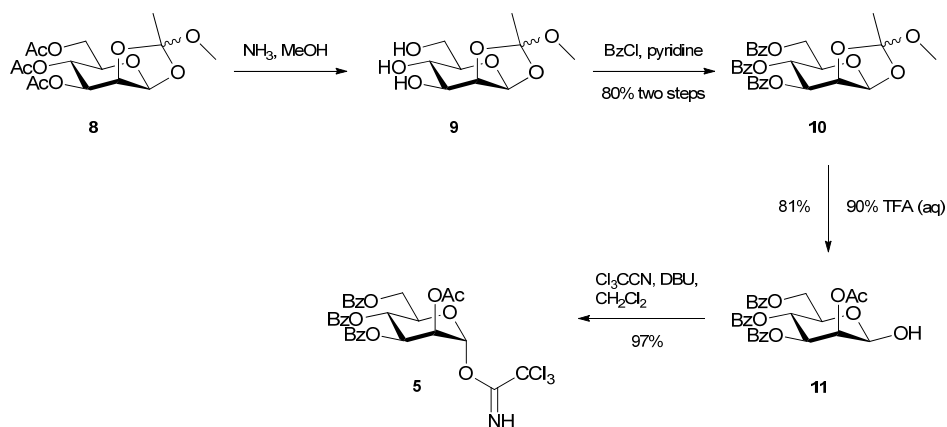
Synthesis of Mannosyl Donor Building Block **5**

The known mannose donor **5**¹²⁴ building block was synthesized using classical carbohydrate methodology. Synthesis started with the peracetylation of *D*-mannose, followed by reaction with HBr in acetic acid to form the mannosyl bromide **7** (Scheme 8).¹²⁵ Subsequent treatment of **7** with 2,6-lutidine produced the crystalline mannose the known 3,4,6-tri-*O*-acetyl-1,2,-*O*-(1-methoxyethylidene)- β -*D*-mannopyranose **8**.¹²⁶



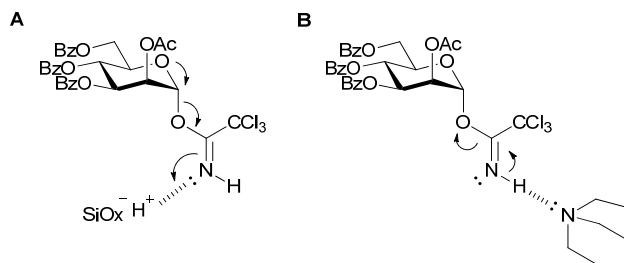
Scheme 8. Synthesis of triacetyl mannose orthoester **8**.

The acetates of the orthoester **8** were removed by ammonolysis and replaced with benzoates to yield the tribenzoate **10** (Scheme 9). The 1,2-orthoester was stereoselectively opened with 90% TFA to produce the reducing sugar **11** as the only product.¹²⁷ Hemiacetal **11** was treated with trichloroacetoneitrile to form imidate donor **5**.^{25, 117}



Scheme 9. Synthesis of mannosyl donor building block **5**.

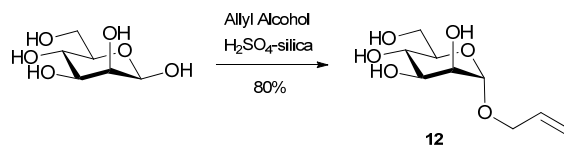
Purification of glycosyl imidates via silica chromatography is usually performed with trace amounts of TEA added to the solvent system in order to neutralize the slight acidity of silica gel which would otherwise activate and degrade the imidate on the column. Surprisingly, the mannosyl imidate **5** quantitatively degraded to the free hydroxyl intermediate **11** when purified with TEA. Purification on silica without TEA yielded the imidate **5** without any degradation. The electron-withdrawing effects of the benzoyl and acetyl esters could reduce the electron density of the imidate, producing the two-fold effect of reducing the nucleophilicity of the imidate nitrogen, and increasing the acidity of the imidate hydrogen. This would explain the stability of the imidate **5** towards silica gel and the reversion to the free hydroxyl intermediate **11** under basic conditions (Scheme 10). The stability of donor **5** is further exemplified by its observed lack of degradation after storage at room temperature over a three month period. The disarming effect of electron withdrawing groups on glycosyl donors is well documented and even exploited in selectively activated glycosylation reactions involving multiple donors.^{128, 129}



Scheme 10. The disarming effects of the ester protecting groups reduce the susceptibility of donor **5** towards acidic activation and trichloroacetamide formation (A) while increasing its susceptibility to basic degradation and reversion to trichloroacetoneitrile (B).

Synthesis of 3,6-Dihydroxy Mannoside Building Block 4

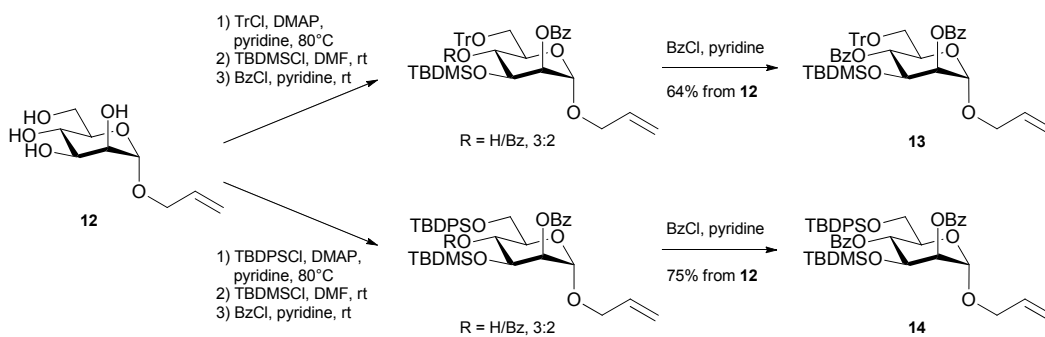
The 3,6-dihydroxy mannoside building block **4**¹¹⁷ was synthesized by following the one-pot method of Kong and coworkers (Scheme 5). The allyl α -D-mannopyranoside **12**¹³⁰ was prepared using the Fischer glycosylation of D-mannopyranose in allyl alcohol utilizing a H₂SO₄-silica catalyst (Scheme 11).¹³¹ Immobilization of sulfuric acid on silica gel allows for the easy removal of the acid catalyst which is problematic with strong mineral acids typically used in the Fischer glycosylation.



Scheme 11. Synthesis of allyl mannoside **12**.

Mannoside **12** was then sequentially treated with TrCl and TBDMSCl to regioselectively protect O6 and O3, respectively, followed by BzCl to protect the remaining 2- and 4-hydroxyls (Scheme 12). Despite faithfully following Kong's one-pot procedure, tetrol **12** gave a mixture of the fully benzoylated product **13** and a 2-O-monobenzoylated product. Removal of the pyridinium salts and reagents via a quick chromatographic purification and repeating the benzoylation produced the 2,4-O-dibenzoylated product **13** in 64% overall yield. A parallel one-pot synthesis was also performed where TrCl was replaced with TBDPSCl to investigate any change in reactivity of the recalcitrant 4-OH towards benzoylation. The outcome was the same, and the stalled 4-O-benzoylation could again be recuperated by first cleaning up the reaction mixture before performing the benzoylation, to produce the TBDPS analogue **14** in 75%

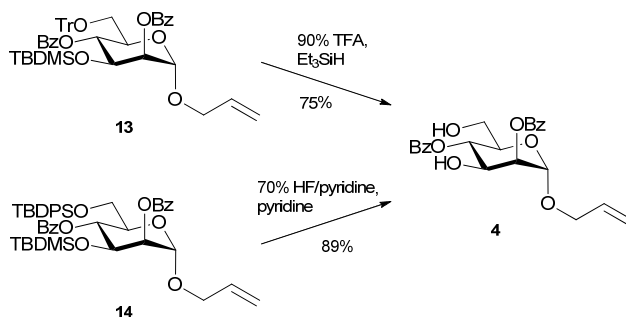
yield. Overall, it was better to purify the reaction intermediate before the addition of BzCl to remove the excess pyridinium salts to ensure a successful benzoylation.



Scheme 12. Attempted one-pot synthesis of the 2,4-di-O-benzoylated intermediates **13** and **14**.

The 2,4-benzoylated product **13** was easier to work with than its TBPDS counterpart **14**, as it is a solid that was easily recrystallized in hexanes, whereas product **14** was a syrup that was difficult to purify.

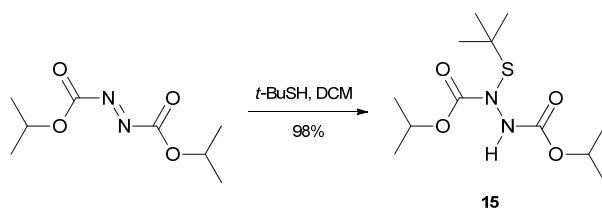
The 3,6-dihydroxy mannoside acceptor **4** was obtained through the simultaneous deprotection of the trityl and/or silyl groups of **13** and **14**, but again requiring deviation from Kong's methodology (Scheme 13). When **13** was treated with 90% TFA (aq), acceptor **4** was obtained *in situ*, but then was quantitatively converted to a 6-O-trityl product upon concentration. This is caused by the trityl cation reacting with the 6-OH as the acid is removed during concentration. The re-tritylation was circumvented by the addition of the cation scavenger Et₃SiH to the reaction mixture,¹³² to yield **4** in 75% yield. In essence, the inclusion or omission of Et₃SiH in the deprotection of **4** can provide access to a 3,6-OH or 3-OH acceptor, respectively. The two silyl protecting groups of **14** were removed with treatment by HF/pyridine (70% HF w/w) overnight to produce **4** in 89% yield. It was observed that the TBDPS group could be selectively removed if the concentration of HF was kept below ~3mM, imparting a route to a 6-OH acceptor. Thus, the 2,4-dibenzoyl intermediates **13** and **14** offer alternative routes to the selectively deprotected 3-OH or 6-OH analogues in addition to the 3,6-di-OH analogue **4**.



Scheme 13. Synthesis of 3,6-dihydroxy building block 4.

Synthesis of Mannosyl Disulfide Building Block 3

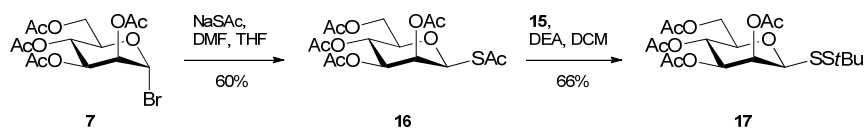
The anomeric disulfide was first installed utilizing the azodicarboxylate transfer reagent **15**, which is useful for producing unsymmetrical disulfides under mild conditions with good yields.^{77, 133} Diisopropyl-*N*-(*tert*-butylsulfanyl)hydrazodicarboxylate **15** was prepared by the reaction of DIAD and 2-methyl-2-propanethiol in DCM (Scheme 14). The reaction proceeded slowly at room temperature and was only nominally increased upon gentle heating (azodicarboxylates may explode upon heating), requiring a week to go to completion. The reduced reaction rate is certainly due to the steric bulk of both the *tert*-butyl and isopropyl groups, as literature reactions between smaller thiols and the less sterically hindered DEAD reagent go to completion with 2-24 hours.¹³³



Scheme 14. Preparation of diisopropyl-*N*-(*tert*-butylsulfanyl)hydrazodicarboxylate **15**.

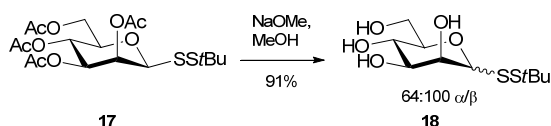
The 1-thio- β -mannopyranoside derivative **16**^{55, 56} was prepared by the nucleophilic displacement of the anomeric α -bromide of the peracetylated mannopyranosyl bromide **7** with sodium thioacetate (Scheme 15). The reaction proceeded smoothly with a 60% isolated yield on a 65g scale after crude purification via flash chromatography and a final purification by recrystallization. The small amount of α -anomer that formed was difficult to remove via chromatography but was entirely

separable upon recrystallization. The β -anomer crystallizes as a white solid while the α -anomer remains in solution, forming a colorless syrup upon concentration.



Scheme 15. Synthesis of mercapto-*tert*-butyl 1-thio-mannoside **17**.

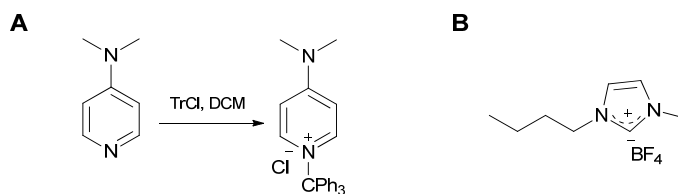
The anomeric *S*-acetate of **16** was removed and reprotected as a *tert*-butyl disulfide by treatment with DEA and reagent **15** in one-pot to produce intermediate **17** in 66% yield as a colorless syrup. Little α -anomer was observed, owing to anomeric thiol's resistance to mutarotation.^{38, 61} A diisopropyl hydrazodicarboxylate byproduct was difficult to remove via chromatography, but could be separated from the product by recrystallization, although not completely. Removal of the acetates under Zemplén conditions generated a 64:100 α/β mixture of the deprotected monosaccharide **18**. The observed anomerization during methanolysis was quite surprising. While anomeric disulfides are not new, most are synthesized using glucose or α -mannose analogues and have reported high yields after having undergone methanolysis, with no note of anomerization.^{77, 134-136} The two anomeric products were not easily separable via either chromatography or recrystallization and were carried through to the next steps as a mixture with the hope that separation of a protected intermediate may be more feasible.



Scheme 16. Deacetylation of mannosides **17**.

The stereochemistry of the two anomers of **18** was determined via multiple standard NMR experiments. The anomeric configuration for mannopyranosides is more difficult than for gluco or galactopyranosides where the proton $^3J_{1,2}$ coupling constant is almost always indicative of α or β configuration. For mannopyranosides, $^3J_{1,2}$ gives values of ~ 0 -2 Hz for either anomer since the H1-H2 dihedral angle is $\sim 60^\circ$ in either case.¹³⁷ However, in ^1H NMR the chemical shift of H3 and H5 is often indicative of anomeric configuration, as an axial orientated heteroatom at C1 is able electrostatically

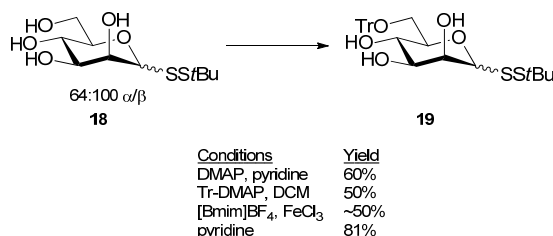
deshield H3 and H5, creating a downfield shift. Chemical shift of the anomeric H1 can also reveal insight towards its orientation, as diamagnetic anisotropy of the C-C and C-O bonds within the ring deshield equatorial orientated hydrogens relative to axial orientated hydrogens.^{138, 139} The intra-ring NOE cross signals between H1 and H3/5 is also helpful in determining the anomeric configuration. Lastly, one-bond $^1J_{C1,H1}$ heteronuclear coupling constants with values above 165 Hz are largely indicative of an axially orientated glycosidic bond, and values below are indicative of a equatorial glycosidic bond.¹⁴⁰ It is important to note that all these NMR elucidations provide general guidelines for determining anomeric configuration and the entire data set should be viewed as whole, as perturbations to ring conformation and complex intramolecular interactions can produce misleading results. Sufficient NMR data will be noted for synthetic targets where confirming the anomeric configuration(s) is important, such as after glycosylation reactions.



Scheme 17. Structures of reagents explored to increase tritylation yield. **A** Formation of 4-dimethylamino-*N*-triphenylmethylpyridinium chloride reagent.¹⁴¹ **B** Structure of 1-butyl-3-methylimidazolium tetrafluoroborate [bmim]BF₄.

The anomeric mixture of disulfide **18** was carried through a similar protection scheme as used for the synthesis of the building block **4** (Scheme 12). The pseudo one-pot protection method was abandoned as the potential to separate the two anomers needed to be investigated after each protection step. Reaction of **18** with TrCl was sluggish with unreliable yields around 50%. Other methods for the preparation of trityl ethers were explored. Tritylation reaction times and yield have been reported to be improved using the electrophilic salt 4-dimethylamino-*N*-triphenylmethylpyridinium chloride (Tr-DMAP),¹⁴¹ prepared from TrCl and DMAP (Scheme 17A).^{142, 143} Reaction of **18** with the TR-DMAP displayed little improvement to yield. The imidazolium-based ionic liquid [bmim]BF₄ (Scheme 17B) was evaluated as a solvent for the tritylation of **18**, as it has been recently shown to increase the yields and rate of formation of trityl ethers with an FeCl₃ catalyst.¹⁴⁴ The catalytic effect of the ionic liquid purported to be due to

the stabilization of the trityl cation formed in the reaction of the TrCl with FeCl₃. Reaction in [bmim]BF₄ gave poor yields, conceivably due to the poor observed solubility of **18** (Scheme 18). Since this reaction was performed, the solubility of various carbohydrates in ionic liquids have been reviewed,¹⁴⁵ revealing a trend of poor solubility for deprotected monosaccharides in ionic liquids with BF₄ anions.

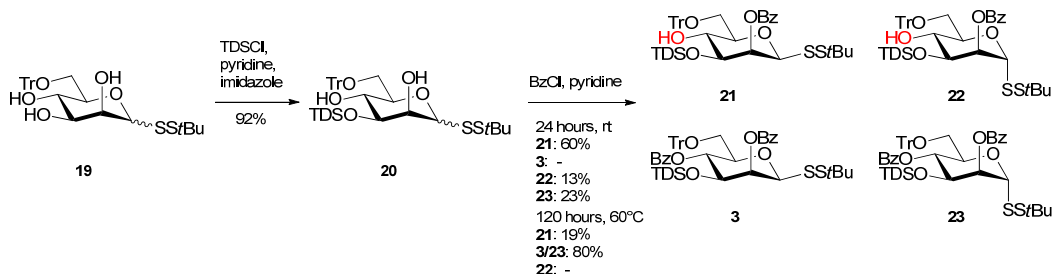


Scheme 18. Comparison of conditions explored to increase the yield of trityl ether formation of mannosyl disulfide **19**.

Ultimately, it was found that the best yield of **19** was achieved in 81% using freshly recrystallized TrCl,¹⁴⁶ although this yield was difficult to reproduce. Under all explored conditions it proved impossible to drive the reaction to completion and unconverted disulfide starting material **18** would be completely recovered. In sharp contrast, the *O*-allyl mannoside **12** was tritylated quantitatively without the need for recrystallized TrCl (Scheme 12). Tritylation did not aid the separation of the α - and β -anomers and **19** was carried onto the next step as an anomeric mixture.

Intermediate **19** was regioselectively silylated using TDSCl in pyridine to afford the 3-*O*-TDS product **20** in 92% yield (Scheme 19). The mixture of anomers was not much more practical to separate after silylation and subjected to benzylation as an α,β -mixture. When **20** was reacted with BzCl in pyridine for 24 hours, a mixture of the β -2-*O*-benzoyl **21**, α -2-*O*-benzoyl **22** and α -2,4-di-*O*-benzoyl **23** products was formed (Scheme 19). The absence of a β -4-*O*-benzylation product (**3**) was surprising as the α -anomer was able to be benzyolated at this position. With all the functionalities of compound **20** are identical except for the anomeric configuration, it must be the orientation of the anomeric center itself that is influencing the reactivity of *O*4. It is known that the 4-OH is the least reactive hydroxyl on the carbohydrate ring, which is further compounded in intermediate **20** by the flanking bulky trityl and silyl groups on *O*6 and *O*3. The anomeric *tert*-butyl disulfide is bulky itself, and in a β -configuration it

could sterically restrict the orientation of the neighbouring 2-*O*-benzoate to occupy space around *O*3, which in turn would force the bulky 3-*O*-silyl group to the unoccupied area surrounding the 4-OH. In essence, the β -disulfide could sterically buttress the neighbouring protecting groups all the way around the sugar ring to shut down reactivity at the 4-OH, which is relieved in an α -configuration.

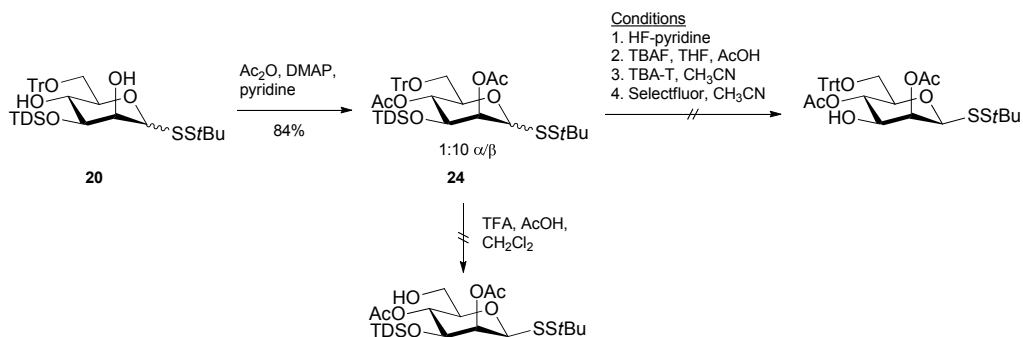


Scheme 19. Silylation and benzylation of intermediate **19** to produce the 3,6-differentially protected building block **3**.

The fully benzoylated β -anomer of **20** was eventually achieved by refluxing **20** with BzCl in pyridine for 5 days, although the reaction did not go to completion. A catalytic amount of 1-methylimidazole was indispensable, having been previously found to aid acylation reactions of sterically hindered alcohols.¹⁴⁷ The di-*O*-benzoylated β -product **3** was difficult to separate from α -anomer **23**. While it would have been technically feasible to separate the incomplete benzylation β -product **21** from the fully benzoylated α -product **23**, and then benzoylate **21** using the optimized conditions to cleanly produce the desired 2,4-di-*O*-benzoyl building block **3**, this entire benzylation procedure is largely impractical.

Acetates were explored as an alternative protecting group to benzoates, as they are sterically smaller and may be able to more efficiently protect the difficult 4-hydroxyl. Intermediate **20** was fully acetylated upon treatment with acetic anhydride in pyridine over 20 hours (Scheme 20). The α,β -anomers of product **24** could only be partially separated by chromatography to afford a 1:10 α/β ratio, as residual α -anomer was exceedingly difficult to remove. There was concern that removal of the trityl or silyl group could lead to migration of the acetates, but the ease of installation of the acetates prompted further investigation. Unfortunately, these concerns were warranted as the common fluoride-based desilylation reagents HF-pyridine, TBAF, TBA-T

and Selectfluor all produced complex mixtures (Scheme 20). Removal of the trityl group under acidic conditions produced the same result. NMR analysis of the crude isolates after chromatography confirmed the migration of acetates. Benzoylation therefore remains the protecting group of choice due to its resistance to migration.

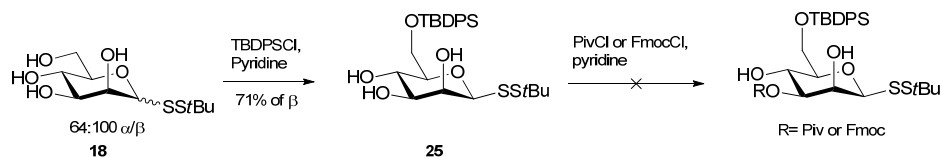


Scheme 20. Synthesis and investigation of the acetylated analogue of building block 3.

At this point, the protection strategy of anomeric disulfide **18** was reevaluated to improve three problematic areas:

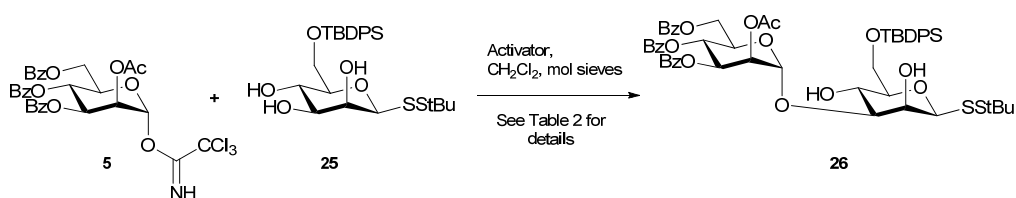
- Poorly yielding incomplete tritylation of **18**
- Reduced reactivity of 4-OH towards benzoylation due to bulky 3-O-silyl protection
- Difficulty isolating the β -anomer following the protection steps

A new protection strategy was therefore explored, starting with the substitution of the trityl group for the selective protection of 6-OH with the bulky silyl TBDPS group, as studied in the synthesis of building block **4** (Scheme 12). It was found that TBDPSCI would fully react with **18**, producing the 6-O-TBDPS product with a 94% yield for the α,β -mixture (Scheme 21). It was noted during chromatographic purification that two forms of product would collect at the top of the test tube fractions as the solvent evaporated – a white powdery solid and a translucent waxy solid. Recrystallization of the pooled fractions with a heptane:EtOAc system allowed for the separation of the α - and β -anomers. The β -product **25** recrystallized as a white powder in 71% recovery from the β -portion of starting material **18**, while the α -product remained in the mother liquor. The TBDPS group solved both the low yielding 6-OH protection and the α,β -separation problems.



Scheme 21. Regioselective protection of intermediate **18**.

A smaller protecting group for the selective protection of the 3-OH was next explored. The protecting group requires significant bulk in order to be selective for the 3-OH, but should be less bulky than TDS in order to facilitate 4-OH benzylation without being sterically shut down. The pivaloyl (Piv) and Fmoc protecting groups both have the medium steric bulk and were evaluated for the regioselectivity when reacted with triol **25**. Both Piv and Fmoc produced complex mixtures upon reaction with **25**, as indicated by TLC, and were not isolated.



Scheme 22. Regioselective glycosylation of triol **25** to produce disaccharide **26**.

As a last resort, **25** was glycosylated using donor **5** to see if there was any regioselectivity with the glycosylation (Scheme 22). Preliminary glycosylations revealed a preference for glycosidic bond formation on the 3-OH of the donor (Table 3, entry 1), confirmed by the heteronuclear coupling between C-1^b and H-3^a. Various glycosylation conditions were explored and a few trends were noted. The glycosylation was very selective for the 3-OH with only trace amounts of the 2-O-linked and 4-O-linked being recovered. The acceptor starting material **25** was recovered under all explored conditions, even when up to two equivalents of donor **5** were used (Table 3, entry 3 & 4). In these cases, the donor was found to react with the excess trichloroacetamide in the reaction mixture, forming an *N*-linked trichloroacetamide. This may explain why the glycosylation cannot be forced to completion with additional donor, as the trichloroacetamide byproduct competes with the acceptor for glycosylation and as the reaction proceeds, the free trichloroacetamide becomes more abundant than the acceptor. There appeared to be a temperature dependence for the formation of the *N*-

linked trichloroacetamide as more was formed at room temperature than at -20 °C, as monitored by TLC (Table 3, entries 3 & 4). Unreacted donor could also be found at lower temperatures, which is not surprising as the stability of this dis-armed donor has already been encountered. The inverse glycosylation procedure,¹⁴⁸ where the donor is slowly added to a premixed solution of acceptor and activator, provided the best yield (Table 3, entry 6).

Table 3. Glycosylation conditions explored for the coupling of donor 5 and acceptor 25.

Entry	Method	Donor:Acceptor Ratio	Activator	Temp	% Yield 26
1	Standard	1:2	TMSOTf	rt	62%
2	Standard	1:1.5 ^a	TMSOTf	0 °C	52%
3	Inverse	1.5:1 ^b	BF ₃ OEt ₂	rt	~43% ^c
4	Inverse	1.5:1 ^b	BF ₃ OEt ₂	-20 °C	~43% ^c
5	Standard	1:1	BF ₃ OEt ₂	rt	67%
6	Inverse	1:1	BF ₃ OEt ₂	0 °C	83%

^a 0.5 equiv. donor 5 added after 1.5 hours

^b 0.5 equiv. donor added after 3 hours

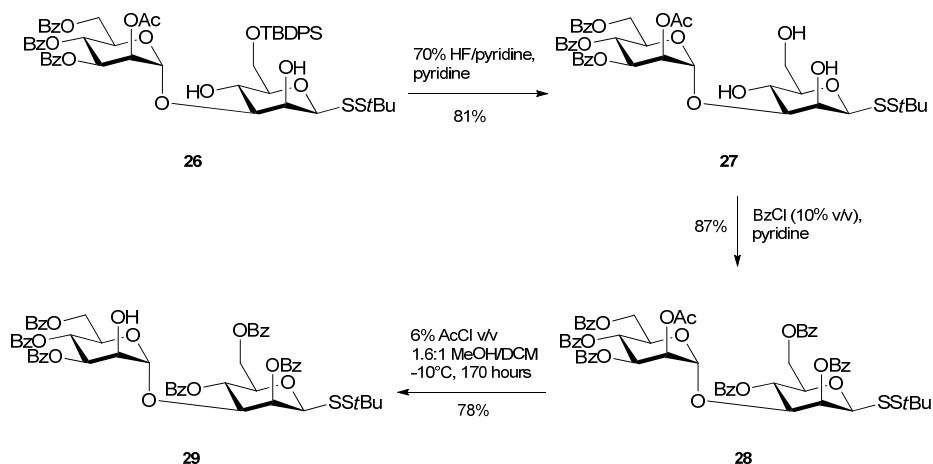
^c Entries 3 and 4 combined for purification

Disaccharide **26** can be utilized in the synthesis of both tetrasaccharide **1** and pentasaccharide **2**. Following the protection of the remaining hydroxyls of **26**, the 2'-*O*-acetate selectively removed to form the acceptor for the synthesis of tetrasaccharide **1**. If the TBDPS group is removed instead of the acetate, the donor intermediate for the synthesis of the pentasaccharide **2** would be formed.

Synthesis of Tetrasaccharide 32

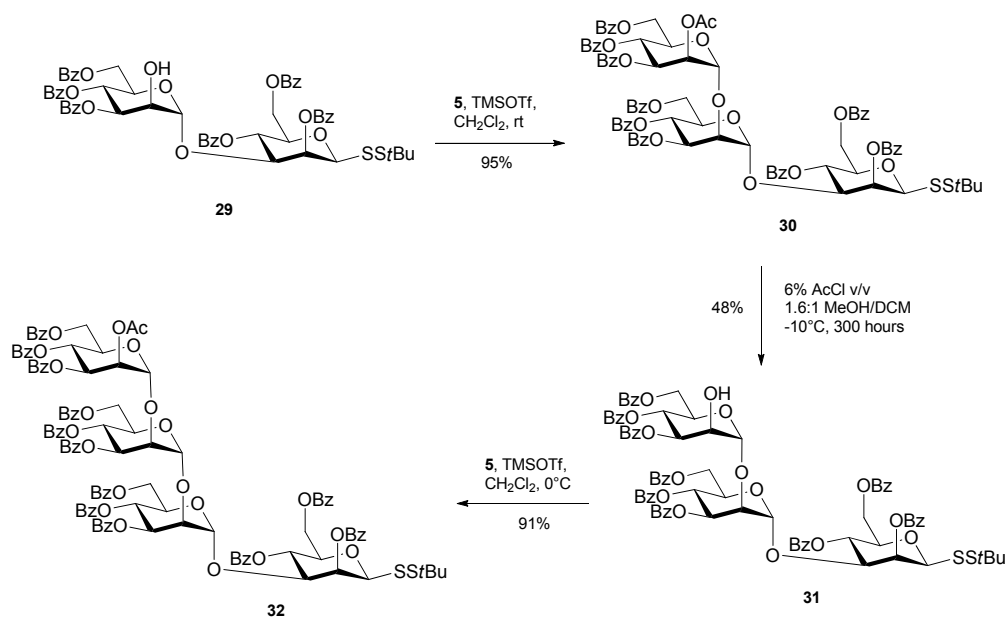
The assembly of the tetrasaccharide was envisioned to involve an iterative 2-*O*-glycosylation strategy using donor **5**, where the participating 2-*O*-acetate group of the donor would be selectively removed after glycosylation to create a selectively protected acceptor for the next glycosylation. The initial acceptor **29** was created from the previously synthesized α -1,3 linked disaccharide **26** (Scheme 23). The silyl group was removed with HF in pyridine to produce the triol **27** in 81% yield. Perbenzoylation required an excess of BzCl (~35 equiv.) at a concentration of 10% v/v to drive the

benzoylation of the unreactive 4-OH. The 2''-O-acetate of **28** was selectively removed by methanolic HCl, prepared by the addition of acetyl chloride to dry methanol.¹²¹ The reaction was monitored by TLC and the conditions adjusted to minimize the accumulation of low R_f debenzoylation side-products. A concentration of 6% AcCl in methanol/DCM at -10 °C was found to be ideal to maintain the selective removal of acetates in good yield (78%), although the reaction time was significantly increased to 170 hours. Starting material **28** was largely recoverable from the small amounts of 2-O- and 4-O-glycosylation products.



Scheme 23. Synthesis of the disaccharide acceptor **29**.

The protected tetrasaccharide **32** was synthesized as outlined in Scheme 24. Glycosylation of 2''-OH disaccharide **29** by donor **5** was performed with TMSOTf activation in CH_2Cl_2 at room temperature to produce the desired trisaccharide **30** in excellent 95% yield. The α -mannopyranosyl stereochemistry of the terminal mannose was confirmed by the $^1J_{\text{C}_1,\text{H}}$ coupling of 171 Hz. The selective deacetylation of **30** with HCl/MeOH, as described above, proceeded sluggishly to yield trisaccharide **31** in only 48% after 300 hours. While the deacetylation could have been optimized by exploring higher temperatures with careful monitoring for debenzoylation side-products, minimizing the degradation of the valuable trisaccharide was the overall goal and was achieved. Very little debenzoylation occurred and nearly quantitative yield of unreacted starting material was recovered. The trisaccharide acceptor **31** was glycosylated by donor **5** to produce the protected target tetrasaccharide **32** in 91% yield. The $^1J_{\text{C}_1''',\text{H}_1''}$ coupling of 175 Hz confirmed the α -mannosylation.

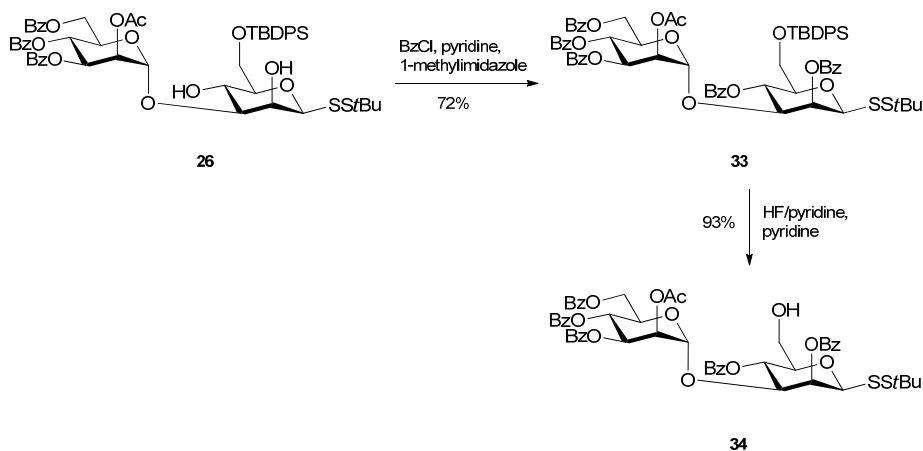


Scheme 24. Synthesis of protected tetrasaccharide analogue **32**.

Optimization of the deacetylation conditions was deemed impractical and was not attempted. Debenzoylation becomes more of a problem with larger oligomers, as there are simply more benzoates that could be removed. A comparison of various literature methods to remove acetates in the presence of benzoates suggests that the method of choice is HCl/MeOH. Notably, Nikolaev and coworkers used methanolic HCl in their synthesis of similar Man α 1 \rightarrow 2Man oligomers and were able to achieve selective deacetylation of a benzoylated di- and trisaccharide in 82% and 85% yield, although reaction times and temperature were not reported.¹²⁴ Other chemoselective reagents have been used to remove *O*-acetates in the presence of *O*-benzoates, such as HBF₄¹⁴⁹ or magnesium methoxide¹⁵⁰ in methanol, and could be explored in the future.

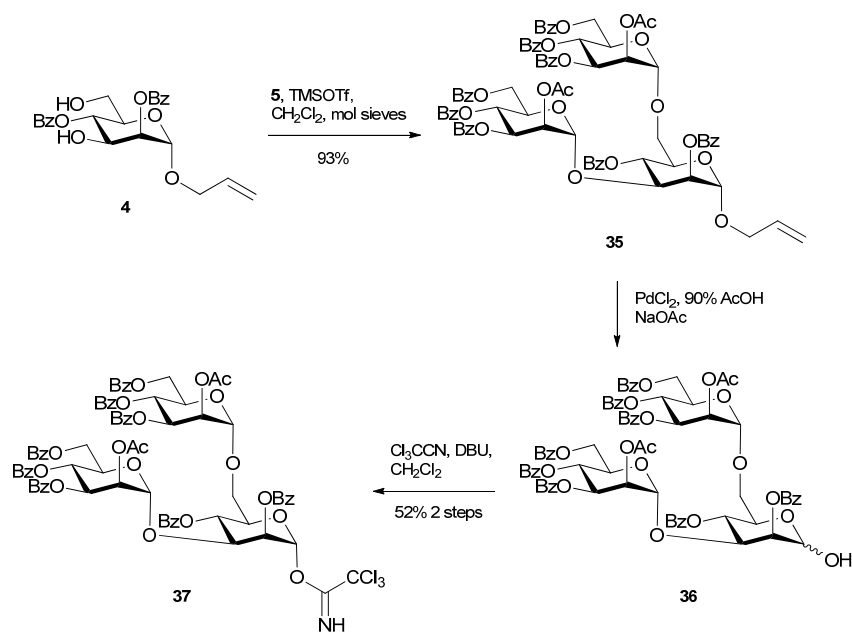
Synthesis of Pentasaccharide **38**

Pentasaccharide **38** was synthesized utilizing a 3 + 2 glycosylation strategy. The disaccharide acceptor **34** was prepared as outlined in Scheme 25. Disaccharide **26** was perbenzoylated, aided by a catalytic amount of 1-methylimidazole to facilitate 4-*O*-benzoylation. The benzoylated product **33** was desilylated by treatment with HF in pyridine to produce the 6-OH disaccharide acceptor **34** in 93% yield.



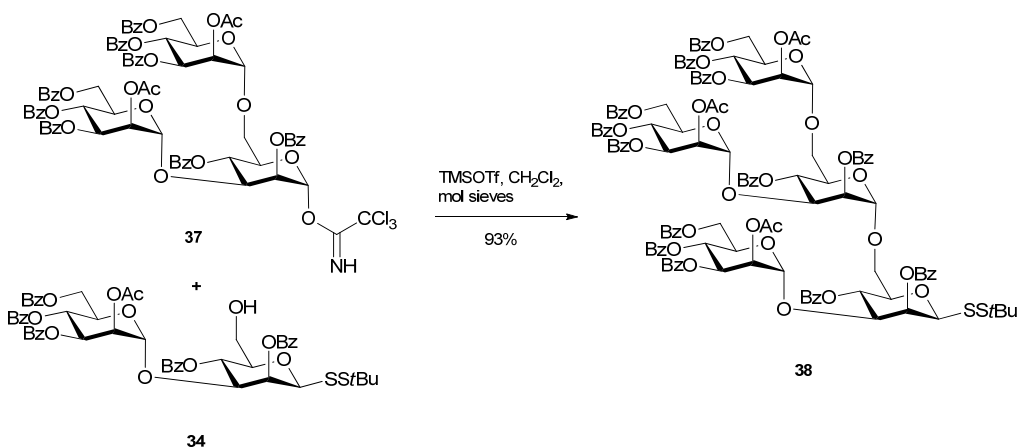
Scheme 25. Synthesis of acceptor disaccharide **34**.

The trisaccharide donor **37** was prepared coupling diol **4** with imidate **5** using TMSOTf as catalyst to give trisaccharide **35**¹¹⁷ in 93% yield (Scheme 26). The newly formed α -1,3 and α -1,6 glycosidic linkages were confirmed by the $^1J_{C1,H1}$ heteronuclear coupling constants of 171 and 175 Hz and position of the linkages by the $^3J_{H1,C3}$ and $^3J_{H1,C6}$ correlations. Deallylation of **35** with PdCl₂ and NaOAc in aqueous acetic acid¹⁵¹ produced a mixture of α - and β -hemiacetal **36** and a 2-oxopropyl side-product. The formation of a Wacker ketone byproduct during anomeric deallylation has been previously reported.¹⁵²⁻¹⁵⁴ The hemiacetal and side-product were difficult to separate from each other via chromatography and were carried onto the next step for separation. Reaction of **36** with trichloroacetonitrile furnished the trisaccharide donor **37** in 52% yield from **35**. In comparison, Kong and coworkers reported an 85% combined yield for these two steps when performed on a nearly identical trisaccharide.¹¹⁷



Scheme 26. Synthesis of 3,6-branched trisaccharide donor **37**.

The pentasaccharide **38** was obtained by the glycosylation of **34** with **37** in 93% yield (Scheme 27). The α -mannopyranoside stereochemistry of the newly formed linkage was confirmed by the heteronuclear $^1J_{C1,H1}$ coupling constant of 175 Hz.



Scheme 27. Glycosylation of disaccharide **34** to form the pentasaccharide target **38**.

Deprotection of Tetrasaccharide **32** and Pentasaccharide **38**

Two steps are required for the deprotection of **32** and **38**: deacylation and disulfide reduction. The order of the deprotection steps was evaluated on monosaccharides **17** and **18** in preparation for the deprotection of oligomers **32** and **38**.

In order to avoid mutarotation and preserve the β -stereochemistry it was reasoned that the cleavage of the disulfide would benefit from being performed after transesterification. Thus, various reducing conditions were investigated on the deacylated monosaccharide **18** as listed in Table 4.

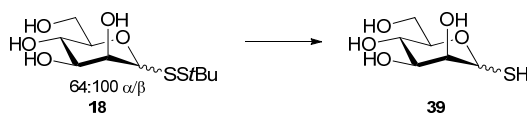


Table 4. Conditions investigated for the disulfide reduction of **18** to form the free thiol **39**.

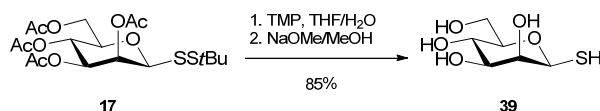
Entry	Solvent	Reagent	Equiv.	Temp	Time	Notes
1	H ₂ O	MESNA	10	rt	24 hrs	Incomplete rxn
2	H ₂ O	2-mercaptoethanol	200	rt	85 hrs	No rxn
3	H ₂ O	TCEP	2	rt	1 hr	Incomplete rxn
4	H ₂ O	TCEP	8.5	rt	1 hr	Complete rxn
5	H ₂ O pH 7.5 ^a	TCEP	2	rt	1 hr	Complete rxn
6	DMF	TCEP	2	rt	1 hr	Incomplete rxn
7	H ₂ O	TCEP	2	90 °C	15 min	Complete rxn
8	H ₂ O pH 7.5 ^a	TCEP-gel	2	rt	1 hr	Incomplete rxn
9	H ₂ O	TMP	4	rt	27 hrs	Incomplete rxn
10	H ₂ O pH 7.5 ^a	TMP	8	rt	1 hr	Complete rxn

^a 0.1 M NaHPO₄ pH 7.50 buffered solution

The most ideal conditions for disulfide reduction were achieved with 8 equivalents of trimethylphosphine (TMP) in pH 7.5 aqueous buffer as monitored by TLC and mass spectrometry (Table 4, Entry 10). Sodium 2-sulfanylethanesulfonate (MESNA) and 2-mercaptoethanol gave incomplete or no reaction (Entries 1 & 2). The bulk of the optimization was performed using tris(2-carboxyethyl)phosphine (TCEP) which revealed the preference for basic conditions (Entries 3 & 5) and the need for 8 or more equivalents of reducing agent at room temperature (Entries 3 & 4). Removing TCEP from product **29** was problematic, and an agarose-immobilized TCEP reagent, which facilitates the removal of the reducing agent, was found to be too costly to use in the excess required to reduce disulfide bonds on scales greater than μg amounts. TMP

performed as well as TCEP under the optimized conditions and was easier to remove under vacuum due to its high volatility.^{††}

Although indicated pure by TLC during reaction, the anomeric thiol **39** degraded upon concentration and lyophilization and gave off a strong hydrogen sulfide smell. It has been observed in the literature that desulfurization can occur during reduction of disulfide bonds with phosphines, especially at higher pH.¹⁵⁵ Neutralizing the reaction with AcOH before lyophilization decreased degradation, but did not eliminate it. The attempted chromatographic purification of the unprotected monosaccharide **39** failed at removing all TMPO, as revealed by NMR, and did not stop the degradation of the product. We conclude that the excess of TMP or TMPO causes decomposition of deprotected 1-thio-mannoses, presumably through desulfurization.



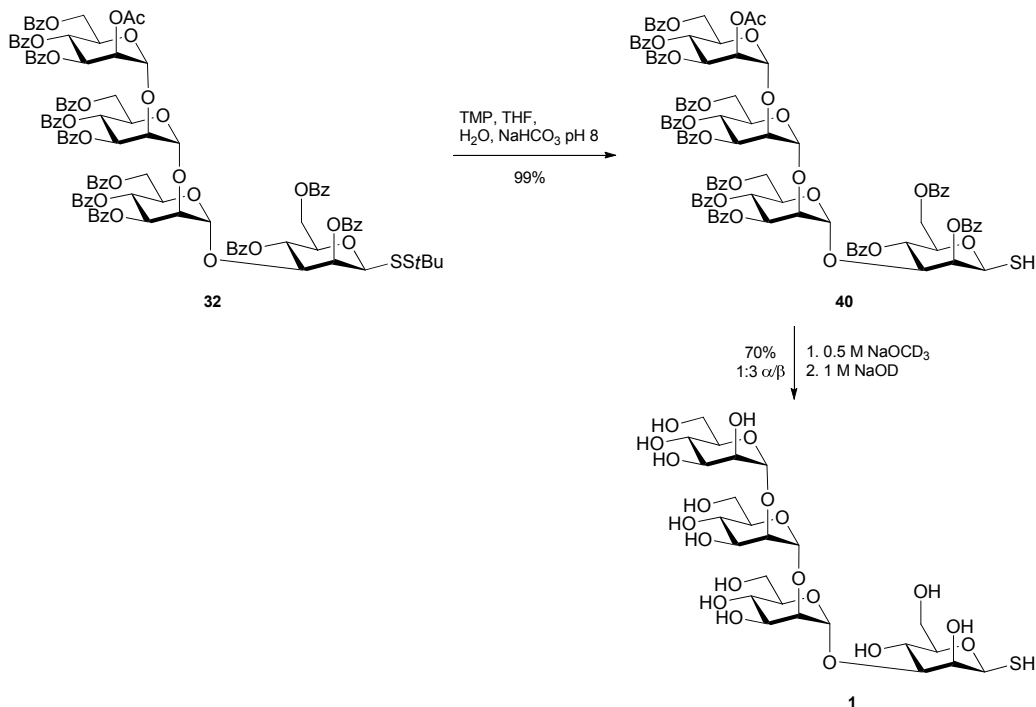
Scheme 28. Reduction and deacetylation of **17** to produce 1-thio- β -mannopyranose **39**.

Reversing the deprotection steps eliminated degradation problems and the anomeric stereochemistry remained intact throughout both procedures (Scheme 28). The reducing agent was easily removed from the acetylated 1-thio-mannose intermediate via chromatography. We therefore used this deprotection methodology for tetrasaccharide **32** and pentasaccharide **38**.

Tetrasaccharide **32** was cleanly converted to free thiol **40** using the described methodology with the complete preservation of the β -stereochemistry (Scheme 29). The subsequent Zemplén deacylation was performed in deuterated solvents in order to monitor the reaction progress via ^1H NMR. Anomerization was observed and the formation of the unwanted α -anomer was found to be more dependant on time than pH, whereas the deacylation was more dependant on pH than reaction time. Thus, the formation of the α -anomer could be kept to the minimum by increasing the amount of base. The 2-*O*-benzoate was extremely resistant to treatment with methoxide, even at 1 M concentrations. The troublesome benzoate was removed by further reaction of the

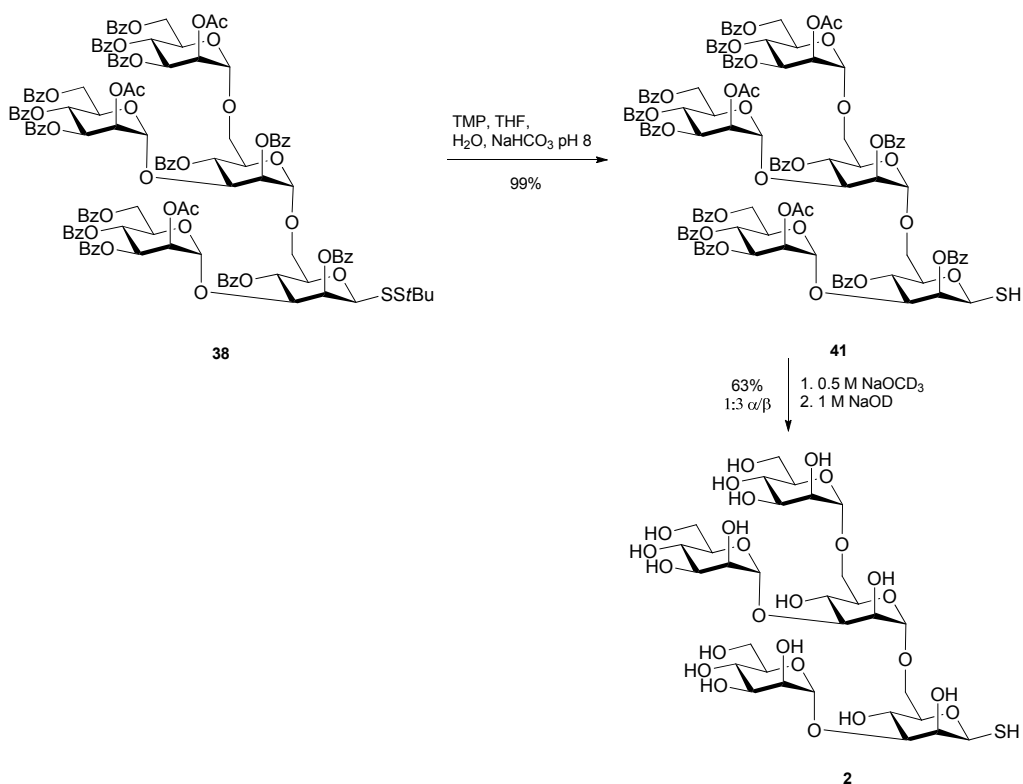
^{††} Trimethylphosphine has a boiling point of 38-39 °C and a vapor pressure of 49.9 kPa @ 20 °C.

worked up mono-benzoylated (*or monobenzoylated?*) intermediate with 1 M NaOD to produce the fully deprotected tetrasaccharide in 70% yield as a 1:3 α/β anomeric mixture. The mixture could be cleanly separated via HPLC to produce tetrasaccharide **1** as the beta-anomer, as verified by anomeric $^1J_{C1,H1}$ heteronuclear coupling constant of 153 Hz.



Scheme 29. Deprotection of tetrasaccharide **32** to yield the target tetrasaccharide **1**.

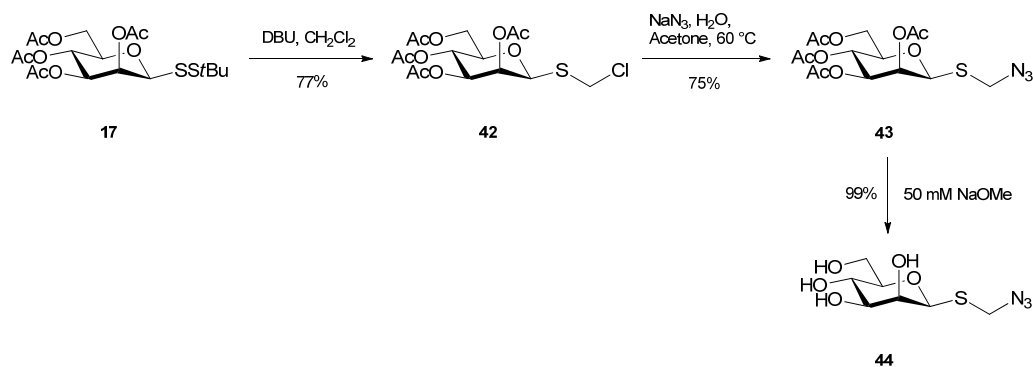
Pentasaccharide **38** was deprotected analogously to tetrasaccharide **32** as outlined in Scheme 30. Treatment with TMP produced the free thiol **41** in quantitative yield. The acyl protecting groups were removed with deuterated methoxide and hydroxide to produce the fully deprotected pentasaccharide in 63% yield with a 1:3 α/β ratio. The β -anomer was acquiesced via HPLC and pentasaccharide **2** verified by the anomeric $^1J_{C1,H1}$ heteronuclear coupling constant of 158 Hz.



Scheme 30. Deprotection of pentasaccharide **38** to yield the target pentasaccharide **2**.

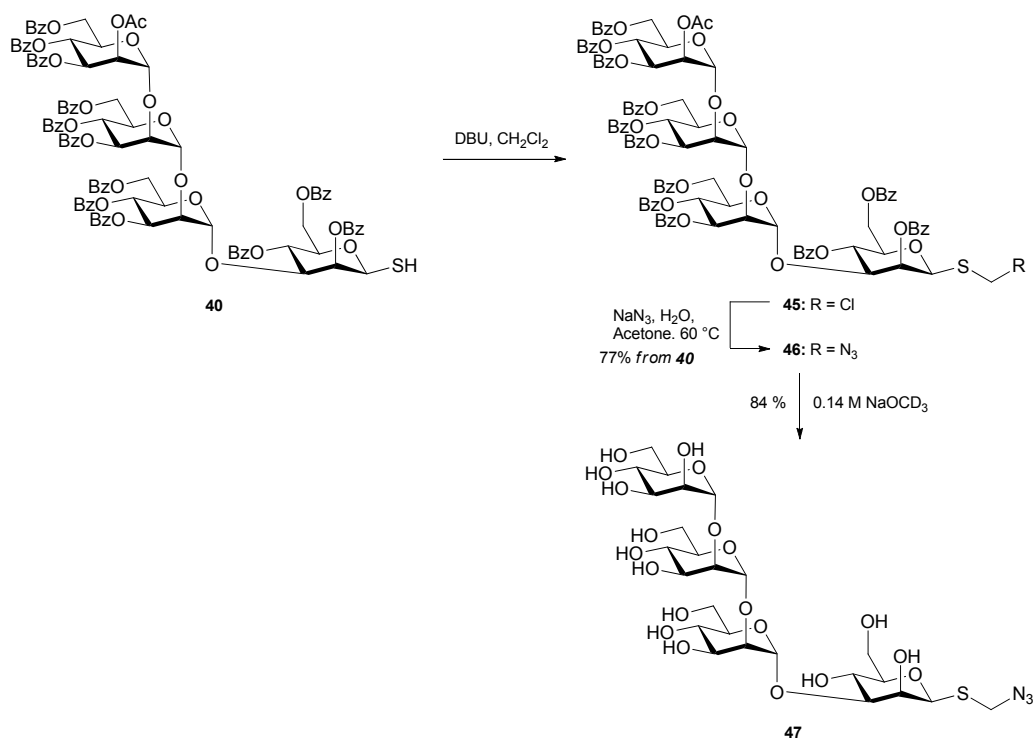
Synthesis of Azidomethyl 1-Thio-Mannopyranosides

During deprotection of disulfide **17** (Scheme 28), trace amounts of dichloromethane were added during optimization in an attempt to enhance solubility of the sugar, leading to the unexpected formation of chloromethyl 1-thio-mannopyranoside **42**. There is literature precedence for the nucleophilic attack of 1-thio-mannopyranoses on dichloromethane.¹⁵⁶ The resultant chloromethyl thioglycosides are of intrinsic interest since they open the door to alternative conjugation strategies. In particular, displacement by azide introduces the option to conjugate the oligosaccharide via the highly efficient azide-alkyne ‘click’ reaction.¹⁵⁷ The small azidomethyl aglycone is also compatible with the originally specified linker strategy which required a short linker in order to better mimic the structure of natural glycoconjugates.



Scheme 31. Formation of the azidomethyl monosaccharide **44**.

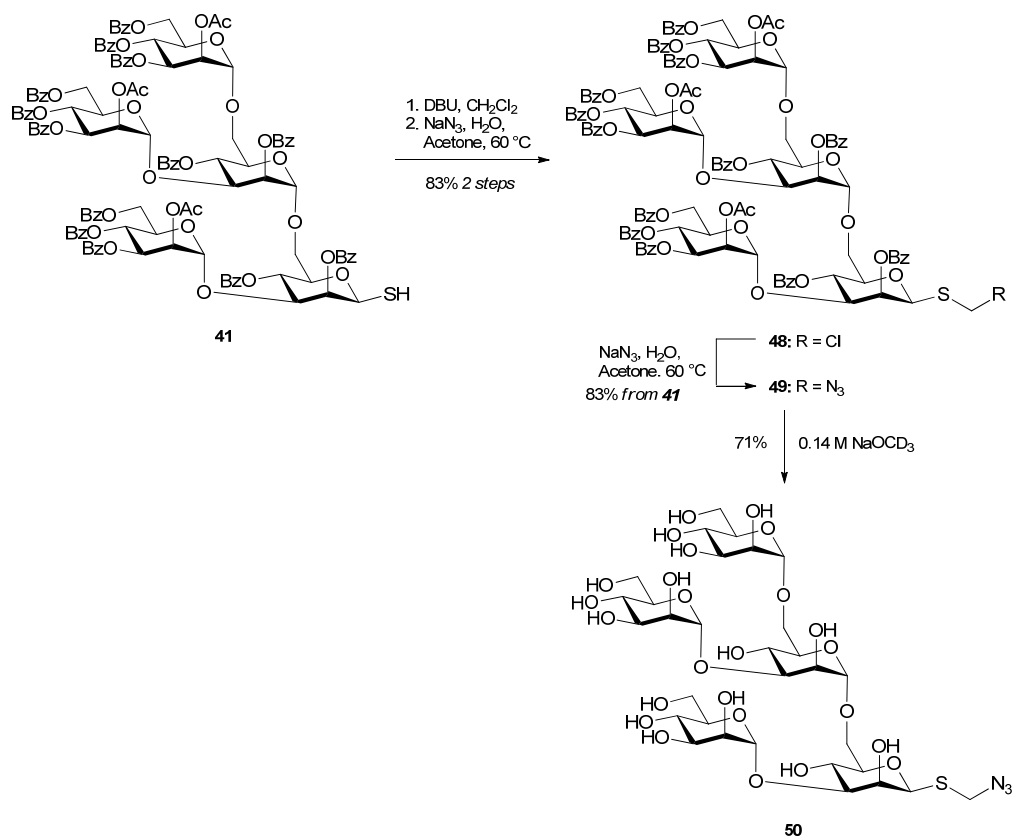
Conversion of the disulfide to the azidomethyl analogues was first performed on monosaccharide **17** as outlined in Scheme 31. Selective cleavage of the *S*-acetate with DBU using dichloromethane as the solvent produced chloromethyl mannoside **42** in 77% yield. The product was stable enough that it could be purified by recrystallization in hexanes:EtOAc. The methylene-linked dimer was not observed. Displacement of the chloride with sodium azide in aqueous acetone afforded the azidomethyl mannoside **43** in 75% yield after recrystallization. Subsequent deacetylation produced mannoside **44** in quantitative yield.



Scheme 32. Formation of azidomethyl tetrasaccharide **47**.

The azidomethyl analogue of tetrasaccharide **1** was synthesized in a similar fashion (Scheme 32). Tetrasaccharide **31** was reacted with dichloromethane in the presence of DBU to produce the chloromethyl mannoside **45**. Unlike the chloromethyl monosaccharide **42**, the chloromethyl tetrasaccharide displayed limited stability and the thioether became exceptionally susceptible to oxidation. A rudimentary chromatographic purification followed by the immediate reaction the chloromethyl tetrasaccharide **45** with sodium azide yielded the azidomethyl product **47** in 77% yield for the two steps. Deacetylation yielded the deprotected tetrasaccharide **48** in 71% yield.

The azidomethyl pentasaccharide equivalent was produced using the same procedure as with tetrasaccharide **46** (Scheme 33). Reaction of 1-thio-pentasaccharide **41** with dichloromethane produced the chloromethyl pentasaccharide **48** which was immediately reacted with sodium azide to create the azidomethyl derivative **49**. Zemplén saponification produced the deprotected pentasaccharide **50** in 71% yield.



Scheme 33. Formation of azidomethyl pentasaccharide 50.

References

1. E. Fischer, *Berichte der deutschen chemischen Gesellschaft* **1891**, 24, 1836-1845.
2. C. S. Hudson, *J. Chem. Educ.* **1941**, 18, 353.
3. R. S. Cahn, C. K. Ingold, *Journal of the Chemical Society* **1951**, 612-622.
4. B. Tollens, *Berichte der deutschen chemischen Gesellschaft* **1883**, 16, 921-924.
5. E. Fischer, *Berichte der deutschen chemischen Gesellschaft* **1895**, 28, 1145-1167.
6. E. Erwig, W. Koenigs, *Berichte der deutschen chemischen Gesellschaft* **1889**, 22, 1464-1467.
7. E. Erwig, W. Koenigs, *Berichte der deutschen chemischen Gesellschaft* **1889**, 22, 2207-2213.
8. T. Charles, *Comptes Rendus* **1895**, 120, 1060-1062.
9. W. Charlton, W. N. Haworth, S. Peat, *Journal of the Chemical Society (Resumed)* **1926**, 89-101.
10. H. D. K. Drew, W. N. Haworth, *Journal of the Chemical Society (Resumed)* **1926**, 2303-2310.
11. R. E. Reeves, *J. Am. Chem. Soc.* **1950**, 72, 1499-1506.
12. E. H. Goodyear, W. N. Haworth, *Journal of the Chemical Society (Resumed)* **1927**, 3136-3146.
13. N. Haworth, M. Stacey, *Annu. Rev. Biochem.* **1948**, 17, 97-114.
14. J. M. Lo-Guidice, M. Lhermitte, *Biomed. Chromatogr.* **1996**, 10, 290-296.
15. J. P. Kamerling, W. Heerma, J. F. G. Vliegenthart, B. N. Green, I. A. S. Lewis, G. Strecker, G. Spik, *Biomed. Mass Spectrom.* **1983**, 10, 420-425.
16. C. Bosso, J. Defaye, A. Heyraud, J. Ulrich, *Carbohydr. Res.* **1984**, 125, 309-317.
17. J. Ø. Duus, C. H. Gotfredsen, K. Bock, *Chem. Rev.* **2000**, 100, 4589-4614.

18. R. U. Lemieux, K. B. Hendriks, R. V. Stick, K. James, *J. Am. Chem. Soc.* **1975**, *97*, 4056-4062.
19. R. U. Lemieux, H. Driguez, *J. Am. Chem. Soc.* **1975**, *97*, 4063-4069.
20. R. U. Lemieux, H. Driguez, *J. Am. Chem. Soc.* **1975**, *97*, 4069-4075.
21. R. U. Lemieux, D. R. Bundle, D. A. Baker, *J. Am. Chem. Soc.* **1975**, *97*, 4076-4083.
22. P. G. M. Wuts, T. W. Green, *Greene's Protective Groups in Organic Synthesis, 4th Edition*, John Wiley & Sons: Hoboken, NJ, **2007**
23. A. Michael, *American Chemistry Journal* **1879**, *1*,
24. E. Fischer, *Berichte der deutschen chemischen Gesellschaft* **1893**, *26*, 2400-2412.
25. R. R. Schmidt, J. Michel, *Angewandte Chemie International Edition in English* **1980**, *19*, 731-732.
26. R. J. Ferrier, R. W. Hay, N. Vethaviyasar, *Carbohydr. Res.* **1973**, *27*, 55-61.
27. D. Kahne, S. Walker, Y. Cheng, D. Van Engen, *J. Am. Chem. Soc.* **1989**, *111*, 6881-6882.
28. L. K. Mydock, A. V. Demchenko, *Org. Biomol. Chem.* **2010**, *8*, 497-510.
29. S. Winstein, R. E. Buckles, *J. Am. Chem. Soc.* **1942**, *64*, 2780-2786.
30. H. Derek, *Chapter 4 Computational Studies of the Role of Glycopyranosyl Oxacarbenium Ions in Glycobiology and Glycochemistry*, in D. M. Whitfield, *Adv. Carbohydr. Chem. Biochem.*, Academic Press, **2009**, p. 83-159
31. J. T. Edward, *Chem. Ind.* **1955**, 1102-1104.
32. R. U. Lemieux, *Abstr. Pap. Am. Chem. Soc.* **1959**, *135*, 5E.
33. R. U. Lemieux, *Pure Appl. Chem.* **1971**, *25*, 527-548.
34. H. S. Isbell, *Annu. Rev. Biochem.* **1940**, *9*, 65-92.
35. S. Winstein, E. Grunwald, *J. Am. Chem. Soc.* **1948**, *70*, 828-837.

36. S. Winstein, E. Grunwald, R. E. Buckles, C. Hanson, *J. Am. Chem. Soc.* **1948**, *70*, 816-821.
37. Y. Ding, M.-O. Contour-Galcerà, J. Ebel, C. Ortiz-Mellet, J. Defaye, *European Journal of Organic Chemistry* **1999**, *1999*, 1143-1152.
38. J. M. MacDougall, X.-D. Zhang, W. E. Polgar, T. V. Khroyan, L. Toll, J. R. Cashman, *J. Med. Chem.* **2004**, *47*, 5809-5815.
39. K. Pachamuthu, R. R. Schmidt, *Chem. Rev.* **2005**, *106*, 160-187.
40. M. L. Uhrig, V. E. Manzano, O. Varela, *European Journal of Organic Chemistry* **2006**, *2006*, 162-168.
41. R. T. Dere, X. Zhu, *Org. Lett.* **2008**, *10*, 4641-4644.
42. M. Fiore, A. Marra, A. Dondoni, *The Journal of Organic Chemistry* **2009**, *74*, 4422-4425.
43. X. Zhu, R. T. Dere, J. Jiang, *Tetrahedron Lett.* **2011**, *52*, 4971-4974.
44. L. W. Melville, *Galactosidases*, in K. Wallenfels, O. P. Malhotra, *Advances in Carbohydrate Chemistry*, Academic Press, **1962**, p. 239-298
45. Z. J. Witczak, R. Chhabra, H. Chen, X.-Q. Xie, *Carbohydr. Res.* **1997**, *301*, 167-175.
46. J. C. Wilson, M. J. Kiefel, D. I. Angus, M. von Itzstein, *Org. Lett.* **1999**, *1*, 443-446.
47. H. Driguez, *ChemBioChem* **2001**, *2*, 311-318.
48. R. R. Kale, H. Mukundan, D. N. Price, J. F. Harris, D. M. Lewallen, B. I. Swanson, J. G. Schmidt, S. S. Iyer, *J. Am. Chem. Soc.* **2008**, *130*, 8169-8171.
49. A. Geyer, G. Hummel, T. Eisele, S. Reinhardt, R. R. Schmidt, *Chemistry – A European Journal* **1996**, *2*, 981-988.
50. B. Aguilera, J. Jiménez-Barbero, A. Fernández-Mayoralas, *Carbohydr. Res.* **1998**, *308*, 19-27.
51. E. Montero, M. Vallmitjana, J. A. Pérez-Pons, E. Querol, J. Jiménez-Barbero, F. J. Cañada, *FEBS Lett.* **1998**, *421*, 243-248.

52. T. Weimar, U. C. Kreis, J. S. Andrews, B. M. Pinto, *Carbohydr. Res.* **1999**, *315*, 222-233.
53. A. Fettke, D. Peikow, M. G. Peter, E. Kleinpeter, *Tetrahedron* **2009**, *65*, 4356-4366.
54. J. R. Rich, D. R. Bundle, *Org. Lett.* **2004**, *6*, 897-900.
55. J. Defaye, H. Driguez, E. Ohleyer, C. Orgeret, C. Viet, *Carbohydr. Res.* **1984**, *130*, 317-321.
56. H. N. Yu, C.-C. Ling, D. R. Bundle, *Journal of the Chemical Society, Perkin Transactions 1* **2001**, 832-837.
57. K. L. Matta, R. N. Girotra, J. J. Barlow, *Carbohydr. Res.* **1975**, *43*, 101-109.
58. Y. Cai, B. P. Roberts, D. A. Tocher, *Journal of the Chemical Society, Perkin Transactions 1* **2002**, 1376-1386.
59. A. Müller, A. Wilhelms, *Berichte der deutschen chemischen Gesellschaft (A and B Series)* **1941**, *74*, 698-705.
60. Z. Pakulski, D. Pierożyński, A. Zamojski, *Tetrahedron* **1994**, *50*, 2975-2992.
61. R. m. Caraballo, L. Deng, L. Amorim, T. Brinck, O. Ramström, *The Journal of Organic Chemistry* **2010**, *75*, 6115-6121.
62. R. T. Dere, Y. Wang, X. Zhu, *Org. Biomol. Chem.* **2008**, *6*, 2061-2063.
63. X. Zhu, R. T. Dere, J. Jiang, L. Zhang, X. Wang, *The Journal of Organic Chemistry* **2011**, *76*, 10187-10197.
64. M. Bodrul Haque, B. P. Roberts, D. A. Tocher, *Journal of the Chemical Society, Perkin Transactions 1* **1998**, 2881-2890.
65. N. Floyd, B. Vijayakrishnan, A. R. Koeppe, B. G. Davis, *Angewandte Chemie-International Edition* **2009**, *48*, 7798-7802.
66. Y. Han, G. Barany, *The Journal of Organic Chemistry* **1997**, *62*, 3841-3848.
67. P. Sieber, B. Kamber, A. Hartmann, A. Jöhl, B. Riniker, W. Rittel, *Helv. Chim. Acta* **1974**, *57*, 2617-2621.

68. R. A. Falconer, *Tetrahedron Lett.* **2002**, *43*, 8503-8505.
69. L. Greffe, M. T. Jensen, F. Chang-Pi-Hin, S. Fruchard, M. J. O'Donohue, B. Svensson, H. Driguez, *Chemistry – A European Journal* **2002**, *8*, 5447-5455.
70. W. I. Patterson, V. du Vigneaud, *J. Biol. Chem.* **1935**, *111*, 393-398.
71. J. E. T. Corrie, J. R. Hlubcek, G. Lowe, *Journal of the Chemical Society, Perkin Transactions 1* **1977**, 1421-1425.
72. Sakakiba.S, Shimonis.Y, Y. Kishida, M. Okada, H. Sugihara, *Bull. Chem. Soc. Jpn.* **1967**, *40*, 2164-&.
73. D. A. J. Ives, *Canadian Journal of Chemistry* **1969**, *47*, 3697-3699.
74. T. L. Cottrell, *The Strengths of Chemical Bonds, 2nd edition*, Butterworths, London, **1958**
75. B. d. Darwent, *National Standard Reference Data Series*, National Bureau of Standards, No. 31: Washington, DC, **1970**
76. M. Adinolfi, D. Capasso, S. Di Gaetano, A. Iadonisi, L. Leone, A. Pastore, *Org. Biomol. Chem.* **2011**, *9*, 6278-6283.
77. G. Hummel, O. Hindsgaul, *Angewandte Chemie International Edition* **1999**, *38*, 1782-1784.
78. B. G. Davis, S. J. Ward, P. M. Rendle, *Chem. Commun. (Camb.)* **2001**, 189-190.
79. C. F. Liang, M. C. Yan, T. C. Chang, C. C. Lin, *J. Am. Chem. Soc.* **2009**, *131*, 3138-3139.
80. M. Mandal, V. Y. Dudkin, X. Geng, S. J. Danishefsky, *Angewandte Chemie International Edition* **2004**, *43*, 2557-2561.
81. P. A. Fernandes, M. J. Ramos, *Chemistry – A European Journal* **2004**, *10*, 257-266.
82. W. W. Cleland, *Biochemistry (Mosc.)* **1964**, *3*, 480-482.
83. J. A. Burns, J. C. Butler, J. Moran, G. M. Whitesides, *The Journal of Organic Chemistry* **1991**, *56*, 2648-2650.

84. D. N. Harpp, J. G. Gleason, J. P. Snyder, *J. Am. Chem. Soc.* **1968**, *90*, 4181-4182.
85. T. Iversen, D. R. Bundle, *Carbohydr. Res.* **1982**, *103*, 29-40.
86. H. H. Bosshard, R. Mory, M. Schmid, H. Zollinger, *Helv. Chim. Acta* **1959**, *42*, 1653-1658.
87. T. Ogawa, K. Katano, M. Matsui, *Carbohydr. Res.* **1978**, *64*, C3-C9.
88. T. Ogawa, K. Sasajima, *Tetrahedron* **1981**, *37*, 2787-2792.
89. K. Kaur, O. Hindsgaul, *Glycoconj. J.* **1991**, *8*, 90-94.
90. S. Oscarson, A.-K. Tidén, *Carbohydr. Res.* **1993**, *247*, 323-328.
91. J. R. Merritt, E. Naisang, B. Fraser-Reid, *The Journal of Organic Chemistry* **1994**, *59*, 4443-4449.
92. S. J. Danishefsky, S. Hu, P. F. Cirillo, M. Eckhardt, P. H. Seeberger, *Chemistry – A European Journal* **1997**, *3*, 1617-1628.
93. P. Grice, S. V. Ley, J. Pietruszka, H. M. I. Osborn, H. W. M. Priepeke, S. L. Warriner, *Chemistry – A European Journal* **1997**, *3*, 431-440.
94. J. Rademann, A. Geyer, R. R. Schmidt, *Angewandte Chemie International Edition* **1998**, *37*, 1241-1245.
95. Y. Du, M. Zhang, F. Kong, *Org. Lett.* **2000**, *2*, 3797-3800.
96. S. Valverde, M. Garcia, A. M. Gomez, J. C. Lopez, *Chem. Commun. (Camb.)* **2000**, 813-814.
97. L. V. Backinowsky, P. I. Abronina, A. S. Shashkov, A. A. Grachev, N. K. Kochetkov, S. A. Nepogodiev, J. F. Stoddart, *Chemistry – A European Journal* **2002**, *8*, 4412-4423.
98. Daniel M. Ratner, Obadiah J. Plante, Peter H. Seeberger, *European Journal of Organic Chemistry* **2002**, *2002*, 826-833.
99. B. Fraser-Reid, J. C. Lopez, K. V. Radhakrishnan, M. V. Nandakumar, A. M. Gomez, C. Uriel, *Chem. Commun. (Camb.)* **2002**, 2104-2105.
100. J. Ning, Y. Yi, F. Kong, *Tetrahedron Lett.* **2002**, *43*, 5545-5549.

101. J. Zhang, F. Kong, *Tetrahedron: Asymmetry* **2002**, *13*, 243-252.
102. R. H. Furneaux, Z. Pakulski, P. C. Tyler, *Canadian Journal of Chemistry* **2002**, *80*, 964-972.
103. N. Smiljanic, S. Halila, V. Moreau, Djedai, amp, x, F. ni-Pilard, *Tetrahedron Lett.* **2003**, *44*, 8999-9002.
104. H.-K. Lee, C. N. Scanlan, C.-Y. Huang, A. Y. Chang, D. A. Calarese, R. A. Dwek, P. M. Rudd, D. R. Burton, I. A. Wilson, C.-H. Wong, *Angewandte Chemie International Edition* **2004**, *43*, 1000-1003.
105. R. Karamanska, B. Mukhopadhyay, D. A. Russell, R. A. Field, *Chem. Commun. (Camb.)* **2005**, 3334-3336.
106. M. Dowlut, D. G. Hall, O. Hindsgaul, *The Journal of Organic Chemistry* **2005**, *70*, 9809-9813.
107. F. A. Jaipuri, N. L. Pohl, *Org. Biomol. Chem.* **2008**, *6*, 2686-2691.
108. A. Pastore, M. Adinolfi, A. Iadonisi, S. Valerio, *Carbohydr. Res.* **2010**, *345*, 1316-1323.
109. Z. Szurmai, L. Balatoni, A. Lipták, *Carbohydr. Res.* **1994**, *254*, 301-309.
110. S. J. Danishefsky, M. T. Bilodeau, *Angewandte Chemie International Edition in English* **1996**, *35*, 1380-1419.
111. S. S. Bhattacharjee, P. A. J. Gorin, *Canadian Journal of Chemistry* **1969**, *47*, 1195-1206.
112. M. Ohlin, R. Johnsson, U. Ellervik, *Carbohydr. Res.* **2011**, *346*, 1358-1370.
113. T. Ogawa, M. Matsui, *Carbohydr. Res.* **1977**, *56*, c1-c6.
114. P. Kováč, *Applications of Stannyl Ethers and Stannylene Acetals to Oligosaccharide Synthesis*, in T. B. Grindley, *Synthetic Oligosaccharides*, American Chemical Society, Washington, D.C., **1994**, p. 51-76
115. T. Ogawa, M. Matsui, *Carbohydr. Res.* **1978**, *62*, C1-C4.
116. N. Teumelsan, X. Huang, *The Journal of Organic Chemistry* **2007**, *72*, 8976-8979.

117. Y. Du, M. Zhang, F. Kong, *Tetrahedron* **2001**, *57*, 1757-1763.
118. J. Kalikanda, Z. Li, *Tetrahedron Lett.* **2010**, *51*, 1550-1553.
119. J. Lawandi, S. Rocheleau, N. Moitessier, *Tetrahedron* **2011**, *67*, 8411-8420.
120. L. Heng, J. Ning, F. Kong, *Journal of Carbohydrate Chemistry* **2001**, *20*, 285-296.
121. N. É. Byramova, M. V. Ovchinnikov, L. V. Backinowsky, N. K. Kochetkov, *Carbohydr. Res.* **1983**, *124*, C8-C11.
122. T. L. Lowary, E. Eichler, D. R. Bundle, *The Journal of Organic Chemistry* **1995**, *60*, 7316-7327.
123. E. J. Grayson, S. J. Ward, A. L. Hall, P. M. Rendle, D. P. Gamblin, A. S. Batsanov, B. G. Davis, *The Journal of Organic Chemistry* **2005**, *70*, 9740-9754.
124. D. V. Yashunsky, V. S. Borodkin, M. A. J. Ferguson, A. V. Nikolaev, *Angewandte Chemie International Edition* **2006**, *45*, 468-474.
125. S. D. Nicholas, F. Smith, *Nature* **1948**, *161*, 349-349.
126. M. Mazurek, A. S. Perlin, *Canadian Journal of Chemistry* **1965**, *43*, 1918-&.
127. N. E. Franks, R. Montgomery, *Carbohydr. Res.* **1968**, *6*, 286-298.
128. D. R. Mootoo, P. Konradsson, U. Udodong, B. Fraser-Reid, *J. Am. Chem. Soc.* **1988**, *110*, 5583-5584.
129. Z. Zhang, I. R. Ollmann, X.-S. Ye, R. Wischnat, T. Baasov, C.-H. Wong, *J. Am. Chem. Soc.* **1999**, *121*, 734-753.
130. F. M. Winnik, J. P. Carver, J. J. Krepinisky, *The Journal of Organic Chemistry* **1982**, *47*, 2701-2707.
131. B. Roy, B. Mukhopadhyay, *Tetrahedron Lett.* **2007**, *48*, 3783-3787.
132. D. A. Pearson, M. Blanchette, M. L. Baker, C. A. Guindon, *Tetrahedron Lett.* **1989**, *30*, 2739-2742.
133. T. Mukaiyama, K. Takahashi, *Tetrahedron Lett.* **1968**, *9*, 5907-5908.

134. D. P. Gamblin, P. Garnier, S. van Kasteren, N. J. Oldham, A. J. Fairbanks, B. G. Davis, *Angewandte Chemie International Edition* **2004**, *43*, 828-833.
135. N. Chakka, B. D. Johnston, B. M. Pinto, *Canadian Journal of Chemistry* **2005**, *83*, 929-936.
136. P. Bonaccorsi, F. Marino-Merlo, A. Barattucci, G. Battaglia, E. Papaiani, T. Papalia, M. C. Aversa, A. Mastino, *Bioorg. Med. Chem.* **2012**, *20*, 3186-3195.
137. M. Karplus, *The Journal of Chemical Physics* **1959**, *30*, 11-15.
138. R. U. Lemieux, R. K. Kullnig, H. J. Bernstein, W. G. Schneider, *J. Am. Chem. Soc.* **1958**, *80*, 6098-6105.
139. A. A. Bothner-By, C. Naar-Colin, *Ann. N. Y. Acad. Sci.* **1958**, *70*, 833-840.
140. K. Bock, C. Pedersen, *Journal of the Chemical Society, Perkin Transactions 2* **1974**, 293-297.
141. O. Hernandez, S. K. Chaudhary, R. H. Cox, J. Porter, *Tetrahedron Lett.* **1981**, *22*, 1491-1494.
142. R. Euzen, V. Ferrières, D. Plusquellec, *Carbohydr. Res.* **2006**, *341*, 2759-2768.
143. T. G. Hansson, N. A. Plobeck, *Tetrahedron* **1995**, *51*, 11319-11326.
144. B. Sreedhar, P. Radhika, B. Neelima, D. V. D. B. Chowdary, M. V. B. Rao, *Synthetic Communications* **2009**, *39*, 3785-3795.
145. M. E. Zakrzewska, E. Bogel-Łukasik, R. Bogel-Łukasik, *Energy & Fuels* **2010**, *24*, 737-745.
146. W. E. Bachmann, *Organic Syntheses, Col. Vol.* **1955**, *3*,
147. Q. P. Wu, H. Liu, H. X. Liu, X. Chen, H. Wang, Q. S. Zhang, Y. Z. Li, *Chemical Research in Chinese Universities* **2010**, *26*, 55-59.
148. R. R. Schmidt, M. Behrendt, A. Toepfer, *Synlett* **1990**, 694-696.
149. V. Pozsgay, *J. Am. Chem. Soc.* **1995**, *117*, 6673-6681.
150. X. Yao-Chang, A. Bizuneh, C. Walker, *Tetrahedron Lett.* **1996**, *37*, 455-458.

151. T. Ogawa, S. Nakabayashi, *Carbohydr. Res.* **1981**, *93*, C1-C5.
152. K. K. Sadozai, T. Kitajima, Y. Nakahara, T. Ogawa, A. Kobata, *Carbohydr. Res.* **1986**, *152*, 173-182.
153. H. P. Wessel, M.-C. Viaud, V. Gardon, *Carbohydr. Res.* **1993**, *245*, 233-244.
154. G. Schüle, T. Ziegler, *Liebigs Annalen* **1996**, *1996*, 1599-1607.
155. I. S. Alferiev, J. M. Connolly, R. J. Levy, *Journal of Organometallic Chemistry* **2005**, *690*, 2543-2547.
156. X. Zhu, R. R. Schmidt, *The Journal of Organic Chemistry* **2004**, *69*, 1081-1085.
157. V. V. Rostovtsev, L. G. Green, V. V. Fokin, K. B. Sharpless, *Angewandte Chemie International Edition* **2002**, *41*, 2596-2599.

CHAPTER 3: Conjugation of the Oligo-Mannose Analogues to Filamentous Phage and their Characterization

Part I: Refining Conjugation Methodology

Preface

Chemical conjugation of ligands to phage conveys additional challenges when compared to ligand conjugations to proteins. Conjugation methodology must consider that the phage is composed of both protein and DNA, which together form the phage quaternary structure- a structure that is held together entirely through non-covalent interactions. In the following sections, purification and characterization techniques are discussed with respect to phage conjugation, followed by the optimization of conjugation reactions with phage.

Purification of Filamentous Phage

Traditionally, double precipitation with polyethylene glycol (PEG) has been a standard technique for purifying filamentous phage,¹ though contaminants can still remain in these phage preparations.² Further purification can be achieved by CsCl density-gradient ultracentrifugation,^{3,4} although contaminant endotoxin from the *E. coli* culture may still remain bound to the phage. These purification techniques are laborious and result in significant loss of phage, making them unsuitable for purification between conjugations.⁵ Size exclusion chromatography has been used more recently as a quick and trivial purification technique for filamentous phage,^{2, 6} making it an attractive choice for this project. Exploratory purifications of a phage/bromophenol blue mixture using Zeba™ Spin Desalting columns with a 40 kDa MW cutoff yielded a near quantitative removal of dye from the phage solution.

It was unknown if the Zeba™ size exclusion columns would remove endotoxin. Endotoxin can be problematic in vaccinations due to the strong immune responses it produces in animals and humans.^{7, 8} Endotoxin is lipopolysaccharide (LPS) which is an integral component of the outer membrane of gram-negative bacteria. As a PAMP, LPS is recognized by PRRs such as LPS binding protein, CD14 and TLR-4,^{9, 10} resulting in the

production of pro-inflammatory cytokines that can provoke systemic inflammation leading to septic shock.¹¹ LPS can be conveniently removed from filamentous phage by treatment with polymixin B.¹² Polymixin B is positively charge cyclic peptide that can bind and inactivate endotoxin.¹³ Interestingly, in a herpes simplex virus (HSV) vaccine study employing a filamentous phage display vaccine it was noted that phage preparations that had been subjected to polymixin B treatment generated considerably lower antibody levels.¹² While residual LPS bound to the phage could produce a beneficial adjuvant effect, the benefit is outweighed by the potential for serious adverse effects.¹⁴

The Zeba™ column was compared with a gel-immobilized polymixin B (Detoxi-Gel™) column for endotoxin removal and recovery of phage. Phage purified by CsCl density-gradient ultracentrifugation were run through each column, with an ~80% recovery of phage from both columns. The eluted phage were analyzed by SDS-PAGE for the presence of exogenous proteins by over-exposing the gel with silver stain (Figure 40). The CsCl density gradient and Zeba™ column purified phage displayed additional banding between the pIII and pVIII bands in comparison to the Detoxi-Gel™ column purified phage. The removal of these bands by polymixin B suggests that these are phage-bound endotoxin, and that size exclusion purification is insufficient to remove endotoxin.

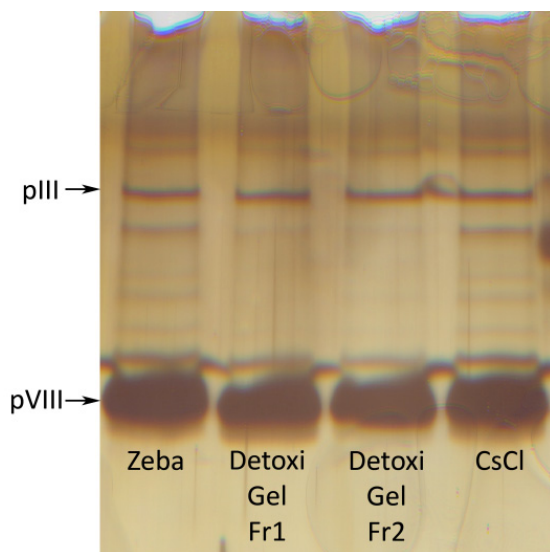


Figure 40. SDS-PAGE of f1.K phage purified by CsCl, Zeba™ Spin Desalting column or Detoxi-Gel™ endotoxin removing column. 2×10^{10} phage loaded per lane.

Quantifying Conjugations to Filamentous Phage

It is important to this project to have an accurate assessment of both the linker addition and the oligosaccharide conjugate addition in order to optimize the conjugation reactions and establish the glycan density. The degree of conjugation of the phage can be determined by either analyzing the whole phage conjugate or the individual pVIII subunits. It is undoubtedly more practical to think of protein concentration in terms of phage concentration, as the concentration of phage can be reliably measured by absorbance measurement or analysis of the phage DNA concentration by gel electrophoresis.³ Quantifying the glycan concentration of a phage glycoconjugate is much more challenging, as the many techniques used to quantify the degree of conjugation of glycoconjugates¹⁵ are either unsuitable for phage or lack the precision desired for this project, as discussed below.

Whole phage glycoconjugates can be analyzed by colorimetric assays or by relying on a detectable tag to extrapolate the conjugation efficiency. There are colorimetric assays for both protein and carbohydrate, such as the Bradford assay or phenol-sulfuric acid assay. The reactions or dyes used in protein assays are dependent on the amino acid composition of the protein and modifications made to the protein, such as glycan addition, often distort the results of these assays.¹⁶ Colorimetric glycan assays would encounter interference from the 2-deoxyribose of the phage DNA, requiring the careful use of phage standards to compensate for this background interference.

An easily detectable molecular label that possesses the same linker chemistry as the glycan can also be used to estimate the conjugation efficiency.^{17, 18} This technique was used to determine the number of attached glycans to a Q β viral particle scaffold, using an easily quantifiable selenium tag with an azide linker to simulate the glycan-azide in the CuAAC conjugation.¹⁹⁻²¹ This is at best an estimate, as the authors even cite *“an experimental error of 10% is typical for independent reactions under identical conditions”*, which is in itself, only an estimate.

Denatured phage conjugates can also be analyzed by gel electrophoresis. The pVIII coat protein can be separated and visualized by SDS-PAGE. If the differentially

conjugated pVIII subunits differ enough in mass and charge to separate on the gel, the different bands could be quantified by densitometry. It is unlikely though that the differing pVIII+linker species would be resolvable by SDS-PAGE, as a phage conjugate using a larger linker was shown to be unresolvable from wt pVIII by Scott and coworkers in a previous study.²² The addition of a small linker adds negligible mass to the pVIII coat protein making it unlikely to resolve any shift in the conjugated protein bands. The addition of a glycan to a protein also causes the protein to move through the gel unpredictably, as the carbohydrate component does not bind SDS, reducing the net charge-to-mass ratio and slowing its migration.²³ If the pVIII+glycan bands were reasonably separable, quantifying the bands would become problematic, as the protein stains used for gel densitometry rely on non-specific binding with the protein, or interact with specific features, such as the charged amino acid side chains. Since the linker addition modifies the positively charged lysine, and the addition of the glycan adds a large polar structural feature to the protein surface, staining of the conjugated pVIII species would give inaccurate readings of band density regardless of the stain used.

Western blots are an alternative approach to detecting glycoconjugates through the use of labeled ligands, such as antibody or ConA. For Western blotting to be useful for quantifying variable degrees of conjugation, the conjugations should not disturb the binding epitope of the detecting ligand, or interfere with ligand binding in general. Quantifying protein from the densitometry results of Western blots has also been questioned, and carries an unknown degree of accuracy.²⁴ High-mannose glycoproteins have been quantified by directly probing electrophoresis gels with labeled ConA, without the need to transfer protein from the gel to nitrocellulose for Western blotting.²⁵⁻²⁷ The accuracy of this method is uncertain, as it is not well utilized for glycan quantification, and would still require accurate protein quantification to determine the degree of glycan conjugation.

Mass spectrometry, particularly MALDI-TOF MS,²⁸ has become a popular technique to quantitatively analyze biomolecules,²⁹⁻⁴⁴ despite concurrent reports of the non-quantitative nature of this method.^{30, 34, 38, 40, 44-49} The main problem of quantifying compounds with MALDI is the reproducibility of the spectrum from shot to shot and

sample to sample. This is generally remedied by using internal standards of known quantity,^{30, 34} which ideally should be composed of the sample itself,^{28, 44} which is not helpful in this study.

Ion suppression also impedes the quantitative performance of all MS.⁵⁰ This refers to how a matrix influences the ionization of solute, making it less likely to ionize, and subsequently be detected. In general, high polarity compounds are more susceptible to ion suppression.⁵¹ The positive mode ionization efficiency of glycoproteins is also inherently lower than their protein counterparts.^{44, 52-54} Negative ion analysis of glycoproteins generally produces weak ion signals but is started to be explored in glycopeptide analysis.⁵⁵ The low ionization efficiency is due in part to the removal of the charged site where the glycan is attached, and the overall negative character of the glycan. Thus, a sample containing a multitude of pVIII glycoconjugates would certainly experience the effects of ion suppression and be unquantifiable due to the variable ionization efficiency of each pVIII glycoconjugate.

To avoid the nuances of ion suppression effects and the inherent variable ionization efficiencies of glycoconjugate, a reverse phase liquid chromatography-UV-mass spectrometry (LC-UV-MS) technique was explored to quantify the glycan loading of the phage. In this system, the differentially conjugated pVIII coat proteins would be separated by reverse phase liquid chromatography, quantified by their UV absorbance, and then identified by mass in the mass spectrometer in positive ion mode(Figure 41). The carbohydrates of the pVIII glycoconjugates do not absorb UV light in the spectral regions used to quantify proteins.^{††} The additional amide bond formed from the linker addition with the amines of the protein may slightly increase the absorption at 210 nm with each conjugation. This should have a negligible effect on absorbance though, as the addition of 1-3 amide bonds is insignificant in comparison to the number of amide bonds already present in pVIII.

^{††} Peptide bonds absorb at a wavelength of 210 nm, although this is dependent on both the individual amino acid^{56, 57} and the peptide bond conformation.⁵⁸ Tryptophan and tyrosine absorb strongly at 280 nm.

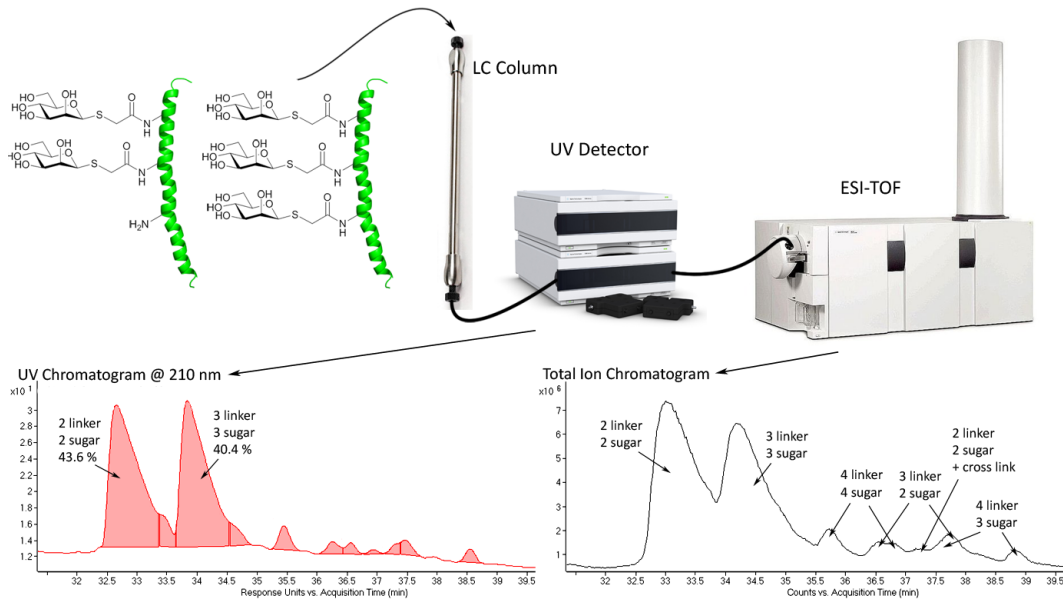


Figure 41. Diagram of the LC-UV-ESI-MS system.

While exploring the feasibility of using LC/MS for phage analysis, it was found that whole phage preparations could be loaded onto the LC column without the need to first denature the phage quaternary structure. The pVIII coat protein only elutes from the column once 38% mobile phase B has been reached. The extreme hydrophobic nature of pVIII lead to the accumulation of phage or phage protein in the C8 OPTI-PAK precolumn, which was apparent from the stepwise buildup of column backpressure in the system with every injection. Replacement of the C8 precolum with a 0.2 μm frit filter solved the pressure increase problem and made the separation and analysis possible.

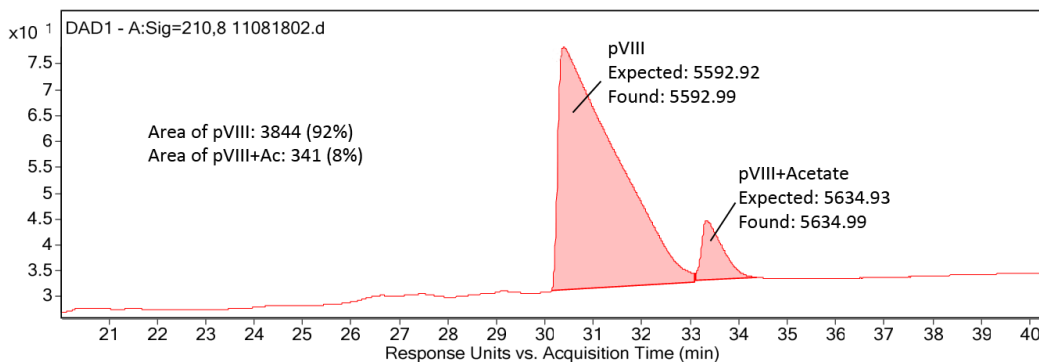


Figure 42. The LC-UV chromatogram of the pVIII coat protein of f1.K phage. The deconvoluted masses of the pVIII subunits representing both peaks are displayed, along with their theoretical masses.

Two Ff phage were to be used in the conjugation studies. The first was f1.K, which was engineered to have an additional lysine residue near the N-terminus of pVIII for chemical conjugation, for a total of three N-terminus amines.⁵⁹ The second phage was f88-4 (f88), which only carried two N-terminus amines for conjugation. The initial analysis of phage also revealed that 8% of pVIII from both phage is acetylated (Figure 42). Lysine and N-terminal acetylation are common post-translational modifications.⁶⁰ ⁶¹ In the context of this project, acetylation removes a potential conjugation site from the pVIII surface.

Perhaps more revealing from this discovery was the good separation that could be achieved between pVIII species that differed by a single small amino acid modification. In practice, this was indeed the case, as multiple pVIII linker conjugates from a single phage sample could be separated, even resolving glycoconjugates that adorn a site of acetylation or oxidation (Figure 43). Multiple conjugates of pVIII that possessed the same degree of conjugation, as determined by their mass, were also eluting from the column independently. These differences in retention time are likely a result of the conjugations occupying different sites on pVIII, and are explored in a subsequent section of this thesis. The level of detail revealed by our LC-UV-MS system made it the clear choice to monitor our conjugations.

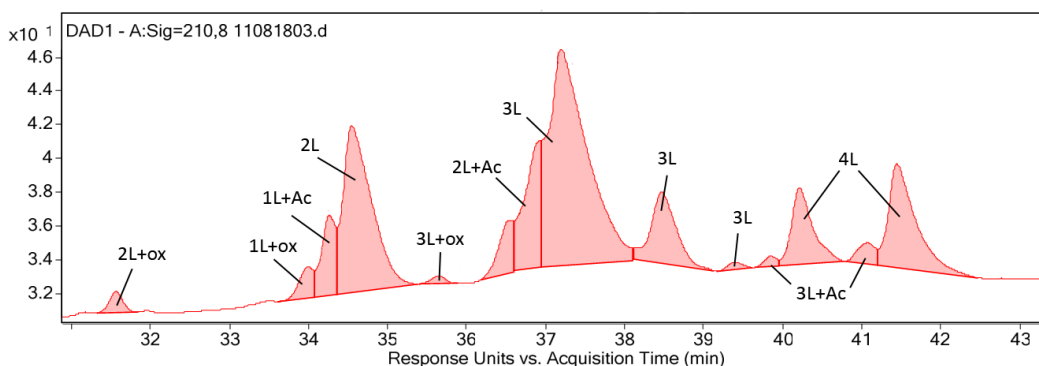
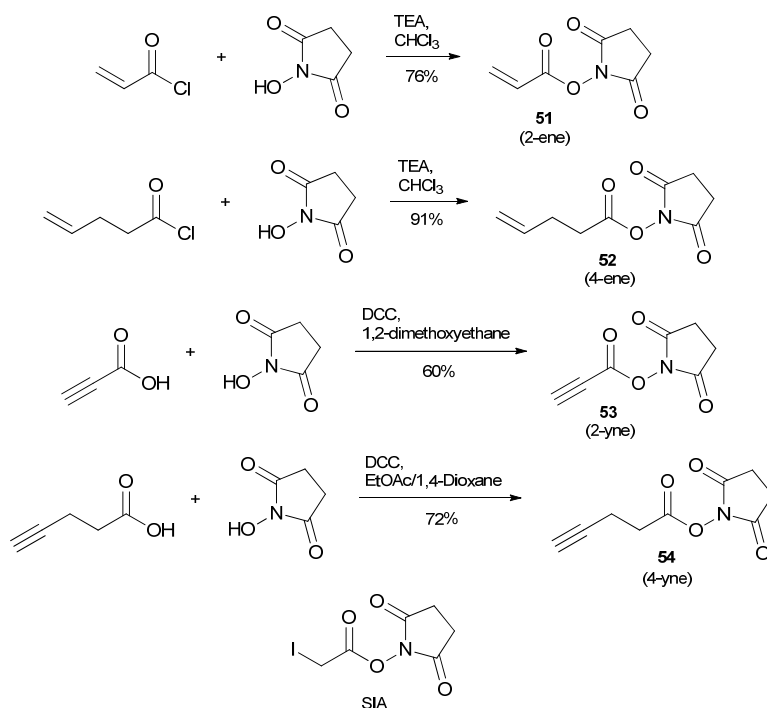


Figure 43. An example LC-UV chromatogram of f1.K phage conjugated with 100 equivalents of linker 54. Each absorbance represents a pVIII conjugate or a cluster of pVIII conjugates. The label of each peak reflects the number of linkers (L) attached to pVIII, as well as any additional acetates (Ac) or oxidation (ox).

Optimization of Linker Additions

With the method for quantifying the degree of conjugation chosen, the optimal conditions for the linker additions and glycoconjugation were determined next. In addition to the original SIA and *N*-(acryloyloxy)succinimide **51** crosslinkers for the haloacetyl and thiol-ene crosslinking strategies, an alkyne functionalized crosslinker was needed to conjugate the azidomethyl 1-thio-mannosides. There was an initial concern that the short linkers would become sterically inaccessible on the phage surface as the glycoconjugation reaction proceeded and the glycan density increased. In preparation for this potential problem, five crosslinkers were investigated: the alkene-functionalized crosslinkers **51** and *N*-(4-pentenyl)oxy)succinimide **52**, the alkyne functionalized crosslinkers *N*-(2-propynyl)oxy)succinimide **53** and *N*-(4-pentynyl)oxy)succinimide **54**, and SIA. Since the only commercially available crosslinker of these five was SIA, the other four were synthesized according to Scheme 34.



Scheme 34. The crosslinkers evaluated in the phage conjugation studies.

In brief, the alkene-functionalized crosslinkers were prepared by the nucleophilic displacement of acryloyl chloride or 4-pentenyl chloride with *N*-hydroxysuccinimide to yield crosslinkers **51** and **52** in 76% and 91% yield. The acid

chlorides of the alkyne precursors were not commercially available, so the carboxylic acid precursors were used instead. Propiolic acid or 4-pentynoic acid was activated with *N,N'*-dicyclohexylcarbodiimide and displaced with *N*-hydroxysuccinimide to yield crosslinkers **53** and **54** in 60% and 72% yield. All four crosslinkers were purified via recrystallization in EtOAc:Hexanes except for **53**, which required additional chromatographic purification using fluorosilica gel.

Reaction between NHS esters and primary amines are ideally performed between physiologic to slightly alkaline conditions (pH 7-9).⁶² Higher pH ranges can lead to unwanted side reactions of the iodoacetate or NHS ester with other amino acids, such as the imidazolyl side chain nitrogens of histadine, the thioether of methionine, and the oxygen of serine.^{62, 63} Thus a neutral pH would be preferred if possible. The initial linker additions performed investigated the effects of pH and time on the degree of conjugation, as well as determined the optimal linker equivalents for the reaction.

The 2-yne crosslinker **53** and SIA were reacted with f1.K phage at pH 7.0 or pH 8.3 for either 3 or 20 hours (Table 5). The degree of conjugation was determined by manually integrating the UV trace at 210 nm to determine the relative abundance of each pVIII+conjugate species. Unsurprisingly, a higher pH correlated with an increased degree in conjugation. Increasing the reaction time appeared to be only beneficial to the linker additions performed at pH 7.0, as no significant increase in conjugation was observed with pH 8.3 reactions longer than 3 hours. Both linkers were able to achieve high degrees of conjugation, averaging between 2.5-3 linkers per pVIII under optimal conditions. The detection of f1.K pVIII with four, and even five, linkers was quite surprising, and suggests that either some of the C-terminal amines were slightly solvent exposed or that the small size of the crosslinkers allow them to penetrate the viral capsid to access the C-terminal amines. Differences in lipophilicity between these two crosslinkers may account for the ability of the short alkynyl crosslinker to produce 4-5 linked pVIII species.

Table 5. The effects of pH and reaction time on the loading of the 2-alkynyl linker on f1.K phage. The pVIII conjugates were categorized based on how many linkers (L) each pVIII possessed. f1.K has three surface exposed N-terminus amines.

Linker	Linker Equiv.	pH	Rxn Time (hours)	Degree of Conjugation of pVIII (%)						Average Linker/pVIII
				No L	1 L	2 L	3 L	4 L	5 L	
2-yne	100	7.0	3	-	2	46	47	5	0.2	2.56
2-yne	100	7.0	20	-	0.5	35	54	10	0.5	2.75
2-yne	100	8.3	3	-	-	18	58	24	1	3.09
2-yne	100	8.3	20	-	-	14	59	26	2	3.15
SIA	100	7.0	3	8	6	52	30	5	-	2.18
SIA	100	7.0	20	-	4	57	34	5	-	2.41
SIA	100	8.3	3	-	-	48	43	8	-	2.57
SIA	100	8.3	20	-	0.6	52	43	5	-	2.52

The optimal equivalents for the linker additions were routinely found to be around 100 equivalents per amine for both f1.K and f88 phage, as less crosslinker would result in unconjugated pVIII species (Table 6). More linker equivalents commonly lead to precipitation in the reaction tube and lower recovery of the phage after purification. This may be a consequence of the increased organic solvent needed to solubilize the water-insoluble crosslinkers.

Table 6. The effects of linker equivalents on the degree of conjugation using the 4-alkynyl crosslinker 54 and f88 phage. The pVIII conjugates were categorized based on how many linkers (L) each pVIII possessed. f88 has two surface exposed amines.

Linker	Linker Equiv.	pH	Time (mins)	Degree of Conjugation (%)				Linker/pVIII
				No L	1L	2L	3L	
4-yne	20	8.3	3	9	77	14	-	1.05
4-yne	40	8.3	3	3	77	19	1	1.18
4-yne	100	8.3	3	0.5	70	27	2	1.30

With the crosslinker chemistry optimized, the five linkers were evaluated for how thoroughly they could coat the f1.K and f88-4 phage (Table 7). All crosslinkers obtained a high degree of conjugation, with the 2-yne crosslinker 53 producing the highest loading for both phage with 3.09 and 1.66 linkers per pVIII_{f1.K} and pVIII_{f88}. Neither phage were able to achieve full loading of their N-terminus conjugation sites, as

indicated by the persistence of the 2-linker pVIII_{f1.K} and 1-linker pVIII_{f88-4} conjugates. Performing a second round of linker additions on previously conjugated phage preparations did not enhance the degree of conjugation significantly. The common N-terminal amine of both phage may be sterically occluded or have limited surface exposure.

Table 7. Linker addition results of f1.K and f88 phage. The phage were reacted with 100 equivalents of linker at pH 8.3 for three hours.

Phage	Linker	Degree of Conjugation of pVIII (%)						Average Linker/ pVIII
		No L	1L	2L	3L	4L	5L	
f1.K	2-ene	-	-	33	50	16	-	2.80
f1.K	4-ene	-	4	59	30	6	-	2.36
f1.K	2-yne	-	-	17	58	24	1	3.09
f1.K	4-yne	-	1	49	41	9	-	2.58
f1.K	SIA	-	-	43	48	9	-	2.66
f88	2-ene	-	45	32	11	-	-	1.42
f88	4-ene	1	49	43	7	-	-	1.56
f88	2-yne	-	23	55	11	-	-	1.66
f88	4-yne	-	61	34	5	-	-	1.44
f88	SIA	3	59	34	3	-	-	1.36

Determining the Sites of pVIII Conjugation

The unexpected occupancy of conjugation sites beyond the three N-terminus amines of f1.K and the two N-terminus amines of f88 prompted an investigation of the crosslinker attachment sites by tandem mass spectrometry (MS/MS). This is a mass spectrometry technique where sequence information about a peptide can be obtained by isolating the desired molecular ion, fragmenting it, and detecting the fragment ions produced. Using MS/MS, fragments of pVIII carrying linker modifications can be identified and the sites modified by linker assigned.

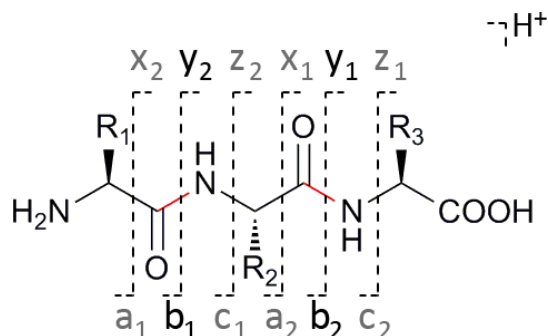


Figure 44. Nomenclature of fragment ions from MS/MS of a peptide. The *a*, *b* and *c* fragments retain the N-terminus and the *x*, *y* and *z* fragments retain the C-terminus. The subscript number is the residue number relative to the terminus that the fragment contains.

The peptide fragments are named according to whether the fragment contains the N- or C-terminus, the type of bond that is cleaved, and the cleavage position along the peptide chain (Figure 44). If the charge is located on the N-terminus fragment, the ion is classified as either *a*, *b* or *c*, depending on the bond that was cleaved. Likewise, if the charge is located on the C-terminus, the ion type is either *x*, *y* or *z*. A subscript number is used to indicate the residue number relative to the terminus that the fragment contains. In this experiment, a low energy collision-induced dissociation (CID) method causes fragmentation of the peptide bond, generating mostly *b* and *y* ions.

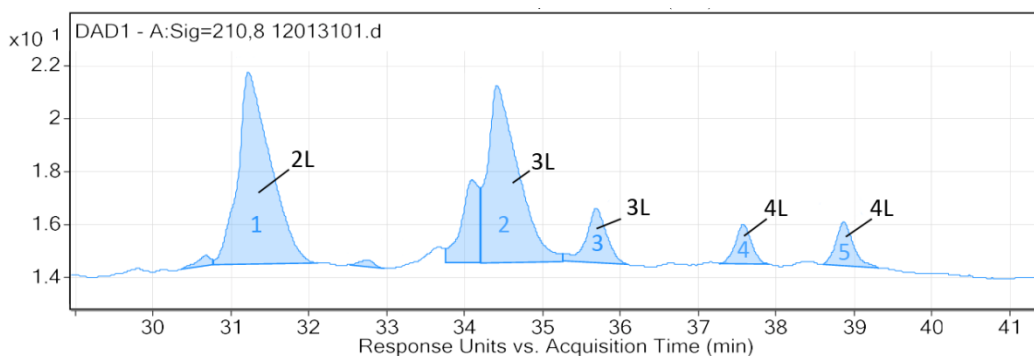
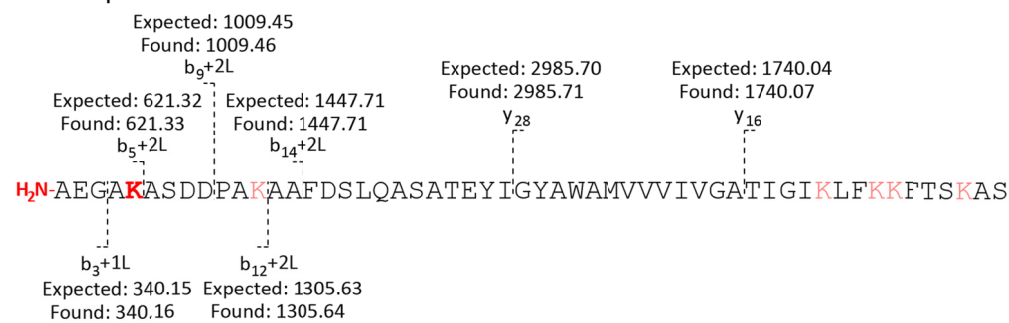


Figure 45. The LC-UV chromatogram of f1.K-(4-yne) linker conjugate. The number of linkers (L) attached to each pVIII conjugate are denoted by the black text. The peaks analyzed by MS/MS are numbered 1-5 in blue text.

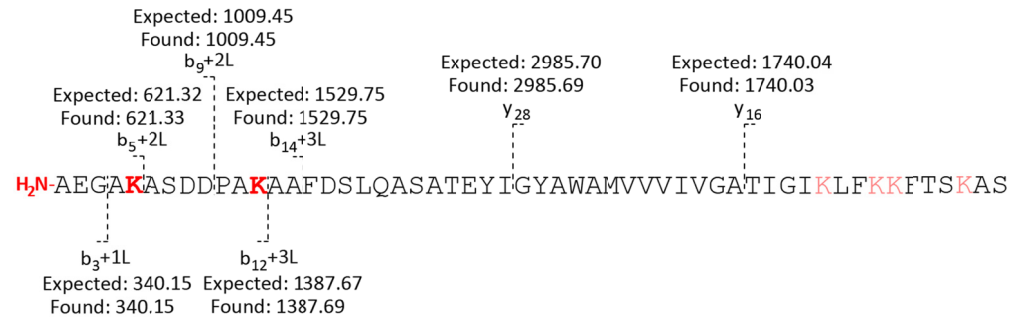
The f1.K-(4-yne) linker conjugate was chosen for MS/MS analysis because of the good separation of the pVIII+(4-yne) conjugates by LC (Figure 45). Each of the five peaks shown in Figure 45 were collected in separate vials and were analyzed by ESI-MS/MS through direct infusion. This allowed for the analysis of peaks correlating to pVIII conjugates of the same mass, but of different retention time. MS/MS analysis of the

two largest UV peaks, 1 and 2, suggests that the N-terminal amine and K5 lysine are preferentially conjugated first, producing the pVIII+2L species of peak 1, followed by conjugation at the K12 lysine to produce the pVIII+3L species of peak 2 (Figure 46). The K12 conjugation was absent on the second pVIII+3L species, represented by peak 3 in the UV chromatogram, and instead carried this conjugation on one of the C-terminus lysines, as indicated by the presence of the $y+1L$ fragment ions (Figure 46). The exact position of this C-terminus lysine could not be identified because of the lack of b or y ions from the C-terminal side of the protein.

Peak 1: pVIII + 2 Linkers



Peak 2: pVIII + 2 Linkers



Peak 3: pVIII + 3 Linkers

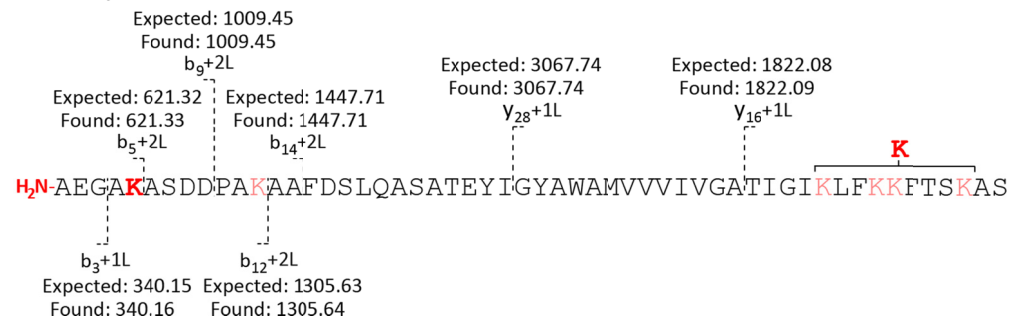
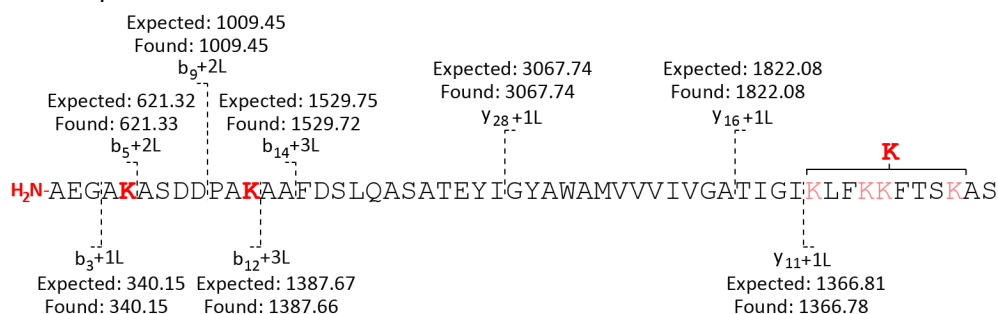


Figure 46. A selection of the fragment ions obtained from the MS/MS results displayed over the pVIII_{f1,K} sequence for the conjugates of peaks 1-3 (Figure 45). The expected masses that include linker (L) are denoted by the +1L or +2L notation appended to the fragment label. Occupied sites of conjugation, either

the lysine (K) amines or N-terminal amine (NH₂), are shown in red. Unused sites of conjugation are highlighted in pink on the pVIII sequence.

The remaining two peaks, 4 and 5, correspond to two different pVIII+4L species. The fragment ions of these pVIII conjugates were similar, displaying a fully conjugated N-terminus with the remaining conjugation on a C-terminus lysine. The difference in retention time of these two pVIII+4L species is thus likely due to a disparity in which C-terminus lysine is conjugated. A complete list of the detected fragment ions and the deconvoluted mass spectra are presented in Appendix A2.

Peak 4: pVIII + 4 Linkers



Peak 5: pVIII + 4 Linkers

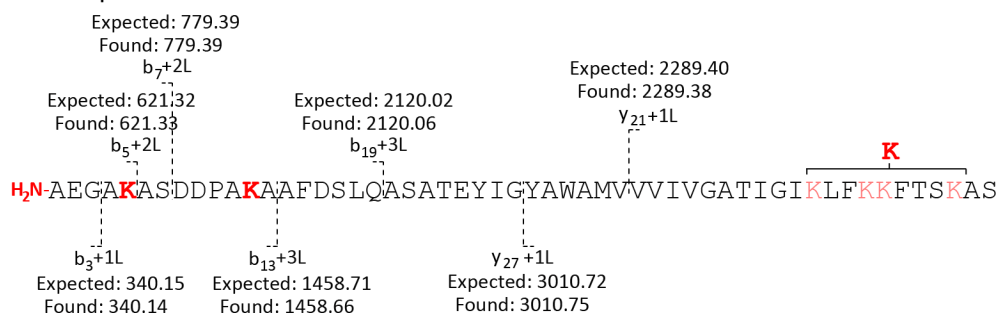


Figure 47. A selection of the fragment ions obtained from the MS/MS analysis are displayed over the pVIII_{f1.K} sequence for the conjugates of peaks 4 and 5 (Figure 45). The expected masses that include linker (L) are denoted by the +1L or +2L notation appended to the fragment label. Occupied sites of conjugation, either the lysine (K) amine or N-terminal amine (NH₂), are shown in red. Unused sites of conjugation are highlighted in pink on the pVIII sequence.

The MS/MS study provides information about the relative reactivity and/or accessibility of the pVIII amines. The N-terminal and K5 lysine are conjugated in all species of pVIII, which is likely due to their accessibility. The K12 lysine of f1.K is sufficiently resistant to conjugation that a C-terminus lysine could experience conjugation before K12, as evidenced by the existence of peak 3 in Figure 46. Subjecting f1.K phage to multiple rounds of linker addition in succession has little effect on

diminishing the pVIII+2L signal, which further exemplifies the resistance of the K12 lysine to conjugation.

Resistance to the complete loading of the N-terminus amines is also observed in the f88 linker additions, where linker loading falters beyond 1.5 conjugates per pVIII (Table 7), despite having two, supposedly exposed, N-terminus amines (Figure 48B). The UV chromatogram of f88-(4-yne) reveals three pVIII+2L species (Figure 48A). The N-terminal amine is likely the most surface accessible and is presumed to be universally conjugated, as seen with f1.K. It is also assumed that the K8 lysine of at least one of the pVIII+2L peaks is occupied, leaving the other two pVIII+2L species with differently occupied C-terminus amines. It would thus appear that the K8 lysine is about as likely to be occupied as the buried C-terminal amines, by comparison of the similar absorbance area of the pVIII+2L peaks in the UV chromatogram. The K8 lysine of pVIII_{f88} is the equivalent to the K12 lysine of pVIII_{f1.K} (Figure 48B), which both display hindered reactivity presumably due to limitations in its accessibility. This is consistent with previous MS/MS studies of M13 phage conjugations with NHS esters.⁶⁴

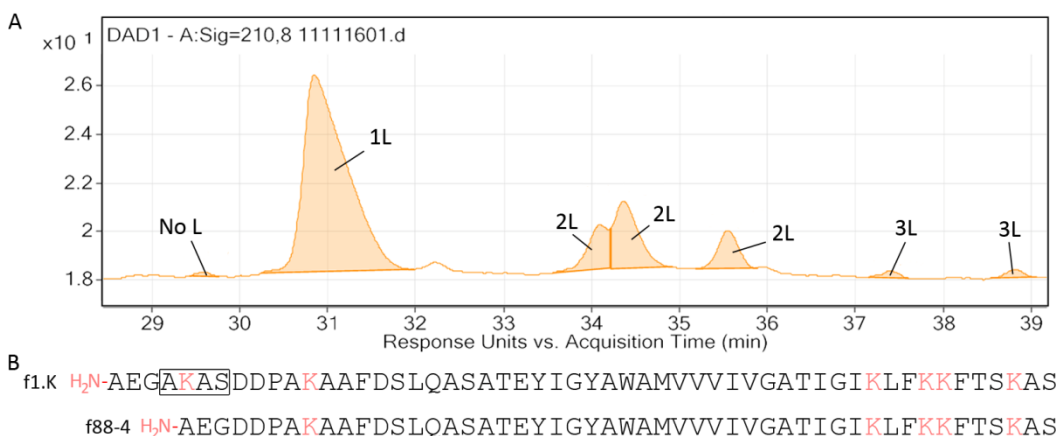


Figure 48. The LC-UV chromatogram of f88-(4-yne) and a comparison of the pVIII sequence of f1.K and f88. **A** | LC-UV trace of f88 phage conjugated with 4-yne crosslinker 54. Each absorbance peak is labeled on the chromatogram to indicate the number of linker (L) conjugations on pVIII. **B** | The pVIII sequence of f1.K and f88-4 are compared. The N-terminal amine and lysines are colored pink. The boxed AKAS sequence was engineered into the f1.K phage by site directed mutagenesis.⁵⁹

Optimization of Glycoconjugation Reactions

The efficiency of the glycoconjugation reactions were next explored, using the five f1.K linker conjugates and the mannopyranosyl thiol **39** and azidomethyl 1-thio-mannopyranoside **44** (Figure 50). These conjugate additions were evaluated in the

same way as the linker additions, using LC-UV-ESI-MS (Figure 41). Good separation of the monosaccharide conjugates by LC was observed (Figure 49), allowing for an accurate quantification of relative abundance of the differentially conjugated pVIII subunits.

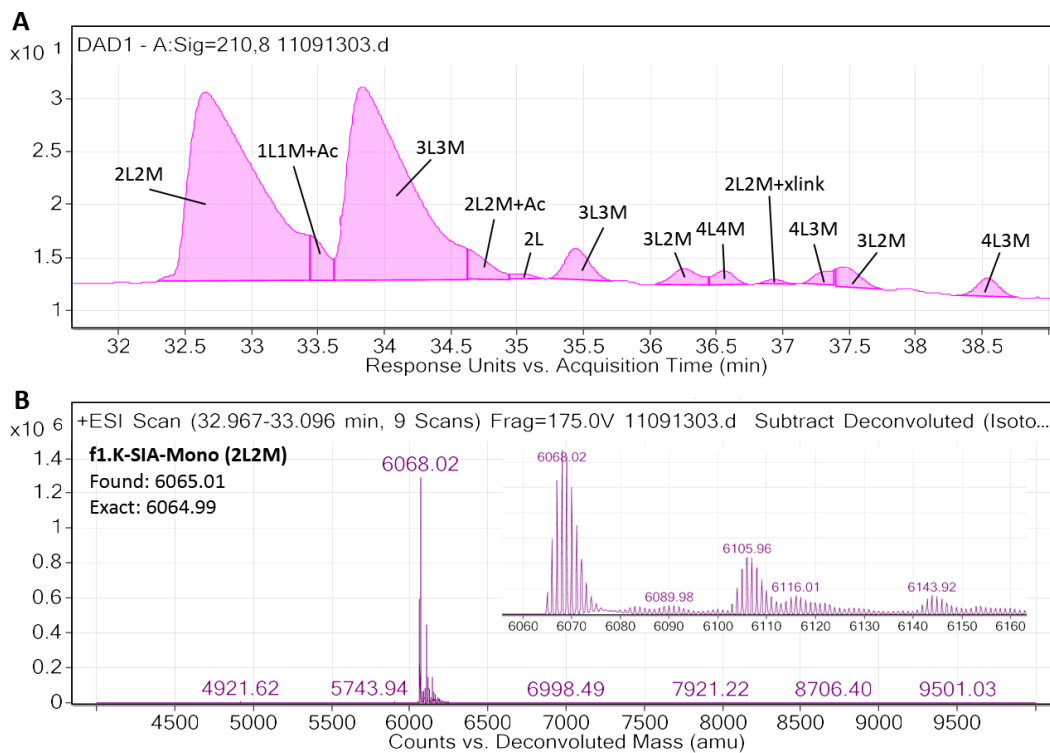


Figure 49. LC-UV-ESI-MS analysis of f1.K-SIA-Mono glycoconjugate. **A**] The UV chromatogram of the f1.K-SIA monosaccharide conjugate, with each peak labeled with the number of linkers (L) and monosaccharide glycans (M) that were present on the pVIII protein. Conjugates containing an acetate (Ac) and an intramolecular crosslink (xlink) are also labeled. **B**] Deconvoluted mass spectrum of the f1.K glycoconjugate containing 2 SIA linkers and 2 monosaccharides (2L2M).

Conjugations using the alkenyl linked phage were performed either through a radical thiol-ene reaction or an anionic thiol Michael addition (Figure 50).⁶⁵ Mannosyl thiol **39** was reacted directly with the electron-deficient alkene of f1.K-(2-ene) as a thiol Michael addition, which has been shown not to require a catalyst.⁶⁶ The f1.K-(4-ene) conjugate, possessing an electron-deficient alkene, was reacted with **39** and the photoinitiator 2,2-azobis(2-methylpropionamide) dihydrochloride (AIBA) under UV light.

Two protocols were evaluated for the copper-catalyzed azide-alkyne cycloaddition (CuAAC) of the f1.K-(2-yne) and f1.K-(4-yne) with azidomethyl mannoside **44** (Figure 50). The first protocol was followed as described by M.G. Finn for the CuAAC

coupling of glycans to Q β capsid.⁶⁷ This method involves the production of the catalytic Cu⁺ ions through the *in situ* reduction of Cu²⁺ with sodium ascorbate. Since biological samples are sensitive to both copper and sodium ascorbate,⁶⁸⁻⁷¹ aminoguanidine and tris(3-hydroxypropyltriazolylmethyl)amine (THPTA)⁵⁵ were employed to protect the protein. Aminoguanidine is used to intercept the byproducts of ascorbate oxidation that can covalently modify or crosslink proteins.⁶⁷ THPTA serves the dual purpose of chelating the Cu⁺ ion to preserve its catalytic +1 oxidation state, and to sacrificially intercept radicals and peroxides derived from Cu/O₂/ascorbate reactions that can oxidize or cleave proteins.⁶⁷ The second protocol produces Cu⁺ ions through the reduction of Cu²⁺ with copper powder and utilizes bathophenanthroline as a Cu⁺ ligand and catalyst.⁷² The reaction solution was degassed with nitrogen prior to the addition of reagents.

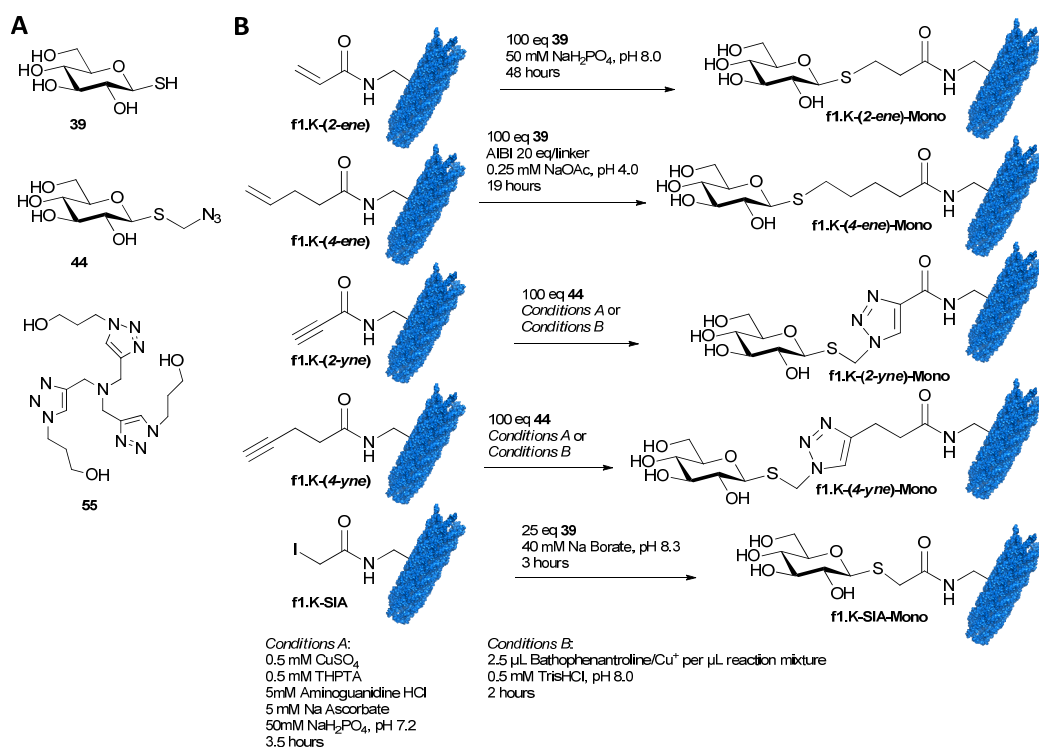


Figure 50. Reaction scheme for the initial monosaccharide conjugations to f1.K phage. A | Mannosyl thiol 39, azidomethyl 1-thio-mannoside 44 and tris(carboxyethyl)phosphine ligand 55 used in the conjugations. B | The conjugation reactions of the f1.K linker conjugates with monosaccharide.

⁵⁵ Synthesized according to the procedure of Finn and coworkers.⁶⁷

The final conjugation was performed with the haloacetyl-derivatized f1.K-SIA phage and mannosyl thiol **39**. To avoid generating free iodine through photolysis, which has the potential to react with tyrosine, histadine and tryptophan residues,⁶² this conjugation was performed in the dark.

The results of the monosaccharide conjugations are displayed in Table 8. The most efficient crosslinker overall was the SIA linker, achieving an average conjugation density of 2.50 monosaccharides per pVIII_{f1.K}, with 94% of the linkers conjugated. Trace amounts of intramolecular crosslinked pVIII were detected for the SIA crosslinked conjugates, which is likely a result of a lysine-bound iodoacetate reacting with a neighbouring lysine on the same pVIII subunit. No UV or MS signal was detected for any intermolecular crosslinked pVIII species.

Table 8. Conjugations of mannose monosaccharides to f1.K phage. 14% and 16% of pVIII conjugates of entries 1 and 2 did not display any monosaccharide.

Entry	Linker	Degree of Conjugation of pVIII (%)									Average Mono/pVIII	Conj. Effic. (%) ^a
		1L1M	2L1M	2L2M	3L1M	3L2M	3L3M	4L2M	4L3M	4L4M		
1	2-ene	-	2	25	0.4	38	15	8	8	-	2.13	76
2	4-ene	-	-	13	-	9	45	7	9	-	2.20	94
3	2-yne	5	2	48	-	19	20	1	6	-	2.21	67
4	4-yne	-	19	15	14	34	15	4	-	-	1.84	71
5	SIA	2	-	47	-	3	42	-	2	4	2.50	94

^a Conjugation efficiency calculated by dividing the average number of glycans per pVIII by the average number of linkers per pVIII (Table 7).

High glycan loading using the f1.K conjugate was able to be achieved with as little as a 5 equivalents of monosaccharide per SIA linker, although 25 equivalents were routinely used. By comparison, it was difficult to obtain complete reaction with the thiol Michael addition and CuAAC reactions using 100 equivalents of monosaccharide (Table 8, Entries 1, 3 & 4). Both thiol-ene and CuAAC reactions were difficult to reproduce, as incomplete conjugations or no conjugation were common. This may be due to the incomplete removal of unreacted linker from the linker addition during size-exclusion chromatography. Dissolved oxygen in the reaction mixtures could also have been a source of poor reproducibility, as it can oxidize the catalytic Cu⁺ in the CuAAC and the mannosyl thiols in the thiol-ene reaction.

Protein degradation was also visible in the mass spectra after the radical initiated thio-ene conjugation and the CuAAC conjugation reactions. The thiol-ene conjugation (Table 8, Entry 2) produced the most degradation, which is expected of a biological sample subjected to a radical reaction. The degraded pVIII subunits produced many overlapping mass peaks that made deconvolution of the extracted mass spectra difficult. The LC separation of the degraded pVIII conjugates was also poor, which reduced the accuracy of integrating the UV absorbance to quantify the incomprehensible mass species. The CuAAC reactions displayed manageable degradation products. More degradation was seen using the bathophenanthroline aided CuAAC reaction, although this conjugation proceeded faster and yielded a greater degree of conjugation than the THPTA aided reaction.

Part II: Preparation of Glycoconjugates for Vaccination

Tetra- and Pentasaccharide Glycoconjugations

A selection of tetra- and pentasaccharide f1.K phage glycoconjugates were produced to be analyzed for their ability to bind 2G12 and ConA. The most promising conjugates were to be used in animal immunization studies. The thiol-ene conjugation strategies were excluded due to protein degradation and low yield. The CuAAC and iodoacetyl conjugation reactions were performed using the optimized conditions from monosaccharide conjugations, using the ascorbate/Cu²⁺ catalytic methodology for the CuAAC reaction. In order to ensure a high degree of conjugation for the CuAAC conjugation, the reaction was performed twice in succession, with an intervening purification step. The reactive equivalents of tetra- and pentasaccharides per linker were reduced to 5:1 for the CuAAC conjugation and 10:1 for the thiol-iodoacetyl conjugation. F88-SIA was also utilized as a carrier in order to assess the effects of lesser glycan density in the binding studies. An additional f1.K-SIA conjugation was performed using a 1:1 mixture of tetra- and pentasaccharide in order to evaluate the effects of glycan heterogeneity in the binding studies.

The tetra- and pentasaccharide conjugates were much less resolvable by LC than the monosaccharide conjugates (Figure 51). The retention times of the pVIII_{f1.K} pentasaccharide conjugates carrying two linkers and two glycans (2L2P) and three linkers and three glycans (3L3P) were too similar to resolve (Figure 51A). The tetrasaccharide equivalents of these conjugates were partially resolvable (Figure 51B). This spectral overlap imposed limitations to the fastidious quantification of the relative number of pVIII species for both f1.K and f88 glycoconjugates. To deal with overlapping absorbances, the area of any given UV absorbance corresponding to two pVIII species was assumed to be the product of equal contribution from both pVIII species. This assumption was made from the observation that for any given absorbance peak composed of two pVIII species, the ion count for both species was roughly equal (Figure 51C), which provides an approximation of the relative abundance of each species. Using this estimation, the UV chromatograms provide an informative overview of the relative abundances of each pVIII conjugate. Overlap of the pVIII_{f88} conjugates was not as

problematic as there are fewer linker-glycan combinations and pVIII_{f88} carries fewer glycans.

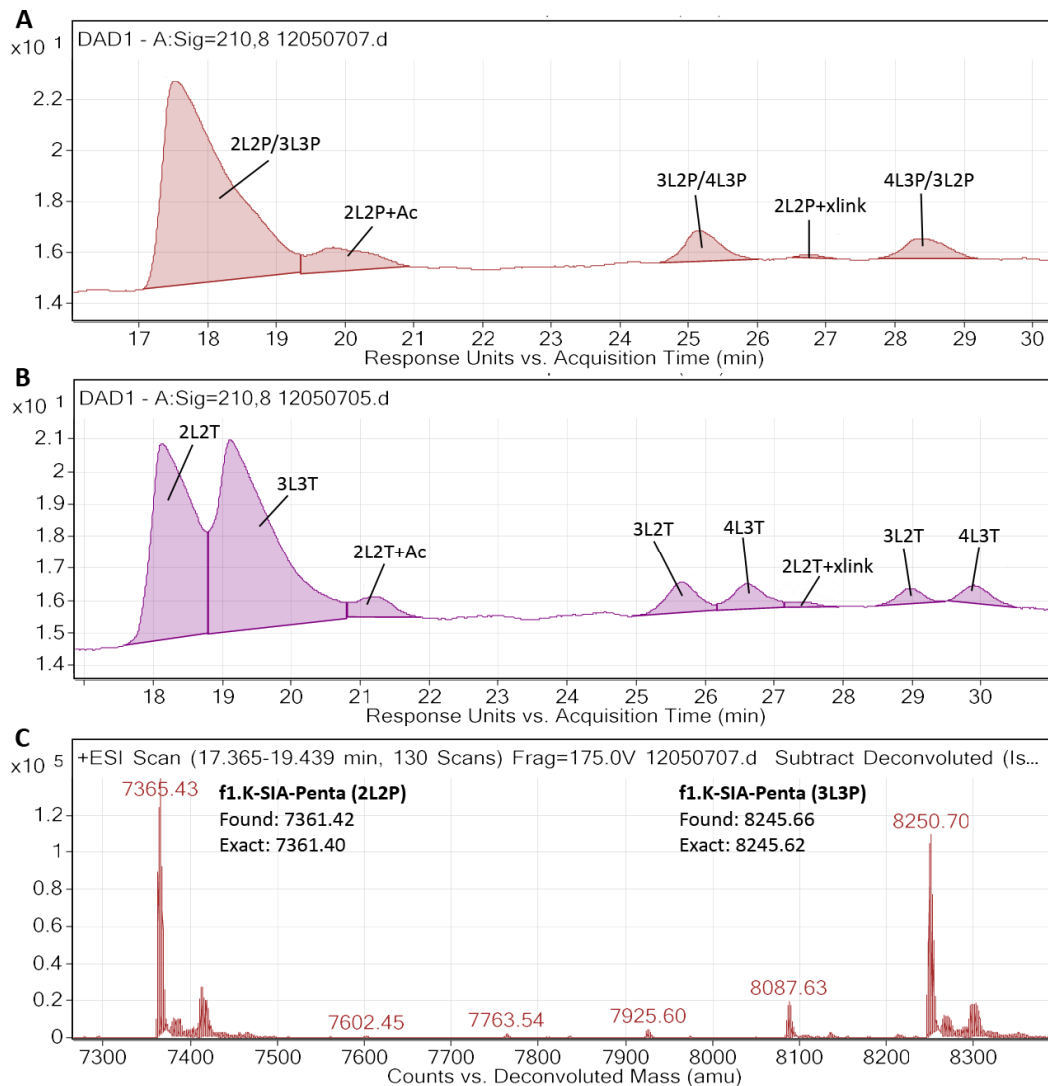


Figure 51. LC-UV chromatograms of the f1.K-SIA-Penta and f1.K-SIA-Tetra conjugates, and a representative deconvoluted mass chromatogram. **A**] The LC-UV chromatogram of f1.K-SIA-Penta conjugate, with peaks labeled by the number of linkers (L) and pentasaccharide (P) associated with the corresponding pVIII conjugate. Acetates (Ac) and intramolecular crosslinkers (xlink) are also noted. **B**] The LC-UV chromatogram of f1.K-SIA-Tetra conjugate with peaks labeled synonymously to the previous chromatogram. **C**] Deconvoluted mass spectrum of the coeluting f1.K glycoconjugates containing 2 linkers/2 pentasaccharides (2L2P) and 3 linkers/3 pentasaccharides (3L3P).

The results of the tetra- and pentasaccharide conjugations with f1.K and f88 phage are shown in Table 9. The remaining conjugations obtained efficiencies of 70% or greater. Overall, the pentasaccharide conjugates displayed a lower average glycan density per pVIII than their tetrasaccharide equivalents, suggesting that the additional

steric mass of the pentasaccharide influences the reaction outcome. The phage conjugates as a whole provide a good range of glycan density for comparison in the ligand binding studies.

Table 9. Glycoconjugation results of f1.K and f88 phage linker conjugates with tetra- and pentasaccharide.

Phage-Linker Conjugate	Reactive Sugar	Degree of Conjugation of pVIII (%)					Average Glycan/pVIII	Conj. Effic. (%) ^a
		1 Glycan	1-2 Glycans	2 Glycans	2-3 Glycans	3 Glycans		
f1.K-(2-yne)	44 (P)	14	-	9	29	57	2.16	70
f1.K-(2-yne)	41 (T)	-	-	28	21	50	2.56	83
f1.K-(4-yne)	44 (P)	-	-	26	63	11	2.17	84
f1.K-(4-yne)	41 (T)	-	6	48	-	46	2.43	94
f1.K-SIA	2 (P)	-	-	9	85	-	2.31	89
f1.K-SIA	1 (T)	-	-	46	-	54	2.54	95
f1.K-SIA	2+1 (P+T)	-	26	11	61	2	2.20	83
f88-SIA	2 (P)	36	60	-	-	-	1.26	93
f88-SIA	1 (T)	77	23	-	-	-	1.16	85

^a Conjugation efficiency calculated by dividing the average number of glycans per pVIII by the average number of linkers per pVIII (Table 7).

β-Glucan Conjugations

Two additional phage glycoconjugates incorporating β-glucan were also produced. β-glucans stimulate the innate immune response through interaction with PRRs, such as dectin-1, displayed on neutrophils, macrophages and dendritic cells.⁷³ The benefits of including β-glucans in vaccine design are just beginning to be appreciated as evidence mounts that β-glucans increase the robustness of the antibody response, recruit T cell help, and regulate the T cell response.⁷⁴⁻⁷⁶

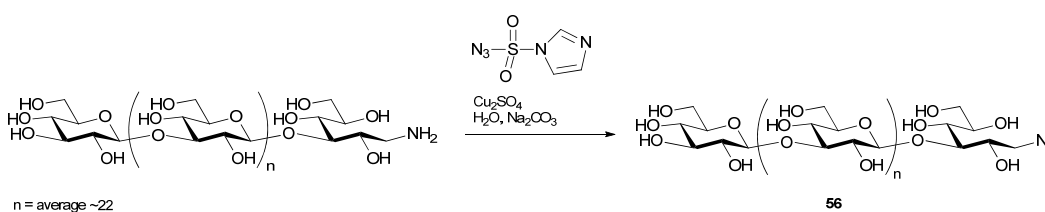
To integrate β-glucan into the phage conjugates, f1.K phage was reacted with SIA and 4-alkynyl crosslinker **54** in a 95:5 ratio (Table 10). The SIA linker would be used to conjugate the tetra- and pentamannosyl thiols **1** and **2**, and the **54** used to conjugate an azide-functionalized β-glucan. This ratio would theoretically coat the phage with a

density of one site for every 24.4 Å in length of phage.^{***} Analysis of the linker addition via LC-UV-MS revealed that the alkyne linker was present in small quantities on all species of pVIII+SIA, although the quantity of heterogeneously linked pVIII could not be verified due to spectral overlap on the UV chromatogram.

Table 10. Degree of conjugation of the heterogenous linker addition of SIA and 4-alkynyl crosslinker **54** to f1.K phage. The number of SIA linkers conjugated to pVIII were used to classify the conjugate species. Linker **54** was present in a small amount on each pVIII-SIA conjugate species.

Phage	Linker	Degree of Conjugation of pVIII (%)				Average SIA/pVIII
		1L	2L	3L	4L	
f1.K	SIA/(4-yne) (95:5)	0.6	56	38	5	2.47

The azido-β-glucan **56** was prepared using previously reductively aminated laminarin derived from a commercially available laminarin source. Laminarin is a polysaccharide composed of repeating β(1→3)-glucans with intermittent β(1→6)-glucans in an approximate 3:1 ratio. The primary amine of **56** was converted to an azide by reaction with five equivalents of the diazo transfer reagent, imidazole-1-sulfonyl azide hydrochloride (Scheme 35).⁷⁷ After 48 hours, the azide product was precipitated in ethanol and the supernatant removed. Removal of the azide transfer reagent was verified by ¹H NMR. The successful transfer of the azide to laminarin was confirmed by the presence of an infrared absorbance band at 2017.31 cm⁻¹.



Scheme 35. Preparation of the azide-functionalized β-glucan **56**.

The heterogeneously linked f1.K-SIA/(4-yne) phage was first conjugated with either tetra- or pentasaccharide **1** or **2** using the conjugation conditions previously described (Table 11). After column purification, the phage were reacted under CuAAC conditions with ~20 equivalents of azido-beta-glucan **56** per alkyne group. LC-UV-MS analysis of the β-glucan-conjugated phage revealed the disappearance of the **54**-linked

^{***} On f1.K phage, every 110 Å length of phage has 90 exposed amines.

pVIII species. Since the conjugation of the large β -glucan structures to the pVIII carrier would greatly suppress ionization, pVIII conjugates carrying β -glucan would be undetectable by MS. Therefore the disappearance of the alkyne linker was used as a confirmation that the CuAAC conjugation was successful.

Table 11. Results of the f1.K conjugation to tetrasaccharide, pentasaccharide and β -glucan 56.

Phage-Linker Conjugate	Reactive Sugar	Degree of Conjugation of pVIII (%)					Average Glycan/pVIII	Conj. Effic. (%) ^a
		1 Glycan	1-2 Glycans	2 Glycans	2-3 Glycans	3 Glycans		
f1.K-SIA/(4-yne)	2 (P)	8 ^b	-	4 ^b	87 ^b	-	2.34	95
f1.K-SIA/(4-yne)	1 (T)	-	4 ^b	44	-	51 ^b	2.47	100
f1.K-SIA/(4-yne)-P	56	10	-	4	86	-	2.33	94
f1.K-SIA/(4-yne)-T	56	-	4 ^b	42	-	54	2.52	102

^a Conjugation efficiency calculated by dividing the average number of glycans per pVIII by the average number of SIA linkers per pVIII (Table 10).

^b pVIII bearing 4-alkynyl crosslinker 54 was observed in these fractions.

Analysis of Phage Integrity

While LC-MS is remarkable for determining the composition of the phage coat protein, this analytical technique reveals little detail about the rest of the phage. It was observed that phage completely lost viability after 30 minutes of exposure to the high concentrations of crosslinkers used in this study. The loss of viability could be due to a number of factors such as the destruction of the genome, an inability to gain entry into the host cell due to pIII modification, or even degradation of the phage quaternary structure.

The DNA of select phage conjugates were analyzed by gel electrophoresis, as shown in Figure 52. Overall, the linker additions appear to leave the genome intact (lanes 4, 7 and 13), but the glycoconjugate additions utilizing the thiol-ene chemistry caused significant degradation (lanes 5, 6, 8 and 9). In contrast, the phage subjected to the SIA conjugation chemistry appear to have suffered little or no DNA damage (lanes 11, 12, 14, 15). Even though a wt phage was not included on the bottom half of the gel for comparison, the consistency of the banding from all SIA-linked phage suggest that SIA linker chemistry had little effect on the genome.

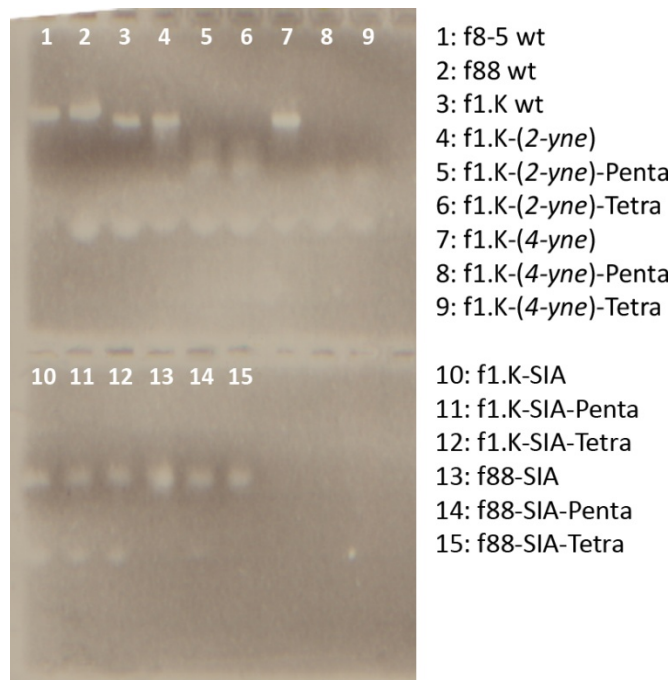


Figure 52. Agarose gel electrophoresis analysis of phage DNA on a 0.8% agarose gel in 4x GBB buffer.⁷⁸ Gel electrophoresis performed by Kevin A. Henry at Simon Fraser University.

Analysis of the phage conjugates by SDS-PAGE revealed a distribution of pVIII species congruent to what was observed by LC-MS (Figure 53). Addition of linker to the coat protein appears to broaden the protein bands, as observed in lanes 3 and 6. The small band seen above pVIII in these lanes could be pVIII dimers formed by the Michael addition between an amine and alkene linker of adjacent pVIII subunits of the phage. The pVIII conjugates displaying two or three glycans were the most abundant as revealed by LC-MS, which correlates well with the banding pattern seen in lanes 4, 5, 7 and 8 (Figure 53). The bands in the lanes containing the pentasaccharide glycoconjugates are also slightly higher than the tetrasaccharide, as would be expected.

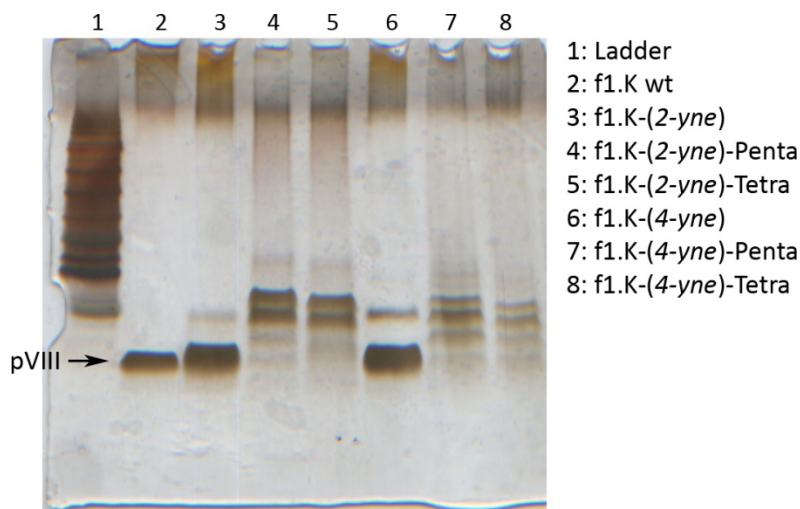


Figure 53. Analysis of phage protein using a modified SDS-PAGE system.⁷⁹ SDS-PAGE performed by Kevin A. Henry at Simon Fraser University.

The quaternary structure was examined using transmission electron microscopy (Figure 54). The conjugated phage were verified as being intact, with relatively little fragmentation observed. Even the phage subjected to the radical thiol-ene reaction conditions exhibited little structural degradation (Figure 54B) despite possessing a highly fragmented genome as revealed by gel electrophoresis (Figure 52, lane 6).

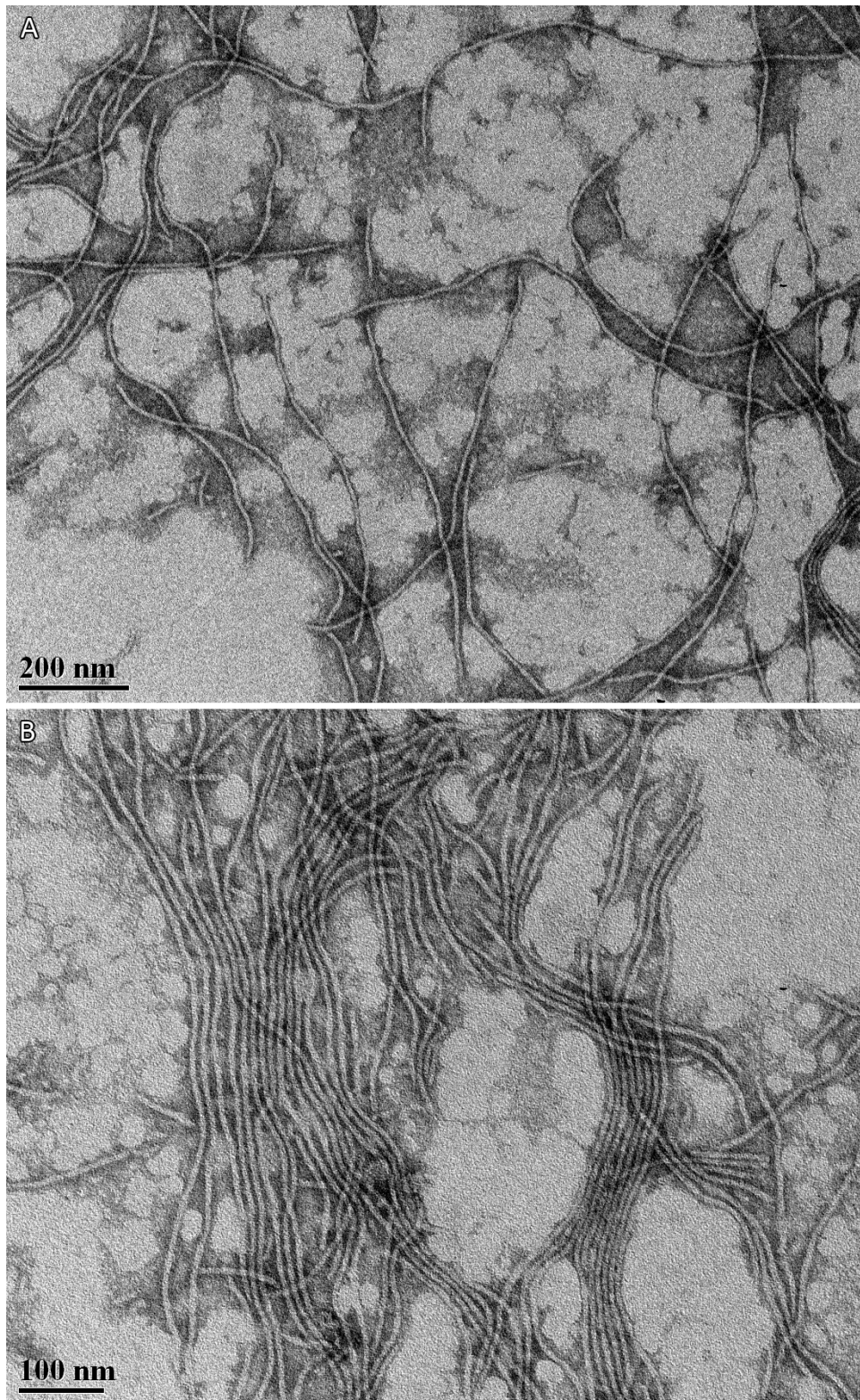


Figure 54. Transmission electron micrographs of f1.K phage particles. A| f1.K-53 phage conjugate observed at 340,000-fold magnification. B| f1.K-(2-*yne*)-Tetra phage glycoconjugate observed at 180,000-fold magnification. The samples were negatively stained with 2% phosphotungstic acid and viewed with a Philips/FEI (Morgagni) Transmission Electron Microscope.

References

1. J. E. Rider, A. B. Sparks, N. Adey, B. and B. K. Kay, *Microbial Methods*, in B. K. Kay, J. Winter, J. McCafferty, *Phage Display of Peptides and Proteins: A Laboratory Manual*, Elsevier Science, **1996**, p. 60
2. M. Y. Zakharova, A. V. Kozyr, A. N. Ignatova, I. A. Vinnikov, I. G. Sherriyakin, A. V. Kolesnikov, *Biotechniques* **2005**, *38*, 194-+.
3. G. P. Smith, J. K. Scott, *Methods Enzymol.* **1993**, *217*, 228-257.
4. K. Korn, H.-H. Foerster, U. Hahn, *Biol. Chem.* **2000**, *381*, 179-181.
5. T. C. Ling, C. M. Loong, W. S. Tan, B. T. Tey, W. M. W. Abdullah, A. Ariff, *Journal of Microbiology* **2004**, *42*, 228-232.
6. S. G. Withers, *Purification and quantitation of bacteriophage M13 using desalting spin columns and digital PCR*
7. D. L. Fraker, M. C. Stovroff, M. J. Merino, J. A. Norton, *J. Exp. Med.* **1988**, *168*, 95-105.
8. Y.-L. Tzeng, A. Datta, V. K. Kolli, R. W. Carlson, D. S. Stephens, *J. Bacteriol.* **2002**, *184*, 2379-2388.
9. R. Medzhitov, P. PrestonHurlburt, C. A. Janeway, *Nature* **1997**, *388*, 394-397.
10. R. Medzhitov, C. A. Janeway, *Cold Spring Harb. Symp. Quant. Biol.* **1999**, *64*, 429-435.
11. J. J. Corrigan, B. M. Bell, *J. Lab. Clin. Med.* **1971**, *77*, 802-&.
12. A. M. Grabowska, R. Jennings, P. Laing, M. Darsley, C. L. Jameson, L. Swift, W. L. Irving, *Virology* **2000**, *269*, 47-53.
13. L. Cardoso, M. Araujo, A. Goes, L. Pacifico, R. Oliveira, S. Oliveira, *Microbial Cell Factories* **2007**, *6*, 1.
14. S. T. Abedon, S. J. Kuhl, B. G. Blasdel, E. M. Kutter, *Bacteriophage* **2011**, *1*, 66-85.
15. H. Geyer, R. Geyer, *Biochimica et Biophysica Acta (BBA) - Proteins & Proteomics* **2006**, *1764*, 1853-1869.

16. C. V. Sapan, R. L. Lundblad, N. C. Price, *Biotechnol. Appl. Biochem.* **1999**, *29*, 99-108.
17. Q. Wang, E. Kaltgrad, T. Lin, J. E. Johnson, M. G. Finn, *Chem. Biol.* **2002**, *9*, 805-811.
18. K. S. Raja, Q. Wang, M. G. Finn, *Chembiochem* **2003**, *4*, 1348-1351.
19. E. Strable, D. E. Prasuhn, A. K. Udit, S. Brown, A. J. Link, J. T. Ngo, G. Lander, J. Quispe, C. S. Potter, B. Carragher, D. A. Tirrell, M. G. Finn, *Bioconjug. Chem.* **2008**, *19*, 866-875.
20. A. Kussrow, E. Kaltgrad, M. L. Wolfenden, M. J. Cloninger, M. G. Finn, D. J. Bornhop, *Anal. Chem.* **2009**, *81*, 4889-4897.
21. R. D. Astronomo, E. Kaltgrad, A. K. Udit, S. K. Wang, K. J. Doores, C. Y. Huang, R. Pantophlet, J. C. Paulson, C. H. Wong, M. G. Finn, D. R. Burton, *Chem. Biol.* **2010**, *17*, 357-370.
22. N. E. van Houten, K. A. Henry, G. P. Smith, J. K. Scott, *Vaccine* **2010**, *28*, 2174-2185.
23. T. N. Peters, *Biochemical Education* **1991**, *19*, 39-39.
24. M. Gassmann, B. Grenacher, B. Rohde, J. Vogel, *Electrophoresis* **2009**, *30*, 1845-1855.
25. Glossman.H, D. M. Neville, *J. Biol. Chem.* **1971**, *246*, 6339-&.
26. J. W. Gurd, W. H. Evans, *Can. J. Biochem.* **1976**, *54*, 477-480.
27. N. Lüthe, H. Plattner, B. Haacke, P. Walther, M. Müller, *Histochem. Cell Biol.* **1986**, *85*, 365-376.
28. E. Szájli, T. Fehér, K. F. Medzihradzky, *Mol. Cell. Proteomics* **2008**, *7*, 2410-2418.
29. R. M. Caprioli, T. B. Farmer, J. Gile, *Anal. Chem.* **1997**, *69*, 4751-4760.
30. W. R. Wilkinson, A. Gusev, A. Proctor, M. Houalla, D. Hercules, *Fresenius' Journal of Analytical Chemistry* **1997**, *357*, 241-248.
31. E. Sugiyama, A. Hara, K.-i. Uemura, *Anal. Biochem.* **1999**, *274*, 90-97.

32. D. M. Desiderio, U. Wirth, J. L. Lovelace, G. Fridland, E. S. Umstot, T. M. D. Nguyen, P. W. Schiller, H. S. Szeto, J. F. Clapp, *J. Mass Spectrom.* **2000**, *35*, 725-733.
33. P. J. Todd, T. G. Schaaff, P. Chaurand, R. M. Caprioli, *J. Mass Spectrom.* **2001**, *36*, 355-369.
34. M. Bucknall, K. C. Fung, M. Duncan, *J. Am. Soc. Mass Spectrom.* **2002**, *13*, 1015-1027.
35. P. Chaurand, S. A. Schwartz, R. M. Caprioli, *Curr. Opin. Chem. Biol.* **2002**, *6*, 676-681.
36. M. Zabet-Moghaddam, E. Heinzle, A. Tholey, *Rapid Commun. Mass Spectrom.* **2004**, *18*, 141-148.
37. D. Bungert, E. Heinzle, A. Tholey, *Anal. Biochem.* **2004**, *326*, 167-175.
38. L. J. Dekker, J. C. Dalebout, I. Siccama, G. Jenster, P. A. Sillevs Smitt, T. M. Luider, *Rapid Commun. Mass Spectrom.* **2005**, *19*, 865-870.
39. T. W. Randolph, B. L. Mitchell, D. F. McLerran, P. D. Lampe, Z. Feng, *Mol. Cell. Proteomics* **2005**, *4*, 1990-1999.
40. A. Tholey, M. Zabet-Moghaddam, E. Heinzle, *Anal. Chem.* **2005**, *78*, 291-297.
41. T. Fujiwaki, M. Tasaka, N. Takahashi, H. Kobayashi, Y. Murakami, T. Shimada, S. Yamaguchi, *Journal of Chromatography B* **2006**, *832*, 97-102.
42. R. Lemaire, J. C. Tabet, P. Ducoroy, J. B. Hendra, M. Salzet, I. Fournier, *Anal. Chem.* **2006**, *78*, 809-819.
43. M. L. Reyzer, R. M. Caprioli, *Curr. Opin. Chem. Biol.* **2007**, *11*, 29-35.
44. N. Floyd, B. Vijayakrishnan, A. R. Koeppe, B. G. Davis, *Angewandte Chemie-International Edition* **2009**, *48*, 7798-7802.
45. S. Trimpin, A. Rouhanipour, R. Az, H. J. Räder, K. Müllen, *Rapid Commun. Mass Spectrom.* **2001**, *15*, 1364-1373.
46. R. Knochenmuss, R. Zenobi, *Chem. Rev.* **2002**, *103*, 441-452.

47. G. Schlosser, G. Pocsfalvi, E. Huszár, A. Malorni, F. Hudecz, *J. Mass Spectrom.* **2005**, *40*, 1590-1594.
48. A. Tholey, E. Heinzle, *Anal. Bioanal. Chem.* **2006**, *386*, 24-37.
49. J. B. Whitfield, *Clin. Chem.* **2007**, *53*, 1-2.
50. T. M. Annesley, *Clin. Chem.* **2003**, *49*, 1041-1044.
51. R. Bonfiglio, R. C. King, T. V. Olah, K. Merkle, *Rapid Commun. Mass Spectrom.* **1999**, *13*, 1175-1185.
52. M. R. Larsen, P. Højrup, P. Roepstorff, *Mol. Cell. Proteomics* **2005**, *4*, 107-119.
53. D. S. Dalpathado, H. Desaire, *Analyst* **2008**, *133*, 731-738.
54. Y. Zhang, E. P. Go, H. Desaire, *Anal. Chem.* **2008**, *80*, 3144-3158.
55. C. C. Nwosu, J. S. Strum, H. J. An, C. B. Lebrilla, *Anal. Chem.* **2010**, *82*, 9654-9662.
56. A. R. Goldfarb, *J. Biol. Chem.* **1953**, *201*, 317-320.
57. K. B. M. L. A. C.B. Anfinsen and T. E. John, *Ultraviolet spectra Of Proteins and Amino Acids*, in D. B. Wetlaufer, *Adv. Protein Chem.*, Academic Press, **1963**, p. 303-390
58. K. Rosenheck, P. Doty, *Proceedings of the National Academy of Sciences* **1961**, *47*, 1775-1785.
59. N. E. van Houten, M. B. Zwick, A. Menendez, J. K. Scott, *Vaccine* **2006**, *24*, 4188-4200.
60. C. Choudhary, C. Kumar, F. Gnad, M. L. Nielsen, M. Rehman, T. C. Walther, J. V. Olsen, M. Mann, *Science* **2009**, *325*, 834-840.
61. S. Zhao, W. Xu, W. Jiang, W. Yu, Y. Lin, T. Zhang, J. Yao, L. Zhou, Y. Zeng, H. Li, Y. Li, J. Shi, W. An, S. M. Hancock, F. He, L. Qin, J. Chin, P. Yang, X. Chen, Q. Lei, Y. Xiong, K.-L. Guan, *Science* **2010**, *327*, 1000-1004.
62. G. T. Hermanson, *Bioconjugate Techniques*, 2nd ed., Academic Press: London, Amsterdam, Burlington, San Diego, **2008**
63. S. Mädler, C. Bich, D. Touboul, R. Zenobi, *J. Mass Spectrom.* **2009**, *44*, 694-706.

64. K. Li, Y. Chen, S. Li, H. G. Nguyen, Z. Niu, S. You, C. M. Mello, X. Lu, Q. Wang, *Bioconjug. Chem.* **2010**, *21*, 1369-1377.
65. C. E. Hoyle, C. N. Bowman, *Angewandte Chemie International Edition* **2010**, *49*, 1540-1573.
66. E. J. Grayson, G. J. L. Bernardes, J. M. Chalker, O. Boutureira, J. R. Koeppel, B. G. Davis, *Angewandte Chemie-International Edition* **2011**, *50*, 4127-4132.
67. V. Hong, S. I. Presolski, C. Ma, M. G. Finn, *Angewandte Chemie International Edition* **2009**, *48*, 9879-9883.
68. S. C. Fry, *Biochem. J.* **1998**, *332*, 507-515.
69. R. H. Nagaraj, D. R. Sell, M. Prabhakaram, B. J. Ortwerth, V. M. Monnier, *Proceedings of the National Academy of Sciences* **1991**, *88*, 10257-10261.
70. Q. Wang, T. R. Chan, R. Hilgraf, V. V. Fokin, K. B. Sharpless, M. G. Finn, *J. Am. Chem. Soc.* **2003**, *125*, 3192-3193.
71. M. R. Levensgood, C. C. Kerwood, C. Chatterjee, W. A. van der Donk, *Chembiochem* **2009**, *10*, 911-919.
72. S. S. Gupta, J. Kuzelka, P. Singh, W. G. Lewis, M. Manchester, M. G. Finn, *Bioconjug. Chem.* **2005**, *16*, 1572-1579.
73. H. S. Goodridge, A. J. Wolf, D. M. Underhill, *Immunol. Rev.* **2009**, *230*, 38-50.
74. I. Caminschi, K. Shortman, *Trends Immunol.* **2012**, *33*, 71-77.
75. W. W. J. Unger, Y. van Kooyk, *Curr. Opin. Immunol.* **2011**, *23*, 131-137.
76. M. A. Johnson, D. R. Bundle, *Chem. Soc. Rev.* **2013**,
77. E. D. Goddard-Borger, R. V. Stick, *Org. Lett.* **2007**, *9*, 3797-3800.
78. L. L. C. Bonnycastle, J. Shen, A. Menendez and J. K. Scott, *General phage methods*, in C. F. Barbas III, D. R. Burton, J. K. Scott, G. J. Silverman, *Phage Display: A Laboratory Manual*, Cold Spring Harbor Laboratory Press, Cold Spring Harbor, NY, **2001**, p. 15.11-15.30
79. M. B. Zwick, A. Menendez, L. L. C. Bonnycastle and J. K. Scott, *Analysis of phage-borne peptides*, in C. F. Barbas III, D. R. Burton, J. K. Scott, G. J. Silverman, *Phage*

Display: A Laboratory Manual, Cold Spring Harbor Laboratory Press, Cold Spring Harbor, NY, **2001**, p. 18, 26-30

CHAPTER 4: Immunization Studies

Part I: Binding Studies of Phage Glycoconjugates

Preparation of Ubiquitin and BSA Glycoconjugates

In order to determine glycan specific antibody titres a heterologous protein was required to display the tetra- and pentasaccharide antigens. A different Ff phage would have been an ideal carrier to display glycans in a similar fashion to f1.K and f88, but antibodies raised against phage have shown significant cross-reactivity with other phage variants.¹ Thus, ubiquitin and BSA were selected as glycan carriers for immunological assays. Ubiquitin was chosen in part because it was similar in molecular weight to pVIII,^{†††} which falls within the resolvable mass range of the LC-MS system, allowing for the same conjugation analysis as the phage. Ubiquitin also has up to seven free amines available for conjugation, allowing for a relatively dense clustering of glycans. Glycan clusters may be important for detecting glycan-specific serum antibodies that were generated from the densely coated phage glycoconjugates. BSA glycoconjugates were also prepared in case the relatively low molecular weight ubiquitin conjugates turned out to be unsuitable for ELISAs.

Ubiquitin glycoconjugates were prepared following the same procedure described for the phage conjugations, using the SIA crosslinker. The equivalents of SIA per amine were reduced to a 4:1 ratio in order to avoid the formation of insoluble protein precipitate and low recovery. Conjugate addition with either tetra- or pentasaccharide **1** and **2** produced the ubiquitin glycoconjugates Ub-(SIA)-Penta and Ub-(SIA)-Tetra with a loading of 5.01 and 4.72 glycans per ubiquitin. BSA glycoconjugates were prepared similarly using the 2-alkynyl crosslinker **54** and tetra- and pentasaccharides **47** and **50**. The degree of conjugation of the resulting BSA-(2-yne)-Penta and BSA-(2-yne)-Tetra conjugates were estimated by MALDI-MS, yielding an average of 42-43 glycans per BSA.

As a side note, the ubiquitin glycoconjugates are a good example of how glycans diminish the ionization efficiency of glycosylated proteins. The UV chromatogram and

^{†††} The MW of pVIII is 5592.9 Da. Ubiquitin has a MW of 8559.6 Da.

total ion chromatogram for each glycoconjugate species displayed different relative abundances for the ubiquitin conjugates as glycan loading increased (Figure 55). The ion count for the ubiquitin species bearing no glycans or 1 glycan was similar to the ion count for the 6-glycan species of ubiquitin (Figure 55A). The UV chromatogram indicated a much higher abundance of the 6-glycan ubiquitin conjugate (Figure 55B), which is a more accurate representation of the ubiquitin glycoconjugate distribution.

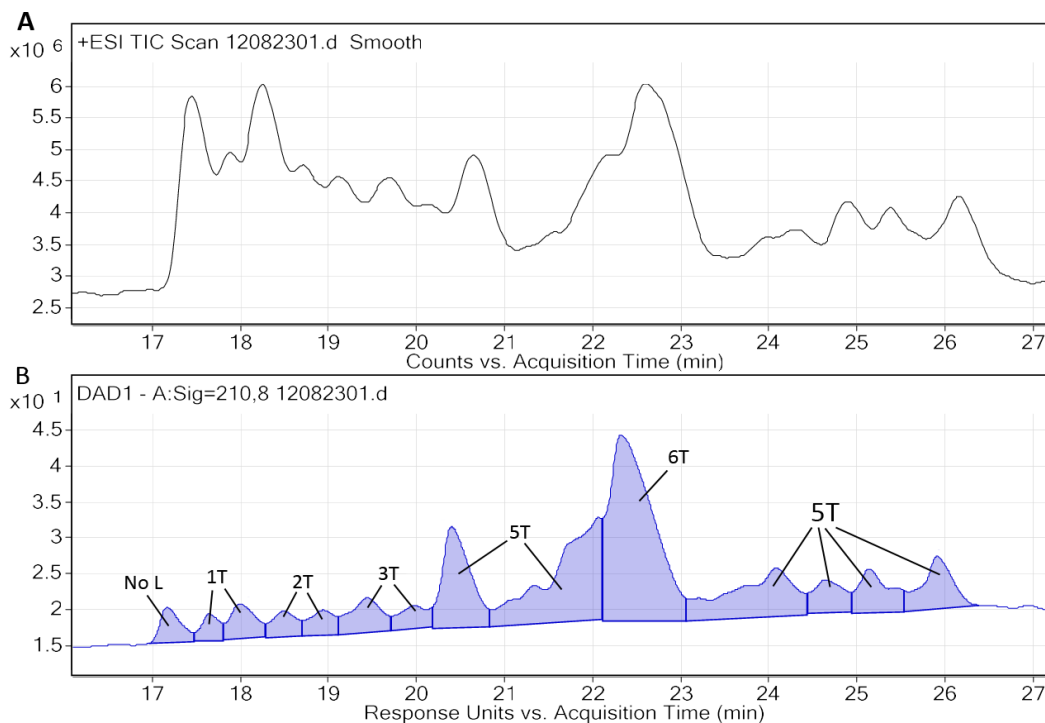


Figure 55. LC-UV and LC-MS chromatograms obtained from Ub-SIA-Tetra. **A** | Total ion chromatogram of Ub-SIA-Tetra. **B** | The UV chromatogram of Ub-SIA-Tetra. The absorbance peaks are labeled corresponding to the number of tetrasaccharides (T) conjugated to ubiquitin.

Ubiquitin Glycoconjugate Binding Studies

Ub-SIA-Penta and Ub-SIA-Tetra were evaluated for their ability to bind concanavalin A (ConA) and the glycan-specific, broadly neutralizing anti-HIV antibody 2G12 by indirect ELISA. ConA is a lectin extracted from the jack-bean, *Canavalia ensiformis*, that binds specifically to terminal α -D-mannosyl and α -D-glucosyl sugars.^{2, 3} 2G12 binds terminal $\text{Man}\alpha 1 \rightarrow 2\text{Man}$ -linked sugars with nanomolar affinity.⁴ Together, these mannose-specific binding proteins were used to verify the presence of the attached oligomannose ligands.

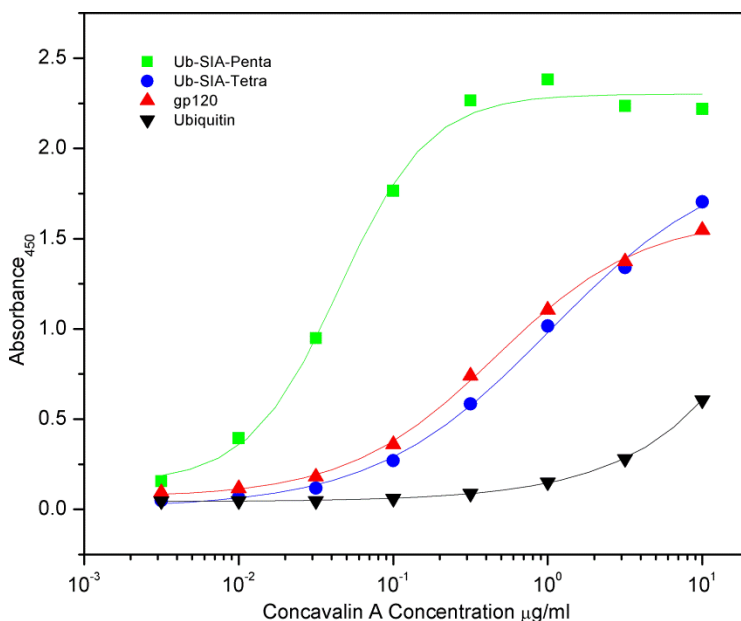


Figure 56. ELISA results of labeled ConA titrated against ubiquitin glycoconjugates and gp120.

The results of an ELISA in which ConA is titrated against immobilized Ub-SIA-Penta and Ub-SIA-Tetra are shown in Figure 56. The pentasaccharide conjugate has a ~25-fold higher relative avidity for ConA than to the tetrasaccharide conjugate. This is understandable since the pentasaccharide hapten has three terminal α -D-mannose moieties versus the one of the tetrasaccharide hapten. Interestingly, the apparent avidity of ConA for Ub-SIA-Tetra was similar to that for gp120_{IIIb}, suggesting a similar displayed density of terminal α -mannose moieties. Since native gp120 is reported to be covered in high-mannose glycans that resemble the pentasaccharide structure, this observation was unexpected, but may be related to the recombinant origin of gp120 used in our ELISAs. As previously discussed, recombinantly produced gp120 displays a greater proportion of complex type glycans, which would reduce the amount of exposed terminal mannose residues, and thus possess fewer binding sites for ConA. The recombinant gp120_{IIIb} protein used in our studies, which is expressed in CHO cells, has been shown to contain 13 complex glycans and 11 high-mannose/hybrid glycans.^{5,6}

Titration of 2G12 against the ubiquitin glycoconjugates revealed a higher relative avidity for the tetrasaccharide conjugate than the pentasaccharide conjugate (Figure 57). This disparity can again be attributed to differences in the hapten structure, as the pentasaccharide does not contain any Man α 1 \rightarrow 2Man-linked moieties that are a

recognition epitope of 2G12. The relative avidity of 2G12 for Ub-SIA-Tetra is an order of magnitude lower than that for gp120_{IIIb}, which is likely due to inferior clustering of the tetrasaccharide glycan on the ubiquitin surface. The 2G12 titration curve for gp120_{IIIb} is identical to that reported in the literature.⁷

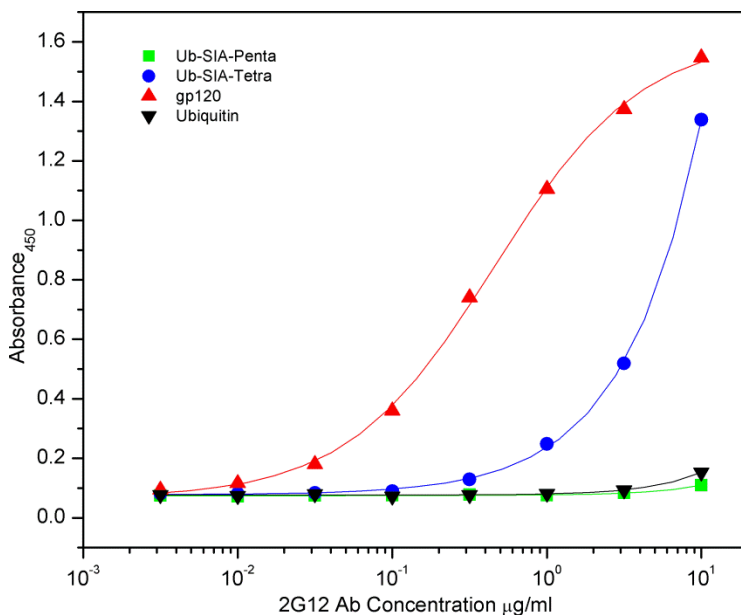


Figure 57. ELISA results of antibody 2G12 titrated against ubiquitin glycoconjugates and gp120.

The combination of these ELISAs suggest that the SIA glycoconjugates will suffice as screening antigens for glycan-specific antibodies produced by immunization of mice. An ideal screening antigen would incorporate an antigenically different carrier that presents the synthetic glycans in a similar density to that of the phage glycoconjugates used for immunization, but no such carrier was available at the time.

Phage Glycoconjugate Binding Studies

The phage conjugates bearing tetra- and pentasaccharide haptens were evaluated by ELISA for binding to ConA and 2G12 binding. Much like with the ubiquitin glycoconjugates, ConA displayed an increased affinity for the pentasaccharide conjugates over the tetrasaccharide conjugates (Figure 58). Likewise, 2G12 displayed a higher affinity for phage bearing the tetrasaccharide hapten over the pentasaccharide hapten (Figure 58). In comparison to gp120_{IIIb}, 2G12 bound the two f1.K-Tetra conjugates utilizing the 2-alkynyl and SIA linkers with a 3-fold lower concentration for

50% binding. Such a comparison may not be so meaningful as it has been observed in the literature that 2G12 binds gp120 of strains JR-FL and JR-CSF in the 0.015 $\mu\text{g}/\text{mL}$ (0.1 nM) range for 50% binding.^{8,9} The glycoform of gp120 is well documented to be both strain and expression system dependent, and these variations in glycoform can impact 2G12 binding.^{10,11}

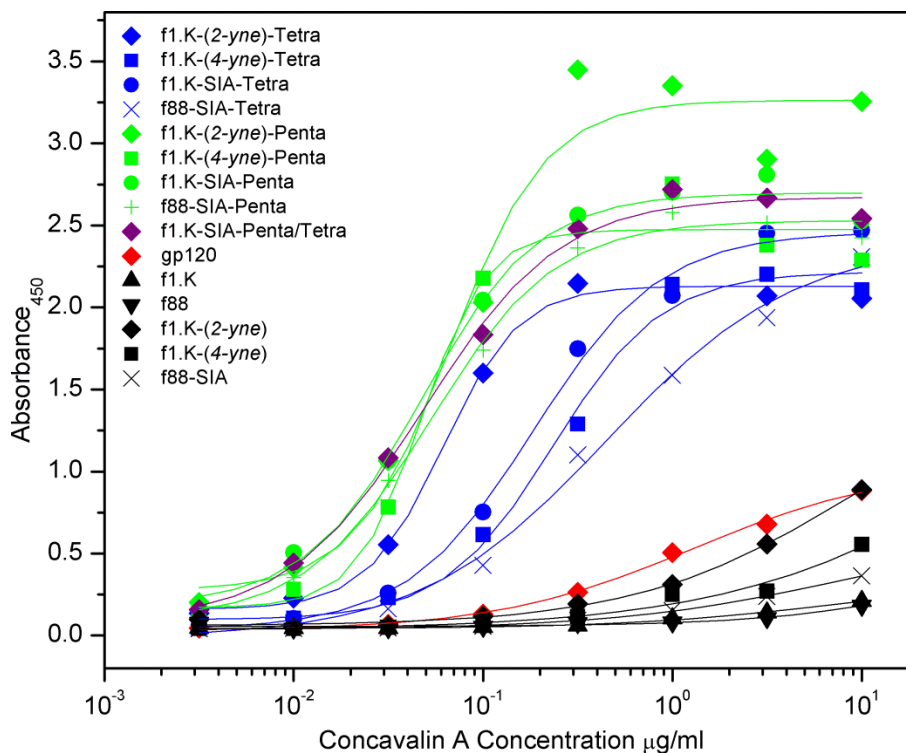


Figure 58. ELISA results of ConA titrated against the phage tetra- and pentasaccharide glycoconjugates.

The lower binding affinity of the f1.K-(4-yne)-Tetra conjugate for 2G12 in comparison to the f1.K-(2-yne)-Tetra and f1.K-SIA-Tetra conjugates may be attributed to differences in conjugation density or linker length. Both the SIA and 2-alkynyl-linked phage conjugates achieved a loading of ~ 2.55 glycans per pVIII subunits, whereas the 4-alkynyl-phage conjugate averaged 2.43 glycans per pVIII subunit. The 4-alkynyl linker is much longer than the SIA linker, and adds an additional two carbons to the spacer chain in comparison to the 2-alkynyl chain. This may increase its flexibility in a way that detracts from the more structurally rigid presentation of the natural glycans. These slight variations in linker length and glycan density may account for the decreased interaction with 2G12, but they are so minimal that any derived correlation should be taken lightly. A more significant correlation can be made between the f1.K-SIA-Tetra

and f88-SIA-Tetra conjugates, where the glycan loading of the f88 phage conjugate is less than half that of the f1.K phage conjugate (2.54 vs 1.16 glycans/pVIII), causing a ~10-fold decrease in avidity for 2G12. The heterogeneously conjugated phage, f1.K-SIA-Penta/Tetra, displayed decreased interaction with 2G12, likely owing to the decreased population of the tetrasaccharide hapten on this conjugate.

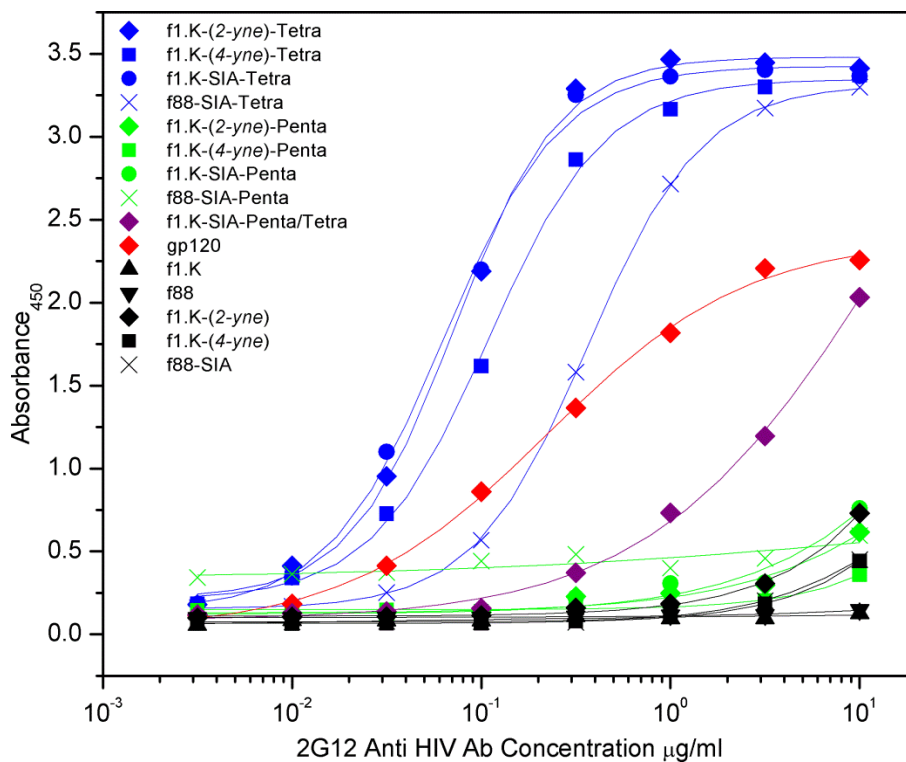


Figure 59. ELISA results of antibody 2G12 titrated against the phage tetra- and pentasaccharide glycoconjugates.

These results highlight the importance of glycan density in correctly mimicking the gp120 surface. Thus, f1.K was chosen as the carrier for its aptitude for glycan clustering. The SIA linker chemistry was chosen for its reliability and its minimalistic linker length. Both the tetrasaccharide and pentasaccharide haptens were intended to be used in mouse immunization studies. Even though 2G12 did not bind the pentasaccharide hapten, the Man5 pentasaccharide is a predominant glycan of native gp120 and may be successful in generating crossreactive antibodies that recognize gp120. The effects of β -glucans on the immunological outcome of the immunizations were also to be explored.

Part II: Mouse Immunizations

Four phage conjugates were used to immunize groups of five mice. Two conjugates were prepared from the Man₅ pentasaccharide, f1.K-SIA-Penta and the related conjugate f1.K-SIA(2-*yne*)-Penta/ β glucan with attached β -glucan for dendritic cell targeting. Two related conjugates were derived from the Man₄ tetrasaccharide, f1.K-SIA-Tetra and e f1.K-SIA(2-*yne*)-Tetra/ β glucan.

ELISA Titrations of Mouse Sera^{*}**

Mice were immunized four times and following the final injection of vaccine, sera were collected and the experiment was terminated. The sera of individual mice were titrated against Ub-SIA-Penta and Ub-SIA-Tetra coated ELISA plates. Mice receiving the f1.K-SIA-Penta vaccines responded most effectively to the conjugate lacking β -glucan. Only one of five mice receiving the conjugate that was intended to target dendritic cells through conjugation with β -glucans gave a strong titre (Figure 60A). The antibody response to both tetrasaccharide conjugates was uniformly low with the majority of end point titres greater than 1:1,000 (Figure 60B). To ensure that the observations of tetrasaccharide conjugates was not an artifact of poor Ub-SIA-Tetra adsorption the ELISA plate, the presence of the ubiquitin was verified by performing a BCA assay in a mock ELISA experiment following the washing steps to establish protein concentration.

^{***} ELISA work was performed by Mrs. Joanna Sadowska.

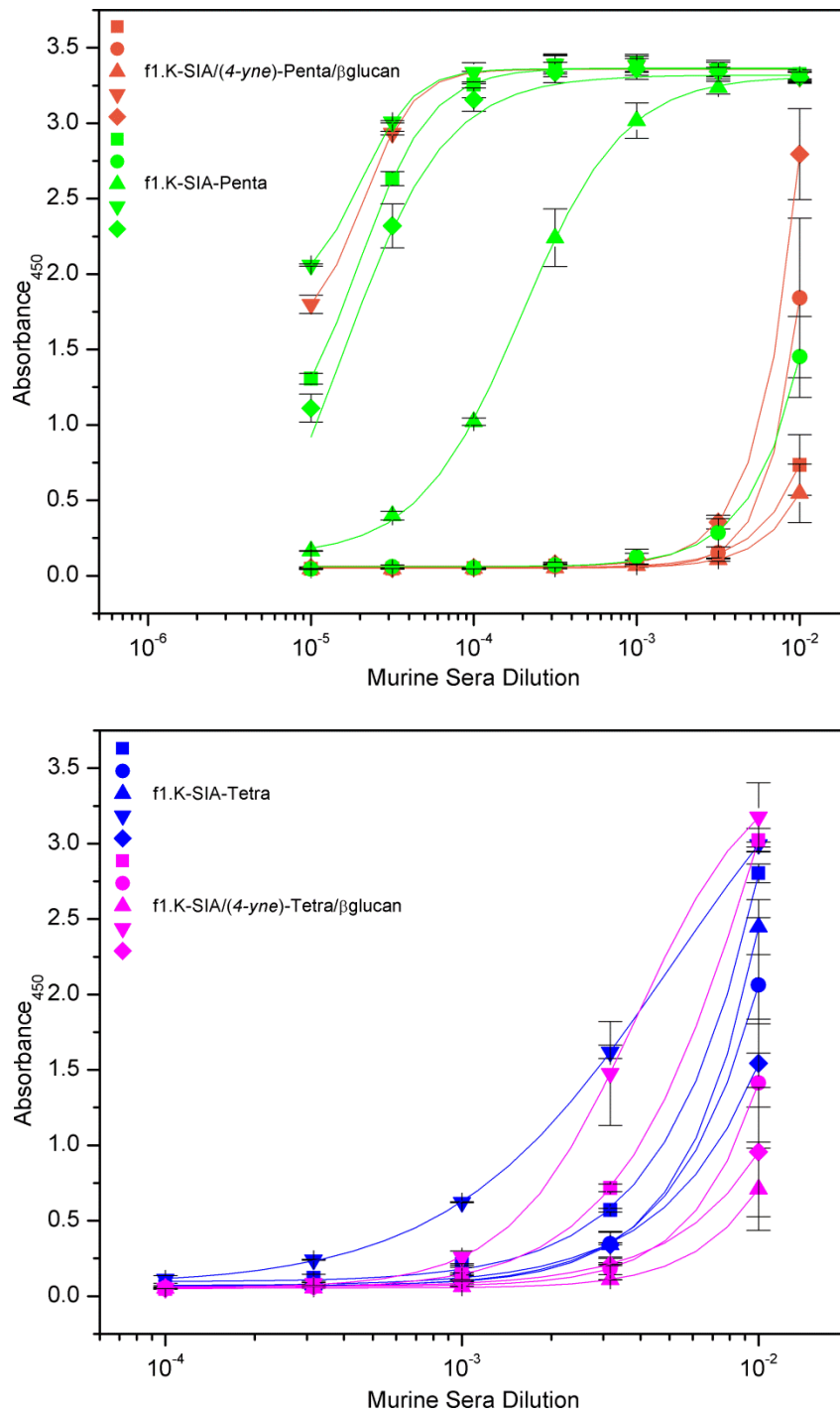


Figure 60. Titration of immune sera against ubiquitin glycoconjugates. A) Serum from mice immunized with f1.K-SIA-Tetra and f1.K-SIA/(4-yne)-Tetra/βglucan titrated against Ub-SIA-Tetra. B) Serum from mice immunized with f1.K-SIA-Penta and f1.K-SIA/(4-yne)-Penta/βglucan titrated against Ub-SIA-Penta. Each colored symbol corresponds to the final-bleed immune sera from individual mice. Data from two repeated ELISAs were averaged and the standard deviation indicated by the error bars.

In total, only 5 out of 20 immunized mice displayed a reasonable titres that exceed 1:1000 against the carbohydrate haptens, and the strongest response was

consistently observed for the pentasaccharide, without β -glucan help. These results were verified with ELISAs where the plates were coated with the BSA-(2-*ylne*)-Penta and BSA-(2-*ylne*)-Tetra conjugates (Figure 61A, B), ruling out any irregularities from using ubiquitin as a carrier.

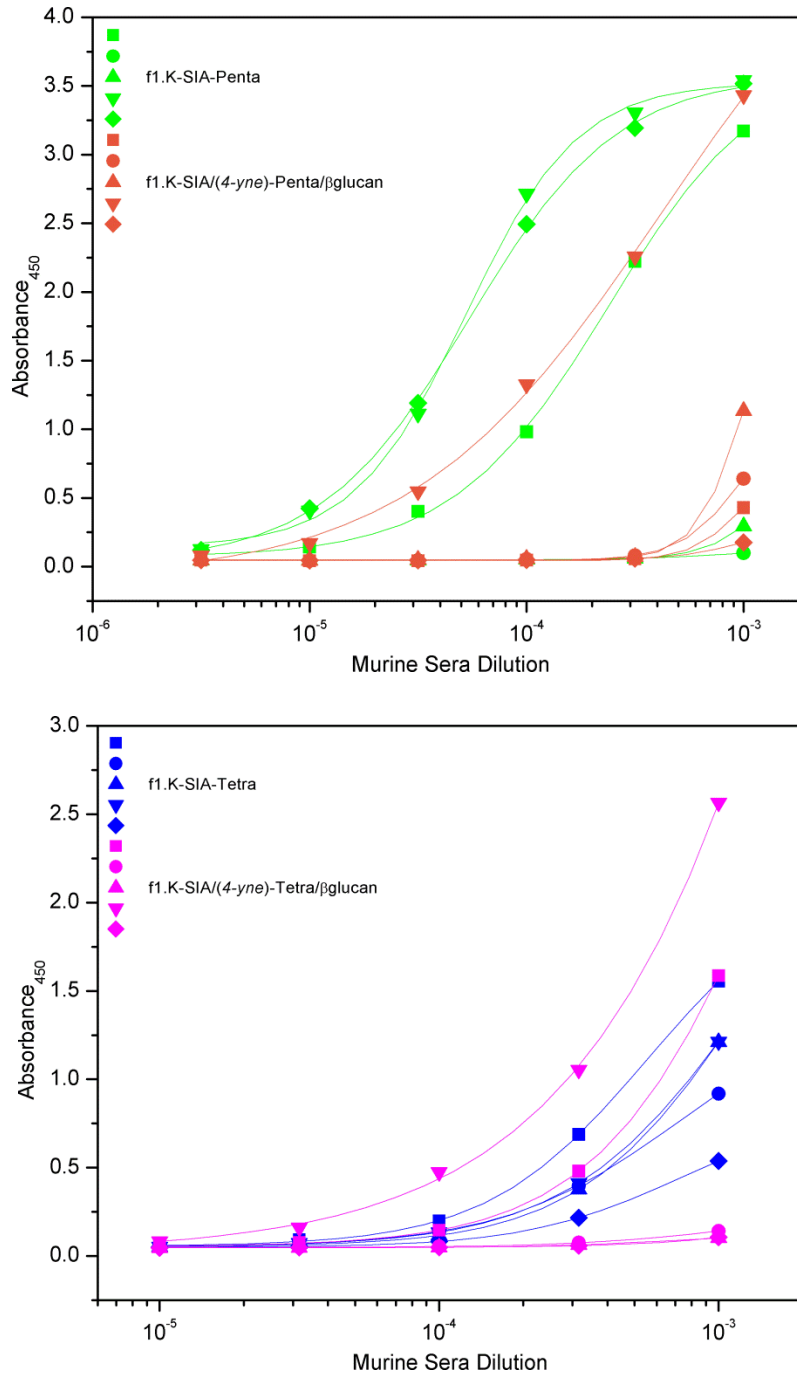


Figure 61. Titration of immune sera against BSA glycoconjugates. A| Sera from f1.K-SIA-Penta and f1.K-SIA/(4-ylne)-Penta/ β glucan immunized mice titred against Ub-(2-ylne)-Penta. B| Sera from f1.K-SIA-Tetra

and f1.K-SIA/(4-*yne*)-Tetra/ β glucan immunized mice titrated against BSA-(2-*yne*)-Tetra. Each colored symbol corresponds to the final-bleed immune sera from an individual mouse.

The ability of anti-mannose serum antibodies to bind to the glycans of gp120 was assessed with recombinant gp120_{III_B} (Figure 62). No significant titres were observed. In all cases the sera failed to titre above 1:1,000, a dilution our lab regards as the threshold for significant anti-hapten responses. This is striking as high titres of anti-mannose antibodies for the f1.K-SIA-Penta immunized mice were produced.

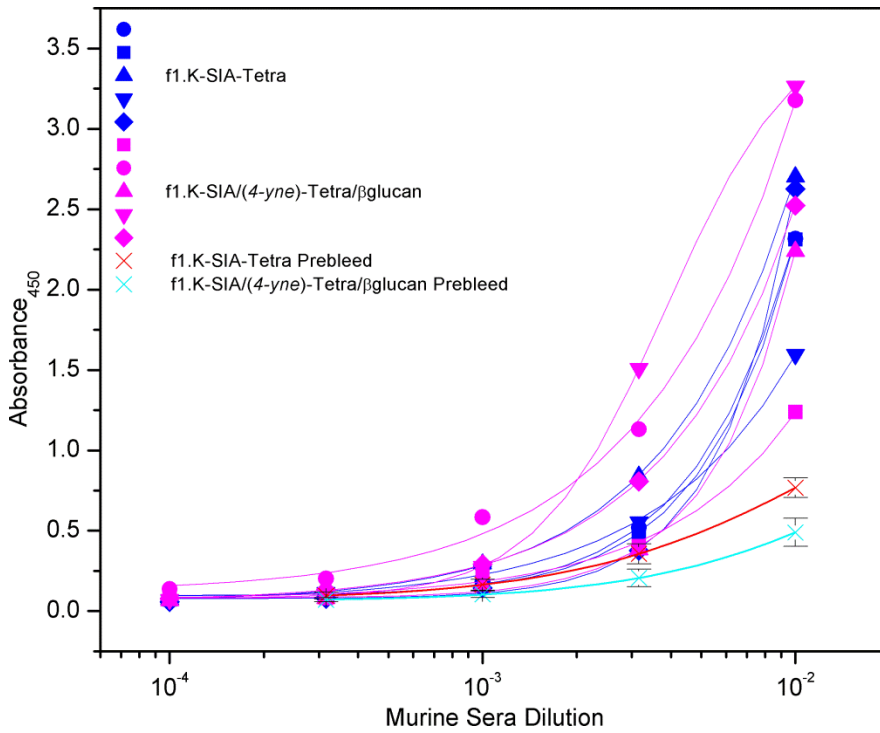
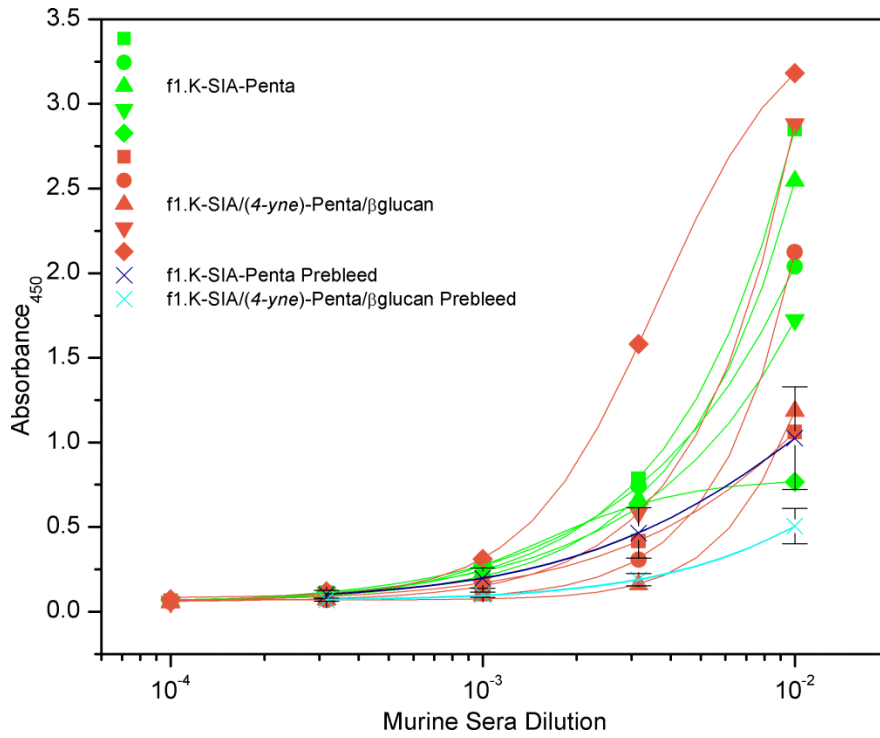


Figure 62. Sera analysis for crossreactive anti-gp120 antibodies. A| Sera from f1.K-SIA-Penta and f1.K-SIA/(4-yne)-Penta/βglucan immunized mice titrated against gp120_{IIIb}. B| Sera from f1.K-SIA-Tetra and f1.K-SIA/(4-yne)-Tetra/βglucan immunized mice titrated against gp120_{IIIb}. Each symbol corresponds to the final-bleed immune sera from an individual mouse. Prebleeds are averaged for each set of mice.

It was noted that abscesses formed at the sites of injection on all the mice. This is likely a reaction to the residual LPS bound to the phage. Abscess formation is an inflammatory response that encapsulates foreign material to contain the spread of infection. This also prevents immune cells from interacting with the pathogen within the capsule structure of the abscess, which could explain why such low antibody titres were observed for the majority of the immunizations.

In order to address the impact of abscess formation on the anti-mannose antibody response, six mice were immunized with surplus phage conjugate from the first immunization that were treated with polymixin B-immobilized resin to remove residual LPS. The β -glucan conjugates were excluded from this side study. The vaccination regime was shorter, consisting of only three immunizations before sera collection and termination. Only half of the mice developed abscesses during the course of the immunization experiment. The sera of individual mice were titrated against Ub-SIA-Penta and Ub-SIA-Tetra coated ELISA plates (Figure 63). One out of three mice receiving the f1.K-SIA-Penta and f1.K-Tetra vaccines produced a significant anti-mannose response. The titres of these responses were lower than the responses observed from the first immunization, which may be due to the lack of the LPS providing an adjuvant effect, or the shortened immunization regimen.

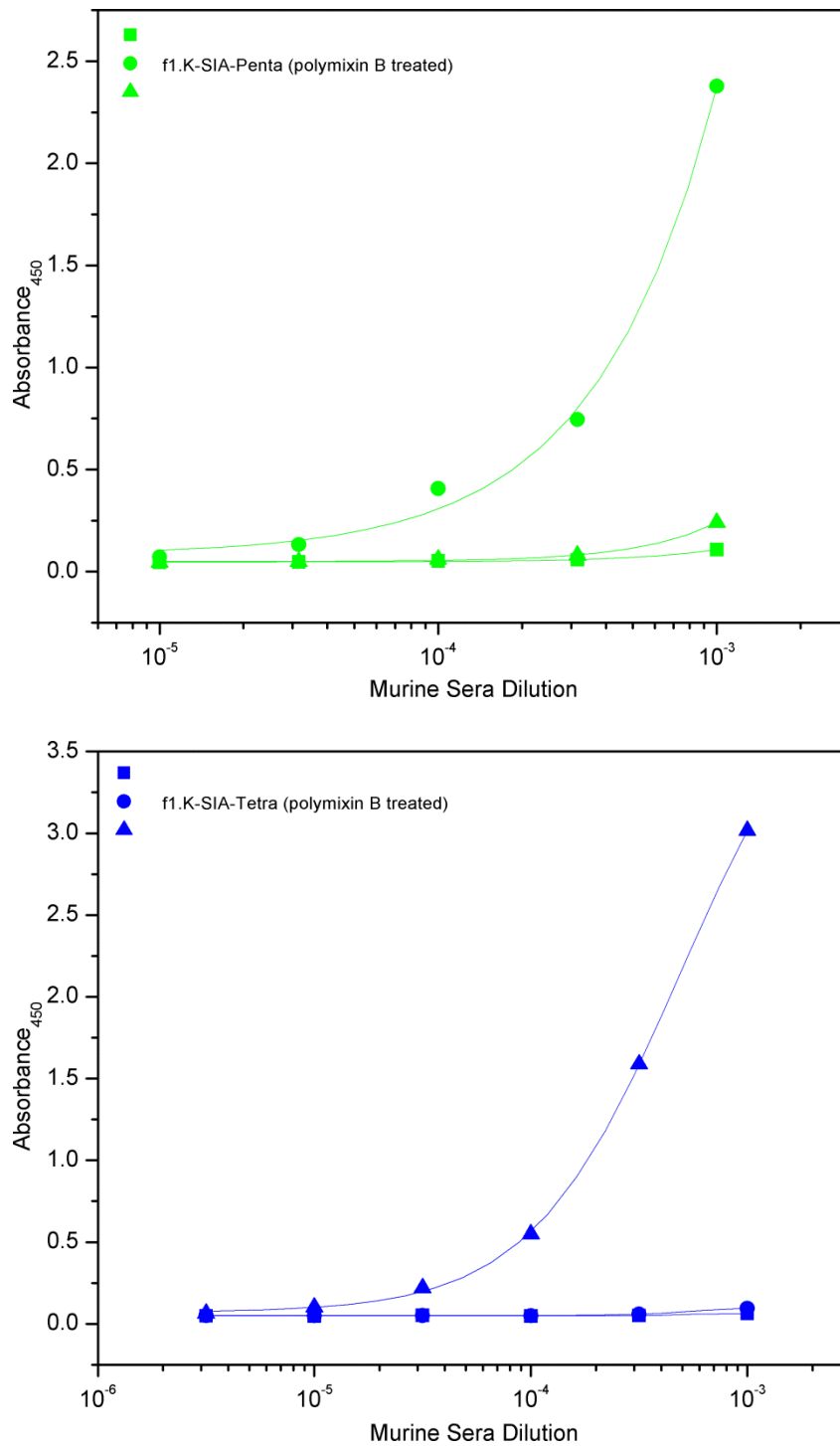


Figure 63. Sera analysis of mice immunized with phage conjugates treated with polymixin B. A| Sera from polymixin B treated f1.K-SIA-Penta and immunized mice titred against Ub-(2-yne)-Penta. B| Sera from polymixin B treated f1.K-SIA-Tetra immunized mice titrated against BSA-(2-yne)-Tetra. Each symbol corresponds to the final-bleed immune sera from an individual mouse.

Concluding remarks

The f1.K carrier is one of the best glycan clustering scaffolds used to mimic gp120 thus far. The f1.K-SIA-Tetra conjugate displayed an apparent 20-fold^{§§§} stronger affinity for 2G12 than the Q β icosahedral virus glycoconjugate (Q β K16M-Man₄) created by M.G. Finn and coworkers.⁹ This increase in binding avidity is likely due to the greater clustering density of oligomannose that was achieved with the f1.K carrier. The repetitive display of the oligomannose structures on f1.K should have been ideal to evoke a strong B cell response, which is a known characteristic of virus particles.^{12, 13} However, only 5 out of 20 mice produced a significant antibody response against the glycan hapten in our first immunization studies (Figure 60). Four of the high titres towards glycan were produced from the f1.K-SIA-Penta conjugate, and the other high titre against the f1.K-SIA/(4yne)-Penta/ β glucan conjugate. The anti-mannose titres obtained from the tetrasaccharide conjugates paled in comparison to their pentasaccharide counterparts. This may be due to a number of reasons, such as the pentasaccharide providing a more structurally distinct recognition epitope due to its relative complexity, or a more densely covered glycan surface was more achievable with the pentasaccharide due to its inherently more bulky biantennary structure. Glycan-specific responses have been raised against the Man₄ structure in two other HIV-1 glycoconjugate vaccines, but these were performed in rabbits.^{9, 14} Literature data as far back as the 1960s has documented strong antibody responses to small oligosaccharide haptens in rabbits and goats.¹⁵ By comparison, there are many reports of poor murine responses to these types of conjugates.¹⁵

The inconsistency of the anti-mannose response may be due to the formation of abscesses sequestering the vaccine from the grasp of the adaptive immune system. The dense covering of the phage surface with high-mannose structures could also potentially mask the virus from the immune system, much like the glycan shield of HIV-1. The high-mannose structures are also recognized by the innate immune system, such as the mannose receptor C-type 1 and DC-SIGN found on macrophages and dendritic cells, or the aptly named serum protein, mannose-binding protein (MBP).¹⁶ These

^{§§§} Half-max binding level of 2G12 titrations against: Q β K16M-Man₄: 10 nM (1.5 μ g/mL).⁹ f1.K-SIA-Tetra: 0.8 μ g/mL (0.5 nM) (Figure 59). Units converted using a MW of 150 kDa for 2G12.

mannose-binding agents have been known to accelerate the clearance of proteins carrying high-mannose glycan from the blood stream.^{17, 18} There is the possibility that the oligomannose phage conjugates used in our immunizations are interacting with the innate immune system in an unexpected way, and are being cleared from the mouse before a sizable immune response could be mounted.

Lastly, the β -glucan did not increase the glycan-specific portion of the antibody response, as indicated by the poor binding to the ubiquitin and BSA conjugates (Figure 60, 7). It could be inferred that the presence of the β -glucan had a suppressive effect on the glycan antibody response, although our data set is too small, and the sera binding results are too inconsistent to draw any firm conclusions. Such a suppressive effect could occur by confusing the innate immune system as to which type of pathogen it is dealing with. β -glucans, which are a component of fungal cell walls, interact with antigen presenting cells, particularly dendritic cells, through the PRR dectin-1. Virus particles also interact with dendritic cells through PRRs, as well as endotoxin derived from *E.coli*, which is residually bound to the phage conjugates. The mode of activation through the specific PRR can produce different types of immune responses.^{19, 20}

References

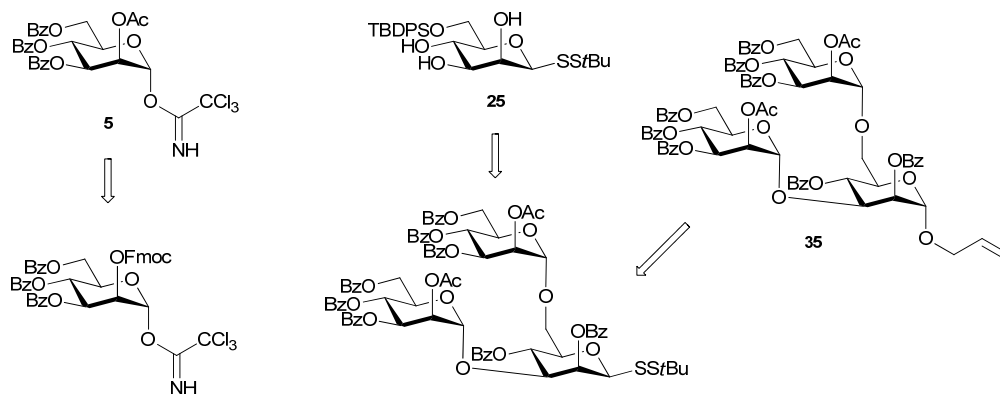
1. N. E. van Houten, K. A. Henry, G. P. Smith, J. K. Scott, *Vaccine* **2010**, *28*, 2174-2185.
2. I. J. Goldstein, C. E. Hollerman, E. E. Smith, *Biochemistry (Mosc.)* **1965**, *4*, 876-883.
3. P. N. Kanellopoulos, K. Pavlou, A. Perrakis, B. Agianian, C. E. Vorgias, C. Mavrommatis, M. Soufi, P. A. Tucker, S. J. Hamodrakas, *J. Struct. Biol.* **1996**, *116*, 345-355.
4. D. A. Calarese, C. N. Scanlan, M. B. Zwick, S. Deechongkit, Y. Mimura, R. Kunert, P. Zhu, M. R. Wormald, R. L. Stanfield, K. H. Roux, J. W. Kelly, P. M. Rudd, R. A. Dwek, H. Katinger, D. R. Burton, I. A. Wilson, *Science* **2003**, *300*, 2065-2071.
5. T. Mizuochi, M. W. Spellman, M. Larkin, J. Solomon, L. J. Basa, T. Feizi, *Biochem. J.* **1988**, *254*, 599-603.
6. C. K. Leonard, M. W. Spellman, L. Riddle, R. J. Harris, J. N. Thomas, T. J. Gregory, *J. Biol. Chem.* **1990**, *265*, 10373-10382.
7. C. N. Scanlan, R. Pantophlet, M. R. Wormald, E. O. Saphire, R. Stanfield, I. A. Wilson, H. Katinger, R. A. Dwek, P. M. Rudd, D. R. Burton, *J. Virol.* **2002**, *76*, 7306-7321.
8. K. J. Doores, Z. Fulton, M. Huber, I. A. Wilson, D. R. Burton, *J. Virol.* **2010**, *84*, 10690-10699.
9. R. D. Astronomo, E. Kaltgrad, A. K. Udit, S. K. Wang, K. J. Doores, C. Y. Huang, R. Pantophlet, J. C. Paulson, C. H. Wong, M. G. Finn, D. R. Burton, *Chem. Biol.* **2010**, *17*, 357-370.
10. A. Trkola, M. Purtscher, T. Muster, C. Ballaun, A. Buchacher, N. Sullivan, K. Srinivasan, J. Sodroski, J. P. Moore, H. Katinger, *J. Virol.* **1996**, *70*, 1100-1108.
11. J. M. Binley, T. Wrin, B. Korber, M. B. Zwick, M. Wang, C. Chappey, G. Stiegler, R. Kunert, S. Zolla-Pazner, H. Katinger, C. J. Petropoulos, D. R. Burton, *J. Virol.* **2004**, *78*, 13232-13252.
12. A. Jegerlehner, A. Tissot, F. Lechner, P. Sebbel, I. Erdmann, T. Kündig, T. Bächli, T. Storni, G. Jennings, P. Pumpens, W. A. Renner, M. F. Bachmann, *Vaccine* **2002**, *20*, 3104-3112.

13. A. C. Tissot, R. Renhofa, N. Schmitz, I. Cielens, E. Meijerink, V. Ose, G. T. Jennings, P. Saudan, P. Pumpens, M. F. Bachmann, *PLoS ONE* **2010**, *5*, e9809.
14. R. D. Astronomo, H. K. Lee, C. N. Scanlan, R. Pantophlet, C. Y. Huang, I. A. Wilson, O. Blixt, R. A. Dwek, C. H. Wong, D. R. Burton, *J. Virol.* **2008**, *82*, 6359-6368.
15. X. Wu, T. Lipinski, F. R. Carrel, J. J. Bailey, D. R. Bundle, *Org. Biomol. Chem.* **2007**, *5*, 3477-3485.
16. K. Takahashi, R. A. B. Ezekowitz, *Clin. Infect. Dis.* **2005**, *41*, S440-S444.
17. L. Liu, A. Stadheim, L. Hamuro, T. Pittman, W. Wang, D. Zha, J. Hochman, T. Prueksaritanont, *Biologicals* **2011**, *39*, 205-210.
18. X. Ji, H. Gewurz, G. T. Spear, *Mol. Immunol.* **2005**, *42*, 145-152.
19. E. M. Carmona, R. Vassallo, Z. Vuk-Pavlovic, J. E. Standing, T. J. Kottom, A. H. Limper, *The Journal of Immunology* **2006**, *177*, 459-467.
20. S. Agrawal, S. Gupta, A. Agrawal, *PLoS ONE* **2010**, *5*, e13418.

CHAPTER 5: Closing Remarks and Future Directions

The research presented in this thesis describes the efforts to create and characterize a mimic of the glycan shield of gp120 utilizing a filamentous phage carrier. The aim was to create a glycoconjugate vaccine that would elicit antibodies with the potential to crossreact with gp120, therein providing protection against HIV-1 infection. While the immunization studies failed in this regard, many worthwhile discoveries were made throughout the project, and questions to be answered.

The synthesis of the mannosyl thiols was initially exasperating due to the unpredictable anomerization, steric size and synthetic limitations imposed by the anomeric disulfide, but were easy to deal with once accustomed to its behavior. The Kong methodology followed for much of the synthesis was unsuitable for the production of 3,6-differentially protected β -mannosides, and even questionable for the production of the originally reported α -mannosides. In hindsight, it is envisioned that a variety of oligomannose structures could be synthesized utilizing just two building blocks (Scheme 36). Replacing the 2-*O*-acetate of donor **5** with a temporary Fmoc protecting group would eliminate the need for the lengthy and problematic selective deacetylation for 2-*O*-glycosylation. Triol **25**, which was the root building block of the entire synthesis, could also be used as a donor as glycosyl disulfides can be reasonably activated with dimethylthiosulfonium triflate.¹ A 3,6-branched trisaccharide based off of **25** could replace the allyl trimannoside **35**, which was difficult to convert to the corresponding trichloroimidate donor **37**. The anomeric disulfide may also be easily switched to an alternative aglycone with differing reactivity, allowing for selective activation of the desired glycosyl disulfide in a glycosylation reaction mixture.



Scheme 36. A concise oligomannose synthetic scheme

The f1.K phage was an ideal carrier for this project, essentially acting as well defined, simplistic polymer that can be easily characterized by analyzing its individual components by LC-UV-MS. Abscess formation during the course of the immunization studies may have detracted from the development of an effective immune response and is a serious limitation if a phage glycoconjugate is to be used in humans. The cause of abscess formations is likely due to an inflammatory response against residual endotoxin from the *E.coli*. Because of the adverse effects to endotoxin in humans, polysaccharide vaccines are recommended to contain less than 2 ng/mL endotoxin.² Removing the endotoxin would also remove its adjuvant effects, which may account for the lower antibody titres observed for the mice immunized with the polymixin B-treated phage conjugates. A potential, safer alternative adjuvant to LPS could be β -glucan. Although studying the effects of β -glucan on vaccination outcome was not the main objective of this immunization study, the inclusion of β -glucan appeared to reduce glycan-specific antibody titres. Further study dedicated to examining the effects of β -glucan density on polymixin treated phage glycoconjugates vaccines on the magnitude and diversity of the antibody response.

The Man₅ pentasaccharide elicited a much higher antibody response than the Man₄ tetrasaccharide. The Man₄ structure is not an ideal structure to use for immunization, as while it may bind 2G12 with high affinity, the purpose of a glycan hapten is to raise antibodies against it that will recognize the pathogen it was derived from. The Man₄ structure is not naturally occurring in the *N*-linked glycosylation pathway, and is not a realistic to expect to derive a protective response from it. It

would be worth exploring the other high-mannose glycans found on native trimeric gp120, particularly Man₆₋₇, in HIV-1 vaccine preparations. Glycoconjugates displaying multiple HIV-1 high-mannan oligomers may be beneficial for mimicking the glycan microheterogeneity found on HIV-1.

Phage glycoconjugates utilizing both the Man₄ and Man₅ glycans failed to produce antibodies that could recognize gp120. The lack of observed cross reactivity may be due to the more processed glycan profile of the recombinant, CHO-derived gp120 used in the ELISAs. A more appropriate capture antigen would be HIV-1 itself, or pseudovirus, although our lab lacks the facilities, training and cell lines to work with these agents. An appropriate native envelope standard is needed for HIV-1 research.

The lack of cross reactivity may also be due to the glycans being presented to the immune system in an irrelevant conformation. In order to elicit broadly neutralizing antibodies that recognize the glycan shield, like 2G12, the glycans should be appropriately orientated, or perhaps limited in conformation, by clustering them in a way that mimics the surface of gp120. The chitobiose core may be essential for establishing the initial glycan epitope for which high-mannose specificity is acquired by the humoral response; however, the exact glycan epitope requirements for recognition may not be as stringent as the epitope requirements to raise anti-mannan antibodies in the first place.

It has been shown through a combination of NMR spectroscopy, molecular modeling, and X-ray crystallography that while high-mannose glycan structures display a high degree of linkage torsional angles, the overall topology of the glycan is relatively conserved.^{3, 4} High-mannose glycans are often stabilized to assume highly ordered structures through extensive protein-carbohydrate interactions and both intra- and intermolecular carbohydrate-carbohydrate interactions.⁵ These localized interactions often uniquely influence the conformation of the glycan, which makes mimicking the glycan shield difficult as the conformation of the densely packed glycans of HIV-1 gp120 is still unknown. Mutational deletions of glycans surrounding the 2G12 epitope have been shown to modestly reduce 2G12 binding,^{6, 7} supporting the need to not only cluster, but accurately orientate the glycans of gp120 in order to be able to elicit cross-reactive antibodies.

References

1. E. J. Grayson, S. J. Ward, A. L. Hall, P. M. Rendle, D. P. Gamblin, A. S. Batsanov, B. G. Davis, *The Journal of Organic Chemistry* **2005**, *70*, 9740-9754.
2. L. A. Brito, M. Singh, *J. Pharm. Sci.* **2011**, *100*, 34-37.
3. P. V. Balaji, P. K. Qasba, V. S. R. Rao, *Glycobiology* **1994**, *4*, 497-515.
4. M. R. Wormald, R. A. Dwek, *Structure* **1999**, *7*, R155-R160.
5. M. Nagae, Y. Yamaguchi, *Int. J. Mol. Sci.* **2012**, *13*, 8398-8429.
6. A. Trkola, M. Purtscher, T. Muster, C. Ballaun, A. Buchacher, N. Sullivan, K. Srinivasan, J. Sodroski, J. P. Moore, H. Katinger, *J. Virol.* **1996**, *70*, 1100-1108.
7. R. W. Sanders, M. Venturi, L. Schiffner, R. Kalyanaraman, H. Katinger, K. O. Lloyd, P. D. Kwong, J. P. Moore, *J. Virol.* **2002**, *76*, 7293-7305.

CHAPTER 6: Experimental

Methods

General Chemical Synthesis

All chemical reagents were of analytical grade and used as obtained from Sigma-Aldrich unless otherwise specified. Solvents used for water sensitive reactions were collected from a PURESOLV solvent purification or were distilled under an inert atmosphere. Unless otherwise noted, all reactions were carried out at room temperature and water sensitive reactions were performed under a positive pressure of argon. Solvents were removed under reduced pressure between 20-40 °C with a rotary evaporator unless otherwise indicated. Molecular sieves (4 Å) were stored in an oven at 500 °C and were cooled *in vacuo* prior to use. Analytical thin layer chromatography (TLC) was conducted on silica gel 60-F₂₅₄ (Merck). TLC plates were visualized under UV light and an anisaldehyde stain composed of 4% H₂SO₄, 1.2% AcOH and 0.4% p-anisaldehyde in ethanol, followed by heating. Amberlite® IR 120 resin (strongly acidic H⁺ form) was used where H⁺ resin is indicated.

Chromatography of Synthetic Compounds

Medium pressure chromatography was conducted using silica gel (230-400 mesh, Silicycle, Montreal) or FluoroFlash® silica gel (40 µm, Fluorous Technologies Incorporated) with flow rates between 5-10 mL/min. Following deprotection, final compounds were purified by HPLC conducted on a Waters Delta 600 system using a Waters 2996 Photodiode Array detector. Separations were performed on a TOSOH TSKgel Amide-80 column with a matched TSKgel Amide-80 column guard using a gradient of water and acetonitrile.

Analytical Procedures

NMR experiments were recorded on Varian INOVA 500 or 600 MHz spectrometers, or on Varian VNMRS 500 or 700 MHz spectrometers equipped with cryogenic probes. The 600 and 700 MHz spectrometers utilize inverse probes (¹H{¹³C/¹⁵N}) allowing for 1200:1 and 7000:1 ¹H sensitivity, respectively. ¹³C NMR was

recorded at approximately 125 MHz. ^1H and ^{13}C NMR chemical shifts, reported in δ (ppm), were referenced to internal residual protonated solvent signals or to external acetone (0.1% ext. acetone @ 2.225 ppm) in the case of D_2O . ^1H and ^{13}C NMR assignments were made with the assistance of COSY, HSQC, HMBC and TOCSY where required. Values of $^2J_{\text{H,H}}$ and $^3J_{\text{H,H}}$ for carbohydrate resonances of defined multiplicity are indicated in Hz. ^1H and ^{13}C NMR chemical shifts are reported to a 100^{th} and 10^{th} of a ppm, except in the case where additional resolution is required to distinguish closely resonating signals.

Electrospray ionization mass spectra were recorded on a Micromass Zabspec TOF mass spectrometer by the analytical services facility at the University of Alberta Department of Chemistry. For high resolution mass determination, spectra were obtained by voltage scan over a narrow range at a resolution of approximately 10^4 .

Optical rotations were determined with a Perkin-Elmer model 241 polarimeter at 22 ± 2 °C using the sodium D-line and are reported in units of $\text{degree} \cdot \text{mL} \cdot \text{g}^{-1} \cdot \text{dm}^{-1}$. Concentrations (c) are reported in mg/mL.

Elemental analysis was performed by the analytical services facility at the University of Alberta Department of Chemistry.

Transmission Electron Microscopy of Filamentous Phage

A 1×10^9 phage/ μL solution of phage in PBS buffer was incubated on a carbon grid for 60 seconds at room temperature and then stained with 2% phosphotungstic acid for 30 seconds. A Philips/FEI (Morgagni) Transmission Electron Microscope with CCD camera was used to take the phage micrographs, with the assistance of the University of Alberta Department of Biological Sciences Microscopy Service Unit.

Phage Conjugation Protocol

Linker addition

To a 100 μL solution of 20 mM borate buffer (mM EDTA, pH 8.3) containing ~ 40 μg phage protein (1.6×10^{12} phage for f88 and f1.K) was added a solution of crosslinker in 2 μL organic solvent. 100 equivalents of crosslinker per reactive amine was used.

Acetonitrile was used to dissolve all linker except SIA, which produced better results using DMSO as the linker solvent. The reaction was rotated at room temperature in the dark for 3 hours. Purified by size exclusion chromatography.

Purification of Phage via Size Exclusion Chromatography

Remove of small molecules from phage preparations was accomplished using Zeba™ spin desalting columns (40K MW cutoff) according to the manufacturer's guidelines. In brief, a 0.5 mL column was washed three times with water and 100 μ L of phage solution loaded onto the resin. A stacker volume of 15 μ L was added and the column centrifuged at 1,500 x g for 2 minutes. The elute phage sample was collected. Equilibrating the column with water will lead to the removal of the buffer solution of the phage sample.

Thiol Michael Conjugation

To a solution 100 μ L solution of \sim 69 μ g phage-linker conjugate (2.6×10^{12} phage for f88 and f1.K) was added 40 μ L of 200 mM phosphate pH 8.0 buffer (final conc. 46 mM) and 25-100 equivalents of mannosyl thiol per available linker. The reaction was rotated at room temperature for 2 days and purified by size exclusion chromatography.

Thiol-ene conjugation

To a solution 125 μ L solution of \sim 44 μ g phage-linker conjugate (1.7×10^{12} phage for f88 and f1.K) was added 30 μ L of 100 mM acetate pH 4.0 buffer (final conc. 24 mM) and 25-100 equivalents of mannosyl thiol per available linker and 0.32 mg (1.2 nmol) AIBA. The reaction was performed in a sealed quartz vial and irradiated with a medium-pressure 125 W Hg-lamp for 3 hours or until the reaction was complete. Purified by size exclusion chromatography.

CuAAC Conjugation: Conditions A

Protocol for the CuAAC coupling followed as described by M.G.Finn.¹ In brief, to a solution 100 μ L solution of \sim 40 μ g phage-linker conjugate (1.6×10^{12} phage for f88 and f1.K) was added 35 μ L of 200 mM phosphate pH 7.2 (final conc. 46 mM), 0.8 μ L of 20 mM CuSO₄, 5-100 equivalents of azidomethyl 1-thio-mannoside per available linker, 1.9

μL of 50 mM THPTA ligand, 7.8 μL of 100 mM aminoguanidine and 7.8 μL of 100mM sodium ascorbate. The reaction was rotated at room temperature for 3 hours and purified by size exclusion chromatography.

CuAAC Conjugation: Conditions B

To a 110 μL solution of ~ 44 μg phage-linker conjugate (1.7×10^{12} phage for f88 and f1.K) was added 33 μL of 200 mM TrisHCl pH 8.0 buffer (final conc. 46 mM) and 5-100 equivalents of azidomethyl 1-thio-mannoside per available linker. The solution was bubbled with argon for 30 minutes and then 3.3 μL of bathophenanthroline/ Cu^+ catalyst added. Reaction mixture rotated at room temperature for 3 hours and purified using size exclusion chromatography.

Bathophenanthroline/ Cu^+ catalyst: 10 mg of $\text{CuSO}_4 \cdot 5\text{H}_2\text{O}$ and 64.4 mg of bathophenanthroline sulfonate were dissolved in 1 mL of 0.2 M TrisHCl, pH 8.0. ~ 50 mg of copper powder is added. Solution must be stored under argon. Formation of a dark green color indicates the successful reduction of Cu^{2+} to Cu^+ .

SIA Conjugation

To a 590 μL solution of ~ 416 μg phage-linker conjugate (1.7×10^{13} phage for f88 and f1.K) was added 120 μL of 200 mM phosphate pH 8.0 buffer (final conc. 34 mM) and 5-25 equivalents of mannosyl thiol per available linker. Reaction mixture rotated at room temperature for 3 hours and purified using size exclusion chromatography.

Phage Quantification

Phage particles in solution were determined by the spectral absorbance at 269 nm using the following relationship formula:²

$$\text{virions/mL} = \frac{(A_{269} - A_{320}) \cdot 6 \times 10^{16}}{\# \text{ of bases/virion}}$$

f1.K phage genome is 6419 bp, and the f88-4 genome is 9234 bp.

Protein Conjugation Protocol

BSA that has been previously treated with iodoacetate to block the free cysteine, or ubiquitin from bovine erythrocytes were used in this protocol. To a solution of 1 mg of protein in 1 mL of 50 mM borate pH 8.3 buffer with 5 mM EDTA was added 0.5 mg of crosslinker. Reaction mixture rotated at room temperature for 3 hours and purified using Zeba™ size exclusion columns (7K MW cutoff). Glycoconjugations were performed identically to the phage glycoconjugations with the exception of using only 1-5 equivalents of glycan per linker.

LC-UV-MS protocol

RP-HPLC-UV-MS was performed using an Agilent 1200 SL HPLC System with a ProSwift® RP-4H Analytical column (1×250 mm) (Dionex, USA), thermostated at 60°C, with a buffer gradient system composed 0.1% formic acid in water as mobile phase A and 0.1% formic acid in acetonitrile as mobile phase B. Gradients were optimized separately for the linker labeled proteins and glycoconjugates.

For the separation of protein-linker and protein-linker-monosaccharide analytes an aliquot of 5 µL equivalent to an amount of 2×10^{-10} phage was loaded onto the column at a flow rate of 0.20 mL min^{-1} and an initial buffer composition of 98% mobile phase A and 2% mobile phase B. After injection, the column was washed using the initial loading conditions for 10 minutes to effectively remove salts. Elution of the protein-linker and protein-linker-monosaccharide analytes was done by using a linear gradient from 2% to 30% mobile phase B over a period of 5 minutes, 30% to 50% mobile phase B over a period of 25 minutes, 50% to 95% mobile phase B over a period of 5 minutes, held at 95% mobile phase B for 5 minutes to remove all analytes from the column and 95% to 2% mobile phase B over a period of 5 minutes.

For the separation of protein-linker-tetra and pentasaccharide analytes an aliquot of 5 µL equivalent to an amount of 2×10^{-10} phage was loaded onto the column at a flow rate of 0.25 mL min^{-1} and an initial buffer composition of 90% mobile phase A and 10% mobile phase B. Elution of the protein-linker-polysaccharide analytes was done by using a linear gradient from 10% to 30% mobile phase B over a period of 2 minutes, 30% to 35% mobile phase B over a period of 3 minutes, 35% to 42% mobile phase B over a period of 25 minutes, 43% to 60% mobile phase B over a period of 5 minutes, 60% to

85% mobile phase B over a period of 3 minutes and 85% to 10% mobile phase B over a period of 5 minutes.

UV absorbance was monitored at 210, 214, 254 and 280 nm. Mass spectra were acquired in positive mode of ionization using an Agilent 6220 Accurate-Mass TOF HPLC/MS system (Santa Clara, CA, USA) equipped with a dual sprayer electrospray ionization source with the second sprayer providing a reference mass solution. Mass spectrometric conditions were drying gas 9 L/min at 300°C, nebulizer 30 psi, mass range 100-3000 Da, acquisition rate of ~1.03 spectra/sec, fragmentor 175 V, skimmer 63 V, capillary 3200 V, instrument state 4 GHz High Resolution. Mass correction was performed for every individual spectrum using peaks at m/z 121.0509 and 922.0098 from the reference solution. Data acquisition was performed using the Mass Hunter software package (ver. B.02.01.) Analysis of the HPLC-UV-MS data was done using the Agilent Mass Hunter Qualitative Analysis software (ver. B.04.01).

ESI-MSMS Protocol

ESI-MSMS was performed by direct infusion of the fractions collected after HPLC-UV (described above) using a q-TOF Premier mass spectrometer (Waters, Milford, MA). Infusion was performed using a syringe pump running at a flow rate of 500 nLmin⁻¹. Mass spectra were acquired in positive mode of ionization using the following conditions: source temperature 100°C, capillary voltage 3.6 kV, cone voltage 35.0, desolvation temperature 180 °C, nanoflow gass pressure 0 Bar. Data acquisition was performed between 100 Da and 2000 Da with the collision energy varied manually between 18 eV and 38 eV, using the Mass Lynx software package (V4.1). Deconvolution of the MSMS data was done using the MaxEnt3 algorithm in the Mass Lynx software package (V4.1) followed by manual interpretation of the results.

BCA Assay

BCA assay performed according to the Pierce®BCA Protein Assay (cat 23235).

Phenol-Sulfuric Acid Assay

To a 2 mL sample of glycoconjugate was added 0.05 mL of 80% phenol and 5 mL of H₂SO₄. Samples were left to react for 10 minutes and then cooled to room

temperature. Absorbance readings at 490 nm were compared to a standard curve to determine the concentration of carbohydrates in solution.

Immunization Regimes

24 mice immunized with phage conjugates

Eight week old C57BL/6 female mice were purchased from Charles River Laboratories International Inc.. Five sets of 5 mice received f1.K-(SIA), f1.K-(SIA)-Penta, f1.K-(SIA)-Tetra, f1.K-(SIA/4-yne)-Penta/βG or f1.K-(4-yne)-Tetra/βG. Mice were immunized 4 times with a solution of PBS containing phage via 125 μL subcutaneous and 125 μL intraperitoneal injections. Injection solutions per mouse (250 μL) contained 10 μg of phage protein (4×10^{11} virions for f1.K and f88 phage). Calculations of phage protein are based on the amount of pVIII per virion, which is determined by the genome size (1 pVIII protein for every 2.3-2.4 nucleotides in the phage genome).³ Phage glycoconjugates contained and 3-4 μg of conjugated glycan per mouse injection, based on a conjugate loading of 2.5 glycans per pVIII. Immunizations were performed on weeks 0, 3, 6 and 9, and blood was collected saphenous veins at weeks 0, 4, and 7. The final bleed and euthanasia were performed at week 11.

6 mice immunized with phage conjugates with endotoxin removed

Three mice received f1.K-(SIA)-Penta and three mice received f1.K-(SIA)-Tetra. The same protocol was used as in the immunization of the 24 mice with phage conjugates, with the following exceptions: The phage conjugates were ran through Detoxi-Gel™ to remove endotoxin before preparing the injection solutions. Immunizations were performed on weeks 0, 1 and 3. The final bleed and euthanasia were performed at week 4.

Enzyme Linked Immunosorbent Assay Titrations

Solutions of phage or glycoconjugate were used to coat plates. Maxisorp 96-well plates (Nunc) were incubated overnight at 4 °C with 100 μL per well of one of the following: phage conjugate in PBS ($1.3-1.5 \times 10^{10}$ virions per well); 5 μg/mL BSA conjugate; 5 μg/mL ubiquitin conjugate; 0.1 μg/mL HIV-1_{IIIIB} gp120 recombinant viral protein (produced in CHO cells, NIH AIDS Reagent Program Cat No: 11784); 0.5 μg/mL

HIV-1_{SF162} gp140 recombinant trimer protein (produced in HEK 293F cells, NIH AIDS Reagent Program Cat No: 12026) in PBS. The plates were washed (Molecular Devices Skan Washer 400) 5 times with PBS containing 0.05% Tween-20 (PBST). For titrations performed with phage coated plates, a 3% solution of BSA in PBS was used to block plates by incubating for 30 min at room temperature, for all else blocking was performed with 1% BSA in PBS for 40 min at room temperature. The plates were then washed 5 times with PBST and serially $\sqrt{10}$ dilutions of either 2G12 antibody (produced in CHO cells, NIH AIDS Reagent Program Cat No: 1476), biotinylated ConA or murine sera (diluted with PBST to 1:100) were allowed to bind antigen for 2 hours at room temperature. The plate was washed 5 times with PBST and 100 μ L/well of enzyme conjugate was added as follows:

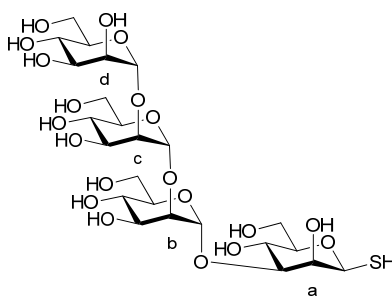
2G12: goat anti-human IgG conjugated to horseradish peroxidase (HRP) (Kirkegaard & Perry Laboratories, 1:5000 dilution in PBST)

Murine sera: goat anti-mouse IgG antibody conjugated to HRP (Kirkegaard & Perry Laboratories, 1:2000 dilution in PBST)

Biotinylated ConA: streptavidin-HRP conjugate diluted to 1:20,000

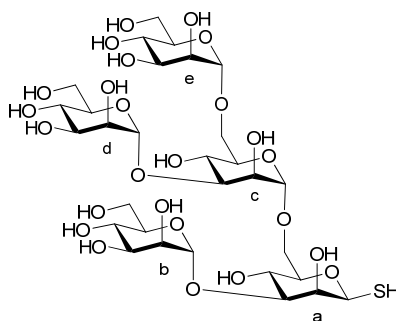
Plates were incubated for 40 minutes before washing 5 times with PBST and addition of a 1:1 mixture of 3,3',5,5'-tetramethylbenzidine (0.4 g/L) and 0.002% H₂O₂ solution (Kirkegaard & Perry Laboratories, 100 μ L). After 15 minutes the reaction was stopped by addition 100 μ L of 1M phosphoric acid. Absorbance was read at 450 nm (Molecular Devices Spectra Max 190 plate reader).

Compounds

**1**

α -D-Mannopyranosyl-(1 \rightarrow 2)- α -D-mannopyranosyl-(1 \rightarrow 2)- α -D-mannopyranosyl-(1 \rightarrow 3)-1-thio- β -D-mannopyranose (1**)**

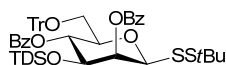
Tetrasaccharide **40** (13.2 mg, 6.7 μ mol) was dissolved in deuterated sodium hydroxide (1 mL, 0.5 M) and the reaction monitored by ^1H NMR. After 2 hours, the reaction was neutralized with H^+ resin, filtered, and concentrated under reduced pressure. The reaction was dissolved in H_2O and lyophilized to remove methyl benzoate. The crude powder was dissolved in deuterated sodium hydroxide (1 mL, 1M) to remove the tenacious 2-*O*-Bz. After 2 hours, the reaction was neutralized with H^+ resin, filtered and lyophilized. Purification of the crude yellow product via HPLC to yield **1** (3.2 mg, 4.7 μ mol, 70%) as a white powder; ^1H NMR (700 MHz, D_2O): δ 5.34 (br. s., 1H, H-1), 5.30 (s, 1H, H-1), 5.05 (s, 1H, H-1), 4.99 (s, 1H, H-1a), 4.11 (br. s., 1H, H-2), 4.08 (br. s., 1H, H-2), 4.07 (br. s., 1H, H-2), 3.26-4.04 (m, 20H), 3.37-3.44 (m, 1H, H-5a); Coupled HSQC (700 MHz, D_2O): δ 103.1/5.05 ($J_{\text{C1}/\text{H1}}$ 172 Hz), 101.7/5.30 ($J_{\text{C1}/\text{H1}}$ 173 Hz), 101.5/5.33 ($J_{\text{C1}/\text{H1}}$ 174 Hz), 82.5/5.00 ($J_{\text{C1a}/\text{H1a}}$ 153 Hz); Anal. calc for $\text{C}_{24}\text{H}_{42}\text{O}_{20}\text{S}$: HR ESIMS $[\text{M}+\text{Na}]^+$: 705.1882, found: 705.1881.



2

α -D-mannopyranosyl-(1 \rightarrow 6)-[α -D-mannopyranosyl-(1 \rightarrow 3)]- α -D-mannopyranosyl-(1 \rightarrow 6)-[α -D-mannopyranosyl-(1 \rightarrow 3)]-1-thio- β -D-mannopyranoside (50)

Pentasaccharide **41** (54.6 mg, 22.6 μ mol) was dissolved in deuterated sodium hydroxide (1 mL, 0.5 M) and the reaction monitored by ^1H NMR. After 2 hours, the reaction was neutralized with H^+ resin, filtered, and concentrated under reduced pressure. The reaction was dissolved in H_2O and lyophilized to remove methyl benzoate. The crude powder was dissolved in deuterated sodium hydroxide (1 mL, 1M) to remove the tenacious 2-*O*-Bz. After 2 hours, the reaction was neutralized with H^+ resin, filtered and lyophilized. Purification of the crude yellow product via HPLC to yield **2** (12.1 mg, 14.2 μ mol, 63%) as a white powder; ^1H NMR (700 MHz, D_2O): δ 5.15 (s, 1H, H-1), 5.10 (s, 1H, H-1), 5.00 (s, 1H, H-1^a), 4.92 (d, 1H, $J_{1,2}$ 1.5 Hz, H-1), 4.87 (d, 1H, $J_{1,2}$ 1.5 Hz, H-1), 4.16 (dd, 1H, $J_{2,3}$ 3.2 Hz, $J_{1,2}$ 1.8 Hz, H-2), 3.64-4.10 (m, 29H); Coupled HSQC (700 MHz, D_2O): δ 103.3/5.10 ($J_{\text{C1}/\text{H1}}$ 172 Hz), 103.0/5.15 ($J_{\text{C1}/\text{H1}}$ 171 Hz), 100.4/4.87 ($J_{\text{C1}/\text{H1}}$ 172 Hz), 101.1/4.92 ($J_{\text{C1}/\text{H1}}$ 172 Hz), 92.1/5.00 ($J_{\text{C1a}/\text{H1a}}$ 158 Hz); Anal. calc for $\text{C}_{30}\text{H}_{52}\text{O}_{25}\text{S}$: HR ESIMS $[\text{M}+\text{Na}]^+$: 867.2411, found: 867.2411.



3 (including 21, 22 and 23)

Mercapto-*tert*-butyl 2,4-di-*O*-benzoyl-3-*O*-*tert*-butyldimethylsilyl-1-thio-6-*O*-triphenylmethyl- β -D-mannopyranoside (3)

To a solution of diol **20** (0.32 g, 0.48 mmol) in pyridine (5 mL) was added benzoyl chloride (0.14 mL, 1.21 mmol) and 1-methylimidazole (1 drop). The reaction was heated to 60 °C for 120 hours, cooled and diluted with EtOAc. The reaction mixture was washed with sat. NaHCO₃, H₂O and brine. The organic was dried over Na₂SO₄ and concentrated under reduced pressure. Purification of the crude product by chromatography (toluene) produced product **3** and **23** as an inseparable mixture (0.37 g, 0.38 mmol, 80%). Intermediates **21** and **22** were also recovered.

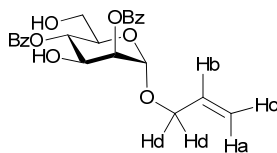
(3) Mercapto-tert-butyl 2,4-di-O-benzoyl-3-O-tert-butyl dimethylsilyl-1-thio-6-O-triphenylmethyl-β-D-mannopyranoside *R*_f 0.65 (toluene); ¹H NMR (500 MHz, CDCl₃): δ 8.16 (m, 2H, ArH), 7.79 (m, 2H, ArH), 7.58 (m, 1H, ArH), 7.54 (m, 1H, ArH), 7.40-7.45 (m, 8H, ArH), 7.38 (m, 2H, ArH), 7.14 (m, 6H, ArH), 7.09 (m, 3H, ArH), 5.84 (d, 1H, *J*_{2,3} 2.8 Hz, H-2), 5.62 (dd, 1H, *J*_{3,4} ≈ *J*_{4,5} 8.8 Hz, H-4), 4.81 (s, 1H, H-1), 4.03 (dd, 1H, *J*_{2,3} 3.1 Hz, *J*_{3,4} 9.1 Hz, H-3), 3.73 (m, 1H, H-5), 3.30 (dd, 2H, H-6), 1.32 (spt, 1H, *J* 7.1 Hz, CH(CH₃)₂), 0.55 (m, 6H, C(CH₃)₂), 0.54 (m, 6H, CH(CH₃)₂), 0.16 (s, 3H, SiCH₃), -0.15 (s, 3H, SiCH₃); ¹³C NMR (126 MHz, CDCl₃): δ 165.8 (C=O), 164.7 (C=O), 143.7 (Ar), 130.1 (Ar), 130.0 (Ar), 128.7 (Ar), 128.4 (Ar), 127.9 (Ar), 127.6 (Ar), 127.3 (Ar), 93.1 (C-1), 86.1 (CPh₃), 78.9 (C-5), 73.9 (C-2), 72.5 (C-3), 69.7 (C-4), 63.1 (C-6), 47.6 (SC(CH₃)₃), 33.8 (CH(CH₃)₂), 30.1 (SC(CH₃)₃), 24.6 (SiCH(CH₃)₂), 19.9 (CH(CH₃)₂), 19.7 (SiC(CH₃)₂), 18.3 (SiC(CH₃)₂), -2.5 (SiCH₃), -3.0 (SiCH₃); Anal. calc for C₅₁H₆₀O₇S₂Si: HR ESIMS [M+Na]⁺: 899.3442, found: 899.3443.

(21) Mercapto-tert-butyl 2-O-benzoyl-3-O-tert-butyl dimethylsilyl-1-thio-6-O-triphenylmethyl-β-D-mannopyranoside *R*_f 0.32 (toluene); ¹H NMR (500 MHz, CDCl₃): δ 8.11 (m, 2H, ArH), 7.52-7.60 (m, 7H, ArH), 7.43 (m, 2H, ArH), 7.31-7.37 (m, 6H, ArH), 7.24-7.30 (m, 3H, ArH), 5.75 (d, 1H, *J*_{1,2} 2.9 Hz, H-2), 4.71 (s, 1H, H-1), 3.97 (dd, 1H, *J*_{3,4} ≈ *J*_{4,5} 8.7 Hz, H-4), 3.72 (dd, 1H, *J*_{2,3} 3.2 Hz, *J*_{3,4} 9.1 Hz, H-3), 3.56-3.63 (m, 1H, H-6), 3.44 (m, 1H, H-5), 3.42 (m, 1H, H-6), 1.96 (br. s, 1H, 4-OH), 1.51 (spt, 1H, *J* 6.8 Hz, CH(CH₃)₂), 1.37 (s, 9H, C(CH₃)₃), 0.75 (s, 3H, C(CH₃)₂), 0.74 (d, 3H, *J* 7.0 Hz, CH(CH₃)₂), 0.74 (d, 3H, *J* 7.0 Hz, C(CH₃)₂), 0.72 (m, 6H, CH(CH₃)₂), 0.21 (s, 3H, SiCH₃), 0.14 (s, 3H, SiCH₃).

(22) Mercapto-tert-butyl 2-O-benzoyl-3-O-tert-butyl dimethylsilyl-1-thio-6-O-triphenylmethyl-α-D-mannopyranoside *R*_f 0.47 (toluene); ¹H NMR (500 MHz, CDCl₃): δ 8.07 (m, 2H, ArH), 7.58 (m, 1H, ArH), 7.52 (m, 6H, ArH), 7.38-7.48 (m, 2H, ArH), 7.22-7.31 (m, 9H, ArH), 5.53 (dd, 1H, *J*_{1,2} 3.1 Hz, *J*_{2,3} 1.8 Hz, H-2), 5.36 (d, 1H, *J*_{1,2} 1.5 Hz, H-1), 4.10 (ddd, 1H, *J*_{3,4} ≈ *J*_{4,5} 9.3 Hz, *J*_{4,OH} 2.7 Hz, H-4), 4.02 (m, 1H, H-5), 3.99 (m, 1H, H-3), 3.53 (dd,

1H, J_{gem} 10.3 Hz, $J_{5,6}$ 2.9 Hz, H-6), 3.40 (dd, 1H, J_{gem} 10.1 Hz, $J_{5,6}$ 3.8 Hz, H-6), 1.95 (d, 1H, $J_{4,\text{OH}}$ 2.7, 4-OH), 1.52 (spt, 1H, J 6.8 Hz, $\text{CH}(\text{CH}_3)_2$), 1.38 (s, 9H, $\text{C}(\text{CH}_3)_3$), 0.76 (s, 3H, $\text{C}(\text{CH}_3)_2$), 0.74 (s, 3H, $\text{C}(\text{CH}_3)_2$), 0.74 (d, 6H, J 6.4, $\text{CH}(\text{CH}_3)_2$), 0.15 (s, 6H, $\text{Si}(\text{CH}_3)_2$).

(23) Mercapto-tert-butyl 2,4-di-O-benzoyl-3-O-tert-butyl dimethylsilyl-1-thio-6-O-triphenylmethyl- α -D-mannopyranoside R_f 0.68 (toluene); ^1H NMR (500 MHz, CDCl_3): δ 8.18 (d, 2H, J_{ortho} 8.4 Hz, ArH), 7.87 (d, 2H, J_{ortho} 7.1 Hz, ArH), 7.61 (t, 1H, J_{ortho} 7.5 Hz, ArH), 7.57 (t, 1H, J_{ortho} 7.5 Hz, ArH), 7.49 (t, 2H, J_{ortho} 7.7 Hz, ArH), 7.38-7.45 (m, 8H, ArH), 7.10-7.15 (m, 6H, ArH), 7.06 (m, 3H, ArH), 5.81 (dd, 1H, $J_{3,4} \approx J_{4,5}$ 9.7 Hz, H-4), 5.63 (dd, 1H, $J_{2,3}$ 2.9 Hz, $J_{1,2}$ 2.0 Hz, H-2), 5.45 (d, 1H, $J_{1,2}$ 1.6 Hz, H-1), 4.31 (m, 1H, H-5), 4.29 (m, 1H, H-3), 3.33 (dd, 1H, J_{gem} 10.4 Hz, $J_{5,6}$ 2.2 Hz, H-6), 3.22 (dd, 1H, J_{gem} 10.4 Hz, $J_{5,6}$ 4.4 Hz, H-6), 1.38 (spt, 1H, J 7.1 Hz, $\text{CH}(\text{CH}_3)_2$), 0.62 (m, 6H, $\text{C}(\text{CH}_3)_2$), 0.59 (m, 6H, $\text{CH}(\text{CH}_3)_2$), 0.11 (s, 3H, SiCH_3), -0.11 (s, 3H, SiCH_3).



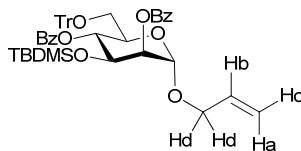
4

Allyl 2,4-di-O-benzoyl- α -D-mannopyranoside (4)

Procedure 1: Monosaccharide **13** (0.144 g, 0.18 mmol) was dissolved in 90% TFA (1 mL) and triethylsilane (60 μL , 0.38 mmol) was added. After 30 minutes, the reaction was concentrated under reduced pressure. Purification of the crude colorless syrup by chromatography (7:3 hexanes/EtOAc) yielded **4** (59 μg , 0.13 mmol, 75%) as a white powder.

Procedure 2: Monosaccharide **14** (0.96 g, 1.23 mmol) was dissolved in pyridine (1.5 mL) and hydrogen fluoride in pyridine (0.15 mL, 70% HF) was added. After 1.5 hours, mass spec analysis revealed that the TBDPS was selectively removed. An additional 0.15 mL of hydrogen fluoride solution was added and the reaction left overnight. The reaction mixture was neutralized with a solution of CaCO_3 suspended in concentrated NaHCO_3 , and filtered through Celite. The elute solution was diluted with CH_2Cl_2 and washed with

NaHCO₃, H₂O and brine. The organic layer was dried over Na₂SO₄ and concentrated under reduced pressure. Purification of the crude product by chromatography (7:2 hexanes/EtOAc) yielded **4** (0.47 g, 1.1 mmol, 89 %) as a white powder. Spectral data agrees with literature values;⁴ $[\alpha]_{\text{D}}^{25}$ -34 (*c* 5.1, CHCl₃); ¹H NMR (498 MHz, CDCl₃): δ 8.06-8.13 (m, 3H, ArH), 7.58-7.64 (m, 2H, ArH), 7.48 (m, 3H, ArH), 5.96 (ddt, 1H, *J*_{trans} 16.8 Hz, *J*_{cis} 11.0 Hz, 2×*J* 5.6 Hz, Hb), 5.52 (dd, 1H, *J*_{3,4} ≈ *J*_{4,5} 10.0 Hz, H-4), 5.44 (dd, 1H, *J*_{2,3} 3.2 Hz, *J*_{1,2} 1.6 Hz, H-2), 5.36 (dq, 1H, *J*_{trans} 17.2 Hz, *J*_{gem} ≈ 2×⁴*J* 1.3 Hz, Ha), 5.27 (dg, 1H, *J*_{cis} 10.3 Hz, *J*_{gem} ≈ 2×⁴*J* 1.2 Hz, Hc), 5.12 (d, 1H, *J*_{1,2} 0.7 Hz, H-1), 4.47 (dd, 1H, *J*_{3,4} 9.7 Hz, *J*_{2,3} 3.3 Hz, H-3), 4.26 (ddt, 1H, *J*_{gem} 12.9 Hz, ³*J* 5.2 Hz, 2×⁴*J* 1.3 Hz, Hd), 4.10 (ddt, 1H, *J*_{gem} 12.9 Hz, ³*J* 6.0 Hz, 2×⁴*J* 1.4 Hz, Hd), 3.99 (ddd, 1H, *J*_{4,5} 9.9 Hz, *J*_{5,6} 3.7 Hz, *J*_{5,6} 2.6 Hz, H-5), 3.82 (dd, 1H, *J*_{gem} 12.1 Hz, *J*_{5,6} 1.3 Hz, H-6), 3.75 (dd, 1H, *J*_{gem} 12.5 Hz, *J*_{5,6} 4.0 Hz, H-6); Anal. calc for C₂₃H₂₄O₈: HR ESIMS [M+Na]⁺: 451.1363, found: 451.1358; Elem. Anal: C, 64.48; H, 5.65; found: C, 64.82; H, 5.65.

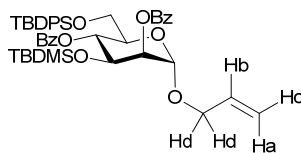


13

Allyl 2,4-di-*O*-benzoyl-3-*O*-*tert*-butyldimethylsilyl-6-*O*-triphenylmethyl- α -D-mannopyranoside (**13**)

A solution of tetrol **12** (0.95 g, 4.33 mmol), trityl chloride (1.51 g, 5.42 mmol) and pyridine (7.5 mL) was heated to 80 °C for 48 hours. The reaction mixture was then cooled to 0 °C (ice-water bath) and TBDMSCl (0.72 g, 4.77 mmol) added in portions over 3 hours. 24 hours later, the reaction was diluted with CH₂Cl₂ and washed with sat. NaHCO₃, H₂O, and brine. The organic layer was dried over Na₂SO₄ and concentrated under reduced pressure. The resulting orange syrup was pushed through a plug of silica to remove the residual salts, yielding the intermediate 2,4-diol as a white solid. The crude intermediate was dissolved in pyridine (8 mL) and benzoyl chloride (1.36 mL, 11.7 mmol) added. After 24 hours, the reaction mixture was diluted with CH₂Cl₂ and washed

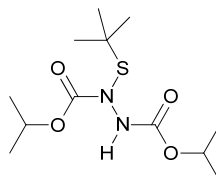
with sat. NaHCO₃, H₂O, and brine. The organic layer was dried over Na₂SO₄ and concentrated under reduced pressure. Purification of the crude product by chromatography (9.7:0.3 toluene/EtOAc) followed by recrystallization (hexanes) yielded **14** (2.46 g, 3.15 mmol, 73%) as a white crystalline solid. Spectral data agrees with literature values;⁴ $[\alpha]_D^{25}$ -28 (c 6.1, CHCl₃); ¹H NMR (500 MHz, CDCl₃): δ 8.15 (m, 2H, ArH), 7.83 (m, 2H, ArH), 7.52-7.62 (m, 2H, ArH), 7.47 (m, 2H, ArH), 7.35-7.43 (m, 8H, ArH), 7.13 (m, 6H, ArH), 7.06 (m, 3H, ArH), 6.03 (ddt, 1H, J_{trans} 16.8 Hz, J_{cis} 11.0 Hz, $2 \times J$ 5.7 Hz, Hb), 5.62 (dd, 1H, $J_{3,4} \approx J_{4,5}$ 9.8 Hz, H-4), 5.38 (dd, 1H, $J_{2,3}$ 3.3 Hz, $J_{1,2}$ 1.7 Hz, H-2), 5.38 (ddt, 1H, J_{trans} 17.2 Hz, $J_{gem} \approx 2 \times J$ 1.4 Hz, Ha), 5.28 (ddt, 1H, J_{cis} 10.5 Hz, $J_{gem} \approx 2 \times J$ 1.3 Hz, Hc), 5.06 (d, 1H, $J_{1,2}$ 0.9 Hz, H-1), 4.35 (ddt, 1H, J_{gem} 13.1 Hz, 3J 5.1 Hz, $2 \times J$ 1.3 Hz, Hd), 4.33 (dd, 2H, $J_{3,4}$ 9.0 Hz, $J_{2,3}$ 3.3 Hz, H-3), 4.16 (ddt, 1H, J_{gem} 13.0 Hz, 3J 6.2 Hz, $2 \times J$ 1.3 Hz, Hd), 4.04 (ddd, 1H, $J_{4,5}$ 10.1 Hz, $J_{5,6}$ 5.3 Hz, $J_{5,6}$ 2.4 Hz, H-5), 3.27 (dd, 1H, J_{gem} 10.5 Hz, $J_{5,6}$ 5.3 Hz, H-6), 3.24 (dd, 1H, J_{gem} 10.5 Hz, $J_{5,6}$ 2.4 Hz, H-6), 0.61 (s, 9H, C(CH₃)₃), 0.02 (s, 3H, SiCH₃), -0.18 (s, 3H, SiCH₃); Anal. calc for C₄₈H₅₂O₈Si: HR ESIMS [M+Na]⁺: 807.3324, found: 807.3318; Elem. Anal: C, 73.44; H, 6.68; found: C, 73.17; H, 6.78.

**14**

Allyl 2,4-di-O-benzoyl-3-O-tert-butylidimethylsilyl-6-O-tert-butylidiphenylsilyl-1-thio-β-D-mannopyranoside (24)

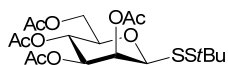
A solution of tetrol **12** (0.95 g, 4.33 mmol), TBDPSCI (1.25 mL, 5.51 mmol) and pyridine (7.5 mL) was heated to 80 °C for 48 hours. The reaction mixture was then cooled to 0 °C (ice-water bath) and TBDMSCI (0.72 g, 4.77 mmol) added in portions over 3 hours. 24 hours later, the reaction was diluted with CH₂Cl₂ and washed with sat. NaHCO₃, H₂O, and brine. The organic layer was dried over Na₂SO₄ and concentrated under reduced pressure. The resulting orange syrup was pushed through a plug of silica to remove the residual salts, yielding the intermediate 2,4-diol as a clear syrup. The crude

intermediate was dissolved in pyridine (8 mL) and benzoyl chloride (1.36 mL, 11.7 mmol) added. After 24 hours, the reaction mixture was diluted with CH_2Cl_2 and washed with sat. NaHCO_3 , H_2O , and brine. The organic layer was dried over Na_2SO_4 and concentrated under reduced pressure. Purification of the crude product by chromatography (9.7:0.3 hexanes/EtOAc) yielded **14** (2.46 g, 3.15 mmol, 73%) as a clear, colorless solid; $[\alpha]_{\text{D}}^{25}$ -16 (c 15.0, CHCl_3); ^1H NMR (600 MHz, CDCl_3): δ 8.11-8.15 (m, 2H, ArH), 7.97-8.00 (m, 2H, ArH), 7.64-7.67 (m, 2H, ArH), 7.55-7.62 (m, 4H, ArH), 7.42-7.47 (m, 4H, ArH), 7.17-7.37 (m, 6H, ArH), 5.98 (ddt, 1H, J_{trans} 16.8 Hz, J_{cis} 11.1 Hz, $2\times^3J$ 5.5 Hz, Hb), 5.72 (dd, 1H, $J_{3,4} \approx J_{4,5}$ 9.8 Hz, H-4), 5.39 (dd, 1H, $J_{2,3}$ 3.3 Hz, $J_{1,2}$ 1.8 Hz, H-2), 5.34 (ddt, 1H, J_{gem} 17.2 Hz, $J_{\text{gem}} \approx 2\times^4J$ 1.4 Hz, Ha), 5.26 (ddt, 1H, J_{cis} 10.4 Hz, $J_{\text{gem}} \approx 2\times^4J$ 1.3 Hz, Hc), 5.04 (d, 1H, $J_{1,2}$ 1.2 Hz, H-1), 4.38 (dd, 1H, $J_{3,4}$ 9.4 Hz, $J_{2,3}$ 3.4 Hz, H-3), 4.29 (ddt, 1H, J_{gem} 13.0 Hz, 3J 5.2 Hz, $2\times^4J$ 1.2 Hz, Hd), 4.10 (ddt, 1H, J_{gem} 13.1 Hz, 3J 6.2 Hz, $2\times^4J$ 1.3 Hz, Hd), 3.99 (ddd, 1H, $J_{4,5}$ 10.1 Hz, $J_{5,6}$ 5.2 Hz, $J_{5,6}$ 1.8 Hz, H-5), 3.85 (dd, 1H, J_{gem} 11.5 Hz, $J_{5,6}$ 5.3 Hz, H-6), 3.77 (dd, 1H, J_{gem} 11.4 Hz, $J_{5,6}$ 2.0 Hz, H-6), 1.03 (s, 9H, $\text{SC}(\text{CH}_3)_3$), 0.63 (s, 9H, $\text{Si}(\text{CH}_3)_3$), 0.04 (s, 3H, SiCH_3), -0.14 (s, 3H, SiCH_3); ^{13}C NMR (126 MHz, CDCl_3): δ 166.1 (C=O), 165.1 (C=O), 135.7 (Ar), 135.6 (Ar), 133.7 (CH=CH₂), 133.3 (Ar), 133.2 (Ar), 133.1 (Ar), 132.9 (Ar), 130.1 (Ar), 130.0 (Ar), 129.9 (Ar), 129.8 (Ar), 129.5 (Ar), 128.4 (Ar), 128.3 (Ar), 127.5 (Ar), 127.5 (Ar), 117.8 (CH=CH₂), 96.8 (C-1), 72.9 (C-2), 71.8 (C-5), 69.7 (C-4), 69.2 (C-3), 68.3 (CH₂CH=CH₂), 63.1 (C-6), 26.7 ($\text{SC}(\text{CH}_3)_3$), 25.3 ($\text{Si}(\text{CH}_3)_3$), 19.2 ($\text{SC}(\text{CH}_3)_3$), 17.6 ($\text{Si}(\text{CH}_3)_3$); Anal. calc for $\text{C}_{45}\text{H}_{56}\text{O}_8\text{Si}_2$: HR ESIMS $[\text{M}+\text{Na}]^+$: 803.3406, found: 803.3414; Elem. Anal: C, 69.20; H, 7.23; found: C, 69.35; H, 7.13.

**15****Diisopropyl-N-(tert-butylsulfanyl)hydrazodicarboxylate (15)**

To a solution of 2-methyl-2-propanethiol (5.5 mL, 48.8 mmol) in CH_2Cl_2 (150 mL) was added diisopropyl azodicarboxylate (10.2 mL, 49.2 mmol) dropwise. The reaction

orange mixture gradually turned yellow over the course of the reaction. After 1 week, the reaction mixture was concentrated under reduced pressure and the yellow syrup purified by chromatography (8:2 hexanes/EtOAc) to yield **15** (13.6 g, 46.3 mmol, 94%) as a colorless syrup. $[\alpha]_{\text{D}}^{25}$ -0.1 (c 16.0 in CHCl_3); ^1H NMR (700 MHz, CDCl_3): δ 7.19-7.35 (br. d., 1H, NH), 4.90 (spt, 1H, J 6.2 Hz, $\text{CH}(\text{CH}_3)_2$), 4.86 (spt, 1H, J 6.1 Hz, $\text{CH}(\text{CH}_3)_2$), 1.27 (br. s., 9H, $\text{C}(\text{CH}_3)_3$), 1.21 (d, 3H, J 6.4 Hz, $\text{C}(\text{CH}_3)_2$), 1.19 (d, 3H, J 6.3 Hz, $\text{C}(\text{CH}_3)_2$); ^{13}C NMR (126 MHz, CDCl_3): δ 157.3 (C=O), 155.3 (C=O), 72.2 ($\text{OCH}(\text{CH}_3)_2$), 70.0 ($\text{OCH}(\text{CH}_3)_2$), 49.9 ($\text{SC}(\text{CH}_3)_3$), 28.8 ($\text{SC}(\text{CH}_3)_3$), 22.0 ($\text{OCH}(\text{CH}_3)_2$), 21.8 ($\text{OCH}(\text{CH}_3)_2$); Anal. calc for $\text{C}_{12}\text{H}_{24}\text{N}_2\text{O}_4\text{S}$: HR ESIMS $[\text{M}+\text{Na}]^+$: 315.1349, found: 315.1349; Elem. Anal: C, 49.29; H, 8.27; N, 9.58; S, 10.97; found: C, 48.69; H, 7.61; N, 9.21; S, 10.56

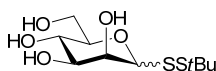


17

Mecapto-*tert*-butyl 2,3,4,6-tetra-*O*-acetyl-1-thio- β -D-mannopyranoside (**17**)

Monosaccharide **16** (17.9 g, 44.1 mmol) was added to a solution of **15** (13.6 g, 46.3 mmol) in CH_2Cl_2 (300 mL) and cooled to 0 °C. Diethylamine (4.8 mL, 46 mmol) was added to the reaction mixture. After 96 hours, reaction was diluted with CH_2Cl_2 and washed with sat. NH_4Cl , sat. NaHCO_3 , H_2O , and brine. The organic was dried over Na_2SO_4 and concentrated under reduced pressure. Purification of the crude product required two rounds of chromatographic purification (6:4 hexanes EtOAc, then 9:1 $\text{CH}_2\text{Cl}_2/\text{EtOAc}$). The bulk of the diisopropyl hydrazodicarboxylate byproduct can be removed through recrystallization (hexanes/EtOAc), yielding **17** (13.1 g, 29.0 mmol, 66%) as a colorless syrup in a 1:22 α/β ratio, containing trace diisopropyl hydrazodicarboxylate; $[\alpha]_{\text{D}}^{25}$ 31 (c 24.3, CHCl_3); ^1H NMR (700 MHz, CDCl_3): δ 5.62 (br. d, 1H, $J_{2,3}$ 2.6 Hz, H-2), 5.20 (dd, 1H, $J_{3,4} \approx J_{4,5}$ 10.0 Hz, H-4), 5.03 (dd, 1H, $J_{3,4}$ 10.1 Hz, $J_{2,3}$ 3.5 Hz, H-3), 4.65 (d, 1H, $J_{1,2}$ 0.9 Hz, H-1), 4.25 (dd, 1H, J_{gem} 12.3 Hz, $J_{5,6}$ 6.1 Hz, H-6), 4.14 (dd, 1H, J_{gem} 12.3 Hz, $J_{5,6}$ 2.3 Hz, H-6), 3.67 (ddd, 1H, $J_{4,5}$ 9.9 Hz, $J_{5,6}$ 6.2 Hz, $J_{5,6}$ 2.3 Hz, H-5), 2.19 (s, 3H, $\text{CH}_3(\text{C}=\text{O})$), 2.07 (s, 3H, $\text{CH}_3(\text{C}=\text{O})$), 2.03 (s, 3H, $\text{CH}_3(\text{C}=\text{O})$), 1.97 (s, 3H, $\text{CH}_3(\text{C}=\text{O})$), 1.34 (s, 9H, $\text{C}(\text{CH}_3)_3$); ^{13}C NMR (176 MHz, CDCl_3): δ 170.6 (C=O), 170.0 (C=O),

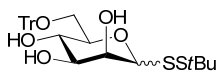
170.0 (C=O), 169.6 (C=O), 92.1 (C-1), 76.9 (C-5), 71.7 (C-3), 70.5 (C-2), 65.6 (C-4), 62.8 (C-6), 47.8 (C(CH₃)₃), 29.9 (C(CH₃)₃), 20.7 (CH₃(C=O)), 20.7 (CH₃(C=O)), 20.6 (CH₃(C=O)), 20.5 (CH₃(C=O)); Anal. calc for C₁₈H₂₈O₉S₂: HR ESIMS [M+Na]⁺: 475.1067, found: 475.1065; Elem. Anal: C, 47.77; H, 6.24; S, 14.17; found: C, 47.98; H, 6.21; S, 13.80.



18

Mecapto-*tert*-butyl 1-thio-D-mannopyranoside (18)

Monosaccharide **17** (10.68 g, 23.6 mmol) was suspended in methanol (110 mL) and 1 M sodium methoxide (0.2 mL) was added. After 4 hours, reaction was neutralized with H⁺ resin, filtered, and concentrated under reduced pressure. Purification of the crude product by recrystallization (hexanes/EtOAc) yielded **18** (6.13 g, 21.5 mmol, 91%) in a 64:100 α/β mixture as a white powder. β-anomer: ¹H NMR (600 MHz, CD₃OD): δ 4.59 (d, 1H, *J*_{1,2} 1.1 Hz, H-1), 4.05 (dd, 1H, *J*_{2,3} 3.4 Hz, *J*_{1,2} 1.0 Hz, H-2), 3.85 (dd, 1H, *J*_{gem} 11.9 Hz, *J*_{5,6} 2.4 Hz, H-6), 3.74 (dd, 1H, *J*_{gem} 11.7 Hz, *J*_{5,6} 5.5 Hz, H-6), 3.61 (dd, 1H, *J*_{3,4} ≈ *J*_{4,5} 9.5 Hz, H-4), 3.45 (dd, 1H, *J*_{3,4} 9.5, *J*_{2,3} 3.3 Hz, H-3), 3.22 (ddd, 1H, *J*_{4,5} 9.7 Hz, *J*_{5,6} 5.1 Hz, *J*_{5,6} 2.4 Hz, H-5), 1.36 (s, 9H, C(CH₃)₃); ¹³C NMR (126 MHz, CD₃OD): δ 94.4 (C-1), 81.4 (H-5), 74.7 (C-3), 72.4 (C-2), 66.5 (C-4), 61.3 (C-6), 46.6 (SC(CH₃)₃), 28.9 (SC(CH₃)₃); α-anomer: ¹H NMR (600 MHz, CD₃OD): δ 5.10 (d, 1H, *J*_{1,2} 1.8 Hz, H-1), 4.10 (dd, 1H, *J*_{2,3} 3.1 Hz, *J*_{1,2} 1.8 Hz, H-2), 3.80-3.83 (m, 1H, H-6), 3.75-3.79 (m, 1H, H-6), 3.73-3.76 (m, 1H, H-5), 3.72 (dd, 1H, *J*_{3,4} ≈ *J*_{4,5} 9.7 Hz, H-4), 3.66 (m, 1H, H-3), 1.36 (s, 9H, C(CH₃)₃); Anal. calc for C₁₀H₂₀O₅S₂: HR ESIMS [M+Na]⁺: 307.0644, found: 307.0641; Elem. Anal: C, 42.23; H, 7.09; S, 22.55; found: C, 42.07; H, 7.05; S, 22.54.



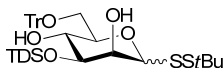
19

Mecapto-*tert*-butyl 1-thio-6-*O*-triphenylmethyl- β -D-mannopyranoside (19)

Tetrol **18** (0.34 g, 1.2 mmol) and TrCl (0.32 g, 1.5 mmol) were dissolved in pyridine (10 mL) and stirred at room temperature. After 68 hours, solid NaHCO₃ was added and the reaction stirred until bubbling ceased. The reaction mixture was diluted with EtOAc and washed with 1 M NaHCO₃, H₂O, and brine. The organic was dried over Na₂SO₄ and concentrated under reduced pressure. Purification of the crude product by chromatography (6:4 CH₂Cl₂/EtOAc) yielded **19** (0.50 g, 0.96 mmol, 81%) in a 64:100 α / β mixture as a white powder;

β -anomer: *R*_f 0.48 (1:9 hexanes/EtOAc); ¹H NMR (500 MHz, CDCl₃): δ 7.42-7.46 (m, 6H, ArH), 7.29-7.34 (m, 6H, ArH), 7.23-7.28 (m, 3H, ArH), 4.54 (d, 1H, *J*_{1,2} 0.9 Hz, H-1), 4.20 (m, 1H, H-2), 3.77 (ddd, 1H, *J*_{3,4} \approx *J*_{4,5} 9.2 Hz, *J*_{4,OH} 2.0 Hz, H-4), 3.55 (ddd, 1H, *J*_{3,4} 9.1 Hz, *J*_{2,3} 5.8 Hz, *J*_{3,OH} 3.6 Hz, H-3), 3.48 (dd, 1H, *J*_{gem} 9.7 Hz, *J*_{5,6} 4.9 Hz, H-6), 3.43 (dd, 1H, *J*_{gem} 9.9 Hz, *J*_{5,6} 5.1 Hz, H-6), 3.37 (ddd, 1H, *J*_{4,5} \approx *J*_{5,6} 10.1, *J*_{5,6} 4.9, H-5), 2.84 (d, 1H, *J*_{4,OH} 2.0 Hz, 4-OH), 2.61 (d, 1H, *J*_{3,OH} 6.2 Hz, 3-OH), 2.47 (d, 1H, *J*_{2,OH} 4.4 Hz, 2-OH), 1.34 (s, 9H, C(CH₃)₃); ¹³C NMR (126 MHz, CDCl₃): δ 143.4 (Ar), 128.6 (Ar), 128.0 (Ar), 127.3 (Ar), 92.6 (C-1), 87.4 (CPh₃), 78.2 (C-5), 74.8 (C-3), 71.5 (C-2), 70.2 (C-4), 64.6 (C-6), 47.7 (SC(CH₃)₃), 30.0 (SC(CH₃)₃); Coupled HSQC (500 MHz, CDCl₃): δ 92.6/4.54 (*J*_{C1/H1} 158 Hz, C-1); Anal. calc for C₂₉H₃₄O₅S₂: HR ESIMS [M+Na]⁺: 549.1740, found: 549.1739; Elem. Anal: C, 66.13; H, 6.51; S, 12.18; found: C, 66.00; H, 6.22; S, 12.07.

α -anomer: *R*_f 0.52 (1:9 hexanes/EtOAc); ¹H NMR (600 MHz, CDCl₃): δ 7.43-7.47 (m, 6H, ArH), 7.30-7.34 (m, 6H, ArH), 7.24-7.27 (m, 3H, ArH), 5.17 (d, 1H, *J*_{1,2} 1.7 Hz, H-1), 4.21 (br. s., 1H, H-2), 3.97 (m, 1H, H-5), 3.83 (m, 1H, H-4), 3.77 (m, 1H, H-3), 3.49 (dd, 1H, *J*_{gem} 9.9 Hz, *J*_{5,6} 4.4 Hz, H-6), 3.40 (dd, 1H, *J*_{gem} 9.8 Hz, *J*_{5,6} 5.8 Hz, H-6), 2.83 (d, 1H, *J*_{4,OH} 2.1 Hz, 4-OH), 2.60 (d, 1H, *J*_{3,OH} 3.4 Hz, 3-OH), 2.46-2.48 (d, 1H, *J*_{2,OH} 3.6 Hz, 2-OH), 1.34 (s, 9H, C(CH₃)₃); ¹³C NMR (126 MHz, CDCl₃): δ 128.6 (Ar), 128.0 (Ar), 127.3 (Ar), 92.5 (C-1), 87.4 (CPh₃), 71.6, 71.55, 71.50, 70.7 (C-2, C-3, C-4, C-5), 64.8 (C-6), 47.8 (SC(CH₃)₃), 30.0 (SC(CH₃)₃); Coupled HSQC (500 MHz, CDCl₃): δ 92.5/5.17 (*J*_{C1/H1} 171 Hz, C-1);

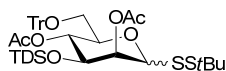


Mecapto-*tert*-butyl 3-*O*-hexyldimethylsilyl-1-thio-6-*O*-triphenylmethyl- β -D-mannopyranoside (20)

Triol **19** (0.15 g, 0.28 mmol) was dissolved in a solution of imidazole (38 mg, 0.56 mmol) and DMF (3 mL). A solution of TDSCI (64 μ L, 0.33 mmol) in DMF (1 mL) was added dropwise to the reaction mixture over 1 hour. After 24 hours, the reaction was diluted with EtOAc and washed with 1 M NaHCO₃, H₂O, and brine. The organic was dried over Na₂SO₄ and concentrated under reduced pressure. Purification of the crude yellow product by chromatography (7:3 hexanes/EtOAc) yielded **20** (0.17 g, 0.26 mmol, 92%) in a 64:100 α/β mixture as a white powder;

β -anomer: *R*_f 0.53 (8:2 hexanes/EtOAc); ¹H NMR (500 MHz, CDCl₃): δ 7.43-7.47 (m, 6H, ArH), 7.28-7.33 (m, 6H, ArH), 7.22-7.26 (m, 3H, ArH), 4.52 (dd, 1H, $J_{1,2} \approx {}^4J_{1,OH}$ 1.5 Hz, H-1), 4.03 (ddd, 1H, $J_{2,3}$ 3.6 Hz, $J_{1,2}$ 1.6 Hz, $J_{2,OH}$ 1.5 Hz, H-2), 3.66 (ddd, 1H, $J_{3,4} \approx J_{4,5}$ 9.2 Hz, $J_{4,OH}$ 2.6 Hz, H-4), 3.57 (dd, 1H, $J_{3,4}$ 8.7 Hz, $J_{2,3}$ 3.6 Hz, H-3), 3.41-3.44 (m, 2H, H-6), 3.37 (m, 1H, H-5), 2.60 (dd, 1H, ${}^4J_{1,OH} \approx J_{2,OH}$ 1.6 Hz, 2-OH), 2.30 (d, 1H, $J_{4,OH}$ 2.7, 4-OH), 1.64 (spt., 1H, J 7.1 Hz, CH(CH₃)₂), 1.35 (s, 9H, C(CH₃)₃), 0.90 (d, 3H, J 6.8, CH(CH₃)₂), 0.89 (d, 3H, J 6.8 Hz, CH(CH₃)₃), 0.86 (s, 6H, C(CH₃)₂), 0.18 (s, 3H, SiCH₃), 0.17 (s, 3H, SiCH₃); ¹³C NMR (126 MHz, CDCl₃): δ 146.9 (Ar), 143.7 (Ar), 143.6 (Ar), 128.7 (Ar), 127.9 (Ar), 127.3 (Ar), 127.1 (Ar), 93.5 (C-1), 82.0 (CPh₃), 78.6 (C-5), 76.0 (C-2), 72.7 (C-3), 69.6 (C-4), 64.9 (C-6), 47.5 (SC(CH₃)₃), 34.2 (CH(CH₃)₂), 30.1 (C(CH₃)₃), 25.0 (SiC(CH₃)₂), 20.5 (CH(CH₃)₂), 20.1 (CH(CH₃)₂), 18.7 (SiC(CH₃)₂), 18.5 (SiC(CH₃)₂), -2.5 (SiCH₃), -2.7 (SiCH₃); Anal. calc for C₃₇H₅₂O₅S₂Si: HR ESIMS [M+Na]⁺: 691.2918, found: 691.2923;

α -anomer: *R*_f 0.50 (8:2 hexanes/EtOAc); ¹H NMR (500 MHz, CDCl₃): δ 7.41-7.52 (m, 6H, ArH), 7.27-7.33 (m, 3H, ArH), 7.21-7.28 (m, 3H, ArH), 5.24 (d, 1H, $J_{1,2}$ 1.3 Hz, H-1), 4.03 (ddd, 1H, $J_{2,3}$ 3.3 Hz, $J_{1,2}$ 1.3 Hz, H-2), 3.97 (ddd, 1H, $J_{5,6}$ 9.4 Hz, $J_{4,5} \approx J_{5,6}$ 4.6 Hz, H-5), 3.83 (dd, 1H, $J_{3,4}$ 8.8 Hz, $J_{2,3}$ 3.3 Hz, H-3), 3.73 (ddd, 1H, $J_{4,5}$ 9.2 Hz, $J_{3,4} \approx J_{4,OH}$ 2.6 Hz, H-4), 3.40 (br. d, 2H, J 4.6 Hz, H-6), 2.67 (d, 1H, $J_{1,2}$ 1.3 Hz, 2-OH), 2.20 (d, 1H, $J_{4,OH}$ 2.9 Hz, 4-OH), 1.65 (spt, 1H, J 7.3 Hz, CH(CH₃)₂), 1.37 (m, 6H, C(CH₃)₃), 0.90 (d, 3H, J 6.8 Hz, CH(CH₃)₂), 0.89 (d, 3H, J 6.8 Hz, CH(CH₃)₂), 0.87 (s, 6H, C(CH₃)₂), 0.18 (br. s., 6H, Si(CH₃)₂);



24

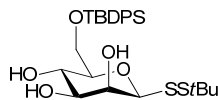
Mecapto-*tert*-butyl 2,4-di-*O*-acetyl-3-*O*-thexyldimethylsilyl-1-thio-6-*O*-triphenylmethyl- β -D-mannopyranoside (24)

Crude diol **20** (0.21g, ~0.32 mmol) was added to a solution of acetic anhydride (1 mL, 10.6 mmol) in pyridine (3 mL). After 24 hours, the reaction mixture was diluted with CH₂Cl₂ and washed with 1 M NaHCO₃, H₂O, and brine. The organic was dried over Na₂SO₄ and concentrated under reduced pressure. Purification of crude product by chromatography (9:1 hexanes/EtOAc) yielded **24** (0.19g, 0.25 mmol, ~83%) in a 1:10 α/β mixture as a white powder;

β -anomer: *R*_f 0.63 (7:3 hexanes/EtOAc); ¹H NMR (600 MHz, CDCl₃): δ 7.46 (m, 6H, ArH), 7.26-7.33 (m, 6H, ArH), 7.21-7.26 (m, 3H, ArH), 5.52 (d, 1H, *J*_{1,2} 2.9 Hz, H-2), 5.00 (dd, 1H, *J*_{3,4} \approx *J*_{4,5} 9.7 Hz, H-4), 4.63 (s, 1H, H-1), 3.75 (dd, 1H, *J*_{3,4} 9.3 Hz, *J*_{2,3} 3.5 Hz, H-3), 3.53 (ddd, 1H, *J*_{4,5} 9.9 Hz, *J*_{5,6} 6.0 Hz, *J*_{5,6} 2.4 Hz, H-5), 3.28 (dd, 1H, *J*_{gem} 10.4 Hz, *J*_{5,6} 5.9 Hz, H-6), 3.08 (dd, 1H, *J*_{gem} 10.5 Hz, *J*_{5,6} 2.3 Hz, H-6), 2.15 (s, 3H, CH₃(C=O)), 1.74 (s, 3H, CH₃(C=O)), 1.53 (spt, 1H, *J* 7.3 Hz, CH(CH₃)₂), 1.40 (s, 9H, C(CH₃)₃), 0.80 (s, 6H, CH(CH₃)₂), 0.75 (s, 6H, C(CH₃)₂), 0.15 (s, 3H, SiCH₃), 0.05 (s, 3H, SiCH₃); ¹³C NMR (126 MHz, CDCl₃): δ 170.0 (C=O), 169.2 (C=O), 143.8 (Ar), 128.8 (Ar), 127.9 (Ar), 127.7 (Ar), 127.3 (Ar), 127.0 (Ar), 92.6 (C-1), 86.8 (CPh₃), 78.8 (C-5), 73.0 (C-2), 71.9 (C-3), 69.2 (C-4), 63.7 (C-6), 47.6 (SC(CH₃)₃), 34.0 (CH(CH₃)₂), 30.1 (C(CH₃)₃), 24.7 (SiC(CH₃)₂), 20.9 (CH(CH₃)₂), 20.8 (CH(CH₃)₂), 20.2 (CH₃(C=O)), 19.9 (CH₃(C=O)), 18.5 (SiC(CH₃)₂), 18.4 (SiC(CH₃)₂), -2.6 (SiCH₃), -3.1 (SiCH₃); Anal. calc for C₄₁H₅₆O₇S₂Si: HR ESIMS [M+Na]⁺: 775.3129, found: 775.3128; Elem. Anal: C, 65.39; H, 7.50; S, 8.52; found: C, 65.13; H, 7.46; S, 8.74.

α -anomer: *R*_f 0.65 (7:3 hexanes/EtOAc); ¹H NMR (500 MHz, CDCl₃): δ 7.47 (m, 6H, ArH), 7.27-7.32 (m, 6H, ArH), 7.20-7.26 (m, 3H, ArH), 5.31-5.34 (m, 1H, H-2), 5.21 (d, 1H, *J*_{1,2} 1.5 Hz, H-1), 5.16 (dd, 1H, *J*_{3,4} \approx *J*_{4,5} 9.7 Hz, H-4), 4.11 (m, 1H, H-5), 4.03 (dd, 1H, *J*_{3,4} 9.3 Hz, *J*_{2,3} 3.3 Hz, H-3), 3.20 (dd, 1H, *J*_{5,6} 5.5 Hz, *J*_{gem} 10.4 Hz, H-6), 3.14 (dd, 1H, *J*_{gem} 10.4 Hz, *J*_{5,6} 2.4 Hz, H-6), 2.13 (s, 3H, CH₃(C=O)), 2.05 (s, 1H, CH₃(C=O)), 1.88 (spt, 1H, *J* 7.3 Hz,

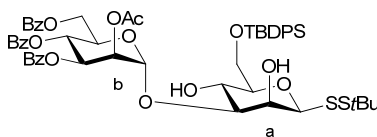
$\text{CH}(\text{CH}_3)_2$, 1.41 (s, 9H, $\text{C}(\text{CH}_3)_3$), 0.81 (d, 6H, J 1.3, $\text{CH}(\text{CH}_3)_2$), 0.76 (m, 6H, $\text{C}(\text{CH}_3)_2$), 0.13 (s, 3H, SiCH_3), 0.07 (s, 3H, SiCH_3)



25

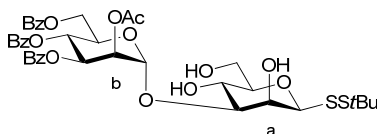
Mecapto-*tert*-butyl 6-*O-tert*-butyldiphenylsilyl-1-thio- β -D-mannopyranoside (25)

Tetrol **18** (2.38 g, 8.4 mmol) was dissolved in pyridine (40 mL) and TBDPSCI (2.4 mL, 9.4 mmol) was slowly added. After 48 hours, the reaction was diluted with toluene and extracted with 1 M NaHCO_3 , H_2O , and brine. The organic layer was dried over Na_2SO_4 and concentrated under reduced pressure. Purification of the crude product by chromatography (6:3 $\text{CH}_2\text{Cl}_2/\text{EtOAc}$) followed by recrystallization (heptane/ EtOAc) yielded **25** (1.86g, 3.57 mmol, 71%) a white crystalline solid; $[\alpha]_D^{25}$ -35 (c 6.2, CH_2Cl_2); ^1H NMR (498 MHz, CDCl_3): δ 7.65-7.70 (m, 4H, ArH), 7.37-7.47 (m, 6H, ArH), 4.53 (s, 1H, H-1), 4.20 (dd, 1H, $J_{2,3} \approx J_{2,\text{OH}}$ 3.8 Hz, H-2), 3.96 (dd, 1H, J_{gem} 10.8 Hz, $J_{5,6}$ 4.8 Hz, H-6), 3.92 (dd, 1H, J_{gem} 10.8 Hz, $J_{5,6}$ 5.8 Hz, H-6), 3.87 (ddd, 2H, $J_{3,4} \approx J_{4,5}$ 9.2 Hz, $J_{4,\text{OH}}$ 1.6 Hz, H-4), 3.58 (ddd, 1H, $J_{3,4}$ 9.3 Hz, $J_{3,\text{OH}}$ 6.2 Hz, $J_{2,3}$ 3.3 Hz, H-3), 3.36 (dt, 2H, $J_{4,5}$ 9.7 Hz, $J_{5,6}$ 5.0 Hz, H-5), 3.09 (d, 2H, $J_{4,\text{OH}}$ 1.8 Hz, 4-OH), 2.58 (d, 2H, $J_{3,\text{OH}}$ 6.4 Hz, 3-OH), 2.38 (d, 2H, $J_{2,\text{OH}}$ 4.8 Hz, 2-OH), 1.30 (s, 9H, $\text{SC}(\text{CH}_3)_3$), 1.06 (s, 9H, $\text{SiC}(\text{CH}_3)_3$); ^{13}C NMR (126 MHz, CDCl_3): δ 135.6 (Ar), 135.6 (Ar), 132.6 (Ar), 132.5 (Ar), 130.0 (Ar), 127.9 (Ar), 92.3 (C-1), 78.7 (C-5), 74.9 (C-3), 71.4 (C-2), 70.3 (C-4), 65.1 (C-6), 47.7 ($\text{SC}(\text{CH}_3)_3$), 29.9 ($\text{SC}(\text{CH}_3)_3$), 26.8 ($\text{SiC}(\text{CH}_3)_3$), 19.2 ($\text{SiC}(\text{CH}_3)_3$); Coupled HSQC (500 MHz, CDCl_3): δ 92.3/4.53 ($J_{\text{C1/H1}}$ 158 Hz, C-1); Anal. calc for $\text{C}_{26}\text{H}_{38}\text{O}_5\text{S}_2\text{Si}$: HR ESIMS $[\text{M}+\text{Na}]^+$: 545.1822, found: 545.1818; Elem. Anal: C, 59.73; H, 7.33; S, 12.27; found: C, 59.12; H, 7.24; S, 12.34.



Mecapto-*tert*-butyl 2-*O*-acetyl-3,4,6-tri-*O*-benzoyl- α -D-mannopyranosyl-(1 \rightarrow 3)-6-*O*-*tert*-butyldiphenylsilyl-1-thio- β -D-mannopyranoside (26)

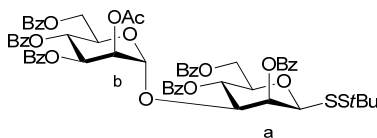
Acceptor **25** (0.32 g, 0.61 mmol) was dissolved in a solution of CH₂Cl₂ (8 mL) containing molecular sieves, cooled to 0 °C, and BF₃·OEt₂ (12 μ L, 96 μ mol) added. A solution of donor **5** (0.42g, 0.61 mmol) in CH₂Cl₂ (5 mL) was added dropwise over 30 minutes to the acceptor solution. After 1 hour, the reaction was quenched with 3 drops of TEA and concentrated under reduced pressure. Purification of the crude product by chromatography (9:1 toluene/EtOAc) yielded **26** (0.53 g, 0.51 mmol, 83%) as a white powder; $[\alpha]_D^{25}$ 25 (c 2.0, CHCl₃); ¹H NMR (500 MHz, CDCl₃): δ 8.01-8.05 (m, 2H, ArH), 7.95-7.99 (m, 2H, ArH), 7.87-7.91 (m, 2H, ArH), 7.70 (m, 4H, ArH), 7.33-7.56 (m, 15H, ArH), 5.90 (dd, 1H, $J_{3,4} \approx J_{4,5}$ 10.1 Hz, H-4^b), 5.82 (dd, 1H, $J_{3,4}$ 10.7 Hz, $J_{2,3}$ 3.7 Hz, H-3^b), 5.62 (dd, 1H, $J_{2,3}$ 3.2 Hz, $J_{1,2}$ 1.9 Hz, H-2^b), 5.34 (d, 1H, $J_{1,2}$ 1.6 Hz, H-1^b), 4.63 (ddd, 1H, $J_{4,5}$ 9.8 Hz, $J_{5,6}$ 5.6 Hz, $J_{5,6}$ 3.1 Hz, H-5^b), 4.59 (dd, 1H, J_{gem} 11.9 Hz, $J_{5,6}$ 2.9 Hz, H-6^b), 4.53 (dd, 1H, J_{gem} 11.7 Hz, $J_{5,6}$ 5.7 Hz, H-6^b), 4.47 (s, 1H, H-1^a), 4.36 (dd, 1H, $J_{2,\text{OH}}$ 5.4 Hz, $J_{2,3}$ 3.4 Hz, H-2^a), 4.12 (ddd, 1H, $J_{3,4} \approx J_{4,5}$ 9.2 Hz, $J_{4,\text{OH}}$ 2.6 Hz, H-4^a), 3.94 (d, 2H, $J_{\text{gem}} \approx J_{5,6}$ 4.8 Hz, H-6^a), 3.67 (dd, 1H, $J_{3,4}$ 9.2 Hz, $J_{2,3}$ 3.2 Hz, H-3^a), 3.34 (ddd, 1H, $J_{4,5}$ 9.3 Hz, $2 \times J_{5,6}$ 4.6 Hz, H-5^a), 2.90 (d, 1H, $J_{4,\text{OH}}$ 2.6 Hz, 4-OH), 2.50 (d, 1H, $J_{2,\text{OH}}$ 5.5 Hz, 2-OH), 2.14 (s, 3H, CH₃(C=O)), 1.29 (s, 9H, SC(CH₃)₃), 1.08 (s, 9H, SiC(CH₃)₃); ¹³C NMR (126 MHz, CDCl₃): δ 169.8 (C=O), 166.3 (C=O), 165.6 (C=O), 165.6 (C=O), 135.7 (Ar), 135.6 (Ar), 133.5 (Ar), 133.3 (Ar), 133.2 (Ar), 132.9 (Ar), 132.7 (Ar), 129.9 (Ar), 129.8 (Ar), 129.7 (Ar), 129.1 (Ar), 128.9 (Ar), 128.5 (Ar), 128.4 (Ar), 127.9 (Ar), 99.3 (C-1^b), 92.7 (C-1^a), 82.9(C-3^a), 79.5 (C-5^a), 71.7 (C-2^a), 69.9, 69.8 (C-2^b, C-3^b), 69.4 (C-5^b), 68.2 (C-4^a), 67.2 (C-4^b), 64.7 (C-6^a), 63.7 (C-6^b), 47.6 (SC(CH₃)₃), 30.0 (SC(CH₃)₃), 26.9 (SiC(CH₃)₃), 20.8 (CH₃(C=O)), 19.3 (SiC(CH₃)₃); Coupled HSQC (500 MHz, CDCl₃): δ 99.3/5.34 ($J_{\text{C1/H1}}$ 177 Hz, C-1^b), 92.7/4.47 ($J_{\text{C1/H1}}$ 157 Hz, C-1^a); Anal. calc for C₅₅H₆₂O₁₄S₂Si: HR ESIMS [M+Na]⁺: 1061.3246, found: 1061.3242; Elem. Anal: C, 63.56; H, 6.01; S, 6.17; found: C, 63.56; H, 6.29; S, 6.17.



27

Mecapto-*tert*-butyl 2-*O*-acetyl-3,4,6-tri-*O*-benzoyl- α -D-mannopyranosyl-(1 \rightarrow 3)-1-thio- β -D-mannopyranoside (27)

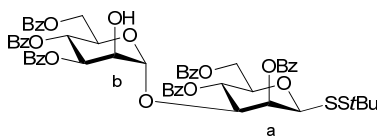
Disaccharide **26** (0.21 g, 0.17 mmol) was dissolved in a pyridine (0.25 mL) and hydrogen fluoride in pyridine (25 μ L, 70% HF) added. The reaction was performed in a polypropylene flask. After 45 minutes, a suspension of CaCO₃ in 1 M NaHCO₃ (0.5 mL) was added and the reaction mixture stirred for 30 minutes. The slurry was filtered through a pad of Celite and the eluted solution concentrated under reduced pressure. Purification of the crude product by chromatography (9:1 toluene/EtOAc) yielded **34** (0.16 g, 0.16 mmol, 93%) as a white solid; $[\alpha]_D^{25}$ 42 (*c* 11.8, CHCl₃); ¹H NMR (500 MHz, CDCl₃): δ 8.01-8.05 (m, 2H, ArH), 7.89-7.93 (m, 2H, ArH), 7.76-7.81 (m, 2H, ArH), 7.51-7.56 (m, 1H, ArH), 7.38-7.48 (m, 3H, ArH), 7.27-7.35 (m, 3H, ArH), 7.09-7.15 (m, 2H, ArH), 5.95 (dd, 1H, $J_{3,4}$ 10.0 Hz, $J_{2,3}$ 3.3 Hz, H-3^b), 5.92 (dd, 1H, $J_{3,4} \approx J_{4,5}$ 9.5 Hz, H-4^b), 5.64 (dd, 1H, $J_{2,3}$ 2.4 Hz, $J_{1,2}$ 1.8 Hz, H-2^b), 5.45 (d, 1H, $J_{1,2}$ 1.6 Hz, H-1^b), 4.76 (ddd, 1H, $J_{4,5}$ 8.9 Hz, $J_{5,6}$ 5.5 Hz, $J_{5,6}$ 3.1 Hz, H-5^b), 4.65 (br. s, 1H, 4-OH^a), 4.56 (dd, 1H, J_{gem} 12.1 Hz, $J_{5,6}$ 3.1 Hz, H-6^b), 4.52 (s, 1H, H-1^a), 4.52 (dd, 1H, J_{gem} 12.3 Hz, $J_{5,6}$ 5.5 Hz, H-6^b), 4.39 (dd, 1H, $J_{2,3}$ 5.9 Hz, $J_{2,\text{OH}}$ 3.3 Hz, H-2^a), 4.30 (m, 1H, H-4^a), 4.16 (m, 1H, 3-OH^a), 3.98 (m, 2H, H-6^a), 3.74 (dd, 1H, $J_{3,4}$ 9.3 Hz, $J_{2,3}$ 3.3 Hz, H-3^a), 3.61 (br. s, 1H, 6-OH^a), 3.31 (ddd, 1H, $J_{4,5} \approx J_{5,6}$ 9.7, $J_{5,6}$ 2.6 Hz, H-5^a), 2.11 (s, 3H, CH₃(C=O)), 1.30 (s, 9H, C(CH₃)₃); ¹³C NMR (126 MHz, CDCl₃): δ 170.3 (C=O), 166.5 (C=O), 166.3 (C=O), 165.6 (C=O), 133.6 (Ar), 133.3 (Ar), 133.2 (Ar), 129.8 (Ar), 129.7 (Ar), 129.7 (Ar), 129.6 (Ar), 128.8 (Ar), 128.7 (Ar), 128.6 (Ar), 128.5 (Ar), 128.3 (Ar), 99.2 (C-1^b), 93.2 (C-1^a), 82.7 (C-3^a), 80.5 (C-5^a), 72.4 (C-2^a), 70.3, 70.1 (C-2^b, C-3^b), 69.4 (C-5^b), 66.9 (C-4^b), 65.4 (C4^a), 63.7 (C-6^b), 61.2 (C-6^a), 47.5 (C(CH₃)₃), 30.0 (C(CH₃)₃), 20.8 (CH₃(C=O)); Anal. calc for C₃₉H₄₄O₁₄S₂: HR ESIMS [M+Na]⁺: 823.2065, found: 823.2053; Elem. Anal: C, 58.49 H, 5.54; S, 8.01; found: C, 57.97 H, 5.87; S, 7.75.



28

Mecapto-*tert*-butyl 2-*O*-acetyl-3,4,6-tri-*O*-benzoyl- α -D-mannopyranosyl-(1 \rightarrow 3)-2,4,6-tri-*O*-benzoyl-1-thio- β -D-mannopyranoside (28)

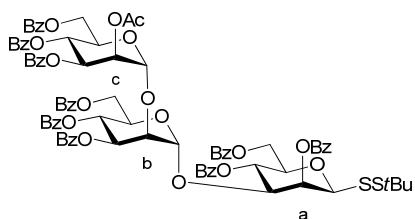
Triol **27** (0.48 g, 0.60 mmol) was dissolved in pyridine (2.5 mL) and cooled to 0 °C (ice-water bath). Benzoyl chloride (2.5 mL, 21.6 mmol) was added in portions and after 1 hour the reaction was removed from the ice bath. After 24 hours total reaction time, the reaction mixture was diluted with toluene and washed with 1 M NaOH, H₂O, and brine. The organic layer was dried over Na₂SO₄ and concentrated under reduced pressure. Purification of the crude product by chromatography (9:1 toluene/EtOAc) yielded **28** (0.53 g, 0.47 mmol, 87%) as a white powder; $[\alpha]_D^{25}$ -39 (c 3.9, CHCl₃); ¹H NMR (600 MHz, CDCl₃): δ 7.25-8.26 (m, 30H, Ar), 6.04 (dd, 1H, $J_{1,2}$ 3.5 Hz, J 1.0 Hz, H-2a), 5.82 (dd, 1H, $J_{3,4} \approx J_{4,5}$ 9.8 Hz, H-4^a), 5.79 (dd, 1H, $J_{3,4} \approx J_{4,5}$ 9.8 Hz, H-4^b), 5.53 (dd, 1H, $J_{3,4}$ 9.7 Hz, $J_{2,3}$ 3.4 Hz, H-3^b), 5.09 (dd, 1H, $J_{2,3}$ 3.4 Hz, $J_{1,2}$ 2.0 Hz, H-2^b), 5.07 (d, 1H, $J_{1,2}$ 1.9 Hz, H-1^b), 4.80 (d, 1H, $J_{1,2}$ 1.2 Hz, H-1^a), 4.80 (ddd, 1H, $J_{4,5}$ 9.8 Hz, $J_{5,6}$ 4.7 Hz, $J_{5,6}$ 2.8 Hz, H-5^b), 4.68 (dd, 1H, J_{gem} 12.3 Hz, $J_{5,6}$ 2.5 Hz, H-6^b), 4.68 (dd, 1H, J_{gem} 12.1 Hz, $J_{5,6}$ 2.5 Hz, H-6^a), 4.53 (dd, 1H, J_{gem} 12.2 Hz, $J_{5,6}$ 4.6 Hz, H-6^b), 4.47 (dd, 1H, J_{gem} 12.2 Hz, $J_{5,6}$ 5.3 Hz, H-6^a), 4.33 (dd, 1H, $J_{3,4}$ 9.8 Hz, $J_{2,3}$ 3.5 Hz, H-3^a), 3.99 (ddd, 1H, $J_{4,5}$ 10.0 Hz, $J_{5,6}$ 5.3 Hz, $J_{5,6}$ 2.9 Hz, H-5^a), 1.78 (s, 3H, CH₃(C=O)), 1.32 (s, 9H, C(CH₃)₃); ¹³C NMR (126 MHz, CDCl₃): δ 166.6 (C=O), 166.5 (C=O), 166.4 (C=O), 165.5 (C=O), 164.9 (C=O), 133.79 (Ar), 133.77 (Ar), 133.70 (Ar), 133.66 (Ar), 133.60 (Ar), 133.50 (Ar), 133.34 (Ar), 133.32 (Ar), 133.26 (Ar), 133.22 (Ar), 133.21 (Ar), 130.63 (Ar), 133.61 (Ar), 130.5 (Ar), 130.18 (Ar), 130.10 (Ar), 130.08 (Ar), 130.06 (Ar), 129.99 (Ar), 129.95 (Ar), 129.2 (Ar) 128.8 (Ar) 128.61 (Ar), 127.8 (Ar), 99.4 (H-1^b), 92.6 (H-1^a), 77.3 (H-3^a), 76.9 (H-5^a), 72.9 (H-2^a), 69.9 (H-5^b), 69.5 (H-2^b), 69.27 (H-3^b), 69.21 (H-4^a), 67.2 (H-4^b), 63.52 (H-6^a), 63.4 (H-6^b), 48.0 (C(CH₃)₃), 30.1 (C(CH₃)₃), 20.4 (CH₃(C=O)); Anal. calc for C₆₀H₅₆O₁₇S₂: HR ESIMS [M+Na]⁺: 1135.2851, found: 1135.2847; Elem. Anal: C, 64.74 H, 5.07; S, 5.76; found: C, 62.62 H, 5.02; S, 5.49.



29

Mecapto-*tert*-butyl 3,4,6-tri-*O*-benzoyl- α -D-mannopyranosyl-(1 \rightarrow 3)-2,4,6-tri-*O*-benzoyl-1-thio- β -D-mannopyranoside (29)

Trisaccharide **28** (0.36 g, 0.32 mmol) was dissolved in CH₂Cl₂ (1.5 mL) and MeOH (2.5 mL) and cooled to -10 °C (HAAKE Fisons chiller). A solution of acetyl chloride (0.25 mL, 2.9 mmol) in MeOH (1 mL) was added dropwise. The reaction was stirred at -10 °C for 170 hours, and quenched with 1 M NaHCO₃. The reaction mixture was extracted three times with EtOAc and the combined organic layer concentrated under reduced pressure. Purification of crude product by chromatography (9.4:0.6 toluene/EtOAc) yielded **29** (0.27 g, 0.25 mmol, 78%) as a white powder; $[\alpha]_D^{25}$ -27 (c 3.0, CHCl₃); ¹H NMR (500 MHz, CDCl₃): δ 7.28-8.27 (m, 30H, Ar), 6.05 (dd, 1H, $J_{2,OH}$ 3.4, $J_{1,2}$ 1.0 Hz, H-2^a), 5.85 (dd, 1H, $J_{3,4} \approx J_{4,5}$ 9.8 Hz, H-4^b), 5.80 (dd, 1H, $J_{3,4} \approx J_{4,5}$ 9.8 Hz, H-4^a), 5.43 (dd, 1H, $J_{3,4}$ 9.5 Hz, $J_{2,3}$ 3.1 Hz, H-3^b), 5.11 (d, 1H, $J_{1,2}$ 1.8 Hz, H-1^b), 4.87 (ddd, 1H, $J_{4,5}$ 9.9 Hz, $J_{5,6}$ 4.6 Hz, $J_{5,6}$ 2.8 Hz, H-5^b), 4.82 (d, 1H, $J_{1,2}$ 1.1 Hz, H-1^a), 4.66 (dd, 1H, J_{gem} 12.2 Hz, $J_{5,6}$ 2.7 Hz, H-6^b), 4.66 (dd, 2H, J_{gem} 12.2 Hz, $J_{5,6}$ 2.8 Hz, H-6^a), 4.56 (dd, 1H, J_{gem} 12.3 Hz, $J_{5,6}$ 4.8 Hz, H-6^b), 4.47 (dd, 4H, J_{gem} 12.3 Hz, $J_{5,6}$ 5.3 Hz, H-6^a), 4.38 (dd, 1H, $J_{3,4}$ 9.8 Hz, $J_{2,3}$ 3.4 Hz, H-3^a), 4.00 (m, 1H, H-5^a), 3.95 (m, 1H, H-2^b), 1.92 (d, 1H, $J_{2,OH}$ 4.2 Hz, 2-OH), 1.32 (s, 9H, C(CH₃)₃); ¹³C NMR (126 MHz, CDCl₃): δ 166.3 (C=O), 166.2 (C=O), 166.0 (C=O), 165.5 (C=O), 165.1 (C=O), 164.8 (C=O), 133.7 (Ar), 133.5 (Ar), 133.3 (Ar), 133.1 (Ar), 133.1 (Ar), 133.0 (Ar), 130.3 (Ar), 129.9 (Ar), 129.8 (Ar), 129.8 (Ar), 129.7 (Ar), 129.4 (Ar), 129.3 (Ar), 129.2 (Ar), 128.7 (Ar), 128.6 (Ar), 128.5 (Ar), 128.4 (Ar), 128.4 (Ar), 128.3 (Ar), 101.3 (C-1^b), 92.3 (C-1^a), 77.2 (C-5^a), 76.6 (C-3^a), 72.8 (C-2^a), 71.8 (C-3^b), 69.6 (C-5^b), 69.3 (C-4^a), 69.1 (C-2^b), 66.8 (C-4^b), 63.4 (C-6^b), 63.3 (C-6^a), 47.8 (C(CH₃)₃), 30.0 (C(CH₃)₃); Anal. calc for C₅₆H₅₄O₁₆S₂: HR ESIMS [M+Na]⁺: 1093.2745, found: 1093.2742.

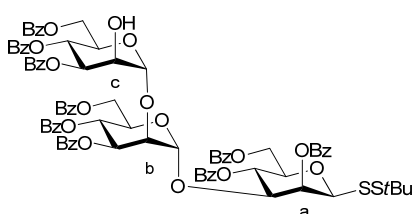


30

Mecapto-*tert*-butyl 2-*O*-acetyl-3,4,6-tri-*O*-benzoyl- α -D-mannopyranosyl-(1 \rightarrow 2)-3,4,6-tri-*O*-benzoyl- α -D-mannopyranosyl-(1 \rightarrow 3)-2,4,6-tri-*O*-benzoyl-1-thio- β -D-mannopyranoside (30)

Donor **5** (0.22 g, 0.33 mmol) and disaccharide acceptor **29** (0.27 g, 0.25 mol) were dissolved in dry CH₂Cl₂ (8 mL), activated molecular sieves added, and TMSOTf (4.6 μ L, 25 μ mol) was added at room temperature. After 1 hours the reaction was quenched with a drop of TEA and the reaction mixture concentrated under reduced pressure. The resulting slurry was purified by chromatography (6:4 heptane/EtOAc) to yield **30** (0.38 g, 0.24 mmol, 95%) as a white powder; $[\alpha]_{\text{D}}^{25}$ -53 (c 6.0, CHCl₃); ¹H NMR (498 MHz, CDCl₃): δ 7.29-8.25 (m, 45H, Ar), 5.93 (dd, 1H, $J_{2,3}$ 3.5 Hz, $J_{1,2}$ 0.7 Hz, H-2^a), 5.88 (dd, 1H, $J_{3,4} \approx J_{4,5}$ 10.0 Hz, H-4^b), 5.71 (dd, 1H, $J_{3,4}$ 9.9 Hz, $J_{2,3}$ 3.3 Hz, H-3^c), 5.64 (dd, 1H, $J_{3,4} \approx J_{4,5}$ 9.8 Hz, H-4^a), 5.61 (dd, 1H, $J_{3,4} \approx J_{4,5}$ 9.9 Hz, H-4^c), 5.51 (dd, 1H, $J_{3,4}$ 9.9 Hz, $J_{2,3}$ 3.3 Hz, H-3^b), 5.33 (d, 1H, $J_{1,2}$ 1.5 Hz, H-1^b), 5.28 (dd, 1H, $J_{2,3}$ 3.1 Hz, $J_{1,2}$ 2.2 Hz, H-2^c), 4.87 (ddd, 1H, $J_{4,5}$ 9.8 Hz, $J_{5,6}$ 5.0 Hz, $J_{5,6}$ 2.7 Hz, H-5^b), 4.71 (dd, 1H, J_{gem} 12.4 Hz, $J_{5,6}$ 5.2 Hz, H-6^b), 4.61 (dd, 1H, J_{gem} 12.3 Hz, $J_{5,6}$ 2.9 Hz, H-6^b), 4.57 (d, 1H, $J_{1,2}$ 0.9 Hz, H-1^a), 4.55 (dd, 1H, J_{gem} 12.1 Hz, $J_{5,6}$ 2.9 Hz, H-6^a), 4.37 (m, 1H, H-5^c), 4.35 (m, 1H, H-6^a), 4.34 (m, 1H, H-6^c), 4.21 (d, 1H, $J_{1,2}$ 1.8 Hz, H-1^c), 4.12 (m, 1H, H-6^c), 3.87 (dd, 1H, $J_{2,3}$ 3.4 Hz, $J_{1,2}$ 1.9 Hz, H-2^b), 3.83 (dd, 1H, $J_{3,4}$ 9.6 Hz, $J_{2,3}$ 3.4 Hz, H-3^a), 3.51 (ddd, 1H, $J_{4,5}$ 10.0 Hz, $J_{5,6}$ 5.3 Hz, $J_{5,6}$ 3.2 Hz, H-5^a), 1.95 (s, 3H, CH₃(C=O)), 1.34 (s, 9H, C(CH₃)₃); ¹³C NMR (126 MHz, CDCl₃): δ 169.1 (C=O), 166.30 (C=O), 166.29 (C=O), 166.25 (C=O), 165.9 (C=O), 166.30 (C=O), 166.28 (C=O), 166.26 (C=O), 166.24 (C=O), 165.15 (C=O), 133.8 (Ar), 133.79 (Ar), 133.78 (Ar), 133.27 (Ar), 133.26 (Ar), 133.24 (Ar), 133.0 (Ar), 132.78 (Ar), 132.73 (Ar), 130.63 (Ar), 130.61 (Ar), 130.56 (Ar), 130.26 (Ar), 130.23 (Ar), 130.14 (Ar), 130.11 (Ar), 130.10 (Ar), 130.09 (Ar), 130.08 (Ar), 130.01 (Ar), 129.61 (Ar), 129.60 (Ar), 129.58 (Ar), 129.57 (Ar), 129.4 (Ar), 129.3 (Ar), 128.85 (Ar), 128.83 (Ar), 128.56 (Ar), 128.55 (Ar), 128.54 (Ar), 128.3 (Ar),

102.8 (C-1^b), 99.7 (C-1^c), 92.5 (C-1^a), 78.8(C-2^b), 77.4 (C-3^a), 76.6 (C-5^a), 73.0 (C-2^a), 70.0 (C-5^c), 69.8 (C-3^b), 69.78 (C-3^c), 69.74 (C-2^c), 69.6 (C-5^b), 67.5 (C-4^b), 5.65 (C-4^a), 5.62 (C-4^c), 64.53 (C-6^b), 63.80 (C-6^c), 63.5 (C-6^a), 48.0 (C(CH₃)₃), 30.3 (C(CH₃)₃), 20.7 (CH₃(C=O)); Coupled HSQC (700 MHz, D₂O): δ 102.8/5.33 ($J_{C1/H1}$ 174 Hz, C-1^b), 99.7/4.21 ($J_{C1/H1}$ 171 Hz, C-1^c), 92.5/4.57 ($J_{C1/H1}$ 158 Hz, C-1^a); Anal. calc for C₈₇H₇₈O₂₅S₂: HR ESIMS [M+Na]⁺: 1609.4160, found: 1609.4160; Elem. Anal: C, 65.82 H, 4.95; S, 4.04; found: C, 65.51; H, 5.13; S, 3.92.

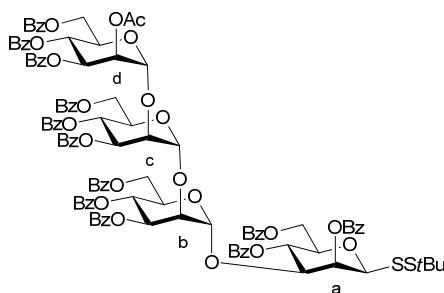


31

Mecapto-*tert*-butyl 3,4,6-tri-*O*-benzoyl- α -D-mannopyranosyl-(1 \rightarrow 2)-3,4,6-tri-*O*-benzoyl- α -D-mannopyranosyl-(1 \rightarrow 3)-2,4,6-tri-*O*-benzoyl-1-thio- β -D-mannopyranoside (31)

Trisaccharide **30** (0.24 g, 0.15 mmol) was dissolved in CH₂Cl₂ (1 mL) and MeOH (1 mL) and cooled to -10 °C (HAAKE Fisons chiller). A solution of acetyl chloride (0.15 mL, 2.1 mmol) in MeOH (0.85 mL) was added dropwise. The reaction was stirred at -10 °C for 2 weeks, and quenched with 1 M NaHCO₃. The reaction mixture was extracted three times with EtOAc and the combined organic layer concentrated under reduced pressure. Purification of crude product by chromatography (9.5:0.5 toluene/EtOAc) yielded **31** (0.11 g, 71 μ mol, 48%) as a white powder; $[\alpha]_D^{25}$ -63 (c 10.4, CHCl₃); ¹H NMR (700 MHz, CDCl₃): δ 7.30-8.26 (m, 45H, Ar), 5.94 (dd, 1H, $J_{2,3}$ 3.4, $J_{1,2}$ 0.9 Hz, H-2^a), 5.88 (dd, 1H, $J_{3,4} \approx J_{4,5}$ 10.0 Hz, H-4^b), 5.67 (dd, 1H, $J_{3,4} \approx J_{4,5}$ 9.9 Hz, H-4^a), 5.65 (dd, 1H, $J_{3,4} \approx J_{4,5}$ 9.8 Hz, H-4^c), 5.58 (dd, 1H, $J_{3,4}$ 9.9 Hz, $J_{2,3}$ 3.1 Hz, H-3^c), 5.46 (dd, 1H, $J_{3,4}$ 9.9 Hz, $J_{2,3}$ 3.4 Hz, H-3^b), 5.36 (d, 1H, $J_{1,2}$ 1.5 Hz, H-1^b), 4.86 (ddd, 1H, J_{gem} 10.0 Hz, $J_{5,6}$ 4.8 Hz, $J_{5,6}$ 2.8 Hz, H-5^b), 4.69 (dd, 1H, J_{gem} 12.4 Hz, $J_{5,6}$ 4.9 Hz, H-6^b), 4.62 (dd, 1H, J_{gem} 12.3 Hz, $J_{5,6}$ 2.5 Hz, H-6^b), 4.59 (d, 1H, $J_{1,2}$ 1.0 Hz, H-1^a), 4.57 (dd, 1H, J_{gem} 12.2 Hz, $J_{5,6}$ 3.0 Hz, H-6^a), 4.39 (dd, 1H, J_{gem} 12.2 Hz,

$J_{5,6}$ 5.2 Hz, H-6^a), 4.36 (m, 1H, H-5^c), 4.34 (m, 1H, H-6^c), 4.18 (d, 1H, $J_{1,2}$ 1.4 Hz, H-1^c), 4.12 (m, 1H, H-6^c), 4.09 (m, 1H, H-2^c), 3.90 (dd, 1H, $J_{2,3}$ 2.8 Hz, $J_{1,2}$ 1.4 Hz, H-2^b), 3.85 (dd, 1H, $J_{3,4}$ 9.7 Hz, $J_{2,3}$ 3.3 Hz, H-3^a), 3.56 (ddd, 1H, $J_{4,5}$ 9.8 Hz, $J_{5,6}$ 5.2 Hz, $J_{5,6}$ 3.1 Hz, H-5^a), 1.65 (d, 1H, $J_{2,OH}$ 4.8 Hz, 2-OH), 1.35 (s, 9H, C(CH₃)₃); ¹³C NMR (126 MHz, CDCl₃): δ 166.5 (C=O), 166.1 (C=O), 166.0 (C=O), 165.9 (C=O), 165.8 (C=O), 165.3 (C=O), 165.1 (C=O), 165.0 (C=O), 164.9 (C=O), 133.8 (Ar), 133.5 (Ar), 133.4 (Ar), 133.4 (Ar), 133.3 (Ar), 133.2 (Ar), 133.1 (Ar), 133.0 (Ar), 133.0 (Ar), 130.3 (Ar), 130.2 (Ar), 130.1 (Ar), 130.0 (Ar), 130.0 (Ar), 130.0 (Ar), 129.9 (Ar), 129.9 (Ar), 129.8 (Ar), 129.7 (Ar), 129.7 (Ar), 129.3 (Ar), 129.3 (Ar), 129.3 (Ar), 129.1 (Ar), 128.9 (Ar), 128.8 (Ar), 128.7 (Ar), 128.7 (Ar), 128.6 (Ar), 128.5 (Ar), 128.4 (Ar), 128.4 (Ar), 128.4 (Ar), 128.3 (Ar), 128.2 (Ar), 101.7 (C-1^c), 100.1 (C-1^b), 92.2 (C-1^a), 78.5 (C-2^b), 77.4 (C-3^a), 76.4 (C-5^a), 72.9 (C-2^a), 72.1 (C-3^c), 70.0 (C-3^b), 69.7 (C-5^c), 69.4 (C-5^b), 69.1 (C-2^c), 68.9 (C-4^a), 67.2 (C-4^b), 66.6 (C-4^c), 64.1 (C-6^b), 63.7 (C-6^a), 63.3 (C-6^c), 47.8 (C(CH₃)₃), 30.1 (C(CH₃)₃); Anal. calc for C₈₅H₇₆O₂₄S₂: HR ESIMS [M+Na]⁺: 1567.4060, found: 1567.4042.

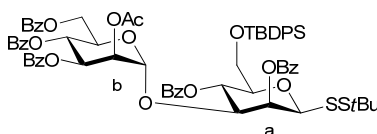


32

Mecapto-*tert*-butyl 2-*O*-acetyl-3,4,6-tri-*O*-benzoyl- α -D-mannopyranosyl-(1 \rightarrow 2)-3,4,6-tri-*O*-benzoyl- α -D-mannopyranosyl-(1 \rightarrow 2)-3,4,6-tri-*O*-benzoyl- α -D-mannopyranosyl-(1 \rightarrow 3)-2,4,6-tri-*O*-benzoyl-1-thio- β -D-mannopyranoside (32)

Donor **5** (45 mg, 66 μ mol) and trisaccharide acceptor **31** (79 mg, 51 μ mol) were dissolved in dry CH₂Cl₂ (0.6 mL), activated molecular sieves added, and the reaction mixture cooled to 0 °C (ice water bath). TMSOTf (1 μ L, 5.5 μ mol) was added and after 1.5 hours the reaction was quenched with a drop of TEA. The reaction mixture was concentrated under reduced pressure and the resulting slurry purified by

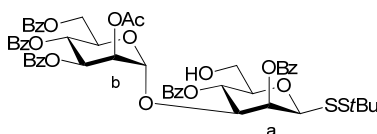
chromatography (7:3 heptane/EtOAc) to yield **32** (95 mg, 46 μ mol, 91%) as a white crystalline solid; $[\alpha]_D^{25}$ -32 (c 43.2, Benzene); ^1H NMR (600 MHz, CDCl_3): δ 7.09-8.32 (m, 60H, Ar), 5.99 (d, 1H, $J_{1,2}$ 3.3 Hz, H-2^a), 5.89 (dd, 1H, $J_{3,4} \approx J_{4,5}$ 9.9 Hz, H-4^b), 5.80 (dd, 1H, $J_{3,4}$ 10.1 Hz, $J_{2,3}$ 2.9 Hz, H-3^c), 5.76 (dd, 1H, $J_{3,4}$ 10.0 Hz, $J_{2,3}$ 3.4 Hz, H-3^d), 5.74 (dd, 1H, $J_{3,4} \approx J_{4,5}$ 7.5 Hz, H-4^c), 5.71 (dd, 1H, $J_{3,4} \approx J_{4,5}$ 9.7 Hz, H-4^a), 5.68 (dd, 1H, $J_{3,4} \approx J_{4,5}$ 10.0 Hz, H-4^d), 5.63 (dd, 1H, $J_{2,3}$ 3.2 Hz, $J_{1,2}$ 1.9 Hz, H-2^d), 5.47 (dd, 1H, $J_{3,4}$ 9.9 Hz, $J_{2,3}$ 3.4 Hz, H-3^b), 5.37 (d, 1H, $J_{1,2}$ 1.2 Hz, H-1^b), 4.89 (ddd, 1H, $J_{4,5}$ 10.0 Hz, $J_{5,6}$ 4.7 Hz, $J_{5,6}$ 2.6 Hz, H-5^b), 4.86 (d, 1H, $J_{1,2}$ 1.3 Hz, H-1^d), 4.71 (dd, 1H, J_{gem} 12.1 Hz, $J_{5,6}$ 5.0 Hz, H-6^b), 4.62 (s, 1H, H-1^a), 4.62 (br. s., 1H, H-1^c), 4.63 (dd, 1H, J_{gem} 12.3 Hz, $J_{5,6}$ 2.6 Hz, H-6^b), 4.58 (dd, 1H, J_{gem} 12.2 Hz, $J_{5,6}$ 2.9 Hz, H-6^a), 4.40 (dd, 1H, J_{gem} 12.2 Hz, $J_{5,6}$ 5.2 Hz, H-6^a), 4.33 (ddd, 1H, $J_{4,5}$ 9.9 Hz, $J_{5,6}$ 6.0 Hz, $J_{5,6}$ 2.0 Hz, H-5^c), 4.26 (d, 1H, $J_{2,3}$ 1.8 Hz, H-2^c), 4.24 (dd, 1H, J_{gem} 12.1 Hz, $J_{5,6}$ 6.0 Hz, H-6^c), 4.13 (br. d, 1H, J_{gem} 12.2 Hz, H-6^c), 4.02 (m, 1H, H-5^d), 4.00 (dd, 1H, $J_{3,4}$ 10.4 Hz, $J_{2,3}$ 3.3 Hz, H-3^a), 3.98 (dd, 1H, J_{gem} 12.6 Hz, $J_{5,6}$ 3.8 Hz, H-6^d), 3.93 (dd, 1H, J_{gem} 12.3 Hz, $J_{5,6}$ 3.5 Hz, H-6^d), 3.90 (br. s., 1H, H-2^b), 3.53 (ddd, 1H, $J_{4,5}$ 9.6 Hz, $J_{5,6}$ 5.0 Hz, $J_{5,6}$ 3.3 Hz, H-5^a), 2.00 (s, 3H, $\text{CH}_3(\text{C}=\text{O})$), 1.36 (s, 9H, $\text{C}(\text{CH}_3)_3$); ^{13}C NMR (126 MHz, CDCl_3): δ 169.0 (C=O), 166.5 (C=O), 166.1 (C=O), 166.1 (C=O), 165.9 (C=O), 165.7 (C=O), 165.7 (C=O), 165.4 (C=O), 165.2 (C=O), 165.2 (C=O), 165.1 (C=O), 165.0 (C=O), 164.6 (C=O), 134.1 (Ar), 133.6 (Ar), 133.4 (Ar), 133.3 (Ar), 133.2 (Ar), 133.1 (Ar), 133.1 (Ar), 133.0 (Ar), 132.8 (Ar), 130.4 (Ar), 130.3 (Ar), 130.0 (Ar), 130.0 (Ar), 130.0 (Ar), 129.8 (Ar), 129.8 (Ar), 129.7 (Ar), 129.7 (Ar), 129.7 (Ar), 129.4 (Ar), 129.4 (Ar), 129.3 (Ar), 129.3 (Ar), 128.9 (Ar), 128.9 (Ar), 128.7 (Ar), 128.7 (Ar), 128.6 (Ar), 128.5 (Ar), 128.5 (Ar), 128.4 (Ar), 128.4 (Ar), 128.3 (Ar), 128.2 (Ar), 100.8 (C-1^c), 100.0 (C-1^b), 99.3 (C-1^d), 92.3 (C-1^a), 78.2 (C-2^b), 76.6 (C-3^a), 76.5 (C-5^a), 75.1 (C-2^c), 72.8 (C-2^a), 71.0 (C-3^c), 69.9 (C-5^c), 69.8 (C-3^b), 69.5 (C-2^d), 69.4 (C-5^b), 69.3 (C-3^d), 69.3 (C-5^d), 68.9 (C-4^a), 67.6 (C-4^d), 67.4 (C-4^b), 66.8 (C-4^c), 64.2 (C-6^a), 64.0 (C-6^c), 63.3 (C-6^a), 63.1 (C-6^d), 47.8 ($\text{C}(\text{CH}_3)_3$), 30.1 ($\text{C}(\text{CH}_3)_3$), 20.6 ($\text{CH}_3(\text{C}=\text{O})$); Coupled HSQC (600 MHz, CDCl_3): δ 100.8/4.62 ($J_{\text{C1/H1}}$ 171 Hz, C-1^c), 100.0/5.37 ($J_{\text{C1/H1}}$ 175 Hz, C-1^b), 99.2/4.86 ($J_{\text{C1/H1}}$ 175 Hz, C-1^d), 92.2/4.62 ($J_{\text{C1/H1}}$ 156 Hz, C-1^a); Anal. calc for $\text{C}_{114}\text{H}_{100}\text{O}_{33}\text{S}_2$: HR ESIMS $[\text{M}+\text{Na}]^+$: 2083.5480, found: 2083.5457;



33

Mercapto-*tert*-butyl 2-*O*-acetyl-3,4,6-tri-*O*-benzoyl- α -D-mannopyranosyl-(1 \rightarrow 3)-2,4-di-*O*-benzoyl-6-*O*-*tert*-butyldiphenylsilyl-1-thio- β -D-mannopyranose (33)

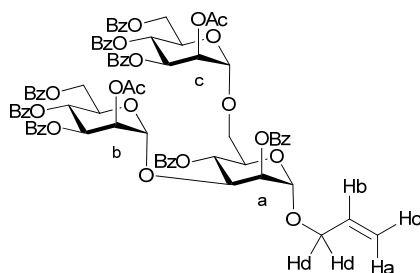
Disaccharide **26** (0.75 g, 0.72 mmol) was dissolved in a solution of pyridine (0.75 mL), benzoyl chloride (0.25 mL, 2.16 mmol) and 1-methylimidazole (1 drop). After 48 hours, the reaction was diluted with CH₂Cl₂ and washed with 1 M NaOH, H₂O and brine. The organic layer was dried over Na₂SO₄ and concentrated under reduced pressure. Purification of the crude product by chromatography (9.7:0.3 toluene/EtOAc) yielded **33** (0.69g, 0.52 mmol, 72%) as a white solid; $[\alpha]_D^{25}$ -40 (*c* 8.1, CHCl₃); ¹H NMR (600 MHz, CDCl₃): δ 7.16-8.30 (m, 35H, ArH), 6.05 (d, 1H, *J*_{2,3} 3.0 Hz, H-2^a), 5.90 (dd, 1H, *J*_{3,4} \approx *J*_{4,5} 9.9 Hz, H-4^a), 5.80 (dd, 1H, *J*_{3,4} \approx *J*_{4,5} 9.8 Hz, H-4^b), 5.55 (dd, 1H, *J*_{3,4} 9.7 Hz, *J*_{2,3} 3.3 Hz, H-3^b), 5.12 (dd, 1H, *J*_{2,3} 3.0 Hz, *J*_{1,2} 2.1 Hz, H-2^b), 5.01 (d, 1H, *J*_{1,2} 1.4 Hz, H-1^b), 4.81 (m, 1H, H-5^b), 4.79 (s, 1H, H-1^a), 4.69 (dd, 1H, *J*_{gem} 12.2 Hz, *J*_{5,6} 2.4 Hz, H-6^b), 4.52 (dd, 1H, *J*_{gem} 12.2 Hz, *J*_{5,6} 4.4 Hz, H-6^b), 4.28 (dd, 1H, *J*_{3,4} 9.9 Hz, *J*_{2,3} 3.4 Hz, H-3^a), 3.86 (m, 2H, H-6^a), 3.68 (ddd, 1H, *J*_{4,5} 9.9 Hz, 2 \times *J*_{5,6} 2.9 Hz, H-5^a), 1.79 (s, 3H, CH₃(C=O)), 1.36 (s, 9H, SiC(CH₃)₃), 1.08 (s, 9H, SiC(CH₃)₃); ¹³C NMR (151 MHz, CDCl₃): δ 168.7 (C=O), 166.2 (C=O), 166.2 (C=O), 165.4 (C=O), 164.7 (C=O), 164.5 (C=O), 135.8 (Ar), 135.6 (Ar), 133.4 (Ar), 133.3 (Ar), 133.1 (Ar), 133.1 (Ar), 133.0 (Ar), 132.8 (Ar), 130.4 (Ar), 130.0 (Ar), 129.9 (Ar), 129.7 (Ar), 129.5 (Ar), 129.5 (Ar), 129.4 (Ar), 129.3 (Ar), 129.2 (Ar), 129.1 (Ar), 128.6 (Ar), 128.5 (Ar), 128.4 (Ar), 128.3 (Ar), 128.2 (Ar), 127.6 (Ar), 127.5 (Ar), 99.1 (C-1^b), 92.4 (C-1^a), 79.7 (C-5^a), 77.5 (C-3^a), 72.7 (C-2^a), 69.6, 69.5, 68.9, 68.4 (C-4^a, C-2^b, C-3^b, C-5^b), 67.0 (C-4^b), 63.1 (H-6^b), 62.6 (H-6^a), 47.7 (SiC(CH₃)₃), 30.0 (SiC(CH₃)₃), 26.7 (SiC(CH₃)₃), 20.3 (CH₃(C=O)), 19.2 (SiC(CH₃)₃); Anal. calc for C₆₉H₇₀O₁₆S₂Si: HR ESIMS [M+Na]⁺: 1269.3767, found: 1269.3765; Elem. Anal: C, 66.43 H, 5.66; S, 5.14; found: C, 66.10; H, 5.61; S, 5.09.



34

Mercapto-*tert*-butyl 2-*O*-acetyl-3,4,6-tri-*O*-benzoyl- α -D-mannopyranosyl-(1 \rightarrow 3)-2,4-di-*O*-benzoyl-1-thio- β -D-mannopyranose (34)

Disaccharide **33** (0.21 g, 0.17 mmol) was dissolved in a pyridine (0.25 mL) and hydrogen fluoride in pyridine (25 μ L, 70% HF) added. The reaction was performed in a polypropylene flask. After 45 minutes, a suspension of CaCO₃ in sat. NaHCO₃ (0.5 mL) was added and the reaction mixture stirred for 30 minutes. The slurry was filtered through a pad of Celite and the eluted solution concentrated under reduced pressure. Purification of the crude product by chromatography (9:1 toluene/EtOAc) yielded **34** (0.16 g, 0.16 mmol, 93%) as a white solid; $[\alpha]_D^{25}$ -63 (*c* 7.2, CHCl₃); ¹H NMR (600 MHz, CDCl₃): δ 7.25-8.28 (m, 25H, ArH), 6.05 (d, 1H, $J_{2,3}$ 3.2 Hz, H-2^a), 5.82 (dd, 1H, $J_{3,4} \approx J_{4,5}$ 9.8 Hz, H-4^b), 5.58 (dd, 1H, $J_{3,4} \approx J_{4,5}$ 9.8 Hz, H-4^a), 5.50 (dd, 1H, $J_{3,4}$ 9.6 Hz, $J_{2,3}$ 3.3 Hz, H-3^b), 5.13 (d, 1H, $J_{1,2}$ 1.5 Hz, H-1^b), 5.09 (dd, 1H, $J_{2,3}$ 2.9 Hz, $J_{1,2}$ 2.1 Hz, H-2^b), 4.80 (s, 1H, H-1^a), 4.77 (ddd, 1H, $J_{4,5}$ 9.9 Hz, $J_{5,6}$ 4.1 Hz, $J_{5,6}$ 3.0 Hz, H-5^b), 4.70 (dd, 1H, J_{gem} 12.2 Hz, $J_{5,6}$ 2.5 Hz, H-6^b), 4.53 (dd, 1H, J_{gem} 12.2 Hz, $J_{5,6}$ 4.4 Hz, H-6^b), 4.36 (dd, 1H, $J_{3,4}$ 9.7 Hz, $J_{2,3}$ 3.5 Hz, H-3^a), 3.84 (ddd, 1H, J_{gem} 12.7 Hz, $J_{5,6}$ 9.5 Hz, $J_{5,6}$ 2.1 Hz, H-6^a), 3.78 (dd, 1H, $J_{5,6}$ 12.8 Hz, $J_{5,6}$ 4.9 Hz, H-6^a), 3.64 (ddd, 1H, $J_{4,5}$ 9.9 Hz, $J_{5,6}$ 4.7 Hz, $J_{5,6}$ 2.3 Hz, H-5^a), 2.62 (dd, 1H, J_{gem} 9.4 Hz, $J_{5,6}$ 5.0 Hz, 6-OH), 1.80 (s, 3H, CH₃(C=O)), 1.38 (s, 9H, SC(CH₃)₃); ¹³C NMR (151 MHz, CDCl₃): δ 168.8 (C=O), 166.2 (C=O), 166.1 (C=O), 166.0 (C=O), 165.4 (C=O), 164.6 (C=O), 133.7 (Ar), 133.6 (Ar), 133.4 (Ar), 133.1 (Ar), 132.9 (Ar), 130.3 (Ar), 129.9 (Ar), 129.7 (Ar), 129.5 (Ar), 129.3 (Ar), 129.1 (Ar), 129.0 (Ar), 128.7 (Ar), 128.5 (Ar), 128.5 (Ar), 128.4 (Ar), 128.2 (Ar), 99.2 (C-1^b), 92.0 (C-1^a), 79.5 (C-5^a), 76.9 (C-3^a), 72.5 (C-2^a), 69.7, 69.4, 69.1, 68.9 (C-4^a, C-2^b, C-3^b, C-5^b), 66.8 (C-4^b), 63.1 (H-6^b), 61.7 (H-6^a), 47.8 (SC(CH₃)₃), 29.9 (SC(CH₃)₃), 20.2 (CH₃(C=O)O); Anal. calc for C₅₃H₅₂O₁₆S₂: HR ESIMS [M+Na]⁺: 1031.2589, found: 1031.2591; Elem. Anal: C, 63.08; H, 5.19; S, 6.36; found: C, 63.07; H, 5.25; S, 6.35.

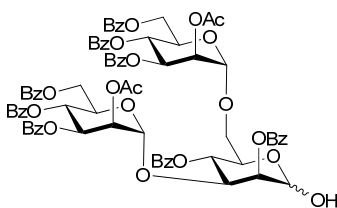


35

Allyl 2-O-acetyl-3,4,6-tri-O-benzoyl- α -D-mannopyranosyl-(1 \rightarrow 6)-[2-O-acetyl-3,4,6-tri-O-benzoyl- α -D-mannopyranosyl-(1 \rightarrow 3)]-2,4-di-O-benzoyl- α -D-mannopyranoside (35)

Donor **5** (1.55 g, 2.28 mmol) and acceptor **4** (0.47 g, 1.09 mol) were dissolved in dry CH_2Cl_2 (18 mL), activated molecular sieves added, and the reaction mixture cooled to 0 °C (ice water bath). TMSOTf (14.5 μL , 73 μmol) was added and after 30 minutes the reaction was removed from the ice bath. Additional TMSOTf (8 μL , 27 μmol) was added after 2 hours total reaction time and the reaction was quenched 30 minutes later with the addition of 3 drops of TEA. The reaction mixture was concentrated under reduced pressure and the resulting slurry purified by chromatography (8:2 hexanes/EtOAc) to yield **35** (1.44g, 0.99 mol, 93%) as a white glassy solid; Spectral data matches literature values;⁴ $[\alpha]_{\text{D}}^{25}$ -5 (c 4.3, CHCl_3); $^1\text{H NMR}$ (600 MHz, CDCl_3): δ 7.26-8.25 (m, 40H, ArH), 5.95 (ddt, 1H, J_{trans} 16.8 Hz, J_{cis} 10.7 Hz, $2 \times J$ 6.0 Hz, Hb), 5.91 (dd, 1H, $J_{3,4} \approx J_{4,5}$ 9.9 Hz, H-4c), 5.85 (dd, 1H, $J_{3,4}$ 10.3 Hz, $J_{2,3}$ 3.0 Hz, H-3^c), 5.83 (dd, 1H, $J_{3,4} \approx J_{4,5}$ 10.1 Hz, H-4^a), 5.79 (dd, 1H, $J_{3,4} \approx J_{4,5}$ 9.8 Hz, H-4^b), 5.68 (dd, 1H, $J_{2,3}$ 3.4 Hz, $J_{1,2}$ 1.6 Hz, H-2^a), 5.57 (dd, 1H, $J_{3,4}$ 9.7 Hz, $J_{2,3}$ 3.3 Hz, H-3^b), 5.50 (dd, 1H, $J_{2,3}$ 3.1 Hz, $J_{1,2}$ 1.8 Hz, H-2^c), 5.43 (dq, 1H, J_{trans} 17.2 Hz, $J_{\text{gem}} \approx 2 \times ^4J$ 1.3 Hz, Ha), 5.30 (dq, 1H, J_{cis} 10.4 Hz, $J_{\text{gem}} \approx 2 \times ^4J$ 1.2 Hz, Hc), 5.18 (d, 1H, $J_{1,2}$ 1.7 Hz, H-1^b), 5.13 (s, 1H, H-1^a), 5.12 (dd, 1H, $J_{2,3}$ 2.8 Hz, $J_{1,2}$ 2.1 Hz, H-2^b), 4.97 (d, 1H, $J_{1,2}$ 1.3 Hz, H-1^c), 4.60 (dd, 1H, $J_{3,4}$ 9.7 Hz, $J_{2,3}$ 3.4 Hz, H-3^a), 4.52 (dd, 1H, J_{gem} 12.1 Hz, $J_{5,6}$ 2.5 Hz, H-6^b), 4.49 (dd, 1H, J_{gem} 11.9 Hz, $J_{5,6}$ 2.5 Hz, H-6^c), 4.45 (ddd, 1H, J_{gem} 9.9 Hz, $J_{5,6}$ 5.2 Hz, $J_{5,6}$ 2.6 Hz, H-5^c), 4.42 (ddd, 1H, J_{gem} 9.8 Hz, $J_{5,6}$ 4.3 Hz, $J_{5,6}$ 2.5 Hz, H-5^b), 4.36 (dd, 1H, J_{gem} 12.0 Hz, $J_{5,6}$ 4.1 Hz, H-6^b), 4.36 (dd, 1H, J_{gem} 11.9 Hz, $J_{5,6}$ 5.2 Hz, H-6^c), 4.34 (ddt, 1H, J_{gem} 12.8 Hz, 3J 5.3 Hz, $2 \times ^4J$ 1.2 Hz, Hd), 4.27 (ddd, 1H, $J_{4,5}$ 9.9 Hz, $J_{5,6}$ 6.4 Hz, $J_{5,6}$ 1.8 Hz, H-5^a), 4.16 (ddt, 1H, J_{gem} 12.8 Hz, 3J 6.2 Hz, $2 \times ^4J$ 1.1 Hz, Hd), 4.10 (dd, 1H, J_{gem} 10.6 Hz, $J_{5,6}$ 6.4 Hz, H-6^a), 3.72 (dd, 1H, J_{gem} 10.6 Hz, $J_{5,6}$ 1.9 Hz, H-6^a), 2.10 (s, 3H, $\text{CH}_3(\text{C}=\text{O})$), 1.88 (s,

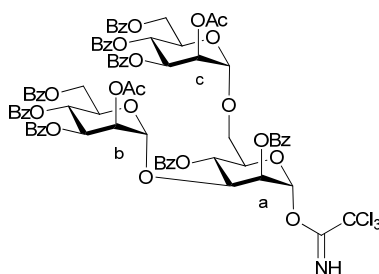
3H, CH₃(C=O)); ¹³C NMR (151 MHz, CDCl₃): δ 169.7 (C=O), 169.0 (C=O), 166.1 (C=O), 166.1 (C=O), 166.0 (C=O), 165.5 (C=O), 165.5 (C=O), 165.2 (C=O), 165.1 (C=O), 164.6 (C=O), 133.5 (Ar), 133.4 (Ar), 133.4 (Ar), 133.2 (Ar), 133.1 (Ar), 133.1 (CH=CH₂), 133.0 (Ar), 132.9 (Ar), 132.9 (Ar), 130.1 (Ar), 129.9 (Ar), 129.9 (Ar), 129.9 (Ar), 129.8 (Ar), 129.8 (Ar), 129.6 (Ar), 129.6 (Ar), 129.6 (Ar), 129.3 (Ar), 129.3 (Ar), 129.2 (Ar), 129.0 (Ar), 128.9 (Ar), 128.9 (Ar), 128.8 (Ar), 128.4 (Ar), 128.4 (Ar), 128.3 (Ar), 128.2 (Ar), 118.7 (CH=CH₂), 99.5 (C-1^b), 97.3 (C-1^c), 96.5 (C-1^a), 76.3 (C-3^a), 72.0 (C-2^a), 69.83, 69.78, 69.71, 69.7, 69.6, 69.1, 68.8, 68.7, 68.6 (C-2^b, C-2^c, C-3^b, C-3^c, C-4^a, C-5^a, C-5^b, C-5^c, CH₂CH=CH₂), 66.9, 66.8, 66.8 (C-4^b, C-4^c, C-6^a), 63.1, 63.0 (C-6^b, C-6^c), 20.7 (CH₃(C=O)), 20.4 (CH₃(C=O)); Coupled HSQC (500 MHz, CDCl₃): δ 99.7/5.18 (*J*_{C1/H1} 171 Hz, C-1^b), 97.6/4.97 (*J*_{C1/H1} 175 Hz, C-1^c), 96.8/5.12 (*J*_{C1/H1} 175 Hz, C-1^a); Anal. calc for C₈₇H₇₂O₂₆: HR ESIMS [M+Na]⁺: 1483.4204, found: 1483.4169;



36

2-*O*-acetyl-3,4,6-tri-*O*-benzoyl- α -D-mannopyranosyl-(1 \rightarrow 6)-[2-*O*-acetyl-3,4,6-tri-*O*-benzoyl- α -D-mannopyranosyl-(1 \rightarrow 3)]-2,4-di-*O*-benzoyl-D-mannopyranose (36)

Trisaccharide **35** (0.73g, 0.5 mmol) was dissolved in a solution of NaOAc (0.5 g, 6 mmol) in AcOH (6.65 mL) and H₂O (0.35 mL). PdCl₂ (0.54 g, 3.0 mmol) was added and the reaction mixture stirred for 10 hours. Palladium black precipitated from the solution over the course of the reaction. The reaction mixture was poured into saturated NaHCO₃ and the aqueous layer was extracted with EtOAc three times. The combined organic phases were dried over Na₂SO₄ and concentrated under reduced pressure. Purification of the crude product by chromatography (8.5:1.5 toluene/EtOAc) yielded trisaccharide **36** as a white powder that was inseparable from a trisaccharide byproduct. Product **36** carried on to the next step without further separation.

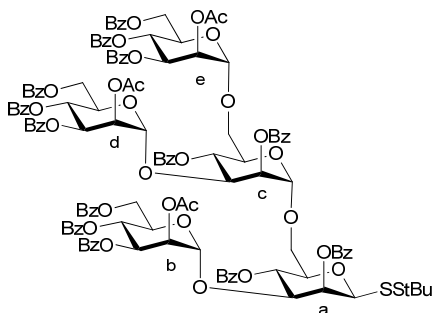


37

2-*O*-acetyl-3,4,6-tri-*O*-benzoyl- α -D-mannopyranosyl-(1 \rightarrow 6)-[2-*O*-acetyl-3,4,6-tri-*O*-benzoyl- α -D-mannopyranosyl-(1 \rightarrow 3)]-2,4-di-*O*-benzoyl- α -D-mannopyranosyl trichloroacetimidate (37)

Trisaccharide **36** (~0.60 g), containing trisaccharide byproduct, was dissolved in a solution of trichloroacetonitrile (0.5 mL, 5.0 mmol) in CH₂Cl₂ (3 mL) and a drop of DBU added. After 24 hours, the reaction mixture was diluted with toluene and concentrated under reduced pressure. Purification of the crude syrup by chromatography (8:2 toluene/EtOAc) yielded **37** (0.41 g, 0.26 mmol, 52% from **35**) as a white foam; [α]_D²⁵ 6 (*c* 8.1, CH₂Cl₂); ¹H NMR (600 MHz, CDCl₃): δ 9.00 (s, 1H, NH), 7.27-8.28 (m, 40H, ArH), 6.56 (d, 1H, *J* 1.4 Hz, H-1^a), 5.95 (dd, 1H, *J*_{3,4} \approx *J*_{4,5} 10.1 Hz, H-4^a), 5.90 (dd, 1H, *J*_{3,4} \approx *J*_{4,5} 10.1 Hz H-4^b), 5.87 (dd, 1H, *J*_{2,3} 3.3 Hz, *J*_{1,2} 2.0 Hz, H-2^a), 5.84 (dd, 1H, *J*_{3,4} \approx *J*_{4,5} 9.8 Hz, H-4^c), 5.81 (dd, 1H, *J*_{3,4} 10.0 Hz, *J*_{2,3} 3.3 Hz, H-3^b), 5.59 (dd, 1H, *J*_{3,4} 9.8 Hz, *J*_{2,3} 3.3 Hz, H-3^c), 5.46 (dd, 1H, *J*_{2,3} 3.2 Hz, *J*_{1,2} 1.8 Hz, H-2^b), 5.24 (d, 1H, *J*_{2,3} 1.7 Hz, H-1^c), 5.17 (dd, 1H, *J*_{2,3} 2.9 Hz, *J*_{1,2} 2.3 Hz, H-2^c), 4.95 (d, 1H, *J*_{1,2} 1.4 Hz, H-1^b), 4.65 (dd, 1H, *J*_{3,4} 9.7 Hz, *J*_{2,3} 3.4 Hz, H-3^a), 4.42-4.50 (m, 5H, H-5^a, H-5^b, H-5^c, H-6^b, H-6^c), 4.38 (dd, 1H, *J*_{gem} 12.2 Hz, *J*_{5,6} 3.2 Hz, H-6^b), 4.36 (dd, 1H, *J*_{gem} 12.4 Hz, *J*_{5,6} 5.2 Hz, H-6^c), 4.09 (dd, 1H, *J*_{gem} 10.9 Hz, *J*_{5,6} 6.2 Hz, H-6^a), 3.78 (dd, 1H, *J*_{gem} 10.9 Hz, *J*_{5,6} 1.9 Hz, H-6^a), 2.10 (s, 3H, CH₃(C=O)), 1.91 (s, 3H, CH₃(C=O)); ¹³C NMR (151 MHz, CDCl₃): δ 169.7 (C=O), 169.0 (C=O), 166.0 (2x C=O), 165.9 (C=O), 165.6 (C=O), 165.4 (C=O), 165.2 (C=O), 165.0 (C=O), 164.7 (C=O), 159.5 (C=NH), 133.8 (Ar), 133.6 (Ar), 133.3 (Ar), 133.3 (Ar), 133.1 (Ar), 133.0 (Ar), 133.0 (Ar), 132.9 (Ar), 130.2 (Ar), 130.0 (Ar), 129.9 (Ar), 129.8 (Ar), 129.8 (Ar), 129.7 (Ar), 129.6 (Ar), 129.6 (Ar), 129.6 (Ar), 129.4 (Ar), 129.3 (Ar), 129.2 (Ar), 128.9 (Ar), 128.9 (Ar), 128.8 (Ar), 128.7 (Ar), 128.5 (Ar), 128.4 (Ar), 128.3 (Ar), 128.3 (Ar), 128.3 (Ar), 128.3 (Ar), 128.2 (Ar), 99.7 (C-1_b), 97.2 (C-

1_c), 94.3 (C-1_a), 90.7 (CCl₃), 76.1 (C-3_a), 72.2 (C-2_a), 70.5, 69.8, 69.8, 69.7, 69.6, 69.1, 68.7, 67.8 (C-2^b, C-2^c, C-3^b, C-3^c, C-4^a, C-5^a, C-5^b, C-5^c), 66.9, 66.6, 66.3 (C-4^b, C-4^c, C-6^a), 63.0, 62.7 (C-6^b, C-6^c), 20.7 (CH₃(C=O)), 20.4 (CH₃(C=O)); Anal. calc for C₈₀H₆₈O₂₆NCl₃: HR ESIMS [M+Na]⁺: 1586.2987, found: 1586.3012; Elem. Anal: C, 61.37; H, 4.38; N, 0.89; found: C, 61.19; H, 4.54; N, 1.05.



38

Mecapto-*tert*-butyl 2-*O*-acetyl-3,4,6-tri-*O*-benzoyl- α -D-mannopyranosyl-(1 \rightarrow 6)-[2-*O*-acetyl-3,4,6-tri-*O*-benzoyl- α -D-mannopyranosyl-(1 \rightarrow 3)]-2,4-di-*O*-benzoyl- α -D-mannopyranosyl-(1 \rightarrow 6)-[2-*O*-acetyl-3,4,6-tri-*O*-benzoyl- α -D-mannopyranosyl-(1 \rightarrow 3)]-2,4-di-*O*-benzoyl-1-thio- β -D-mannopyranoside (38)

Trisaccharide donor **37** (84.6 mg, 54 μ mol) and disaccharide acceptor **34** (53 mg, 53 μ mol) were dissolved in dry CH₂Cl₂ (0.7 mL), activated molecular sieves added, and the reaction mixture cooled to 0 °C (ice water bath). TMSOTf (1 μ L, 5.5 μ mol) was added and after 30 minutes the reaction was quenched with a drop of TEA. Reaction mixture was concentrated under reduced pressure and the resulting slurry purified by chromatography (9:1 toluene/EtOAc) to yield **38** (0.119 g, 49 μ mol, 93%) as a white glassy solid; $[\alpha]_D^{25}$ -10 (c 9.1, CHCl₃); ¹H NMR (700 MHz, CDCl₃): δ 7.24-8.27 (m, 65H, ArH), 6.08 (dd, 1H, $J_{2,3}$ 3.5 Hz, $J_{1,2}$ 1.1 Hz, H-2^a), 5.95 (dd, 1H, $J_{3,4} \approx J_{4,5}$ 10.0 Hz, H-4^c), 5.89 (dd, 1H, $J_{3,4} \approx J_{4,5}$ 10.0 Hz, H-4^e), 5.84 (dd, 1H, $J_{3,4}$ 10.4 Hz, $J_{2,3}$ 3.1 Hz, H-3^e), 5.83 (dd, 1H, $J_{3,4} \approx J_{4,5}$ 9.6 Hz, H-4^d), 5.82 (dd, 1H, $J_{3,4} \approx J_{4,5}$ 10.0 Hz, H-4^b), 5.79 (dd, 1H, $J_{3,4} \approx J_{4,5}$ 10.0 Hz, H-4^a), 5.76 (dd, 1H, $J_{2,3}$ 3.4 Hz, $J_{1,2}$ 1.6 Hz, H-2^c), 5.59 (dd, 1H, $J_{3,4}$ 9.8 Hz, $J_{2,3}$ 3.3 Hz, H-3^d), 5.54 (dd, 1H, $J_{3,4}$ 9.6 Hz, $J_{2,3}$ 2.9 Hz, H-3^b), 5.46 (dd, 1H, $J_{2,3}$ 3.1 Hz, $J_{1,2}$ 1.9 Hz, H-2^e), 5.23

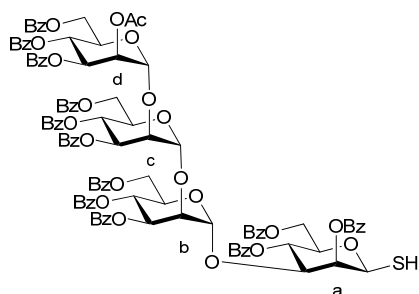
(d, 1H, $J_{1,2}$ 1.9 Hz, H-1^d), 5.18 (dd, 1H, $J_{2,3}$ 3.1 Hz, $J_{1,2}$ 2.1 Hz, H-2^d), 5.12 (d, 1H, $J_{1,2}$ 1.2 Hz, H-1^c), 5.10(br. s, 1H, H-1^b), 5.10 (dd, 1H, $J_{2,3}$ 3.3 Hz, $J_{1,2}$ 1.9 Hz, H-2^b), 4.83 (d, 1H, $J_{1,2}$ 1.2 Hz, H-1^a), 4.80 (d, 1H, $J_{1,2}$ 1.8 Hz, H-1^e), 4.80 (ddd, 1H, $J_{4,5}$ 9.6 Hz, $J_{5,6}$ 4.0 Hz, $J_{5,6}$ 3.0 Hz, H-5^b), 4.72 (dd, 1H, J_{gem} 12.2 Hz, $J_{5,6}$ 2.6 Hz, H-6^b), 4.64 (dd, 1H, $J_{3,4}$ 9.7 Hz, $J_{2,3}$ 3.5 Hz, H-3^c), 4.52 (dd, 1H, J_{gem} 12.2 Hz, $J_{5,6}$ 4.4 Hz, H-6^b), 4.51 (dd, 1H, J_{gem} 13.3 Hz, $J_{5,6}$ 4.0 Hz, H-6^d), 4.38 (dd, 1H, J_{gem} 11.9 Hz, $J_{5,6}$ 2.4 Hz, H-6^e), 4.36 (dd, 1H, $J_{3,4}$ 10.0 Hz, $J_{2,3}$ 3.7 Hz, H-3^a), 4.34-4.37 (m, 2H, H-5^d, H-6^a), 4.35 (ddd, 1H, $J_{4,5}$ 9.5 Hz, $J_{5,6}$ 4.8 Hz, $J_{5,6}$ 2.9 Hz, H-5^e), 4.28 (dd, 1H, J_{gem} 11.8 Hz, $J_{5,6}$ 5.1 Hz, H-6^e), 4.24 (ddd, 1H, $J_{4,5}$ 10.2 Hz, $J_{5,6}$ 5.1 Hz, $J_{5,6}$ 2.0 Hz, H-5^c), 4.18 (dd, 1H, J_{gem} 11.1 Hz, $J_{5,6}$ 6.1 Hz, H-6^a), 4.01 (dd, 1H, J_{gem} 10.8 Hz, $J_{5,6}$ 5.2 Hz, H-6^c), 3.92 (ddd, 1H, $J_{4,5}$ 10.0 Hz, $J_{5,6}$ 6.2 Hz, $J_{5,6}$ 1.8 Hz, H-5^a), 3.75 (dd, 1H, J_{gem} 11.1 Hz, $J_{5,6}$ 1.6 Hz, H-6^a), 3.49 (dd, 1H, J_{gem} 10.6 Hz, $J_{5,6}$ 1.9 Hz, H-6^c), 2.10 (s, 3H, CH₃(C=O)), 1.92 (s, 3H, CH₃(C=O)), 1.77 (s, 3H, CH₃(C=O)), 1.38 (s, 9H, C(CH₃)₃); ¹³C NMR (176 MHz, CDCl₃): δ 169.5 (C=O), 168.9 (C=O), 168.7 (C=O), 166.2 (C=O), 166.2 (C=O), 166.1 (C=O), 166.0 (C=O), 165.9 (C=O), 165.6 (C=O), 165.6 (C=O), 165.4 (C=O), 165.2 (2×C=O), 165.1 (C=O), 164.6 (C=O), 164.6 (C=O), 133.5 (Ar), 133.4 (Ar), 133.3 (Ar), 133.1 (Ar), 133.1 (Ar), 133.0 (Ar), 133.0 (Ar), 132.9 (Ar), 132.9 (Ar), 130.2 (Ar), 130.2 (Ar), 130.0 (Ar), 130.0 (Ar), 130.0 (Ar), 129.9 (Ar), 129.8 (Ar), 129.8 (Ar), 129.7 (Ar), 129.7 (Ar), 129.7 (Ar), 129.6 (Ar), 129.5 (Ar), 129.5 (Ar), 129.4 (Ar), 129.3 (Ar), 129.2 (Ar), 129.2 (Ar), 129.1 (Ar), 129.1 (Ar), 128.9 (Ar), 128.9 (Ar), 128.7 (Ar), 128.6 (Ar), 128.5 (Ar), 128.4 (Ar), 128.4 (Ar), 128.3 (Ar), 128.3 (Ar), 128.2 (Ar), 128.2 (Ar), 100.0 (C-1^d), 99.3 (C-1^b), 97.6 (C-1^c), 97.3 (C-1^e), 92.0 (C-1^a), 77.7, 77.4 (C-3^c, C-5^a), 77.4 (C-3^a), 72.6 (C-2^a), 71.9 (C-2^c), 70.1, 69.67, 2×69.67, 69.5, 2×69.4, 69.3, 69.0, 68.7, 68.6 (C-4^a, C-2^b, C-3^b, C-5^b, C-5^c, C-2^d, C-3^d, C-5^d, C-2^e, C-3^e, C-5^e), 67.9 (C-4^c), 66.9 (C-4^b), 66.74 (C-6^a), 66.66 (C-4^d, C-4^e), 66.0 (C-6^c), 63.1, 63.0, 62.8 (C-6^b, C-6^d, C-6^e), 47.9 (C(CH₃)₃), 29.9 (C(CH₃)₃), 20.7 (CH₃(C=O)), 20.4 (CH₃(C=O)), 20.2 (CH₃(C=O)); Coupled HSQC (700 MHz, CDCl₃): δ 100.0/5.23 ($J_{\text{C1/H1}}$ 174 Hz, C-1^d), 99.3/5.10 ($J_{\text{C1/H1}}$ 177 Hz, C-1^b), 97.6/5.12 ($J_{\text{C1/H1}}$ 175 Hz, C-1^c), -97.3/4.80 ($J_{\text{C1/H1}}$ 175 Hz, C-1^e), 92.0/4.83 ($J_{\text{C1/H1}}$ 157 Hz, C-1^a); Anal. calc for C₁₃₁H₁₁₈O₄₁S: HR ESIMS [M+Na]⁺: 2433.6482, found: 2433.6434.



39

 β -D-mannopyranosyl thiol (39)

Monosaccharide **17** (25 mg, 55 μ mol) was dissolved in a 1 M solution of trimethylphosphine in THF (0.64 mL, 0.64 mmol) and a 1 M solution of NaHCO_3 (0.46 mL, pH 9) added and stirred vigorously. After 1.5 hours, the reaction mixture was neutralized with dilute AcOH and extracted with EtOAc three times and the organic layer concentrated under reduced pressure. Phosphine impurities were removed by chromatographic purification (1:1 hexanes/EtOAc). The free thiol intermediate was suspended in MeOH (0.5 mL) and a 1 M solution of sodium methoxide (55 μ L) added. After 45 minutes, the resulting precipitate was collect by filtration and washed with ice cold methanol, yielding **39** (10.5 mg, 47 μ mol, 85%) as a sodium salt. Spectral data matched literature values;⁵ ^1H NMR (600 MHz, D_2O): δ 4.97 (s, 6H, H-1), 3.82 (dd, 1H, $J_{3,4}$ 12.1 Hz, $J_{2,3}$ 1.3 Hz, H-3), 3.61-3.68 (m, 3H, H-2, 2 \times H-6), 3.56 (dd, 1H, $J_{3,4} \approx J_{4,5}$ 9.6 Hz, H-4), 3.32 (m, 1H, H-5); ^{13}C NMR (126 MHz, D_2O): δ 83.1 (C-1), 81.1 (C-5), 76.0, 75.7 (C-2, C-3), 67.7 (C-4), 62.4 (C-6); Coupled HSQC (600 MHz, D_2O): δ 83.1/4.97 ($J_{\text{C1/H1}}$ 154 Hz, C-1); Anal. calc for $\text{C}_6\text{H}_{11}\text{O}_5\text{SNa}$: HR ESIMS [$\text{M}-\text{Na}$] $^-$: 195.0333, found: 195.0327; Elem. Anal: C, 33.0%; H, 5.08; S, 14.70; found: C, 33.00; H, 5.95; S, 12.96.

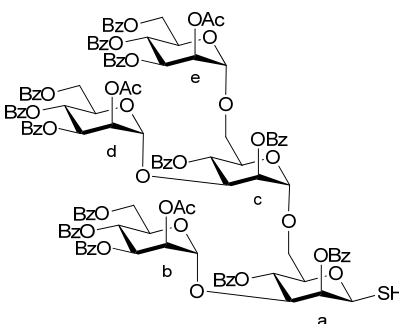


40

2-O-acetyl-3,4,6-tri-O-benzoyl- α -D-mannopyranosyl-(1 \rightarrow 2)-3,4,6-tri-O-benzoyl- α -D-mannopyranosyl-(1 \rightarrow 2)-3,4,6-tri-O-benzoyl- α -D-mannopyranosyl-(1 \rightarrow 3)-2,4,6-tri-O-benzoyl-1-thio- β -D-mannopyranose (40)

Tetrasaccharide **32** (21.5 mg, 10 μ mol) was dissolved in a 1 M solution of trimethylphosphine in THF (1 mL, 1 mmol) and a 1 M solution of NaHCO₃ (1 mL, pH 9) added and stirred vigorously. After 1.5 hours, the reaction mixture was neutralized with dilute AcOH and extracted with EtOAc three times and the organic layer concentrated under reduced pressure. Purification of the crude product by chromatography (1:1 heptane/EtOAc) yielded **40** (20.4 mg, 10 μ mol, 99%) as a white powder; $[\alpha]_{\text{D}}^{25}$ -45 (c 7.0, CHCl₃); ¹H NMR (700 MHz, CDCl₃): δ 7.06-8.34 (m, 60H, Ar), 5.84 (dd, 1H, $J_{3,4} \approx J_{4,5}$ 9.9 Hz, H-4^b), 5.81 (dd, 1H, $J_{2,3}$ 3.4 Hz, $J_{1,2}$ 0.9 Hz, H-2^a), 5.79 (dd, 1H, $J_{3,4}$ 10.2 Hz, $J_{2,3}$ 3.0 Hz, H-3^c), 5.78 (dd, 1H, $J_{3,4} \approx J_{4,5}$ 9.9 Hz, H-4^a), 5.75 (dd, 1H, $J_{2,3}$ 3.4 Hz, H-3^d), 5.75 (dd, 1H, $J_{3,4} \approx J_{4,5}$ 9.9 Hz, H-4^c), 5.67 (dd, 1H, $J_{3,4} \approx J_{4,5}$ 10.1 Hz, H-4^d), 5.62 (dd, 1H, $J_{2,3}$ 3.3, $J_{1,2}$ 1.8 Hz, H-2^d), 5.48 (dd, 1H, $J_{3,4}$ 9.8 Hz, $J_{2,3}$ 3.3 Hz, H-3^b), 5.35 (d, 1H, $J_{1,2}$ 1.5 Hz, H-1^b), 4.92 (ddd, 1H, $J_{4,5}$ 10.1 Hz, $J_{5,6}$ 5.8 Hz, $J_{5,6}$ 2.6 Hz, H-5^b), 4.86 (d, 1H, $J_{1,2}$ 1.5 Hz, H-1^d), 4.73 (dd, 1H, J_{gem} 12.2 Hz, $J_{5,6}$ 5.8 Hz, H-6^b), 4.67 (dd, 1H, $J_{1,51}$ 10.1 Hz, $J_{1,2}$ 1.0 Hz, H-1^a), 4.63 (s, 1H, H-1^c), 4.61 (dd, 1H, J_{gem} 9.2 Hz, $J_{5,6}$ 2.6 Hz, H-6^b), 4.59 (dd, 1H, J_{gem} 12.2 Hz, $J_{5,6}$ 3.1 Hz, H-6^a), 4.34 (dd, 1H, J_{gem} 12.3 Hz, $J_{5,6}$ 4.4 Hz, H-6^a), 4.29 (ddd, 1H, $J_{4,5}$ 9.8, $J_{5,6}$ 5.9 Hz, $J_{5,6}$ 2.2 Hz, H-5^c), 4.25 (dd, 1H, $J_{2,3}$ 2.7, $J_{1,2}$ 2.1 Hz, H-2^c), 4.20 (dd, 1H, J_{gem} 12.1 Hz, $J_{5,6}$ 6.1 Hz, H-6^c), 4.11 (br. d, 1H, J_{gem} 11.9 Hz, H-6^c), 4.08 (dd, 1H, $J_{3,4}$ 9.9 Hz, $J_{2,3}$ 3.3 Hz, H-3^a), 4.02 (dt, 1H, $J_{4,5}$ 9.9 Hz, $J_{5,6}$ 4.0 Hz, H-5^d), 3.96 (d, 2H, $J_{5,6}$ 3.2 Hz, H-6^d), 3.88 (dd, 1H, $J_{2,3}$ 2.7 Hz, $J_{1,2}$ 1.5 Hz, H-2^b), 3.57 (dt, 1H, $J_{4,5}$ 10.0 Hz, $2 \times J_{5,6}$ 3.7 Hz, H-5^a), 2.59 (d, 1H, $J_{1,51}$ 10.1 Hz, SH), 1.99 (s, 3H, CH₃(C=O)O); ¹³C NMR (126 MHz, CDCl₃): δ 168.9 (C=O), 166.4 (C=O), 166.1 (C=O), 166.0 (C=O), 165.9 (C=O), 165.7 (C=O), 165.7 (C=O), 165.4 (C=O), 165.3 (C=O), 165.1 (C=O), 165.1 (C=O), 165.0 (C=O), 164.7 (C=O), 134.1 (Ar), 133.8 (Ar), 133.4 (Ar), 133.3 (Ar), 133.3 (Ar), 133.2 (Ar), 133.2 (Ar), 133.1 (Ar), 133.1 (Ar), 133.0 (Ar), 133.0 (Ar), 132.9 (Ar), 132.9 (Ar), 132.8 (Ar), 130.3 (Ar), 130.3 (Ar), 130.0 (Ar), 130.0 (Ar), 130.0 (Ar), 130.0 (Ar), 129.9 (Ar), 129.9 (Ar), 129.9 (Ar), 129.8 (Ar), 129.8 (Ar), 129.7 (Ar), 129.7 (Ar), 129.7 (Ar), 129.4 (Ar), 129.4 (Ar), 129.3 (Ar), 129.3 (Ar), 129.3 (Ar), 129.1 (Ar), 128.9 (Ar), 128.9 (Ar), 128.9 (Ar), 128.8 (Ar), 128.6 (Ar), 128.6 (Ar), 128.5 (Ar), 128.5 (Ar), 128.4 (Ar), 128.4 (Ar), 128.4 (Ar), 128.3 (Ar), 128.3 (Ar), 128.2 (Ar), 100.7 (C-1^c), 100.0 (C-1^b), 99.3 (C-1^d), 78.1 (C-2^b), 76.9 (C-1^a), 76.7 (C-3^a), 76.6 (C-5^a), 75.1 (C-2^c), 74.1 (C-2^a), 71.0 (C-3^c), 69.9 (C-5^c), 69.78 (C-3^b), 69.74 (C-5^b), 69.4 (C-2^d), 69.3 (C-3^d), 69.3 (C-5^d), 68.5 (C-4^a), 67.6 (C-4^d), 67.4 (C-4^b), 66.7 (C-4^c), 64.4 (C-6^b), 63.9 (C-6^c), 63.07 (C-6^a), 63.03 (C-6^d), 20.6 (CH₃C=O); Coupled HSQC (700 MHz, CDCl₃): δ 100.7/4.63

($J_{C1/H1}$ 175 Hz, C-1^c), 99.98/5.35 ($J_{C1/H1}$ 178 Hz, C-1^b), 99.3/4.85 ($J_{C1/H1}$ 176 Hz, C-1^d), 76.94/4.67 ($J_{C1/H1}$ 152 Hz, C-1^a); Anal. calc for C₁₁₀H₉₂O₃₃S: HR ESIMS [M+Na]⁺: 1995.5134, found: 1995.5105.

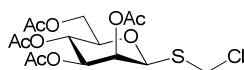


41

2-O-acetyl-3,4,6-tri-O-benzoyl- α -D-mannopyranosyl-(1 \rightarrow 6)-[2-O-acetyl-3,4,6-tri-O-benzoyl- α -D-mannopyranosyl-(1 \rightarrow 3)]-2,4-di-O-benzoyl- α -D-mannopyranosyl-(1 \rightarrow 6)-[2-O-acetyl-3,4,6-tri-O-benzoyl- α -D-mannopyranosyl-(1 \rightarrow 3)]-2,4-di-O-benzoyl- β -D-mannopyranosyl thiol (41)

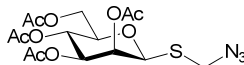
Pentasaccharide **38** (20.5 mg, 8.5 μ mol) was dissolved in a 1 M solution of trimethylphosphine in THF (1 mL, 1 mmol) and a 1 M solution of NaHCO₃ (1 mL, pH 9) added and stirred vigorously. After 30 minutes, the reaction mixture was neutralized with dilute AcOH and extracted with EtOAc three times and the organic layer concentrated under reduced pressure. Purification of the crude product by chromatography (1:1 heptane/EtOAc) yielded **41** (19.7 mg, 8.5 μ mol, 99%) as a white powder; ¹H NMR (700 MHz, CDCl₃): δ 7.26 (m, 65H, ArH), 5.87 (d, 1H, $J_{2,3}$ 2.4 Hz, H-2^a), 5.86 (dd, 1H, $J_{3,4} \approx J_{4,5}$ 10.0 Hz, H-4^e), 5.85 (dd, 1H, $J_{3,4} \approx J_{4,5}$ 9.4 Hz, H-4^a), 5.84 (dd, 1H, $J_{3,4} \approx J_{4,5}$ 9.8 Hz, H-4^d), 5.83 (dd, 1H, $J_{3,4} \approx J_{4,5}$ 10.0 Hz, H-4^c), 5.78 (dd, 1H, $J_{3,4}$ 10.1 Hz, $J_{2,3}$ 3.3 Hz, H-3^e), 5.73 (dd, 1H, $J_{2,3}$ 3.5 Hz, $J_{1,2}$ 1.7 Hz, H-2^c), 5.74 (dd, 1H, $J_{3,4} \approx J_{4,5}$ 9.8 Hz, H-4^b), 5.57 (dd, 1H, $J_{3,4}$ 9.8 Hz, $J_{2,3}$ 3.2 Hz, H-3^d), 5.51 (dd, 1H, $J_{3,4}$ 9.6 Hz, $J_{2,3}$ 3.4 Hz, H-3^b), 5.35 (dd, 1H, $J_{2,3}$ 3.3 Hz, $J_{1,2}$ 1.8 Hz, H-2^e), 5.23 (d, 1H, $J_{1,2}$ 2.0 Hz, H-1^d), 5.18 (dd, 1H, $J_{2,3}$ 3.3 Hz, $J_{1,2}$ 2.0 Hz, H-2^d), 5.11 (d, 1H, $J_{1,2}$ 1.4 Hz, H-1^c), 5.10 (dd, 1H, $J_{2,3}$ 3.4 Hz, $J_{1,2}$ 1.9 Hz, H-2^b), 5.05 (d, 1H, $J_{1,2}$ 2.0 Hz, H-1^b), 4.88 (dd, 1H, $J_{1,SH}$ 10.4 Hz, $J_{1,2}$ 1.2 Hz, H-1^a), 4.85 (ddd, 1H,

$J_{4,5}$ 10.0 Hz, $J_{5,6}$ 5.3 Hz, $J_{5,6}$ 2.5 Hz, H-5^b), 4.71 (d, 1H, $J_{1,2}$ 1.8 Hz, H-1^e), 4.65 (dd, 1H, J_{gem} 11.4 Hz, $J_{5,6}$ 2.5 Hz, H-6^b), 4.63 (dd, 1H, $J_{3,4}$ 9.9 Hz, $J_{2,3}$ 3.5 Hz, H-3^c), 4.58 (dd, 1H, J_{gem} 12.2 Hz, $J_{5,6}$ 5.3 Hz, H-6^b), 4.53 (dd, 1H, J_{gem} 13.0 Hz, $J_{5,6}$ 3.5 Hz, H-6^d), 4.40 (dd, 1H, J_{gem} 11.2 Hz, $J_{5,6}$ 2.5 Hz, H-6^e), 4.38 (dd, 1H, $J_{3,4}$ 9.9 Hz, $J_{2,3}$ 3.2 Hz, H-3^a), 4.36 (ddd, 1H, $J_{4,5}$ 9.8 Hz, $J_{5,6}$ 5.3 Hz, $J_{5,6}$ 2.4 Hz, H-5^d), 4.29-4.33 (m, 2H, H-5^d, H-6^d), 4.28 (dd, 1H, J_{gem} 11.8 Hz, $J_{5,6}$ 5.2 Hz, H-6^e), 4.20 (ddd, 1H, $J_{4,5}$ 10.2 Hz, $J_{5,6}$ 6.0 Hz, $J_{5,6}$ 2.0 Hz, H-5^c), 4.15 (dd, 1H, J_{gem} 11.2 Hz, $J_{5,6}$ 5.3 Hz, H-6^a), 3.94 (dd, 1H, J_{gem} 10.4 Hz, $J_{5,6}$ 5.8 Hz, H-6^c), 3.94 (ddd, 1H, $J_{4,5}$ 9.9 Hz, $J_{5,6}$ 5.1 Hz, $J_{5,6}$ 1.7 Hz, H-5^a), 3.79 (dd, 1H, J_{gem} 11.2 Hz, $J_{5,6}$ 1.9 Hz, H-6^a), 3.37 (dd, 1H, J_{gem} 10.5 Hz, $J_{5,6}$ 2.0 Hz, H-6^c), 2.70 (d, 1H, $J_{1,\text{SH}}$ 10.4 Hz, SH), 2.07 (s, 3H, CH₃(C=O)), 1.95 (s, 3H, CH₃(C=O)), 1.75 (s, 3H, CH₃(C=O)); ¹³C NMR (126 MHz, CDCl₃): δ 169.6 (C=O), 169.0 (C=O), 168.6 (C=O), 166.3 (C=O), 166.2 (C=O), 166.1 (C=O), 166.0 (C=O), 166.0 (C=O), 165.6 (C=O), 165.6 (C=O), 165.5 (C=O), 165.2 (C=O), 165.2 (C=O), 165.1 (C=O), 164.6 (C=O), 164.6 (C=O), 133.7 (Ar), 133.5 (Ar), 133.5 (Ar), 133.4 (Ar), 133.2 (Ar), 133.1 (Ar), 133.0 (Ar), 132.9 (Ar), 132.9 (Ar), 130.2 (Ar), 130.2 (Ar), 130.0 (Ar), 130.0 (Ar), 130.0 (Ar), 129.9 (Ar), 129.8 (Ar), 129.8 (Ar), 129.7 (Ar), 129.7 (Ar), 129.7 (Ar), 129.6 (Ar), 129.6 (Ar), 129.5 (Ar), 129.4 (Ar), 129.4 (Ar), 129.4 (Ar), 129.2 (Ar), 129.1 (Ar), 129.1 (Ar), 129.0 (Ar), 128.9 (Ar), 128.9 (Ar), 128.8 (Ar), 128.7 (Ar), 128.5 (Ar), 128.5 (Ar), 128.4 (Ar), 128.4 (Ar), 128.4 (Ar), 128.3 (Ar), 128.2 (Ar), 128.2 (Ar), 100.1 (C-1^d), 99.3 (C-1^b), 97.6 (C-1^c), 97.1 (C-1^e), 77.9 (C-5^a), 77.8 (C-3^c), 77.7 (C-3^a), 77.5 (C-1^a), 74.2 (C-2^a), 71.9 (C-2^c), 70.0, 69.8, 69.7, 69.68, 69.62, 69.4, 69.35, 69.31, 68.9, 68.8, 68.3, 68.1, 67.1, 66.7, 66.6, 66.5, 66.2 (C-4^a, C-6^a, C-2^b, C-3^b, C-4^b, C-5^b, C-4^c, C-5^c, C-6^c, C-2^d, C-3^d, C-4^d, C-5^d, C-2^e, C-3^e, C-4^e, C-5^e), 63.3 (C-6^b), 63.0 (C-6^e), 62.8 (C-6^d), 20.7 (CH₃(C=O)), 20.5 (CH₃(C=O)), 20.2 (CH₃(C=O)); Coupled HSQC (700 MHz, CDCl₃): δ 100.1/5.23 ($J_{\text{C1/H1}}$ 175 Hz, C-1^d), 99.3/5.05 ($J_{\text{C1/H1}}$ 176 Hz, C-1^b), 97.6/5.11 ($J_{\text{C1/H1}}$ 176 Hz, C-1^c), 97.1/4.71 ($J_{\text{C1/H1}}$ 176 Hz, C-1^e), 77.9/4.88 ($J_{\text{C1/H1}}$ 163 Hz, C-1^a); Anal. calc for C₁₂₇H₁₁₀O₄₁S: HR ESIMS [M+Na]⁺: 2345.6135, found: 2345.6132.



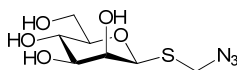
Chloromethyl 2,3,4,6-tri-*O*-acetyl-1-thio- β -D-mannopyranoside (42)

To a solution of compound **17** (0.218 g, 0.537 mmol) in CH₂Cl₂ (10 mL) was added DBU (96 μ L, 0.642 mmol). After 18 hours, reaction was diluted with toluene and concentrated under reduced pressure. Purification of the crude yellow syrup by chromatography (1:1 hexanes/EtOAc) followed by recrystallization yielded **42** (0.17 g, 0.414 mmol, 77%) as a white crystalline solid; m.p.: 133.83 °C; $[\alpha]_D^{25}$ -158 (c 8.5, CHCl₃); ¹H NMR (600 MHz, CDCl₃): δ 5.54 (dd, 1H, $J_{2,3}$ 3.5 Hz, $J_{1,2}$ 0.8 Hz, H-2), 5.30 (dd, 1H, $J_{3,4} \approx J_{4,5}$ 10.0 Hz, H-4), 5.14 (dd, 1H, $J_{3,4}$ 10.0 Hz, $J_{2,3}$ 3.5 Hz, H-3), 5.11 (d, 1H, $J_{1,2}$ 0.8 Hz, H-1), 4.95 (d, 1H, J_{gem} 11.9 Hz, SCH₂Cl), 4.67 (d, 1H, J_{gem} 11.9 Hz, SCH₂Cl), 4.31 (dd, 1H, J_{gem} 12.3 Hz, $J_{5,6}$ 5.8 Hz, H-6), 4.18 (dd, 1H, J_{gem} 12.3 Hz, $J_{5,6}$ 2.4 Hz, H-6), 3.78 (ddd, 1H, $J_{4,5}$ 10.0 Hz, $J_{5,6}$ 5.8 Hz, $J_{5,6}$ 2.4 Hz, H-5), 2.19 (s, 3H, CH₃(C=O)), 2.10 (s, 3H, CH₃(C=O)), 2.06 (s, 3H, CH₃(C=O)), (s, 3H, CH₃(C=O)); ¹³C NMR (151 MHz, CDCl₃): δ 170.6 (C=O), 169.9 (2x C=O), 169.6 (C=O), 79.7 (C-1), 76.9 (C-5), 71.8 (C-3), 69.7 (C-2), 65.7 (C-4), 62.5 (C-6), 45.9 (SCH₂Cl), 20.7 (C=O), 20.7 (C=O), 20.6 (C=O), 20.5 (C=O); Anal. calc for C₁₅H₂₁ClO₉S: HR ESIMS [M+Na]⁺: 435.0487, found: 435.0480; Elem. Anal: C, 43.64; H, 5.13; S, 7.77; found: C, 43.67; H, 5.13; S, 7.84.

**43****Azidomethyl 2,3,4,6-tri-*O*-acetyl-1-thio- β -D-mannopyranoside (43)**

Compound **42** (0.132 g, 0.32 mmol) was dissolved in a solution of 2:1 acetone/H₂O (3 mL) and NaN₃ (83 mg, 1.3 mmol) added. After 24 hours at reflux, the reaction mixture was cooled and diluted with EtOAc, washed with H₂O, then brine, and dried over Na₂SO₄. The organic layer was concentrated under reduced pressure and the crude powder purified by chromatography (1:1 hexanes/EtOAc) followed by recrystallization (EtOAc/heptane) to yield **43** (0.10 g, 0.24 mmol, 75%) as a white crystalline solid; m.p.: 100.65 °C; $[\alpha]_D^{25}$ -175 (c 6.5, CHCl₃); ¹H NMR (500 MHz, CDCl₃): δ 5.56 (dd, 1H, J 3.5 Hz, $J_{1,2}$ 1.1 Hz, H-1), 5.31 (dd, 1H, $J_{3,4} \approx J_{4,5}$ 10.0 Hz, H-4), 5.13 (dd, 1H, $J_{3,4}$ 10.1 Hz, $J_{2,3}$ 3.5 Hz,

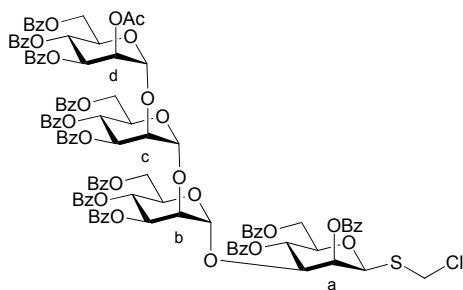
H-3), 5.02 (d, 1H, $J_{1,2}$ 1.1 Hz, H-1), 4.45 (d, 2H, J_{gem} 3.5 Hz, SCH₂N₃), 4.31 (dd, 1H, $J_{4,5}$ 12.4 Hz, $J_{5,6}$ 6.0 Hz, H-6), 4.19 (dd, 1H, J_{gem} 12.3 Hz, $J_{5,6}$ 2.4 Hz, H-6), 3.77 (ddd, 1H, $J_{4,5}$ 10.1 Hz, $J_{5,6}$ 5.9 Hz, $J_{5,6}$ 2.6 Hz, H-5), 2.23 (s, 3H, CH₃(C=O)), 2.11 (s, 3H, CH₃(C=O)), 2.08 (s, 3H, CH₃(C=O)), 2.02 (s, 3H, CH₃(C=O)); ¹³C NMR (126 MHz, CDCl₃): δ 170.6 (C=O), 170.0 (C=O), 170.0 (C=O), 169.6 (C=O), 80.2 (C-1), 76.9 (C-5), 71.8 (C-3), 70.0 (C-2), 65.6 (C-4), 62.6 (C-6), 51.9 (SCH₂N₃), 20.8 (CH₃(C=O)), 20.7 (CH₃(C=O)), 20.6 (CH₃(C=O)), 20.6 (CH₃(C=O)); Anal. calc for C₁₅H₂₁N₃O₉S: HR ESIMS [M+Na]⁺: 442.0891, found: 442.0886; Elem. Anal: C, 42.96; H, 5.05; N, 10.02; S, 7.65; found: C, 43.08; H, 5.16; N, 10.16; S, 7.63.



44

Azidomethyl 1-thio-β-D-mannopyranoside (44)

To a suspension of compound **43** (0.10 g, 0.24 mmol) in MeOH (3 mL) was added NaOMe (0.15 mL, 1 M). After 10 mins, the reaction was neutralized with H⁺ resin, filtered, and concentrated under reduced pressure. The resulting syrup was dissolved in H₂O and lyophilized to produce **44** (63.9 mg, 0.25 mmol, quantitative yield) as a white powder; ¹H NMR (600 MHz, D₂O): δ 5.04 (s, 1H, H-1), 4.58 (d, 1H, J_{gem} 13.5 Hz, SCH₂N₃), 4.50 (d, 1H, J_{gem} 13.2 Hz, SCH₂N₃), 4.07 (d, 1H, $J_{2,3}$ 3.1 Hz, H-2), 3.91 (dd, 1H, J_{gem} 12.3 Hz, $J_{5,6}$ 2.2 Hz, H-6), 3.73 (dd, 1H, J_{gem} 12.3 Hz, $J_{5,6}$ 6.0 Hz, H-6), 3.68 (dd, 1H, $J_{3,4}$ 9.7 Hz, $J_{2,3}$ 3.5 Hz, H-3), 3.62 (dd, 1H, $J_{3,4} \approx J_{4,5}$ 9.7 Hz, H-4), 3.43 (ddd, 1H, $J_{4,5}$ 9.6 Hz, $J_{5,6}$ 6.1 Hz, $J_{5,6}$ 2.2 Hz, H-5); ¹³C NMR (126 MHz, D₂O): δ 84.2 (C-1), 81.3 (C-5), 74.7 (C-3), 72.8 (C-2), 67.5 (C-4), 62.0 (C-6), 53.1 (SCH₂N₃); Coupled HSQC (600 MHz, D₂O): δ 84.2/5.04 ($J_{\text{C1/H1}}$ 156 Hz, C-1); Anal. calc for C₇H₁₃N₃O₅S: HR ESIMS [M+Na]⁺: 274.0468, found: 274.0464; Elem. Anal: C, 33.46; H, 5.21; N, 16.72; S, 12.76; found: C, 33.52; H, 6.40; N, 16.14; S, 12.64.

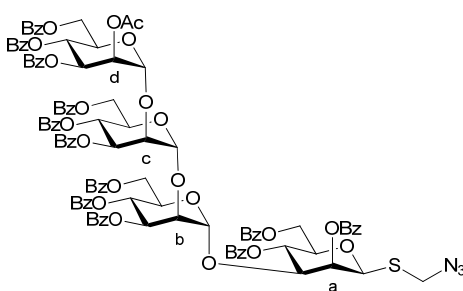


45

Chloromethyl 2-*O*-acetyl-3,4,6-tri-*O*-benzoyl- α -D-mannopyranosyl-(1 \rightarrow 2)-3,4,6-tri-*O*-benzoyl- α -D-mannopyranosyl-(1 \rightarrow 2)-3,4,6-tri-*O*-benzoyl- α -D-mannopyranosyl-(1 \rightarrow 3)-2,4,6-tri-*O*-benzoyl-1-thio- β -D-mannopyranoside (45)

To a solution of tetrasaccharide **40** (20.4 mg, 10.3 μ mol) in CH_2Cl_2 (5 mL) was added DBU (6 μ L, 20 μ mol). After 2 hours, reaction was diluted with toluene and concentrated under reduced pressure. Crude product **45** was sensitive to oxidation and unstable on silica gel and was used immediately for the next step; $[\alpha]_{\text{D}}^{25}$ -70 (*c* 16.9, CHCl_3); ^1H NMR (700 MHz, CDCl_3): δ 7.10-8.28 (m, 60H, Ar), 5.86 (d, 1H, $J_{2,3}$ 3.5 Hz, H-2^a), 5.85 (dd, 1H, $J_{3,4} \approx J_{4,5}$ 9.5 Hz, H-4^b), 5.81 (dd, 1H, $J_{3,4}$ 10.1 Hz, $J_{2,3}$ 3.1 Hz, H-3^c), 5.76 (dd, 1H, $J_{3,4}$ 10.1 Hz, $J_{2,3}$ 3.6 Hz, H-3^d), 5.76 (dd, 1H, $J_{3,4} \approx J_{4,5}$ 9.5 Hz, H-4^a), 5.72 (dd, 1H, $J_{3,4} \approx J_{4,5}$ 10.1 Hz, H-4^c), 5.68 (dd, 1H, $J_{3,4} \approx J_{4,5}$ 9.9 Hz, H-4^d), 5.63 (dd, 1H, $J_{2,3}$ 3.2 Hz, $J_{1,2}$ 1.9 Hz, H-2^d), 5.44 (dd, 1H, $J_{3,4}$ 9.9 Hz, $J_{2,3}$ 3.3 Hz, H-3^b), 5.39 (s, 1H, H-1^b), 5.05 (s, 1H, H-1^a), 5.04 (d, 1H, J_{gem} 11.8 Hz, SCH_2Cl), 4.86 (s, 1H, H-1^d), 4.77 (ddd, 1H, $J_{4,5}$ 9.8 Hz, $J_{5,6}$ 5.7 Hz, $J_{5,6}$ 2.6 Hz, H-5^b), 4.72 (dd, 1H, J_{gem} 12.2 Hz, $J_{5,6}$ 5.5 Hz, H-6^b), 4.70 (d, 1H, J_{gem} 11.6 Hz, SCH_2Cl), 4.59 (dd, 1H, J_{gem} 12.0 Hz, $J_{5,6}$ 2.8 Hz, H-6^a), 4.58 (dd, 1H, J_{gem} 12.0 Hz, $J_{5,6}$ 2.2 Hz, H-6^b), 4.56 (s, 1H, H-1^c), 4.41 (m, 1H, H-5^c), 4.40 (dd, 1H, J_{gem} 12.5 Hz, $J_{5,6}$ 5.7 Hz, H-6^a), 4.37 (dd, 1H, J_{gem} 11.7 Hz, $J_{5,6}$ 6.8 Hz, H-6^c), 4.26 (br. s., 1H, H-2^c), 4.20 (br. d, 1H, J_{gem} 11.6 Hz, H-6^c), 3.99 (dd, 1H, $J_{3,4}$ 9.3 Hz, $J_{2,3}$ 3.73 Hz, H-3^a), 3.98 (m, 1H, H-5^d), 3.95 (m, 1H, H-6^d), 3.92 (s, 1H, H-2^b), 3.89 (m, 1H, H-6^d), 3.50 (ddd, 1H, $J_{4,5}$ 9.6 Hz, $J_{5,6}$ 5.5 Hz, $J_{5,6}$ 3.0 Hz, H-5^a), 1.99 (s, 3H, $\text{CH}_3(\text{C}=\text{O})$); ^{13}C NMR (176 MHz, CDCl_3): δ 168.9 (C=O), 166.4 (C=O), 166.0 (C=O), 165.9 (C=O), 165.6 (C=O), 165.6 (C=O), 165.4 (C=O), 165.1 (C=O), 165.1 (C=O), 164.9 (C=O), 164.6 (C=O), 134.2 (Ar), 133.6 (Ar), 133.4 (Ar), 133.3 (Ar), 133.2 (Ar), 133.2 (Ar), 133.1 (Ar), 133.1 (Ar), 132.9 (Ar), 132.8 (Ar), 130.2 (Ar), 130.0 (Ar), 130.0 (Ar), 129.9 (Ar), 129.9 (Ar), 129.8 (Ar), 129.7 (Ar), 129.7 (Ar), 129.6 (Ar), 129.6 (Ar), 129.4 (Ar), 129.4 (Ar), 129.2

(Ar), 129.2 (Ar), 129.2 (Ar), 129.1 (Ar), 128.9 (Ar), 128.8 (Ar), 128.8 (Ar), 128.7 (Ar), 128.7 (Ar), 128.5 (Ar), 128.4 (Ar), 128.4 (Ar), 128.3 (Ar), 128.2 (Ar), 128.2 (Ar), 128.1 (Ar), 101.0 (C-1^c), 100.1 (C-1^b), 99.2 (C-1^d), 79.2 (C-1^a), 78.5 (C-2^b), 76.60 (C-3^a), 76.55 (C-5^a), 74.8 (C-2^c), 71.7 (C-2^a), 71.0 (C-3^c), 69.9 (C-5^c), 69.7 (C-3^b), 69.5 (C-5^b), 69.4 (C-2^d), 69.1 (C-3^d), 69.1 (C-4^a), 68.8 (C-5^d), 67.7 (C-4^d), 67.3 (C-4^b), 66.8 (C-4^c), 64.3 (C-6^b), 64.1 (C-6^c), 63.0 (C-6^a), 63.0 (C-6^d), 46.0 (SCH₂Cl), 20.5 (CH₃(C=O)); Anal. calc for C₁₁₁H₉₃ClO₃₃S: HR ESIMS [M+Na]⁺: 2043.4901, found: 2043.4887.

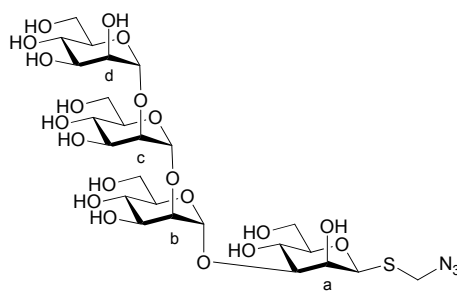


46

Azidomethyl 2-O-acetyl-3,4,6-tri-O-benzoyl- α -D-mannopyranosyl-(1 \rightarrow 2)-3,4,6-tri-O-benzoyl- α -D-mannopyranosyl-(1 \rightarrow 2)-3,4,6-tri-O-benzoyl- α -D-mannopyranosyl-(1 \rightarrow 3)-2,4,6-tri-O-benzoyl-1-thio- β -D-mannopyranoside (46)

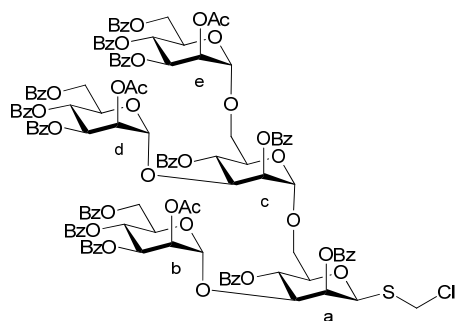
Crude tetrasaccharide **45** (~10.3 μ mol) was dissolved in acetone (3 mL) and 15 mg (0.23 mmol) of NaN₃ added. Reaction was heated to 60 °C and H₂O was added dropwise until the solution became homogenous. After 24 hours at 60 °C, the reaction mixture was cooled and diluted with EtOAc, washed with H₂O, then brine, and dried over Na₂SO₄. The organic layer was concentrated under reduced pressure and the crude yellow powder purified by chromatography (9.7:0.3 toluene/acetonitrile) to yield **49** (16 mg, 7.89 μ mol, 77% from **40**) as a white solid; [α]_D²⁵ -70 (c 8.7, CHCl₃); ¹H NMR (700 MHz, CDCl₃): δ 7.09-8.29 (m, 60H, ArH), 5.88 (dd, 1H, $J_{3,4} \approx J_{4,5}$ 10.0 Hz, H-4^b), 5.86 (dd, 1H, $J_{2,3}$ 3.5, $J_{1,2}$ 0.5 Hz, H-2^a), 5.80 (dd, 1H, $J_{3,4}$ 10.2 Hz, $J_{2,3}$ 3.1 Hz, H-3^c), 5.79 (dd, 1H, $J_{3,4} \approx J_{4,5}$ 9.8 Hz, H-4^a), 5.76 (dd, 1H, $J_{3,4}$ 10.1 Hz, $J_{2,3}$ 3.5 Hz, H-3^d), 5.74 (dd, 1H, $J_{3,4} \approx J_{4,5}$ 10.1 Hz, H-4^c), 5.68 (dd, 1H, $J_{3,4} \approx J_{4,5}$ 9.9 Hz, H-4^d), 5.62 (dd, 1H, $J_{2,3}$ 3.2 Hz, $J_{1,2}$ 1.8 Hz, H-2^d), 5.46 (dd, 1H, $J_{3,4}$ 9.8 Hz, $J_{2,3}$ 3.4 Hz, H-3^b), 5.39 (d, 1H, $J_{1,2}$ 1.5 Hz, H-1^b), 4.91 (d, 1H, $J_{1,2}$ 0.5

Hz, H-1^a), 4.86 (d, 1H, $J_{1,2}$ 1.4 Hz, H-1^d), 4.76 (ddd, 1H, $J_{4,5}$ 9.9 Hz, $J_{5,6}$ 4.9 Hz, $J_{5,6}$ 2.8 Hz, H-5^b), 4.69 (dd, 1H, J_{gem} 12.1 Hz, $J_{5,6}$ 4.9 Hz, H-6^b), 4.62 (br. s, 1H, H-1^c), 4.62 (dd, 1H, J_{gem} 12.2 Hz, $J_{5,6}$ 3.0 Hz, H-6^b), 4.61 (dd, 1H, J_{gem} 12.5 Hz, $J_{5,6}$ 2.8 Hz, H-6^a), 4.50 (d, 1H, J_{gem} 13.3 Hz, SCH₂N₃), 4.39 (dd, 1H, J_{gem} 12.2 Hz, $J_{5,6}$ 5.2 Hz, H-6^a), 4.38 (d, 1H, J_{gem} 13.1 Hz, SCH₂N₃), 4.35 (ddd, 1H, $J_{4,5}$ 10.0 Hz, $J_{5,6}$ 6.3 Hz, $J_{5,6}$ 2.2 Hz, H-5^c), 4.29 (dd, 1H, J_{gem} 12.0 Hz, $J_{5,6}$ 6.2 Hz, H-6^c), 4.26 (dd, 1H, $J_{2,3}$ 2.8 Hz, $J_{1,2}$ 1.9 Hz, H-2^c), 4.17 (br. d, 1H, J_{gem} 11.8 Hz, H-6^c), 4.04 (dd, 1H, $J_{3,4}$ 9.8 Hz, $J_{2,3}$ 3.2 Hz, H-3^a), 4.00 (dt, 1H, $J_{4,5}$ 9.9 Hz, $2 \times J_{5,6}$ 4.1 Hz, H-5^d), 3.95 (dd, 1H, J_{gem} 12.1 Hz, $J_{5,6}$ 4.3 Hz, H-6^d), 3.92 (br. s., 1H, H-2^b), 3.91 (dd, 1H, J_{gem} 13.7 Hz, $J_{5,6}$ 3.2 Hz, H-6^d), 3.57 (ddd, 1H, $J_{4,5}$ 9.8 Hz, $J_{5,6}$ 5.0 Hz, $J_{5,6}$ 3.2 Hz, H-5^a), 2.00 (s, 3H, CH₃(C=O)); ¹³C NMR (125 MHz, CDCl₃): δ 169.0 (C=O), 166.5 (C=O), 166.1 (C=O), 166.0 (C=O), 166.0 (C=O), 165.7 (C=O), 165.4 (C=O), 165.1 (C=O), 165.0 (C=O), 164.7 (C=O), 134.1 (Ar), 133.6 (Ar), 133.4 (Ar), 133.3 (Ar), 133.3 (Ar), 133.2 (Ar), 133.1 (Ar), 133.0 (Ar), 132.8 (Ar), 130.3 (Ar), 130.0 (Ar), 130.0 (Ar), 130.0 (Ar), 129.9 (Ar), 129.7 (Ar), 129.7 (Ar), 129.7 (Ar), 129.6 (Ar), 129.5 (Ar), 128.9 (Ar), 128.7 (Ar), 128.7 (Ar), 128.6 (Ar), 128.5 (Ar), 128.5 (Ar), 128.5 (Ar), 128.4 (Ar), 128.4 (Ar), 128.3 (Ar), 128.3 (Ar), 128.2 (Ar), 100.9 (C-1^c), 100.2 (C-1^b), 99.2 (C-1^d), 80.0 (C-1^a), 78.2 (C-2^b), 77.2 (C-3^a), 76.6 (C-5^a), 75.0 (C-2^c), 72.0 (C-2^a), 71.0 (C-3^c), 69.9 (C-5^c), 69.8 (C-3^b), 69.5 (C-5^b), 69.4 (C-2^d), 69.2 (C-3^d), 69.2 (C-4^a), 68.8 (C-5^d), 67.7 (C-4^d), 67.3 (C-4^b), 66.9 (C-4^c), 64.2 (C-6^b), 64.0 (C-6^c), 63.1 (C-6^a, C-6^d), 51.8 (SCH₂N₃), 20.6 (CH₃(C=O)); Coupled HSQC (700 MHz, CDCl₃): δ 100.9/4.61 ($J_{\text{C1/H1}}$ 174 Hz, C-1^c), 100.1/5.39 ($J_{\text{C1/H1}}$ 177 Hz, C-1^b), 99.2/4.86 ($J_{\text{C1/H1}}$ 176 Hz, C-1^d), 80.0/4.91 ($J_{\text{C1/H1}}$ 156 Hz, C-1^a); Anal. calc for C₁₁₁H₉₃N₃O₃₃S: HR ESIMS [M+Na]⁺: 2050.5304, found: 2050.5232.



Azidomethyl α -D-mannopyranosyl-(1 \rightarrow 2)- α -D-mannopyranosyl-(1 \rightarrow 2)- α -D-mannopyranosyl-(1 \rightarrow 3)-1-thio- β -D-mannopyranoside (47)

Tetrasaccharide **46** (14 mg, 6.9 μ mol) was suspended in deuterated methanol (1 mL) and deuterated sodium methoxide (0.14 mL, 1 M) added. Reaction was monitored by ^1H NMR. After 20 hours, the reaction was neutralized with H^+ resin and the solvent removed under reduced pressure. The orange syrup was purified via HPLC to yield **47** (4.3 mg, 5.83 μ mol, 84%) as a white powder; $[\alpha]_{\text{D}}^{25}$ -10 (c 5.1, H_2O); ^1H NMR (700 MHz, D_2O): δ 5.37 (d, 1H, $J_{1,2}$ 1.5 Hz, H-1^b), 5.31 (d, 1H, $J_{1,2}$ 1.5 Hz, H-1^c), 5.06 (s, 1H, H-1^a), 5.05 (d, 1H, $J_{1,2}$ 1.5 Hz, H-1^d), 4.59 (d, 1H, J_{gem} 13.3 Hz, SCH_2N_3), 4.52 (d, 1H, J_{gem} 13.4 Hz, SCH_2N_3), 4.23 (d, 1H, $J_{2,3}$ 3.1 Hz, H-2^a), 4.11 (dd, 1H, $J_{2,3}$ 3.1 Hz, $J_{1,2}$ 1.9 Hz, H-2^c), 4.09 (dd, 1H, $J_{2,3}$ 3.2 Hz, $J_{1,2}$ 1.7 Hz, H-2^b), 4.07 (dd, 1H, $J_{2,3}$ 3.3 Hz, $J_{1,2}$ 1.9 Hz, H-2^d), 3.99 (dd, 1H, $J_{3,4}$ 9.6 Hz, $J_{2,3}$ 3.3 Hz, H-3^b), 3.96 (dd, 1H, $J_{3,4}$ 9.3 Hz, $J_{2,3}$ 3.3 Hz, H-3^c), 3.93 (dd, 1H, J_{gem} 12.5 Hz, $J_{5,6}$ 2.2 Hz, H-6^a), 3.90 (m, 1H, H-6^b), 3.87 (m, 1H, H-6^d), 3.86 (dd, 1H, J_{gem} 12.5 Hz, $J_{5,6}$ 1.7 Hz, H-6^c), 3.84 (dd, 1H, $J_{3,4}$ 9.5 Hz, $J_{2,3}$ 3.4 Hz, H-3^d), 3.78 (dd, 1H, $J_{3,4}$ 9.7 Hz, $J_{2,3}$ 3.2 Hz, H-3^a), 3.77 (dd, 1H, J_{gem} 11.7 Hz, $J_{5,6}$ 6.0 Hz, H-6^c), 3.74-3.78 (m, 2H, H-5^b, H-6^b), 3.75 (m, 1H, H-6^a), 3.75 (dd, 1H, $J_{3,4} \approx J_{4,5}$ 9.4 Hz, H-4^a), 3.73-3.79 (m, 2H, H-5^d, H-6^d), 3.73 (m, 1H, H-5^c), 3.70 (dd, 1H, $J_{3,4} \approx J_{4,5}$ 9.4 Hz, H-4^b), 3.70 (dd, 1H, $J_{3,4} \approx J_{4,5}$ 9.4 Hz, H-4^c), 3.64 (dd, 1H, $J_{3,4} \approx J_{4,5}$ 9.7 Hz, H-4^d), 3.49 (ddd, 1H, $J_{4,5}$ 9.1 Hz, $J_{5,6}$ 6.0 Hz, $J_{5,6}$ 2.1 Hz, H-5^a); ^{13}C NMR (126 MHz, D_2O): δ 102.2 (C-1^d), 100.7 (C-1^c), 100.7 (C-1^b), 83.2 (C-1^a), 81.3 (C-3^a), 80.4 (C-5^a), 78.6 (C-2^b), 78.5 (C-2^c), 73.4 (C-5^b), 73.2 (C-5^c), 73.2 (C-5⁺), 71.5 (C-2^a), 70.3 (C-3^d), 70.1 (C-3^b), 70.0 (C-3^c), 70.0 (C-2^d), 67.0 (C-4^c), 66.9 (C-4⁺), 66.8 (C-4^d), 65.9 (C-4^a), 61.1 (C-6^d), 61.0 (C-6^a, C-6^b, C-6^c), 52.2 (SCH_2N_3); Coupled HSQC (700 MHz, D_2O): δ 102.3/5.05 ($J_{\text{C1/H1}}$ 172 Hz, C-1^d), 100.70/5.30 ($J_{\text{C1/H1}}$ 173 Hz, C-1^c), 100.66/5.36 ($J_{\text{C1/H1}}$ 174 Hz, C-1^b), 83.2/5.06 ($J_{\text{C1/H1}}$ 156 Hz, C-1^a); Anal. calc for $\text{C}_{25}\text{H}_{43}\text{N}_3\text{O}_{20}\text{S}$: HR ESIMS $[\text{M}+\text{Na}]^+$: 760.2053, found: 760.2045.

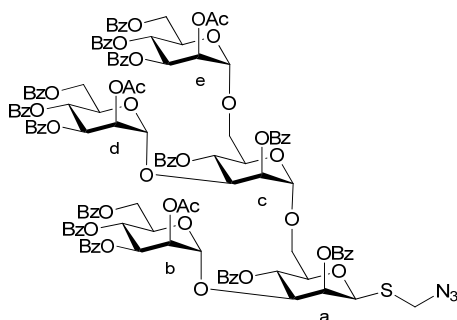


48

Chloromethyl 2-*O*-acetyl-3,4,6-tri-*O*-benzoyl- α -D-mannopyranosyl-(1 \rightarrow 6)-[2-*O*-acetyl-3,4,6-tri-*O*-benzoyl- α -D-mannopyranosyl-(1 \rightarrow 3)]-2,4-di-*O*-benzoyl- α -D-mannopyranosyl-(1 \rightarrow 6)-[2-*O*-acetyl-3,4,6-tri-*O*-benzoyl- α -D-mannopyranosyl-(1 \rightarrow 3)]-2,4-di-*O*-benzoyl-1-thio- β -D-mannopyranoside (48)

To a solution of pentasaccharide **41** (20 mg, 8.6 μ mol) in CH_2Cl_2 (5 mL) was added DBU (3 μ L, 20 μ mol). After 2.5 hours, reaction was diluted with toluene and concentrated under reduced pressure. Crude product **48** was sensitive to oxidation and unstable on silica gel and was used immediately for the next step; ^1H NMR (600 MHz, cdCl_3): δ 7.26 (s, 65H, Ar), 6.00 (dd, 1H, $J_{2,3}$ 3.5 Hz, $J_{1,2}$ 0.9 Hz, H-2^a), 5.85 (dd, 1H, $J_{3,4} \approx J_{4,5}$ 9.9 Hz, H-4^e), 5.85 (dd, 1H, $J_{3,4} \approx J_{4,5}$ 9.6 Hz, H-4^c), 5.83 (dd, 1H, $J_{3,4} \approx J_{4,5}$ 9.8 Hz, H-4^a), 5.81 (dd, 1H, $J_{3,4} \approx J_{4,5}$ 9.8 Hz, H-4^b), 5.75 (dd, 1H, $J_{3,4}$ 9.9 Hz, $J_{2,3}$ 3.2 Hz, H-3^e), 5.76 (dd, 1H, $J_{3,4} \approx J_{4,5}$ 9.9 Hz, H-4^d), 5.71 (dd, 1H, $J_{2,3}$ 3.5 Hz, $J_{1,2}$ 1.7 Hz, H-2^c), 5.57 (dd, 1H, $J_{3,4}$ 9.7 Hz, $J_{2,3}$ 3.3 Hz, H-3^b), 5.49 (dd, 1H, $J_{3,4}$ 9.6 Hz, $J_{2,3}$ 3.4 Hz, H-3^d), 5.36 (dd, 1H, $J_{2,3}$ 3.4 Hz, $J_{1,2}$ 1.7 Hz, H-2^e), 5.32 (d, 1H, $J_{1,2}$ 1.0 Hz, H-1^a), 5.21 (d, 1H, $J_{1,2}$ 2.1 Hz, H-1^b), 5.16 (dd, 1H, $J_{2,3}$ 3.3 Hz, $J_{1,2}$ 2.1 Hz, H-2^b), 5.14 (d, 1H, $J_{1,2}$ 1.8 Hz, H-1^c), 5.14 (d, 1H, J_{gem} 11.8 Hz, SCH_2Cl), 5.10 (d, 1H, $J_{1,2}$ 2.1 Hz, H-1^d), 5.08 (dd, 1H, $J_{2,3}$ 3.4 Hz, $J_{1,2}$ 2.0 Hz, H-2^d), 4.77 (d, 1H, $J_{1,2}$ 1.7 Hz, H-1^e), 4.77 (d, 1H, J_{gem} 11.8 Hz, SCH_2Cl), 4.66 (ddd, 1H, $J_{4,5}$ 9.9 Hz, $J_{5,6}$ 4.8 Hz, $J_{5,6}$ 2.8 Hz, H-5^d), 4.63 (dd, 1H, J_{gem} 11.8 Hz, $J_{5,6}$ 2.9 Hz, H-6^d), 4.62 (dd, 1H, $J_{3,4}$ 9.9 Hz, $J_{2,3}$ 3.2 Hz, H-3^c), 4.50 (dd, 1H, J_{gem} 12.3 Hz, $J_{5,6}$ 3.1 Hz, H-6^b), 4.49 (dd, 1H, J_{gem} 12.1 Hz, $J_{5,6}$ 4.2 Hz, H-6^d), 4.45 (dd, 1H, $J_{3,4}$ 9.7 Hz, $J_{2,3}$ 3.4 Hz, H-3^a), 4.38 (dd, 1H, J_{gem} 11.7 Hz, $J_{5,6}$ 2.5 Hz, H-6^e), 4.33-4.36 (m, 1H, H-5^e), 4.32-4.35 (m, 1H, H-6^b), 4.30-4.34 (m, 1H, H-5^b), 4.28 (dd, 1H, $J_{4,5}$ 11.7 Hz, $J_{5,6}$ 5.2 Hz, H-6^e), 4.22 (ddd, 1H, $J_{4,5}$ 10.2 Hz, $J_{5,6}$ 5.7 Hz, $J_{5,6}$ 2.9 Hz, H-5^c), 4.17 (dd, 1H, J_{gem} 11.1 Hz, $J_{5,6}$ 6.1 Hz, H-6^a), 4.03 (ddd, 1H, $J_{4,5}$ 10.0 Hz, $J_{5,6}$ 6.3 Hz, $J_{5,6}$ 2.2 Hz, H-5^a), 3.98 (dd, 1H,

J_{gem} 10.7 Hz, $J_{5,6}$ 5.4 Hz, H-6^c), 3.79 (dd, 1H, J_{gem} 11.4 Hz, $J_{5,6}$ 2.2 Hz, H-6^a), 3.50 (dd, 1H, J_{gem} 10.6 Hz, $J_{5,6}$ 2.8 Hz, H-6^c), 2.09 (s, 3H, CH₃(C=O)), 1.92 (s, 3H, CH₃(C=O)), 1.76 (s, 3H, CH₃(C=O)); ¹³C NMR (176 MHz, CDCl₃): δ 169.5 (C=O), 168.9 (C=O), 168.7 (C=O), 166.1 (C=O), 166.1 (C=O), 166.1 (C=O), 165.9 (C=O), 165.9 (C=O), 165.6 (C=O), 165.5 (C=O), 165.3 (C=O), 165.2 (C=O), 165.2 (C=O), 165.1 (C=O), 164.6 (C=O), 164.5 (C=O), 133.6 (Ar), 133.5 (Ar), 133.5 (Ar), 133.3 (Ar), 133.3 (Ar), 133.3 (Ar), 133.1 (Ar), 133.0 (Ar), 133.0 (2×Ar), 132.9 (Ar), 132.9 (2×Ar), 130.1 (Ar), 130.1 (Ar), 130.0 (Ar), 130.0 (Ar), 129.9 (Ar), 129.9 (Ar), 129.7 (Ar), 129.7 (Ar), 129.7 (Ar), 129.6 (Ar), 129.5 (Ar), 129.5 (Ar), 129.3 (Ar), 129.3 (Ar), 129.3 (Ar), 129.1 (Ar), 129.0 (Ar), 129.0 (Ar), 128.9 (Ar), 128.9 (Ar), 128.9 (Ar), 128.6 (Ar), 128.6 (Ar), 128.5 (Ar), 128.4 (Ar), 128.4 (Ar), 128.3 (Ar), 128.3 (Ar), 128.2 (Ar), 128.2 (Ar), 128.1 (Ar), 100.0 (C-1^d), 99.4 (C-1^b), 97.4 (C-1^c), 97.3 (C-1^e), 80.5 (C-1^a), 77.9 (C-5^a), 77.7 (C-3^a), 77.1 (C-3^b), 71.9, 71.9 (C-2^a, C-2^c), 69.9, 69.7, 69.59, 69.57, 69.51, 2×69.3, 69.2, 68.9, 68.8, 68.6, 68.5 (C-4^a, C-2^b, C-3^b, C-5^b, C-4^c, C-5^c, C-2^d, C-3^d, C-5^d, C-2^e, C-3^e, C-5^e), 66.9 (C-6^a), 66.8, 66.7, 66.6 (C-4^b, C-4^d, C-4^e), 66.5 (C-6^c), 63.2, 62.9, 62.8 (C-6^b, C-6^d, C-6^e), 46.4 (SCH₂Cl), 20.7 (CH₃(C=O)), 20.4 (CH₃(C=O)), 20.2 (CH₃(C=O)); Anal. calc for C₁₂₈H₁₁₁ClO₄₁S: HR ESIMS [M+Na]⁺: 2393.5902, found: 2393.5850.

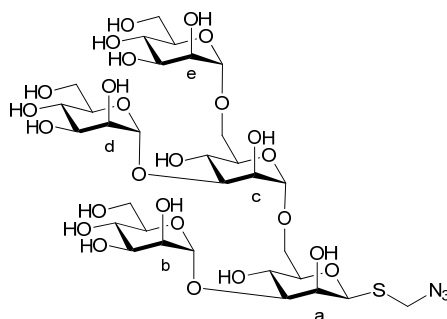


49

Azidomethyl 2-O-acetyl-3,4,6-tri-O-benzoyl- α -D-mannopyranosyl-(1 \rightarrow 6)-[2-O-acetyl-3,4,6-tri-O-benzoyl- α -D-mannopyranosyl-(1 \rightarrow 3)]-2,4-di-O-benzoyl- α -D-mannopyranosyl-(1 \rightarrow 6)-[2-O-acetyl-3,4,6-tri-O-benzoyl- α -D-mannopyranosyl-(1 \rightarrow 3)]-2,4-di-O-benzoyl-1-thio- β -D-mannopyranoside (49)

Crude pentasaccharide **48** (~8.6 μmol) was dissolved in acetone (2 mL) and 3 mg (46 μmol) of NaN_3 added. Reaction was heated to 60 °C and H_2O was added dropwise until the solution became homogenous. After 20 hours at 60 °C, the reaction mixture was cooled and diluted with EtOAc and washed with H_2O , then brine, and dried over Na_2SO_4 . The organic layer was concentrated under reduced pressure and the crude yellow powder purified by chromatography (9.6:0.4 toluene/acetonitrile) to yield **49** (12 mg, 7.15 μmol , 83% from **41**) as a white solid; $[\alpha]_{\text{D}}^{25}$ -49 (c 12.0 in CHCl_3); ^1H NMR (700 MHz, CDCl_3): δ 7.21-8.21 (m, 65H, Ar), 5.97 (dd, 1H, $J_{2,3}$ 3.5 Hz, $J_{1,2}$ 0.9 Hz, H-2^a), 5.84 (dd, 1H, $J_{3,4} \approx J_{4,5}$ 10.0 Hz, H-4^c), 5.83 (dd, 1H, $J_{3,4} \approx J_{4,5}$ 10.2 Hz, H-4^e), 5.80 (dd, 1H, $J_{3,4} \approx J_{4,5}$ 9.6 Hz, H-4^b), 5.79 (dd, 1H, $J_{3,4} \approx J_{4,5}$ 9.4 Hz, H-4^a), 5.76 (dd, 1H, $J_{3,4} \approx J_{4,5}$ 9.8 Hz, H-4^d), 5.73 (dd, 1H, $J_{3,4}$ 10.1 Hz, $J_{2,3}$ 3.2 Hz, H-3^e), 5.68 (dd, 1H, $J_{2,3}$ 3.4 Hz, $J_{1,2}$ 1.7 Hz, H-2^c), 5.55 (dd, 1H, $J_{3,4}$ 9.7 Hz, $J_{2,3}$ 3.3 Hz, H-3^b), 5.47 (dd, 1H, $J_{3,4}$ 9.5 Hz, $J_{2,3}$ 3.4 Hz, H-3^d), 5.34 (dd, 1H, $J_{2,3}$ 3.2 Hz, $J_{1,2}$ 1.7 Hz, H-2^e), 5.19 (d, 1H, $J_{1,2}$ 1.9 Hz, H-1^b), 5.14 (d, 1H, $J_{1,2}$ 0.8 Hz, H-1^a), 5.14 (dd, 1H, $J_{2,3}$ 3.3 Hz, $J_{1,2}$ 1.9 Hz, H-2^b), 5.11 (d, 1H, $J_{1,2}$ 1.4 Hz, H-1^c), 5.08 (d, 1H, $J_{2,3}$ 1.9 Hz, H-1^d), 5.06 (dd, 1H, $J_{2,3}$ 3.4 Hz, $J_{1,2}$ 2.1 Hz, H-2^d), 4.76 (d, 1H, $J_{1,2}$ 1.5 Hz, H-1^e), 4.66 (s, 1H, H-5^d), 4.63-4.66 (m, 1H, H-6^d), 4.58-4.61 (dd, 1H, $J_{3,4}$ 9.7 Hz, $J_{2,3}$ 3.4 Hz, H-3^c), 4.56 (d, 1H, J_{gem} 13.4 Hz, SCH_2N_3), 4.47-4.50 (m, 1H, H-6^b), 4.47 (dd, 1H, J_{gem} 12.2 Hz, $J_{5,6}$ 4.5 Hz, H-6^d), 4.43 (d, 1H, J_{gem} 13.4 Hz, SCH_2N_3), 4.38-4.41 (dd, 1H, $J_{3,4}$ 9.7 Hz, $J_{2,3}$ 3.5 Hz, H-3^a), 4.33-4.36 (m, 1H, H-6^e), 4.32-4.34 (m, 1H, H-5^e), 4.31-4.34 (m, 1H, H-6^b), 4.29-4.32 (m, 1H, H-5^b), 4.24-4.27 (m, 1H, H-6^e), 4.20 (ddd, 1H, $J_{4,5}$ 10.1 Hz, $J_{5,6}$ 5.4 Hz, $J_{5,6}$ 2.9 Hz, H-5^c), 4.14 (dd, 1H, J_{gem} 11.4 Hz, $J_{5,6}$ 6.3 Hz, H-6^a), 3.97 (dd, 1H, J_{gem} 10.6 Hz, $J_{5,6}$ 5.4 Hz, H-6^c), 3.95 (ddd, 1H, $J_{4,5}$ 10.1 Hz, $J_{5,6}$ 6.3 Hz, $J_{5,6}$ 2.1 Hz, H-5^a), 3.75 (dd, 1H, J_{gem} 11.3 Hz, $J_{5,6}$ 1.8 Hz, H-6^a), 3.49 (dd, 1H, J_{gem} 10.6 Hz, $J_{5,6}$ 2.8 Hz, H-6^c), 2.07 (s, 3H, $\text{CH}_3(\text{C}=\text{O})$), 1.91 (s, 3H, $\text{CH}_3(\text{C}=\text{O})$), 1.74 (s, 3H, $\text{CH}_3(\text{C}=\text{O})$); ^{13}C NMR (176 MHz, CDCl_3): δ 169.5 (C=O), 169.0 (C=O), 168.7 (C=O), 166.2 (C=O), 166.1 (C=O), 166.1 (C=O), 166.0 (C=O), 165.9 (C=O), 165.57 (C=O), 165.56 (C=O), 165.3 (C=O), 165.2 (C=O), 165.17 (C=O), 165.15 (C=O), 164.61 (C=O), 164.55 (C=O), 133.6 (Ar), 133.5 (Ar), 133.5 (Ar), 133.3 (Ar), 133.3 (Ar), 133.1 (Ar), 133.1 (Ar), 133.0 (Ar), 132.9 (Ar), 130.2 (Ar), 130.1 (Ar), 130.0 (Ar), 129.93 (Ar), 129.90 (Ar), 129.8 (Ar), 129.71 (Ar), 129.67 (Ar), 129.6 (Ar), 129.5 (Ar), 129.5 (Ar), 129.4 (Ar), 129.33 (Ar), 129.29 (Ar), 129.18 (Ar), 129.17 (Ar), 129.03 (Ar), 128.99 (Ar), 128.98 (Ar), 128.92 (Ar), 128.89 (Ar), 128.67 (Ar), 128.65 (Ar), 128.5 (Ar), 128.46 (Ar), 128.45 (Ar), 128.42 (Ar), 128.35 (Ar), 128.26 (Ar), 128.21 (Ar), 128.18 (Ar), 100.0 (C-

1^d), 99.4 (C-1^b), 97.6 (C-1^c), 97.3 (C-1^e), 80.9 (C-1^a), 77.9 (C-5^a), 77.6 (C-3^a), 77.0 (C-3^c), 72.2, 71.9 (C-2^a, C-2^c), 70.0, 69.7, 2×69.6, 69.6, 69.3, 69.34, 69.33, 69.0, 68.9, 68.6, 68.5 (C-4^a, C-2^b, C-3^b, C-5^b, C-4^c, C-5^c, C-2^d, C-3^d, C-5^d, C-2^e, C-3^e, C-5^e), 67.1 (C-6^a), 66.9, 66.7, 66.6 (C-4^b, C-4^d, C-4^e), 66.5 (C-6^c), 63.1, 63.0, 62.9 (C-6^b, C-6^d, C-6^e), 51.9 (SCH₂N₃), 20.7 (CH₃(C=O)), 20.5 (CH₃(C=O)), 20.2 (CH₃(C=O)); Coupled HSQC (700 MHz, D₂O): δ 100.0/5.08 (*J*_{C1/H1} 175 Hz, C-1^d), 99.4/5.19 (*J*_{C1/H1} 176 Hz, C-1^b), 97.6/5.11 (*J*_{C1/H1} 175 Hz, C-1^c), 97.3/4.76 (*J*_{C1/H1} 176 Hz, C-1^e), 80.9/5.14 (*J*_{C1/H1} 155 Hz, C-1^a); Anal. calc for C₁₂₈H₁₁₁N₃O₄₁S: HR ESIMS [M+Na]⁺: 2400.6306, found: 2400.6308.

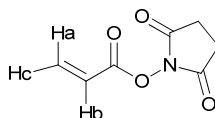


50

Azidomethyl α -D-mannopyranosyl-(1→6)-[α -D-mannopyranosyl-(1→3)]- α -D-mannopyranosyl-(1→6)-[α -D-mannopyranosyl-(1→3)]-1-thio- β -D-mannopyranoside (50)

Pentasaccharide **49** (15 mg, 6.3 μ mol) was suspended in deuterated methanol (1 mL) and deuterated sodium methoxide (0.14 mL, 1 M) added. Reaction was monitored by ¹H NMR. After 20 hours, the reaction was neutralized with H⁺ resin and the solvent removed under reduced pressure. The yellow syrup was purified via HPLC to yield **50** (4.0 mg, 4.45 μ mol, 71%) as a white powder; ¹H NMR (700 MHz, D₂O): δ 5.15 (d, 1H, *J*_{1,2} 1.4 Hz, H-1^d), 5.12 (d, 1H, *J*_{1,2} 1.2 Hz, H-1^b), 5.07 (s, 1H, H-1^a), 4.91 (d, 1H, *J*_{1,2} 1.3 Hz, H-1^e), 4.87 (d, 1H, *J*_{1,2} 1.5 Hz, H-1^c), 4.60 (d, 1H, *J*_{gem} 13.4 Hz, SCH₂N₃), 4.49 (d, 1H, *J*_{gem} 13.4 Hz, SCH₂N₃), 4.27 (d, 1H, *J*_{2,3} 3.5 Hz, H-2^a), 4.16 (dd, 1H, *J*_{2,3} 3.2 Hz, *J*_{1,2} 1.9 Hz, H-2^c), 4.09 (dd, 1H, *J*_{2,3} 3.4 Hz, *J*_{1,2} 1.7 Hz, H-2^b), 4.07 (dd, 1H, *J*_{2,3} 3.4 Hz, *J*_{1,2} 1.7 Hz, H-2^d), 3.99 (dd, 1H, *J*_{2,3} 3.4 Hz, *J*_{1,2} 1.7 Hz, H-2^e), 3.97-4.00 (m, 1H, H-6^c), 3.96 (dd, 1H, *J*_{gem} 11.3 Hz, *J*_{5,6} 4.8

H_z, H-6^a), 3.93 (dd, 1H, $J_{3,4}$ 9.5 Hz, $J_{2,3}$ 3.5 Hz, H-3^c), 3.90 (s, 1H, H-6^b), 3.89 (dd, 1H, $J_{3,4}$ 9.5 Hz, $J_{2,3}$ 3.4 Hz, H-3^b), 3.89 (m, 1H, H-3^d), 3.91 (m, 1H, H-6^c), 3.88-3.91 (m, 1H, H-6^e), 3.89 (m, 1H, H-5^c), 3.87-3.89 (m, 1H, H-4^c), 3.87 (dd, 1H, $J_{3,4} \approx J_{4,5}$ 9.8 Hz, H-4^a), 3.84 (dd, 1H, $J_{3,4}$ 9.2 Hz, $J_{2,3}$ 3.4 Hz, H-3^e), 3.81 (dd, 1H, $J_{3,4}$ 9.9 Hz, $J_{2,3}$ 3.5 Hz, H-3^a), 3.79 (br. s., 1H, H-6^a), 3.76 (dd, 1H, J_{gem} 12.4 Hz, $J_{5,6}$ 5.9 Hz, H-6^e), 3.75-3.77 (m, 1H, H-6^c), 3.75-3.80 (m, 2H, H-6^d, H-6^d), 3.68-3.71 (m, 1H, H-5^e), 3.66-3.70 (m, 1H, H-5^d), 3.68 (dd, 1H, $J_{3,4} \approx J_{4,5}$ 9.9 Hz, H-4^d), 3.64-3.68 (m, 1H, H-4^e), 3.65 (ddd, 1H, $J_{4,5}$ 9.9 Hz, $J_{5,6}$ 5.3 Hz, $J_{5,6}$ 1.9 Hz, H-5^a); ¹³C NMR (176 MHz, D₂O): δ 103.3 (C-1^b), 103.1 (C-1^d), 100.4 (C-1^c), 100.1 (C-1^e), 84.7 (C-1^a), 82.4 (C-3^a), 79.4 (C-3^c), 79.2 (C-5^a), 74.2, 74.1, 73.5, 72.3, 71.7, 71.4, 2 \times 71.2, 70.9, 70.85, 70.8, 70.3, 67.61, 2 \times 67.56 (C-2^a, C-2^b, C-3^b, C-4^b, C-5^b, C-2^c, C-5^c, C-2^d, C-3^d, C-4^d, C-5^d, C-2^e, C-3^e, C-4^e, C-5^e), 66.6 (C-4^c), 66.5 (C-6a), 66.4 (C-4^a), 66.1 (C-6^c), 61.8, 2 \times 61.8 (C-6^b, C-6^d, C-6^e), 53.3 (SCH₂N₃); Coupled HSQC (700 MHz, D₂O): δ 103.3/5.12 ($J_{\text{C1/H1}}$ 176 Hz, C-1^b), 103.1/5.15 ($J_{\text{C1/H1}}$ 175 Hz, C-1^d), 100.4/4.87 ($J_{\text{C1/H1}}$ 175 Hz, C-1^c), 100.0/4.91 ($J_{\text{C1/H1}}$ 174 Hz, C-1^e), 84.7/5.07 ($J_{\text{C1/H1}}$ 157 Hz, C-1^a); Anal. calc for C₃₁H₅₃N₃O₂₅S: HR ESIMS [M+Na]⁺: 922.2581, found: 922.2573.

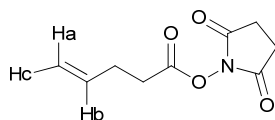


51

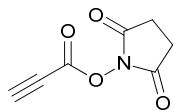
***N*-(acryloyloxy)succinimide (51)**

Acryloyl chloride (1 mL, 11.8 mmol) was added dropwise to a solution of *N*-hydroxysuccinimide (1.36 g, 11.8 mmol), TEA (1.8 mL, 13.0 mmol) and CHCl₃ (10 mL) at 0 °C (ice-water bath). After 20 h, the reaction was diluted with CHCl₃ and the organic layer washed with H₂O, then brine, and dried over Na₂SO₄. The organic layer was concentrated under reduced pressure. The crude yellow crystals were passed through a short silica column and the eluted fractions recrystallized with hexanes/EtOAc to yield **51** (1.52 g, 9.0 mmol, 76%) as a white crystalline solid; m.p.: 71.52 °C; ¹H NMR (498 MHz, cdcl₃): δ 6.70 (dd, 1H, J_{trans} 17.2 Hz, J_{gem} 0.9 Hz, Ha), 6.32 (dd, 1H, J_{trans} 17.4 Hz, J_{cis} 10.6 Hz, Hb), 6.16 (dd, 1H, J_{cis} 10.6 Hz, J_{gem} 0.9 Hz, Hc), 2.86 (br. s., 4H, 2 \times CH₂(C=O)); ¹³C NMR

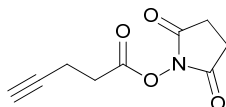
(126 MHz, CDCl₃): δ 169.0 (C=O), 161.1 (C=O), 136.2 (C=C), 123.0 (C=C), 25.6 (CH₂C=O); Anal. calc for C₇H₇NO₄: HR ESIMS [M+Na]⁺: 192.0267, found: 192.0264; Elem. Anal: C, 49.71; H, 4.17; N, 8.28; found: C, 49.72; H, 4.08; N, 8.19.

**52*****N*-(4-pentenyl)succinimide (52)**

4-Pentenyl chloride (1 mL, 8.9 mmol) was added dropwise to a solution of *N*-hydroxysuccinimide (1.04 g, 8.9 mmol), TEA (1.36 mL, 9.9 mmol) and CHCl₃ (10 mL) at 0 °C (ice-water bath). After 20 h, the reaction was diluted with CHCl₃ and the organic layer washed with H₂O, then brine, dried (Na₂SO₄) then concentrated under reduced pressure. The crude brown syrup was passed through a short silica column and the eluted fractions recrystallized with hexanes/EtOAc to yield **52** (1.58 g, 8.0 mmol, 91%) as a white crystalline solid; m.p.: 49.01 °C; ¹H NMR (500 MHz, CDCl₃): δ 5.85 (ddt, 1H, J_{trans} 17.0 Hz, J_{cis} 10.3 Hz, $2 \times J$ 6.5 Hz, Hb), 5.13 (dq, 1H, J_{trans} 17.1 Hz, $3 \times J$ 1.6 Hz, Ha), 5.08 (ddt, 1H, J_{cis} 10.2 Hz, J_{gem} 1.6 Hz, $2 \times J$ 1.3 Hz, Hc), 2.83 (br. s., 4H, CH₂(C=O)N), 2.71 (t, 2H, J 7.6 Hz, CH₂(C=O)O), 2.46-2.52 (m, 1H, CH₂C=C); ¹³C NMR (126 MHz, CDCl₃): δ 169.1 (C=O), 135.2 (C=C), 116.6 (C=C), 30.4 (CH₂), 28.4 (CH₂), 25.6 (CH₂); Anal. calc for C₉H₁₁NO₄: HR ESIMS [M+Na]⁺: 220.0580, found: 220.0576; Elem. Anal: C, 54.82; H, 5.62; N, 7.10; found: C, 54.84; H, 5.50; N, 7.09.

**53*****N*-(2-propynyl)succinimide (53)**

A solution of propiolic acid (1 mL, 15.4 mmol), *N*-hydroxysuccinimide (1.81 g, 15.4 mmol) and DCC (3.22 g, 15.4 mmol) in 1,2-dimethoxyethane (100 mL) stirred at room temperature for 20 hours. After the reaction, the mixture was filtered through Celite to remove the bulk dicyclohexylurea, and the collected solution concentrated under reduced pressure. The brown syrup was purified on a FluoroFLASH® silica gel column (1:1 hexanes/EtOAc) to yield and recrystallized with hexanes/EtOAc to yield **53** (1.54 g, 9.24 mmol, 60%) as a white crystalline solid; m.p.: 49.01 °C; ¹H NMR (600 MHz, CDCl₃): δ 3.30 (s, 1H, C≡CH), 2.87 (s, 4H, CH₂C=O); ¹³C NMR (126 MHz, CDCl₃): δ 168.1 (C=O), 147.8 (C=O), 81.9 (C≡C), 70.3 (C≡C), 25.6 (CH₂C=O); Anal. calc for C₇H₅NO₄: HR ESIMS [M+Na]⁺: 190.0111, found: 190.0111.

**54**

***N*-(4-pentyloxy)succinimide (54)**

To a 0 °C (ice-water bath) solution of 4-pentynoic acid (0.5 g, 4.84 mmol) and *N*-hydroxysuccinimide (0.57 g, 4.84 mmol) in 1:1 EtOAc:1,2-dioxane (60 mL) was added DCC (1.01 g, 4.90 mmol) in a single portion. The reaction mixture was allowed to warm to room temperature overnight. After 20 hours, the mixture was filtered through Celite and the collected solution diluted with EtOAc and washed with H₂O and brine. The organic layer was concentrated under reduced pressure and recrystallized with hexanes/EtOAc to yield **54** (0.68 g, 3.49 mmol, 72%) as a white crystalline solid; m.p.: 74.20 °C; ¹H NMR (498 MHz, CDCl₃): δ 2.88 (t, 2H, *J* 7.9 Hz, CH₂(C=O)O), 2.84 (br. s., 4H, CH₂(C=O)N), 2.62 (td, 4H, *J* 7.5, *J* 2.7 Hz, CH₂C≡C), 2.04 (t, 1H, *J* 2.7 Hz, C≡CH); ¹³C NMR (126 MHz, CDCl₃): δ 168.9 (C=O), 167.0 (C=O), 80.8 (C≡C), 70.0 (C≡C), 30.3 (CH₂), 25.6 (CH₂), 14.1 (CH₂); Anal. calc for C₉H₁₁NO₄: HR ESIMS [M+Na]⁺: 218.0424, found: 218.0424; Elem. Anal: , 55.39; H, 4.65; N, 7.18; found: C, C, 55.13; H, 4.65; N, 7.35.

References

1. V. Hong, S. I. Presolski, C. Ma, M. G. Finn, *Angewandte Chemie International Edition* **2009**, *48*, 9879-9883.
2. C. F. Barbas III, D. R. Burton, J. K. Scott, G. J. Silverman, *Phage Display: A Laboratory Manual*, Cold Spring Harbor Laboratory Press: Cold Spring Harbor, NY, **2001**
3. D. A. Marvin, L. C. Welsh, M. F. Symmons, W. R. P. Scott, S. K. Straus, *J. Mol. Biol.* **2006**, *355*, 294-309.
4. Y. Du, M. Zhang, F. Kong, *Tetrahedron* **2001**, *57*, 1757-1763.
5. N. Floyd, B. Vijayakrishnan, A. R. Koeppe, B. G. Davis, *Angewandte Chemie-International Edition* **2009**, *48*, 7798-7802.

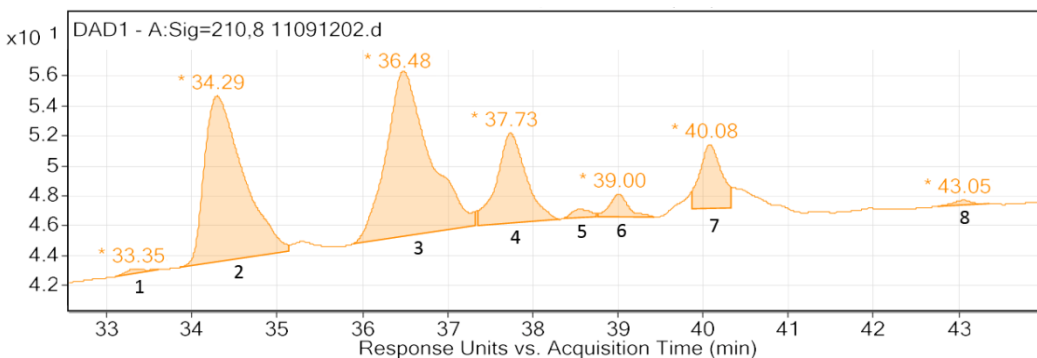
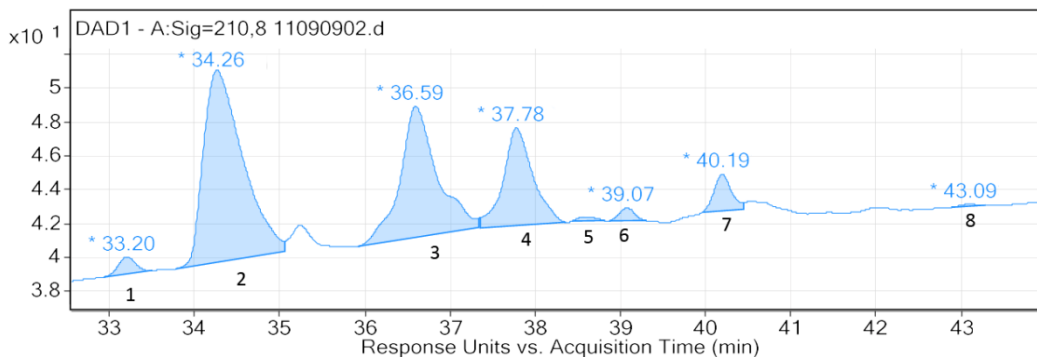
Appendices

Appendix List

Appendix A1 – LC-UV chromatograms and integration tables	262
[LC-UV chromatograms used to determine the degree of conjugation of phage and ubiquitin conjugates. See Chapter 3, Parts I and II; Chapter 4, Part I]	
Appendix A2 – MS/MS analysis of f1.K-(4-yne)	286
[MS/MS analysis of f1.K-(4-yne) to determine the occupied conjugation sites. See Chapter 3, Part I.]	
Appendix A3 – MALDI MS of BSA conjugates	292
[MALDI MS spectra used to determine the degree of hapten incorporation on BSA conjugates. See Chapter 4, Part I.]	
Appendix A4 – NMR data of select compounds	293
[NMR data for new compounds reported in Chapter 6 that do not have combustion analysis.]	

Appendix A1

LC-UV chromatograms and corresponding pVIII conjugates of f1.K linker additions with 2-alkynyl crosslinker **53** for determining the optimal pH and reaction times (Table 5).



3 hours pH 7.0

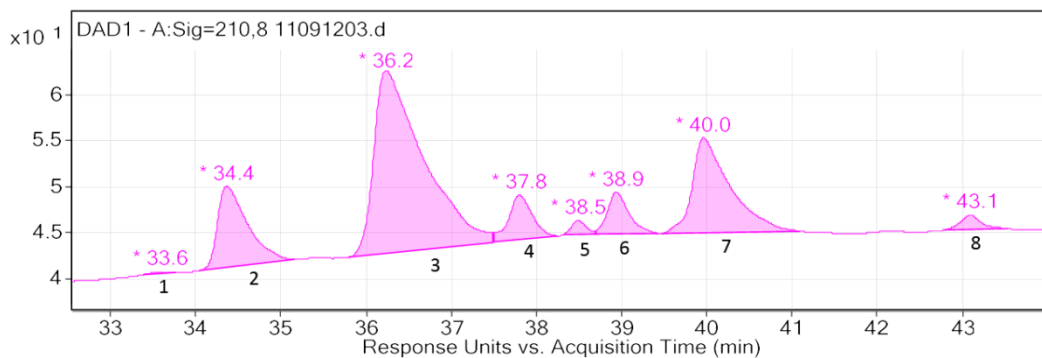
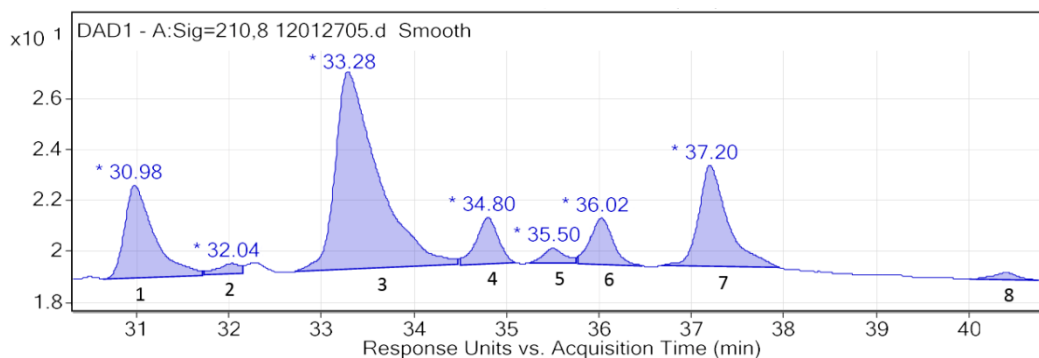
f1.K-(2-yne)		11090902	
Peak #	Identity	Area	% Area
1	1L	14.6	1.8%
2	2L	362.4	45.5%
3	3L	235.0	29.5%
4	3L	139.1	17.5%
5	3L	3.4	0.4%
6	4L	9.4	1.2%
7	4L	30.9	3.9%
8	5L	1.5	0.2%
Total Area:		796.2	

20 hours pH 7.0

f1.K-(2-yne)		11091202	
Peak #	Identity	Area	% Area
1	1L	4.5	0.5%
2	2L	350.6	34.9%
3	3L	392.1	39.0%
4	3L	144.7	14.4%
5	3L	8.4	0.8%
6	4L	23.2	2.3%
7	4L	75.9	7.6%
8	5L	5.0	0.5%
Total Area:		1004.4	

Remnants of pVIII protein from a previous run are visible in the LC-UV trace (between peaks 2 and 3, and surrounding peak 7) and were not included in the integration.

LC-UV chromatograms and corresponding pVIII conjugates of f1.K linker additions with 2-alkynyl crosslinker **53** for determining the optimal pH and reaction times (Table 5), continued.



3 hours pH 8.3

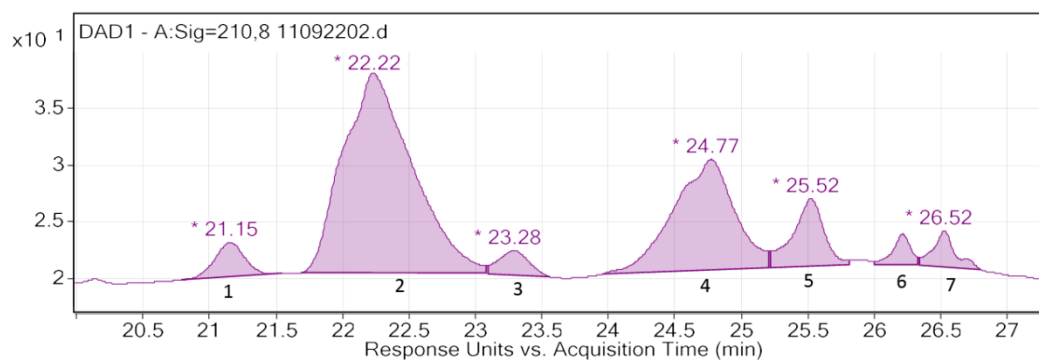
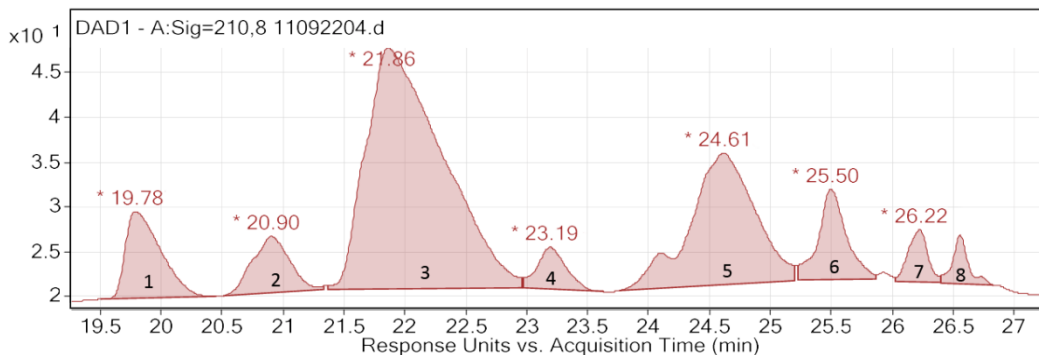
f1.K-(2-yne)		12012705	
Peak #	Identity	Area	% Area
1	2L	81.1	16.2%
2	2L	7.1	1.4%
3	3L	251.2	49.9%
4	3L	30.4	6.0%
5	3L	9.4	1.9%
6	4L	31.3	6.2%
7	4L	87.3	17.4%
8	5L	5.4	1.1%
Total Area:		503.0	

20 hours pH 8.3

f1.K-(2-yne)		11091203	
Peak #	Identity	Area	% Area
1	2L, 3L+16	2.4	0.2%
2	2L	215.8	13.8%
3	3L	804.9	51.6%
4	3L	92.8	6.0%
5	3L	17.7	1.1%
6	4L	79.5	5.1%
7	4L	321.6	20.6%
8	5L	26.6	1.7%
Total Area:		1561.2	

Remnants of pVIII protein from a previous run are visible in the LC-UV trace (between peaks 2 and 3) and were not included in the integration.

LC-UV chromatograms and corresponding pVIII conjugates of f1.K linker additions with SIA crosslinker for determining the optimal pH and reaction time (Table 5).



3 hours pH 7.0

f1.K-SIA **11092204**

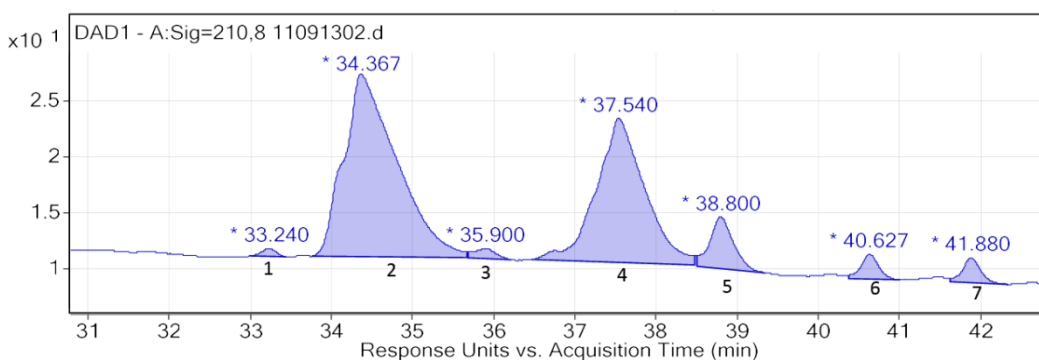
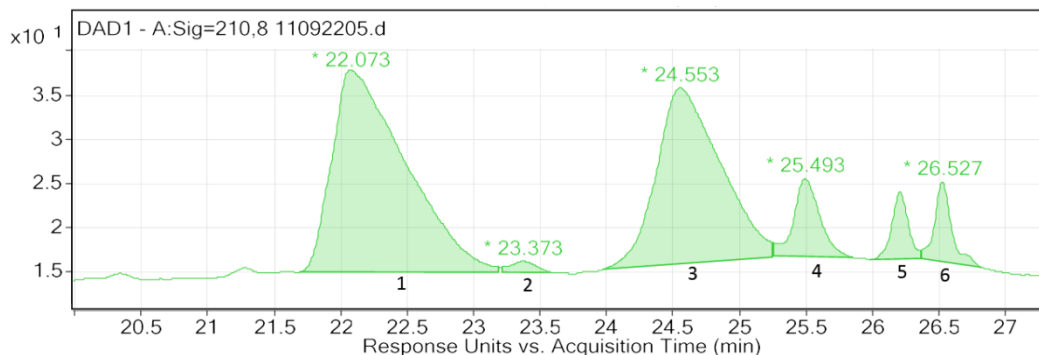
Peak #	Identity	Area	% Area
1	pVIII	194.9	8.1%
2	1L	134.2	5.6%
3	2L	1138.0	49.0%
4	2L	76.8	3.2%
5	3L	548.7	22.7%
6	3L	162.5	6.7%
7	4L	65.6	2.7%
8	4L	48.9	2.0%
Total Area:		2415.0	

20 hours pH 7.0

f1.K-SIA **11092202**

Peak #	Identity	Area	% Area
1	1L	46.5	3.9%
2	2L	640.5	53.6%
3	2L	34.33	2.9%
4	3L	313.7	26.3%
5	3L	97.3	8.1%
6	4L	25.2	2.1%
7	4L	36.8	3.1%
Total Area:		1194.3	

LC-UV chromatograms and corresponding pVIII conjugates of f1.K linker additions with SIA crosslinker for determining the optimal pH and reaction times (Table 5), continued.



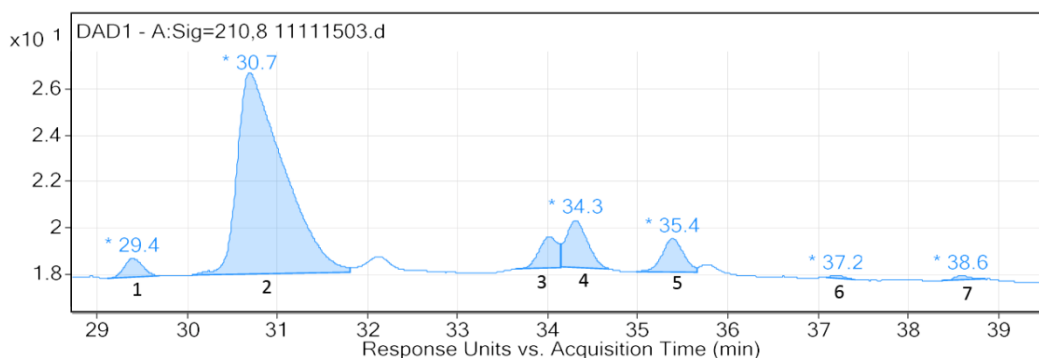
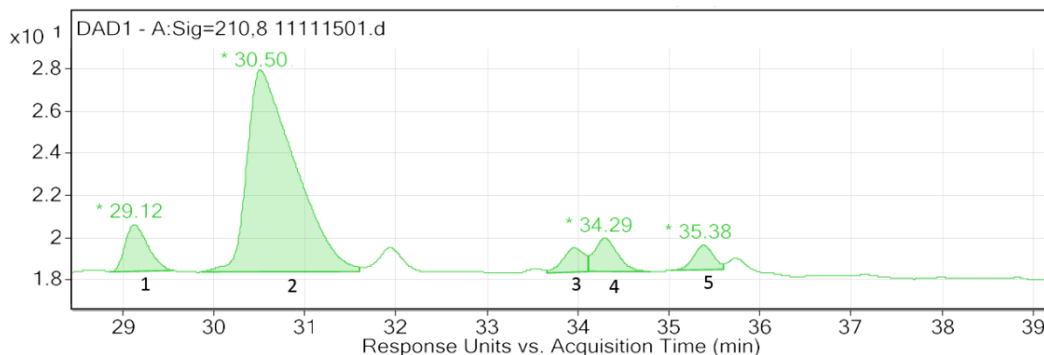
3 hours pH 8.3

f1.K-SIA		11092205	
Peak #	Identity	Area	% Area
1	2L	884.2	48.1%
2	2L	16.9	0.9%
3	3L	670.3	36.4%
4	3L	121.9	6.6%
5	4L	65.9	3.6%
6	4L	80.8	4.4%
		Total Area: 1840.0	

20 hours pH 8.3

f1.K-SIA		11091302	
Peak #	Identity	Area	% Area
1	1L	8.8	0.6%
2	2L	741.4	50.6%
3	2L	16.6	1.1%
4	3L	537.5	36.7%
5	3L	93.4	6.4%
6	4L	33.8	2.3%
7	4L	34.6	2.4%
		Total Area: 1466.1	

LC-UV chromatograms and corresponding pVIII conjugates of f88 linker additions with 4-alkynyl crosslinker **54** for determining the optimal linker equivalents (Table 6).



20 linker equiv

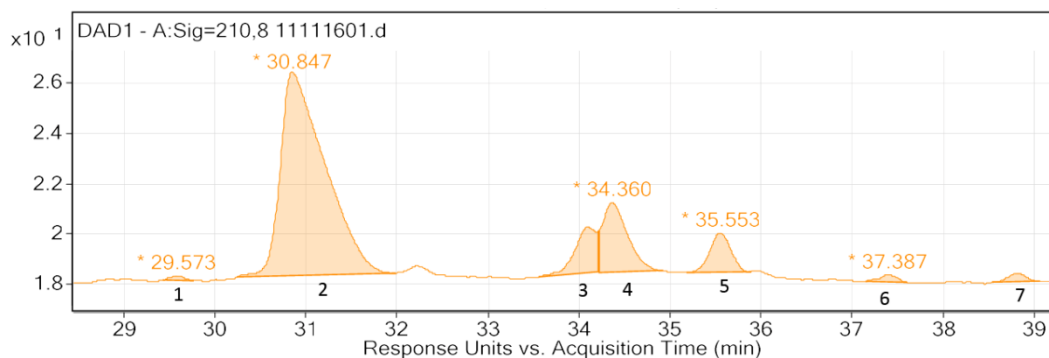
f88-(4-yne)		11111501	
Peak #	Identity	Area	% Area
1	pVIII	38.9	8.5%
2	1L	351.2	77.1%
3	2L	19.3	4.2%
4	2L	28.1	6.2%
5	2L	18.1	4.0%
Total Area:		455.6	

40 linker equiv

f88-(4-yne)		11111503	
Peak #	Identity	Area	% Area
1	pVIII	11.4	2.8%
2	1L	310.9	77.1%
3	2L	19.8	4.9%
4	2L	33.4	8.3%
5	2L	24.0	6.0%
6	3L	1.3	0.3%
7	3L	2.2	0.5%
Total Area:		403.0	

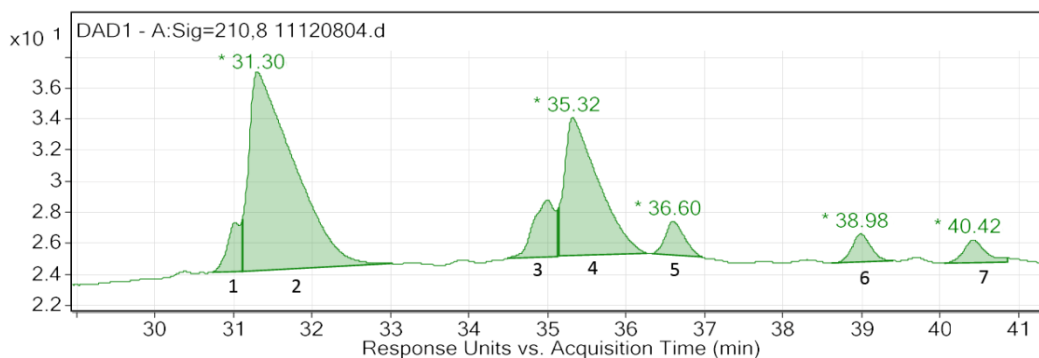
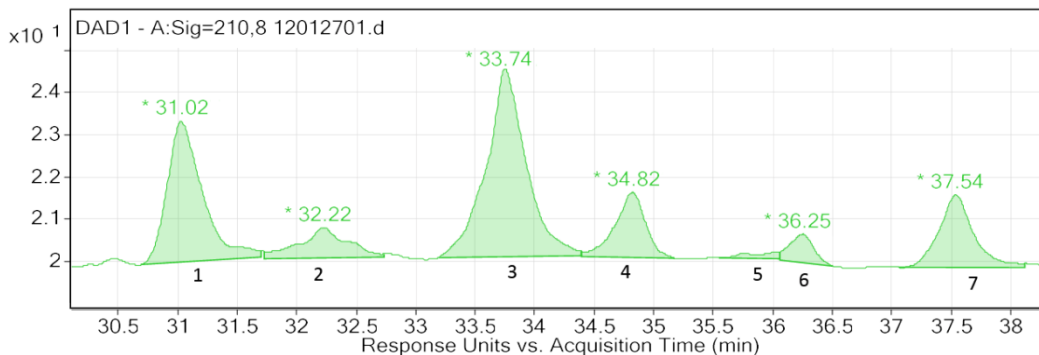
Remnants of pVIII protein from a previous run are visible in the LC-UV trace (between peaks 2 and 3, and the shoulder of peaks 3 and 5) and were not included in the integration.

LC-UV chromatograms and corresponding pVIII conjugates of f88 linker additions with 4-alkynyl crosslinker **54** for determining the optimal linker equivalents (Table 6), continued.



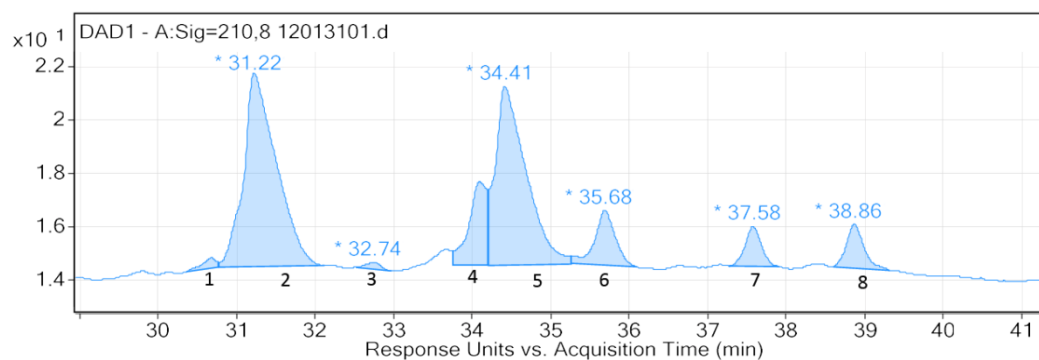
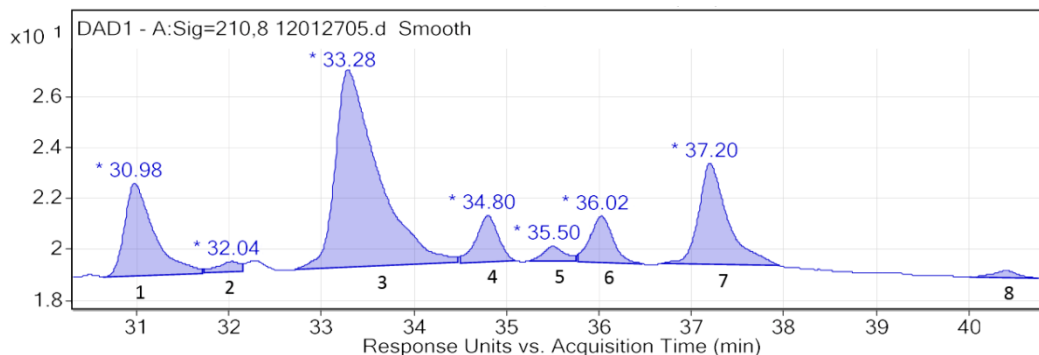
100 linker equiv		11111601	
Peak #	Identity	Area	% Area
1	pVIII	1.9	0.48%
2	1L	276.2	70.12%
3	2L	30.3	7.69%
4	2L	52.2	13.24%
5	2L	25.1	6.38%
6	3L	3.8	0.96%
7	3L	4.5	1.13%
Total Area:		393.9	

LC-UV chromatograms and corresponding pVIII conjugates of optimized f1.K linker additions (Table 7).



f1.K-(2-ene)				f1.K-(4-ene)			
Peak #	Identity	Area	% Area	Peak #	Identity	Area	% Area
1	2L	69.2	25.7%	1	1L+42	40.1	4.1%
2	2L	20.2	7.5%	2	2L	509.2	51.8%
3	3L	105.0	39.0%	3	2L+42	70.3	7.2%
4	3L	27.6	10.3%	4	3L	266.3	27.1%
5	3L	2.7	1.0%	5	3L	37.1	3.8%
6	4L	9.5	3.5%	6	4L	29.8	3.0%
7	4L	34.9	13.0%	7	4L	29.6	3.0%
Total Area:		269.0		Total Area:		982.5	

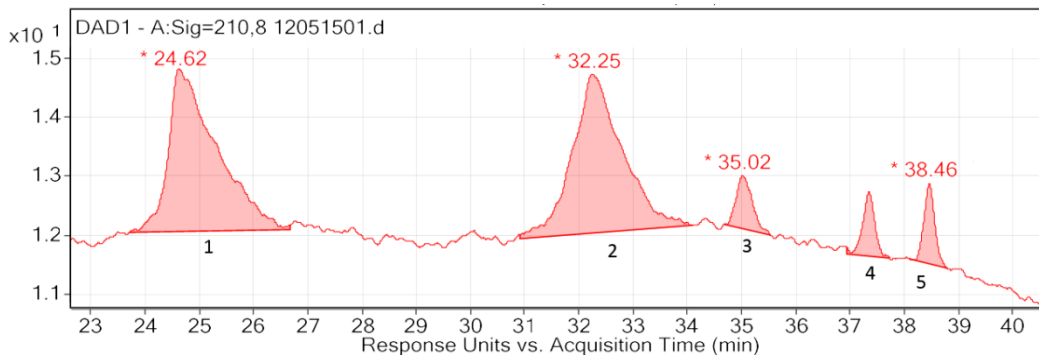
LC-UV chromatograms and corresponding pVIII conjugates of optimized f1.K linker additions (Table 7), continued.



f1.K-(2-yne)				f1.K-(4-yne)			
Peak #	Identity	Area	% Area	Peak #	Identity	Area	% Area
1	2L	81.1	16.1%	1	1L+42	4.9	0.9%
2	2L	7.1	1.4%	2	2L	211.8	39.3%
3	3L	251.2	49.9%	3	2L	3.3	0.6%
4	3L	30.4	6.0%	4	2L+42	49.2	9.1%
5	3L	9.4	1.9%	5	3L	184.1	34.2%
6	4L	31.3	6.2%	6	3L	38.1	7.1%
7	4L	87.3	17.4%	7	4L	21.5	4.0%
8	5L	5.4	1.1%	8	4L	25.7	4.8%
Total Area:		503.0		Total Area:		538.6	

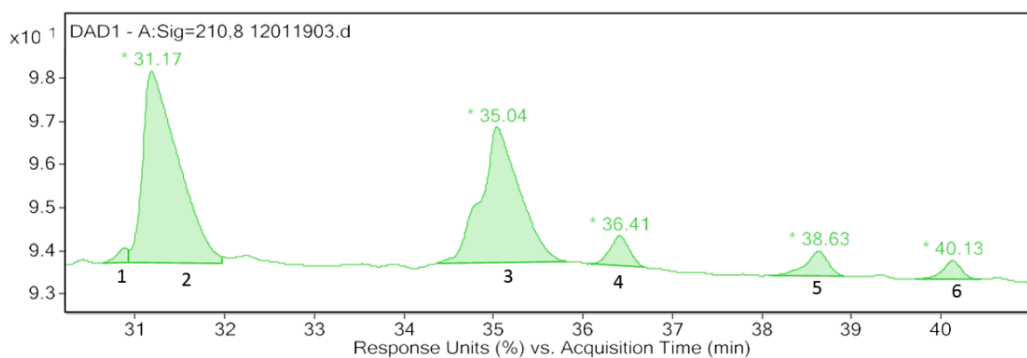
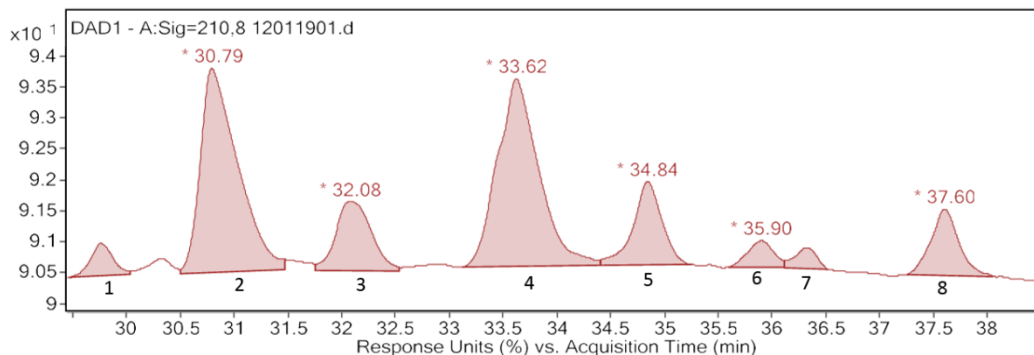
Remnants of phage from a previous run are visible in the LC-UV trace (between peaks 2 and 3 of 12012705, and peaks 3 and 4 of 12013101) and were not included in the integration.

LC-UV chromatograms and corresponding pVIII conjugates of optimized f1.K linker additions (Table 7), continued.



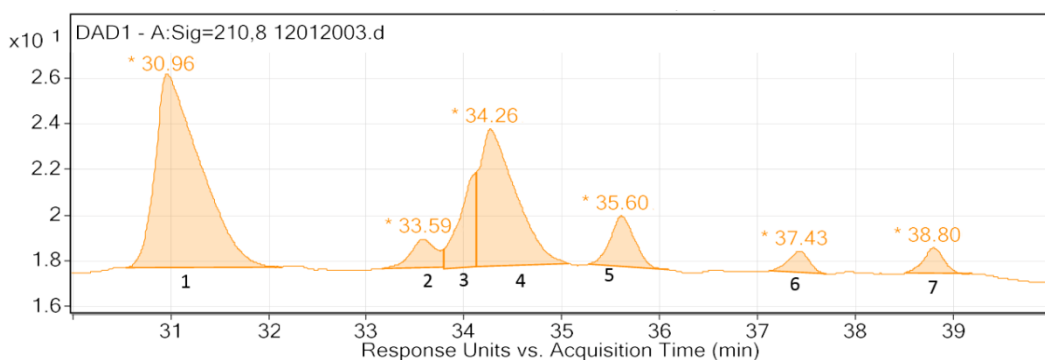
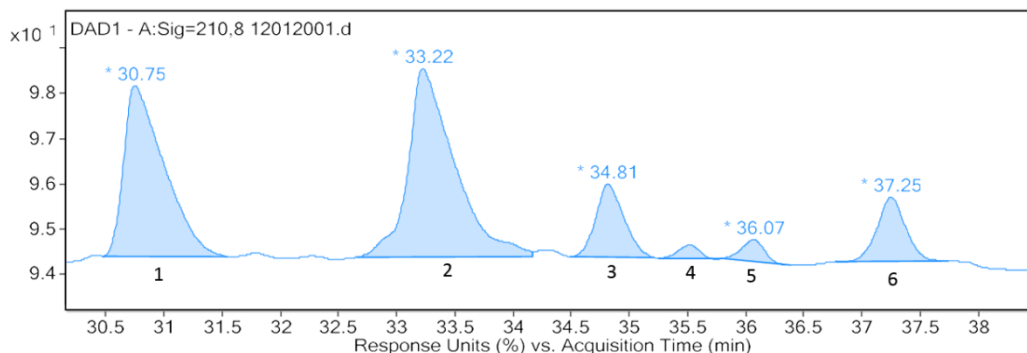
f1.K-SIA		12051501	
Peak #	Identity	Area	% Area
1	2L	171.9	42.9%
2	3L	173.9	43.4%
3	3L	18.6	4.7%
4	4L	17.0	4.3%
5	4L	19.1	4.8%
Total Area:		400.5	

LC-UV chromatograms and corresponding pVIII conjugates of optimized f88 linker additions (Table 7).



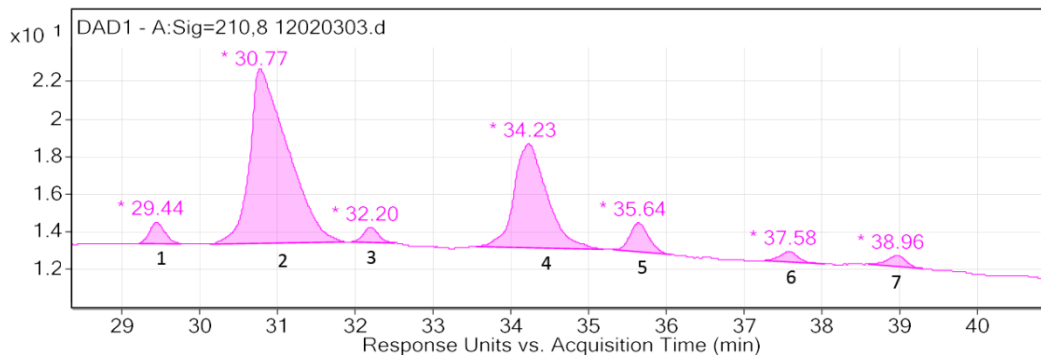
f88-(2-ene)				f88-(4-ene)			
Peak #	Identity	Area	% Area	Peak #	Identity	Area	% Area
1	1L+18	12.5	3.0%	1	pVIII+42	5.4	1.2%
2	1L	133.2	31.7%	2	1L	215.4	49.4%
3	1L	43.3	10.3%	3	2L	167.5	38.5%
4	2L	136.2	32.5%	4	2L	18.5	4.2%
5	2L	41.8	10.0%	5	3L	18.1	4.1%
6	3L+18	12.0	2.9%	6	3L	10.8	2.5%
7	3L	8.0	1.9%	Total Area:		435.6	
8	3L	32.5	7.7%				
Total Area:		419.5					

LC-UV chromatograms and corresponding pVIII conjugates of optimized f1.K linker additions (Table 7), continued.



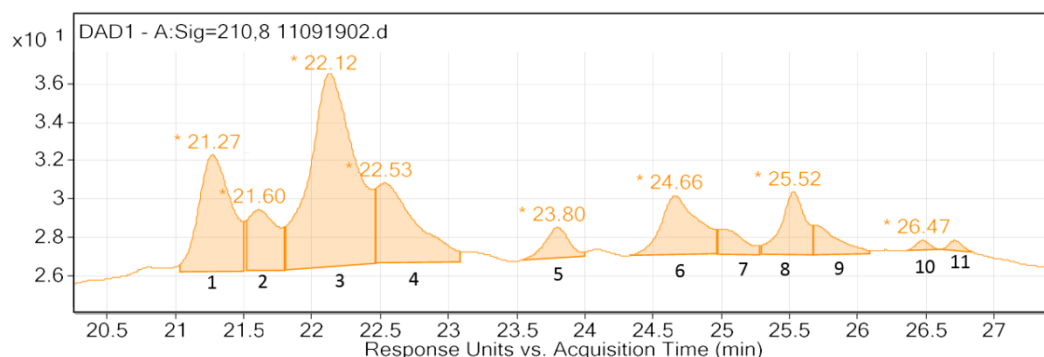
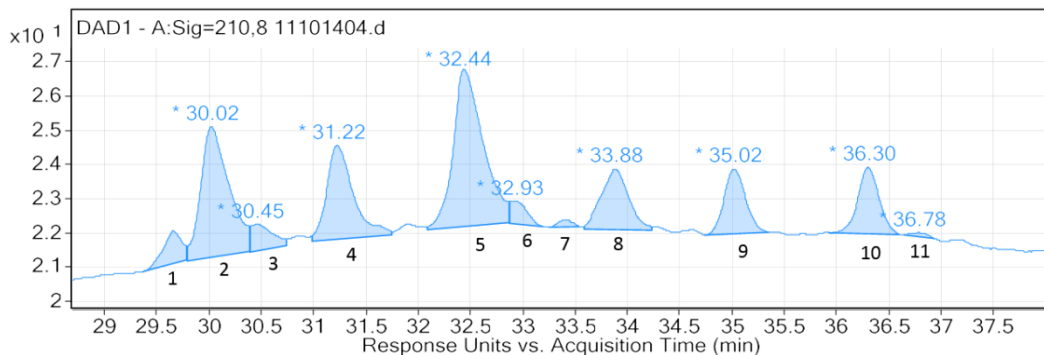
f88-(2-yne)				12012001				f88-(4-yne)				12012003			
Peak #	Identity	Area	% Area	Peak #	Identity	Area	% Area	Peak #	Identity	Area	% Area	Peak #	Identity	Area	% Area
1	1L	150.8	33.9%	1	1L	271.7	48.3%	1	1L	271.7	48.3%	1	1L	271.7	48.3%
2	2L	192.9	43.4%	2	1L+17	23.2	4.1%	2	1L+17	23.2	4.1%	2	1L+17	23.2	4.1%
3	2L	44.9	10.1%	3	1L+42	48.5	8.6%	3	1L+42	48.5	8.6%	3	1L+42	48.5	8.6%
4	2L	6.1	1.4%	4	2L	150.8	26.8%	4	2L	150.8	26.8%	4	2L	150.8	26.8%
5	3L	10.7	2.4%	5	2L	38.1	6.8%	5	2L	38.1	6.8%	5	2L	38.1	6.8%
6	3L	39.7	8.9%	6	3L	13.8	2.5%	6	3L	13.8	2.5%	6	3L	13.8	2.5%
Total Area:		445.0		Total Area:		562.0		Total Area:		562.0		Total Area:		562.0	

LC-UV chromatograms and corresponding pVIII conjugates of optimized f1.K linker additions (Table 7), continued.



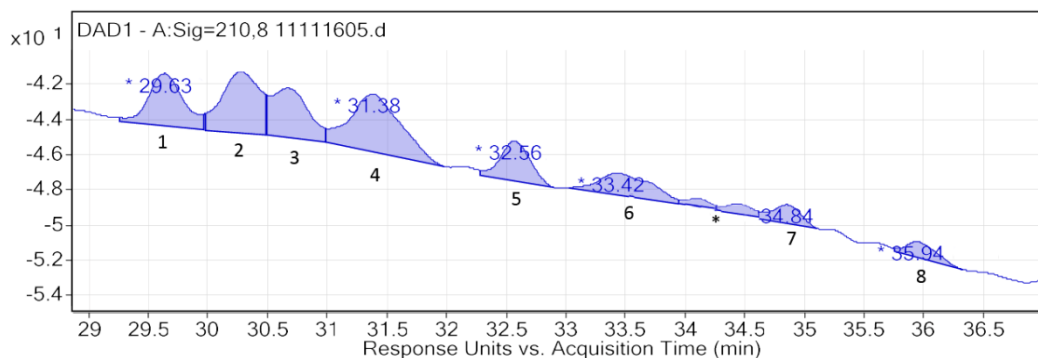
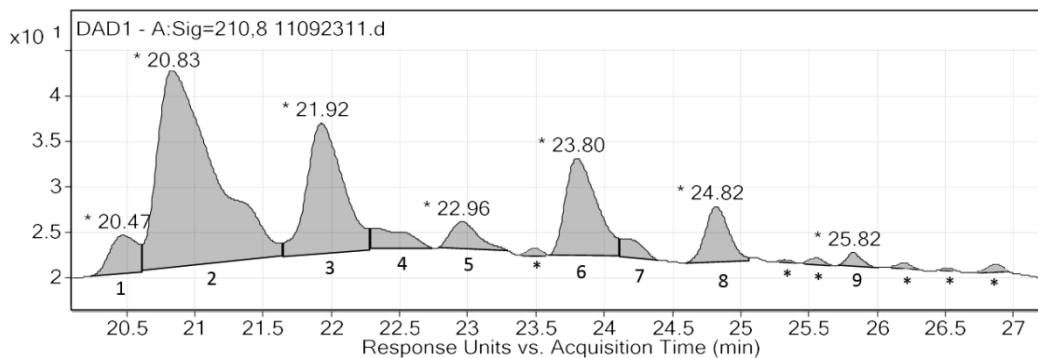
f88-SIA		12020303	
Peak #	Identity	Area	% Area
1	pVIII	15.6	2.82%
2	1L	318.1	57.44%
3	1L	10.8	1.94%
4	2L	164.6	29.71%
5	2L	25.9	4.68%
6	3L	9.2	1.66%
7	3L	9.7	1.74%
Total Area		553.8	

LC-UV chromatograms and corresponding pVIII glycoconjugates of f1.K conjugated to monosaccharide **39** (Table 8).



f1.K-(2-ene)-Mono				f1.K-(4-ene)-Mono			
Peak #	Identity	Area	% Area	Peak #	Identity	Area	% Area
1	1L	11.9	3.55%	1	2L	101.0	16.10%
2	2L2M	72.2	21.61%	2	3L3M+16	45.9	7.32%
3	2L2M	10.9	3.25%	3	3L3M	235.2	37.47%
4	3L3M	48.6	14.54%	4	2L2M+42	83.3	13.28%
5	3L2M	92.8	27.78%	5	3L2M	19.9	3.16%
6	2L1M+42	7.2	2.16%	6	4L3M	58.7	9.35%
7	2L	2.0	0.59%	7	3L2M+42	16.8	2.68%
8	3L2M	32.6	9.76%	8	4L2M	40.8	6.50%
9	4L3M	27.2	8.14%	9	3L2M+42	19.2	3.05%
10	4L2M	27.5	8.23%	10	4L2M	3.4	0.54%
11	3L1M+42	1.3	0.39%	11	5L3M	3.5	0.56%
Total Area:		334.2		Total Area:		627.6	

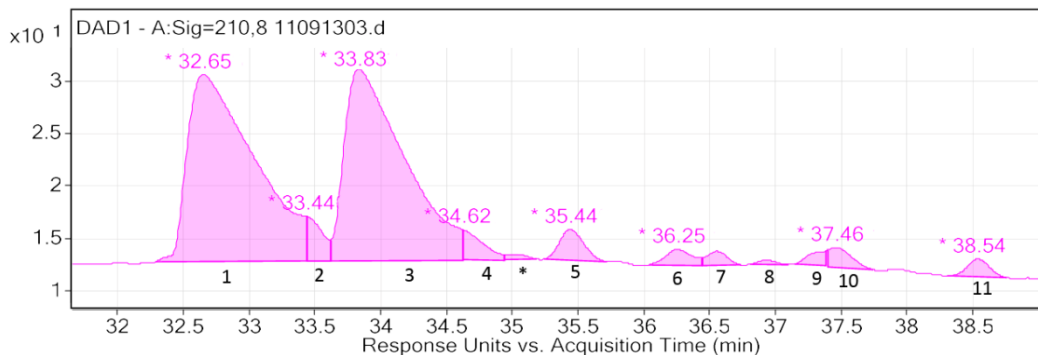
LC-UV chromatograms and corresponding pVIII glycoconjugates of f1.K conjugated to monosaccharide **44** (Table 8).



f1.K-(2-yne)-Mono 11092311				f1.K-(4-yne)-Mono 11111605			
Peak #	Identity	Area	% Area	Peak #	Identity	Area	% Area
1	1L1M	60.2	4.6%	1	2L2M	61.1	15.0%
2	2L2M	626.6	47.6%	2	2L1M	76.4	18.7%
3	3L3M	270.0	20.5%	3	3L3M	60.1	14.7%
4	3L2M+48	40.6	3.1%	4	3L2M	97.0	23.8%
5	3L2M	41.7	3.2%	5	3L2M	39.7	9.7%
6	3L2M	171.1	13.0%	6	3L1M	40.0	9.8%
7	2L1M+42	22.0	1.7%	7	3L1M	18.0	4.4%
8	4L3M	73.9	5.6%	8	4L2M	15.8	3.9%
9	4L2M	11.3	0.9%	Total Area:		408.0	
Total Area:		1317.3					

* These fractions were unidentifiable by mass.

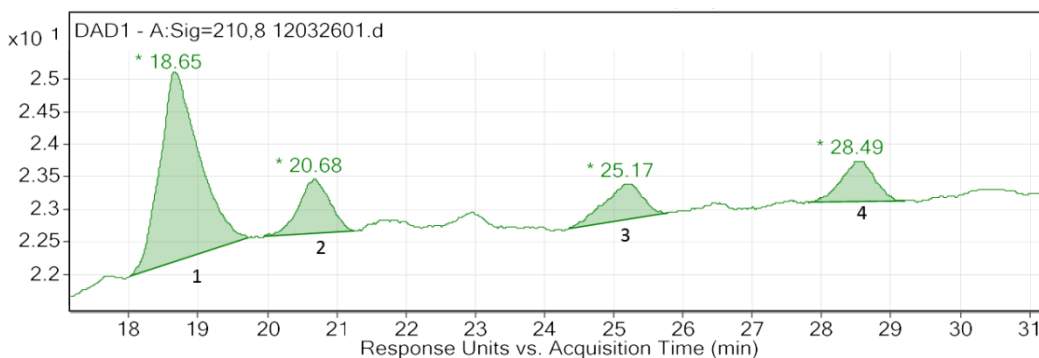
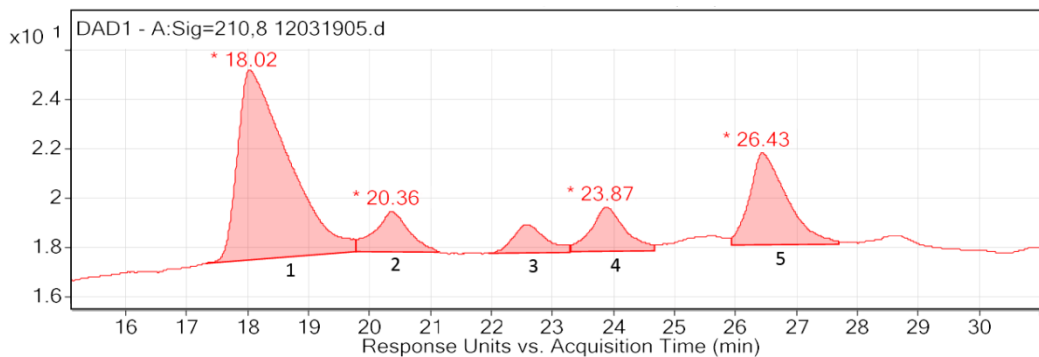
LC-UV chromatograms and corresponding pVIII glycoconjugates of f1.K conjugated to monosaccharide **39** (Table 8).



f1.K-SIA-Mono			11091303
Peak #	Identity	Area	% Area
1	2L2M	635.1	44.89%
2	1L1M+42	30.3	2.14%
3	3L3M	588.7	41.61%
4	2L2M+42	29.2	2.06%
5	4L4M	37.9	2.68%
6	3L2M	21.4	1.51%
7	4L4M	14.1	1.00%
8	2L2M	3.9	0.27%
9	4L3M	12.3	0.87%
10	3L2M	22.1	1.56%
11	4L3M	19.8	1.40%
Total Area		1414.6	

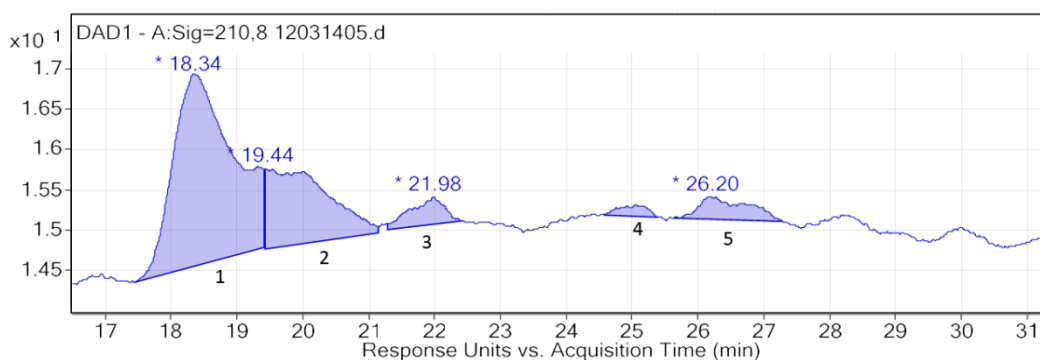
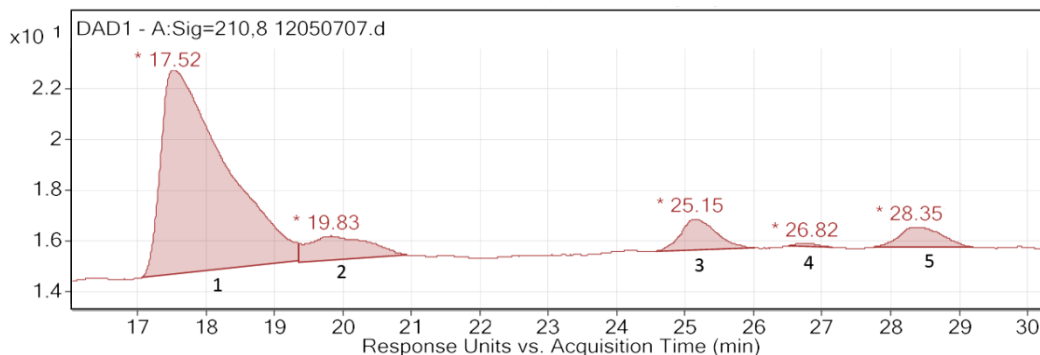
* This fraction was unidentifiable by mass.

LC-UV chromatograms and corresponding pVIII glycoconjugates of f1.K conjugated to pentasaccharide **44** (Table 9).



f1.K-(2-yne)-Penta				f1.K-(4-yne)-Penta			
Peak #	Identity	Area	% Area	Peak #	Identity	Area	% Area
1	2L2P, 3L3P	445.2	56.8%	1	2L2P, 3L3P	115.4	62.8%
2	1L1P	65.0	8.3%	2	2L2P	26.1	14.2%
3	2L1P	43.4	5.5%	3	3L2T	21.3	11.6%
4	3L2P	70.6	9.0%	4	4L3T	20.9	11.4%
5	3L2P, 4L3P	159.9	20.4%	Total Area:		183.7	
Total Area:		784.0					

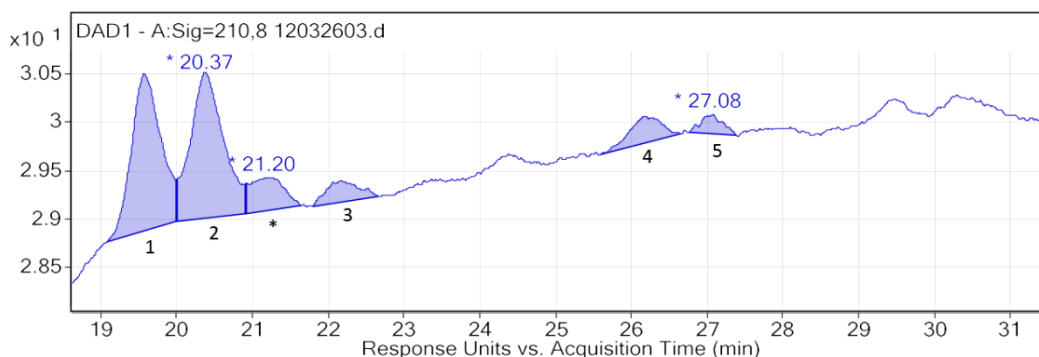
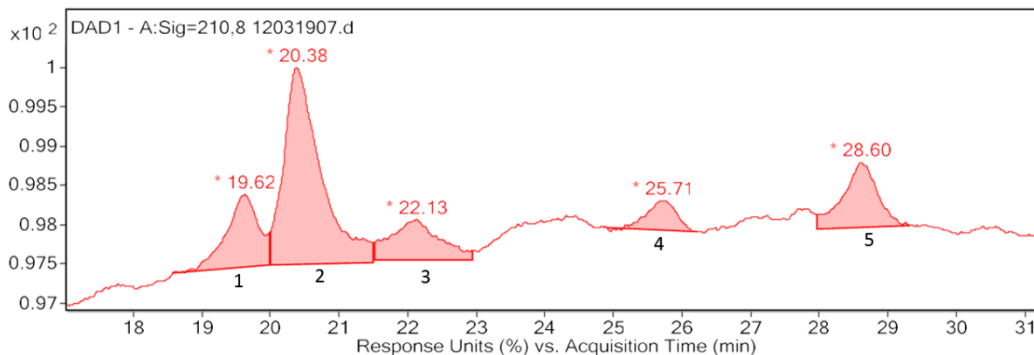
LC-UV chromatograms and corresponding pVIII glycoconjugates of f1.K conjugated to pentasaccharide **2**, and both pentasaccharide **2** and tetrasaccharide **1** (Table 9).



f1.K-SIA-Penta				f1.K-SIA-Penta/Tetra			
Peak #	Identity	Area	% Area	Peak #	Identity	Area	% Area
1	2L2P, 3L3P	525.7	79.2%	1	2L2P, 2L1P1T	149.3	61.5%
2	2L2P+42	58.2	8.8%	2	2L1P	62.1	25.6%
3	3L2P, 4L3P	43.6	6.6%	3	2L2P+58	12.4	5.1%
4	2L2P	2.6	0.4%	4	3L3P	4.3	1.8%
5	3L2P, 4L3P	33.8	5.1%	5	2L2P	14.5	6.0%
Total Area:		663.9		Total Area:		242.6	

For f1.K-SIA-Penta/Tetra, the pentasaccharide was the most predominant glycan on all the pVIII conjugates. Mixtures of the pentasaccharide and tetrasaccharide were found in all the peaks, with peak 1 containing the largest tetrasaccharide fraction.

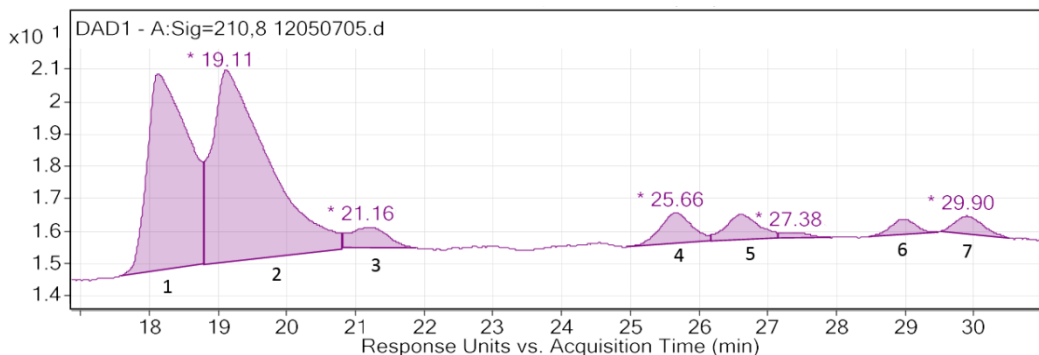
LC-UV chromatograms and corresponding pVIII glycoconjugates of f1.K conjugated to tetrasaccharide **41** (Table 9).



f1.K-(2-yne)-Tetra				f1.K-(4-yne)-Tetra			
Peak #	Identity	Area	% Area	Peak #	Identity	Area	% Area
1	2L2T	30.8	16.0%	1	2L2T	44.2	40.7%
2	3L3T	95.7	49.7%	2	3L3T	45.8	42.1%
3	2L1T, 2L2T+42	25.8	13.4%	3	2L1T, 2L2T+42	6.6	6.1%
4	3L2T	11.1	5.8%	4	3L2T	8.1	7.4%
5	4L3T	29.4	15.2%	5	4L3T	4.0	3.7%
Total Area: 192.8				Total Area: 108.7			

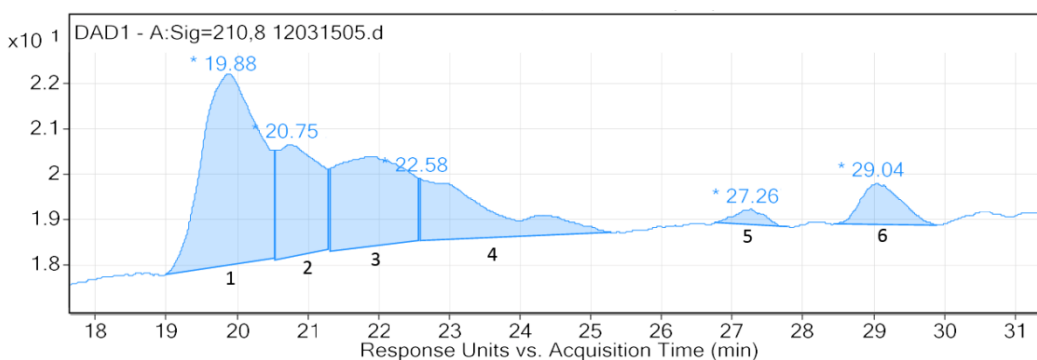
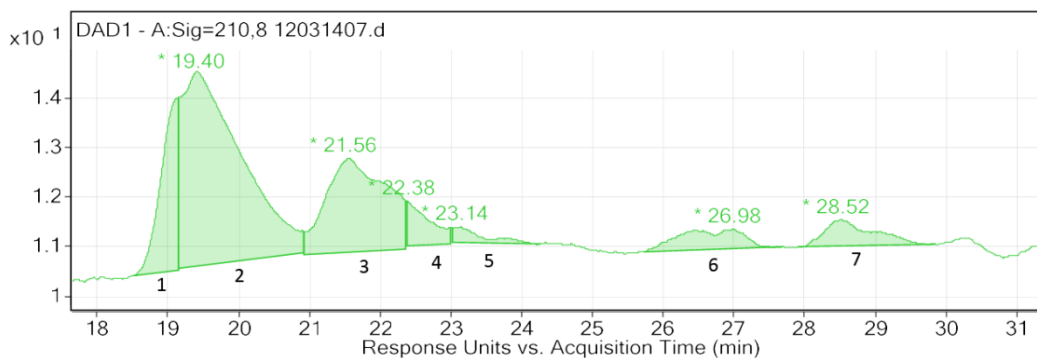
* This fraction was unidentifiable by mass.

LC-UV chromatograms and corresponding pVIII glycoconjugates of f1.K conjugated to tetrasaccharide **1** (Table 9).



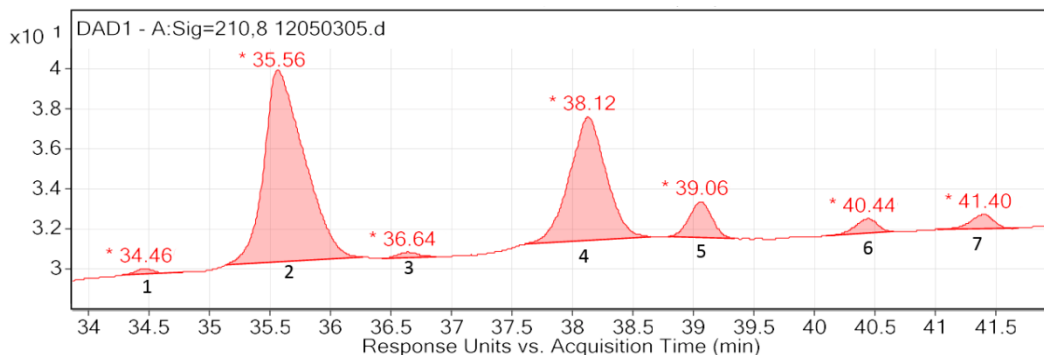
f1.K-SIA-Tetra		12050705	
Peak #	Identity	Area	% Area
1	2L2T	254.3	36.9%
2	3L3T	330.5	48.0%
3	2L2T+42	24.2	3.5%
4	3L2T	29.6	4.3%
5	4L3T	22.2	3.2%
6	3L2T	12.0	1.7%
7	4L3T	15.9	2.3%
Total Area:		688.7	

LC-UV chromatograms and corresponding pVIII glycoconjugates of f88 conjugated to pentasaccharide **2** and tetrasaccharide **1** (Table 9).



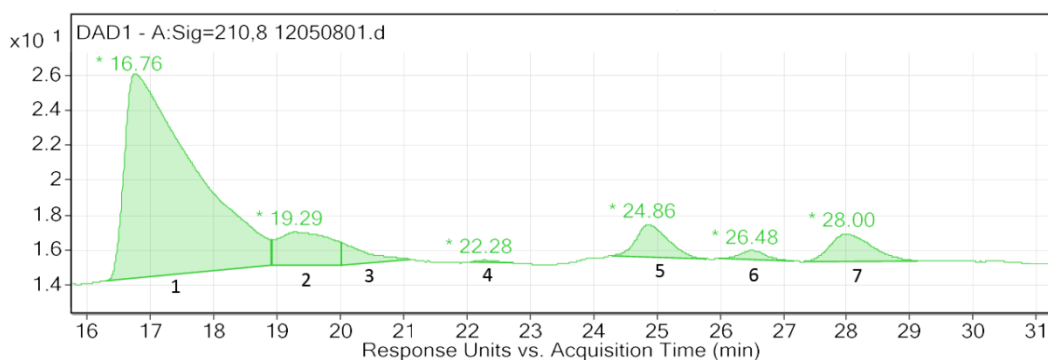
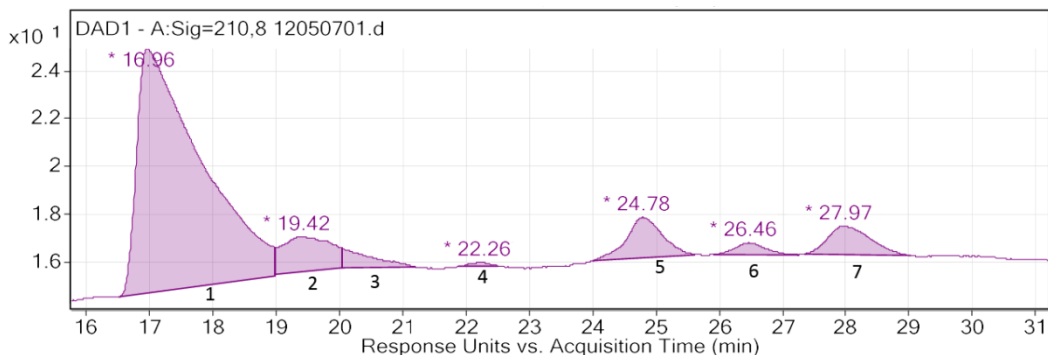
f88-SIA-Penta				f88-SIA-Tetra			
Peak #	Identity	Area	% Area	Peak #	Identity	Area	% Area
1, 2	1L1P, 2L2P	288.1	60.0%	1	1L1T	235.9	38.8%
3	1L1P (deg)	112.6	23.5%	2	2L2T	137.8	22.7%
4	pVIII+42	19.6	4.1%	3	1L1T (deg)	66.9	11.0%
5	1L1P+58	8.9	1.9%	4	1L1T	121.5	20.0%
6	2L1P	25.8	5.4%	5	2L1T	9.4	1.6%
7	1L1P+xlink	24.8	5.2%	6	1L1T+xlink	35.8	5.9%
Total Area:		479.8		Total Area:		607.4	

LC-UV chromatograms and corresponding f1.K conjugates following the linker addition with SIA and 4-alkynyl crosslinker **54** (Table 10).



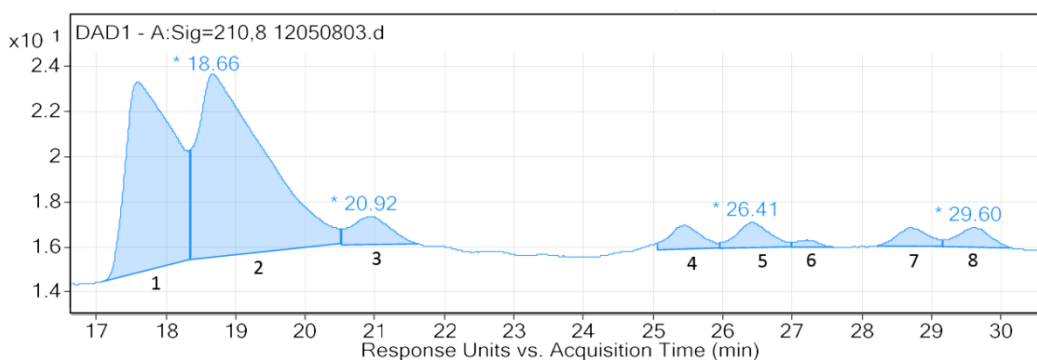
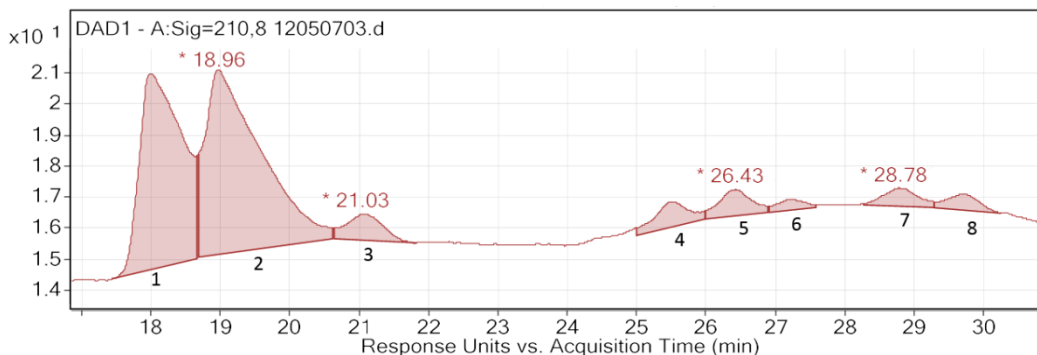
f1.K-SIA/(4-yne)		12050305	
Peak #	Identity	Area	% Area
1	1SIA, 1YNE	2.5	0.6%
2	2SIA	222.6	55.5%
3	2SIA	3.5	0.9%
4	3SIA, 2SIA+1YNE	130.4	32.5%
5	3SIA, 2SIA+1YNE	23.6	5.9%
6	4SIA, 3SIA+1YNE	8.9	2.2%
7	4SIA, 3SIA+1YNE	9.5	2.4%
Total Area:		401.0	

LC-UV chromatograms and corresponding pVIII glycoconjugates of f1.K conjugated to first pentasaccharide **2**, then β -glucan **56** (Table 11).



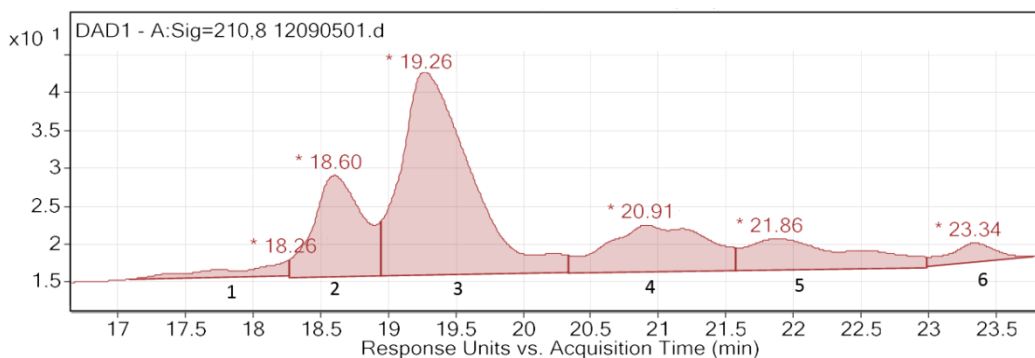
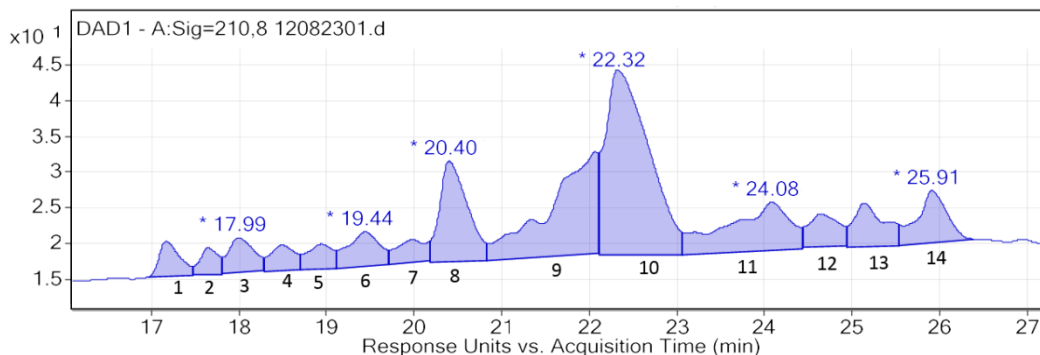
f1.k-SIA/(4-yne)-Penta				f1.k-SIA/(4-yne)-Penta/ β glucan			
Peak #	Identity	Area	% Area	Peak #	Identity	Area	% Area
1	2L2P+3L3P	718.0	74.4%	1	2L2P, 3L3P	889.8	74.7%
2	1L1P+42	78.7	8.2%	2	1L1P+42	110.7	9.3%
3	2L2P+1YNE	25.9	2.7%	3	2L2P	33.9	2.9%
4	1L1P+1YNE	3.1	0.3%	4	1L1P	2.6	0.2%
5	3L2P, 4L3P, 2L2P+1YNE	66.8	6.9%	5	3L2P, 4L3P	65.8	5.5%
6	2L2P+xlink	16.5	1.7%	6	2L2P+xlink	15.2	1.3%
7	2L2P, 3L3P, 2L2P+1YNE	56.0	5.8%	7	2L2P, 3L3P	72.7	6.1%
Total Area:		964.9		Total Area:		1190.6	

LC-UV chromatograms and corresponding pVIII glycoconjugates of f1.K conjugated to first tetrasaccharide **1**, then β -glucan **56** (Table 11).



f1.k-SIA/(4-yne)-Tetra 12050703				f1.k-SIA/(4-yne)-Tetra/ β glucan 12050803			
Peak #	Identity	Area	% Area	Peak #	Identity	Area	% Area
1	2L2T	267.0	36.4%	1	2L2T	402.2	35.7%
2	3L3T	332.2	45.2%	2	3L3T	543.0	48.2%
3	1L1T, 1L1T+YNE, 2L2T+1YNE	30.9	4.2%	3	2L12, 1L1T+YNE (trace)	48.8	4.3%
4	3L2T	28.6	3.9%	4	3L2T	33.7	3.0%
5	4L3T	28.2	3.8%	5	4L3T	37.6	3.3%
6	2L2T+xlink	9.9	1.3%	6	2L2T+xlink	6.9	0.6%
7	3L2T	20.9	2.9%	7	3L2T	26.0	2.3%
8	4L3T, 3L3T+YNE	16.9	2.3%	8	4L3T, 3L3T	28.9	2.6%
Total Area:		734.4		Total Area:		1127.0	

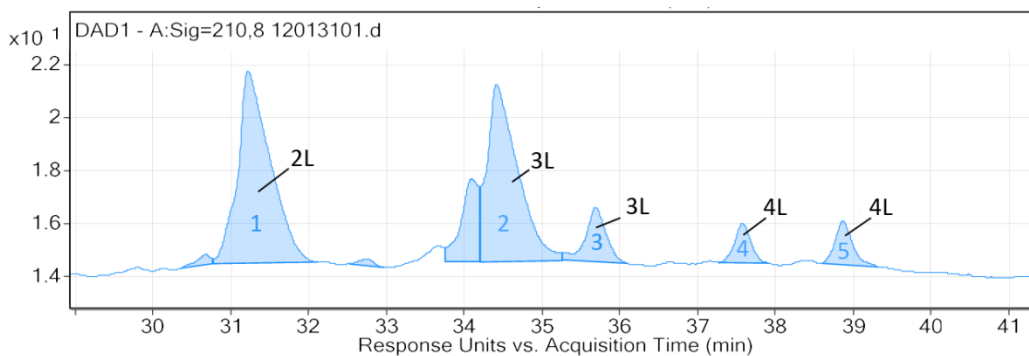
LC-UV chromatograms and corresponding ubiquitin conjugates following the linker addition with SIA and tetrasaccharide **1** or pentasaccharide **2** glycoconjugation.



Ub-SIA-Tetra				Ub-SIA-Penta			
Peak #	Identity	Area	% Area	Peak #	Identity	Area	% Area
1		81.5	2.62%	1	3,4,5	60.1	3.03%
2		54.5	1.75%	2	4,5	346.0	17.42%
3		97.8	3.15%	3	5,6	960.7	48.37%
4		70.0	2.25%	4	3,4,5,6	325.6	16.40%
5		71.2	2.29%	5	5	231.7	11.67%
6		123.3	3.97%	6	5	61.9	3.11%
7		74.8	2.41%	Total Area:		1985.9	
8		313.2	10.08%				
9		550.9	17.73%				
10		892.7	28.72%				
11		341.4	10.98%				
12		110.7	3.56%				
13		149.3	4.80%				
14		176.8	5.69%				
Total Area:		3108.0					

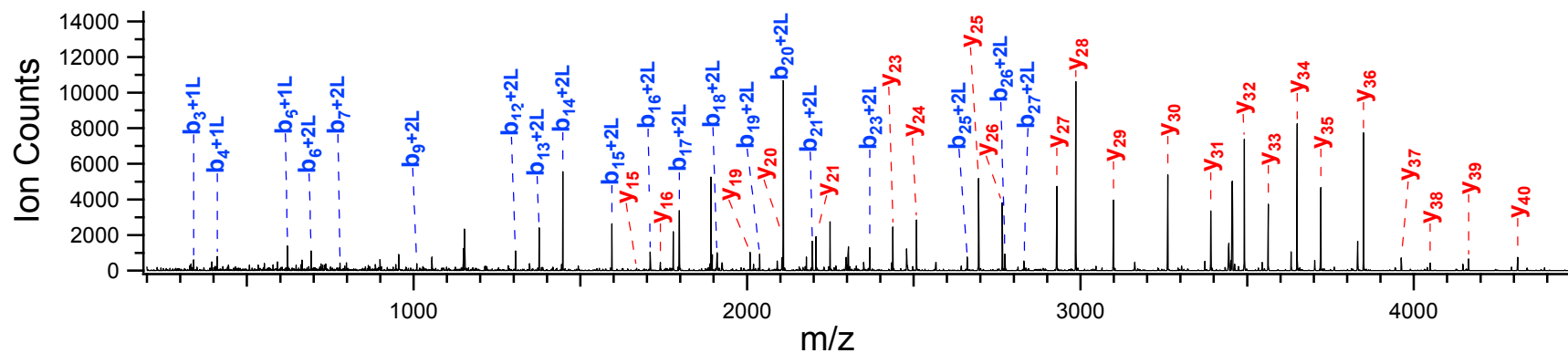
Appendix A2

The MS/MS analysis data of the differentially conjugated pVIII species of the phage f1.K-(4-*yne*) linker conjugate. The five major peaks, as shown in the below LC-UV trace were collected and analyzed by MS/MS.



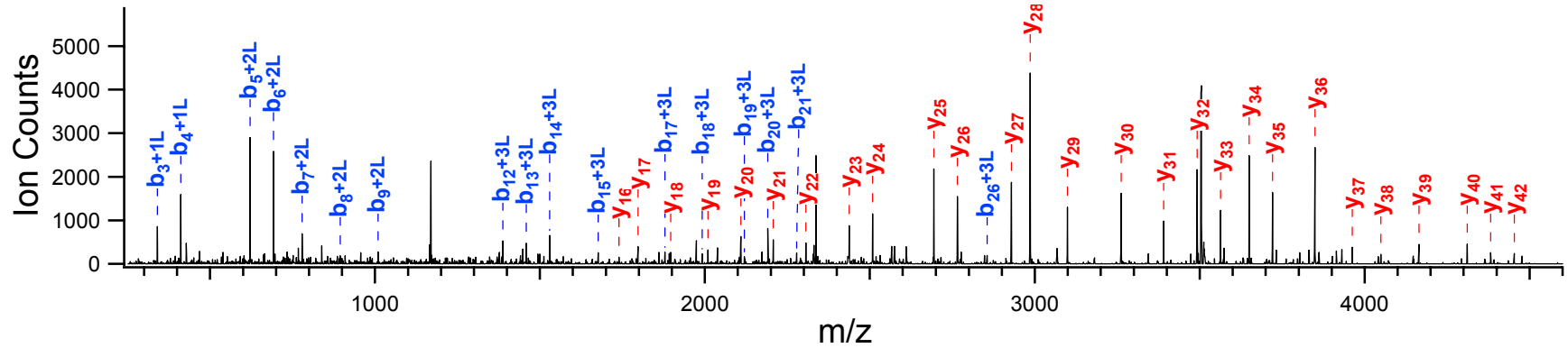
The deconvoluted mass spectra and accompanying tables of *b* and *y* fragment ion are presented on the follow pages for each of the five fractions.

Fraction 1



b+3L	b+2L	b+1L	b		pVIII	y	y+1L	b+3L	b+2L	b+1L	b	pVIII	y	y+1L		
322.17	240.12	158.08	76.04	1	A	54	--	3075.45	2993.41	2911.36	2829.32	28	Y	27	2928.68	3010.72
447.21	365.17	283.13	201.09	2	E	53	5522.89	3146.48	3064.44	2982.40	2900.36	29	A	26	2765.62	2847.66
504.23	422.19	340.15	258.11	3	G	52	5393.85	3332.56	3250.52	3168.48	3086.44	30	W	25	2694.58	2776.62
575.27	493.23	411.19	329.15	4	A	51	5336.83	3403.60	3321.56	3239.52	3157.47	31	A	24	2508.50	2590.54
703.37	621.32	539.28	457.24	5	K	50	5265.79	3534.64	3452.60	3370.56	3288.52	32	M	23	2437.46	2519.50
774.40	692.36	610.32	528.28	6	A	49	5137.70	3633.71	3551.67	3469.63	3387.58	33	V	22	2306.42	2388.46
861.44	779.39	697.35	615.31	7	S	48	5066.66	3732.78	3650.74	3568.69	3486.65	34	V	21	2207.35	2289.39
976.46	894.42	812.38	730.34	8	D	47	4979.63	3831.85	3749.80	3667.76	3585.72	35	V	20	2108.28	2190.33
1091.49	1009.45	927.41	845.36	9	D	46	4864.60	3944.93	3862.89	3780.85	3698.80	36	I	19	2009.22	2091.26
1188.54	1106.50	1024.46	942.42	10	P	45	4749.57	4044.00	3961.96	3879.92	3797.87	37	V	18	1896.13	1978.17
1259.58	1177.54	1095.50	1013.45	11	A	44	4652.52	4101.02	4018.98	3936.94	3854.89	38	G	17	1797.06	1879.11
1387.67	1305.63	1223.59	1141.55	12	K	43	4581.48	4172.06	4090.02	4007.97	3925.93	39	A	16	1740.04	1822.08
1458.71	1376.67	1294.63	1212.59	13	A	42	4453.39	4273.11	4191.06	4109.02	4026.98	40	T	15	1669.00	1751.05
1529.75	1447.71	1365.66	1283.62	14	A	41	4382.35	4386.19	4304.15	4222.11	4140.06	41	I	14	1567.96	1650.00
1676.82	1594.77	1512.73	1430.69	15	F	40	4311.31	4443.21	4361.17	4279.13	4197.08	42	G	13	1454.87	1536.91
1791.84	1709.80	1627.76	1545.72	16	D	39	4164.25	4556.29	4474.25	4392.21	4310.17	43	I	12	1397.85	1479.89
1878.88	1796.83	1714.79	1632.75	17	S	38	4049.22	4684.39	4602.35	4520.31	4438.26	44	K	11	1284.77	1366.81
1991.96	1909.92	1827.88	1745.83	18	L	37	3962.19	4797.47	4715.43	4633.39	4551.35	45	L	10	1156.67	1238.71
2120.02	2037.98	1955.93	1873.89	19	Q	36	3849.10	4944.54	4862.50	4780.46	4698.42	46	F	9	1043.59	1125.63
2191.06	2109.01	2026.97	1944.93	20	A	35	3721.04	5072.64	4990.60	4908.55	4826.51	47	K	8	896.52	978.56
2278.09	2196.05	2114.00	2031.96	21	S	34	3650.01	5200.73	5118.69	5036.65	4954.61	48	K	7	768.43	850.47
2349.12	2267.08	2185.04	2103.00	22	A	33	3562.97	5347.80	5265.76	5183.72	5101.67	49	F	6	640.33	722.37
2450.17	2368.13	2286.09	2204.05	23	T	32	3491.94	5448.85	5366.81	5284.76	5202.72	50	T	5	493.26	575.30
2579.21	2497.17	2415.13	2333.09	24	E	31	3390.89	5535.88	5453.84	5371.80	5289.75	51	S	4	392.21	474.26
2742.28	2660.24	2578.19	2496.15	25	Y	30	3261.85	5663.98	5581.93	5499.89	5417.85	52	K	3	305.18	387.22
2855.36	2773.32	2691.28	2609.24	26	I	29	3098.78	5735.01	5652.97	5570.93	5488.89	53	A	2	177.09	259.13
2912.38	2830.34	2748.30	2666.26	27	G	28	2985.70	--	--	--	--	54	S	1	106.05	188.09

Fraction 2

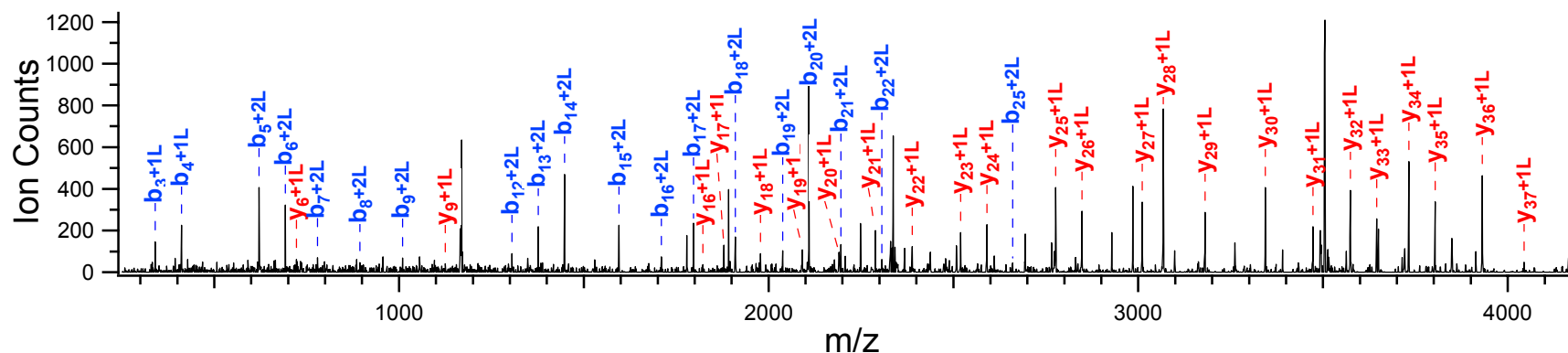


b+3L	b+2L	b+1L	b	pVIII	y	y+1L
322.17	240.12	158.08	76.04	1 A 54	--	--
447.21	365.17	283.13	201.09	2 E 53	5522.89	5604.93
504.23	422.19	340.15	258.11	3 G 52	5393.85	5475.89
575.27	493.23	411.19	329.15	4 A 51	5336.83	5418.87
703.37	621.32	539.28	457.24	5 K 50	5265.79	5347.83
774.40	692.36	610.32	528.28	6 A 49	5137.70	5219.74
861.44	779.39	697.35	615.31	7 S 48	5066.66	5148.70
976.46	894.42	812.38	730.34	8 D 47	4979.63	5061.67
1091.49	1009.45	927.41	845.36	9 D 46	4864.60	4946.64
1188.54	1106.50	1024.46	942.42	10 P 45	4749.57	4831.61
1259.58	1177.54	1095.50	1013.45	11 A 44	4652.52	4734.56
1387.67	1305.63	1223.59	1141.55	12 K 43	4581.48	4663.52
1458.71	1376.67	1294.63	1212.59	13 A 42	4453.39	4535.43
1529.75	1447.71	1365.66	1283.62	14 A 41	4382.35	4464.39
1676.82	1594.77	1512.73	1430.69	15 F 40	4311.31	4393.36
1791.84	1709.80	1627.76	1545.72	16 D 39	4164.25	4246.29
1878.88	1796.83	1714.79	1632.75	17 S 38	4049.22	4131.26
1991.96	1909.92	1827.88	1745.83	18 L 37	3962.19	4044.23
2120.02	2037.98	1955.93	1873.89	19 Q 36	3849.10	3931.14
2191.06	2109.01	2026.97	1944.93	20 A 35	3721.04	3803.09
2278.09	2196.05	2114.00	2031.96	21 S 34	3650.01	3732.05
2349.12	2267.08	2185.04	2103.00	22 A 33	3562.97	3645.02
2450.17	2368.13	2286.09	2204.05	23 T 32	3491.94	3573.98
2579.21	2497.17	2415.13	2333.09	24 E 31	3390.89	3472.93
2742.28	2660.24	2578.19	2496.15	25 Y 30	3261.85	3343.89
2855.36	2773.32	2691.28	2609.24	26 I 29	3098.78	3180.83
2912.38	2830.34	2748.30	2666.26	27 G 28	2985.70	3067.74

m/z

b+3L	b+2L	b+1L	b	pVIII	y	y+1L
3075.45	2993.41	2911.36	2829.32	28 Y 27	2928.68	3010.72
3146.48	3064.44	2982.40	2900.36	29 A 26	2765.62	2847.66
3332.56	3250.52	3168.48	3086.44	30 W 25	2694.58	2776.62
3403.60	3321.56	3239.52	3157.47	31 A 24	2508.50	2590.54
3534.64	3452.60	3370.56	3288.52	32 M 23	2437.46	2519.50
3633.71	3551.67	3469.63	3387.58	33 V 22	2306.42	2388.46
3732.78	3650.74	3568.69	3486.65	34 V 21	2207.35	2289.39
3831.85	3749.80	3667.76	3585.72	35 V 20	2108.28	2190.33
3944.93	3862.89	3780.85	3698.80	36 I 19	2009.22	2091.26
4044.00	3961.96	3879.92	3797.87	37 V 18	1896.13	1978.17
4101.02	4018.98	3936.94	3854.89	38 G 17	1797.06	1879.11
4172.06	4090.02	4007.97	3925.93	39 A 16	1740.04	1822.08
4273.11	4191.06	4109.02	4026.98	40 T 15	1669.00	1751.05
4386.19	4304.15	4222.11	4140.06	41 I 14	1567.96	1650.00
4443.21	4361.17	4279.13	4197.08	42 G 13	1454.87	1536.91
4556.29	4474.25	4392.21	4310.17	43 I 12	1397.85	1479.89
4684.39	4602.35	4520.31	4438.26	44 K 11	1284.77	1366.81
4797.47	4715.43	4633.39	4551.35	45 L 10	1156.67	1238.71
4944.54	4862.50	4780.46	4698.42	46 F 9	1043.59	1125.63
5072.64	4990.60	4908.55	4826.51	47 K 8	896.52	978.56
5200.73	5118.69	5036.65	4954.61	48 K 7	768.43	850.47
5347.80	5265.76	5183.72	5101.67	49 F 6	640.33	722.37
5448.85	5366.81	5284.76	5202.72	50 T 5	493.26	575.30
5535.88	5453.84	5371.80	5289.75	51 S 4	392.21	474.26
5663.98	5581.93	5499.89	5417.85	52 K 3	305.18	387.22
5735.01	5652.97	5570.93	5488.89	53 A 2	177.09	259.13
--	--	--	--	54 S 1	106.05	188.09

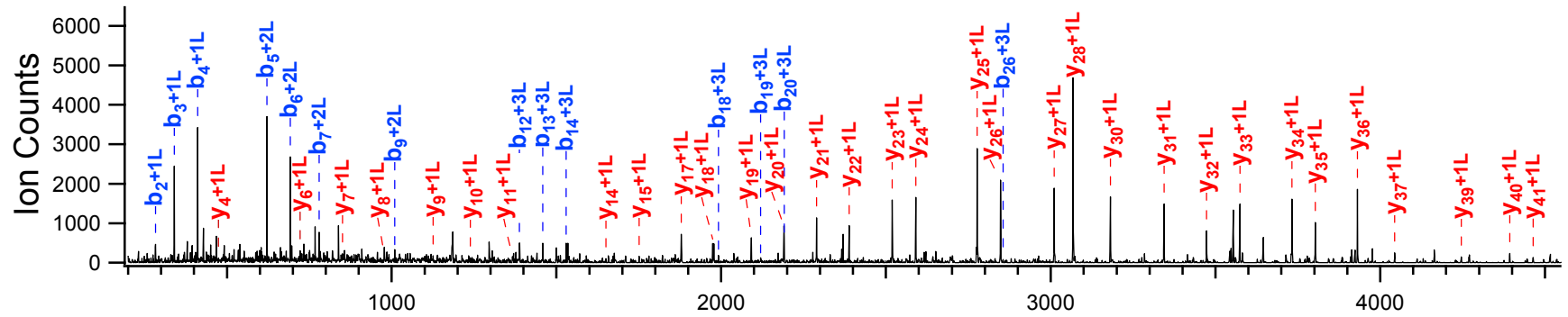
Fraction 3



b+3L	b+2L	b+1L	b	pVIII	y	y+1L	
322.17	240.12	158.08	76.04	1	A	54	--
447.21	365.17	283.13	201.09	2	E	53	5522.89
504.23	422.19	340.15	258.11	3	G	52	5393.85
575.27	493.23	411.19	329.15	4	A	51	5336.83
703.37	621.32	539.28	457.24	5	K	50	5265.79
774.40	692.36	610.32	528.28	6	A	49	5137.70
861.44	779.39	697.35	615.31	7	S	48	5066.66
976.46	894.42	812.38	730.34	8	D	47	4979.63
1091.49	1009.45	927.41	845.36	9	D	46	4864.60
1188.54	1106.50	1024.46	942.42	10	P	45	4749.57
1259.58	1177.54	1095.50	1013.45	11	A	44	4652.52
1387.67	1305.63	1223.59	1141.55	12	K	43	4581.48
1458.71	1376.67	1294.63	1212.59	13	A	42	4453.39
1529.75	1447.71	1365.66	1283.62	14	A	41	4382.35
1676.82	1594.77	1512.73	1430.69	15	F	40	4311.31
1791.84	1709.80	1627.76	1545.72	16	D	39	4164.25
1878.88	1796.83	1714.79	1632.75	17	S	38	4049.22
1991.96	1909.92	1827.88	1745.83	18	L	37	3962.19
2120.02	2037.98	1955.93	1873.89	19	Q	36	3849.10
2191.06	2109.01	2026.97	1944.93	20	A	35	3721.04
2278.09	2196.05	2114.00	2031.96	21	S	34	3650.01
2349.12	2267.08	2185.04	2103.00	22	A	33	3562.97
2450.17	2368.13	2286.09	2204.05	23	T	32	3491.94
2579.21	2497.17	2415.13	2333.09	24	E	31	3390.89
2742.28	2660.24	2578.19	2496.15	25	Y	30	3261.85
2855.36	2773.32	2691.28	2609.24	26	I	29	3098.78
2912.38	2830.34	2748.30	2666.26	27	G	28	2985.70

b+3L	b+2L	b+1L	b	pVIII	y	y+1L	
3075.45	2993.41	2911.36	2829.32	28	Y	27	2928.68
3146.48	3064.44	2982.40	2900.36	29	A	26	2765.62
3332.56	3250.52	3168.48	3086.44	30	W	25	2694.58
3403.60	3321.56	3239.52	3157.47	31	A	24	2508.50
3534.64	3452.60	3370.56	3288.52	32	M	23	2437.46
3633.71	3551.67	3469.63	3387.58	33	V	22	2306.42
3732.78	3650.74	3568.69	3486.65	34	V	21	2207.35
3831.85	3749.80	3667.76	3585.72	35	V	20	2108.28
3944.93	3862.89	3780.85	3698.80	36	I	19	2009.22
4044.00	3961.96	3879.92	3797.87	37	V	18	1896.13
4101.02	4018.98	3936.94	3854.89	38	G	17	1797.06
4172.06	4090.02	4007.97	3925.93	39	A	16	1740.04
4273.11	4191.06	4109.02	4026.98	40	T	15	1669.00
4386.19	4304.15	4222.11	4140.06	41	I	14	1567.96
4443.21	4361.17	4279.13	4197.08	42	G	13	1454.87
4556.29	4474.25	4392.21	4310.17	43	I	12	1397.85
4684.39	4602.35	4520.31	4438.26	44	K	11	1284.77
4797.47	4715.43	4633.39	4551.35	45	L	10	1156.67
4944.54	4862.50	4780.46	4698.42	46	F	9	1043.59
5072.64	4990.60	4908.55	4826.51	47	K	8	896.52
5200.73	5118.69	5036.65	4954.61	48	K	7	768.43
5347.80	5265.76	5183.72	5101.67	49	F	6	640.33
5448.85	5366.81	5284.76	5202.72	50	T	5	493.26
5535.88	5453.84	5371.80	5289.75	51	S	4	392.21
5663.98	5581.93	5499.89	5417.85	52	K	3	305.18
5735.01	5652.97	5570.93	5488.89	53	A	2	177.09
--	--	--	--	54	S	1	106.05

Fraction 4

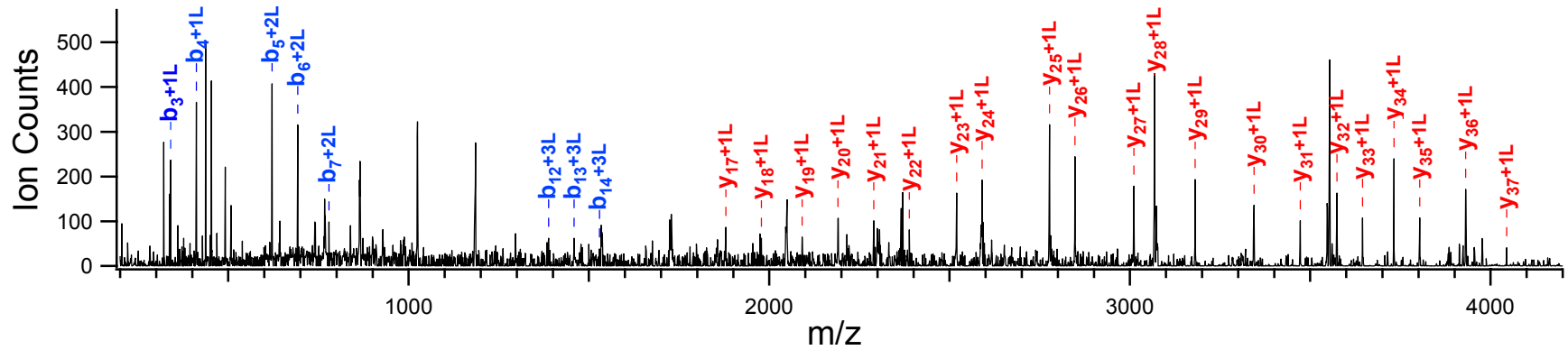


b+3L	b+2L	b+1L	b	pVIII	y	y+1L		
322.17	240.12	158.08	76.04	1	A	54	---	---
447.21	365.17	283.13	201.09	2	E	53	5522.89	5604.93
504.23	422.19	340.15	258.11	3	G	52	5393.85	5475.89
575.27	493.23	411.19	329.15	4	A	51	5336.83	5418.87
703.37	621.32	539.28	457.24	5	K	50	5265.79	5347.83
774.40	692.36	610.32	528.28	6	A	49	5137.70	5219.74
861.44	779.39	697.35	615.31	7	S	48	5066.66	5148.70
976.46	894.42	812.38	730.34	8	D	47	4979.63	5061.67
1091.49	1009.45	927.41	845.36	9	D	46	4864.60	4946.64
1188.54	1106.50	1024.46	942.42	10	P	45	4749.57	4831.61
1259.58	1177.54	1095.50	1013.45	11	A	44	4652.52	4734.56
1387.67	1305.63	1223.59	1141.55	12	K	43	4581.48	4663.52
1458.71	1376.67	1294.63	1212.59	13	A	42	4453.39	4535.43
1529.75	1447.71	1365.66	1283.62	14	A	41	4382.35	4464.39
1676.82	1594.77	1512.73	1430.69	15	F	40	4311.31	4393.36
1791.84	1709.80	1627.76	1545.72	16	D	39	4164.25	4246.29
1878.88	1796.83	1714.79	1632.75	17	S	38	4049.22	4131.26
1991.96	1909.92	1827.88	1745.83	18	L	37	3962.19	4044.23
2120.02	2037.98	1955.93	1873.89	19	Q	36	3849.10	3931.14
2191.06	2109.01	2026.97	1944.93	20	A	35	3721.04	3803.09
2278.09	2196.05	2114.00	2031.96	21	S	34	3650.01	3732.05
2349.12	2267.08	2185.04	2103.00	22	A	33	3562.97	3645.02
2450.17	2368.13	2286.09	2204.05	23	T	32	3491.94	3573.98
2579.21	2497.17	2415.13	2333.09	24	E	31	3390.89	3472.93
2742.28	2660.24	2578.19	2496.15	25	Y	30	3261.85	3343.89
2855.36	2773.32	2691.28	2609.24	26	I	29	3098.78	3180.83
2912.38	2830.34	2748.30	2666.26	27	G	28	2985.70	3067.74

m/z

b+3L	b+2L	b+1L	b	pVIII	y	y+1L		
3075.45	2993.41	2911.36	2829.32	28	Y	27	2928.68	3010.72
3146.48	3064.44	2982.40	2900.36	29	A	26	2765.62	2847.66
3332.56	3250.52	3168.48	3086.44	30	W	25	2694.58	2776.62
3403.60	3321.56	3239.52	3157.47	31	A	24	2508.50	2590.54
3534.64	3452.60	3370.56	3288.52	32	M	23	2437.46	2519.50
3633.71	3551.67	3469.63	3387.58	33	V	22	2306.42	2388.46
3732.78	3650.74	3568.69	3486.65	34	V	21	2207.35	2289.39
3831.85	3749.80	3667.76	3585.72	35	V	20	2108.28	2190.33
3944.93	3862.89	3780.85	3698.80	36	I	19	2009.22	2091.26
4044.00	3961.96	3879.92	3797.87	37	V	18	1896.13	1978.17
4101.02	4018.98	3936.94	3854.89	38	G	17	1797.06	1879.11
4172.06	4090.02	4007.97	3925.93	39	A	16	1740.04	1822.08
4273.11	4191.06	4109.02	4026.98	40	T	15	1669.00	1751.05
4386.19	4304.15	4222.11	4140.06	41	I	14	1567.96	1650.00
4443.21	4361.17	4279.13	4197.08	42	G	13	1454.87	1536.91
4556.29	4474.25	4392.21	4310.17	43	I	12	1397.85	1479.89
4684.39	4602.35	4520.31	4438.26	44	K	11	1284.77	1366.81
4797.47	4715.43	4633.39	4551.35	45	L	10	1156.67	1238.71
4944.54	4862.50	4780.46	4698.42	46	F	9	1043.59	1125.63
5072.64	4990.60	4908.55	4826.51	47	K	8	896.52	978.56
5200.73	5118.69	5036.65	4954.61	48	K	7	768.43	850.47
5347.80	5265.76	5183.72	5101.67	49	F	6	640.33	722.37
5448.85	5366.81	5284.76	5202.72	50	T	5	493.26	575.30
5535.88	5453.84	5371.80	5289.75	51	S	4	392.21	474.26
5663.98	5581.93	5499.89	5417.85	52	K	3	305.18	387.22
5735.01	5652.97	5570.93	5488.89	53	A	2	177.09	259.13
--	--	--	--	54	S	1	106.05	188.09

Fraction 5

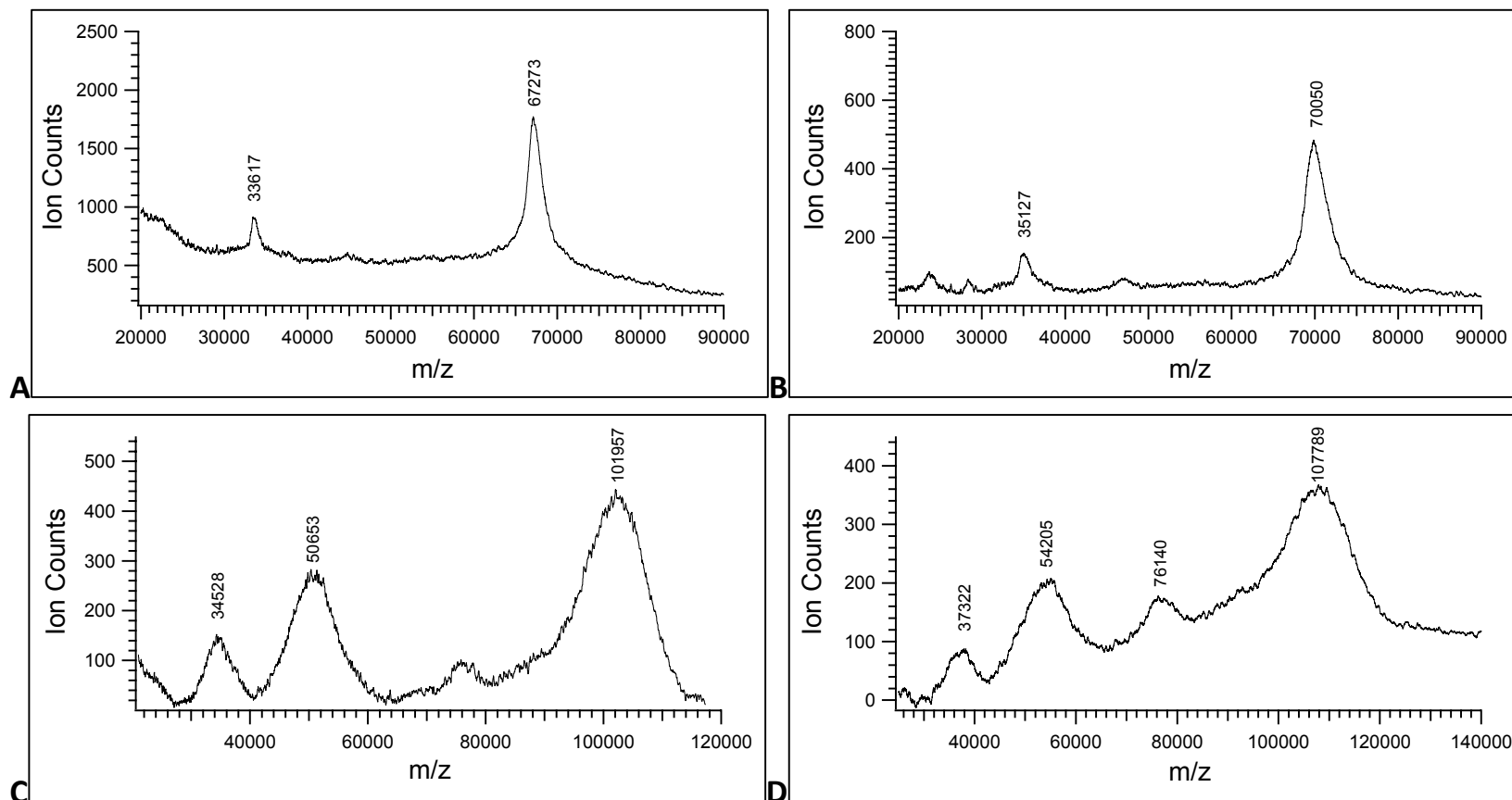


b+3L	b+2L	b+1L	b	pVIII	y	y+1L
322.17	240.12	158.08	76.04	1 A 54	---	---
447.21	365.17	283.13	201.09	2 E 53	5522.89	5604.93
504.23	422.19	340.15	258.11	3 G 52	5393.85	5475.89
575.27	493.23	411.19	329.15	4 A 51	5336.83	5418.87
703.37	621.32	539.28	457.24	5 K 50	5265.79	5347.83
774.40	692.36	610.32	528.28	6 A 49	5137.70	5219.74
861.44	779.39	697.35	615.31	7 S 48	5066.66	5148.70
976.46	894.42	812.38	730.34	8 D 47	4979.63	5061.67
1091.49	1009.45	927.41	845.36	9 D 46	4864.60	4946.64
1188.54	1106.50	1024.46	942.42	10 P 45	4749.57	4831.61
1259.58	1177.54	1095.50	1013.45	11 A 44	4652.52	4734.56
1387.67	1305.63	1223.59	1141.55	12 K 43	4581.48	4663.52
1458.71	1376.67	1294.63	1212.59	13 A 42	4453.39	4535.43
1529.75	1447.71	1365.66	1283.62	14 A 41	4382.35	4464.39
1676.82	1594.77	1512.73	1430.69	15 F 40	4311.31	4393.36
1791.84	1709.80	1627.76	1545.72	16 D 39	4164.25	4246.29
1878.88	1796.83	1714.79	1632.75	17 S 38	4049.22	4131.26
1991.96	1909.92	1827.88	1745.83	18 L 37	3962.19	4044.23
2120.02	2037.98	1955.93	1873.89	19 Q 36	3849.10	3931.14
2191.06	2109.01	2026.97	1944.93	20 A 35	3721.04	3803.09
2278.09	2196.05	2114.00	2031.96	21 S 34	3650.01	3732.05
2349.12	2267.08	2185.04	2103.00	22 A 33	3562.97	3645.02
2450.17	2368.13	2286.09	2204.05	23 T 32	3491.94	3573.98
2579.21	2497.17	2415.13	2333.09	24 E 31	3390.89	3472.93
2742.28	2660.24	2578.19	2496.15	25 Y 30	3261.85	3343.89
2855.36	2773.32	2691.28	2609.24	26 I 29	3098.78	3180.83
2912.38	2830.34	2748.30	2666.26	27 G 28	2985.70	3067.74

b+3L	b+2L	b+1L	b	pVIII	y	y+1L
3075.45	2993.41	2911.36	2829.32	28 Y 27	2928.68	3010.72
3146.48	3064.44	2982.40	2900.36	29 A 26	2765.62	2847.66
3332.56	3250.52	3168.48	3086.44	30 W 25	2694.58	2776.62
3403.60	3321.56	3239.52	3157.47	31 A 24	2508.50	2590.54
3534.64	3452.60	3370.56	3288.52	32 M 23	2437.46	2519.50
3633.71	3551.67	3469.63	3387.58	33 V 22	2306.42	2388.46
3732.78	3650.74	3568.69	3486.65	34 V 21	2207.35	2289.39
3831.85	3749.80	3667.76	3585.72	35 V 20	2108.28	2190.33
3944.93	3862.89	3780.85	3698.80	36 I 19	2009.22	2091.26
4044.00	3961.96	3879.92	3797.87	37 V 18	1896.13	1978.17
4101.02	4018.98	3936.94	3854.89	38 G 17	1797.06	1879.11
4172.06	4090.02	4007.97	3925.93	39 A 16	1740.04	1822.08
4273.11	4191.06	4109.02	4026.98	40 T 15	1669.00	1751.05
4386.19	4304.15	4222.11	4140.06	41 I 14	1567.96	1650.00
4443.21	4361.17	4279.13	4197.08	42 G 13	1454.87	1536.91
4556.29	4474.25	4392.21	4310.17	43 I 12	1397.85	1479.89
4684.39	4602.35	4520.31	4438.26	44 K 11	1284.77	1366.81
4797.47	4715.43	4633.39	4551.35	45 L 10	1156.67	1238.71
4944.54	4862.50	4780.46	4698.42	46 F 9	1043.59	1125.63
5072.64	4990.60	4908.55	4826.51	47 K 8	896.52	978.56
5200.73	5118.69	5036.65	4954.61	48 K 7	768.43	850.47
5347.80	5265.76	5183.72	5101.67	49 F 6	640.33	722.37
5448.85	5366.81	5284.76	5202.72	50 T 5	493.26	575.30
5535.88	5453.84	5371.80	5289.75	51 S 4	392.21	474.26
5663.98	5581.93	5499.89	5417.85	52 K 3	305.18	387.22
5735.01	5652.97	5570.93	5488.89	53 A 2	177.09	259.13
---	---	---	---	54 S 1	106.05	188.09

Appendix A3

MALDI-MS deconvoluted spectra of BSA (A), BSA-(2-yne) (B), BSA-(2-yne)-Tetra (C) and BSA-(2-yne)-Penta (D). Each linker addition adds a net mass of 59.99 Da. Each tetrasaccharide and pentasaccharide conjugated adds a net mass of 737.22 and 899.27 Da.



Appendix A4

¹H NMR of compound **1**

¹H NMR overlay of α and β anomers of compound **1**

¹H NMR overlay of α and β anomers of compound **2**

¹H NMR of compound **28**

¹H NMR of compound **29**

¹H NMR of compound **31**

¹H NMR of compound **32**

1D TOCSY overlay of compound **32**

¹H NMR of compound **35**

¹H NMR of compound **38**

1D TOCSY overlay of compound **38**

¹H NMR of compound **40**

¹H NMR of compound **41**

¹H NMR of compound **45**

1D TOCSY overlay of compound **45**

¹H NMR of compound **46**

¹H NMR of compound **47**

1D TOCSY overlay of compound **47**

¹H NMR of compound **49**

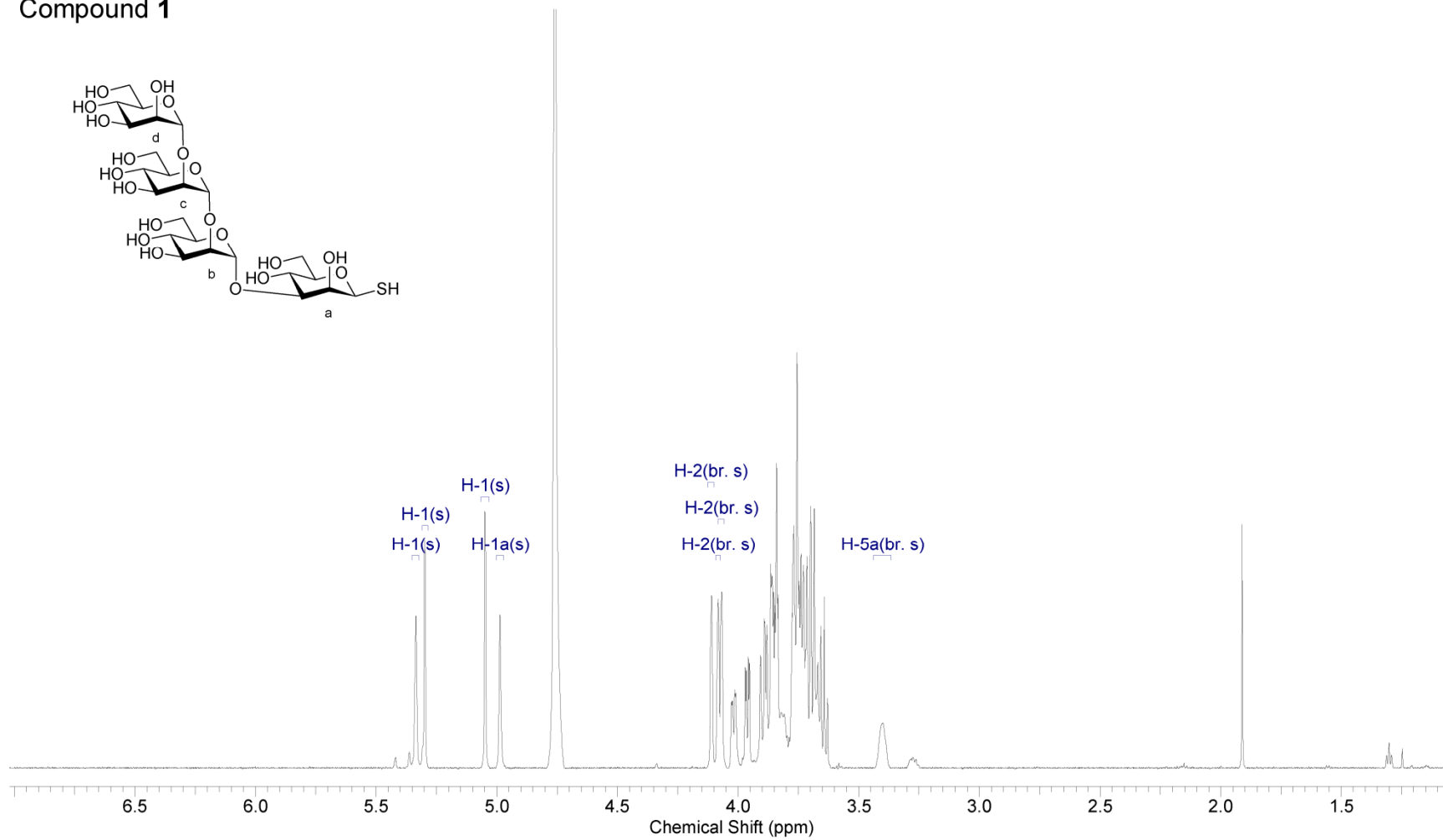
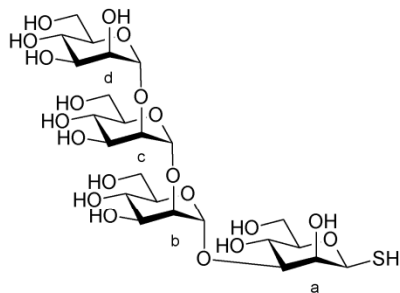
1D TOCSY overlay of compound **49**

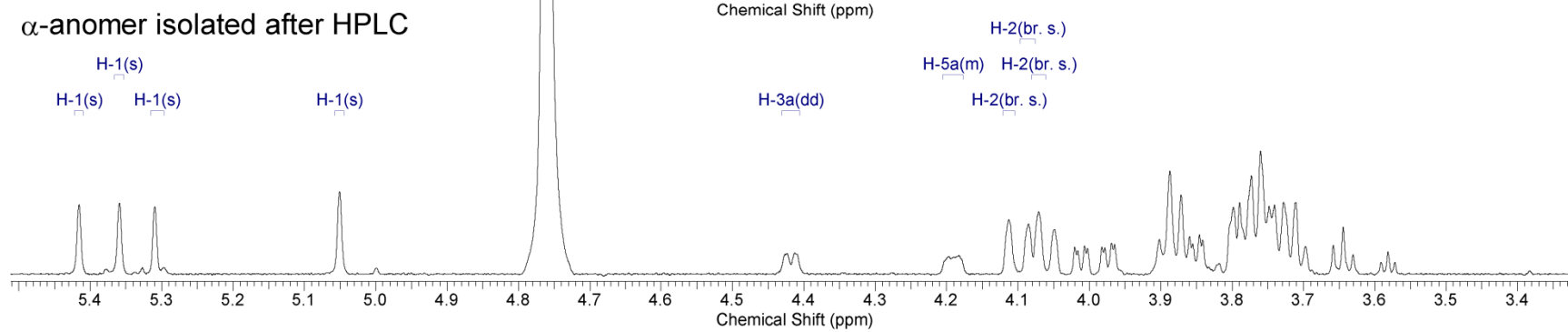
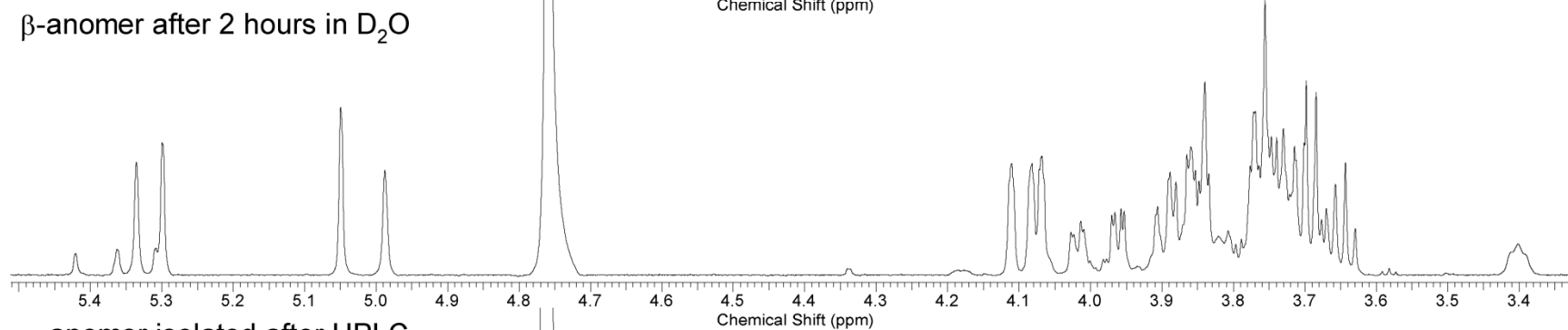
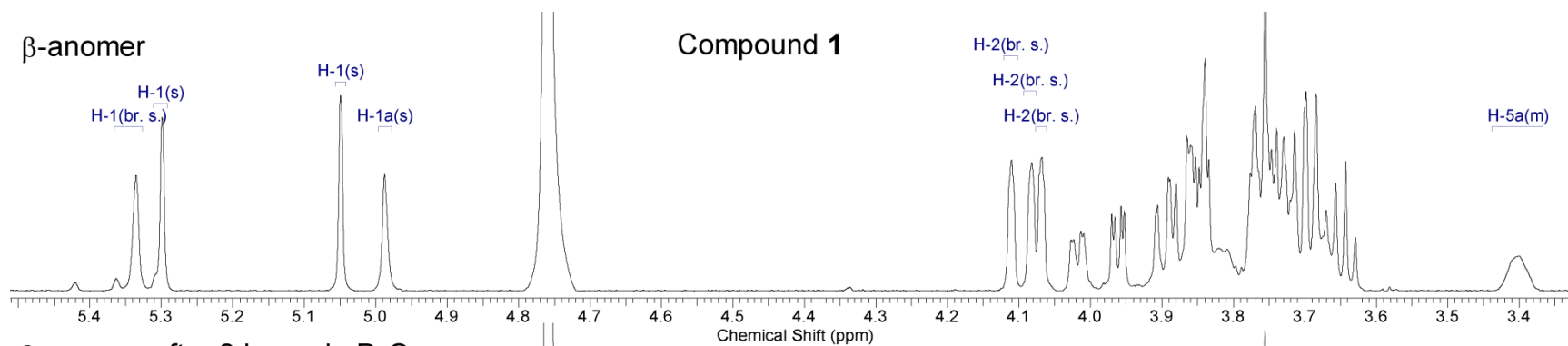
¹H NMR of compound **50**

1D TOCSY overlay of compound **50**

JB-06-57 Tetra-SH 49m4 699.740 MHz H1 1D in d2o (ref. to external acetone @ 2.225 ppm), temp 27.5 C -> actual temp = 27.0 C, coldid probe

Compound 1

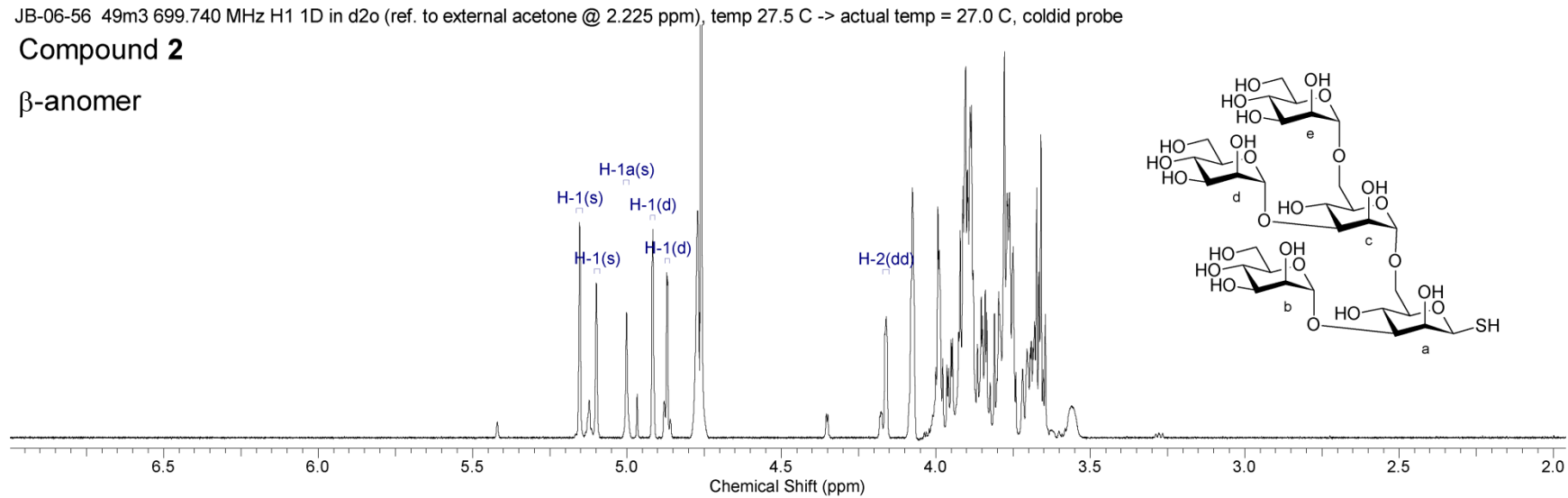




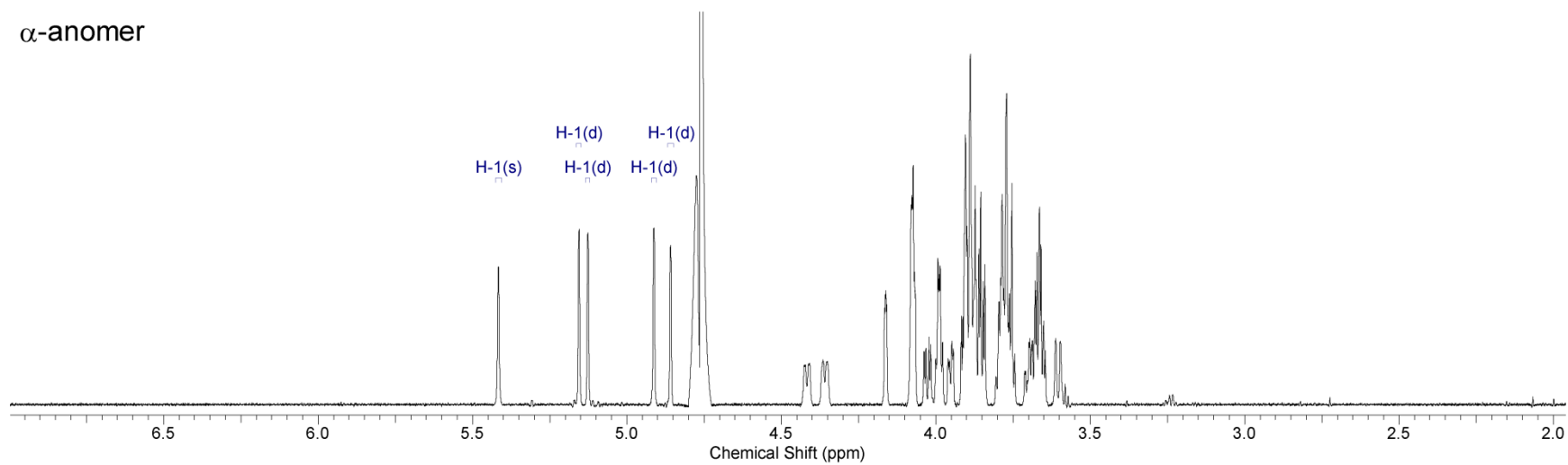
JB-06-56 49m3 699.740 MHz H1 1D in d2o (ref. to external acetone @ 2.225 ppm), temp 27.5 C -> actual temp = 27.0 C, coldid probe

Compound 2

β -anomer



α -anomer

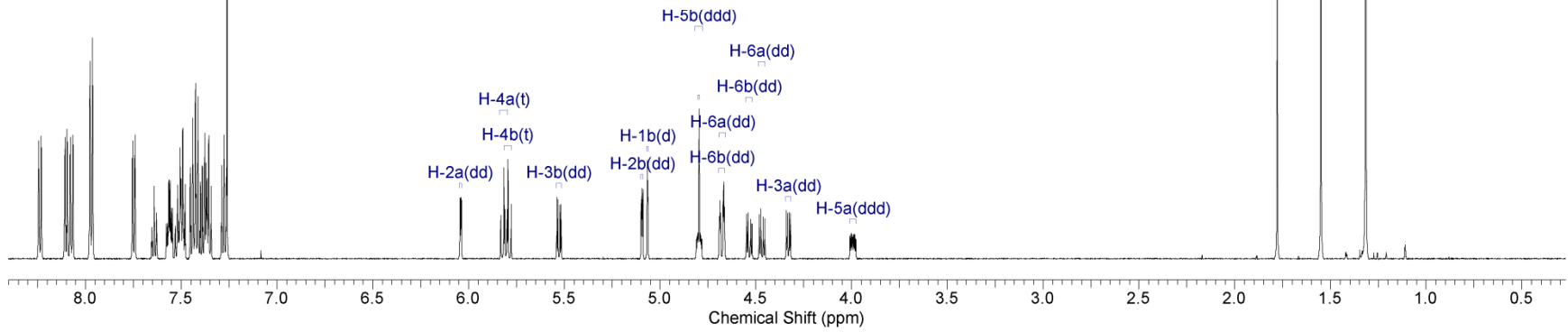
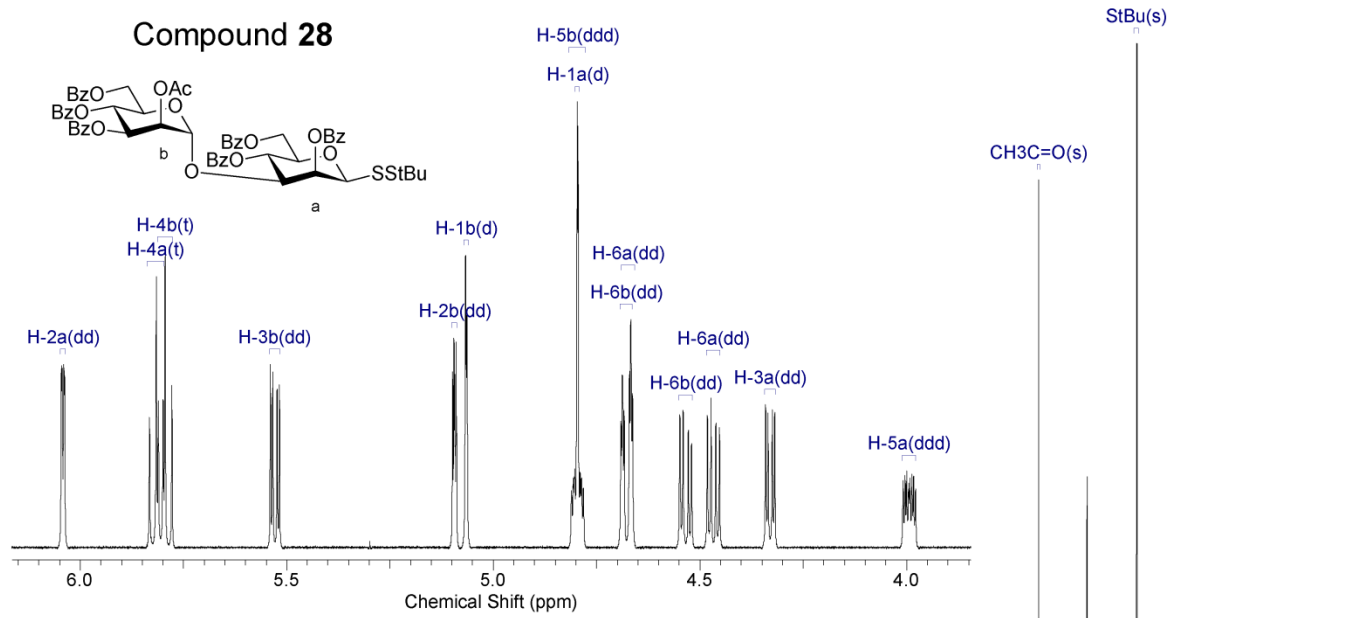
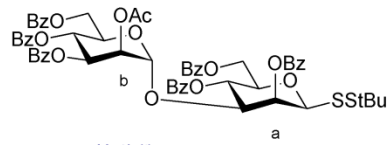


Ar(m)

JB-05-39 599.926 MHz H1 1D in cdcl3 (ref. to CDCI3 @ 7.26 ppm), temp 25.8 C -> actual temp = 27.0 C, autoxid probe

CDCI3

Compound 28

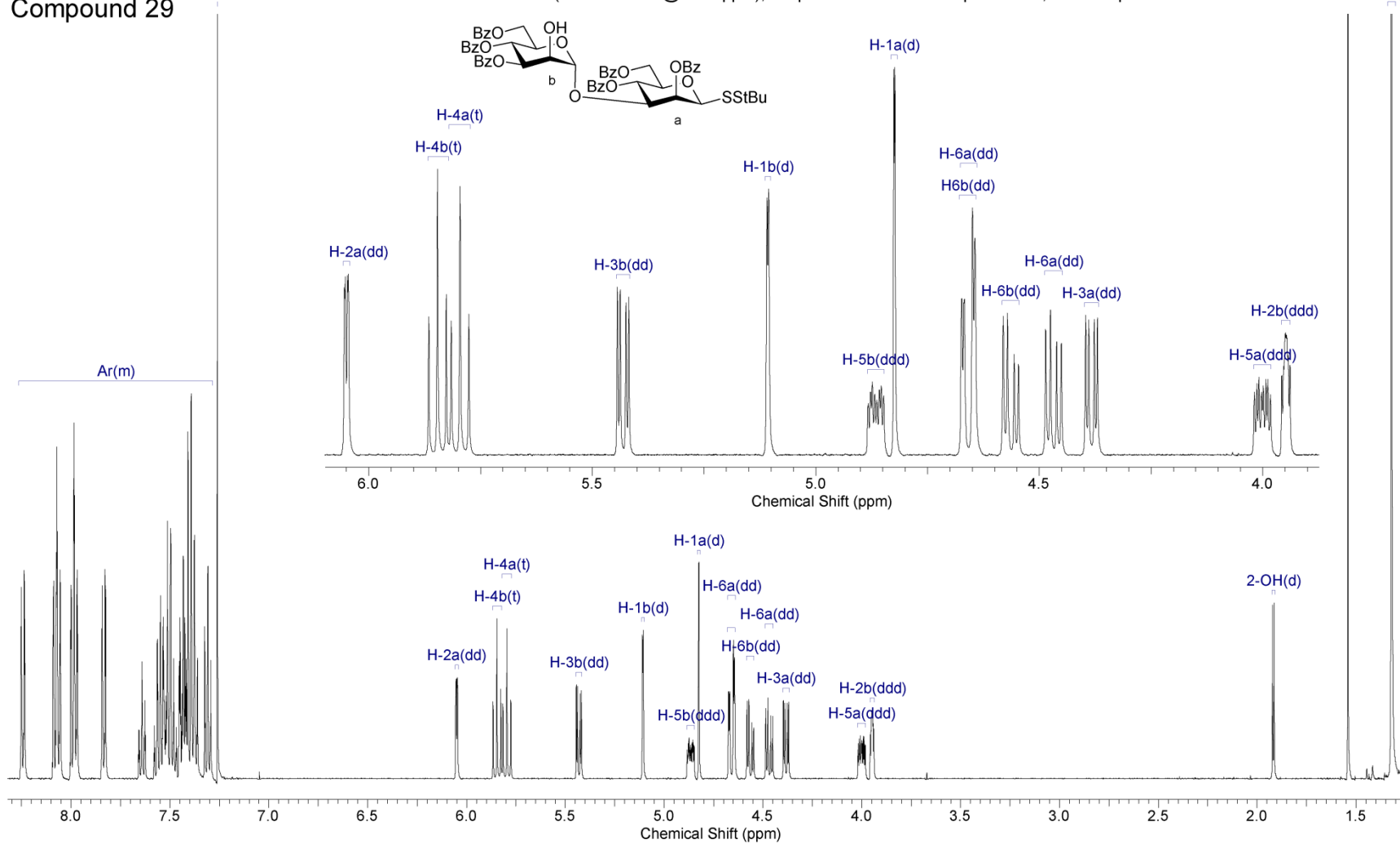


Compound 29

CDC13 JB-05-30 499.815 MHz H1 1D in cdcl3 (ref. to CDC13 @ 7.26 ppm), temp 27.7 C -> actual temp = 27.0 C, cold dual probe

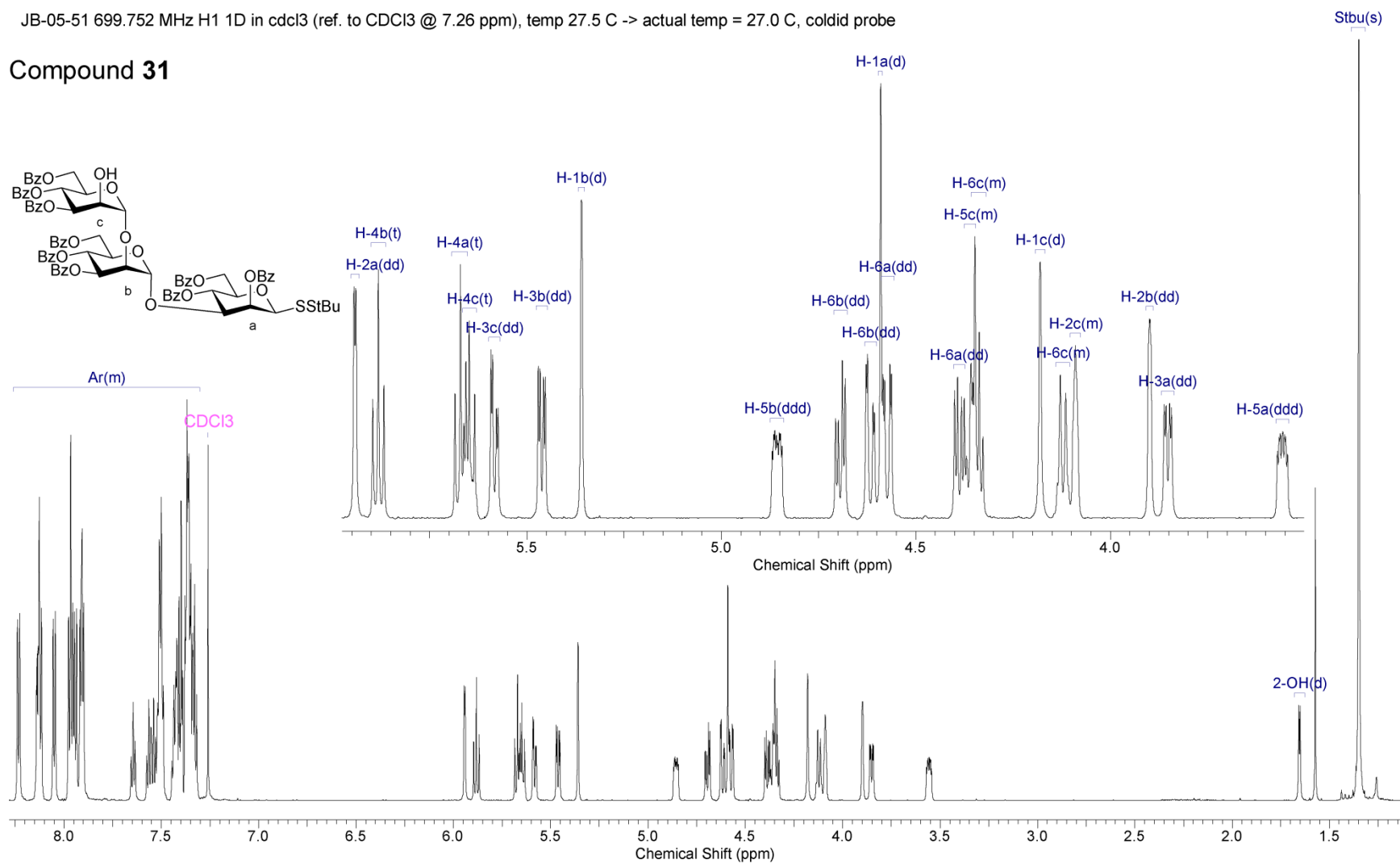
StBu(s)

Appendices

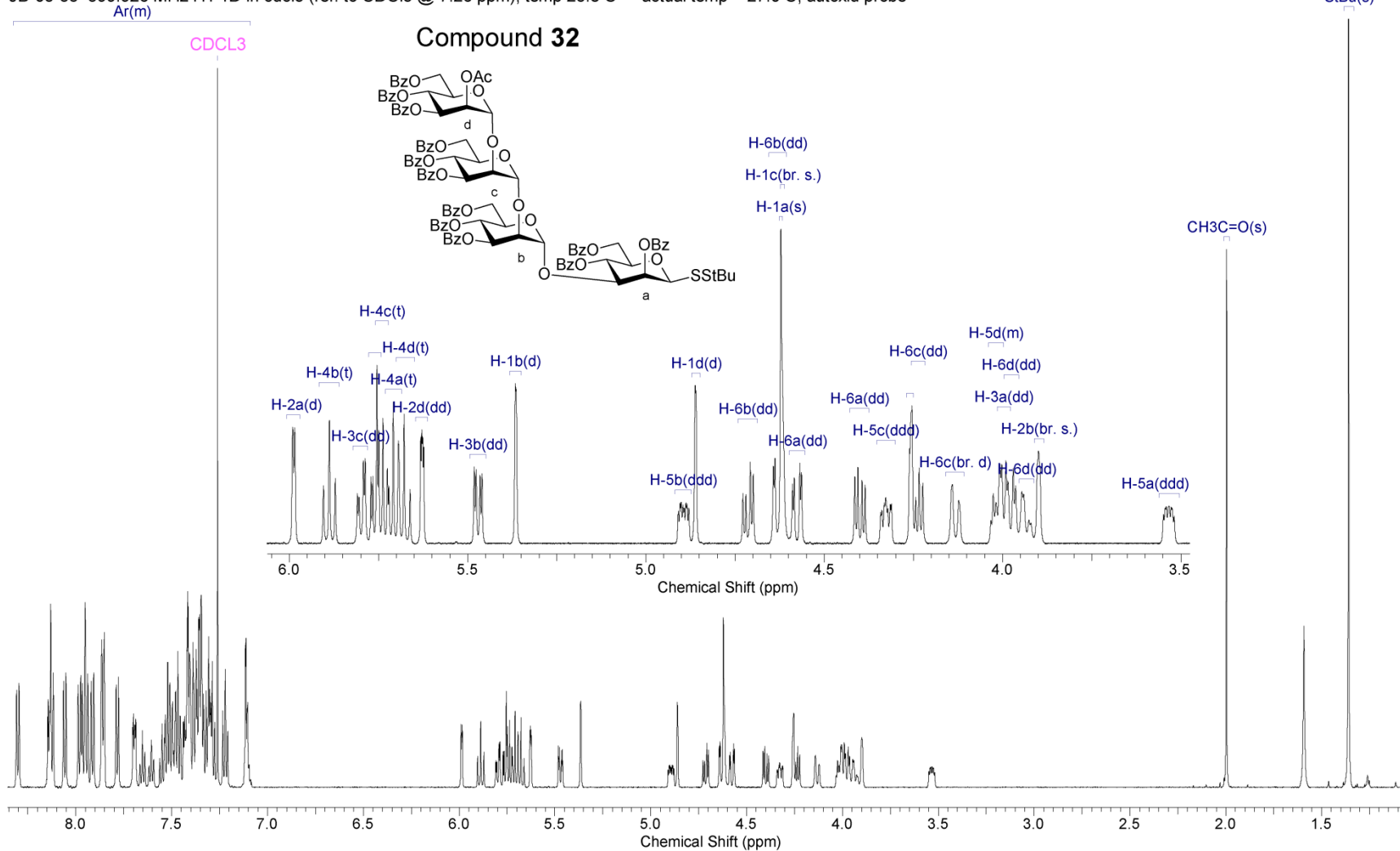


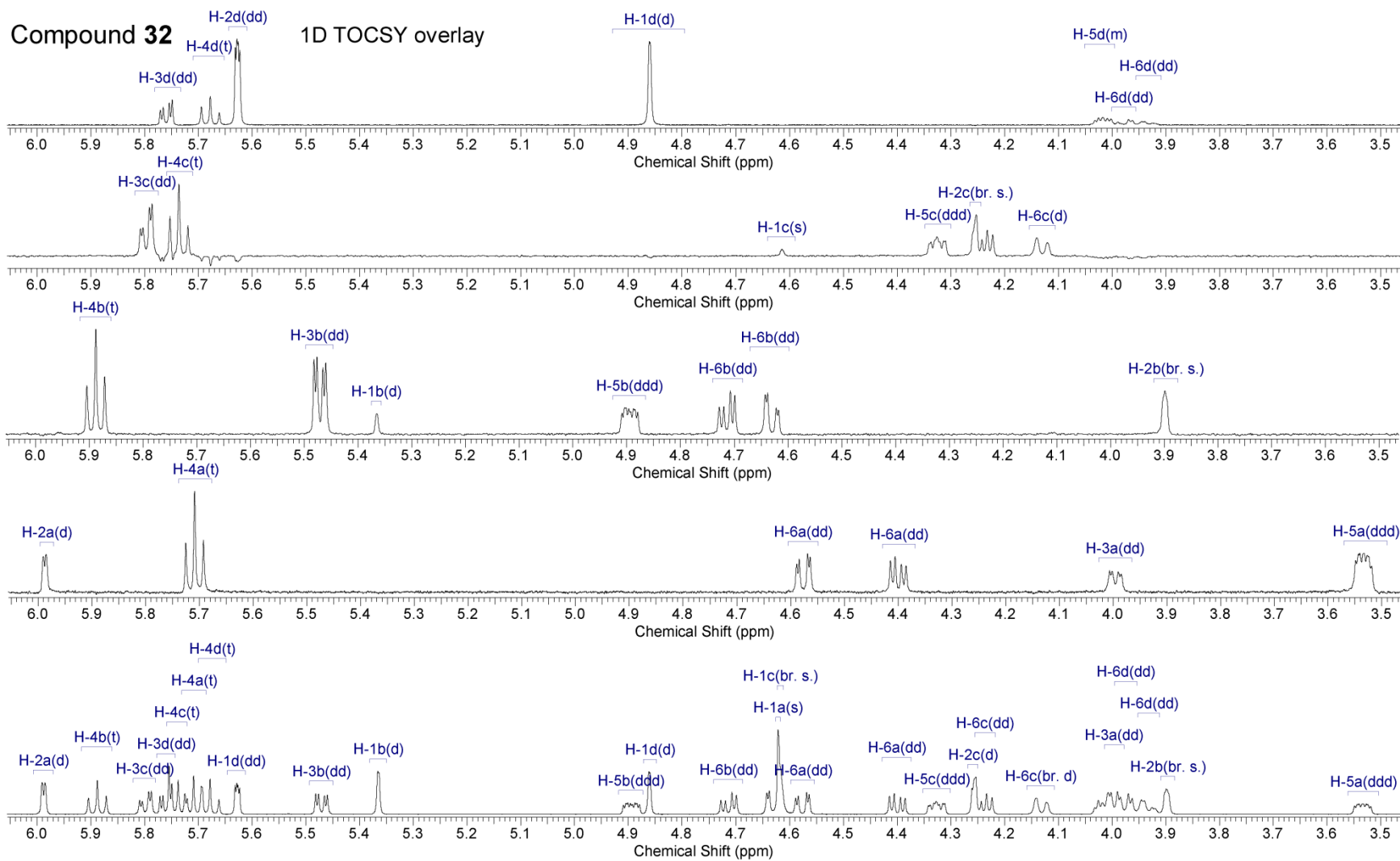
JB-05-51 699.752 MHz H1 1D in cdcl3 (ref. to CDCl3 @ 7.26 ppm), temp 27.5 C -> actual temp = 27.0 C, coldid probe

Compound 31



JB-05-55 599.926 MHz H1 1D in cdcl3 (ref. to CDCl3 @ 7.26 ppm), temp 25.8 C -> actual temp = 27.0 C, autoxid probe



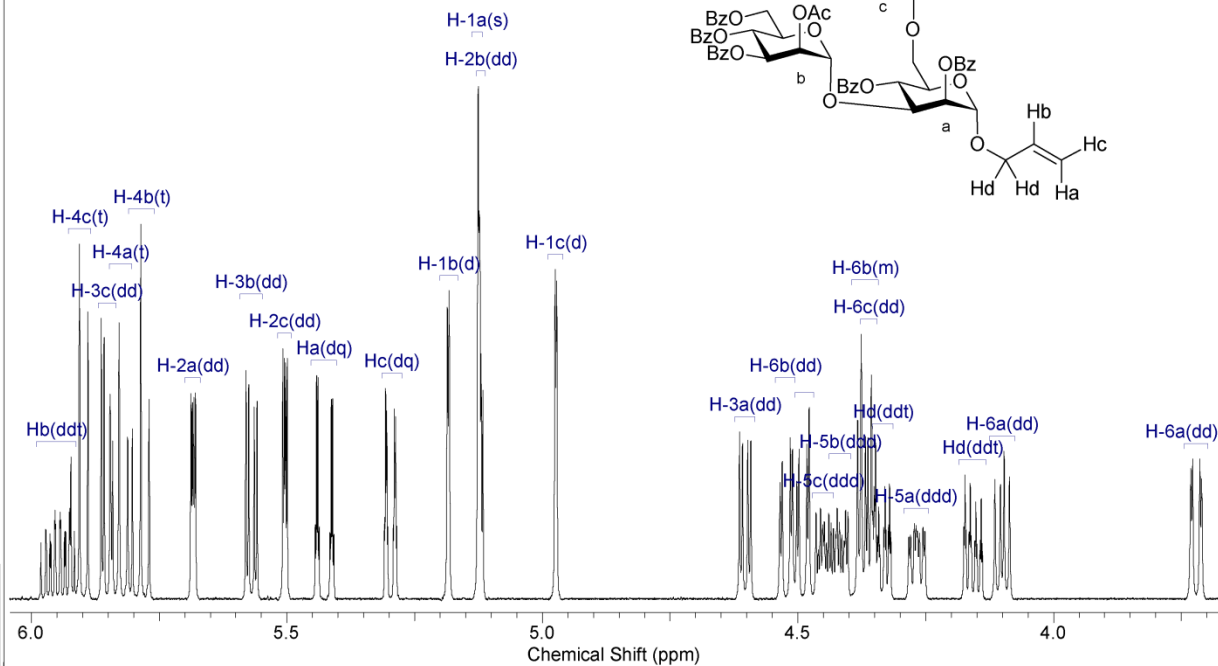
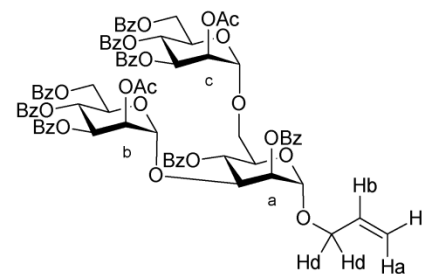


ArH(m)

JB-05-84 599.926 MHz H1 1D in cdcl3 (ref. to CDCl3 @ 7.26 ppm), temp 25.8 C -> actual temp = 27.0 C, autodox probe

Compound 35

CH3(C=O)(s)

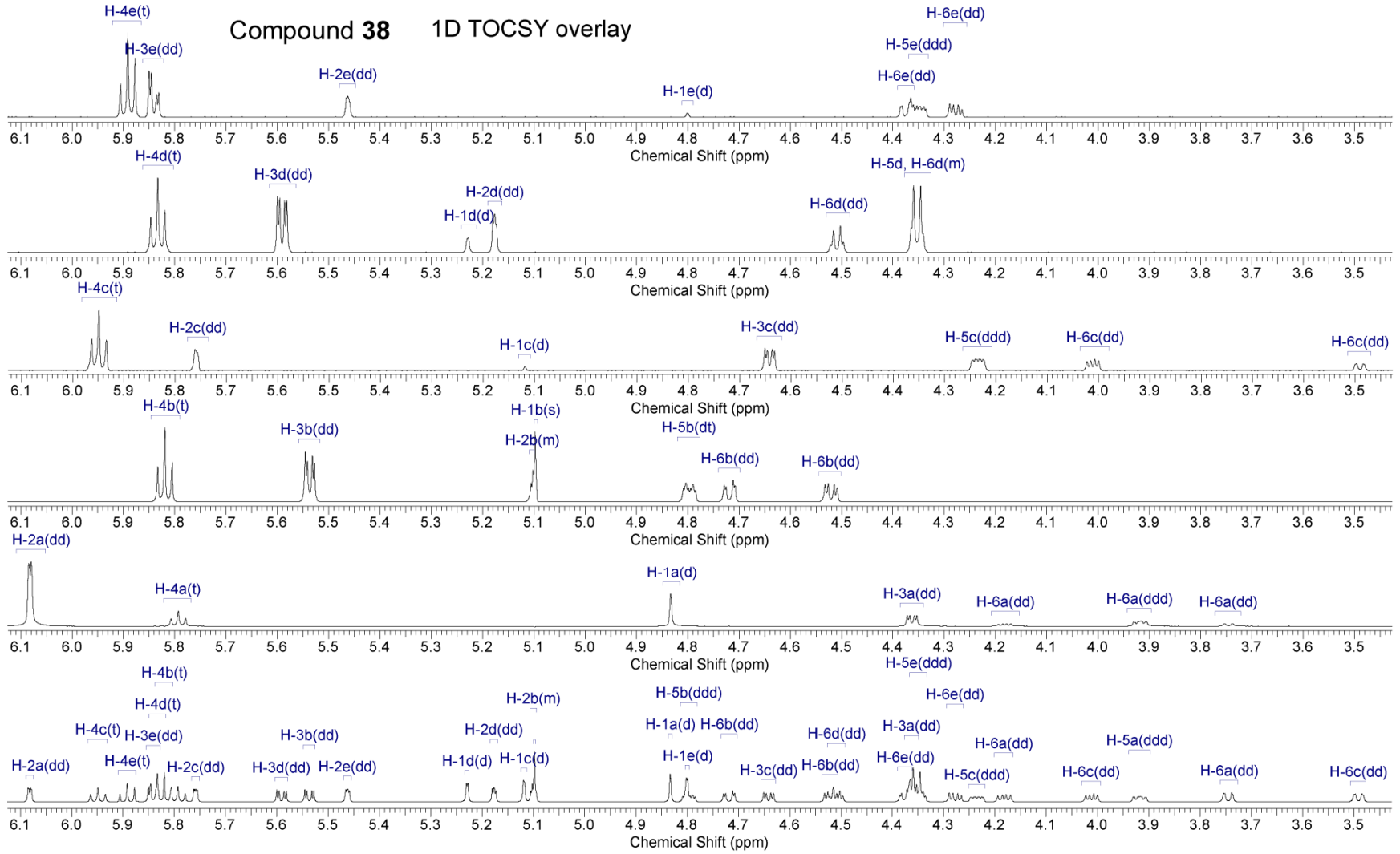


6.0 5.5 5.0 4.5 4.0
Chemical Shift (ppm)

CH3(C=O)(s)

H-6a(dd)

Chemical Shift (ppm)

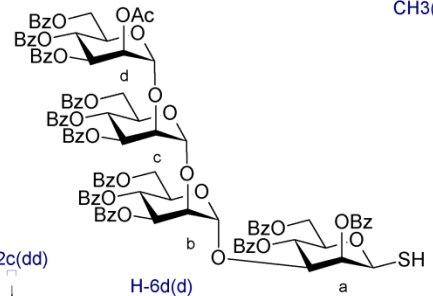


Ar(m)

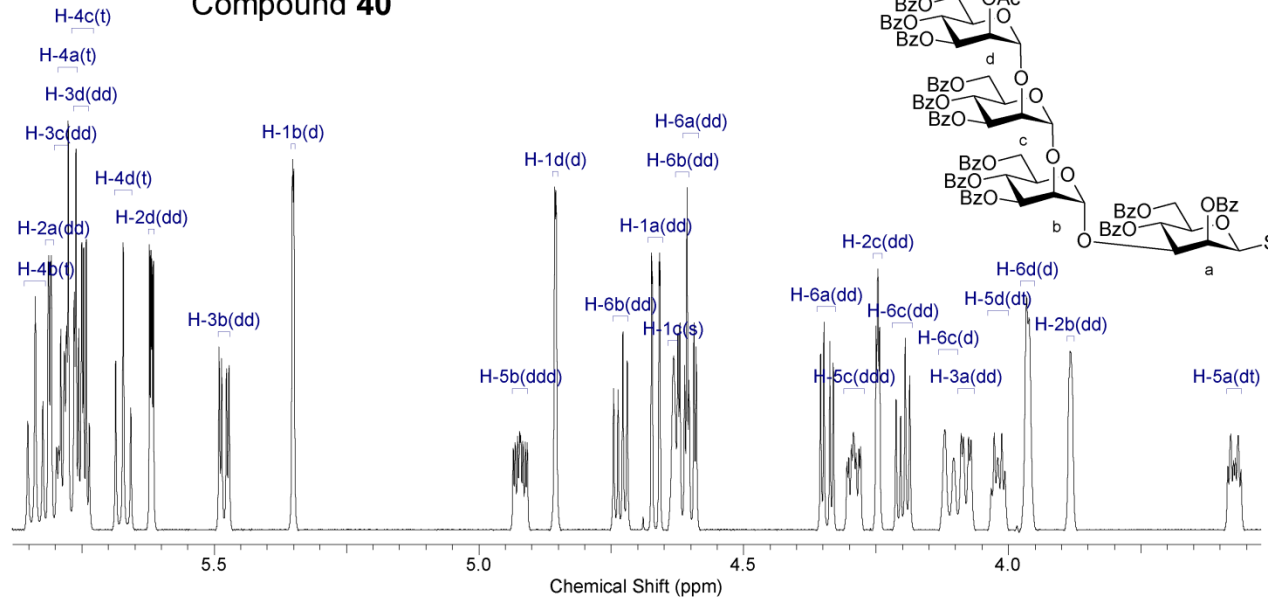
JB-06-46 699.738 MHz H1 1D in cdcl3 (ref. to CDCl3 @ 7.26 ppm), temp 27.5 C -> actual temp = 27.0 C, coldid probe

CDCl3

Compound 40

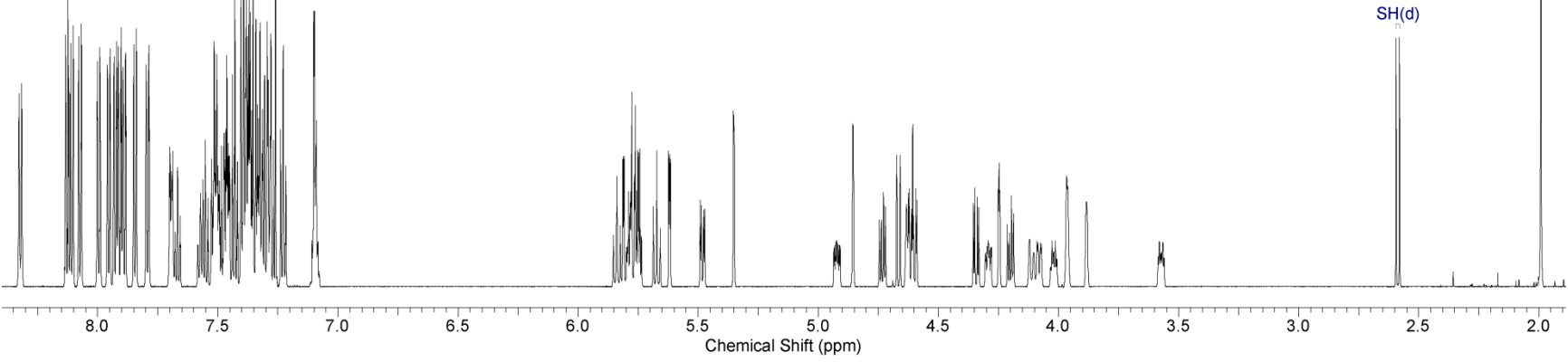


CH3(C=O)(s)



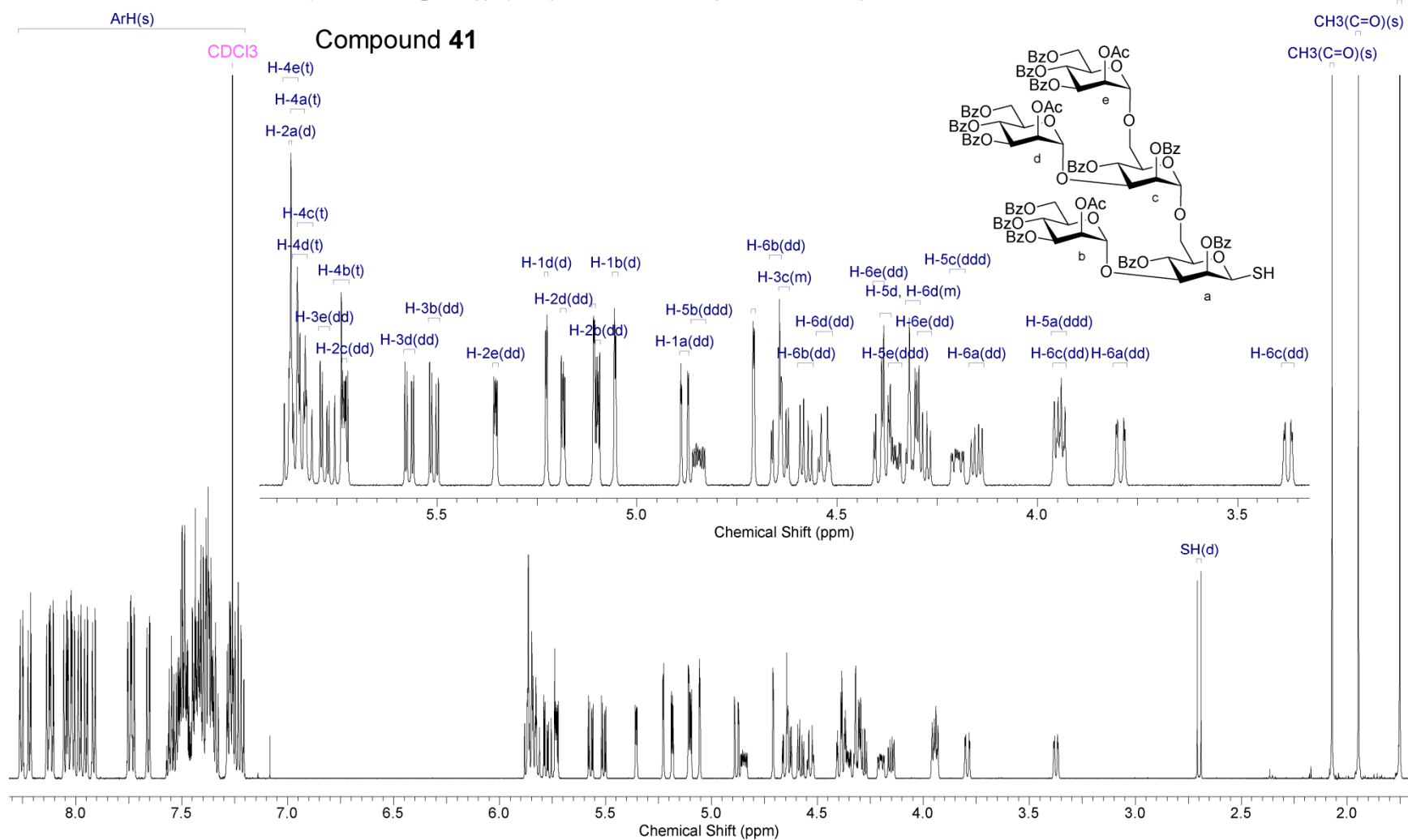
Chemical Shift (ppm)

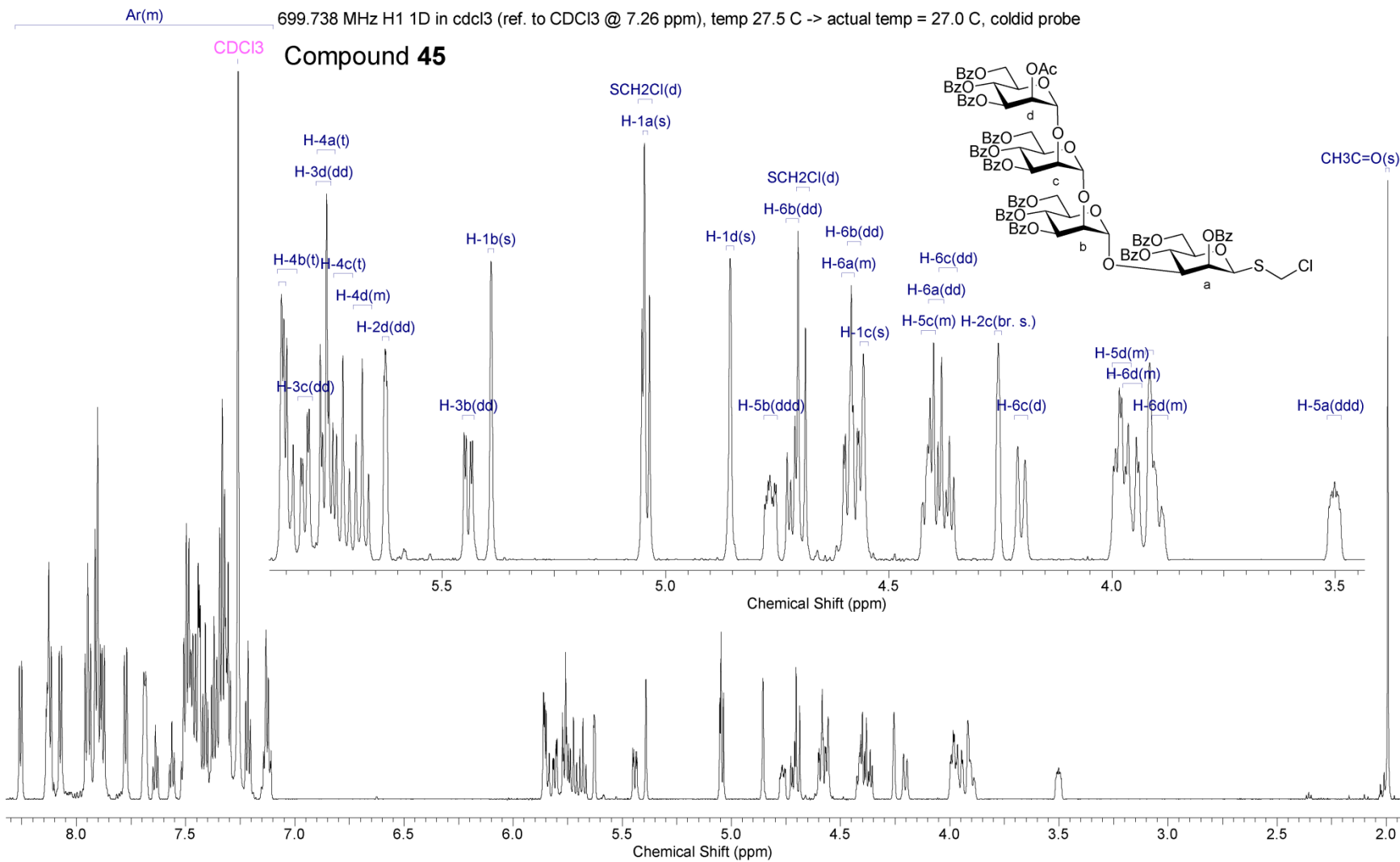
SH(d)

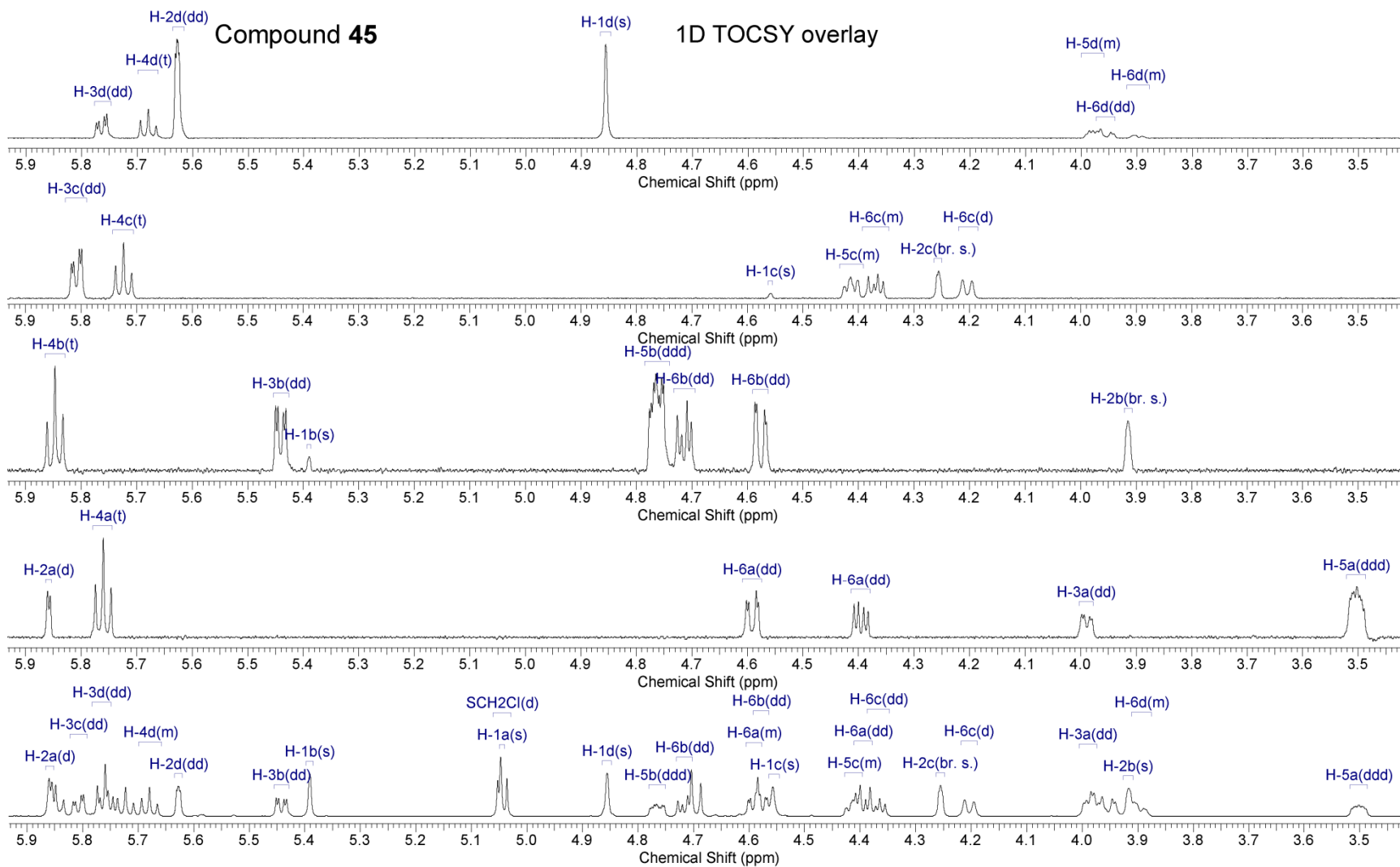


Chemical Shift (ppm)

JB-06-45 599.926 MHz H1 1D in cdcl3 (ref. to CDCl3 @ 7.26 ppm), temp 25.8 C -> actual temp = 27.0 C, autoxid probe





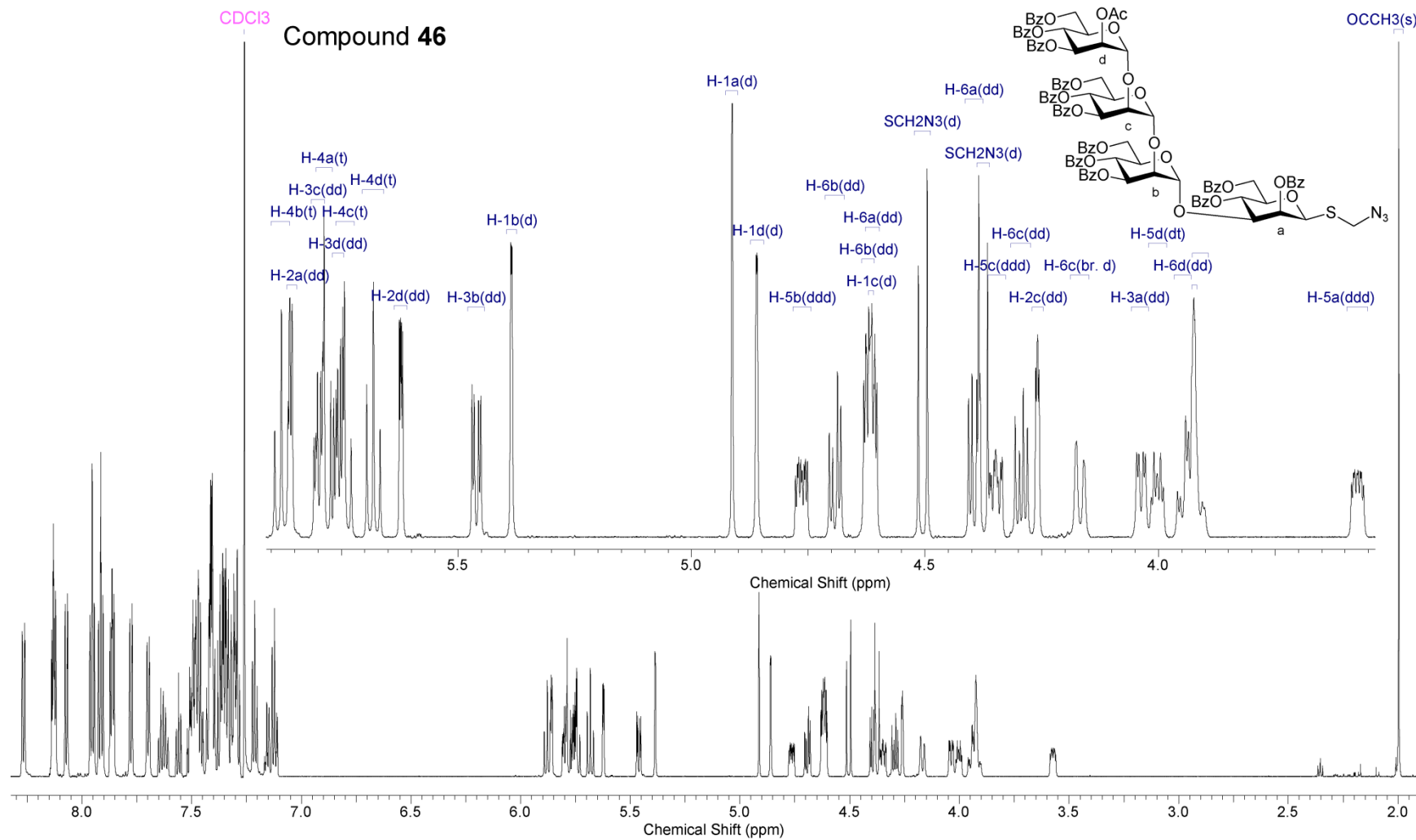


ArH(m)

JB-06-44 699.738 MHz H1 1D in cdcl3 (ref. to CDCl3 @ 7.26 ppm), temp 27.5 C -> actual temp = 27.0 C, coldid probe

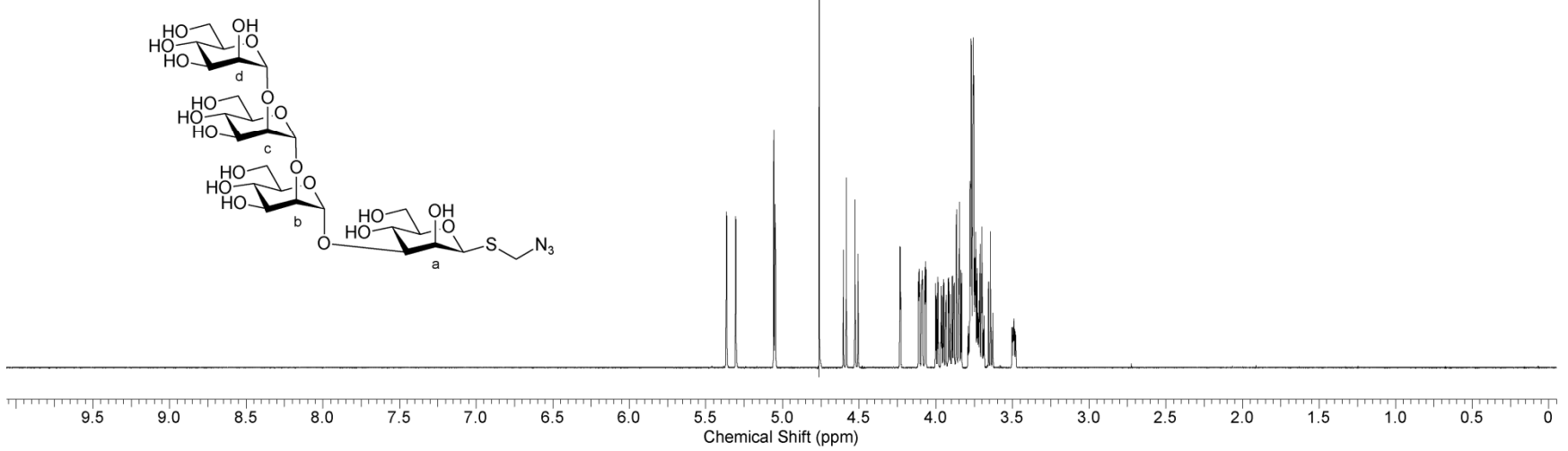
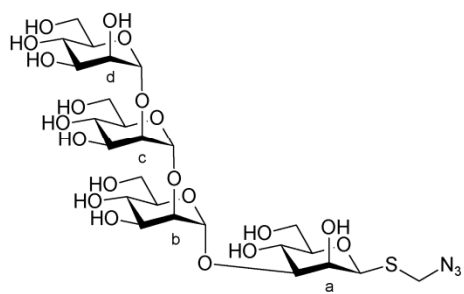
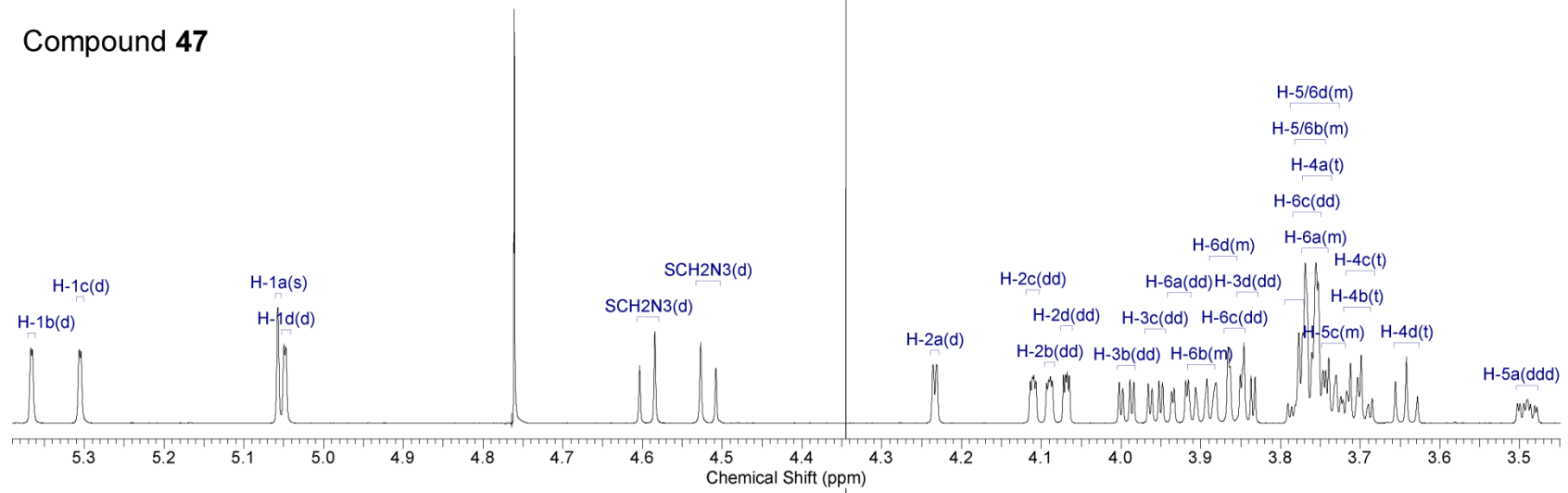
CDCl3

Compound 46

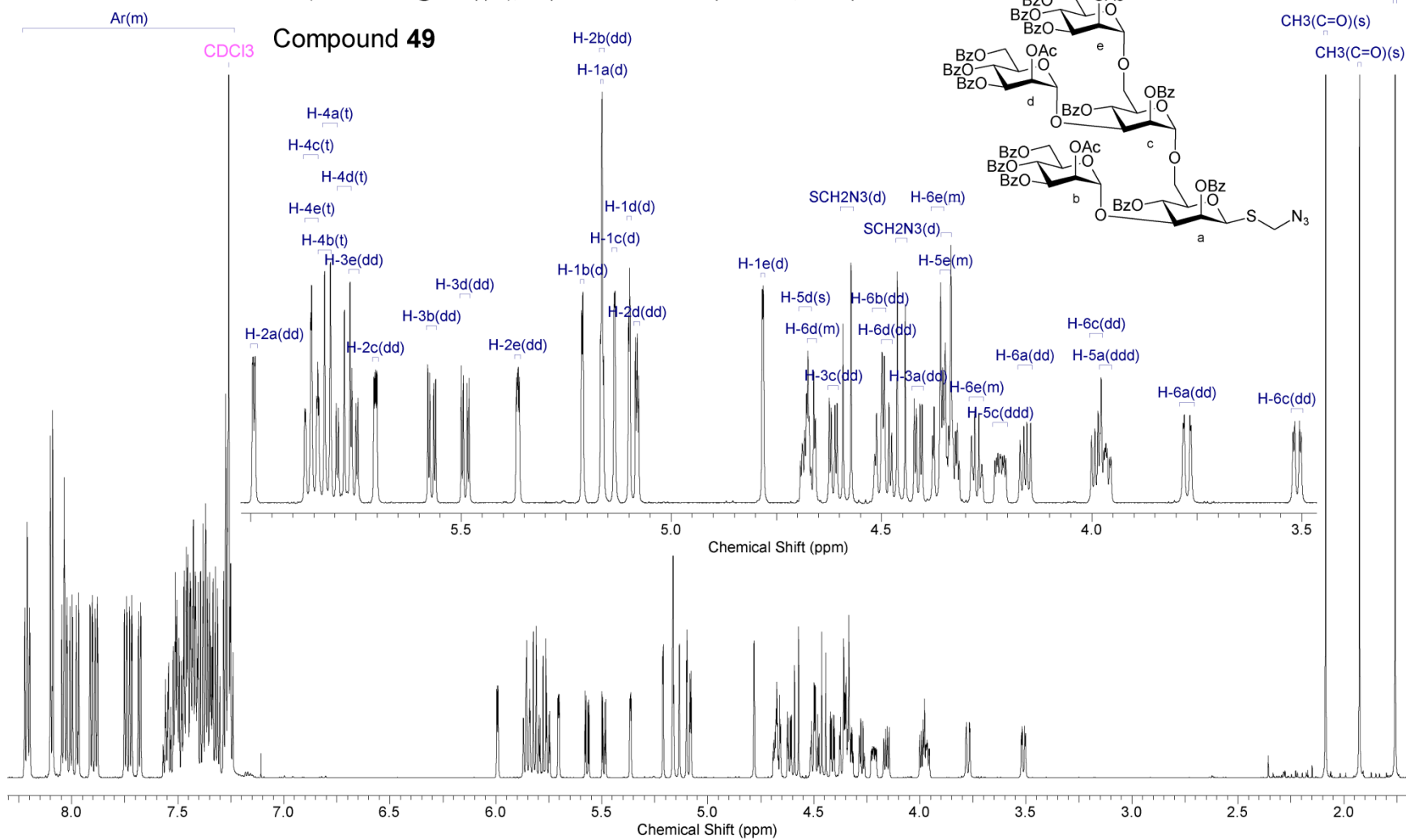


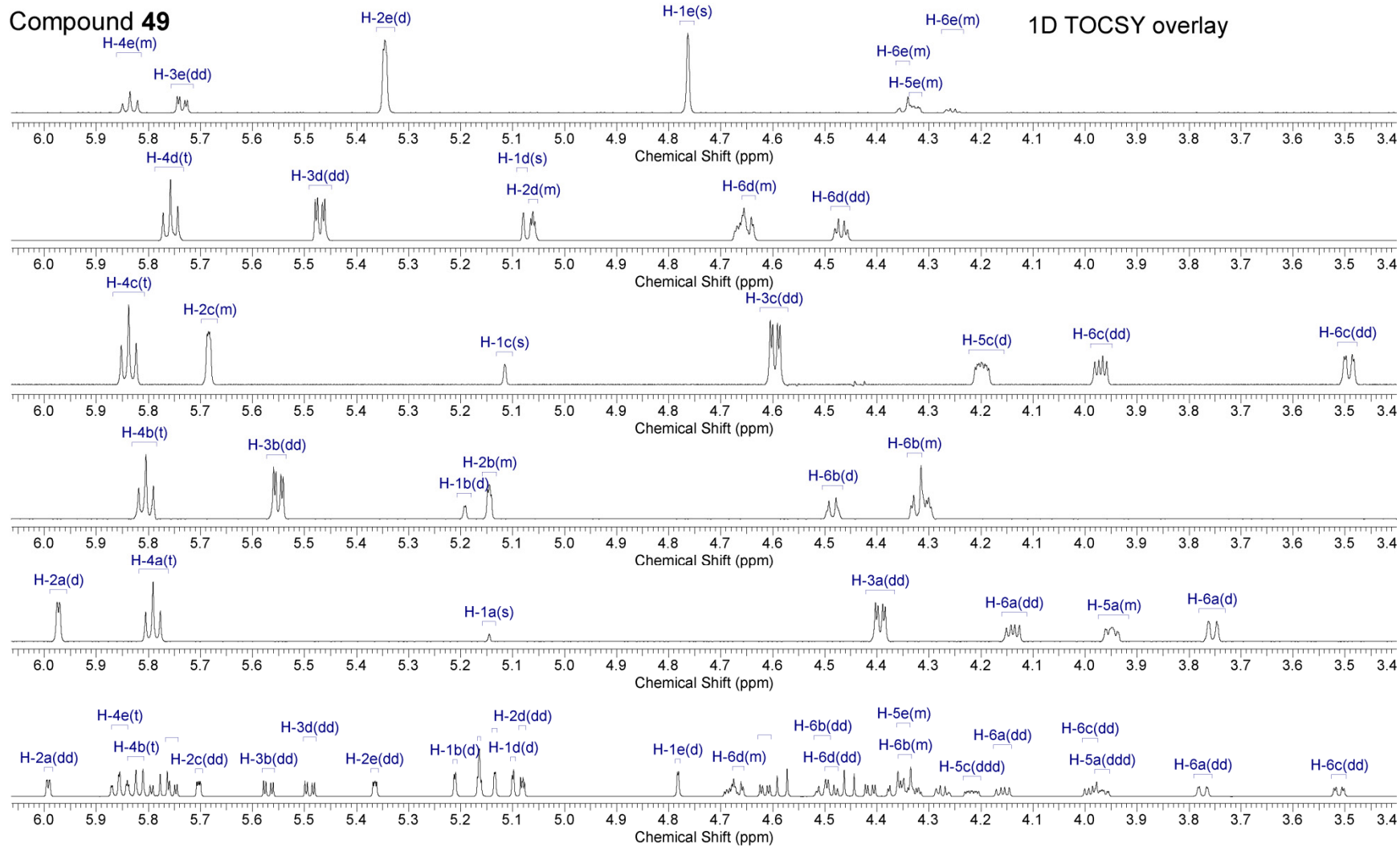
JB-06-52 44 min HPLC fraction 699.740 MHz H1 1D in d2o (ref. to external acetone @ 2.225 ppm), temp 27.5 C -> actual temp = 27.0 C, coldid probe

Compound 47



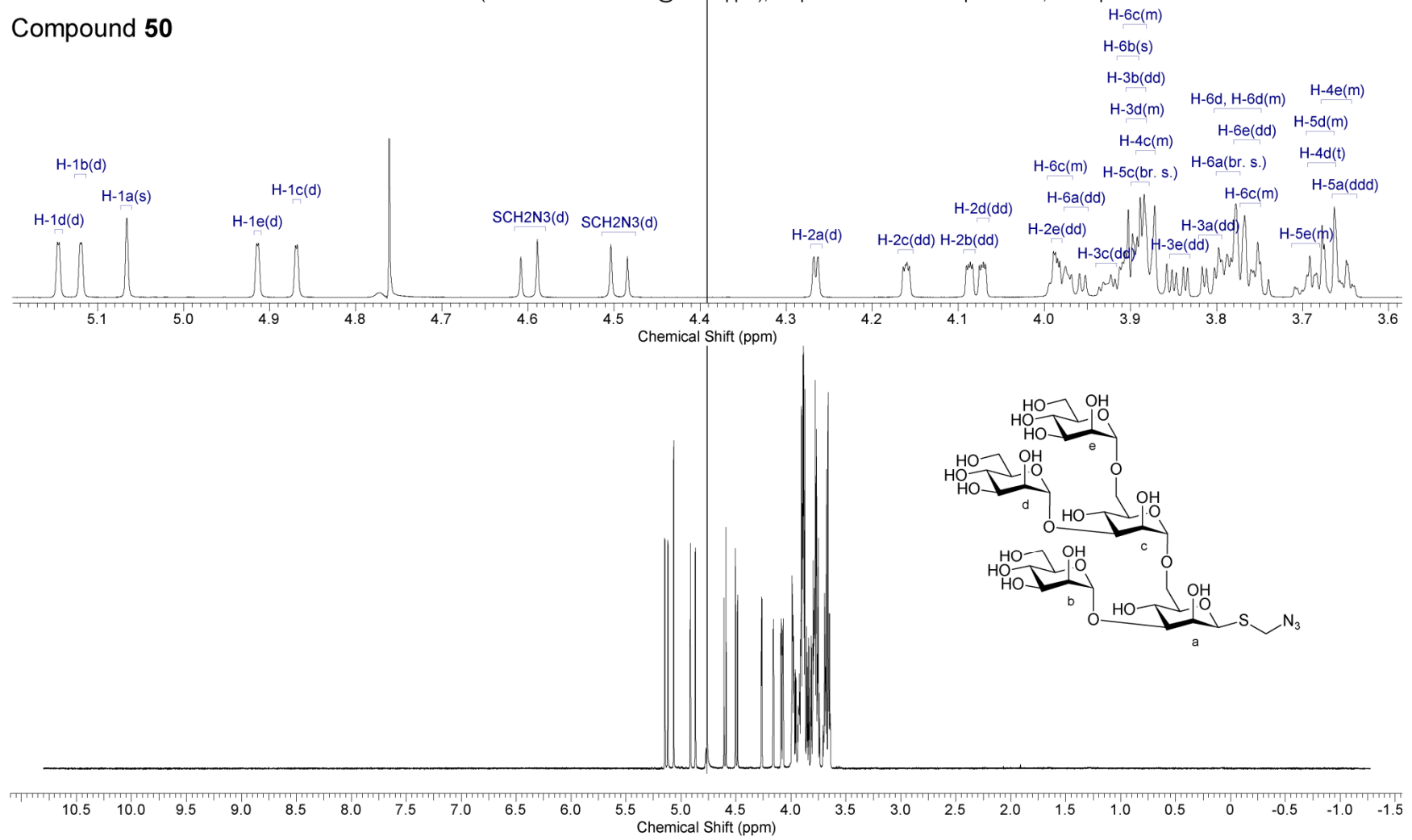
JB-06-50 699.738 MHz H1 1D in cdcl3 (ref. to CDCl3 @ 7.26 ppm), temp 27.5 C -> actual temp = 27.0 C, coldid probe





JB-06-53 59 minute HPLC fraction 699.740 MHz H1 1D in d2o (ref. to external acetone @ 2.225 ppm), temp 27.5 C -> actual temp = 27.0 C, coldid probe

Compound 50



Compound **50** 1D TOCSY overlay

